THE PHYSICAL SOCIETY

REPORTS ON PROGRESS IN PHYSICS

VOLUME XIX (1956)

EXECUTIVE EDITOR
A. C. STICKLAND

Price to non-Fellows £2 10*s. net* (*Postage* 1*s.* 8*d.*)
Price to Fellows (*one copy*) £1 7*s.* 6*d. net* (*Postage* 1*s.* 8*d.*)

Published by
THE PHYSICAL SOCIETY
1 Lowther Gardens, Prince Consort Road
London S.W.7
1956

Printed by John Wright and Sons Ltd.
The Stonebridge Press, Bath Road, Bristol 4

CONTENTS

	PAGE
Preface	iv
The Kinetic Theory of Monatomic Liquids at Ordinary Temperatures. By G. H. A. Cole	1
The Proton Synchrotron. By J. P. Blewett	37
Radioactive Methods for Determining Geological Age. By L. H. Ahrens	80
Infra-red Absorption in Semiconductors. By H. Y. Fan	107
Aero-thermoacoustics. By O. K. Mawardi	156
Some Aspects of Diffraction Theory and their Application to the Ionosphere. By J. A. Ratcliffe	188
Some Topics in Neutron Diffusion Theory. By J. H. Tait	268
New Lens Systems. By C. G. Wynne	298
The Macroscopic Theory of Irreversibility. By R. O. Davies	326

PREFACE

The *Reports on Progress in Physics* is under the general supervision of the Papers Committee of the Physical Society. The Members of the Papers Committee were as follows:

Chairman:—Professor H. Jones.

Honorary Papers Secretary:—Dr. H. H. Hopkins.

Ordinary Members:—The President (Professor H. S. W. Massey), Professor W. E. Burcham, Dr. E. H. S. Burhop, Mr. C. H. Collie, Dr. A. H. Cooke, Professor S. Devons, Professor C. Domb, Dr. W. Ehrenberg, Dr. F. C. Frank, Mr. D. W. Fry, Mr. R. C. Horner, Professor F. Llewellyn Jones, Professor G. O. Jones, Dr. H. G. Kuhn, Professor R. E. Peierls, Mr. E. S. Shire, Dr. R. W. B. Stephens, Dr. H. Wilman, Dr. C. G. Wynne.

Reports published in the Volume are also being issued as individual articles, at prices depending on their length. Information may be obtained from the offices of the Society.

A. C. STICKLAND,
Secretary–Editor.

THE KINETIC THEORY OF MONATOMIC LIQUIDS AT ORDINARY TEMPERATURES

By G. H. A. COLE
University College London

CONTENTS

PAGE

§ 1. Introduction 2
§ 2. Molecular order in liquids 3

I. Uniform Systems

§ 3. The theory of molecular order in uniform liquids 6
3.1. The pair distribution in statistical mechanics 6
3.2. The superposition approximation 9
3.3. The cell model 10
3.4. The calculation of thermodynamic functions 11
§ 4. Comparison between theory and experiment 13
4.1. Equations using the pair distribution 13
4.1.1. Analytical methods 13
4.1.2. Numerical methods 14
4.2. Critique of the superposition approximation 15
4.3. Equations from the cell model 16
§ 5. Surface tension 17

II. Non-uniform Systems

§ 6. The element of irreversibility 19
§ 7. The theory of molecular order in non-uniform liquids 20
7.1. The Fokker–Planck equation 20
7.2. The friction constants 23
7.3. The Smoluchowski equation 24
7.4. The Born and Green equations 25
§ 8. Momentum and energy flow 26
§ 9. Calculations of the transport coefficients 27
9.1. The theory of Born and Green 27
9.2. The theory of Kirkwood 27
9.3. The theory of Eisenschitz 30
§ 10. Conclusion 33
Acknowledgment 34
References 35

Abstract. In the last ten years new and successful attempts have been made at constructing a satisfactory theory of liquids which is able to include uniform or non-uniform conditions. For uniform systems the problem is the mathematical one of applying to the liquid state the well-established principles of statistical mechanics. For non-uniform systems, where the principles of statistical mechanics are inapplicable, the problem is first to derive principles of as wide validity for these systems as those of statistical mechanics for uniform systems. Solutions of both problems are now available which have led to quantitative calculations for monatomic liquids, and which can provide also semi-quantitative information for polyatomic liquids. This modern work is reviewed in the present article with a view to determining the achievements and deficiencies of the theory. It is concluded that at last a correct kinetic theory of monatomic liquids has been established which can be expected to lead to a full understanding of the liquid state.

§ 1. Introduction

The aim of the kinetic theory can be taken as being the calculation of the gross properties of matter from the properties of the constituent molecules, using only the principles of molecular dynamics. The theory of liquids has for a long time been in an unsatisfactory state, as compared with the corresponding theories of solids and dilute gases, owing to the difficulties associated with treating the motion of a system of interacting particles which does not have simplifying features. In the last decade new attempts have been made at constructing a molecular theory of fluids, and encouraging progress can be claimed as a result.

In the theory it is necessary to distinguish clearly between systems that are in equilibrium and those that are not. This distinction, whose importance was recognized by Fowler (1939), has often been neglected. The macroscopic properties of a uniform system are described by thermodynamic functions that can be calculated from molecular data by an appeal to the well-established principles of statistical mechanics. The necessary molecular data, such as the intermolecular force, can be regarded as known to sufficient accuracy for this purpose at the present time. These general principles apply to all equilibria, and to the interphase regions. Their application, however, has been severely restricted by purely mathematical difficulties, which are particularly troublesome for liquids.

A system that is not in equilibrium moves irreversibly towards this state at a rate specified by a set of transport coefficients ; for a simple system these are the coefficients of viscosity, thermal conduction, diffusion, and so on. A macroscopic theory of irreversible thermodynamics has now been established to treat such non-uniform systems (see, for example, the review by Davies (1956) in the present volume). The corresponding microscopic theory cannot be based on statistical mechanics, even though the non-uniformities may be arbitrarily small, and in the problem of calculating the transport coefficients from molecular data it is first necessary to find principles of as wide validity for non-uniform systems as those of statistical mechanics in the theory of uniform systems. While, therefore, the problem of treating uniform systems is one of mathematics, which has been alleviated to some extent by the introduction of electronic computing techniques, the problem of non-uniform systems is still one of physics.

The present report falls naturally, therefore, into two parts. In the first, which follows a consideration of liquid molecular order (§ 2), attention is given to the equilibrium properties. The theory of molecular order is treated by invoking the principles of statistical mechanics (§ 3). First, expressions for the pair distributions in phase- and configuration-space are obtained (§ 3.1). It is seen that, due solely to mathematical difficulties, the evaluation of the expressions can at present be achieved only by the introduction of an auxiliary hypothesis ; this hypothesis is introduced into the theory in § 3.2. An alternative, mathematically simpler but theoretically less satisfactory, treatment of molecular order is that of the cell model ; this model is discussed in § 3.4. Finally (§ 3.5), the way in which the knowledge of the molecular order leads to values of the thermodynamic quantities of the system is explained. In § 4 the theory is compared with experiment (§ 4.1 and § 4.3), and the position of the auxiliary hypothesis

in the theory is briefly considered (§ 4.2). The first part then ends with a brief review of the treatment of surface tension (§ 5).

In the second part attention is directed to the theory of non-uniform systems, the particular importance of the element of irreversibility being stressed (§ 6). The central problem of the non-uniform theory, namely, the calculation of the non-uniform distribution functions, forms the topic of the next paragraph (§ 7). In § 8 the expressions for the flow of momentum and of energy describing the flux necessary for the establishment of uniformity throughout the liquid are explained, and finally (in § 9) the calculations of the transport coefficients that have been made so far are considered. The report ends with a brief summary (§ 10).

In order to keep the report to a reasonable length it is necessary to restrict its scope in several respects. Firstly, only theories in which details of the intermolecular force plays an important role have been considered. This has meant that those aspects of the cell model associated with Eyring (1936), and Eyring and Hirschfelder (1937), have had to be left out, as have also the researches using the ' hole ' model of Fürth (1941), such as that of Auluck and Kothari (1944, 1945).

Secondly, it has not been possible to include a discussion of the highly interesting work on the processes of condensation (which has already been adequately treated elsewhere by Eisenschitz (1947), Mayer and Mayer (1946), and de Boer (1952 a)), or of melting (Herzfeld and Goeppert-Mayer (1934), Born (1939), Lennard-Jones and Devonshire (1939 a, b), Frenkel (1946); see also § 7 of the review of de Boer (1952 b)).

A full quantum theory of liquids can hardly be formulated until the corresponding classical theory is available. The modifications of the results of the classical theory necessary to account for quantum effects have already been considered by de Boer (1948), and de Boer and Lunbeck (1948). In a recent paper Prigogine (1954) has reviewed the interesting attempts to extend a classical model of liquids to the realm of quantum physics. Attempts to understand the properties of the quantum liquid helium II using purely quantum methods have been in many ways disappointing, although the recent work of Feynman (1953 a, b, c, 1954, 1955), and more particularly of Bogolyobev and Zubarev (1955), and of Chester (1953, 1954 a, b) suggest that interesting results can ultimately be expected. It is, however, clear from all this work that an understanding of quantum liquids involves no general principles of physics that are not already needed for an understanding of classical liquids. For this reason the report is subjected to the third restriction that emphasis will be placed on classical liquids, quantum theory being introduced only where it is needed for a clearer assessment of the classical theory.

§ 2. Molecular Order in Liquids

A consideration of the experimental data which give information about the structure of the liquid state is necessary before passing on to the theory of liquids itself. This topic forms the subject of the present paragraph.

In the modern theory the three states of matter are conveniently distinguished by considerations of molecular order. According to this general view, a liquid is characterized by short-range order; in this respect it differs from a solid, where the order is long-ranged, and from a dilute gas, where the molecules are

completely disordered. Consequently the methods developed for calculating the properties of liquids have involved a knowledge of the molecular spatial distribution.

The spatial distribution of the molecules of a liquid in equilibrium is revealed by x-ray diffraction experiments (see, for example, Gingrich (1943) for details of these experiments). In these experiments a monochromatic x-ray beam of known wavelength is focused on to the liquid, and the diffracted beam is analysed. A range of liquids has been tested in this way, and the technique is well established. (Recently experiments have been reported in which the spatial distribution is derived from the diffraction of neutrons by a liquid: see, for example, Henshaw, Hurst and Pope (1953), and Vineyard (1954).)

Monatomic liquids diffract x-rays to form an intensity pattern in many ways similar to that formed by a fine powder of crystallites. There is one principal diffuse ring, and possibly one or more weaker rings. The mean radius of the primary ring has been associated with the molecular radius and in this way molecular dimensions have been arrived at that agree with independent determinations. Similar intensity curves result from polyatomic molecules; these more general data do not affect the present report which is restricted to simple liquids.

The initial interpretation of the full x-ray curves emphasized the close similarity between the data for liquids and for crystalline powders. This comparison led Stewart (1930) to postulate the existence of 'cybotactic groups' in a liquid, the liquid being regarded as a special form of crystalline powder. An alternative interpretation of the x-ray experiments, according to which the liquid is given a blurred crystal structure, was considered by Prins (1931), Prins and Petersen (1936) and Bernal (1937). The absence of long-range order in a liquid is, in this way, accounted for within the framework of crystal physics; this approach is likely to be particularly useful in the region of melting (Frenkel 1946). The crystal model was put into a form more acceptable for liquids by Guggenheim (1932) in the cell model, a model used by many subsequent authors. In the model explicit account is taken of the empirical result that each liquid molecule, although constrained by its neighbours to remain in a small volume of space, is nevertheless not so firmly held by its neighbours as to eliminate small irregular movement. (The cell model is explained in § 3.)

A more general interpretation of the experimental data which is not based on a crystal model is that involving the pair distribution function only. This function is derivable directly from the x-ray intensity data already described by a Fourier transform (cf. Gingrich 1943). For simple molecules interacting with central forces the number of particles contained in a spherical shell of thickness dr, and distant r from some arbitrary molecule chosen as origin, is written

$$dn = 4\pi\rho_0 g(r)\, r^2\, dr \qquad \ldots\ldots(2.1)$$

where ρ_0 is the mean number density. The function $g(r)$ is called the radial distribution function, sometimes simply referred to as the pair distribution. Since the liquid shows only short ranged order the condition

$$\lim_{r\to\infty} g(r) = 1 \qquad \ldots\ldots(2.2)$$

must be imposed on $g(r)$. In figure 1 is drawn a curve for dn which is typical of monatomic liquids.

If the molecular force is non-central a pair distribution can also be defined by analogy with (2.1), but now it is a function not only of r, but also of the orientation angles ϑ, φ :

$$dn = \int_0^{2\pi} \int_0^{\pi} \rho_0 g(r, \vartheta, \varphi) r^2 \sin \vartheta \, dr \, d\vartheta \, d\varphi. \qquad \ldots\ldots(2.3)$$

When g is independent of the angles (2.3) reduces to (2.1), and it is this situation that largely interests us in this report.

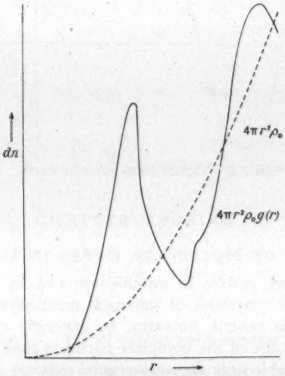

Figure 1. Typical curve for dn.

For a liquid in equilibrium the mean relative force on a molecular pair, that is the mean of the difference of the forces on each molecule separately due to all other molecules, does not vanish, even though the mean force on each molecule may be zero. The mean relative force has been equated to the negative gradient of a mean potential Φ related to the pair distribution according to

$$\Phi(\mathbf{r}) = -kT \log g(\mathbf{r}) \qquad \ldots\ldots(2.4)$$

where T is the temperature, and k is Boltzmann's constant.

For a liquid that is not in equilibrium it is assumed that the mean potential again defines the force determining the actual molecular movement.

The form of the mean potential curve for a typical liquid is shown in figure 2. According to the definition (2.4), a maximum in the function $g(r)$ corresponds to a minimum of the function Φ. At zero distance the mean potential has a very large, though finite, first maximum, which is likely to be indistinguishable from the potential of the actual molecular interaction at these small separation distances. Corresponding to the principal diffuse ring of the x-ray curves, the

mean potential has a first minimum. Secondary maxima and minima occur at larger distances corresponding to the weaker rings of the x-ray intensity pattern. These features are reproduced with decreasing amplitude for increasing distance, ultimately disappearing, the mean potential approaching zero. This knowledge of the structure of liquids, derived from experimental data, must form the basis for all theories of the liquid state.

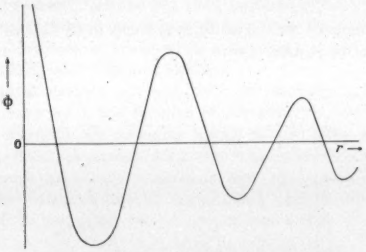

Figure 2. Typical mean potential curve.

I. UNIFORM SYSTEMS

§ 3. The Theory of Molecular Order in Uniform Liquids

The properties of any system in equilibrium can be obtained in principle from an application of the methods of statistical mechanics. The wide range of validity of these methods cannot, however, be generally exploited because they involve a detailed knowledge of the complete partition function, defined by equation (3.5), which is available only for very special systems of which the ideal gas is virtually the only example. Certainly for liquids a complete evaluation of the partition function is totally impracticable. Progress for liquids has been made by circumventing the difficulties associated with such an evaluation. It will be shown in § 3.4 that a knowledge of the pair distribution function is sufficient for calculating the thermodynamic properties of a uniform system, as was first inferred by Bernal (1937). Accordingly it is sufficient in the theory to replace the evaluation of the complete partition function by the relatively simpler problem of the evaluation of the pair distribution function.

3.1. *The Pair Distribution in Statistical Mechanics*

The liquid may be regarded as an assembly of N interacting particles contained in a volume V. The normalized probability distribution for the simultaneous occurrence of the N momenta and N position vectors is denoted by $f^{(N)}(\mathbf{p}, \mathbf{r})$. According to the general principles of statistical mechanics this function has the form (see, for instance, Tolman 1938, p. 58):

$$f^{(N)}(\mathbf{p}, \mathbf{r}) = \frac{1}{Z} \exp\left\{-\frac{H}{kT}\right\} \qquad \ldots\ldots(3.1)$$

where H is the energy function (Hamiltonian) of the system. The potential energy of the system of N particles, $\psi(1, 2, \ldots N)$, is written as the sum of the $\frac{1}{2}N^2$ contributions of pairs of molecules :

$$\psi(1, 2, \ldots N) = \tfrac{1}{2} \sum_{i=1}^{N} \sum_{\substack{j=1 \\ i \neq j}}^{N} \psi(i, j) \qquad \ldots\ldots(3.2)$$

where $\psi(i, j)$ is the potential energy of the molecular pair (i, j). This potential function is for central forces a function of the separation distance $r_{ij} (= |\mathbf{r}_i - \mathbf{r}_j|)$ alone, and is known to have the form shown in figure 3. For distances in the

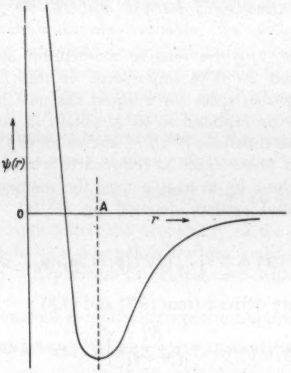

Figure 3. Typical true interaction potential curve.

region OA the force is repulsive, expressing the property of molecular impenetrability, and for larger values of r is attractive. Analytic expressions for $\psi(i, j)$ are available that are of sufficient accuracy for most purposes, of which the Lennard-Jones (1937) expression

$$\psi(r) = a\left[\left(\frac{b}{r}\right)^{12} - \left(\frac{b}{r}\right)^{6}\right] \qquad \ldots\ldots(3.3)$$

is the most widely used.† The Hamiltonian energy function is to be written

$$H(\mathbf{p}, \mathbf{r}) = \sum_{i=1}^{N} \frac{p_i^2}{2m} + \tfrac{1}{2} \sum_{i=1}^{N} \sum_{\substack{j=1 \\ j \neq i}}^{N} \psi(i, j). \qquad \ldots\ldots(3.4)$$

Z in (3.1) is called the partition function and is defined by the expression

$$Z = \int \ldots \int \exp\left\{-\frac{H}{kT}\right\} d\mathbf{p}\, d\mathbf{r} \qquad \ldots\ldots(3.5)$$

the integrations being made over all molecules and over all space. $f^{(N)}$ is in this way normalized to unity

$$\int \ldots \int f^{(N)}\, d\mathbf{p}_1 \ldots d\mathbf{p}_N\, d\mathbf{r}_1 \ldots d\mathbf{r}_N = 1. \qquad \ldots\ldots(3.6)$$

† a and b are adjustable parameters.

By averaging (3.1) over the subspace of $N-1$ molecules the singlet distribution function $f^{(1)}$ is obtained which is the distribution function of importance in the theory of dilute gases

$$f^{(1)}(x, y, z, p_x, p_y, p_z) = \int \dots \int f^{(N)}(\mathbf{p}, \mathbf{r})\, d\mathbf{p}_2 d\mathbf{p}_3 \dots d\mathbf{p}_N d\mathbf{r}_2 d\mathbf{r}_3 \dots d\mathbf{r}_N. \quad \dots\dots(3.7)$$

By averaging (3.1) over the subspace of $N-2$ molecules the doublet distribution function of the remaining pair, numbered 1 and 2, is obtained

$$f^{(2)}(x_{12}, y_{12}, z_{12}, p_{x_{12}}, p_{y_{12}}, p_{z_{12}}) = \int \dots \int f^{(N)}(\mathbf{p}, \mathbf{r})\, d\mathbf{p}_3 d\mathbf{p}_4 \dots d\mathbf{p}_N d\mathbf{r}_3 d\mathbf{r}_4 \dots d\mathbf{r}_N \quad \dots\dots(3.8)$$

where $x_{12}, y_{12}, z_{12}, p_{x_{12}}, p_{y_{12}}, p_{z_{12}}$ are relative momentum and position coordinates of the molecules 1 and 2. The importance of this distribution function in momentum–position (phase) space for a liquid has now been recognized.

The procedure can be repeated so as to obtain in succession the remainder of the set of distribution functions $f^{(3)}$, $f^{(4)}$, and so on to $f^{(N-1)}$.

The distribution in phase space is reduced to a distribution in the position (configuration) space alone by averaging over the momenta. The configuration distribution for the total system, denoted by $n^{(N)}(\mathbf{r})$, is then obtained from $f^{(N)}$ according to

$$n^{(N)}(\mathbf{r}) = N! \int \dots \int f^{(N)}(\mathbf{p}, \mathbf{r})\, d\mathbf{p}_1 d\mathbf{p}_2 \dots d\mathbf{p}_N. \quad \dots\dots(3.9)$$

Similarly $n^{(1)}$ and $n^{(2)}$ are derived from (3.7) and (3.8):

$$n^{(1)}(x, y, z) = \frac{N!}{(N-1)!} \int f^{(1)}(\mathbf{p}_1, \mathbf{r}_1)\, d\mathbf{p}_1 \quad \dots\dots(3.10)$$

and

$$n^{(2)}(x_{12}, y_{12}, z_{12}) = \frac{N!}{(N-2)!} \iint f^{(2)}(\mathbf{p}_1, \mathbf{p}_2, \mathbf{r}_1, \mathbf{r}_2)\, d\mathbf{p}_1 d\mathbf{p}_2. \quad \dots\dots(3.11)$$

Inserting (3.8) into (3.11) gives the complete expression for $n^{(2)}$

$$n^{(2)} = \frac{N!}{(N-2)!} \int \dots \int f^{(N)}(\mathbf{p}, \mathbf{r})\, d\mathbf{p}_1 \dots d\mathbf{p}_N d\mathbf{r}_3 \dots d\mathbf{r}_N \quad \dots\dots(3.12)$$

where $f^{(N)}$ is given by (3.1).

$n^{(2)}$ is here exactly the pair distribution whose significance for liquids was recognized in § 2. By repeating the averaging procedure followed so far expressions for the distribution function $n^{(3)}$

$$n^{(3)} = \frac{N!}{(N-3)!} \int \dots \int f^{(N)}\, d\mathbf{p}_1 \dots d\mathbf{p}_N d\mathbf{r}_4 \dots d\mathbf{r}_N \quad \dots\dots(3.13)$$

and for $n^{(4)}, n^{(5)}, \dots n^{(N-1)}$ are obtained.

The relations derived above can be applied also to quantum systems. Quantum phase space distribution functions, first introduced by Wigner (1932), take the place of the corresponding classical functions and the equations (3.7) and (3.8) remain strictly valid, although now the possibility arises that the reduced distribution functions $f^{(1)}, f^{(2)}, \dots$ may become negative. Using the analytical methods

developed independently by Moyal (1949) and Irving and Zwanzig (1951), the arguments developed so far for classical systems can be applied also to quantum systems without the necessity of any major modifications.

3.2. *The Superposition Approximation*

In the expression (3.12) for the pair distribution the integration over the momenta can readily be carried out irrespective of whether the system that it refers to is a solid, liquid or gas. This is not so for the integration over the coordinates, and for a liquid the evaluation of (3.12) for $n^{(2)}$ is just as intractable as the evaluation of the full partition function (3.5), even if the most advanced electronic computing techniques are available. In order to make progress, therefore, it is necessary to introduce a new simplifying hypothesis into the theory. Such an hypothesis, and one which has been adopted by many authors, is the superposition approximation first formulated by Kirkwood (1935) (see also Kirkwood and Boggs 1942). According to this hypothesis the correlation between a group of molecules can be replaced by the product of the correlations between small numbers of molecules. For a group of three molecules the hypothesis is written as

$$n^{(3)}(1,2,3) = n^{(2)}(1,2)\,n^{(2)}(1,3)\,n^{(2)}(2,3) \qquad \ldots\ldots(3.14)$$

and amounts to the assumption that the probability of the occurrence of a given configuration of three molecules is equal to the probability of the occurrence of the three pairs separately. Expression (3.14) has been widely used in the theory of liquids.

Applied to a group of four molecules the superposition approximation hypothesis is

$$n^{(4)}(1,2,3,4) = n^{(3)}(1,2,3)\,n^{(3)}(1,2,4)\ldots n^{(3)}(2,3,4). \qquad \ldots\ldots(3.15)$$

Similar expressions are assumed to apply to molecular groups of $5, 6, \ldots$ components. The merit of the hypothesis must rest on the comparison of the predictions it leads to with experiment (cf. § 4.2). The hypothesis in the form (3.14) has been used by Born and Green, and independently by Kirkwood, to derive an integro-differential equation for $n^{(2)}$.

Inserting (3.1) and (3.4) into (3.12), using (3.13) and finally differentiating with respect to the vector distance (with molecule 1 chosen as origin), there results the integro-differential equation

$$\frac{\partial n^{(2)}(1,2)}{\partial \mathbf{r}_{12}} + \frac{1}{kT}\frac{\partial \psi(1,2)}{\partial \mathbf{r}_{12}}\,n^{(2)}(1,2) = -\frac{N}{kT}\int \frac{\partial \psi(1,3)}{\partial \mathbf{r}_{13}}\,n^{(3)}(1,2,3)\,d\mathbf{r}_{13}. \qquad \ldots\ldots(3.16)$$

Both $n^{(2)}$ and $n^{(3)}$ occur in this equation; if $n^{(3)}$ is known as function of $n^{(2)}$ (3.16) is reduced to an equation involving $n^{(2)}$ alone. This reduction is made possible by the hypothesis (3.14), and by its use the non-linear integro-differential equation for $n^{(2)}$

$$\frac{\partial}{\partial \mathbf{r}_{12}}\left[\log n^{(2)}(1,2) + \frac{1}{kT}\psi(1,2)\right] = -\frac{N}{kT}\int \frac{\partial \psi(1,3)}{\partial \mathbf{r}_{13}}\,n^{(2)}(1,3)\,n^{(2)}(2,3)\,d\mathbf{r}_{13} \qquad \ldots\ldots(3.17)$$

results. This equation is due to Born and Green (1946).

An equivalent equation has been given by Kirkwood and Boggs (1942). The total potential energy is now arranged in a form that allows the interaction between a chosen molecule, labelled molecule 1, and its neighbours to be varied:

$$\psi(1,2,\ldots N) = \xi \sum_{i=2}^{N} \psi(1,i) + \sum_{i=2}^{N} \sum_{j>i}^{N} \psi(i,j). \qquad \ldots\ldots(3.18)$$

Here ξ is a continuous coupling parameter that is continuous in the range 0 to 1. When $\xi = 0$ the molecule 1 is completely isolated; when $\xi = 1$ the interaction with the neighbours is complete. By following through an argument identical with that leading to (3.16), except that now differentiation is performed with respect to ξ, the Kirkwood equation

$$\frac{\partial}{\partial \xi}[\log n^{(2)}(1,2,\xi)] + \frac{\psi(1,2)}{kT} = -\frac{N}{kT}\int \psi(1,3)[n^{(3)}(1,2,3,\xi) - n^{(2)}(1,2,\xi)]\, d\mathbf{r}_{13} \qquad \ldots\ldots(3.19)$$

results. It will be seen later (cf. § 4.1.2) that both (3.17) and (3.19) lead to essentially the same function $n^{(2)}$.

Although (3.17), or its analogue (3.19), is valid for systems where ψ is also a function of the orientation angles, in this case its form is particularly cumbersome. If the angular dependence is not too strong it is more convenient to express ψ in the form

$$\psi(r,\vartheta,\varphi) = \psi_0(r) + \psi_1(r,\vartheta,\varphi) \qquad \ldots\ldots(3.20)$$

where ψ_1 is to be treated as a perturbing term. Writing

$$n^{(2)}(r,\vartheta,\varphi) = n_0^{(2)}(r)\,[1 + \delta(r,\vartheta,\varphi)] \qquad \ldots\ldots(3.21)$$

where δ is small, then δ is obtained from a simple expansion of the right-hand side of (3.9), and $n_0(r)$ from (3.17) (see, for example, Cole 1952).

An extension of the arguments of this section to the quantum theory has not yet been achieved; Chester (1954 b) has shown that an equation of the type (3.17) is inapplicable in this case.

3.3. *The Cell Model*

To restrict the theory to simple mathematics only the liquid molecular order has sometimes been considered in terms of the cell model, already met with in § 2. This approach, which was developed before the methods of the last section, is hardly reducible to any single set of postulates, and is of interest very largely because of its simplicity. (For full details of the theory the reader is referred to the reviews of Rowlinson and Curtiss (1951), and de Boer (1952 b, 1953 b).) The aim of the method is to obtain a simple expression for the partition function for a liquid which is as good an approximation as possible to the correct expression (3.7).

Each molecule of the liquid is assumed to be constrained by its neighbours to move in a small volume of space, called a cell. The mean potential inside the cell depends upon the mean positions of the remaining molecules in a way that can be calculated. The procedure, which is closely similar to that of the

self-consistent field of quantum physics, yields a mean potential function which corresponds to that defined by (2.4) provided the latter is assumed to suffer a cut-off at a distance equal to the radius of the cell.

Originally (Lennard-Jones and Devonshire 1937, 1938) each cell was assumed to contain one molecule only, and there were assumed to be no vacant cells. The homogeneity of the model leads to an identity of cells. For calculating the mean potential of the force in each cell the molecular interaction (restricted to nearest neighbours only) is taken to be given by (3.3). The neighbouring molecules are assumed to remain in mean positions located on the virtual face-centred crystal lattice. With this molecular arrangement the coordination number z (the number of nearest neighbours to each molecule) is 12. The total potential energy of the liquid molecules of this model is found to be the sum of the potential energies for each molecule at the centre of its cell, ψ_0, and the energies due to molecular movement within the cell, $\psi(r)$. The partition function is accordingly

$$Z = A \exp\left\{-\tfrac{1}{2} z \frac{N}{kT} \psi_0\right\} v_f^N \qquad \ldots\ldots(3.22)$$

where A is a normalization constant. v_f, called the free volume, is given by

$$v_f = \int_0^{r_{\max}} \exp\left\{-\frac{z}{kT} \psi(r)\right\} 4\pi r^2 \, dr. \qquad \ldots\ldots(3.23)$$

$r_{\max}$ is related to the molecular volume v ($= V/N$) according to $4\pi {r_{\max}}^3/3 = v$. In the limit of vanishing density ($v_f = V/N$, $\psi_0 = 0$), Z given by (3.22) does not approach the known form for a dilute gas; to correct this fault Lennard-Jones and Devonshire introduced *ad hoc* the necessary factor e^N. These authors further considered the possibility of reduced coordination numbers; such a reduction contradicts the initial crystal form, modifications of the virtual lattice structure being required if a reduced coordination number is to be used.

Further modifications have been made by a number of authors and the work is still in progress. The possibility of the number of cells exceeding the number of molecules has been considered by Cernuschi and Eyring (1939), Ono (1947), Peek and Hill (1950), Rowlinson and Curtiss (1951), and Arakawa (1954). Alternatively the possibility of one cell containing more than one molecule has been considered (Janssens and Prigogine 1950, Pople 1951). Finally, correlations of motion between molecules in neighbouring cells have been taken into account (de Boer 1953 a, Cohen, de Boer and Salsburg 1955). A partition function is derived which includes not only the motion of single molecules in single cells, but also the motion of pairs of molecules in a cluster of two neighbouring cells.

Recently the model has been applied to quantum systems by Prigogine (1954), particularly with a view to treating the anomalous properties of liquid helium II. This extension represents an attempt to use a tractable theory which passes to the conventional classical form at high temperatures.

3.4. *The Calculation of Thermodynamic Functions*

According to the principles of statistical mechanics the thermodynamic functions characterizing a uniform system, such as the pressure p, the internal

energy U, and the chemical potential μ, are related to the partition function by the equations

$$F = -kT \log Z, \qquad \ldots\ldots(3.24)$$

$$p = -\left.\frac{\partial F}{\partial V}\right|_{T,N}; \quad U = \frac{1}{T}\left.\frac{\partial F}{\partial (1/T)}\right|_{V,N}; \quad \mu = \left.\frac{\partial F}{\partial N}\right|_{T,V}. \qquad \ldots\ldots(3.25)$$

Here F is the Helmholtz free energy. These equations apply to all equilibria, and can relate to both classical and quantal systems. In applying them to liquids without making arbitrary assumptions concerning the form of Z it is necessary to attempt their rearrangement in terms of the pair distribution. The method of achieving this has been given by Green (1947).

In the rearrangement of the equations (3.25) to show explicitly the dependence on $n^{(2)}$, the essential difficulty is carrying out the differentiation with respect to the volume appearing in the expression for the pressure. This difficulty was overcome by Green, who showed that the differentiation can be performed by using the artifice of expressing the position coordinates as fractions of a characteristic length of the containing vessel. Green gives the equations

$$p = \frac{N}{V}kT - \frac{1}{6V}\int_0^\infty n^{(2)}(1,2)\frac{\partial \psi(1,2)}{\partial \mathbf{r}_{12}} r_{12}\, d\mathbf{r}_{12} \qquad \ldots\ldots(3.26)$$

$$U = \frac{N}{V}\frac{3}{2}kT + \frac{1}{2}\int_0^\infty n^{(2)}(1,2)\,\psi(1,2)\, d\mathbf{r}_{12}. \qquad \ldots\ldots(3.27)$$

The first term in each expression relates to the motion of single molecules; the second term involves the interaction of molecular pairs. The relative importance of the two terms changes with the density. The first term is the important term for dilute gases; as the density increases the second term makes a contribution whose importance increases until it finally becomes the controlling term for a liquid. The equations are, therefore, to be expected to cover the region of condensation. It should be noticed that whereas the gradient of the intermolecular potential appears in the expression for the pressure, the intermolecular potential itself appears in the expression for the total energy.

As an alternative to (3.26) and (3.27) a partition function derived from the cell model, such as (3.22), can be inserted directly into (3.24) and (3.25). This leads to the formulae for p and U:

$$p = -\tfrac{1}{2}Nz\frac{\partial \psi_0}{\partial V} + RT\frac{\partial}{\partial V}(\log v_f) \qquad \ldots\ldots(3.28)$$

$$U = NkT - kN\frac{\partial}{\partial (1/T)}\log v_f + \frac{1}{2}\frac{zN}{T}\frac{\partial \psi_0}{\partial (1/T)}. \qquad \ldots\ldots(3.29)$$

Changes in the initial model cause also changes in these expressions by means of the partition function, and for this reason the cell model can hardly be claimed to lead to unique expressions for the thermodynamic functions. This is to be contrasted with the expressions (3.26) and (3.27), which are determined by essentially a single parameter. When the pair interaction potential $\psi(i,j)$ is given,

$n^{(2)}$ can be uniquely calculated using (3.17) or (3.19); inserting this function into (3.26) and (3.27) gives explicitly unique equations of state without an evaluation of the partition function.

§ 4. Comparison between Theory and Experiment

The theory that has been developed so far is able to make predictions of the thermodynamic functions that can be compared with the corresponding experimental data. Such a test of the theory has been made by several authors, and this comparison is considered now.

4.1. *Equations using the Pair Distribution*

In order to make use of (3.26) and (3.27) it is necessary to know the equilibrium pair distribution corresponding to a given intermolecular potential function ψ, so that a solution of (3.17), or alternatively (3.19), must be available. Such a solution has been given by several authors in an analytic or in a numerical form. We consider these two applications separately.

4.1.1. *Analytical methods.*

The mathematical theory of non-linear integro-differential equations is not yet sufficiently developed to allow a complete analytic solution of (3.17), or of (3.19), to be obtained. If a solution of these equations is required in terms of analytic functions approximations must be introduced into the solution procedure.

For this purpose Green (1947), in solving (3.17), assumed that $n^{(2)}$ is related to a small unknown function $\alpha(r)$ according to

$$n^{(2)}(r) = \exp\left\{-\frac{\psi(r)}{kT}\right\}\{1+\alpha(r)\}. \qquad \ldots\ldots(4.1)$$

By inserting (4.1) into (3.17) an equation for the unknown function $\alpha(r)$ results, the initial problem of calculating $n^{(2)}$ being replaced by that of calculating $\alpha(r)$. Since $\alpha(r)$ is small the new equation can be made linear by neglecting terms of the order of α^2 or above, and assuming further that in certain terms of the equation $\alpha(r)$ is to be replaced by an average value written $\epsilon-1$.

The solution given by Green,† which is possibly only semi-qualitative, is

$$\alpha(r) = \frac{1}{\sqrt{(2\pi)}}\frac{1}{r}\int_0^\infty \frac{\epsilon^2 r_{23}\sin(rr_{23})}{\lambda-\epsilon\beta(r_{23})}\,dr_{23} \qquad \ldots\ldots(4.2)$$

where $n^{(1)}\lambda = (2\pi)^{-3/2}$ and $\beta(r_{23})$ is given by

$$\beta(r_{23}) = \frac{1}{\sqrt{(2\pi)}}\frac{1}{r_{23}}\int_0^\infty r_{23}\left[\exp\left\{-\frac{\psi(2,3)}{kT}\right\}-1\right]\sin(rr_{23})\,dr.$$

Rodriguez (1948) improved the solution to some extent by writing in place of (4.1),

$$n^{(2)}(r) = \exp\left\{-\frac{\psi(r)}{kT}+\alpha(r)\right\},$$

† This solution has been criticized by Scoins (1952): his alternative solution seems to show a longer ranged molecular order than that usually assumed. The result, however, does not appear to affect the main arguments used in this report.

essentially applying again Green's procedure. McLellan (1952 a) attempted a further improvement by solving (3.17) in its non-linear form using a power series expansion in place of $\alpha(r)$:

$$n^{(2)}(r) = \exp\left\{-\frac{\psi(r)}{kT}\right\}\left[1+\sum_{j=1}^{\infty} a_j r^j\right],$$

the problem of determining $n^{(2)}$ now being reduced to that of finding the coefficients a_j of the series expansion. (For details of the methods the reader is referred to Green 1952, p. 80.) These various analytical expressions for $n^{(2)}$ lead to curves that show qualitative agreement with experimental data for liquids. Such analytic solutions, involving as they do the use of several purely mathematical approximations, are hard to assess in physical terms, and predictions based on them, such as the analytical criteria claimed for distinguishing between the liquid and vapour phases, must be subjected to careful scrutiny.

Rodriguez (1948) used his analytical solution for the construction of fluid isotherms, and the same test has been applied by McLellan (1952 a). Agreement with experiment is satisfactory at the low density region (corresponding to the vapour) but in the true liquid region the agreement is not good. Further, the calculated critical data are too low by some 10%.

4.1.2. *Numerical methods.*

The worst difficulties associated with the analytical calculations are avoided by using numerical methods. In a number of papers Kirkwood and his school have given details of their use of the theory in conjunction with electronic computational procedures. These calculations are perhaps the best that are at present available for the properties of uniform liquids, though even now agreement with experiment is not always convincing.

Numerical solutions of both equations (3.17) and (3.19) have been obtained in several steps. First Kirkwood and Boggs (1942), and later Kirkwood, Mann and Alder (1950) showed that the solution of (3.19) for a hard sphere model exhibits the same general features as the experimental x-ray curves, of which figure 1 is typical. This simplified model, accounting only for the strong intermolecular repulsive force, was modified by Kirkwood, Lewinson and Alder (1952) to include also the attractive forces. These authors do this by assuming a hard core model of radius r_0, with a superposed Lennard-Jones potential (3.3) for $r > r_0$, adapted to argon. With this potential, numerical solutions of both the Born and Green equation (3.17) and the Kirkwood equation (3.19) were obtained over a range of density and temperature. The two equations lead to essentially the same solution, the most significant difference being that $n^{(2)}$ calculated from (3.17) has a first maximum some 10% smaller than that obtained from (3.19). Although the solutions agree in their main features with the experimental curves for argon, such a comparison is not sufficient to allow the superiority of one solution over the other to be recognized.

The pair distribution has been inserted by Kirkwood, Lewinson and Alder into (3.26) and (3.27) adapted to argon. Although a reduced (p, V) diagram is obtained which agrees well with the experimental fluid isotherms, showing also the liquid–vapour transition region, the more critical test of constructing a

(pV/T, density) diagram is not entirely satisfactory. At low densities (near the critical point) the calculated pressure and internal energy agree with experiment to some 20%, but in the high density region (near the freezing point) comparison with experiment is disappointing. The calculated and experimental values (due to Kirkwood, Lewinson and Alder 1952) are shown in figure 4.

More accurate calculations of the thermodynamic functions could be expected to result from a more accurate knowledge of the pair distribution. It is suggestive to treat the solutions of (3.17), or (3.19), as a first approximation to the correct function, and to apply a procedure for obtaining higher approximations. No

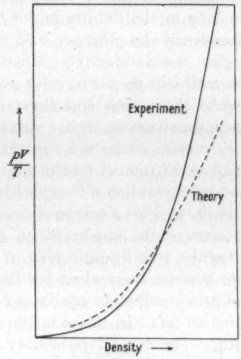

Figure 4.

such general procedure seems available at the present time, although a tentative procedure of empirical correction has been used by Zwanzig, Kirkwood, Stripp and Oppenheim (1953 a). These authors modify the calculated pair distribution by small, arbitrary, amounts to a form which, when inserted into (3.26), or (3.27), gives a pressure or an internal energy in agreement with experiment. It appears that such agreement can be achieved if $n^{(2)}(r)$ is written $n^{(2)}(cr)$, c being a scale factor that depends upon both the temperature and the density. The introduction of this scale factor without relating it to the intermolecular potential in an explicit way is most unsatisfactory; a new parameter is introduced, but our aim must always be the elimination of arbitrary parameters from the theory.

4.2. *Critique of the Superposition Approximation*

Agreement between theory and experiment for the liquid region is not as good as might be expected from the theory, although the agreement improves as the critical region is reached. This leads us to seek in the theory any approximations which might not be accurate enough. It has been seen in § 3 that the theory is a logical, and rigorous, extension of the already well established principles of statistical mechanics as far as equation (3.16) for $n^{(2)}$. In arranging this equation into a convenient form for evaluation it has been necessary to

introduce the superposition hypothesis (3.14) which may well now be suspected. The fact that it is valid for dilute gases, and in a certain sense also for solids, is no justification for using it in the liquid region.

The validity of the approximation for liquids has been discussed by several authors, though no final conclusion has yet been reached. Salsburg, Zwanzig and Kirkwood (1953) and, independently, Klein and Prigogine (1953 a) have found the superposition approximation to be exact for a one-dimensional model, where the associated formulae can be evaluated analytically in closed form, but have not extended their work to three dimensions. Rushbrooke and Scoins (1951, 1953) have studied the approximation from the standpoint of molecular clusters and find it valid so long as the density is not too high. A similar conclusion was reached independently by Nijboer and van Hoove (1951). The recent calculations of the pair distribution by Alder, Frenkel and Lewinson (1955) using a Monte Carlo method† do not involve a superposition approximation. The agreement between these data and those calculated from formulae involving the superposition approximation is not decisive since the comparison is made in the lower density region where the superposition approximation can be expected to be valid. This conclusion is reinforced by the agreement between these data and those obtained by expanding $n^{(2)}$ explicitly in powers of the density (see, for example, de Boer 1949, p. 354) since such an expansion applies only to a dense gas. None of the tests of the superposition approximation applied so far, therefore, is significant for the true liquid region.

Two possibilities seem to present themselves for further study. The first is an extension of the Monte Carlo method to enable it to treat systems of higher density than have been treated so far. In this way the superposition approximation could be dispensed with. The second possibility is the application of the superposition approximation in the form (3.15). An equation for $n^{(3)}$, equivalent to (3.16) for $n^{(2)}$, can be derived from (3.13), and this non-linear equation will contain on the right-hand side the function $n^{(4)}(1, 2, 3, 4)$ under the integral sign. By applying (3.15) a solution for $n^{(3)}$ can, in principle, be found, and this solution can then be inserted directly into the right-hand side of (3.16) to obtain $n^{(2)}$. Very extensive numerical work would be involved in such a procedure, but the inaccuracies introduced into the calculations by a superposition approximation should be reduced in this way. Future work on the theory of uniform systems must be centred around the problem of replacing, or eliminating the need for, the superposition approximation (3.14).

4.3. *Equations from the Cell Model*

The possibility of any comparison between theory and experiment in the normal sense does not exist for the cell model, its aim so far being to repeat experimental data as nearly as possible by a gradual modification of the initial model. By this process of gradual evolution of the initial assumptions critical data for argon and neon have been obtained from equations of the type (3.28) and (3.29) which agree well with the experimental data (see, for example, de Boer 1952 b).

† For details of the Monte Carlo method for liquids and its present range of application, see Metropolis, Rosenbluth, Rosenbluth, Teller and Teller (1953), and Rosenbluth and Rosenbluth (1954).

§ 5. Surface Tension

So far we have considered the properties of a uniform liquid of infinite extent; we now turn to the calculation of the boundary properties, such as surface tension γ and surface energy U_s, in terms of the intermolecular force. Calculations of this type have so far been restricted almost entirely to the interface between a simple liquid and its vapour.

For an equilibrium system the principles of statistical mechanics can be invoked, as was first done by Fowler (1937), and subsequently by Kirkwood and Buff (1949) and MacLellan (1952 b, 1953). The calculation of the superficial properties is far from a simple matter owing to the difficulty of specifying accurately the molecular order in the interface region. Although macroscopically the region of phase separation can be regarded as a well-defined surface, from a microscopic point of view this is not so. The molecular order characteristic of one phase changes gradually into that characteristic of the other phase; the interphase region is therefore a finite zone of gradually changing molecular order and density. The way in which the order, represented by the pair distribution, changes across this zone is not known from experimental or theoretical data, so that the calculations of surface tension and surface energy must be somewhat arbitrary.

Fowler (1937) was the first author to derive expressions for the surface tension and surface energy of a simple liquid–vapour interface in terms of the intermolecular potential and the pair distribution on the basis of statistical mechanics and thermodynamics, and his formulae have still not been superseded for purposes of practical application. In his paper he gives also a theoretical justification of the empirical formulae of Macleod:

$$\gamma = \text{const.}\,(\rho_{\text{liq}} - \rho_{\text{vap}})^2 \qquad \ldots\ldots(5.1)$$

and of Sugden:

$$P = \frac{M\gamma^{1/4}}{\rho_{\text{liq}} - \rho_{\text{vap}}} \qquad \ldots\ldots(5.2)$$

(where M is the molecular weight, and P the parachor) in the region of the critical point; the wide experimental range of application of (5.1) and (5.2) gives the theory a greater significance. Fowler assumes a plane surface of liquid–vapour separation, and calculates the surface free energy as one half of the work necessary to overcome the adhesion linking two semi-infinite columns of unit area of the liquid. The intermolecular potential and the pair distribution specify the adhesion force.

By these means the surface tension is found to be

$$\gamma = \frac{\pi}{8}\left(\frac{N}{V}\right)^2 \int_0^\infty r^4 n^{(2)}(r)\,\frac{\partial\psi(r)}{\partial r}\,dr \qquad \ldots\ldots(5.3)$$

where $n^{(2)}$ is the pair distribution in the liquid. The surface energy, expressed as the excess energy resulting from the formation of a liquid–vapour interface from an infinite column of liquid, is given as

$$U_s = -\pi \int_0^\infty r^3 \psi(r) \left\{ \left(\frac{N}{V}\right)^2 n^{(2)}(r) - \frac{2NN_1}{V^2}\, n_2^{(2)}(r) + \left(\frac{N_1}{V}\right)^2 n_1^{(2)}(r) \right\} dr. \qquad \ldots\ldots(5.4)$$

Here N_1 is the number of vapour molecules in volume V, $n_1^{(2)}$ the pair distribution in the vapour, and $n_2^{(2)}$ is the (essentially unknown) pair distribution in the separation surface. In the region of the critical temperature T_c Fowler assumes that $n^{(2)}$, $n_1^{(2)}$ and $n_2^{(2)}$ are linear functions of the dimensionless variable $\mathcal{T} = (T_c - T)/T_c$:

$$n^{(2)} = g_c(r) + G(r)\mathcal{T}\ ; \quad n_1^{(2)} = g_c(r) + G_1(r)\mathcal{T}\ ; \quad n_2^{(2)} = g_c(r) + G_2(r)\mathcal{T} \qquad \ldots\ldots(5.5)$$

and an application of (5.4) involves a specification of the functions $G_1(r)$ and $G_2(r)$.

Fowler further derives for the parachor the expression

$$P^4 = \frac{B}{4A^2}\frac{N_A{}^4}{T_c} \qquad \ldots\ldots(5.6)$$

where N_A is Avogadro's number, A is a constant equal to $(N/V - N_1/V)^2(T_c - T)^{-1}$, and B, which is nearly a constant, is related simply to the pair distributions $n^{(2)}, n_1^{(2)}, n_2^{(2)}$, and to the intermolecular potential. By making some rather arbitrary but plausible assumptions concerning the coefficients $G(r)$, $G_1(r)$ and $G_2(r)$ of $\mathcal{T}$ in (5.5), Fowler calculates the value of the parachor for argon, P_A and mercury, P_{Hg}. He finds for P_A the value 62, to be compared with the empirical value 52·5; for P_{Hg} the calculated value is 63 against an empirical value of 53. This agreement can be considered satisfactory. Fowler in his paper does not calculate values for γ or U_s.

Kirkwood and Buff (1949), and independently MacLellan (1952, 1953), derived expressions for the surface tension and surface energy by alternative methods, their expressions differing from those of Fowler in including also terms involving the variation of the pair distribution through the interface. Since this variation is not yet known the formulae are reduced to the Fowler form (5.3) and (5.4) when numerical values are calculated. MacLellan extended the calculations to apply also to the interface between a fluid and the walls of the container.

Kirkwood and Buff calculate values for the surface tension and surface energy of argon at 90°K, and compare their values with experiment: they find γ(calc) = 14·9, compared with γ(expt) = 11·9; U_s(calc) = 27·2 compared with U_s(expt) = 35·0. The agreement is not entirely unsatisfactory since the calculated values depend critically on details of the pair distribution.

Table 1. Surface Tension and Surface Energy for Argon (*after* Stanfield)

T (°K)	γ (dyn cm^{-1})		U_s (dyn cm)	
	expt.	calc.	expt.	calc.
90	11·86	14·05	34·39	26·89
123	4·35	10·62	29·02	18·19
149	0·16	4·85	13·80	7·64

The comparison between theory and experiment has recently been extended by Stanfield (1954)† who made measurements of γ and U_s for argon over a range of temperature. He compared these values with those calculated from (5.3) and

† Dr Eisenschitz brought this work to my notice.

(5.4) using an empirically corrected pair distribution, and his results are contained in table 1, the values for $T = 90°\text{K}$ differing only slightly from those of Kirkwood and Buff. Agreement between theory and experiment is poor, but is probably as good as can be expected until the molecular order in the interfacial zone can be determined.

II. NON-UNIFORM SYSTEMS

§ 6. The Element of Irreversibility

It has been assumed by all authors that the same molecular properties control the irreversible approach to equilibrium as determine the equilibrium condition itself, although the molecular order of a non-uniform system cannot be obtained by an application of the principles of statistical mechanics. The element of irreversibility is present in spite of the inherent reversibility of the associated molecular dynamics.

The theories so far developed for non-uniform systems have been restricted to either steady, or only slowly varying, small non-uniformities of temperature, or macroscopic flow, or, possibly, the concentration. Although the molecular order may be only slightly distorted by such small non-uniformities the effect of any deviation from uniformity, however small it may be, is far-reaching. The principles of statistical mechanics do not contain any element of irreversibility and so are powerless in the treatment of such systems. In order to take account of non-uniformities it is necessary to formulate a new principle, or principles, which introduce explicitly the element of irreversibility into the theory.† No such general formulation has yet been made, although four special solutions are available that give some indication of the characteristics that any general formulation must have. These special solutions occur (i) in the theory of dilute gases (Boltzmann collision numbers) (see, for example, Chapman and Cowling 1954); (ii) in the semi-macroscopic theory of the Brownian motion (Einstein 1926); (iii) in the classical theory of heat conduction in a crystal (Peierls 1929); and (iv) in the quantum-mechanical time-dependent perturbation theory. These four independent theories have three characteristics in common in the way that they introduce the irreversible element, viz.: (1) each uses the theory of Markoff stochastic processes; (2) each involves a time interval which cannot be infinitesimally small nor indefinitely large; and (3) mean square increments of variables are strictly proportional to the magnitude of the time interval itself, and not to its square or any other power. It is to be expected that these three characteristics will be present in any general theory of non-uniform systems, and in particular that they will play a prominent role in the theory of non-uniform liquids.

Recently Kirkwood (1946) has shown how a non-uniform liquid can be treated by the methods of the kinetic theory, and his work can claim considerable success. In the theory of Kirkwood (to be explained in § 7) the irreversibility is introduced by considering the correlation of the force on each liquid molecule at subsequent times; provided the time interval between two measurements of the force is larger than a characteristic value no correlation is to exist between them. The

† The implication in the recent papers of Klein and Prigogine (1953 b, c) that the superposition approximation has been used in such a role is incorrect; nowhere in the previous literature has a necessary connection been assumed between the superposition approximation and irreversibility.

theory treats the liquid in terms of the theory of Markoff stochastic processes, and leads to molecular phase increments that are proportional to the time interval that determines the correlation of the force. It therefore contains the three characteristics that we deduced before as being important in any theory of non-uniform systems.

Further work is required before a completely general statement of an irreversibility principle is finally formulated. A detailed analysis of the features of Markoff stochastic processes along the lines of that made by M. L. Green (1952) may be useful in leading to such a formulation. The hypothesis of Kirkwood appears to be the most satisfactory one at the present time for insertion in the theory of liquids, and is likely to be contained in any final formulation. Certainly it is at present the only one that has allowed values of the transport coefficients to be calculated by a strict application of the methods of the kinetic theory, and agreement between such calculated values and experiment, although not perfect, is by no means discouraging.

§ 7. The Theory of Molecular Order in Non-uniform Liquids

The molecular order in a non-uniform system is expressed in terms of distribution functions in phase- and configuration-space, and if the non-uniformities are small, these distribution functions are related to the corresponding uniform distributions in a simple way. As in the uniform theory, the non-uniform configurational distributions are derived from the phase distributions by averaging over the momenta; reduced distribution functions for groups of molecules are obtained by averaging over the partial phase or configuration of the remainder. The importance in the equilibrium theory of the interaction between molecular pairs makes it natural to assume, at least at first, that the corresponding interaction will prove significant in the non-uniform theory. The non-uniform pair distribution in configuration space, $g^{(2)}(r, \vartheta, \varphi, t)$† will be assumed to be related to the corresponding uniform function according to

$$g^{(2)}(r, \vartheta, \varphi, t) = n^{(2)}(\mathbf{r})\,[1 + \omega(r, \vartheta, \varphi, t)] \qquad \ldots\ldots(7.1)$$

where $\omega(r, \vartheta, \varphi, t)$ is a small term; it is angle and time dependent in a way dictated by the non-uniformity imposed on the system. $\omega(r, \vartheta, \varphi, t)$ must be calculated from the theory, experimental techniques for its determination not being available.

The central problem of the theory of non-uniform liquids, therefore, is the calculation of the molecular distribution functions, and particularly the pair distribution. Kirkwood (1946), and independently Born and Green (1946, 1947 a), have given methods for doing this. Since Kirkwood's method has led to definite results but the Born and Green method has not yet done so, we place emphasis on the theory of Kirkwood in the following pages, considering his method first.

7.1. *The Fokker–Planck Equation*

Kirkwood bases his theory on equations similar to those met with in the theory of the Brownian motion (see, for example, Chandrasekhar 1943), and in

† $g^{(2)}$ is not to be confused with the radial distribution function introduced in § 2, and written there $g(r)$, which is a special case of the *equilibrium* pair distribution $n^{(2)}$.

his paper derives first the Langevin equation, which forms the starting-point of the conventional theory of the Brownian movement, and then shows how the theory is to be generalized to include pair, triplet, ... distribution functions. One important result of the theory is that it gives, for the first time, an expression for the Stokes friction constant of classical hydrodynamics in terms of the intermolecular force.

The normalized non-uniform probability distribution function at time t for a liquid regarded as an assembly of N interacting particles contained in a volume V is denoted by $f^{(N)}(\mathbf{p}, \mathbf{r}, t)$. It satisfies the Liouville equation :

$$\frac{\partial f^{(N)}}{\partial t} + \sum_{i=1}^{N}\left[\frac{1}{m}(\mathbf{p}_i . \nabla_{\mathbf{r}_i} f^{(N)}) + (\mathbf{F}_i . \nabla_{\mathbf{p}_i} f^{(N)})\right] = 0 \qquad \ldots\ldots(7.2)$$

where $\mathbf{F}_i$ is the force acting on the ith particle. Equation (7.2) is applicable to both uniform and non-uniform systems, an element of irreversibility not yet having been introduced.

To derive the reduced distribution function for a group of $h(<N)$ molecules, $f^{(h)}(1, 2, ..., h\,;\, t)$, (7.2) is integrated over the phase space of the remainder $(\mathbf{P}, \mathbf{R})$:

$$\int \ldots \int \left\{\frac{\partial f^{(N)}}{\partial t} + \sum_{i=1}^{N}\left[\frac{1}{m}(\mathbf{p}_i . \nabla_{\mathbf{r}_i} f^{(N)}) + (\mathbf{F}_i . \nabla_{\mathbf{p}_i} f^{(N)})\right]\right\} d\mathbf{P}\, d\mathbf{R} = 0. \qquad \ldots\ldots(7.3)$$

In order to introduce the irreversibility element into the theory, Kirkwood invokes a coarse-graining in the time. To achieve this (7.3) is integrated over a time interval τ that is microscopically large, and yet macroscopically small in a way to be made more precise later (cf. § 7.2). In his initial paper Kirkwood (1946) carried through two time smoothing operations. The first is to obtain a time smoothed probability function $\bar{f}^{(h)}$ related to $f^{(h)}$ according to

$$\bar{f}^{(h)}(1, 2, ..., h, t) = \frac{1}{\tau}\int_{-\tau}^{0} f^{(h)}(1, 2, ..., h, t + t_1)\, dt_1.$$

Kirkwood asserts that it is $\bar{f}^{(h)}$ that is to have significance in measurements. The second time average ensures that the theory relates to irreversible systems. Eisenschitz (1951) pointed out that only the second time average is necessary for the development of the theory, and that the complication of replacing $f^{(h)}$ by $\bar{f}^{(h)}$ is not essential for this purpose. Consequently only a single time averaging need be introduced.

Integrating (7.3) over the time gives :

$$\tau\left\{\frac{\partial \bar{f}^{(h)}}{\partial t} + \sum_{i=1}^{h}\frac{\mathbf{p}_i}{m} . \nabla_{\mathbf{r}_i} f^{(h)}\right\} = -\sum_{i=1}^{N}\int_{-\tau}^{0}\int \mathbf{F}_i . \nabla_{\mathbf{p}_i} f^{(N)}\, d\mathbf{P}\, d\mathbf{R}\, dt$$
$$- \sum_{i=h+1}^{N}\int_{-\tau}^{0}\int \frac{\mathbf{p}_i}{m} . \nabla_{\mathbf{r}_i} f^{(h)}\, d\mathbf{P}\, d\mathbf{R}\, dt. \qquad \ldots\ldots(7.4)$$

It is now assumed that during the time interval τ changes in macroscopic molecular position are small : the last term on the right-hand side of (7.4) is therefore put equal to zero. By writing $\mathbf{F}_i = d\mathbf{p}_i/dt$, the remaining term on the right-hand side of (7.4) can be rearranged :

$$\int_{-\tau}^{0} \mathbf{F}_i . \nabla_{\mathbf{p}_i} f^{(N)}\, dt = \int_{-\tau}^{0} \frac{d\mathbf{p}_i}{dt} . \nabla_{\mathbf{p}_i} f^{(N)}\, dt = \nabla_{\mathbf{p}_i} f^{(N)} \Delta\mathbf{p} \qquad \ldots\ldots(7.5)$$

the last step resulting from the assumption that $f^{(N)}$ changes by only a small amount during the time interval τ; $\Delta\mathbf{p}$ is the change in momentum of the ith particle during the time τ. (7.4) is consequently :

$$\tau\left\{\frac{\partial f^{(h)}}{\partial t}+\sum_{i=1}^{h}\frac{\mathbf{p}_i}{m}.\nabla_{\mathbf{r}_i}f^{(h)}\right\}=(N-h)\iint f^{(N)}(\mathbf{p},\mathbf{r},t)\,d\mathbf{P}\,d\mathbf{R}-f^{(h)} \quad \ldots\ldots(7.6)$$

$f^{(N)}$ is now written explicitly in terms of the product of the distribution function for the group of h molecules, and the distribution function for the remaining $N-h$ molecules :

$$f^{(N)}(\mathbf{p},\mathbf{r},\mathbf{P},\mathbf{R};t)=f^{(h)}(\mathbf{p},\mathbf{r};t)f^{(N-h)}(\mathbf{P},\mathbf{R},t:\mathbf{p},\mathbf{r}) \quad \ldots\ldots(7.7)$$

so that $$\tau\left\{\frac{\partial f^{(h)}}{\partial t}+\frac{\mathbf{p}}{m}.\nabla_{\mathbf{r}}f^{(h)}\right\}=-f^{(h)}+(N-h)\iint f^{(h)}(\mathbf{p}t)f^{(N-h)}(\mathbf{P},\mathbf{R},\mathbf{p}:\mathbf{p})\,d\mathbf{P}\,d\mathbf{R}$$
$\ldots\ldots(7.8)$

where $\mathbf{p}$ is in this equation the momentum of the $3h$-dimensional momentum space of the group of h molecules. This form of the equation is due to Eisenschitz (1952 b, 1954), and differs from that first given by Kirkwood ; it is preferable because it shows explicitly the Markoff form of the integral equation for the theory.

If $f^{(N-h)}$ is independent of the time, and the integration in (7.8) is made over phase elements of constant $\Delta\mathbf{p}$, then (7.8) has the form of the integral equation appearing in Einstein's formulation of the theory of the Brownian motion. $f^{(N-h)}$ is now to be considered as simply related to a transition probability ; its time-independence amounts to the assumption that the molecules surrounding the arbitrary group of h molecules are in a steady state. The validity of this assumption is to be judged by the comparison of the predictions that follow from it with experimental data.

The forms of (7.8) of present interest are those for which $h=1$ and $h=2$. When $h=1$, and the density is small enough, (7.8) has been shown by Born and Green (1946) and by Kirkwood (1947) to reduce to the Maxwell–Boltzmann equation used as a basis for the theory of non-uniform dilute gases (Chapman and Cowling 1954). Both the restriction to binary encounters and the hypothesis of molecular chaos are essential features of the theory that are not applicable to liquids. However, for liquids, when the density is no longer small, (7.8) takes on a simple form since $\Delta\mathbf{p}$ is now small. By following the procedure well known in the theory of the Brownian movement (cf. Chandrasekhar 1943, ch. 1, p. 31), (7.8) can be reduced to an equation of the Fokker–Planck type :

$$\tau\left\{\frac{\partial f^{(1)}}{\partial t}+\frac{\mathbf{p}}{m}.\nabla_{\mathbf{r}}f^{(1)}\right\}=-\frac{\partial}{\partial\mathbf{p}}.(\overline{\Delta\mathbf{p}}f^{(1)})+\frac{1}{2}\frac{\partial^2}{\partial\mathbf{p}^2}.(\overline{\Delta\mathbf{p}^2}f^{(1)})+\frac{\partial^2}{\partial p_i\partial p_j}(\overline{\Delta p_i\Delta p_j}f^{(1)})+\ldots$$
$\ldots\ldots(7.9)$

where $\overline{\Delta\mathbf{p}}$, $\overline{\Delta\mathbf{p}^2}$, $\overline{\Delta p_i\Delta p_j}$ are respectively the mean, the mean square, and the mean component product of the momentum increments in the time interval τ. Evaluation of the mean values gives the following results (Eisenschitz 1951) :

$$\overline{\Delta\mathbf{p}}=-\beta^{(1)}\mathbf{p}\tau\,;\quad \overline{\Delta\mathbf{p}^2}=2\beta^{(1)}kT\tau\,;\quad \overline{\Delta p_i\Delta p_j}=\mathrm{O}(\tau^2) \quad \ldots\ldots(7.10)$$

with $$\beta^{(1)}=\frac{1}{mkT}\int_{-\tau}^{0}\overline{\mathbf{F}(t).\mathbf{F}(t+t')}\,dt'. \quad \ldots\ldots(7.11)$$

$\beta^{(1)}$ has dimensions (time)$^{-1}$. It is further found that

$$\overline{\Delta \mathbf{p}^n} = O(\tau^2); \quad \overline{\Delta p_i \Delta p_j \Delta p_k} = O(\tau^2) \qquad \ldots\ldots(7.12)$$

where $n > 2$. Only the first and second mean moments are of order τ, so that these two factors alone need be retained: that $\overline{\Delta \mathbf{p}^2}$ is proportional to τ and not to τ^2 is important since it is this particular time dependence that is characteristic of systems containing an irreversible mechanism.

If the liquid has a flow velocity $\mathbf{v}$, the mean momentum increment to be inserted into (7.9) becomes

$$\overline{\Delta \mathbf{p}} = -\beta(\mathbf{p} - m\mathbf{v})\tau. \qquad \ldots\ldots(7.13)$$

$\mathbf{v}$ or T may be arbitrary functions of the position, the solution of (7.9) giving the appropriate non-uniform singlet distribution.

The mean values (7.10) have the same form as those describing the translational Brownian movement if $\beta^{(1)}$ is associated with the hydrodynamical friction constant.

The method is at once applicable to the calculation of higher order distribution functions. Equation (7.8) has been used to obtain explicitly the Fokker–Planck equation for the pair distribution (Eisenschitz 1954). In this case the molecular interaction is to be split into two parts, viz. one part which describes the interaction between the two molecules of a representative pair in the absence of the remaining molecules, and a second part which describes the interaction of each molecule of the pair separately with the remainder.

The mean moments equivalent to (7.10) again are found, but now there are two types of terms. One relates to the centre of gravity of the pair, and the other to the momentum increment relative to the neighbours. In $\beta^{(2)}$ two different functions can now be distinguished, viz.

$$\beta_1^{(2)} = \frac{1}{mkT} \int_{-\tau}^{0} \overline{\mathbf{F}(t) . \mathbf{F}(t+t')}\, dt' \qquad \ldots\ldots(7.14)$$

where $\mathbf{F} = \frac{1}{2}[\mathbf{F}(1,2) + \mathbf{F}(2,1)]$

and

$$\gamma_1^{(2)} = \frac{1}{mkT} \int_{-\tau}^{0} \overline{\mathbf{F}^*(t) . \mathbf{F}^*(t+t')}\, dt' \qquad \ldots\ldots(7.15)$$

where $\mathbf{F}^* = \sum_{j=3}^{N} [\mathbf{F}(2,j) - \mathbf{F}(1,j)]$.

$\beta_1^{(2)}$ relates to the actual pair interaction, and $\gamma_1^{(2)}$ to the relative interaction.

The extension of the theory to quantum theory has also begun. Irving and Zwanzig (1951) have derived the quantum analogue of (7.6) and Eisenschitz (1952 a) has extended the work by deriving the quantum expression corresponding to the classical equation (7.9). Attempts along similar lines have been made by several Japanese authors (Mori and Ono 1952, Mori 1953, Ono 1954).

7.2. *The Friction Constants*

In order that (7.9) shall describe a non-uniform system it is necessary that $\beta^{(1)}$ defined by (7.11) shall be interpreted as the hydrodynamical Stokes friction constant. Kirkwood (1946) ensured this interpretation by introducing a principle of irreversibility which plays for liquids a role equivalent to the hypothesis of

molecular chaos in the theory of dilute gases. According to Kirkwood it is to be assumed that the force on a given molecule at time t is statistically independent of the force at a previous time t_0, provided that the interval $|t-t_0|$ is larger than some critical value τ. Expressed analytically it is postulated that:

$$\begin{aligned} \overline{\mathbf{F}(t_0).\mathbf{F}(t)} &= 0 \quad \text{for} \quad |t-t_0|>\tau \\ &\neq 0 \quad \text{for} \quad |t-t_0|<\tau \end{aligned} \qquad \ldots\ldots(7.16)$$

the bar denoting an average over all remaining molecular momenta and co-ordinates. The critical time interval τ is to be large compared with the time of extended molecular encounters, and yet small compared with the period of the Poincaré cycle when events become virtually reversible. With this hypothesis $\beta^{(1)}$, related to (7.16) by (7.11), approaches a constant value as $t-t_0$ is increased beyond the value τ, and exhibits the characteristic behaviour of a friction constant. The hypothesis (7.16) is applicable immediately to liquid molecular groupings of higher order and ensures that (7.14) and (7.15) ultimately become constants.

Expressions for the friction constants, of which (7.11) is typical, for the first time relate the friction constant explicitly to the molecular interaction, and represent an important new result of the modern theory. Unfortunately it has not so far proved possible to evaluate the expressions even for the simplest liquid system. In particular the range of conditions over which they can be interpreted as friction constants has not been fully discussed, although it can be expected to be wide. In a general way it is realized that the friction effect must arise from the apparent asymmetric molecular velocities relative to a chosen molecule, as has been recognized for the case of gravitationally interacting stars (Chandrasekhar 1943), and for ionized gases (Cohen, Spitzer and McR. Routly 1950). It is not yet possible to adapt these particle trajectory methods to the liquid state. Kirkwood (1946), as a tentative approximation only, replaced the force correlation function by a gaussian curve. In a later paper (Kirkwood, Buff and Green 1949) Kirkwood quotes the expression

$$[\beta^{(1)}]^2 = \frac{4\pi\rho}{a_0}\int_0^\infty r^2 n^{(2)}(r)\left[\frac{d^2\psi}{dr^2}+\frac{2}{r}\frac{d\psi}{dr}\right]dr$$

where a_0 is half the distance between nearest neighbours. The value so obtained for liquid argon of $\beta^{(1)} = 4{\cdot}84\times10^{-10}$ g sec^{-1} is close to the experimental Stokes' constant, but this agreement must not be over-emphasized owing to the approximations involved in the calculation. The lack of techniques for calculating the friction constant from molecular data is at the present time one of the serious breaks in the development of the theory; it is all the more unsatisfactory since, as was pointed out by Eisenschitz (1952 b), the friction constants appropriate to correlations between different numbers of molecules are likely to differ in both magnitude and temperature dependence.

7.3. *The Smoluchowski Equation*

The determination of the non-uniform distribution functions from the Fokker–Planck equations is greatly simplified for systems in which the time interval τ is small enough, that is for which the friction constant is large enough, as was first shown by Kramers (1940) for the case of the Brownian motion, and used by

Kirkwood, Buff and Green (1949) for liquids. In this case the momenta reach essentially an equilibrium distribution in the time interval τ, but the position coordinates do not. Accordingly to sufficient approximation the non-uniform phase distribution can be replaced by the product of a Maxwell–Boltzmann term for the momenta, and a non-uniform configurational distribution function $g(\mathbf{r}, t)$.† $g(\mathbf{r}, t)$ is determined by solving the Smoluchowski equation in configuration space :

$$\frac{\partial g}{\partial t} = \frac{1}{\beta m}\{\nabla_r[(\nabla_r \Phi)g] + \nabla_r{}^2(kTg)\}$$

(cf. Chandrasekhar 1943, ch. 2, p. 41). In this equation $-(1/\beta m)\nabla_r \Phi$ is the mean displacement, and $kT/\beta m$ is the mean square displacement per unit time. The problem of solving a differential equation in phase space is replaced by the simpler problem of solving a differential equation in configuration space.

To determine the pair distribution for a fluid with flow velocity $\mathbf{v}$ it is therefore necessary to determine only the relative pair distribution in configuration space, $g^{(1)}(\mathbf{r}, t)$, by solving the Smoluchowski equation

$$\frac{\partial g^{(1)}}{\partial t} = \frac{1}{\beta^{(2)} m}\{\nabla_r[(\nabla_r \Phi - \beta^{(2)} m\mathbf{v})g^{(1)}] + \nabla_r{}^2(kTg^{(1)})\}. \quad \ldots\ldots(7.17)$$

The application of (7.17) to particular non-uniform systems is made by specifying $\mathbf{v}$ or T as functions of the coordinates, and possibly the time. The boundary conditions to be imposed on the solution are to be obtained from physical criteria.

Recently Suddaby (1954) has considered in detail the replacement of the Fokker–Planck equation (7.9), where $f^{(1)}$ is now the relative pair distribution in phase, by the Smoluchowski equation (7.17). By expanding (7.9) in inverse powers of the friction constant he obtains (7.17) as a first term ; a second term, proportional to β^{-2}, is found to involve a fourth order differential equation. Although it appears that (7.17) is a sufficient approximation to the correct equation (7.9) for the liquid region, the fourth order equation is important in testing the form of the boundary conditions to be imposed on the solution ; we will return to this point later (§ 9.3).

7.4. *The Born and Green Equations*

Born and Green (1947 a, b) attempted to apply directly the equation (7.6) to the calculation of non-uniform liquid properties without the explicit introduction of an irreversibility principle. Such a procedure cannot lead directly to transport coefficients since (7.6), which is essentially only a rearrangement of (7.2), would lead directly to mean square increments of momentum or position that are proportional to τ^2, and not to τ itself. The τ^2 dependence does not allow a distinction between past and future times to be made, and so cannot appear in any theory of non-uniform systems. The need to introduce an irreversibility postulate into the Born and Green system of equations has now been recognized by H. S. Green (1952, p. 216), but his proposal for introducing such a postulate has so far only been explicitly stated in a form applicable to a theory of gases.

† This function must not be confused with the radial distribution function which in the accepted notation is $g(r)$.

§ 8. Momentum and Energy Flow

When the non-uniform distribution functions are known the flow of momentum, or energy, necessary to establish uniform conditions in a fluid can be calculated. For small non-uniformities these fluxes are proportional respectively to the velocity gradient, and to the temperature gradient, so that their calculation from molecular data leads at once to values for the viscosity coefficient, and to the thermal conduction coefficient. Expressions for the momentum and energy fluxes have been given by Born and Green (1947 a), and by Irving and Kirkwood (1950); they result from a deduction of the equations of classical hydrodynamics from the molecular distribution functions.

Expressions for the momentum or energy conservation derived in terms of molecular variables are compared with the corresponding hydrodynamical expressions term by term. In this way Irving and Kirkwood obtain the divergence of the momentum flux, and the divergence of the energy flux. In order to obtain the fluxes themselves a further argument is required which appears to be rather arbitrary. The momentum flux is defined to an arbitrary tensor of vanishing divergence, and the heat flux is defined to the curl of an arbitrary vector field. These integration factors are fixed so as to lead to expressions of the momentum flow and the heat flow that are in agreement with the conventional definitions of these quantities for fluids.

If $\mathbf{P}$ is the momentum flux tensor, and $\mathbf{Q}$ is the energy flux vector, Irving and Kirkwood give the dependence on the central intermolecular force as

$$\mathbf{P} = \frac{N}{V}\overline{m(\mathbf{vv})} - \frac{N^2}{2V}\left\langle\frac{d\psi}{dr}\frac{\mathbf{rr}}{r}\right\rangle \qquad \ldots\ldots(8.1)$$

$$\mathbf{Q} = \frac{N}{V}\overline{m(\mathbf{v}v^2)} + \frac{N^2}{2V}\left\langle\overline{\psi\mathbf{v}} - \overline{\left(\frac{d\psi}{dr}\frac{\mathbf{r}}{r}(\mathbf{r}.\mathbf{v})\right)}\right\rangle. \qquad \ldots\ldots(8.2)$$

ψ is here the *equilibrium* potential of pair interaction. The bars in (8.1) and (8.2) stand for averages over the non-equilibrium pair distribution, averages over the corresponding equilibrium distribution vanishing.

The physical meaning of the expressions (8.1) and (8.2) are as follows. N/V and $N^2/2V$ are respectively the number of single molecules and molecular pairs per unit fluid volume. The first term in each expression therefore is the contribution due to single molecules, which is the predominant contribution in gases; the second term is the contribution due to molecular pairs, and is the predominant term in liquids.

The first term in each expression is well known from the kinetic theory of dilute gases. The second term is less familiar. According to (8.1) the contribution of each representative pair to the momentum flux is the product of the intermolecular force $-d\psi/dr$ and the intermolecular distance r. The corresponding contribution to the energy flux is in two parts. First there is the product of the intermolecular potential and the relative velocity; secondly the product of the intermolecular distance and the work done against the intermolecular force.

By using equivalent arguments Born and Green derived the same expression (8.1) for $\mathbf{P}$; their expression for $\mathbf{Q}$ differs from (8.2) in that the term $(\overline{\psi\mathbf{v}})$ is not included. The agreement as to the expression for $\mathbf{P}$, coupled with the fact that

Falkenhagen (1931) using elementary arguments derived much earlier an expression of the same type in connection with the viscosity of electrolytic solutions, gives confidence in (8.1).

The disagreement as to the exact expression for $\mathbf{Q}$ is not satisfactory since the disputed term is likely to make a significant contribution. The discrepancy appears, however, to have been resolved in a very recent paper of Eisenschitz (1955).† This author approaches the problem by way of an extension of the virial theorem, and confirms the expression (8.1). The expression (8.2) for $\mathbf{Q}$ remains formally the same, the interpretation of the term $(\overline{\phi \mathbf{v}})$ being changed. It is now to refer to the mass centre of the representative pair, and not to a single molecule. It has been shown by Irving and Zwanzig (1951), and by Eisenschitz (1955) that (8.1) and (8.2) (in both the old and new form) are applicable also to quantum systems.

In carrying through the averages associated with the pair contributions in (8.1) and (8.2) a simplification is possible. In (8.2) the momenta, occurring by way of the flow, can be replaced by expressions involving the distribution of coordinates only; the momenta do not occur at all in (8.1). Consequently the contributions to the momentum or energy flow that are of importance in liquids can be calculated if the configurational pair distribution only is known. For calculating the fluxes for liquids to sufficient accuracy, therefore, it is sufficient at first to know the solution of the Smoluchowski equation (7.17), the solution of the full Fokker–Planck equation not being necessary. This represents an important reduction in the computational work.

§ 9. Calculations of the Transport Coefficients

The theories developed so far have been used by a number of authors to calculate the viscosity, or thermal conduction, of monatomic liquids, principally liquid argon taken as the typical classical monatomic liquid. We turn now to this experimental test of the theory.

9.1. *The Theory of Born and Green*

These authors have not developed their theory to the stage of providing calculated data for the transport coefficients. They have, however, given a 'preliminary' discussion of viscosity based on dimensional arguments (Born and Green 1947 a) from which they arrive at a simple qualitative expression for the viscosity. This expression contains an exponential temperature dependence of the type suggested by Andrade (1934) on empirical grounds, but the argument cannot be regarded as a proof of the correctness of this temperature dependence.

9.2. *The Theory of Kirkwood*

Kirkwood and his co-workers have applied the arguments of §§ 7 and 8 to the calculation of the viscosity and thermal conduction of argon near its critical point in a number of papers, giving values that can be compared with experiment.

For the viscosity (Kirkwood, Buff and Green 1949, Zwanzig, Kirkwood, Stripp and Oppenheim 1953 b) conditions of steady laminar flow with velocity $\mathbf{v}$

† My thanks are due to this author for telling me of his work in advance of publication.

are assumed, the non-uniform and uniform pair distributions being related according to (7.1). The small distortion due to the flow, $\omega(r, \vartheta, \varphi)$, is taken as being due to two separate effects, viz. a shear flow effect and a contraction flow effect. The first effect only is present in an incompressible liquid. The condition of laminar flow imposes on $\omega(r, \vartheta, \varphi)$ the angular dependence $P_2^1(\cos\vartheta)\sin\varphi$, where $P_2^1(\cos\vartheta)$ is an associated spherical harmonic. The radial part of the distortion is written as $\chi_1 + \chi_2 \operatorname{div} \mathbf{v}$, χ_1 and χ_2 being two unknown functions to be determined by the condition that (7.1) is a solution of the Fokker–Planck equation (7.9) in the phase space of relative pairs. This equation in phase space is reduced to two equations in configuration space which determine two configuration functions ω_1 and ω_2 which replace the phase functions χ_1 and χ_2. ω_1 and ω_2 satisfy the Smoluchowski equations

$$\frac{d}{dr}\left(r^2 n^{(2)} \frac{d\omega_1}{dr}\right) - 6n^{(2)}\omega_1 = \frac{6kT}{\beta} r^3 \frac{dn^{(2)}}{dr} \qquad \ldots\ldots(9.1)$$

subject to the (weak) boundary conditions

$$\left.\begin{aligned} \omega_1(r) &= 0 \qquad r = \infty \\ d\omega_1/dr &= 0 \qquad r = 0 \end{aligned}\right\} \qquad \ldots\ldots(9.2)$$

and

$$\frac{d}{dr}\left(r^2 n^{(2)} \frac{d\omega_2}{dr}\right) = \frac{6kT}{\beta} r^3 \frac{dn^{(2)}}{dr} - \frac{18kT}{\beta} r^2 \frac{dn^{(2)}}{d(\log n^{(1)})} \qquad \ldots\ldots(9.3)$$

subject to the conditions $d\omega_1/dr = 0$, $r = 0$ and $r = \infty$. The momentum flux calculated from (8.1) is compared with the corresponding Newtonian macroscopic expression and this leads Kirkwood, Buff and Green to the following formulae for the liquid shear viscosity η and bulk viscosity Ξ:

$$\eta = \frac{2\pi}{15kT}\frac{\beta}{V}\frac{N^2}{2V}\int_0^\infty n^{(2)}(\mathbf{r})\frac{d\psi}{d\mathbf{r}}\omega_1(\mathbf{r})\, r^3\, d\mathbf{r} \qquad \ldots\ldots(9.4)$$

$$\Xi = \frac{2\pi}{9kT}\frac{\beta}{V}\frac{N^2}{2V}\int_0^\infty n^{(2)}(\mathbf{r})\frac{d\psi}{d\mathbf{r}}\omega_2(\mathbf{r})\, r^3\, d\mathbf{r}. \qquad \ldots\ldots(9.5)$$

If the equilibrium pair distribution and the true interaction potential are known, η is determined when the solution of (9.1) is known, or Ξ is determined when the solution of (9.3) is known. Kirkwood, Buff and Green used (9.4) to calculate the ratio η/β for liquid argon at 90°K, using an analytic form of $n^{(2)}$ chosen both for its mathematical simplicity and for its close agreement with the experimental x-ray curves of argon over the important first maximum region. The molecular interaction potential was taken to be (3.3). A value $\eta/\beta = 2{\cdot}63 \times 10^6$ was obtained which, after the introduction of a preliminary estimate of β, gave a value for η of $1{\cdot}27 \times 10^{-3}$ poise. This value was later modified by Zwanzig, Kirkwood, Stripp and Oppenheim. These authors used a radial distribution function in numerical form, modified according to their 'stretching' procedure explained previously (§ 4.1.2). By applying numerical methods these authors find a best value of $\eta/\beta = 2{\cdot}4 \times 10^6$; by using a trajectory method, they claim $\beta \sim 3{\cdot}5 \times 10^{-10}\,\mathrm{sec}^{-1}$, giving a final value $\eta = 0{\cdot}84 \times 10^{-3}$ poise, a smaller value than that obtained

by Kirkwood, Buff and Green. The experimental value of the viscosity for argon near its normal boiling point is $\eta = 2{\cdot}39 \times 10^{-3}$ poise. Both the calculated values, although of the correct order of magnitude, are too small, the modified pair distribution leading to worse agreement with experiment.

A value of the bulk viscosity is given by Zwanzig, Kirkwood, Stripp and Oppenheim as $\Xi = 0{\cdot}42 \times 10^{-3}$ poise. This value must be regarded with caution since the calculation of Ξ according to (9.5) depends in a very sensitive way on the details of the pair distribution $n^{(2)}$. The use of $n^{(2)}$ in the form $n^{(2)}(cr)$ is not likely to lead to a reliable form either for $n^{(2)}$ or for Ξ. In spite of this, (9.5) is important in relating for the first time the bulk viscosity to the intermolecular force in an explicit way. (For further details of the theory of the bulk viscosity the reader is referred to the printed report of the discussion on "The First and Second Viscosities of Fluids", organized by the Royal Society, and held on 29th April 1954 (*Proc. Roy. Soc.* A, **226**, pp. 1–69), see particularly p. 24 (R. O. Davies).)

The thermal conduction of liquid argon at its normal boiling point has been calculated by Zwanzig, Kirkwood, Oppenheim and Alder (1954), using the (uncorrected) expression for the heat flow (8.2). The intermolecular potential has the form (3.3). These authors arrive at an expression for the heat flow :

$$\mathbf{Q} = \mathbf{Q}_K + \mathbf{Q}_V \qquad \ldots\ldots(9.6)$$

where

$$\mathbf{Q}_K = \frac{Nm^2}{2}\int_0^\infty |\mathbf{p} - m\mathbf{v}|^2 (\mathbf{p} - m\mathbf{v}) f^{(1)}(\mathbf{p}, \mathbf{r}, t)\, d\mathbf{p} \qquad \ldots\ldots(9.7)$$

and

$$\mathbf{Q}_V = \frac{1}{2}\int_0^\infty \left[\psi(r) + \frac{\mathbf{r}.\mathbf{r}}{r}\frac{d\psi(r)}{dr}\right][\mathbf{j}_1^{(2)} - \mathbf{v}n^{(2)}]\, d\mathbf{r}. \qquad \ldots\ldots(9.8)$$

$\mathbf{Q}_K$ is the average transport vector of kinetic energy of single molecules relative to the macroscopic fluid velocity, and $\mathbf{Q}_V$ is the average transport vector of potential energy.

$\mathbf{j}_1^{(2)}$ is the flow vector of a single particle in the presence of a second :

$$\mathbf{j}_1^{(2)}(\mathbf{r}_1, \mathbf{r}_2 ; t) = N^2 \iint \frac{\mathbf{p}_1}{m} f^{(2)}(\mathbf{p}, \mathbf{r} ; t)\, d\mathbf{p}_1 d\mathbf{p}_2. \qquad \ldots\ldots(9.9)$$

According to the new interpretation by Eisenschitz, explained in § 8, this vector should relate not to the particle motion but to the motion of the centre of mass of a pair. For a liquid the term $\mathbf{Q}_V$ gives the significant contribution. The evaluation of $\mathbf{Q}_V$ according to (9.8) requires a knowledge of $f^{(2)}$, and this is obtained by these authors using the Fokker–Planck equation.

The thermal conductivity λ is related to the heat flow according to $\mathbf{Q} = \lambda \Delta T = (\lambda_K + \lambda_V)\Delta T$ where ΔT is the temperature gradient. To calculate λ, Zwanzig, Kirkwood, Oppenheim and Alder expand the function $(\mathbf{j}_1^{(2)} - n^{(2)}\mathbf{v})$ in powers of the temperature gradient ; after averaging over the angles they arrive at the expression

$$\lambda = \frac{\pi kT}{3\beta}(n^{(1)})^2 \int_0^\infty \left(r\frac{d\psi}{dr} - \psi\right) r^3 n^{(2)}(r) \frac{d}{dr}\left[\frac{\partial}{\partial T}\log n^{(2)}(r)\right] dr$$

$$+ \frac{\pi kT}{\beta}(n^{(1)})^2 \left[\frac{\partial}{\partial T}\int_0^\infty \left(r^2\psi - r^3\frac{d\psi}{dr}\right) n^{(2)}(r)\, dr\right]. \qquad \ldots\ldots(9.10)$$

The authors quote for β the value $3{\cdot}53 \times 10^{-10}$ g sec^{-1}, and this gives for argon the value of the thermal conduction $\lambda = 2{\cdot}4 \times 10^{-4}$ cal g^{-1} sec^{-1} deg^{-1}. This is to be compared with the experimental value $\lambda = 2{\cdot}9 \times 10^{-4}$ cal g^{-1} sec^{-1} deg^{-1}. The remarkable agreement is, however, very probably coincidental since Zwanzig, Kirkwood, Stripp and Alder give in their paper the effect on the calculation of replacing $n^{(2)}(r)$ by $n^{(2)}(1{\cdot}026r)$; they find $\lambda = 4{\cdot}1 \times 10^{-4}$ cal g^{-1} sec^{-1} deg^{-1}, which is 1·7 times the previous value. The corresponding friction constant is given as $2{\cdot}85 \times 10^{-10}$. Apparently the value of λ depends very critically on the exact details of the pair distribution.

Since the calculations give η/β and $\lambda\beta$, the friction constant does not appear in the product $\eta\lambda$. Using the calculated data it is found that $\eta\lambda = 2{\cdot}1 \times 10^{-7}$, which is to be compared with the experimental value $6{\cdot}9 \times 10^{-7}$. The calculated value of $\eta\lambda$ is therefore too small by a factor of about 3. This discrepancy might be reduced when the new expression for the heat flow (cf. § 8) is used in place of (9.8).

9.3. *The Theory of Eisenschitz*

Eisenschitz (1949) derived expressions for the viscosity and thermal conduction of a simple liquid in terms of the friction constant from a single formulation which differs from Kirkwood in several respects, the characteristic temperature dependences now resulting from the different boundary conditions appropriate to the two cases. His formulae are sufficiently simple to allow evaluation in numerical terms. The non-uniform pair distribution to be used in evaluating (8.1) or (8.2) is derived from the Smoluchowski equation (7.17), which is to be solved in accordance with boundary conditions to eliminate anisotropy of flow (viscosity), or infinite heat flow (thermal conduction).

For calculating viscosity the small distortion term in (7.1) for steady laminar flow is factorized :

$$\omega(r, \vartheta, \varphi) = u(r)\, \mathrm{P}_2^1(\cos\vartheta) \sin\varphi, \qquad \ldots\ldots(9.11)$$

$u(r)$ being a solution of the radial Smoluchowski equation

$$\frac{d^2u}{dr^2} + \left(\frac{2}{r} - \frac{1}{kT}\frac{d\Phi}{dr}\right)\frac{du}{dr} - \frac{6u}{r^2} = -\frac{\beta a m}{(kT)^2} r \frac{d\Phi}{dr}. \qquad \ldots\ldots(9.12)$$

Φ is here the equilibrium mean potential of interaction, and $a/2$ the rate of shear. The strong boundary conditions

$$du/dr = 0\,; \qquad r^3 u = 0 \qquad (r = \infty) \qquad \ldots\ldots(9.13)$$

were applied. With ω determined in this way (8.1) is to be evaluated : for laminar flow in the xy plane this leads to the expression for the shear viscosity :

$$\eta = -\frac{N^2}{2V}\frac{2}{a}\int_0^\infty n^{(2)} \frac{d\Phi}{dr} u(r) \frac{\partial\phi}{\partial r} r^3 \sin^3\vartheta \cos^2\vartheta \sin\varphi \, dr\, d\vartheta\, d\varphi \qquad \ldots\ldots(9.14)$$

ϕ being the true potential. This expression is formally the same as Kirkwood's (9.4), but $\omega_1(r)$ and $u(r)$ are calculated according to quite different boundary conditions. $u(r)$ is proportional to β (according to (9.12)) so that (9.14) gives the ratio η/β. By choosing the two constants appearing in $u(r)$ in conformity with the conditions at infinity, (9.13), Eisenschitz finds that one of them has the magnitude $\exp(\epsilon/kT)$, where ϵ has the dimensions of an energy and a magnitude

comparable with that appearing in Andrade's formula: further, this magnitude determines also that of η. Whereas the strong boundary conditions (9.13) fix the value of this constant, the weak conditions (9.2) of Kirkwood leave it completely undetermined. Putting this constant zero for the Kirkwood boundary conditions, Cole (1952) has found numerical values of $\eta a/(N^2/V)$ from (9.14) appropriate to the conditions (9.2) and (9.13), using data similar to that for argon. He finds that the latter conditions lead to a value about 14 times that given by the former. Further, it appears that if the molecular data are varied in a way that may be interpreted as due to temperature change, the value of (9.14) changes in a way that is comparable with the known strong dependence of η on temperature if the strong boundary conditions are used; these conclusions could be made more positive if the temperature dependence of the friction constant were known.

The validity of the alternative boundary conditions (9.2) of Kirkwood (the weak boundary conditions) or (9.13) (the strong boundary conditions) has been considered in detail by Eisenschitz and Suddaby (1953), see also Suddaby (1954). The strong conditions lead to a function that becomes infinite at $r = 0$, the Smoluchowski equation not being a satisfactory approximation to the correct Fokker–Planck equation in this region. This has no effect on the viscosity, since in the calculation of the momentum flux the product $n^{(2)}u(r)$ occurs, and $n^{(2)}$ either vanishes exponentially as r approaches zero, or else becomes arbitrarily small; the momentum flux remains finite. The weak conditions of Kirkwood, while avoiding this singularity in the pair distribution, lead to anisotropy, which is not observed experimentally. In order to distinguish between the two possibilities, Suddaby solved the Fokker–Planck equation:

$$\frac{\partial f^{(1)}}{\partial t}+\frac{\mathbf{p}}{m}.\frac{\partial f^{(1)}}{\partial \mathbf{r}}+\mathbf{F}.\frac{\partial f^{(1)}}{\partial \mathbf{p}}=m\beta\left\{\frac{\partial}{\partial \mathbf{p}}[(\mathbf{p}-m\mathbf{v})f^{(1)}]+kT\frac{\partial^2 f^{(1)}}{\partial \mathbf{p}^2}\right\} \quad \ldots\ldots(9.15)$$

in powers of $1/\beta$, the first approximation being the Smoluchowski equation (7.17). The next approximation, which is a fourth order equation, has a solution which, it appears, can only be made unique by the application of the strong boundary conditions. While the question of boundary conditions cannot be regarded as finally settled, there are strong reasons at the present time for preferring the strong conditions of Eisenschitz to the weak conditions of Kirkwood.

The theory has been extended by Eisenschitz and Cole (1954) (see also Cole 1952) to account for the effect of a steady transverse electric field on the viscosity of a polar liquid, such as chloroform. Reliable experimental data are now available (Andrade and Dodd 1951, Andrade and Hart 1954) so that a direct comparison with experiment can be made. Such a comparison is particularly significant because Andrade and Dodd show in their paper that elementary arguments cannot explain the results.

The slight molecular asymmetry (implied by the presence of a dipole moment μ) is neglected as a first approximation, and the intermolecular force is assumed central with a superposed dipole force. The expression for the momentum flux (8.1) is modified to include also the electric field F, and the pair distribution function necessary for its evaluation is again taken as (7.1). The small term ω is now dependent also on the field, and is derived by solving the Smoluchowski equation (7.17) applying the strong boundary conditions (9.13).

The equilibrium mean potential includes now both an angular term, and the field, being augmented by a term arising from a dipole–dipole–field interaction of the form

$$b\frac{\mu^4F^2}{(kT)^3}\frac{P_2(\cos\vartheta)}{r^3}$$

where r is the length of the line of centres of a pair, and ϑ is the angle between this direction and the field; $P_2(\cos\vartheta)$ is a spherical harmonic, and b is a numerical factor whose value depends on the number of neighbours. This orientation effect influences the viscosity: if $\Delta\eta$ is the viscosity increment it is found that

$$\frac{\Delta\eta}{\eta}=g\frac{\mu^4F^2}{(kT)^3} \qquad \ldots\ldots(9.16)$$

the friction constant, which is found to be essentially unaffected by the electric field, not appearing in this expression. g is a numerical factor calculated from the theory. The quantity $g\mu^4/(kT)^3$ is to be equated with the 'visco-electric constant' of Andrade and Dodd. The effect of the field is to increase the viscosity, the increase being proportional to the square of the field strength. This result is in agreement with experiment; the experimental data are not sufficient to allow a test for the dependence of the visco-electric constant on the value of the dipole moment.

Eisenschitz and Cole subjected (9.16) to a large number of numerical checks and the ratio $\Delta\eta/\eta F^2$ was found to be insensitive to the details of the pair distribution, although η was found to be very sensitive. This suggests that $\Delta\eta/\eta$ can be expected to be virtually independent of the temperature.

Finally these authors applied (9.16) to the case of liquid chloroform where the molecular asymmetry is small. Since the pair distribution function for this liquid is not known, a plausible curve was constructed from density data which had a form compatible with known curves for other monatomic liquids. This rather arbitrary procedure was justified by the results of the numerical tests. The final result for chloroform (with F in e.s.u.), $\Delta\eta/\eta=20{\cdot}8\times10^{-8}$, is to be compared with the experimental result of Andrade and Dodd (1951) for chloroform: $17{\cdot}0\times10^{-8}$. The experimental results available for chlorobenzene and amyl acetate are very similar to that for chloroform: although no calculations were made, it would appear that the theory is well compatible with these results.

Although (9.16) would at first sight suggest that the viscosity of a non-polar liquid would remain unaffected by the presence of an electric field, the molecular dipole induced by the field invalidates this conclusion. Although the predicted effect is much smaller for a non-polar than for a polar liquid, it is not actually zero. For the non-polar liquid benzene (the only non-polar liquid tested by Andrade and Dodd), the induced dipole leads to a predicted value of the visco-electric constant not much less than 10^{-8}, whereas Andrade and Dodd find experimentally that it could hardly be larger than 10^{-9}. To account for this discrepancy Eisenschitz and Cole suggest that forces not so far considered in the theory should be taken into account, such as the repulsive overlap forces, and indicate how the inclusion of such forces could be expected to resolve the discrepancy for benzene, without interfering with the result for chloroform.

To calculate the thermal conduction Eisenschitz (1949) considered the case of a linear temperature gradient along the z-axis of a Cartesian frame, $T = T_0(1+cz)$. Using (7.1) and (8.2) the heat flow is found to good approximation to be

$$\mathbf{j} = -\frac{kn^{(2)}}{\beta m}\left[T_0 \operatorname{grad}\omega + \left(1+\frac{\Phi}{kT}\right)\operatorname{grad} T\right]. \qquad \ldots\ldots(9.17)$$

ω, the distortion of the pair distribution, can be factorized in the form $\omega(r,\vartheta,\varphi) = v(r)\cos\vartheta$ where $v(r)$ is a solution of the radial Smoluchowski equation

$$\frac{d^2v}{dr^2}+\left(\frac{2}{r}-\frac{1}{kT}\frac{d\Phi}{dr}\right)\frac{dv}{dr}-\frac{2v}{r^2} = \frac{c\Phi}{(kT)^2}\frac{d\Phi}{dr} \qquad \ldots\ldots(9.18)$$

subject to the boundary conditions at infinity :

$$\frac{dv}{dr} = -c\,; \quad \frac{v}{r} = -c \quad (r=\infty). \qquad \ldots\ldots(9.19)$$

To recover the form of Zwanzig, Kirkwood, Oppenheim and Alder (apart from the entirely unknown dependence of the equilibrium pair distribution which is not included), the factor $1+\Phi/kT$ is replaced by Φ/kT.

The coefficient of the z-component of the energy flow, evaluated using (9.18) and (9.19), leads to the liquid thermal conduction coefficient :

$$\lambda = -\frac{N^2}{2V}\int_0^\infty\left\{\left(r\frac{d\Phi}{dr}-\Phi\right)\left[\frac{1}{b}\frac{dv}{dr}+\frac{\Phi}{kT}+1\right]\cos^2\vartheta + \left(\tfrac{1}{2}r\frac{d\Phi}{dr}-\Phi\right)\left[\frac{1}{b}\frac{v}{r}+\frac{\Phi}{kT}+1\right]\sin^2\vartheta\right\}\frac{n^{(2)}r}{kT}\sin\vartheta\,dr\,d\vartheta\,d\varphi \qquad \ldots\ldots(9.20)$$

where T_0 has been replaced by T. This gives the product $\lambda\beta$ in terms of intermolecular data. Eisenschitz finds that neither of the two constants in $v(r)$ has a magnitude as large as $\exp(\epsilon/kT)$, and in this way confirms the experimentally established difference in the dependence of η and λ on the temperature.

The product $\eta\lambda$ calculated by Orton (1955) from (9.14) and (9.20) using data for liquid argon gives a value about one-third that found experimentally ; this is virtually the same as Kirkwood's value and will in any case have to be amended in the light of the new expression to replace (8.2).

§ 10. Conclusion

A brief indication of the achievements and deficiencies of the theory at the present time would perhaps be of use. For uniform systems the well established principles of statistical mechanics are strictly applicable, and for liquids their use has involved the circumvention of purely mathematical difficulties by the introduction of an additional hypothesis, viz. the so-called superposition approximation. While this hypothesis has led to a calculated pair distribution that shows the essential features of the experimental curves obtained from x-ray measurements, it has not so far given calculated data to the accuracy required in calculations of the equations of state for the true liquid region. Future work, it would appear, must be centred around either a reintroduction of this additional hypothesis into the established theory, or else the elimination of the need for its introduction ; the former course seems likely to be the more profitable.

In the treatment of non-uniform systems, where the principles of statistical mechanics do not apply, the introduction of the property of irreversibility by the hypothesis of Kirkwood (cf. § 7.2, eqn. (7.16)) has led to significant progress. With its use the kinetic theory has given for the first time calculated values for the liquid viscosity and thermal conduction coefficients that are derived solely from molecular data. Further, the hydrodynamical friction constant appearing in these formulae is given explicitly in terms of the intermolecular force, although again mathematical difficulties have so far prevented its evaluation for liquids. Calculated values of the transport coefficients of the correct order of magnitude have been obtained, and satisfactory numerical agreement can be expected when once a reliable value of the friction constant is available. Nevertheless, the theory has accounted for the quite different temperature dependence of viscosity and thermal conduction in a natural way, in terms of the different boundary conditions that the appropriate solution of a certain differential equation must satisfy. The theory has not confirmed the early hope that the empirical exponential temperature dependence would prove especially significant. The strong temperature dependence, which is not obtained in exponential form, results only from a full application of the theory, and is not immediately apparent from expressions such as (9.4) or (9.14). In leading to an expression for the bulk viscosity, (9.5), the theory has given a result that could not have been expected from the more elementary procedures.

So far it has been possible to apply only two absolute experimental checks on the non-uniform theory that do not involve the friction constant, viz. the calculation of the product $\eta\lambda$, and the calculation of the effect of an electric field on the viscosity. In the first case the comparison is rather disappointing but might well be improved when the more correct expression for the heat flux, which has only recently been given by Eisenschitz, is used. In the second case, the electric field effect on the viscosity of a polar liquid, the friction constant does not appear if the result is given in relative form, so that the calculated value is absolute in this sense. The satisfactory agreement with experiment in the case of liquid chloroform, made all the more pleasing by the inability of elementary theories to account for the result, is to some extent marred by the need to appeal to the action of forces not included in the calculations in order to explain the experimentally null result for the non-polar liquid benzene.

It can, however, be claimed that at last the foundations of a correct kinetic theory of liquids have been laid which is able to include both uniform and non-uniform conditions. Further, the theory as developed for monatomic liquids contains also semi-quantitatively many of the properties of polyatomic liquids in so far as these properties are not due to the internal molecular properties themselves. Much work still remains to be done before we can claim to understand the liquid state fully, but the methods that can be expected to lead to such an understanding seem now to be available.

ACKNOWLEDGMENT

It is a pleasure to thank Dr. Eisenschitz for a full and extremely helpful discussion of the manuscript.

References

Alder, B. J., Frankel, S. P., and Lewinson, V. A., 1955, *J. Chem. Phys.*, **23**, 4.

Andrade, E. N. da C., 1934, *Phil. Mag.*, **17**, 497, 698.

Andrade, E. N. da C., and Dodd, C., 1951, *Proc. Roy. Soc.* A, **214**, 494.

Andrade, E. N. da C., and Hart, J., 1954, *Proc. Roy. Soc.* A, **225**, 463.

Arakawa, K., 1954, *J. Phys. Soc. Japan*, **9**, 647.

Auluck, F. C., and Kothari, D. S., 1944, *Proc. Nat. Inst. Sci. India*, **10**, 397 ; 1945, *Proc. Camb. Phil. Soc.*, **41**, 180.

Bernal, J. D., 1937, *Trans. Faraday Soc.*, **33**, 27.

de Boer, J., 1948, *Physica*, **14**, 139 ; 1949, *Rep. Progr. Phys.*, **12**, 305 (London : Physical Society) ; 1952 a, *Changements de Phases* (Paris : Société de Chimie Physique) ; 1952 b, *Proc. Roy. Soc.* A, **215**, 4 ; 1953 a, *Proceedings of the International Conference on Theoretical Physics, Kyoto and Tokyo*, September 1953 (Tokyo : Science Council of Japan) ; 1953 b, *Suppl. Nuovo Cim.*, **10**, 225.

de Boer, J., and Lunbeck, R. J., 1948, *Physica*, **14**, 510, 520.

Bogolyobov, N., and Zubarev, D., 1955, *J. Expt. Theor. Phys. U.S.S.R.*, **28**, 121.

Born, M., 1939, *J. Chem. Phys.*, **7**, 591.

Born, M., and Green, H. S., 1946, *Proc. Roy. Soc.* A, **188**, 10 ; 1947 a, *Ibid.*, **190**, 455 ; 1947 b, *Ibid.*, **191**, 168.

Cernuschi, F., and Eyring, H., 1939, *J. Chem. Phys.*, **7**, 547.

Chandrasekhar, S., 1943, *Rev. Mod. Phys.*, **15**, 2.

Chapman, S., and Cowling, T. G., 1954, *The Mathematical Theory of Non-uniform Gases*, 2nd Edn. (Cambridge : University Press).

Chester, G. V., 1953, *Phys. Rev.*, **93**, 606 ; 1954 a, *Ibid.*, **94**, 246 ; 1954 b, *Ph.D. Thesis*, University of London.

Cohen, E. G. D., de Boer, J., and Salsburg, Z. W., 1955, *Physica*, **11**, 1.

Cohen, R. S., Spitzer, L., and McR. Roulty, P., 1950, *Phys. Rev.*, **80**, 230.

Cole, G. H. A., 1952, *Ph.D. Thesis*, University of London.

Davies, R. O., 1956, *Rep. Progr. Phys.*, **19**, 326 (London : Physical Society).

Einstein, A., 1926, *Investigations on the Theory of Brownian Movement* (London : Methuen).

Eisenschitz, R., 1947, *Sci. Progr.*, **35**, 470 ; 1949, *Proc. Phys. Soc.* A, **52**, 41 ; 1951, *Nature, Lond.*, **167**, 216 ; 1952 a, *Phil. Mag.*, **43**, 804 ; 1952 b, *Proc. Roy. Soc.* A, **215**, 29 ; 1954, *Kolloidzschr.*, **139**, 38 ; 1955, *Phys. Rev.*, **99**, 1059.

Eisenschitz, R., and Cole, G. H. A., 1954, *Phil. Mag.*, **45**, 394.

Eisenschitz, R., and Suddaby, A., 1953, *Proc. 2nd Int. Congr. Rheol.* (London : Butterworths Scientific Publications), p. 320.

Eyring, H., 1936, *J. Chem. Phys.*, **4**, 283.

Eyring, H., and Hirschfelder, J., 1937, *J. Chem. Phys.*, **45**, 249.

Falkenhagen, H., 1931, *Phys. Z.*, **32**, 745.

Feynman, R., 1953 a, *Phys. Rev.*, **90**, 1116 ; 1953 b, *Ibid.*, **91**, 1291 ; 1953 c, *Ibid.*, **91**, 1301 ; 1954, *Ibid.*, **94**, 262 ; 1955, *Progress in Low Temperature Physics*, Vol. I (Amsterdam : North-Holland Publishing Co.), p. 17.

Fowler, R. H., 1937, *Proc. Roy. Soc.* A, **159**, 229 ; 1939, *Nature, Lond.*, **144**, 993.

Frenkel, J., 1946, *Kinetic Theory of Liquids* (Oxford : Clarendon Press).

Fürth, R., 1941, *Proc. Camb. Phil. Soc.*, **37**, 252, 276, 281.

Gingrich, N. S., 1943, *Rev. Mod. Phys.*, **15**, 90.

Green, H. S., 1947, *Proc. Roy. Soc.* A, **189**, 103 ; 1952, *Molecular Theory of Fluids* (Amsterdam : North-Holland Publishing Co.).

Green, M. L., 1952, *J. Chem. Phys.*, **20**, 1281.

Guggenheim, E. A., 1932, *Proc. Roy. Soc.* A, **135**, 181.

Henshaw, D. G., Hurst, D. G., and Pope, N. K., 1953, *Phys. Rev.*, **92**, 1229.

Herzfeld, J. F., and Goeppert-Mayer, M., 1934, *Phys. Rev.*, **46**, 995.

Irving, J. H., and Kirkwood, J. G., 1950, *J. Chem. Phys.*, **18**, 17.

Irving, J. H., and Zwanzig, R. W., 1951, *J. Chem. Phys.*, **19**, 1173.

Janssens, P., and Prigogine, I., 1950, *Physica*, **16**, 895.

KIRKWOOD, J. G., 1935, *J. Chem. Phys.*, **3**, 300; 1946, *Ibid.*, **14**, 180; 1947, *Ibid.*, **15**, 72.
KIRKWOOD, J. G., and BOGGS, M. B., 1942, *J. Chem. Phys.*, **10**, 394.
KIRKWOOD, J. G., and BUFF, F. P., 1949, *J. Chem. Phys.*, **17**, 338.
KIRKWOOD, J. G., BUFF, F. P., and GREEN, M. S., 1949, *J. Chem. Phys.*, **17**, 988.
KIRKWOOD, J. G., LEWINSON, V. A., and ALDER, B. J., 1952, *J. Chem. Phys.*, **20**, 929.
KIRKWOOD, J. G., MAUN, E. K., and ALDER, B. J., 1950, *J. Chem. Phys.*, **18**, 1040.
KLEIN, G., and PRIGOGINE, I., 1953 a, *Physica*, **19**, 74; 1953 b, *Ibid.*, **19**, 89; 1953 c, *Ibid.*, **19**, 1053.
KRAMERS, H. A., 1940, *Physica*, **7**, 234.
LENNARD-JONES, J. E., 1937, *Physica*, **4**, 941.
LENNARD-JONES, J. E., and DEVONSHIRE, A. F., 1937, *Proc. Roy. Soc.* A, **163**, 63; 1938, *Ibid.*, **164**, 1; 1939 a, *Ibid.*, **169**, 317; 1939 b, *Ibid.*, **170**, 464.
MCLELLAN, A. G., 1952 a, *Proc. Roy. Soc.* A, **210**, 509; 1952 b, *Ibid.*, **213**, 274; 1953, *Ibid.*, **217**, 92.
MAYER, J. E., and GOEPPERT-MAYER, M., 1946, *Statistical Mechanics* (New York: John Wiley).
METROPOLIS, N., ROSENBLUTH, M., ROSENBLUTH, A., TELLER, A., and TELLER, E., 1953, *J. Chem. Phys.*, **21**, 1087.
MORI, H., 1953, *Progr. Theor. Phys.* (*Univ. Kyoto*), **9**, 473.
MORI, H., and ONO, S., 1952, *Progr. Theor. Phys.* (*Univ. Kyoto*), **8**, 327.
MOYAL, J. E., 1949, *Proc. Camb. Phil. Soc.*, **45**, 99.
NIJBOER, B., and VAN HOOVE, L., 1951, *Proc. Acad. Sci. Amst.* B, **54**, 256.
ONO, S., 1947, *Mem. Fac. Engng Kyushu*, **10**, 190; 1954, *Progr. Theor. Phys.* (*Univ. Kyoto*), **12**, 113.
ORTON, B. R., 1955, *M.Sc. Thesis*, University of London.
PEEK, H. M., and HILL, F. L., 1950, *J. Chem. Phys.*, **18**, 1252.
PEIERLS, R., 1929, *Ann. Phys., Lpz*, **3**, 1055.
POPLE, J. A., 1951, *Phil. Mag.*, **41**, 459.
PRIGOGINE, I., 1954, *Advanc. Phys.*, **3**, 131.
PRINS, J. A., 1931, *Naturwissenschaften*, **19**, 435.
PRINS, J. A., and PETERSEN, H., 1936, *Physica*, **3**, 147.
RODRIGUEZ, A. E., 1948, *Proc. Roy. Soc.* A, **196**, 73.
ROSENBLUTH, M., and ROSENBLUTH, A., 1954, *J. Chem. Phys.*, **22**, 881.
ROWLINSON, J. S., and CURTISS, C. F., 1951, *J. Chem. Phys.*, **19**, 1519.
RUSHBROOKE, G. S., and SCOINS, H. I., 1951, *Phil. Mag.*, **42**, 582; 1953, *Proc. Roy. Soc.* A, **216**, 203.
SALSBURG, Z. W., ZWANZIG, R. W., and KIRKWOOD, J. G., 1953, *J. Chem. Phys.*, **21**, 1098.
SCOINS, H. I., 1952, *Phil. Mag.*, **43**, 806.
STANFIELD, D., 1954, *Ph.D. Thesis*, University of Bristol.
STEWART, G. W., 1930, *Rev. Mod. Phys.*, **2**, 116.
SUDDABY, A., 1954, *Ph.D. Thesis*, University of London.
TOLMAN, R. C., 1938, *Principles of Statistical Mechanics* (Oxford: Clarendon Press).
VINEYARD, G. H., 1954, *J. Chem. Phys.*, **22**, 1665.
WIGNER, E., 1932, *Phys. Rev.*, **40**, 749.
ZWANZIG, R. W., KIRKWOOD, J. G., OPPENHEIM, I., and ALDER, B. J., 1954, *J. Chem. Phys.*, **22**, 783.
ZWANZIG, R. W., KIRKWOOD, J. G., STRIPP, K. F., and OPPENHEIM, I., 1953 a, *J. Chem. Phys.*, **21**, 1268; 1953 b, *Ibid.*, **21**, 2050.

THE PROTON SYNCHROTRON

By J. P. BLEWETT
Brookhaven National Laboratory, Upton, N.Y., U.S.A.

CONTENTS

	PAGE
§ 1. Introduction	38
§ 2. History of the proton synchrotron	39
§ 3. Proton dynamics in the conventional proton synchrotron	42
3.1. Protons on the equilibrium orbit	42
3.2. Betatron oscillations	42
3.3. Phase oscillations	43
3.4. Gas scattering	45
§ 4. Proton synchrotron parameters	46
§ 5. The Birmingham 1-GeV proton synchrotron	48
5.1. Magnet	48
5.2. Injection	49
5.3. Radio-frequency system	49
5.4. Vacuum system	50
5.5. Operation and experimental programme	51
§ 6. The Brookhaven 3-GeV Cosmotron	52
6.1. Magnet	53
6.2. Injection	54
6.3. Radio-frequency system	55
6.4. Vacuum system	56
6.5. Operation and experimental programme	57
§ 7. The Berkeley 6-GeV Bevatron	59
7.1. Magnet	59
7.2. Injection	61
7.3. Radio-frequency system	61
7.4. Vacuum system	62
7.5. Operation and experimental programme	62
§ 8. Comparison of existing proton synchrotrons	63
§ 9. The Canberra 10-GeV air-cored proton synchrotron project	64
§ 10. Alternating-gradient focusing	65
10.1. Betatron oscillations in alternating-gradient fields	66
10.2. Effects of misalignments in the alternating-gradient synchrotron	69
10.3. Phase stability in the alternating-gradient synchrotron	69
§ 11. The Brookhaven 25-GeV alternating-gradient proton synchrotron project	70
11.1. The electron analogue	71
11.2. Magnet	72
11.3. Injection	73
11.4. Radio-frequency system	73
11.5. Vacuum system	74
§ 12. The CERN 25-GeV alternating-gradient proton synchrotron project	74
§ 13. The Midwest fixed-field alternating-gradient principle (FFAG)	75
§ 14. Conclusion	77
Acknowledgments	77
References	77

Abstract. Three proton synchrotrons are now in operation in the energy range above 1000 MeV (1 GeV). A 1-GeV machine has been constructed at the University of Birmingham and 3- and 6-GeV machines are located at the Brookhaven National Laboratory (N.Y.) and the Berkeley Radiation Laboratory (California). In this report a general description of

these three synchrotrons is preceded by a brief presentation of the applicable proton dynamics. A survey is also included of the salient features of a 10-GeV air-cored proton synchrotron under construction at Canberra (Australia).

The discovery of alternating-gradient focusing has made possible the design of proton synchrotrons in the 10 to 50 GeV range. The dynamics of protons in alternating-gradient fields are discussed and design data are presented for machines to be constructed by Brookhaven and by the European Organization for Nuclear Research in Geneva, Switzerland. A novel application of the new focusing method evolved by the Midwest Universities Research Association (U.S.A.) is also explained.

§ 1. Introduction

The discovery in the cosmic radiation of K-mesons and other particles having masses about 1000 times that of the electron and of hyperons whose masses are greater than that of the proton has made it clear that an understanding of fundamental nuclear processes must await the accumulation of experimental data on the exact masses and properties of these particles. For their production under controlled laboratory conditions proton energies are needed in excess of 1000 million electron volts (1 GeV). Protons can, in principle, be accelerated to reach these energies by the linear accelerator, the synchrocyclotron or the proton synchrotron.

A linear accelerator for 3 GeV would be about 3000 feet long and would require hundreds of megawatts of pulsed power at a fixed frequency in the neighbourhood of 200 Mc/s. A synchrocyclotron for 3 GeV would require a fixed magnetic field of the order of 20 000 gauss over a region 50 feet in diameter. The proton synchrotron requires a ring-shaped magnet supplying fields which vary from zero to about 14 000 gauss in one second, but these fields have a radial extent of only about two feet around the proton orbit. Average beam intensities in the linear accelerator and the synchrocyclotron would be about 1 microampere; in the proton synchrotron the average current is about 1000 times less but is still quite adequate for the desired studies of single events attending nuclear collisions. The cost of a 3-GeV proton synchrotron would be about £2 000 000, while either of the other machines would cost at least ten times as much. It appears, therefore, that the proton synchrotron is by far the best bargain.

In its ' conventional ' form the proton synchrotron has been notably successful in the range from 1 to 6 GeV and its new modification using alternating-gradient focusing gives promise of much higher energies. Present designs are aimed at 25 GeV and future designs seem to be limited only by the financial resources of the builder.

In the synchrotron, the charged particles make repeated circuits of the same closed orbit during acceleration. This orbit may be circular, or short field-free straight sections may be included at intervals so that the orbit is only approximately circular. The curved parts of the orbit lie in regions where a vertical magnetic field is maintained; as the particle energy increases the field is increased in such a way that the orbit does not change. Acceleration of the particles takes place at one or more insulated gaps across which is applied a radio-frequency electric field.

By a mechanism to be discussed later, a fraction of the order of one half of the particles will be trapped around accelerating phases of this field and will then travel on orbits whose radius is determined only by the frequency of the accelerating signal. This frequency must be a harmonic of the frequency of revolution of the particles, so, if the orbit is to remain fixed in position, the frequency must increase as the particle velocity increases. Consequently, either the magnetic field cycle must be controlled from the frequency cycle or the frequency cycle must be determined by information from the magnetic field or from the dynamic position of the particle orbit. Since magnet power supplies are very cumbersome and not susceptible to precise control, the latter expedient has been chosen in all cases.

At this point another advantage of the proton synchrotron becomes evident. At any desired proton energy between injection and the maximum available energy, the proton beam can be brought inward or outward to a target at a rate determined only by the rate of change of the accelerating frequency. Pulses at the target can be made to last some tens of milliseconds so that fast counter systems can derive several pieces of information during one acceleration cycle.

Since acceleration in the proton synchrotron requires a period of the order of one second during which the particles make many revolutions of their orbit, it is evidently impossible to inject so accurately that further forces are unnecessary to restore the protons to their orbit. These forces are introduced by appropriate shaping of the magnetic field so that particles which are not injected exactly on the so-called ' equilibrium orbit ' will undergo stable oscillations around that orbit. Since these forces were first studied in connection with the betatron, the oscillations around the equilibrium orbit are usually known as ' betatron oscillations '.

It is patently impossible to tailor the frequency cycle of the accelerating signal so accurately that the particles will always arrive at the correct phase of the accelerating signal. Fortunately a self-synchronizing mechanism exists whereby particles arriving at the wrong phase restore themselves to the correct accelerating phase. Incorrect phase of the accelerating wave produces energy errors which, in turn, result in excursions away from the equilibrium orbit. The period of revolution on the new orbit differs from that on the equilibrium orbit and results in phase shifts in the revolution pattern which act to correct the acceleration phase. The excursions during which this correction takes place are known as ' phase oscillations ' or ' synchrotron oscillations '.

The dimensions of the synchrotron magnet gap are determined by the expected amplitudes of the betatron and phase oscillations. These oscillations are discussed in some detail in §§ 3 and 10.

Brief introductions to the theory and design of the proton synchrotron are available in the article of Fremlin and Gooden (1950) in the *Reports on Progress in Physics* and in Livingston's recent book *High-energy Accelerators* (1954).

§ 2. History of the Proton Synchrotron

The published history of the proton synchrotron begins with the appearance of the paper of Oliphant, Gooden and Hide (1947) describing the proposed design and beginning of construction of the accelerator at the University of Birmingham.

A suggestion had been made by Oliphant in 1943 that charged particles could be accelerated in a magnetic accelerator in which, in contrast to the cyclotron, the radius of the particle orbit is held constant by variation of the magnetic field. No assurance of the continued synchronism of the revolving particles with the accelerating field existed at the time, but this doubt was removed by the discovery of the principle of phase stability by Veksler (1945) and McMillan (1945). Electron synchrotrons following the proposal of Veksler and McMillan were soon shown to be feasible but the proton synchrotron presented a number of technical difficulties associated with the design of large dynamic magnets and with the necessity for modulating the frequency of the accelerating signal over a large factor as the proton velocity increased from a small fraction of the velocity of light at injection up to almost the velocity of light at energies in the Gev range.

The Birmingham group in their 1947 paper presented possible solutions of the various design problems and proposed a machine for acceleration of protons to energies slightly higher than 1 Gev. During the same year the accelerator group at the newly formed Brookhaven National Laboratory in the U.S.A. made a study of accelerator designs for proton energies of several Gev and concluded that the proton synchrotron was the most useful and practical machine for this energy range (Livingston, Blewett, Green and Haworth 1950). The same conclusion had been reached at the Berkeley Radiation Laboratory of the University of California (Brobeck 1948). In 1948 the U.S. Atomic Energy Commission authorized construction at Brookhaven of a 3-Gev proton synchrotron (later known as the ' Cosmotron ') and at Berkeley of a 6-Gev proton synchrotron (known as the ' Bevatron ').

Although these three machines are basically the same, their design and construction differ in many ways. The Birmingham machine is circular while the American machines are both divided into four quadrants separated by field-free straight sections which are used for auxiliary equipment. The Birmingham and Brookhaven machines both utilize C-shaped magnets with the magnet return inside the proton orbit. In the Berkeley machine the magnet is roughly symmetrical about the orbit with magnet returns both inside and outside the orbit. Injection in the Birmingham machine is at 460 kev from a voltage doubling set ; at Brookhaven the injector is a 4-Mev Van de Graaff electrostatic accelerator ; at Berkeley injection is at 10 Mev from a linear accelerator. The radio-frequency accelerating systems of the three machines differ widely one from another. Many other points of difference will appear in the subsequent discussion of the particular machines.

The first successful acceleration to energies greater than 1 Gev was at Brookhaven in May 1952. By June the energy was increased to 2·2 Gev and during 1953 the design energy of 3 Gev was reached. In the meantime the Birmingham group had suffered the loss of two of its senior group and had been plagued by post-war procurement difficulties and by a serious shortage of manpower. In spite of this, and as a result of superhuman efforts on the part of an insufficient staff, successful operation at 1 Gev was achieved in July of 1953. The Bevatron was completed early in 1954 and proton energies of 5 Gev were reached in March of that year. It now operates successfully up to its design energy of 6 Gev.

It now appears that 6 GeV may not long continue to be the highest accelerated proton energy available for nuclear research. At the August 1955 United Nations sponsored International Conference on the Peaceful Uses of Atomic Energy held in Geneva, V. Veksler, of the Lebedev Physical Institute of the Academy of Sciences, Moscow, announced that a 10-GeV proton synchrotron will be completed in the U.S.S.R. during 1956. The magnet for this machine is 180 feet in diameter and weighs about 36 000 tons; in external appearance it is very similar to the magnet of the Bevatron. The magnet aperture is approximately 2 feet by 6 feet. Injection is from a 9-MeV linear accelerator. Acceleration takes place at two radio-frequency stations. The acceleration cycle lasts 3·3 seconds and is repeated 10 times per minute. Work on this machine has been in progress for four years and was preceded by construction of a working model which accelerated protons to 180 MeV. Successful operation of the 10-GeV machine will probably yield the highest proton energies ever to be attained with the conventional proton synchrotron.

At the Australian National University a proposal was advanced in 1950 for a combined machine called the 'cyclosynchrotron' (Oliphant 1950) in which protons were to be accelerated to 200 MeV by a synchrocyclotron which then became the injector for a 2-GeV air-cored proton synchrotron around the synchrocyclotron periphery. These plans have now been abandoned in favour of the 10-GeV air-cored proton synchrotron discussed in § 9.

By 1952 the proton synchrotron appeared to be approaching an economic upper limit of the order of 15 GeV. Unknown to most accelerator builders, however, a proposal for reduction of the particle oscillation amplitudes had been buried in the patent literature since 1949. Christofilos, in Athens, had proposed the new alternating-gradient method but had not published his work. The same principle was rediscovered at Brookhaven three years later by Courant, Livingston and Snyder (1952) and synchrotron designs based on its use were evolved for energies up to 100 GeV. Investigations at the Atomic Energy Research Establishment, Harwell, and elsewhere, of the limitations of the method, and economic evaluations, led to a choice at Brookhaven of 25 GeV as a reasonable energy for tests of the new method. Design work at Brookhaven is proceeding actively on this machine and construction will be begun during 1956.

The year 1952 was marked also by the formation of the European Council for Nuclear Research (CERN) which immediately laid plans for construction of a large proton synchrotron in its proposed laboratory in Geneva, Switzerland. The original plan for a 10-GeV version of the Cosmotron was abandoned with the discovery of alternating-gradient focusing and the CERN group, after design studies closely paralleling those at Brookhaven, decided in 1953 to construct a 25-GeV alternating-gradient machine.

The CERN schedule is very similar to that of the Brookhaven group and both machines should be ready for test by 1960.

At the 1955 Geneva United Nations Conference Veksler announced that design studies for alternating gradient machines are in progress in the U.S.S.R. and are aimed, at present, at a 30-GeV proton synchrotron. Magnet model studies are already in progress for this machine. The Moscow group has been particularly concerned with the possibility of avoiding the necessity for passing the

phase transition (cf. § 10.3) and has demonstrated that reversal of the magnetic field at intervals over short sections of the magnet ring can make it possible to eliminate the phase transition at the expense of a slight increase in aperture and orbit circumference. (The orbit theory for this magnet configuration has been published by V. V. Vladimirskii and E. K. Tarasov (1955).)

§ 3. Proton Dynamics in the Conventional Proton Synchrotron

3.1. *Protons on the Equilibrium Orbit*

The radius of curvature R of the path of a proton of total energy W (expressed in electron volts) in a magnetic field of B webers per square metre (units of 10 000 gauss) is given by

$$R = \frac{(W^2 - W_0^2)^{1/2}}{Bc} \text{ metres} \qquad \ldots\ldots(1)$$

where W_0 is the rest energy of the proton (938 MeV) and c is the velocity of light in metres per second.

The figures in table 1, derived from equation (1), indicate the relative size of proton synchrotrons for various energies if the peak magnetic field is 14 000 gauss.

Table 1

Peak kinetic energy (GeV)	1	3	6	10	25
Peak total energy (GeV)	1·938	3·938	6·938	10·938	25·938
Radius of curvature (m)	4·0	9·1	16·4	25·9	61·7

The accelerating frequency cycle will depend on the variation of proton velocity with magnetic field. The accelerating frequency will be proportional to the proton velocity or to the ratio v/c. In terms of the proton energy, v/c is given by

$$v/c = \{1 - (W_0/W)^2\}^{1/2}. \qquad \ldots\ldots(2)$$

Numerical values derived from (2) are shown in table 2.

Table 2

Kinetic energy (GeV)	0·1	0·2	0·5	1·0	3·0	6·0
v/c	0·43	0·57	0·76	0·88	0·97	0·99

The frequency cycle can be determined as a function of the rising magnetic field by combination of (1) and (2). It is found that the frequency rises rapidly at first and then flattens out as the proton velocity approaches the velocity of light. The higher the final energy, the more the frequency variation will be concentrated in the early part of the cycle. In the 3-GeV Cosmotron, for example, 95% of the frequency variation takes place during the first half of the acceleration cycle (cf. figure 1).

3.2. *Betatron Oscillations*

Radial and vertical stability of the equilibrium orbit are achieved by making the magnetic field B_z at the orbit decrease with radius r according to the relation

$$B_z = B_0(r/R)^{-n} \qquad \ldots\ldots(3)$$

where R is the radius of curvature of the equilibrium orbit and B_0 is the field at radius R. To satisfy Maxwell's equations the radial field component B_r must have the form

$$B_r = (-nz/r)\,B_z + \text{higher order terms in } z/r. \qquad \ldots\ldots(4)$$

The radial and axial motions of the particle follow from the force equations

$$\frac{d}{dt}\left(m\frac{dr}{dt}\right) - \frac{mv^2}{r} = -evB_z \qquad \ldots\ldots(5)$$

$$\frac{d}{dt}\left(m\frac{dz}{dt}\right) = evB_r. \qquad \ldots\ldots(6)$$

We replace r by $R+x$ in the first of these relations and assume that x and z are small compared with R and that m and v are sensibly constant during the period under consideration. From (5) and (6) we now find

$$\frac{d^2x}{dt^2} + (1-n)\,\omega_0^2 x = 0 \qquad \ldots\ldots(7)$$

$$\frac{d^2z}{dt^2} + n\omega_0^2 z = 0 \qquad \ldots\ldots(8)$$

where ω_0 is the frequency of revolution of the protons. Equations (7) and (8) describe oscillations which are stable provided only that

$$0 < n < 1. \qquad \ldots\ldots(9)$$

Their frequency is of the order of half of the revolution frequency. More refined considerations concerned with possible resonances between radial, vertical and orbital motions make it desirable to operate with n in the range between 0·5 and 0·8.

A more exact evaluation of the oscillation amplitudes during acceleration shows that the betatron oscillations are damped as the magnetic field rises; the oscillation amplitude is proportional to $B^{-1/2}$.

3.3. *Phase Oscillations*

For simplicity we shall consider the phase oscillations in a circular machine in which the orbits are not complicated by the presence of field-free sectors. We shall assume that acceleration takes place at a single localized gap across which a radio-frequency voltage $V\sin(h\omega t)$ is applied; h is an integer and represents the harmonic order of the wave, i.e. the ratio of wave frequency to proton revolution frequency. The frequency of this signal will be assumed to vary so that as a hypothetical 'equilibrium particle' is accelerated it arrives always at the same phase ϕ_0 of the wave. The field due to this gap can be analysed into a series of travelling wave components circulating around the machine in both directions. It is easy to see that the interactions of the protons and the various travelling wave components will average out to zero except in the case of the one component which travels with the same velocity as the protons in the same direction as the protons are travelling. If s represents distance travelled by the protons, this component can be represented by

$$E_s = \frac{V}{2\pi r}\sin\left(h\int\omega\,dt - h\int\frac{\omega}{v}\,ds + \phi_0\right) \qquad \ldots\ldots(10)$$

where v is the wave velocity and hence the velocity of the 'equilibrium proton' and is represented by

$$v = r\omega. \qquad \ldots\ldots(11)$$

We shall now demonstrate that a choice of parameters can be made such that small errors in phase will not eventually cause the protons to fall out of step with the accelerating wave.

If the proton is travelling on the equilibrium orbit at the equilibrium phase ϕ_0, ω and v must have been adjusted so that

$$\int \omega\, dt = \int \frac{\omega}{v}\, ds. \qquad \ldots\ldots(12)$$

Suppose now that the particle has a momentum error Δp. The velocity error $\Delta \dot{s} (= \dot{s} - v)$ will be given in terms of Δp by

$$\Delta \dot{s}/v = (1 - v^2/c^2)\, \Delta p/p. \qquad \ldots\ldots(13)$$

This momentum error will cause the proton to travel on a different orbit having a new radius r which differs from the equilibrium orbit radius R by an amount which we represent by Δr. Since $p = B_z e r$, and B_z is defined in terms of r by equation (3), we can show that

$$\Delta p/p = (1 - n)\, \Delta r/R. \qquad \ldots\ldots(14)$$

The phase of the non-equilibrium particle will differ from the equilibrium phase ϕ_0 by an amount δ given by

$$\begin{aligned} \delta &= h\int \omega\, dt - h\int ds/r \\ &= h\int \omega\, dt - h\int \dot{s} dt/r \qquad \ldots\ldots(15) \\ &= h\int \omega\, dt - h\int (v + \Delta \dot{s})\, dt/(R + \Delta r). \end{aligned}$$

If we take derivatives with respect to time and expand, keeping only first-order terms

$$\frac{d\delta}{dt} = -h\omega(\Delta \dot{s}/v - \Delta r/R). \qquad \ldots\ldots(16)$$

From (13), (14) and (16)

$$\frac{d\delta}{dt} = -h\omega\left(1 - \frac{v^2}{c^2} - \frac{1}{1-n}\right)\frac{\Delta p}{p}. \qquad \ldots\ldots(17)$$

We are now ready to substitute in the equation of motion

$$\frac{dp}{dt} = eE_s + eE' \qquad \ldots\ldots(18)$$

where the second term on the right represents the electric field due to the fact that the orbit includes a changing magnetic flux. E' is given by

$$E' = \frac{1}{r}\int \frac{\partial B}{\partial t}\, r\, dr. \qquad \ldots\ldots(19)$$

From (10), (15) and (18)

$$(R+\Delta r)\frac{d}{dt}(p+\Delta p)=\frac{eV}{2\pi}\sin(\phi_0+\delta)+e(R+\Delta r)(E'+\Delta E'). \quad \ldots\ldots(20)$$

If Δp and its derivatives are zero, Δr and $\Delta E'$ will vanish and

$$R\frac{dp}{dt}=\frac{eV}{2\pi}\sin\phi_0+eRE'. \quad \ldots\ldots(21)$$

This is the relation describing the motion of the equilibrium proton. From (3), (17), (19), (20) and (21)

$$\frac{d}{dt}\left[\frac{pd\delta/dt}{h\omega\{1-v^2/c^2-1/(1-n)\}}\right]=-\frac{eV\delta\cos\phi_0}{2\pi R}. \quad \ldots\ldots(22)$$

This is the relation which describes the behaviour of the phase of the non-equilibrium particle. Since n must lie between zero and one for stability in the radial and vertical betatron oscillations, the quantity $1/(1-n)$ will always be greater than unity and for stability in the phase oscillations $\cos\phi_0$ must be negative. Since $\sin\phi_0$ must be positive to permit acceleration ϕ_0 must lie between 90° and 180°. If these conditions are satisfied, equation (22) describes a stable, weakly damped oscillation in phase.

The frequency of this oscillation for existing proton synchrotrons is of the order of 1 kc/s. Associated with the phase oscillation is a radial oscillation whose amplitude is derivable by rewriting (17) and (14) in the form

$$\frac{\Delta r}{R}=-\frac{d\delta/dt}{h\omega}\left[\frac{1}{(1-n)(1-v^2/c^2)-1}\right]. \quad \ldots\ldots(23)$$

For existing proton synchrotrons (23) indicates a radial oscillation having an amplitude of several inches and damping somewhat more rapidly than do the phase oscillations. In existing machines $h=1$. Equation (23) indicates that a higher harmonic order than unity would decrease the aperture required to contain the radial synchrotron oscillations.

A more rigorous treatment of the various orbital oscillations is given by Twiss and Frank (1949), who present a simultaneous solution of the betatron and phase oscillations. Since the frequencies of the oscillations differ by a factor of the order of several hundred, however, the above treatment is sufficiently accurate for all but the most exacting design considerations.

3.4. *Gas Scattering*

Protons in the circulating beam in the synchrotron can be lost in a variety of ways by interactions with the residual gas in the vacuum chamber. The most important losses are due to multiple, small-angle elastic (Rutherford) scattering. Losses due to single scattering through larger angles are much less important. Inelastic scattering due to nuclear disintegration processes causes losses which are quite negligible compared with the elastic scattering processes. The various losses have been analysed in detail by Blachman and Courant (1948, 1949 a, b) and by Courant (1953).

Blachman and Courant show that the maximum mean square amplitude of betatron oscillations induced by gas scattering is proportional to the quantity

$$\frac{(\text{orbit radius})^3 \times (\text{residual gas pressure})}{(\text{injection energy}) \times (\text{energy gain per revolution})}.$$

Gas scattering is most effective at injection. The build-up of gas-scattering amplitudes is rapidly overcome by the damping of the betatron oscillations; the gas-scattering amplitude reaches a maximum for an energy of about four times the injection energy, after which it decreases to become negligible at high energies.

From the gas-scattering theory it is possible, for a given machine, to estimate the gas pressure for gas-scattering loss of a given fraction of the proton beam. For a 10% loss of beam, the theory indicates that the gas pressure in the Cosmotron and in the Bevatron must be less than 8×10^{-6}. In the Birmingham proton synchrotron the pressure must be less than 2×10^{-6} because of the relatively low injection energy.

Experimental verifications of this theory are difficult, partly because of such obscuring factors as misalignments of the magnetic field pattern and partly because of a lack of information about the composition of the residual gas in a vacuum chamber assembled with gaskets of organic materials. When these factors are taken into account it can be said that the theory has been verified at least to within a factor of two.

§ 4. Proton Synchrotron Parameters

The basic choices of design parameters for a proton synchrotron are rigidly circumscribed by the above considerations. Magnetic fields must be accurately maintained over apertures large enough to contain the betatron oscillations associated with injection errors, gas scattering and magnet misalignments; space must also be provided for the radial motions associated with the phase oscillations. The fields over this aperture must fall within stable limits from the low fields appropriate for injection to the high final fields. Neither eddy currents nor remanent-field effects must materially perturb the field at injection. The final field must not be so high that magnetic saturation will distort the field pattern so that the beam becomes unstable.

In view of these limitations it is not surprising that the three existing machines have quite similar operating parameters particularly in so far as magnet operation is concerned. Table 3 summarizes the design parameters for these machines. Figure 1 shows the variation, during the accelerating cycle, of magnetic field, frequency of revolution of protons and proton energy for the three machines.

The most serious problems in proton synchrotron design are evident from table 3. The first major problem is associated with the very large size of the magnet. In the gap of so large a magnet at full field, energies of tens of millions of joules are stored. To store this energy in one second or so requires a very large power supply. To reduce the field to zero rapidly in preparation for another cycle of operation this energy must be removed and either dissipated or stored elsewhere.

Mechanical problems encountered in magnet erection are very serious because of the large forces to be expected in the presence of so much stored energy. In spite of these forces, the faces of the magnet gap must be aligned to a fraction of a millimetre in order that the field pattern indicated by equation (3) shall be maintained within the limits prescribed by equation (9).

Table 3

	Birmingham	Cosmotron	Bevatron
Final proton energy (Gev)	1·0	3·0	6·4
Radius of orbit (m)	4·5	9·2	15·2
Lengths of straight sections (m)	0	3·0	6·1
Injection energy (Mev)	0·46	3·7	9·8
Magnetic field at injection (gauss)	227	295	300
Final magnetic field (gauss)	12600	13800	16000
Vertical extent of magnet gap (cm)	21	22·4	30
Radial extent of magnet gap (cm)	50	91	122
Weight of magnet (tons)	810	1650	10000
Frequency of revolution of protons :			
at injection (kc/s)	330	330	360
at full energy (kc/s)	9300	4200	2500
Proton energy gain per revolution (ev)	240	1000	1500
Time required for acceleration (sec)	1·0	1·0	2·0
Repetition rate (cycles per minute at full energy)	6	12	10

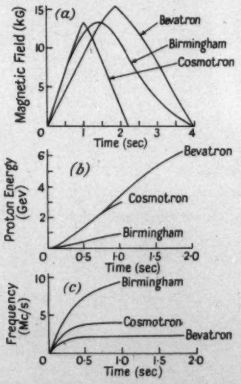

Figure 1. Proton synchrotron parameters as functions of time : (*a*) magnetic field ; (*b*) proton energy ; (*c*) radio frequency in accelerating system (equal to frequency of revolution of protons).

The radio-frequency accelerating gap must support a voltage of the order of 1000 volts over a frequency range of the order of ten to one in spite of space limitations which would hold the gap reactance to only a few ohms at the operating frequency. This voltage must be supplied from a source whose frequency tracks

a relativistic relation between proton velocity and magnetic field within limits of a fraction of one per cent.

The solutions which have been found for these problems will now be discussed in detail.

§ 5. The Birmingham 1-Gev Proton Synchrotron

A general view of the Birmingham proton synchrotron is given in Plate I. In the foreground are the high-voltage electrodes of the injection system. The magnet structure in the background stands about 8 feet high. The radio-frequency power amplifier is visible at the left.

A general description of the Birmingham proton synchrotron was published by Hibbard (1950) and successful operation was announced in *Nature* in 1953 (Birmingham 1953). Operating characteristics have been discussed by Moon, Riddiford and Symonds (1955), Ledley and Riddiford (1955) and Riddiford, van der Raay and Coe (1955).

5.1. *Magnet*

The Birmingham magnet is shown in cross-section in figure 2. Eddy current effects in the varying field are kept within tolerable limits by lamination. The magnet proper consists of 800 tons of low-carbon steel plates $\frac{1}{2}$ inch thick. These

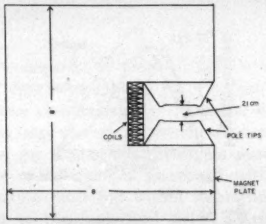

Figure 2. Cross section through the magnet of the Birmingham proton synchrotron.

plates are arranged in a circle so that they touch at the inside edge and the wedge-shaped spaces between them are partly filled by wedge-shaped steel plates. The pole tips are constructed of insulated soft-iron plates, $\frac{1}{8}$ inch thick, and are carefully aligned so that the gap dimensions are maintained to better than 0·005 inch. The gap contour was determined by electrolytic tank measurements to give an n-value of 0·7.

The magnet winding consists of 144 turns of stranded conductor arranged in 6 parallel coils of 24 turns each. The mean dissipation of 182 kw in the winding and 50 kw in the magnet iron is removed by air cooling.

At peak field the magnetic stored energy is about 7×10^6 joules. This energy is supplied by a pair of 1100-volt d.c. generators connected in parallel and driven by a 1500-h.p. induction motor. Coupled to the generators is a 36-ton flywheel; total energy storage in the rotating system is 55×10^6 joules. The magnet cycle is initiated by connection of generators to magnet through an ignitron which is

PLATE I. The 1-Gev proton synchrotron at the University of Birmingham.

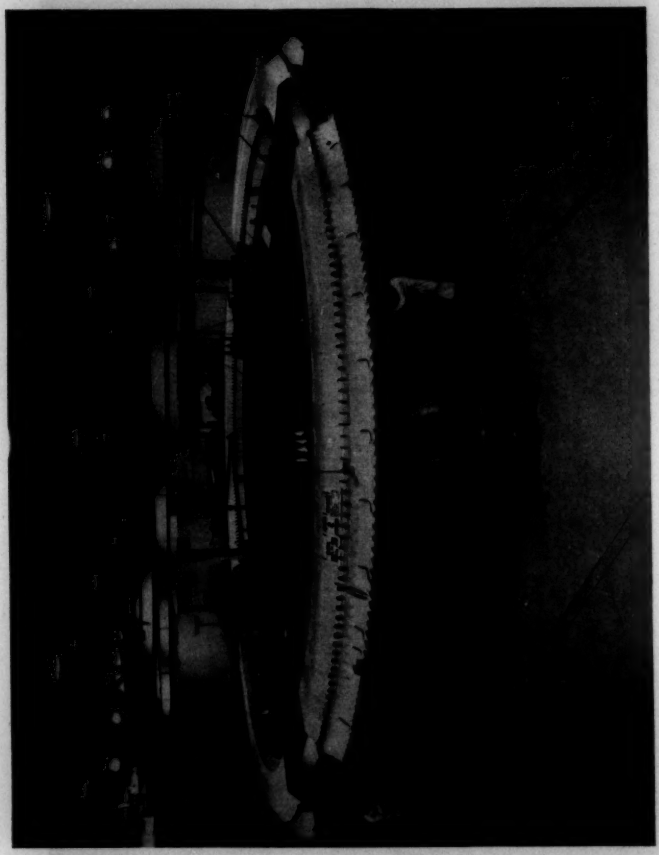

PLATE II. The Brookhaven 3-Gev Cosmotron before addition of the shielding wall.

short-circuited by rapid closure of nine 600-amp contactors before its rating is exceeded. Since the magnet presents an approximately inductive load, the current rises roughly linearly to its peak value of 12 000 amps in one second. During the rise of magnet current, the generator excitation is reversed at a time such that the current rise is checked at 12 000 amperes and decreases to zero about 4 seconds after the start of the cycle. By this means the relatively small fraction of the magnetic stored energy which has not been dissipated in the magnet or the power supply is restored to the flywheel. This cycle is repeated once every 10 seconds.

5.2. *Injection*

When the field in the magnet gap has reached the appropriate value for injection, a signal derived from a peaking strip in the magnetic field triggers a radio-frequency ion source which yields a peak proton current of 0·7 ma. The protons are accelerated by a Cockcroft–Walton set to an energy of 460 kev and approach the synchrotron along a tangent to their initial orbit. A $\frac{1}{8}$-inch thick mumetal cone provides shielding from the stray field of the magnet up to the point where the beam enters a set of electrostatic guide plates which maintain the tangential path through the external regions of the magnetic field up to the point of release. When the beam is released it enters on a spiral orbit of somewhat greater initial radius than the final equilibrium orbit. Since the magnetic field is rising the proton orbit shrinks at a rate of about 3 mm per revolution and so clears the injection system on further revolutions. Injection continues during about 70 revolutions of the proton beam. During this period the injection energy is increased linearly by about 30 kev so that the injected beam continues to have the appropriate energy for the injection orbit in spite of the rise of the magnetic field.

5.3. *Radio-frequency System*

The frequency of the field which accelerates the protons varies during the acceleration cycle from 330 kc/s to 9·2 Mc/s. The signal is generated in a beat-frequency oscillator whose frequency is governed by the field in the synchrotron magnet through a control system of great electrical and mechanical complexity. Its essential features are as follows (cf. Hibbard 1950, Hibbard, Caro and Freeman 1954).

The beat-frequency oscillator consists of a fixed 32-Mc/s oscillator and a variable 32–22 Mc/s oscillator. Both oscillators use quarter-wave lines as tuning elements but the resonant system of the variable-frequency oscillator includes a rotating capacitor cut very precisely to give the desired cycle. The vane of this capacitor rotates at a speed accurately proportional to the synchrotron magnet voltage. If the magnet voltage does not reproduce precisely, an electromechanical synchronizer can accelerate or retard the speed of rotation of the vane. Comparisons between capacitor speed and magnet voltage are made every 10 milliseconds through an optical system which includes a fixed light beam and one of 120 miniature mirrors, each located to 2 seconds of arc on a circle around the shaft of the capacitor rotor. Signals from the optical system are compared with a sequence of pulses controlled by the magnet voltage, and the output of the

comparison circuit is used to vary the speed of the motor which drives the capacitor.

The output of the beat-frequency oscillator is amplified and applied to a metallic lining inside a portion of the vacuum chamber of the synchrotron. This lining constitutes an accelerating electrode or ' drift tube ' occupying 96° of the total circumference of the chamber and protons are accelerated both on entering and on leaving this electrode. Thus, it functions in much the same fashion as the dee of a cyclotron. The accelerating electrode, or ' Cee ', has so high a capacity to its surroundings that, at its top frequency, its driving point reactance is only 3·8 ohms. Such a load is not easily driven to its operating voltage of 240 volts by an amplifier of reasonable size, so the Cee capacitance is resonated by a variable inductance which consists of a tapered coil that is plunged during each cycle into a pool of mercury. The coil moves at such a rate that those turns of inductance, which are not short circuited by the mercury, present the correct reactance to keep the Cee-inductance system resonant. Although an inductance range of 2000 to 1 would be required for resonance over the whole frequency range, the Cee reactance is high enough at the low frequencies that an inductance variation of about 1000 to 1 has been found to be adequate. Performance of this inductor has now been found to be unsatisfactory due to occasional adherence of mercury drops to the winding and it is expected that it will shortly be replaced by a saturable ferrite inductor.

Although the low-level frequency-control system is synchronized with the magnet, and operates whether or not a beam is present, the high-level amplifier is not operated until protons have been injected. The first protons to reach the inner wall of the vacuum chamber are collected on a current probe. This signal is used to activate the power amplifier because these protons arrive at about the instant when the main proton beam has reached the centre of the vacuum chamber. By this means the need for accurate stabilization of the injection energy is removed.

5.4. *Vacuum System*

When the parameters of the Birmingham machine are inserted in the gas-scattering relation (see § 3.4), it is found that about 10% of the protons should be lost at a pressure of 2×10^{-6} mm of mercury. For pressures above this the loss should increase very rapidly. Actually the beam has been found to be several times more sensitive to pressure than was anticipated from the theory. This is partly due to magnet misalignments and partly because the phase oscillations do not damp as rapidly as expected (probably because of small errors in the radio-frequency control system) and considerable loss is attributable to scattering in the radial direction. In any case the beam is effectively lost if the pressure rises above 2×10^{-6} mm and best operation of the machine is achieved when the pressure is held below 8×10^{-7} mm.

The vacuum chamber (Riddiford 1951) is constructed of sixty short pipes of electrical porcelain, 2·8 cm thick and having an approximately rectangular cross section, with internal dimensions 10 cm vertically by 36 cm radially. To avoid collection of charge on the inside of the chamber, without at the same time providing for circulation of large eddy currents, the internal surface of the chamber

is coated with a layer of platinum having a resistance of one ohm per square. Possible deleterious effects due to bare spots in this coating are guarded against by a preliminary glazing of the inside wall with a conducting glaze of resistance of 1 megohm per square. The chamber sections and their conducting coatings are joined by rubber gasket rings and metal spring contacts.

The system is evacuated by five, carefully baffled, oil-diffusion pumps each having a speed of 2000 litres per second. These pumps are arranged almost symmetrically around the ring at the points where most gas evolution is expected.

Six air locks are included in the system for insertion of targets and three re-entrant tubes are used for irradiation of materials and photographic emulsions.

5.5. *Operation and Experimental Programme*

The best accelerated beam intensity attained is about 5×10^9 protons per pulse with average pulse-to-pulse fluctuations of about a factor of two. The beam can be cut to about 2% of its peak intensity, for experiments which require it, by restricting the vertical aperture. The beam intensity is monitored by an induction electrode; this is an insulated plate over which the beam passes. As the pulsating beam approaches the plate, charges flow to the plate from an external circuit and supply a signal of an appreciable fraction of a volt which is easily measured. In this way the beam intensity can be continuously observed without interception of protons. If two electrodes are used, one inside the equilibrium orbit and one outside, the relative induced charges give an indication of the radial position of the beam. This technique, which was first used at Brookhaven, is now included in the Birmingham synchrotron.

Shielding of this machine for protection of personnel has been a serious problem, since the machine is built in a small room around which are disposed a number of offices and laboratories. Until more shielding can be added the only solution to this problem is a limitation of the hours of operation of the machine—a very serious drawback in view of the number of experiments contemplated.

The dimensions of the proton beam at various stages of the acceleration cycle have been studied by rapid introduction of diaphragms (Riddiford, van der Raay and Coe 1955), by introduction of a crystal scintillator (Ledley and Riddiford 1955), and by observations of radioactivity in targets (Moon, Riddiford and Symonds 1955). It appears that the high-energy beam is about 2 cm both in radial and in vertical extent.

Both inside and outside targets are used. The inside targets are fixed in position inside the region required during acceleration and the beam is contracted to their position by the rising magnetic field after the accelerating field has been turned off. The outside targets are driven into position after injection and the beam is expanded to strike them by turning off the accelerating field after the magnetic field has reached its peak and is decreasing, or by making appropriate changes in the radio-frequency cycle. Because of the finite extent of the beam and because its radius contracts or expands rather slowly under the conditions described, pulses of particles from the targets last from 5 to 30 milliseconds so that fast counters can register several counts during one pulse.

Although all experimental work to date has been done on beams scattered out from the targets, plans are under way for ejection of the beam by a method similar to that used with the Brookhaven Cosmotron (Piccioni *et al.* 1955).

Experimental techniques now in use at Birmingham include the study of tracks in nuclear emulsions, observation of tracks in an 18-inch high-pressure hydrogen-filled cloud chamber in a pulsed field of 13 000 gauss, and measurements with coincidence counter telescopes. Published results include studies on nuclear interactions and star formation in photographic emulsions for 600-Mev protons (Lock and March 1955) and for 950-Mev protons (Lock, March, Muirhead and Rosser 1955). Cloud chamber studies have been made of p–p interactions in the same energy range. Elastic and inelastic interactions have been observed; in the latter case evidence has been found for an excited state of the nucleon (similar evidence has been found at Brookhaven, cf. § 6.5). In addition to these techniques which involve observations of individual particles, a substantial amount of work has been done on radiochemistry of various elements in the 200–950-Mev range. The first result of this work is an excitation curve for the reaction $^{12}C\,(p, pn)^{11}C$.

§ 6. The Brookhaven 3-Gev Cosmotron

Plate II is a photograph of the Brookhaven Cosmotron taken before the present shielding wall was constructed. The 4-Mev, pressurized, electrostatic injector is visible in the centre background. Protons are injected into the field-free straight section in the left background and circulate counterclockwise in the machine. The next straight section (at the extreme left of the photograph) was originally used for beam detection equipment, but this apparatus has now been moved into the injection straight section, and the second straight section is occupied by targets and beam-ejection components. The targets in this section emit beams into an area uncomfortably close to several occupied laboratories; consequently they are used for cloud-chamber experiments which operate at a much reduced intensity of beam. The third straight section, at the extreme right of the photograph, is used for high-intensity beam targets. Beams from these targets pass through openings in the shielding wall into the experimental area or out, through the building wall, into an outdoor area where several cloud chambers are housed in temporary structures or trailers. The last straight section, in the right background (and partly hidden in the photograph by a building column), is occupied by the radio-frequency accelerating unit. A plan view of the Cosmotron is shown in figure 3.

The Cosmotron was described in great detail in a series of 27 papers in a complete issue of the *Review of Scientific Instruments* (M. H. Blewett *et al.* 1953). At the time this description appeared, the machine was operating at 2·2 Gev. Correction windings, which had been included on the faces of the magnet poles to correct for magnet saturation, had not yet been powered. During 1953 the pole-face windings were brought into operation and the final energy was raised to its present, and final, value of 3 Gev. The machine was operated about 80 hours per week during 1953 and 1954 until November 1954, when a short circuit developed in one of the magnet windings. During a five-month shutdown for repairs a number of changes and improvements were made with the result that

present operation appears to be completely free from pulse-to-pulse fluctuations. The machine is now operating 24 hours per day, five days per week, with periodic scheduled shutdowns for maintenance and rearrangement of experimental facilities.

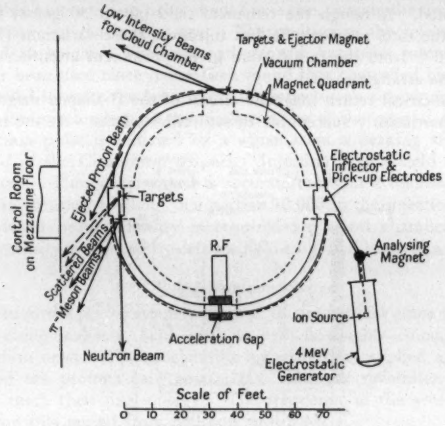

Figure 3. Plan view of the components of the Cosmotron.

6.1. *Magnet*

The Cosmotron magnet is shown in cross section in figure 4. In this magnet it has been possible, by raising the current to high density in water-cooled coils, to decrease the exciting coil's cross section to the point where it can be set in a linear extension of the magnet gap. This improves the efficiency of the magnet design since the field, in principle, is uniform up to the surface of the coil. In practice, eddy current and saturation effects produce some perturbation at the surface of the winding but only over a space which is used for coil clamps and vacuum-chamber walls. A return winding is situated half above, and half below, the outer edge of the gap. The addition of this winding, which is omitted in the Birmingham magnet, results in a 25% reduction in magnet stored energy and reduces external fields to almost negligible proportions.

The magnet is composed of 288 blocks, each of which is a stack of twelve $\frac{1}{2}$-inch laminations. Each block was stacked and then machined as a unit. The gap contour was evolved by analysis and modelling to give an n-value of 0·6, and consists of a central section where the gap increases linearly by about 0·010 inch per inch, and a region about 4 inches in the radial direction where the gap is closed to its inner height. This configuration adds about an inch to the radial extent of the useful field. The wedge-shaped spaces between the blocks are left vacant. The blocks are connected to form a single structure by welded tie-bars.

The blocks were each given very extensive magnetic tests and then were arranged around the magnet ring in an order that would give minimum variation in those magnetic values which might cause perturbations of the beam. Remanent fields varied, from block to block, over a wider range than the other magnetic properties tested. Although the remanent field (about 30 gauss) is only about one-tenth of the total magnetic field at injection, these variations (in some cases as much as 20% from the mean) were given prominent attention in the determination of the arranging order.

The asymmetrical return magnetic circuit of the C-shaped magnet makes the field pattern particularly susceptible to saturation effects. As the iron saturates,

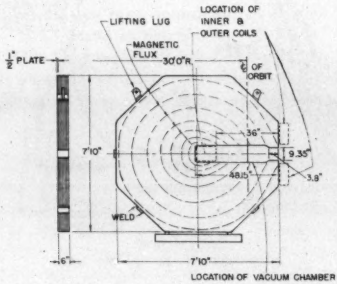

Figure 4. Cross section through the magnet of the Brookhaven Cosmotron.

the radial rate of decrease of the field increases and the n-value increases to the point where the beam is no longer stable for fields of about 11 000 gauss. The field can be corrected, however, by a distributed current on the pole faces. This current must be increased rapidly as further saturation sets in, and 14 000 gauss was chosen as the highest field for which correction was economically feasible. This correction corresponds to an increase in final proton energy from 2·2 to about 3 GeV.

At peak field the energy stored in the field of the Cosmotron magnet is about 12×10^6 joules. Before the magnet is energized this energy is stored in a flywheel as in the Birmingham machine. The power supply is not a d.c. generator as in the Birmingham case, however, but consists of a 12-phase a.c. generator and an ignitron rectifier bank. When the magnet reaches peak field the ignitron firing phase is retarded by about 150° ; this has the effect of reversing the voltage on the magnet and the magnet's stored energy flows back through the alternator, now acting as a motor, into the flywheel. The main advantage of this system lies in the ability to reverse voltage in a small fraction of a second and so to cut down dissipation in the magnet.

6.2. *Injection*

The Cosmotron injector is a horizontal, pressurized, electrostatic generator that is rated at 4 MeV but ordinarily operated at about 3·7 MeV. The proton beam originates in a cold-cathode ion source and is analysed after acceleration

by a magnetic field which deflects the proton beam toward the inflection assembly while the hydrogen molecular beam is allowed to fall on a split plate which is part of the energy control system for the electrostatic machine. The proton beam then undergoes an electrostatic deflection of 30° to emerge in the Cosmotron vacuum chamber tangent to an orbit about ten inches outside the final equilibrium orbit in the centre of the magnet gap. The position of the injector is variable in radius and in height. The latter adjustment has been found unnecessary and has never been used since it has been found that controlled betatron oscillations can be used to make the beam clear the inflector on subsequent revolutions even though the injector lies on the median plane of the magnet gap.

The injection pulse is initiated by a signal from a peaking strip located in the stray field of the Cosmotron magnet. Injection is at a field in the gap of about 300 gauss. The peaker signal is accurate to about 2 microseconds, corresponding to an accuracy to about one part in 10 000 in the injection field.

When reduced beam intensity is required for cloud chamber experiments the injected intensity is reduced by defocusing the injected beam in a magnetic lens.

6.3. *Radio-frequency System*

After injection the proton beam is allowed to circulate for some tens of revolutions in the rising magnetic field until its path is roughly coincident with the final equilibrium orbit. The accelerating signal is then applied across an insulated gap and the protons gain about 1000 volts per revolution until, in one second, they reach their final energy. The frequency of the accelerating signal changes during this period from 330 kc/s to 4·2 Mc/s.

The radio-frequency system of the Cosmotron differs from that of the Birmingham machine in almost every respect. It is completely electrical; no dependence is placed on mechanical timing or controls. The primary signal is derived from the magnetic field through a circuit which includes eight large pick-up windings that are buried in the pole-face windings, an electronic integrator which yields a signal proportional to the field, and a non-linear network which distorts the field signal into a current appropriate for tuning a saturable inductance in the tank circuit of an oscillator.

The non-linear control network has its characteristic controlled by a series of biased diodes which begin to pass current when the field signal reaches a series of preset values. Originally, 28 diode correction points were included. This number will be increased slightly in a new modification of the control system.

The saturating core for the oscillator is shaped from a ferrite ring in such a way that no coupling exists between the radio-frequency and saturating windings. The core is immersed in oil whose temperature is held constant to 0·1°C.

The original low-level system was rather susceptible to miscellaneous electrical noises. It has now been rebuilt in a compact and well shielded cabinet and appears to be free from external disturbances.

The oscillator output is amplified in a broad-band amplifier culminating in a pair of 75-kw transmitting valves. It is then applied directly across an insulated gap in the vacuum chamber. The same difficulties with low shunt impedance were met with this system as were found with the Birmingham machine. In the Cosmotron, they were solved by making the gap part of a re-entrant cavity structure

which is heavily loaded with about a ton of ferrite whose low-frequency permeability is about 1000. This raises the driving impedance of the cavity to a value whose average over the cycle is approximately 100 ohms. Series and shunt resonances in this system and its associated circuits were adjusted to give a fairly flat impedance–frequency characteristic over the operating range.

The broad-band system used in the Cosmotron has some advantages of simplicity in operation. These advantages are offset to a considerable extent by its lack of discrimination against harmonics in the accelerating wave, and it seems probable that some rudimentary tuning will eventually be included.

The sequence of operations during the accelerating cycle begins, so far as the radio-frequency system is concerned, by the activation slightly before injection of the frequency-control system. The power amplifier is turned on when the injected beam reaches the centre of the magnet gap, and is turned off when the beam has reached its desired energy.

6.4. *Vacuum System*

In each quadrant of the Cosmotron, a single vacuum chamber 50 feet long is curved to fit the magnet periphery. This chamber is rectangular in cross section, having solid, stainless steel, vertical walls and laminated horizontal walls.

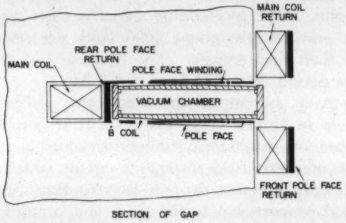

Figure 5. Cross section through the vacuum chamber of the Cosmotron.

It is shown in cross section in figure 5. The upper and lower walls are made up of insulated bars of stainless steel, 2 inches wide, and $\frac{3}{4}$ inch thick at their centre section. These walls are made vacuum-tight by cover sheets of low-vapour-pressure rubber (Myvaseal). The deflection under vacuum of these 36-inch long bars is $\frac{3}{16}$ inch. The 2-inch width of the bars is the maximum permissible if eddy current distortions of the field are to be held to harmless proportions.

Since about 2 inches of vertical aperture is lost by the members of this chamber many attempts were made to design a thinner structure supported from the magnet, but all such designs were rejected on the basis of their mechanical complexity.

In the two target straight sections, the vacuum chamber expands to internal dimensions of 2 ft by 4 ft to allow room for the various targets and auxiliary equipment. The injection straight section includes an even larger vacuum box of an irregular shape designed to house the inflection system. In the acceleration

straight section, the vacuum chamber continues with approximately unchanged inside dimensions. In all straight sections expansion joints are included at the point where the vacuum chamber leaves the magnet.

The vacuum chamber is evacuated by twelve 20-inch oil-diffusion pumps. Pressure is maintained below 5×10^{-6} mm, although very little gas scattering is observed at pressures twice as high as this.

In spite of its mechanical complexity and its hundreds of feet of vacuum gasketing, this chamber has performed very satisfactorily. Only once in three years of operation has it been necessary to remove a vacuum chamber quadrant to repair a vacuum leak.

6.5. *Operation and Experimental Programme*

The performance of the Cosmotron has exceeded expectation to the extent that shielding has been a more serious problem than was expected. During the preliminary operation, radiation surveys indicated that an eight-foot concrete wall must be interposed between the machine and the operating personnel. Provision had been made for such a wall, but soon after its installation rapid improvement of the machine made the protection of this wall marginal. A concrete roof has now been raised over the main target straight section and the adjacent parts of the magnet and, for the present, the radiation level in the control room is slightly below tolerance. A Brookhaven Laboratory report is available on the *Health Physics Program for the Brookhaven Cosmotron* (Cowan and Handloser 1953).

The beam intensity is now stable at a level of 5×10^{10} protons per pulse. In full-energy operation the cycle is repeated every 5 seconds. For lower final energies, the cycle can be repeated more frequently up to a maximum of about 30 pulses per minute.

After the preliminary test period, which lasted for about eight months, the machine entered a period of 16-hour-per-day operation, five days per week. Scheduled one-week shutdowns for maintenance and experimental rearrangement took place every five to seven weeks. During operation, shutdowns due to machine failures finally required less than 10% of the operating time and, at this point, the turn-on and turn-off time became an appreciable fraction of the operating day. In addition, the demands of the experimental programme grew so great that, at one time, some 67 experiments using the machine were in progress. The machine was then put on 24-hour-per-day operation, five days per week; turn-on and turn-off periods now occur only once per week.

Simultaneous experiments have been made possible by sequencing of beam pulses and target operations. For example, during a counter experiment using a high-intensity beam, one pulse per minute is accelerated at reduced intensity and deflected to a separate target to provide a beam for an expansion cloud chamber which cannot use the more frequent pulses.

For experimental use several beams are available. An intense exchange-neutron beam including neutrons up to almost the full incident proton energy is emitted in the forward direction from all targets, mesons of all varieties and scattered protons are allowed to emerge at various angles from targets in the straight sections and negative π-meson beams are analysed by the stray field

of the Cosmotron magnet and are focused at various points at distances of the order of 20 feet from the machine. Intensities of the meson beam are of the order of 5 per cm^2 per pulse. In addition to these beams an ejected proton beam is now available (Piccioni *et al.* 1955). This has been accomplished by shrinking the accelerated proton beam until it passes through a lucite target in which it undergoes a sufficient energy loss that it is displaced inward about 4 inches on its next revolution. It then enters the 6000-gauss field of an electromagnet, 30 inches long, which gives it a sufficient outward deflection that it emerges from the machine one quadrant later. If necessary, a second magnet is to be installed at the point of emergence to give the ejected beam an additional outward deflection of 8 degrees. Preliminary tests of this system show that almost half of the circulating proton beam will be emitted through an area 2 inches high and 5 inches wide. The ejected beam will be re-focused by a lens consisting of two quadrupole magnets (cf. § 10).

For the most part, the beams from the Cosmotron have been used in studies of single events occurring when a proton, deuteron, or other atomic nucleus, is struck by a high-energy proton, neutron or π-meson. These events are observed in arrays of counter telescopes, in cloud chambers or bubble chambers, or in photographic emulsions. It has been found that all of the known heavy mesons and hyperons can be produced by particles in the range below 3 Gev and a great deal of new information has been accumulated regarding the masses, production and decay processes of the various heavy unstable particles. In addition to the single event studies, a number of radiochemical investigations have been made of the disintegration schemes of various nuclei under high-energy proton bombardment. A number of papers have appeared describing these experiments, and a number more are in preparation. In the following paragraphs we mention only a few of the results already reported.

Typical of the work using counter telescopes are a series of measurements of the scattering of pions by hydrogen and other nuclei (Lindenbaum and Yuan 1953, 1955, Shapiro, Leavitt and Chen 1953, Cool, Madansky and Piccioni 1954). When total cross section for scattering of pions by protons is plotted against pion energy a sharp peak appears at 0·2 Gev; this peak is believed to indicate the existence of a short-lived excited state of the nucleon. Further evidence for the existence of this excited state can be adduced from measurements of production cross sections for π-mesons by 2·3 Gev protons (Yuan and Lindenbaum 1954). Using a pair of counter telescopes, Smith, McReynolds and Snow (1955) have studied elastic p–p scattering in the range from 0·44 to 1·0 Gev. Coor *et al.* (1955) have measured nuclear cross sections for 1·4 Gev neutrons with results which indicate a nuclear density distribution intermediate between uniform and gaussian. When these results are compared with those from high-energy electron scattering, it is possible to conclude that the spatial distribution of protons in the nucleus is very closely the same as the neutron distribution (Williams 1955).

Probably the most impressive conclusion to be drawn from the cloud-chamber studies is that hyperon production, either by protons or pions, is usually accompanied by production of a K-meson. This has been demonstrated both for charged and neutral hyperons by Block *et al.* (1955), Fowler *et al.* (1955) and Walker (1955). General cloud chamber studies of events involving high-energy

neutrons and pions (Fowler *et al.* 1953 a, b, 1954 a, b, Walker *et al.* 1955, Eisberg *et al.* 1955) have yielded information about elastic scattering of pions and production of mesons and V-tracks.

Photographic emulsions have been exposed in the various external beams and have been inserted into the circulating proton beam of the Cosmotron. Stars of various types appear in considerable profusion and have been analysed in great numbers. Heavy meson tracks have been measured in sufficient numbers that it now appears that the masses of the various K-mesons are almost, if not exactly, identical (Hill, Salant and Widgoff 1955). Various events involving interaction of 0·5 Gev negative mesons and emulsion nuclei have been analysed by Blau and Caulton (1954).

Under bombardment by 0·4–3-Gev protons, atomic nuclei undergo a profusion of reactions resulting in production of nuclei of much lower atomic numbers (observations on disintegration of Al, for example, are described by Friedlander, Hudis and Wolfgang (1955)). The most surprising generalization to be drawn from this work is that most excitation functions for production of nuclei lower in the periodic table are very weakly energy-dependent from 0·5 to 3 Gev. Another interesting radiochemical study was made by Fireman and Rowland (1955) on tritium production by 2·2-Gev protons on nitrogen and oxygen. The results were compared with the concentration of natural tritium and the conclusion was drawn that the natural tritium can be attributed to nuclear disintegrations by cosmic rays.

§ 7. The Berkeley 6-Gev Bevatron

Plate III is a photograph of the Bevatron as seen from a gallery high on the wall of the almost circular building which houses the machine. The tank in the foreground is the vacuum chamber of the 10-Mev linear accelerator injector. One quadrant away, to the right, is the straight section which includes the radio-frequency accelerating unit. The straight section at the left of the picture houses beam monitoring equipment. The tower in the centre of the ring is a support for two radial 30-ton cranes. In the region behind this tower is the straight section which, with neighbouring regions of the vacuum chamber, encloses the various target assemblies. Outside the target region the machine is shielded by a concrete wall which encloses about half of the circumference of the machine. (Plate III faces page 64.)

Detailed descriptions of the Bevatron and its operation are, as yet, available only in *University of California Radiation Laboratory Reports* (Cork and Lofgren 1954, Lofgren and Heard 1955, and Cork, Chupp and Lofgren 1955). A design report, now very much out of date, was published at the beginning of construction (Brobeck 1948) and a short report was published by Lofgren (1950) on the operation of a quarter-scale model which preceded the construction of the Bevatron.

7.1. *Magnet*

The Bevatron magnet is shown in cross section in figure 6. It was very conservatively designed to be operated, if necessary, at reduced energy with a very large aperture. This would have been accomplished by leaving out the pole tips. Data on aperture requirements which became available with the

successful operation of the Cosmotron made it evident that this was unnecessary and the aperture was reduced to its present size of 1 foot by 4 feet.

The circulating beam of protons is completely enclosed throughout the magnet quadrants by the two magnet return paths. This geometry is much less sensitive to saturation effects than that of the Cosmotron magnet and the magnetic field pattern is satisfactory up to fields of 16 000 gauss at the equilibrium orbit rather than 13 800 gauss as in the Cosmotron magnet corrected by its pole-face windings.

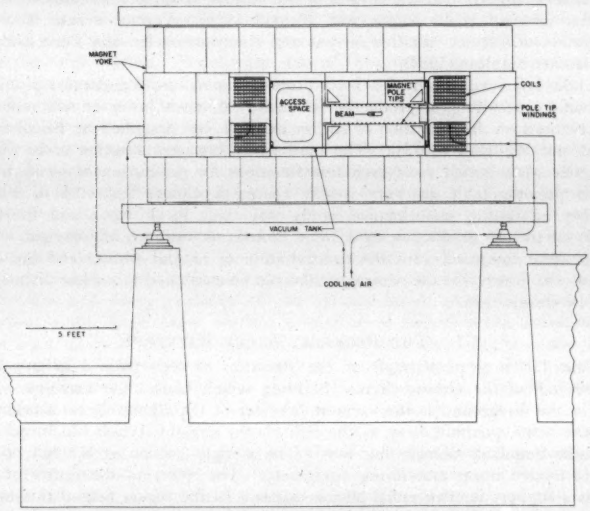

Figure 6. Cross section through the magnet of the Bevatron.

The total magnet weight is 10 000 tons. The yoke is assembled from 288 slabs each made up of $\frac{1}{2}$-inch laminations. In the pole tips, the lamination thickness is reduced to $\frac{1}{4}$ inch to minimize eddy-current perturbations. The magnetizing windings are stranded cables and are air-cooled (the exit vents of the air-cooling system are visible in Plate III at both ends of the injection straight section). Extra windings are included on the pole tips as shown in figure 6, and serve to trim the magnetic field pattern. These windings have been found to be essential since the machine operates dangerously close to $n = 0{\cdot}5$, at which value a resonance between vertical and horizontal oscillations is possible.

The magnet power supply for the Bevatron consists of two units, each almost identical with the Cosmotron power supply. The magnet voltage drops during excitation from 18 000 volts at zero current to 12 000 volts one second later at a full current of 8300 amperes. The stored energy in the magnetic field at full excitation is 80×10^6 joules.

This enormous magnet standing about 14 feet high and over 130 feet in diameter is, to a visitor, a very impressive sight; it is quite evident that proton synchrotrons of this type cannot be scaled up to energies much over 15 Gev without presenting almost insuperable mechanical problems.

7.2. *Injection*

The Bevatron injector is a 10-Mev linear accelerator of conventional design. It is the only Bevatron component which, thus far, has had a published description (Cork 1955). Several milliamperes of protons from a cold-cathode ion source are first accelerated by a 500-kev Cockcroft–Walton generator and are then deflected through an angle of 20° and separated from other ions by a magnetic field. Before entering the linear accelerator the protons pass through a ' buncher ': a gap excited at the linear accelerator's radio frequency and a drift space. The buncher operates on the same principle as a klystron cavity and drift tube, and causes the protons to concentrate in the neighbourhood of the stable phase of the linear accelerator; its inclusion results in an increase, by a factor of three, in the intensity of the beam captured by the linear accelerator.

The linear accelerator operates at 200 Mc/s; 42 drift tubes are included in its 18-foot length and grid focusing is employed throughout.

After leaving the linear accelerator the proton beam, now reduced to about 200 microamperes, is focused by a series of quadrupole magnetic lenses (cf. § 10) and enters a 35° electrostatic inflector similar in its operation to the inflector in the Cosmotron. Injection continues during about 100 revolutions of the circulating beam in the Bevatron.

7.3. *Radio-frequency System*

After injection, the proton beam spirals inward in the rising magnetic field to the centre of the vacuum chamber where it is captured by the turn-on of the radio-frequency accelerating signal. The initial rate of revolution of the protons in the equilibrium orbit, and hence the initial frequency of the accelerating signal, is 360 kc/s. At a final energy of 6 Gev, this frequency has increased to 2·5 Mc/s. The radio-frequency system of the Bevatron is described in a Radiation Laboratory report by Winningstad *et al.* (1952).

The primary frequency source is an oscillator in whose resonant circuit is included an inductance which is varied by saturating its ferrite core by current shunted from the main Bevatron magnet. This gives a frequency which varies in approximately the same fashion as does the protons' revolution frequency during acceleration. Correction to the exact characteristic is made by extra saturating current supplied from an adjustable non-linear network in which bias voltages on a series of diodes can be changed to make small modifications in the frequency–magnetic field characteristic.

After amplification the radio-frequency signal is applied to a drift tube, 11 feet long, through which the proton beam passes. As it enters and as it leaves the drift tube, the proton beam experiences an acceleration or deceleration; because of the time lapse during passage through the tube a net acceleration is achieved at the correct phase. In order that the protons can gain the requisite 1500 ev per turn the applied voltage on the drift tube must be 22 kv. Better efficiency

could have been achieved in a longer drift tube but space requirements in the straight-section tank limit the available space. The drift tube presents a very low reactance corresponding to its 450 pF capacity and the impedance of the system is raised to manageable values by a large ferrite-cored shunt inductance. The drift-tube–inductance circuit is kept in resonance by a servo system which compares the phases of the signals at grid and plate of the final amplifier. Dissipation in the resonant system is of the order of 20 kw.

7.4. *Vacuum System*

The outline of the vacuum chamber is indicated by heavy lines in figure 6. It is a very complicated structure fabricated from sheets of stainless steel, insulated from one another to prevent the flow of large eddy currents. The top and bottom sheets lie between the magnet yoke and the pole tips so that the pole tips and pole-face windings are in the vacuum. To repair leaks in the chamber it is necessary to dismantle part of the magnet structure; fortunately leaks do not appear very frequently. The upper pole tip is supported by structural members attached to the lower pole tip. At one side, between poles and winding, is an access space through which personnel can crawl around the complete circumference of the ring.

The chamber is evacuated by twenty-four 32-inch diffusion pumps distributed among the four straight sections. The pumps are located below the straight-section tanks and are connected directly through the lower walls of these tanks.

The straight-section tanks are large enough that, when they are open to the atmosphere, several men can work inside without crowding. Each tank is especially designed for its particular function. For example, the target tank includes a re-entrant tube in which photographic emulsions can be exposed without breaking the vacuum.

7.5. *Operation and Experimental Programme*

Although the operation of the Bevatron is very impressive and pulses of 10^{10} protons are sometimes available, some difficulties still remain and it cannot be said that the shakedown period is yet completed. Large pulse-to-pulse fluctuations still remain; for experimental purposes the beam is reduced during acceleration to a predetermined level by introduction of noise into the radio-frequency control system. Some faults still occur in the magnet's power supply and work is continuing on the ignitron firing circuits. The radio-frequency system is still undergoing improvements to remove stray disturbances which perturb the frequency control and result in beam loss. The machine is, however, in full operation for experimental use and its regularity of operation improves daily.

Beams for experimental use originate in targets either in the target straight section or in the vacuum chamber upstream from this point. Most of these targets are moved into the beam during the later stages of the acceleration period. A very interesting experimental facility is a ' beam ' of K-mesons which is focused by a quadrupole magnet lens system adjacent to the target straight section.

Many exposures of photographic emulsions in the beams from the Bevatron have been made for groups of physicists in the United States and elsewhere, and

published discussions of the tracks observed should be forthcoming during 1955 and 1956. Some preliminary observations of K-meson properties and masses have already appeared (Birge *et al.* 1955, Chupp *et al.* 1955).

For use with the Bevatron a 10-inch liquid-hydrogen bubble chamber is under construction and design studies are in progress for a similar chamber 6 feet long operating in a field of 20 000 gauss.

During 1955 a large fraction of the experimental programme of the Bevatron was devoted to a search for the negative proton. Negative particles from Bevatron targets are analysed in momentum by electromagnets, and velocity is determined by time of flight in counter telescopes and by response of Cerenkov counters. A successful culmination of this search was announced in October of 1955, at which time more than 50 particles had been observed having negative charge and mass between 0·95 and 1·05 times the proton mass. The threshold for production of these particles appears to lie between 4 and 5 Gev.

§ 8. Comparison of Existing Proton Synchrotrons

Enough experience has now been accumulated with the three operating proton synchrotrons for an evaluation to be made of the relative advantages of those design features which differ from one machine to another. It should, in short, be possible to design a new machine in the 1–6 Gev range which combines the best features of all three existing machines. The conclusions stated below will be controversial to some extent but each can be supported by arguments of appreciable cogency.

The hypothetical machine would have a C-shaped magnet. The better magnetic efficiency of the Bevatron magnet is more than offset by the better accessibility and flexibility in experimental use of the other machines in which particle beams can emerge at almost all azimuths. This C magnet should have a return winding outside the gap both for improved magnetic efficiency and for reduction of the large external fields which are very troublesome in the Birmingham machine.

The aperture available to the beam could be cut in both directions to about two-thirds of the relative aperture available in the Cosmotron; this would cut the weight of the magnet steel to half.

Straight sections are very useful and should be included. They could be safely increased in length by at least 20% over those used in the Cosmotron and the Bevatron.

A polyphase a.c. generator and rectifier system is much more efficient for the magnet power supply than a d.c. generator since dissipation in the magnet is cut drastically by the more rapid reversal of magnet voltage at the peak of the magnet cycle. The a.c. system is, in addition, more flexible in operation.

The frequency-control system in the Cosmotron appears to be the simplest of the three and appears to be adequate, although direct frequency control from the radial position of the beam may eventually be more reliable (cf. § 11.4). The accelerating unit should be tuned, as in the Birmingham machine and the Bevatron, so that the harmonic content of the accelerating signal with its attendant loss of beam can be held to negligible proportions.

As an injector the electrostatic machine appears to have advantages at present but the linear accelerator art is advancing so rapidly that a linear accelerator may well be the best choice in the near future.

The control and laboratory areas should be removed at least 100 feet from the machine and room should be included for high shielding walls up to 15 or 20 feet thick. The experimental area should be at least 100 feet square, and should be covered by a crane of at least 20 tons capacity. On these points the Birmingham machine and the Cosmotron are very deficient. The Bevatron has not been in operation long enough to make a good evaluation of its experimental facilities.

The pulse-rate should be as high as possible so that the very time-consuming experiments using counter telescopes can be completed in rapid sequence.

§ 9. The Canberra 10-Gev Air-cored Proton Synchrotron Project

In an attempt to achieve high energies without the very large expenditures necessary for machines of the type already described, the group under the direction of Professor M. L. Oliphant at the Australian National University in Canberra has designed and has under construction a 10-Gev proton synchrotron of a completely unconventional design. The radius of the proton orbit has been reduced to 12 ft by increasing the peak magnetic field to 100 000 gauss!

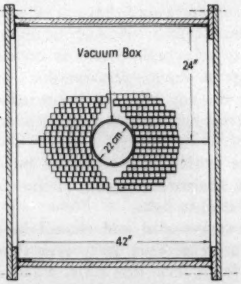

Figure 7. Cross section through the magnet of the proposed Canberra 10-Gev air-cored proton synchrotron.

Iron is obviously of very little use in the magnet, which will consist only of an array of conductors suitably arranged as shown in figure 7 to give the correct field distribution. Alternating-gradient focusing has been considered for this machine but seems to present insufficient advantage; the machine will operate as a conventional proton synchrotron. The magnet conductors are water-cooled and are connected in parallel in eight groups so that the winding consists essentially of four turns outside and four turns inside the orbit; the currents in the two four-turn windings flow in opposite directions. At peak field the current will

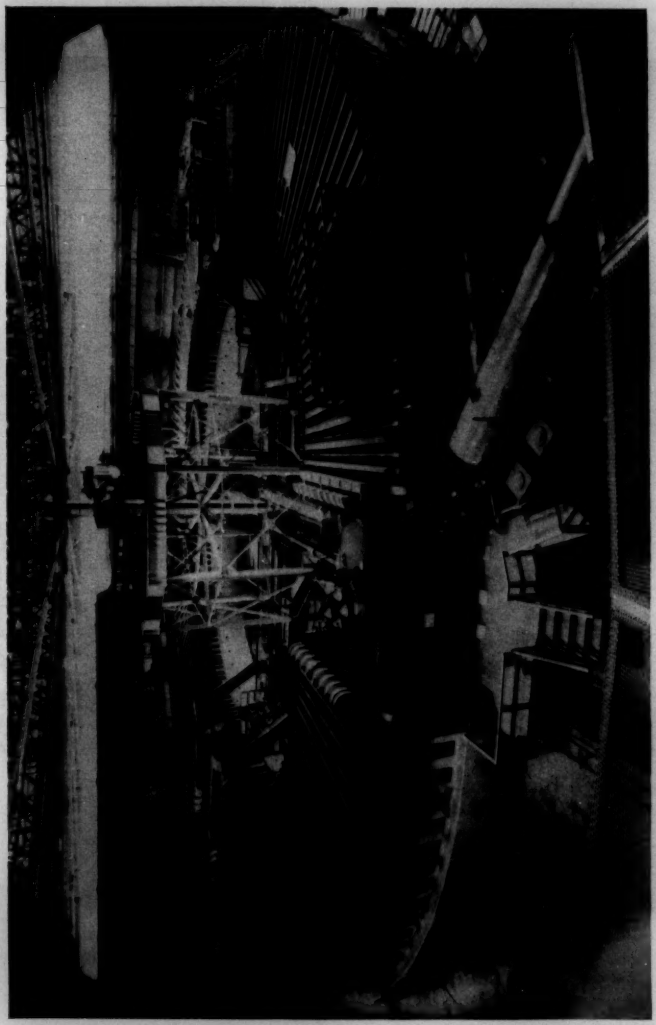

PLATE III. The 6-Gev Bevatron at the University of California Radiation Laboratory.

PLATE IV. The Brookhaven electron analogue with the vacuum covers removed.

be $1{\cdot}5 \times 10^6$ amperes. The force between the two groups of conductors will be repulsive and will have a peak value of about 45 tons per inch of length. To restrain these forces the coils will be supported in shaped holes cut in closely spaced, vertical, duralumin plates, each $\frac{1}{2}$ inch thick. The magnet will be broken into four quadrants separated by 6-ft straight sections. In addition to the local bursting forces there will be a maximum tension in each quadrant of 750 tons. The steel box enclosing the dural plates and shown in figure 7 sustains this tension and transmits it to the quadrant ends.

The power supply for this magnet will be a homopolar generator in which four steel discs, 139 inches in diameter and $10\frac{1}{2}$ inches thick, rotate at 900 rev min^{-1} in a magnetic field of 16 000 gauss. Contact with the discs will be made by jets of liquid sodium ; the rotor will be enclosed in an atmosphere of dry nitrogen. A $\frac{1}{8}$-scale model of this machine has already been built and tested using mercury-jet contacts.

When the magnet is pulsed its field will rise to peak in 0·65 second on a damped sinusoidal wave. The current will be turned off as the current passes its first zero. During this cycle about three-quarters of the energy stored in the generator rotor will be dissipated in the magnet. To restore the rotor to full speed the generator will be run as a homopolar motor for a period of 10 minutes.

Injection will be from an 8-Mev 26-inch cyclotron which will use the magnet from the homopolar generator model. Beam inflection and acceleration techniques will follow the conventional lines already described in connection with other proton synchrotrons.

While it cannot be denied that this is an intriguing project it seems probable that difficulties will be experienced, not only with the limited strength of the conventional materials of construction, but also with the low repetition rate. The latter drawback will be felt most strongly during the period when the machine is brought into operation and the various parameters are under continuous adjustment. It is to be hoped that these difficulties will be brought under control and that this daring project will arrive at a successful conclusion.

§ 10. Alternating-gradient Focusing

A beam of positively charged particles travelling parallel to the z axis of a rectangular coordinate system can be focused in the xz plane by an electric field of constant gradient whose x component has the form $E_x = kx$. But, since $\text{div}\, E = 0$, the y component of E must have a gradient of opposite sign and the beam will automatically be defocused in the yz plane. It can rather easily be shown that this situation is generally true. There is no combination of electric or magnetic fields in free space which will yield simultaneous focusing in all planes through the axis of a rectilinear beam.

If the beam travels on a curved path the situation is slightly changed by terms introduced in the equations of motion by the centrifugal force. In this case focusing is possible for the rather narrow limits of field distribution indicated by equation (9) in our previous discussion of betatron oscillations. The focusing forces provided in this way are relatively weak, however, and the apertures required to contain the excursions of protons from the equilibrium orbit of a

conventional synchrotron are relatively large. These dimensions scale almost directly with the final proton energy of the machine and, as a result, a Cosmotron scaled up to yield 30-Gev protons would have a total magnet weight of 2 million tons. It appears that the economic limit to such scaling operations is not much above 15 Gev.

Fortunately the upper attainable proton energy has again been raised by the discovery of the 'alternating-gradient', or 'strong-focusing', principle. This principle was discovered by Christofilos in Athens in 1949 (cf. Courant *et al.* 1953). His work was not published and the principle was rediscovered by Courant, Livingston and Snyder (1952). These authors point out that successive application of strong focusing and defocusing forces of the same order of magnitude can result in a very strong net focusing. The principle is, perhaps, most easily understood through the optical analogy: the combination of a focusing and a defocusing lens, of equal focal lengths, may be so arranged that, for either lens coming first, the net focal length of the combination is positive.

10.1. *Betatron Oscillations in Alternating-gradient Fields*

The lenses used in alternating-gradient focusing are regions of transverse electric or magnetic fields in which the field varies linearly in a direction normal to the direction of propagation of the particle beam. For a beam travelling in the z direction, we shall now investigate the deflections when the beam travels first for a distance d through a region where the magnetic field has components $B_x = B'y$ and $B_y = B'x$ (since curl $B = 0$) and then immediately travels for a distance d through a region where $B_x = -B''y$ and $B_y = -B''x$. B' and B'' are assumed to be constant. It will be assumed also that the particle velocity v in the z direction is large compared with its velocities in the x and y directions. We shall consider only the motion in the x direction: the conclusions reached will be equally valid for the y motions.

If the particle enters this field array with a displacement x_0 and a velocity in the x-direction of $(dx/dt)_0$, its displacement and velocity x_1 and $(dx/dt)_1$, after travelling through the two field regions, will be given by the transformation matrix

$$\begin{pmatrix} x_1 \\ \left(\frac{dx}{dt}\right)_1 \end{pmatrix} = \begin{pmatrix} \cos\theta'\cosh\theta'' + \frac{k''}{k'}\sin\theta'\sinh\theta'' & \frac{1}{k''}\cos\theta'\sinh\theta'' + \frac{1}{k'}\sin\theta'\cosh\theta'' \\ -k'\sin\theta'\cosh\theta'' + k''\cos\theta'\sinh\theta'' & -\frac{k'}{k''}\sin\theta'\sinh\theta'' + \cos\theta'\cosh\theta'' \end{pmatrix} \begin{pmatrix} x_0 \\ \left(\frac{dx}{dt}\right)_0 \end{pmatrix}$$

$$= (M)\begin{pmatrix} x_0 \\ (dx/dt)_0 \end{pmatrix} \qquad \ldots\ldots(24)$$

where $k'^2 = eB'v/m$, $k''^2 = eB''v/m$, $\theta' = k'd/v$, and $\theta'' = k''d/v$.

The matrix M defined by equation (24) has a unit determinant. Therefore, it can be expressed in terms of three parameters. A convenient choice is

$$M = \begin{pmatrix} \cos\mu + A\sin\mu & B\sin\mu \\ -\frac{(1+A^2)\sin\mu}{B} & \cos\mu - A\sin\mu \end{pmatrix}. \qquad \ldots\ldots(25)$$

This matrix has the property that successive applications of the indicated transformation are governed by the law

$$M(A, B, \mu)^k = M(A, B, k\mu). \qquad \ldots\ldots(26)$$

Evidently a particle, traversing a succession of pairs of lenses of the type described, will undergo a stable oscillatory motion only if μ is real. Consequently the condition for stable motion through a succession of alternating-gradient lenses is $-1 < \cos\mu < 1$ or, in terms of the original parameters,

$$-1 < \cos\left(\frac{eB'}{m}\right)^{1/2}\frac{d}{v}\cosh\left(\frac{eB''}{m}\right)^{1/2}\frac{d}{v} + \frac{B''-B'}{2(B'B'')^{1/2}}\sin\left(\frac{eB'}{m}\right)^{1/2}\frac{d}{v}\sinh\left(\frac{eB''}{m}\right)^{1/2}\frac{d}{v} < 1. \qquad \ldots\ldots(27)$$

This relation defines a region of stability for alternating-gradient magnetic focusing.

Focusing by electric fields having alternating gradients is equally effective. It is necessary in the above discussion only to substitute E'/v for B' and E''/v for B'' and the stability relation (27) is applicable to the electric case.

In the proton synchrotron, focusing is accomplished by magnetic fields. Since a magnetic field is also required to maintain the approximately circular proton path, it is usual to combine the bending and focusing fields so that the field in the region of the proton orbit has the form

$$B_z = B_0 + B'(r-R). \qquad \ldots\ldots(28)$$

This relation is usually written in the form

$$B_z = B_0[1 + n(1-r/R)] \qquad \ldots\ldots(29)$$

so that the parameter n is defined by

$$n = -RB'/B_0. \qquad \ldots\ldots(30)$$

For small displacements from the equilibrium orbit, this definition of n is approximately the same as that used in the conventional synchrotron (equation (3) above).

The radial component of magnetic field is (since curl $B = 0$)

$$B_r = -nB_0 z/R. \qquad \ldots\ldots(31)$$

The orbit of the proton through these fields now follows from a succession of solutions of equations of the form of (7) and (8) above in which the value of n alternates between values of n' and $-n''$. The procedure for establishing the region of stability is the same as that derived above for linear motion and yields the stability relations :

in the vertical direction :

$$-1 < \cos\frac{\pi\sqrt{n'}}{N}\cosh\frac{\pi\sqrt{n''}}{N} + \frac{n''-n'}{(n'n'')^{1/2}}\sin\frac{\pi\sqrt{n'}}{N}\sinh\frac{\pi\sqrt{n''}}{N} < 1 \qquad \ldots\ldots(32)$$

in the radial direction :

$$-1 < \cosh\frac{\pi(n'-1)^{1/2}}{N}\cos\frac{\pi(n''+1)^{1/2}}{N} + \frac{2+n''-n'}{[(n'-1)(n''+1)]^{1/2}}\sinh\frac{\pi(n'-1)^{1/2}}{N}\sin\frac{\pi(n''+1)^{1/2}}{N} < 1 \qquad \ldots\ldots(33)$$

where N is the total number of periods of the alternating-gradient system of which the magnet ring is composed, N sectors having gradients described by n' and N having gradients described by $-n''$. The necktie-shaped region of stability is shown in terms of the parameters n'/N^2 and n''/N^2 in figure 8.

It is now evident that the stable region includes n-values much higher than the upper limit of unity imposed in the conventional synchrotron. In the individual sectors, accordingly, the protons experience focusing or de-focusing forces which are stronger by orders of magnitude than the focusing forces experienced

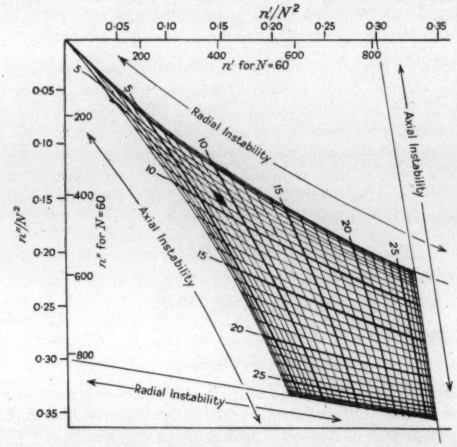

Figure 8. Stability diagram for alternating-gradient focusing in a synchrotron with no straight sections. The lines which cross-hatch the area of stability are the integral resonances for the case of $N = 60$. Values of ν at the resonances are indicated for every fifth resonance along the edge of the region of stability. Fractional integral and other resonances are not shown in this diagram. The small black diamond is the region in which the Brookhaven 25-Gev machine would operate if no straight sections were included. Inclusion of straight sections has the general effect of shifting the whole pattern slightly toward smaller values of n.

in the conventional synchrotron. It remains to be shown that the total effective restoring forces are stronger in the alternating-gradient case than in the conventional case. This is easily seen from an evaluation of the frequency of betatron oscillations. From the definition of the parameter μ in equation (25) and from the behaviour of the transformation matrix indicated in equation (26) it is evident that μ represents a phase shift through one pair of lens elements. When successive applications of the transformation matrix yield a total phase shift of 2π, the system is restored to its original condition and one betatron oscillation has been completed. Consequently the total number ν of betatron oscillations during one revolution of the machine will be given by

$$\nu = N\mu/2\pi. \qquad \ldots\ldots(34)$$

For reasonable values of N and μ it is possible to include a number of betatron oscillations in one revolution. In the conventional machine, on the other hand, equations (7) and (8) indicate that only a fraction of a betatron oscillation will be included in one revolution. Since excursions from the orbit for a given initial error in direction will be proportional to the betatron wavelength it is evident that effective restoring forces are an order of magnitude greater in the alternating-gradient machine than in the conventional machine.

10.2. *Effects of Misalignments in the Alternating-gradient Synchrotron*

Early optimism regarding the capabilities of alternating-gradient focusing for reducing synchrotron apertures to negligible proportions by the use of extremely high n values was tempered somewhat by the results of a study of effects of misalignments of focusing elements by Adams, Hine and Lawson (1953). These authors drew attention to the fact that although the net focusing force in an alternating-gradient system is relatively strong, it is not nearly as strong as the individual forces which follow in sequence to give the net effect. Small misalignments in individual focusing elements are, accordingly, magnified into very large orbit deviations. This is particularly true when the number of betatron oscillations during one revolution around the machine is approximately integral. In this case a resonant build-up of betatron-oscillation amplitude takes place and the beam is lost. At the resonant betatron frequency even the smallest misalignment results in rapid loss of the beam.

The sensitivity to misalignment decreases with a decrease in n value and, hence, in the number of betatron wavelengths per revolution. Designs which now appear practicable allow for not more than ten, or so, oscillations per revolution. Even in this case alignment of magnet units must be accurate to better than one millimetre.

For any machine the resonant n values must be computed and avoided. The stability diagram now becomes cross-hatched, as indicated in figure 8 (for the particular case of $N = 60$), by a number of lines at which resonant instability occurs. Operation is possible only within one of the small diamond-shaped areas between resonances. The safe operating region is found to be still further restricted by other subsidiary resonances which will not be discussed here (cf. CERN 1953).

10.3. *Phase Stability in the Alternating-gradient Synchrotron*

In the alternating-gradient synchrotron a proton whose momentum differs from that of the equilibrium proton will no longer travel on a circular orbit. The new orbit will consist of an alternation of sinusoidal and hyperbolic-functional deviations from a circular orbit of a new radius. When this orbit is traced it is found that the radius of the new average circular orbit differs from that of the equilibrium orbit by an amount Δr given approximately by

$$\nu^2 \Delta r/R = \Delta p/p. \qquad \ldots\ldots(35)$$

This relation replaces equation (14) in the analysis of phase oscillations in the conventional proton synchrotron. Otherwise the analysis of phase oscillations is

identical with the conventional analysis and the final equation for phase oscillations takes the form (to be compared with equation (22))

$$\frac{d}{dt}\left(\frac{pd\delta/dt}{\omega(1-v^2/c^2-1/\nu^2)}\right)=-\frac{eVh\delta\cos\phi_0}{2\pi R}. \qquad \ldots\ldots(36)$$

The consequences of this equation are somewhat more complex than those in the conventional case since $1/\nu^2$ will generally be less than unity. Accordingly, for stability $\cos\phi_0$ must be positive up to an energy E_{tr} for which

$$1-v^2/c^2=1/\nu^2 \qquad \ldots\ldots(37)$$

so that

$$E_{tr}=m_0c^2\nu. \qquad \ldots\ldots(38)$$

Above this energy, $\cos\phi_0$ must be negative. For stable operation the phase of the accelerating wave must be shifted discontinuously at this transition energy from a point on the rising side of the wave to a corresponding point on the falling side of the wave. The behaviour of the proton beam as this transition is passed has been the subject of considerable study and it appears that the transition can be made with safety and without radial excursions of the beam greater than those experienced earlier in the accelerating cycle.

§ 11. The Brookhaven 25-Gev Alternating-Gradient Proton Synchrotron Project

The Brookhaven Accelerator Development Department under the direction of L. J. Haworth has made several design studies for alternating-gradient proton

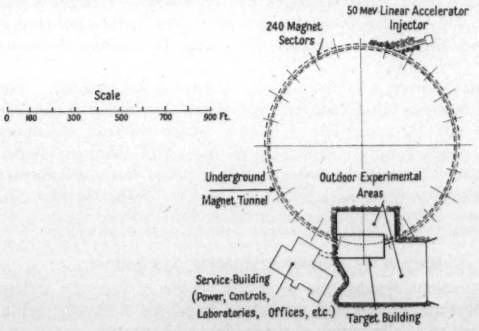

Figure 9. Plan view of the components of the proposed 25-Gev alternating-gradient proton synchrotron.

synchrotrons having final energies up to 100 Gev. Analyses have been made of construction costs as a function of proton energy and attempts have been made to estimate the scientific usefulness of protons in the various energy ranges. A final choice of 25 Gev has been made and construction has been approved by the U.S. Atomic Energy Commission. It is estimated that the machine will cost slightly more than $20 000 000 and will take about six years to build.

The field index n in this machine will be about 350, and the number N of elements in the alternating gradient system will be 60; this will result in a ν of 8·75 betatron oscillations per revolution.

The magnet will be divided into 240 sectors, each about 8 ft long, disposed around a ring 840 ft in diameter. It will be enclosed in a ring-shaped tunnel which will expand at one point into a target building about 100 ft by 200 ft in dimensions. The general configuration of the machine is indicated in figure 9.

11.1. *The Electron Analogue*

Before starting construction of the proton synchrotron the Brookhaven group has constructed a 10-Mev alternating-gradient electron synchrotron using electrostatic bending and focusing. This device is in no sense a model for the larger machine. It is merely a precise analogue computer for obtaining a more accurate solution of the equations of motion of charged particles in alternating-gradient fields than can easily be done using other computing machines. Controlled misalignments can be inserted and their effects studied. Acceleration will be continued through the phase transition at 3 Mev so that radio-frequency techniques for achieving stability during transition can be tested. This machine is now in operation and tests are beginning. Thus far, theoretical predictions have been verified in all cases tested.

Plate IV is a photograph of a section of the analogue lens system taken before the vacuum housings were installed. The primary bending and focusing elements are 80 pairs of shaped electrodes disposed around a circle 45 ft in diameter. One electrode of each lens element has a hyperbolic cross section and the other has a right-angle cross section with faces lying along the asymptotes of the hyperbola formed by the other electrode. This configuration gives an electric field with an accurately linear gradient. One of these elements can be seen in the foreground of Plate IV. Arranged at intervals between the bending lenses are sixteen quadrupole lenses whose electrodes make up a family of rectangular hyperbolae. These lenses provide fields with uniform gradients which can be used for focusing without bending the beam. By changing the bias voltage on the lenses, the effective n value of the machine can be changed sufficiently to take it through several resonances. Also included are several sextupole and octupole lenses which can introduce controlled non-linearities into the field pattern so that effects of magnet saturation can be simulated. Induction pick-up electrodes and removable probes are mounted on each of the sixteen vacuum housings.

Injection in this machine is at 1 Mev from an electrostatic accelerator. Acceleration will take place at one point in a ferrite-loaded cavity unit similar to that used on the Cosmotron.

The first tests with this machine have not included acceleration. An injected beam is allowed to coast in the machine over some thousands of revolutions with the bending lenses held at a constant potential. With the quadrupole lenses, resonances have been observed which cause immediate loss of the beam. In every case the resonances have precisely the expected values.

Note added in proof: In December, 1955, the electron beam in the electron analogue was accelerated through the phase transition energy. Later tests showed that the phase transition can be passed with no appreciable loss of beam.

11.2. *Magnet*

The magnet for the 25-GeV proton synchrotron will have approximately the configuration shown in figure 10. The pole contour, designed for a maximum area of useful field, has been determined by relaxation calculations of fields both in the air gap and in the iron and has been checked by construction of a series of models. The dotted line in the diagram indicates the pole contour for the next magnet sector which will have the opposite gradient. The various magnet sectors will be arranged around the ring in a complicated sequence, some with return legs inside and some with return legs outside the orbit. This is to permit maximum use of targets in the experimental area. The magnet sectors will be separated by straight sections of various lengths for the various radio-frequency accelerating stations, beam detection electrodes, quadrupole correction lenses, etc.

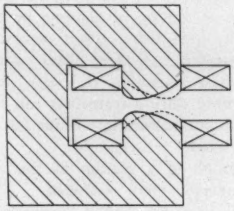

Figure 10. Cross section through the magnet of the proposed Brookhaven 25-GeV alternating-gradient proton synchrotron. The dotted line represents the pole contour for the next magnet sector in which the magnetic-field gradient is reversed. The dimensions of this magnet are not yet fixed ; its height will probably be of the order of 36 inches.

A possible sequence of elements involves 12 ' unit cells ' each including 20 magnet sectors. Within the cell, if the directions of the field gradients are represented by plus and minus signs and the straight sections are represented by numbers which correspond to their length in feet, the sequence runs as follows :

$$+2-5-2+2+10-2-2+5+2-5-2+5+2-2-10+2+2-5-2+5.$$

This disposition is fixed by detailed studies of proton orbits modified by the various requirements for straight section access.

The total magnet weight will be about 3000 tons. Its degree of lamination is not yet decided but the laminations will certainly have a maximum thickness less than $\frac{1}{2}$ inch. The magnet must be very accurately and stably located on its foundation ; r.m.s. misalignments within a betatron wavelength must be less than 0·020 inch. For this reason extensive studies of foundation stability and soil mechanics will be completed before the building construction is started. Loading studies on the Long Island sand which will serve as a base indicate that the tolerances can be met, if necessary by supporting the magnet on piles driven to a depth of 40 to 50 feet.

The power supply for this magnet will be similar in design and ratings to that used for the Cosmotron magnet. More attention must be paid to the first ten milliseconds of the cycle in this case since injection will occur at 100 gauss

rather than 300 gauss as in the Cosmotron. Since the beginning of the cycle will be perturbed by a variety of transients due to ignitron commutation, eddy current effects and propagation of wave fronts around the half-mile circumference of the machine, some consideration has been given to the possible use of a saturating reactor in series with the magnet to slow down the initial rate of rise.

11.3. *Injection*

The proton beam will be injected at an energy of 50 Mev by a linear accelerator. Several different linear accelerator configurations have been explored and the final design choices have not yet been made. It seems probable that the beam will receive a pre-acceleration to 750 kev by a Cockcroft–Walton set, will pass through a buncher and will then travel about 110 feet through the linear accelerator. Since grid focusing results in serious attenuation of the beam, focusing will be either by pulsed quadrupole or permanent quadrupole magnets. Permanent-magnet gradients of more than 1000 gauss per cm have been set up in cylinders, made of Ferroxdure and similar materials, of 1 inch inside diameter and less than 2 inches outside diameter, by impulse magnetization using a quadrupole magnetizing coil inside the cylinder. For magnetization of these materials in such geometries peak currents must yield over 100 000 ampere-turns in the magnetizer.

If the rate of rise of the magnetic field in the synchrotron is of the order of 10 000 gauss per second, the radius of the orbit of the injected beam will shrink about 1 mm per revolution. It is possible that betatron oscillations could be tailored to induce the beam to clear an outside inflector during sufficient revolutions for the equilibrium orbit to clear a practicable inflector structure. If this is not possible, or if the rate of rise of the magnetic field is reduced, it may be necessary to apply the inflecting field across the whole vacuum chamber. In this case injection can last during only one revolution since the field must be removed before it can perturb the protons on their second revolution. This is the injection method used in the electron analogue.

11.4. *Radio-frequency System*

Since the 50-Mev injected beam has about one-third of the velocity of light, the frequency must change during the cycle by three to one. The beam reaches relativistic velocities rather early in the cycle, so the frequency rises rapidly at first and then becomes almost constant; during the latter half of the one-second acceleration cycle, the frequency varies by less than one part in 400. The phase transition will take place at about 8 Gev, after about one-third of the acceleration period.

The frequency tolerances which must be met by the control system are so severe, particularly around the phase transition, that there seems little hope of using a programmed cycle as has been done in conventional machines. The frequency must be derived from information from the proton beam. The simplest method for accomplishing this appears to be one in which the accelerating signal is derived from a pick-up electrode through which the beam passes. This signal is then amplified and applied to the accelerating unit. Errors in this frequency will then correspond to errors in the radial position of the beam. These errors

will be corrected by using the differential output of pick-up electrodes, inside and outside the proton orbit, to control a phase shifter in the amplifier which supplies the accelerating units. This method has been tested on the Cosmotron with satisfactory results and will be used on the electron analogue.

The frequency of revolution of the proton beam varies from 125 kc/s, at injection, to 375 kc/s at 25 Gev. To reduce the amplitude of the phase oscillations, the 12th harmonic of the revolution frequency will be used in acceleration; thus, the radio-frequency range will be from 1·5 to 4·5 Mc/s. The accelerating units will be ferrite-loaded cavities, tuned to resonance by d.c. saturation of the ferrite. Ferrites with satisfactory properties are now available and a test cavity is under construction.

Accelerating units will be located in twelve of the twenty-four ten-foot straight sections. The average proton energy gain per revolution will be about 70 kev; this will be equally distributed among the accelerating stations so that each must supply about 6 kev per revolution. To maintain phase stability peak gap voltages will be about twice this figure. The power requirements for the radio-frequency system during acceleration will be of the order of 500 kw.

11.5. *Vacuum System*

Because of the high injection energy and the rapid energy gain of the protons, gas-scattering problems will not be serious in the 25-Gev accelerator even at pressures as high as 10^{-5} mm (cf. § 3.4). In spite of the rather slow pumping speed through the restricted area of the vacuum chamber it should be possible to separate diffusion pumping stations by as much as 50 feet.

The vacuum chamber will probably be a stainless-steel pipe of approximately elliptical cross section with maximum inside dimensions of 7 cm vertically and 15 cm radially. Evacuation tests on sample sections of these dimensions indicate that a minimum wall thickness to withstand atmospheric pressure is 0·062 inch. With this wall thickness the vertical dimension decreased $\frac{1}{8}$ to $\frac{3}{16}$ inch under evacuation.

Eddy currents in this pipe will cause sufficient magnetic-field distortion to require correction for injection fields. Adequate correction is possible by attaching conductors, carrying constant currents of a few amperes, near the inner and outer radial limits of the chamber (the currents travel in the azimuthal direction along the chamber wall).

§ 12. The CERN 25-Gev Alternating-Gradient Proton Synchrotron Project

An operation, which closely parallels the Brookhaven 25-Gev project, is also under way in Geneva, Switzerland, where the European Organization for Nuclear Research is constructing a new laboratory to house a large synchrocyclotron and a 25-Gev proton synchrotron. This laboratory is a co-operative effort on the part of twelve European nations. The proton synchrotron project was initiated in 1952 under the direction of O. Dahl of Norway and is now directed by J. B. Adams of Great Britain. The design phase of this project is approaching completion and construction of the machine building is already in progress. The accelerator is scheduled for completion at the end of 1959.

A published description of the CERN machine design as it existed in 1953 is available in the published *Lectures on the Theory and Design of an Alternating-gradient Proton Synchrotron*, edited by M. H. Blewett (CERN 1953). Since that publication, the design energy has been dropped from 30 to 25 GeV and many lesser changes have been made in the proposed design.

A close and very friendly co-operation has continued from the initiation of the Brookhaven and CERN projects between the two groups involved. Design conclusions reached independently have been checked between the two groups and some results have followed from co-operative efforts. It is, therefore, not surprising that the two designs are strikingly similar in most essentials. Some differences in technique exist and, where no unique method applies, these differences have been encouraged in order that more experience may be gained by operation of the two machines.

Since the two machines are so similar in basic features the CERN machine will not be discussed in detail. We shall merely point out a few of the more important features in which it differs from the Brookhaven design.

The aperture in the CERN machine is slightly larger than that in the Brookhaven case. The vertical height of the magnet gap in the CERN magnet is 10 cm compared with about 8 cm in the Brookhaven magnet. There seems no doubt that the Brookhaven aperture is adequate for eventual operation but the extra cost of steel for the CERN magnet may be offset by greater ease and speed in bringing the machine into operation.

The CERN radio-frequency group has evolved a complex, but very ingenious, frequency-programming system which depends on information derived from a Hall-effect sample in the magnetic field. Only small corrections, if any, will need to be made to this frequency programme. The Brookhaven group hopes to derive all frequency-control information directly from the proton beam.

Both machines will use 50-MeV linear accelerator injectors; the CERN group has been able to bring the injector close to the main building complex while the Brookhaven group has been forced, by terrain considerations, to locate their injector on the opposite side of the ring from all other equipment centres (see figure 9).

The two groups have entirely different foundation stability problems since the CERN machine will have foundation supports directly from a soft sandstone 'bedrock', while the Brookhaven machine will be built on a layer of sand 1500 feet thick.

It might be thought that the setting up of such an international laboratory as that at CERN would be attended by such political and language difficulties as to present a real impediment to the progress of a major project such as this one. During a six-month visit to the CERN group the author was able to observe that no such impediments exist. The progress of the CERN 25-GeV machine may be expected to be rapid and successful.

§ 13. The Midwest Fixed-field Alternating-gradient Principle (FFAG)

In 1953 a group of scientists, from universities in the area of the United States within a distance of about 500 miles from Chicago, met to consider the design of

a large accelerator for use by their respective institutions. In 1954 this group organized itself as the 'Midwest Universities Research Association' (MURA). From early speculations along more or less conventional lines, this group rapidly turned to the evolution of more radical ideas, the most important of which is the 'Fixed-field Alternating-gradient' (FFAG) technique. The ideas evolved were presented in January 1955 at the New York meeting of the American Physical Society (Symon 1955). No detailed publication is yet available, but a comprehensive paper is in preparation for submission to one of the journals of the American Physical Society (cf. also MURA 1955).

This group realized that the high gradients, permissible in an alternating-gradient accelerator, make possible the construction of a d.c. magnet which can contain orbits of protons from injection to multi-GeV energies. Alternating gradients can be included if the beam is bent alternately to the right and to the left. The orbit can have a generally circular configuration if bending in one direction is not as strong as the bending in the other direction. This design, now described as the FFAG Mark I, had been given brief consideration at Brookhaven and later, at the University of Tokyo, but was dismissed because of the increased magnet size and length over the accepted design with a varying magnetic field. The MURA group, whose evolution of this idea was quite independent, gave the proposal further study and pointed out its advantages of easier frequency control and high average beam intensity resulting from an increased repetition rate of the acceleration cycle. The FFAG idea evolved through a series of variations to the FFAG Mark V in which alternating-gradient focusing is included in a circular d.c. magnet by the inclusion on the pole faces of a set of spiral ridges. The imposing problem of the dynamics of a proton oscillating around a spiral equilibrium orbit in the field of these ridges is now being investigated by the MURA group. Results, thus far, are encouraging and FFAG Mark V may soon become a design for an accelerator in the GeV range.

The advantages of this proposal are, primarily, those of a fixed-field magnet compared with a magnet in which fields are varied from low to high values. Eddy current, remanent-field and saturation troubles are eliminated. Also, successions of accelerated pulses can be very rapid. Continuous operation is not possible since the radio frequency must still be cycled as the proton velocity increases. These advantages are balanced against an increased magnet size and cost; the total magnet aperture in the Mark V magnet is about 1 metre in the radial direction. Magnet power will also be increased by an appreciable factor, although the magnet power supply will probably be simpler than that in a conventional synchrotron.

A small model of FFAG Mark I is being built at the University of Michigan. Electrons will be accelerated in this model by a betatron technique from 25 kev to 500 kev. The FFAG Mark V method has been considered by several groups for use in synchrocyclotrons which could be converted to continuously operating fixed-frequency cyclotrons by making the average field match the relativistic increase in mass.

A FFAG Mark V proton synchrotron appears feasible if the orbit analysis gives satisfactory results. For 20 GeV, for example, the magnet of such a machine would weigh about 3500 tons and would require a continuous power of 2×10^6 watts.

§ 14. Conclusion

The proton synchrotron art is now well established and new machines in the Gev range will probably appear in some profusion during the coming decade. For example, design studies are already well advanced, under the direction of S. D. Winter in the Saclay Laboratory of the French C.E.A., for a 1·5-Gev proton synchrotron of conventional design. At Princeton, U.S.A., a 2-Gev machine has been proposed by M. G. White and his associates for operation at 30 cycles per second to yield a beam of average intensity many times that of the Cosmotron. M. S. Livingston and others, in a joint M.I.T.–Harvard group, have designed a 10–15-Gev alternating-gradient proton synchrotron but have now turned their attention to the design of a 5-Gev electron accelerator.

In magnitude, cost and complexity, the proton synchrotron is a device beyond the wildest dreams of pre-war physicists. Construction of the Brookhaven Cosmotron, for example, cost about $7 000 000; it consumed about 300 man–years in the design and construction group, and many more in the Laboratory's general shop and service groups and in the factories of co-operating manufacturers. At the peak of construction, the project staff consisted of more than 80 persons. The mere maintenance and operation of such a machine for experimental use costs about $1 000 000 per year and requires a large staff for 24-hour-a-day operation.

These luxurious operations are not without their sobering concomitants. It is no longer possible to undertake the construction of an accelerator of this class without the support of a well-organized group of physicists skilled in the arts of electricity and magnetism, a versatile staff of electrical and mechanical engineers, and the assurance of continued and lavish financial support for the operation and experimental use of the device when its construction has been completed.

Acknowledgments

The author is indebted for much of the information presented above to a number of his colleagues and correspondents, including J. Laslett of the MURA group, E. J. Lofgren of the Berkeley Radiation Laboratory, M. L. Oliphant and L. U. Hibbard of the Australian National University, L. Riddiford of the University of Birmingham and many of his past and present associates with the CERN group, the Brookhaven Cosmotron Department and the Brookhaven Accelerator Development Department.

References

Adams, J. B., Hine, M. G. N., and Lawson, J. D., 1953, *Nature, Lond.*, **171**, 926.

Birge, R. W., Haddock, R. P., Kerth, L. T., Peterson, J. R., Sandweiss, J., Stork, D. H., and Whitehead, M. N., 1955, *Phys. Rev.*, **99**, 329.

Birmingham, 1953, *Nature, Lond.*, **172**, 704.

Blachman, N. M., and Courant, E. D., 1948, *Phys. Rev.*, **74**, 140; 1949 a, *Ibid.*, **75**, 315; 1949 b, *Rev. Sci. Instrum.*, **20**, 596.

Blau, M., and Caulton, M., 1954, *Phys. Rev.*, **96**, 150.

Blewett, M. H., *et al.*, 1953, *Rev. Sci. Instrum.*, **24**, 723–870.

Block, M. M., Harth, E. M., Fowler, W. B., Shutt, R. P., Thorndike, A. M., and Whittemore, W. L., 1955, *Phys. Rev.*, **99**, 261.

BROBECK, W. M., 1948, *Rev. Sci. Instrum.*, **19**, 545.
CERN, 1953, *Lectures on the Theory and Design of an Alternating-gradient Proton Synchrotron* (M. H. BLEWETT, Ed.) (Geneva: CERN Proton Synchrotron Group, Institut de Physique).
CHUPP, W. W., GOLDHABER, G., GOLDHABER, S., GOLDSACK, S. J., LANUTTI, J. E., SMITH, F. M., and WEBB, F. H., 1955, *Phys. Rev.*, **99**, 335.
COOL, R. L., MADANSKY, L., and PICCIONI, O., 1954, *Phys. Rev.*, **93**, 249, 637.
COOR, T., HILL, D. A., HORNYAK, W. F., SMITH, L. W., and SNOW, G., 1955, *Phys. Rev.*, **98**, 1369.
CORK, B., 1955, *Rev. Sci. Instrum.*, **26**, 210.
CORK, B., and LOFGREN, E. J., 1954, *University of California Radiation Laboratory Reports* UCRL–2646, UCRL–2692.
CORK, B., CHUPP, W., and LOFGREN, E. J., 1955, *University of California Radiation Laboratory Report* UCRL–2954.
COURANT, E. D., 1953, *Rev. Sci. Instrum.*, **24**, 836.
COURANT, E. D., LIVINGSTON, M. S., and SNYDER, H. S., 1952, *Phys. Rev.*, **88**, 1190.
COURANT, E. D., LIVINGSTON, M. S., SNYDER, H. S., and BLEWETT, J. P., 1953, *Phys. Rev.*, **91**, 202.
COWAN, F. P., and HANDLOSER, J. S., 1953, *Brookhaven National Laboratory Report* 264 (T–43).
EISBERG, L. M., FOWLER, W. B., LEA, R. M., SHEPHARD, W. D., SHUTT, R. P., THORNDIKE, A. M., and WHITTEMORE, W. L., 1955, *Phys. Rev.*, **97**, 797.
FIREMAN, E. L., and ROWLAND, F. S., 1955, *Phys. Rev.*, **97**, 780.
FOWLER, W. B., SHUTT, R. P., THORNDIKE, A. M., and WHITTEMORE, W. L., 1953 a, *Phys. Rev.*, **90**, 1126; 1953 b, *Ibid.*, **91**, 1287; 1954 a, *Ibid.*, **93**, 861; 1954 b, *Ibid.*, **95**, 1026; 1955, *Ibid.*, **98**, 121.
FREMLIN, J. H., and GOODEN, J. S., 1950, *Rep. Progr. Phys.*, **13**, 295 (London: Physical Society).
FRIEDLANDER, G., HUDIS, J., and WOLFGANG, R. L., 1955, *Phys. Rev.*, **99**, 263.
HIBBARD, L. U., 1950, *Nucleonics*, **7** (4), 30.
HIBBARD, L. U., CARO, D. E., and FREEMAN, J. Y., 1954, *J. Sci. Instrum.*, **31**, 139.
HILL, R. D., SALANT, E. O., and WIDGOFF, M., 1955, *Phys. Rev.*, **99**, 229.
LEDLEY, B., and RIDDIFORD, L., 1955, *Proc. Phys. Soc.* A, **68**, 836.
LINDENBAUM, S. J., and YUAN, L. C. L., 1953, *Phys. Rev.*, **92**, 1578; 1955, *Ibid.*, **100**, 306.
LIVINGSTON, M. S., 1954, *High-energy Accelerators* (New York: Interscience Publishers).
LIVINGSTON, M. S., BLEWETT, J. P., GREEN, G. K., and HAWORTH, L. J., 1950, *Rev. Sci. Instrum.*, **21**, 7.
LOCK, W. O., and MARCH, P. V., 1955, *Proc. Roy. Soc.* A, **230**, 222.
LOCK, W. O., MARCH, P. V., MUIRHEAD, H., and ROSSER, W. G. V., 1955, *Proc. Roy. Soc.* A, **230**, 215.
LOFGREN, E. J., 1950, *Science*, **111**, 295.
LOFGREN, E. J., and HEARD, H. G., 1955, *University of California Radiation Laboratory Report* UCRL–2822.
MCMILLAN, E. M., 1945, *Phys. Rev.*, **68**, 143.
MOON, P. B., RIDDIFORD, L., and SYMONDS, J. L., 1955, *Proc. Roy. Soc.* A, **230**, 204.
MURA, 1955, *Phys. Today*, **8** (2), 6.
OLIPHANT, M. L., 1950, *Nature, Lond.*, **165**, 466.
OLIPHANT, M. L., GOODEN, J. S., and HIDE, G. S., 1947, *Proc. Phys. Soc.*, **59**, 666.
PICCIONI, O., CLARK, D., COOL, R., FRIEDLANDER, G., and KASSNER, D., 1955, *Rev. Sci. Instrum.*, **26**, 232.
RIDDIFORD, L., 1951, *J. Sci. Instrum.*, Supplement No. 1, 47.
RIDDIFORD, L., VAN DER RAAY, H. B., and COE, R. F., 1955, *Proc. Phys. Soc.* A, **68**, 489.
SHAPIRO, A. M., LEAVITT, C. P., and CHEN, F. F., 1953, *Phys. Rev.*, **92**, 1073.
SMITH, L. W., MCREYNOLDS, A. W., and SNOW, G. A., 1955, *Phys. Rev.*, **98**, 1167.
SYMON, R., 1955, *Phys. Rev.*, **98**, 1152, abstract D2 (see also abstracts D3, D4, and D5).
TWISS, R. Q., and FRANK, N. H., 1949, *Rev. Sci. Instrum.*, **20**, 1.
VEKSLER, V., 1945, *J. Phys. U.S.S.R.*, **9**, 153.

VLADIMIRSKII, V. V., and TARASOV, E. K., 1955, *Doklady Akad. Nauk, S.S.S.R.*

WALKER, R. M., PRESTON, R. S., FOWLER, E. C., and KRAYBILL, H. L., 1955, *Phys. Rev.*, **97**, 1086.

WALKER, W. D., 1955, *Phys. Rev.*, **98**, 1407.

WILLIAMS, R. W., 1955, *Phys. Rev.*, **98**, 1387.

WINNINGSTAD, C. N., PAXSON, D., ANDERSON, O., KERNS, Q., and RIEDEL, J., 1952, *University of California Radiation Laboratory Report* UCRL–1750.

YUAN, L. C. L., and LINDENBAUM, S. J., 1954, *Phys. Rev.*, **93**, 1431.

RADIOACTIVE METHODS FOR DETERMINING GEOLOGICAL AGE

By L. H. AHRENS
Department of Geology and Mineralogy, Oxford

CONTENTS

	PAGE
§ 1. Introduction	81
§ 2. The lead method	82
2.1. Analytical procedures	82
2.2. Lead age distributions	84
2.3. Extending the scope of the lead method	87
(i) Accessory minerals from igneous rocks	87
(ii) Lead ores	89
2.4. Use of the ratio $\frac{206}{238}$	89
§ 3. The helium method	91
§ 4. Methods based on the radioactivity of the alkali metals K and Rb	93
4.1. The strontium method	93
4.2. The argon method	95
§ 5. Potential methods	97
§ 6. A comparison of the ages of the oldest minerals with estimates of the age of the earth, meteorites, solar system, elements and universe	99
§ 7. Selected references on methods and techniques not discussed	102
7.1. Dating of ocean sediments	102
7.2. Use of photographic emulsion for age determinations	102
7.3. Indirect methods for determining geological age	102
References	103

Abstract. Research on the use of radioactive methods for determining the absolute ages of minerals, rocks and meteorites has developed with great vigour since World War II. Much of this expansion of application has been due to the introduction of a variety of sensitive and precise analytical procedures. The lead method remains the most highly developed of all methods, but difficulty of interpreting lead age distributions has been a major problem. Recent interpretation of these distributions on a basis of lead deficiency leads to the conclusion that most recommended lead ages are under-estimates and that the scale of geological time, now based on the lead method, should be expanded considerably. Investigations demonstrating the surficial concentration of uranium and thorium around mineral grains and within their cracks and fissures has been most helpful for the helium and lead methods.

Several new methods are in various stages of development and those based on the radioactivity of rubidium and potassium appear to be the most promising. The simple nature of alkali metal radioactivity is a fundamental consideration in their favour. The strontium method, though still somewhat restricted in application, appears to be particularly satisfactory for determining the ages of very early pre-Cambrian minerals, whereas the argon method shows promise of wide application to common potassium minerals; uncertainty of the branching ratio β/e for ^{40}K remains a problem. Long life of parents and other considerations seem to rule out the possibility of utilizing the radioactivity of several elements such as tellurium, bismuth, indium and samarium.

Several possible indirect methods (radiation damage, thermoluminescence and cube edge variation) are being developed for the purpose of determining the geological age of a mineral, but have not been considered in this review.

§ 1. Introduction

Attempts to determine the absolute ages of minerals by means of natural radioactivity go back to the first decade of this century. It was assumed that the decay rate of a radioactive element would not be influenced by geological processes and hence would remain uniform throughout its lifetime. In this case standard equations for radioactive decay could be made to apply, namely,

$$N = N_0 e^{-\lambda t}$$

or

$$t = \frac{2{\cdot}303}{\lambda} \log_{10}\left(\frac{N_0}{N}\right)$$

where t is the geological age of the mineral, that is, the time at which a mineral containing a significant concentration of radioactive element crystallized; N_0 is the number of atoms of radioactive element in the mineral at that time (t years ago) and N the number now.† Although the possibility of a time relativity has been raised—when we go back several thousands of millions of years—and also a possibility that t measured by different decay processes might not be strictly comparable, the fundamental assumption of uniformity of decay rate of all nuclear decay processes throughout geological time does not seem to be in serious question and for the purpose of this review will be regarded as valid.

By the beginning of World War II considerable progress had been made on the use of the two classical methods—lead and helium—and the status just before that time has been covered by Holmes' (1937) readable *Age of the Earth*. Since World War II impressive efforts have been made to develop radioactive methods, but though encouraging, progress in actual application of these methods has not always been equally impressive. The lead method in particular, and the helium method to a lesser extent, have continued to develop vigorously, but in addition a host of new modifications and methods have blossomed forth, each with its particular sphere of application. With such a variety of tools, it has now become possible to tackle virtually the whole range of geological time, beginning with archaeological time of a thousand years or so ago and extending back into the very earliest pre-Cambrian of some 3×10^9 years ago, an age approaching that of the earth itself. The task of adequate review of progress in all aspects of all radioactive methods for determining geological age is not easily accomplished in an article of this length, and it will therefore be necessary to define which specific topics will be covered. Choice of subject is somewhat arbitrary and is dictated partly by the author's familiarity with a topic and partly whether it is well suited for review; in the main, emphasis will be on direct methods.

We will begin with the lead method, which as a single method is the most highly developed and continues to develop vigorously. The helium method, the second of the classical methods, will be considered very briefly. No other method has perhaps had so many ups and downs and its present status is not easily reviewed. This method has, however, recently been thoroughly and authoritatively discussed by Hurley (1954), who includes most of the early observations

† The ratio N_0/N may be obtained from the measured concentration ratio of parent to daughter isotopes. If p% and d% are measured concentrations of parent and daughter isotopes, respectively, then N_0/N is given by $(p+d)/p \times$ the ratio of the mass numbers of the respective parent and daughter isotopes.

and traces its development up to its present state. We will pass next to two recent methods (strontium and argon), both based on alkali metal radioactivity and just coming into application, and after reviewing the prospects of some potential methods ($^{40}K \rightarrow {}^{40}Ca$; natural fission and others) go on to compare the age of the earth's oldest minerals with some estimates of the ages of meteorites, elements, universe and the earth itself. Work at the very other end of the age scale, that is, of archaeological material by induced activity of ^{14}C, is not discussed; see Libby (1955) for a detailed and recent discussion. A final section gives references only to recent papers on (i) methods for determining the ages of ocean sediments, (ii) the use of photographic techniques for estimating age, and (iii) indirect age methods—cube edge variation, radiation damage, etc.

Recent accounts of the use of radioactive methods for determining geological age may be found in Rankama (1954), Faul (1954), Bullard and Wilson (1954) and Kohman and Saito (1954).

§ 2. The Lead Method

2.1. *Analytical Procedures*

The most significant single development not only for the lead age method but in age research as a whole has been the introduction of mass spectrometric methods in place of laborious atomic weight determinations for estimating the proportion of non-radiogenic lead (Nier 1939, Nier *et al.* 1941). The quantitative isotope information so provided has led to the possibility of estimating age by means of each specific parent–daughter ratio ($^{206}Pb/^{238}U$, $^{207}Pb/^{235}U$, $^{208}Pb/^{232}U$) as well as by means of the ratio $^{207}Pb/^{206}Pb$,† which also is time-sensitive because of the differing half-lives of the respective parents ($^{235}U = 7{\cdot}1 \times 10^8$ years and $^{238}U = 4{\cdot}5 \times 10^9$ years). It will be recalled that lead age estimates were once based on chemical analysis only—now often referred to as the chemical or 'crude' estimate—and except when used for reconnaissance or as a rapid procedure for dating accessory minerals of igneous rocks (see p. 87) such crude ages have been replaced entirely by the use of specific parent : daughter isotope ratios. Some workers carry out complete analyses (chemical and isotopic), whereas a few have been inclined to rely on $\frac{207}{206}$ ratios only (no chemical analysis) on the grounds that this ratio alone serves as a valid estimate of age; this assumption is controversial and we come back to it later after reviewing further progress in the development of analytical methods.

Refinement of mass spectrometric procedure itself has progressed impressively. The accuracy achieved by Nier and others who first used mass spectrometric procedures for age research was high and adequate for the purpose and later developments have been mainly in the direction of sensitivity and broadening scope of application. Collins *et al.* (1951, 1954) and Dibeler and Mohler (1951) chose to employ Pb tetramethyl, a gas, in place of PbI_2 used by Nier and coworkers, and claim advantages of speed and absence of memory effect. Other Pb compounds have been used successfully. Farquhar *et al.* (1953) compared results obtained from solid (PbI_2 and $PbCl_2$) and gas (Pb tetramethyl) samples and report satisfactory agreement.

† Abbreviations $\frac{208}{206}$, $\frac{207}{235}$, $\frac{208}{232}$ and $\frac{207}{206}$ will be used hereafter.

A combination of mass spectrometric and isotope dilution procedures has been most effective. As an example, Tilton *et al.* (1952) and Tilton (1954) have been able to determine thorium down to about 1 microgramme quantities and to within about 1½%, using a mass spectrometer–isotope dilution procedure with ^{230}Th as carrier. This development is highly significant as many of the earlier Th determinations seem to be seriously in error, particularly at low concentrations, and it now becomes possible to determine Th precisely in accessory minerals such as zircon (see, for example, Carnegie Institution 1954). Microgramme quantities of lead have also been determined mass spectrometrically (Hess *et al.* 1953). The use of combined mass spectrometer–isotope dilution procedures may be compared with an equally effective application for the strontium and argon methods (see below). The use of isotope dilution procedures, including their application to the determination of the geological age of minerals, has been reviewed by Inghram (1954).

Several other analytical techniques have been introduced during the post-war period. Holmes and Smales (1948) successfully employed a polarographic procedure for the determination of total lead and uranium in monazite, Smales (1952) has developed a procedure for the determination of low uranium concentrations in rocks and minerals by activation in the Harwell pile, and a similar procedure for thorium is described by Jenkins (1954). Larsen and co-workers (1952, 1953, and unpublished) used optical spectrochemical methods (for details see Waring and Worthing 1953) for the determination of lead in zircon down to concentrations of a few parts per million; that is, concentrations of lead which are likely to be found in zircons as young as about 20×10^6 years or so. A similar general procedure has been used by workers at Massachusetts Institute of Technology (Ahrens and co-workers, unpublished) and is being employed elsewhere. Fluorimetric and colorimetric methods for handling a wide uranium range (lower limit ~ 10 parts/10^6 U) in rocks and minerals are described by Adams and Maeck (1954).

Various sensitive procedures have been employed by Dalton and co-workers for the determination of the very low concentrations of uranium and thorium usually present in meteorites: alpha counting of radon and thoron in a concentrate of radium (^{225}Ra and ^{224}ThX) in a carrier precipitate of $BaSO_4$, counting of thorium C + C′ alpha particles in thorium B separated from chemically isolated thorium (Dalton *et al.* 1953, 1954), fluorimetric determinations of chemically isolated uranium (Dalton *et al.* 1953, 1954). The accuracy of the uranium determination is improved by the addition of ^{233}U as tracer (Dalton *et al.* 1954). Patterson *et al.* (1953) developed an isotope dilution–mass spectrometric procedure using enriched ^{235}U as carrier (see also Hess *et al.* 1953).

Although attention has been focused on the recent introduction of various sensitive analytical procedures we should not overlook the fact that wet methods of chemical analysis still serve satisfactorily for the determination of U, Th and total Pb when present at high concentrations, as in uraninites for example.

To sum up: the development of analytical procedures applicable to the lead method has been most satisfactory (under *favourable* conditions, analytical error should not exceed $\sim 1\%$, Kulp *et al.* 1954), and although further investigations are naturally required, a lot of what requires to be done is much a matter of detail.

We pass now to review the central problem of the lead method which is not in nearly so satisfactory a state; namely, lead age distributions, their nature and their cause. This particular aspect of age research is highly significant as although the lead method is the most highly developed and widely applied of all methods, the validity of individual estimates of age depend not only on the accuracy of the analytical data but also on their interpretation.

2.2. *Lead Age Distributions*

The first mass spectrometric determinations (Nier 1938, Nier *et al.* 1941) indicated that $t(\frac{207}{235})$, $t(\frac{206}{238})$, $t(\frac{208}{232})$ and $t(\frac{207}{206})$ were rarely in full agreement and this has been confirmed by subsequent observations. Figures 1 and 2 serve to illustrate the nature and magnitude of lead age distributions. Figure 1 relates

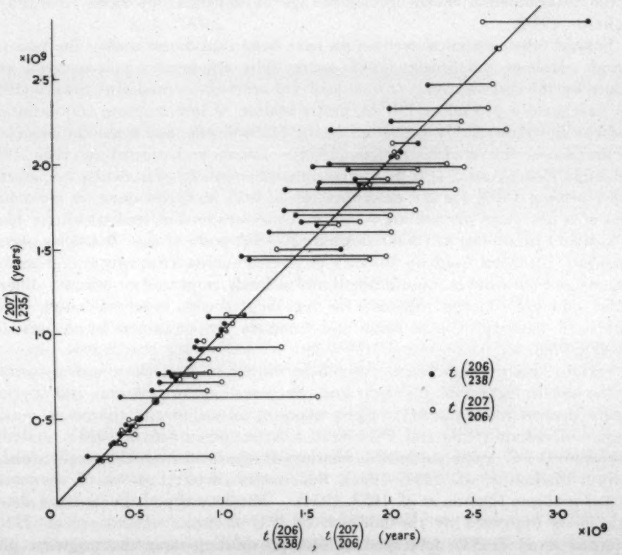

Figure 1. Lead age distributions [$t(\frac{206}{238})$, $t(\frac{207}{235})$ and $t(\frac{207}{206})$] of some 53 specimens. For the majority of specimens, the distribution is $t(\frac{207}{235}) > t(\frac{206}{238}) > t(\frac{207}{206})$. For some observations on $t(\frac{206}{238})$, see figure 2.

$t(\frac{207}{235})$ as ordinate to $t(\frac{206}{238})$ and $t(\frac{207}{206})$ as abscissa for most published age determinations (data mainly from Faul 1954); $t(\frac{208}{232})$ has been omitted because many earlier estimates of $t(\frac{208}{232})$, particularly in Th-poor minerals, are likely to be inaccurate either because of faulty analysis or because of uncertainty of constitution of primary lead—see Louw (1955) for example. Although these two points must of course be borne in mind when $t(\frac{208}{232})$ is considered, the causes are not regarded as fundamental and as Th determinations can now apparently be carried

out with better accuracy it seems more satisfactory in some respects to omit $t(\frac{208}{232})$ from figure 1. Figure 2 may, however, serve as an indication of the relationship between $t(\frac{208}{232})$ and the uranium–lead ages; this particular age pattern is considered in detail a little later.

Figures 1 and 2 indicate that the majority of age distributions have $t(\frac{207}{206}) > t(\frac{207}{235}) > t(\frac{206}{238}) > t(\frac{208}{232})$; some have $t(\frac{206}{238}) > t(\frac{207}{235}) > t(\frac{207}{206})$ and in some specimens there is complete agreement.

Gain or loss of parent or daughter is the usually suggested cause for internal disagreement (see, for example, Holmes 1948, also Rankama 1954, fig. 75.1 and p. 384). Consider the majority distribution $t(\frac{207}{206}) > t(\frac{207}{235}) > t(\frac{206}{238})$ first. Wickman (1942) discussed the possible escape of emanation (radon, actinon and thoron) either by recoil or simple diffusion; he considered a diffusion escape as the more likely of the two possibilities but that significant loss only of Rn would take place because its half-life (3·825 days) was substantially greater than that of Tn (54·5 seconds) and An (3·92 seconds). Escape of Rn would depress $t(\frac{206}{238})$, elevate $t(\frac{207}{206})$ but leave $t(\frac{207}{235})$ unchanged; thus, such a mechanism seemed feasible to account for the $t(\frac{207}{206}) > t(\frac{207}{235}) > t(\frac{206}{238})$ distributions, and many workers (Holmes, several papers, Kulp *et al.* 1954, Louw 1955) have since assumed significant Rn escape and recommended $t(\frac{207}{235})$. Wickman (1942) drew attention to the observations of Föyn (1938), who demonstrated that emanation from bröggerite was easily measurable and increased steeply with decrease in particle size. Several other measurements of emanation loss have been made (Kulp *et al.* 1954, Horne and Davidson 1954, Gilletti and Kulp 1955, Eckelmann and Kulp 1956), which indicate that whereas secondary minerals such as carnotite may apparently lose 20% or so emanation, such loss is evidently so small, often 1% or so, in primary radioactive minerals that it cannot account for the large internal age disagreement. This has led to the search for some other possible cause for the $t(\frac{207}{206}) > t(\frac{207}{235}) > t(\frac{206}{238})$ age distribution. Holmes (1954) observed that the age relationships of some Rhodesian monazites could be most satisfactorily explained by an assumption of loss of lead as a whole and not deficiency of 206 alone due to radon loss. Age data on the three Rhodesian monazites together with some other specimens which will be considered in detail are given in table 1. These have been plotted in

Table I. 'Age' Calculations of the most primitive Monazites and Uraninites

Specimens and locality	Age ($\times 10^6$ years) $\frac{204}{238}$	$\frac{207}{235}$	$\frac{208}{232}$	$\frac{207}{206}$	Con-vergent
Monazite, Ebonite Tantalum Claims, Bikita District, S. Rhodesia	2675	2680	2645	2680	2680
Monazite, Jack Tin Claims, north of Salisbury, S. Rhodesia	2260	2470	1940	2650	2680
Monazite, Irumi Hills, N. Rhodesia	2040	2330	1390	2620	2680
Monazite, Antsirabe, Madagascar	1400	1850	610	2420	2680
Monazite, Huron Claim pegmatite, south-east Manitoba	3217	2839	1827	2590	—
Uraninite, Huron Claim pegmatite, south-east Manitoba	1564	1985	1273	2475	2680
Uraninite, Dominion Reefs, Klerksdorp, Transvaal	1678	2200	3672	2730	~2930

figure 2 (Ahrens 1955 a). This age pattern has been discussed by Ahrens (1955 a, b), who concludes that variable lead deficiency, brought about either by loss of lead itself or intermediate members of a decay chain, has been the cause and that the high degree of order in the pattern points to physical control, rather than chemical, of varying lead deficiency. The high degree of order in the Rhodesia pattern raises the question (Ahrens 1955 b) as to whether some other process rather than one of escape, may be the cause.

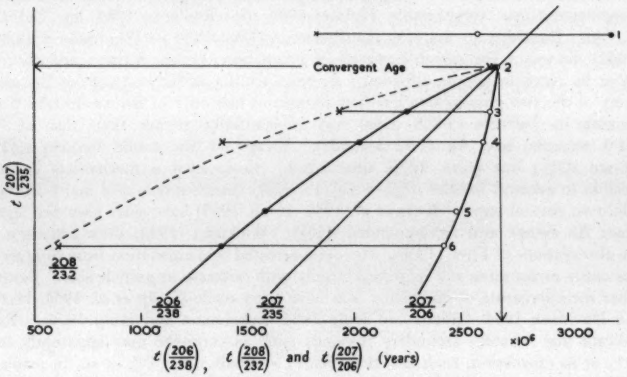

Figure 2. The Rhodesia age pattern : 1, monazite, Huron Claim, Manitoba ; 2, 3 and 4, monazite, Rhodesia (Bikita, Salisbury and Irumi, respectively) ; 5, uraninite, Huron Claim, Manitoba ; 6, monazite, Antsirabe, Madagascar. Varying lead deficiency is one suggested cause of the development of this pattern.

For participants of the Rhodesia pattern, the ratio N_{207}/N_{235} appears to be linearly related to N_{206}/N_{238} (figure 3) and perhaps also N_{208}/N_{232} (Ahrens 1955 b). Use has been made of this relationship to indicate that all lead isotopes are not equally deficient and that the order is 208 (greatest deficiency) > 207 > 206. Eckelmann and Kulp (1956) have examined the age distributions of several specimens of pitchblende from Lake Athabasca and find that in all specimens $t\left(\frac{207}{206}\right) > t\left(\frac{207}{235}\right) > t\left(\frac{206}{238}\right)$; they conclude that loss of lead and not of radon is the cause of internal disagreement. This observation may be contrasted with the earlier writings of Kulp and co-workers (see above, for example).

It has been suggested (Ahrens 1955 a, b) that the age of each participating specimen of the Rhodesia pattern is the same (2680×10^6 years) and that this age, the *convergent* age, is given by the point of convergence. (General support for close similarity of age between Rhodesian and Manitoban pegmatites has come from the strontium method (Ahrens 1949, Ahrens and Macgregor 1951, Davis and Aldrich 1953, Nicolaysen *et al.* 1953 and Nicolaysen 1954).)

An assumption that most age distributions of figure 1 are participants of age patterns of the Rhodesia type (figure 2) leads to the conclusion (Ahrens 1955 b)

that the majority of lead age estimates are under-estimates and that the lead age scale for measuring time should be expanded; this would bring it roughly into line with the strontium age scale which has heretofore been regarded as in error but which may in fact have been a closer approach to the true scale of geological time.

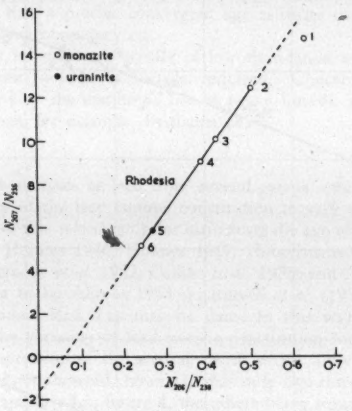

Figure 3. Pb–U isotope ratios for participants of the Rhodesia pattern. Numbering of points as in figure 2.

2.3. *Extending the Scope of the Lead Method*

(i) *Accessory minerals from igneous rocks.*

The extension of the lead method to accessory minerals from igneous rocks (Larsen *et al.* 1952, 1953) has been a great step forward in the application of radioactive methods as the lead method is no longer confined for the most part to pegmatites and to pitchblende veins.

The accessory minerals zircon, sphene, apatite and some rare earth minerals, including monazite, are the principal hosts to U and Th in igneous rocks. A favourable feature about these minerals is that although their structures readily accept U and Th they tend to reject the entry of Pb^{2+} mainly because its size and charge are unsuitable. As a result, it has been possible to employ rapid methods without isotope analysis control as well as refined procedures based on complete analyses. Larsen *et al.* (1952, 1953) were the first to publish a set of ages based on the rapid procedure; these determinations have since been augmented by many others and some 85 are listed by Faul (1954). A thick source count is made of total activity and total lead is determined, as for example by a spectrochemical procedure (Waring and Worthing 1953). An approximate age is obtained from the relationship $t = K(\mathrm{Pb})/\alpha$ where t is age, (Pb) total lead and K a constant which is 2600 for U alone and 1990 for Th alone.

In zircon, activity is due mainly to U. It should be recalled that chemical ages [total Pb/(U + Th)] are often low† in uraninite and monazite and that Pb ages are likely therefore to be under-estimates, particularly in the pre-Cambrian, unless a significant proportion of rock lead is present in the mineral.

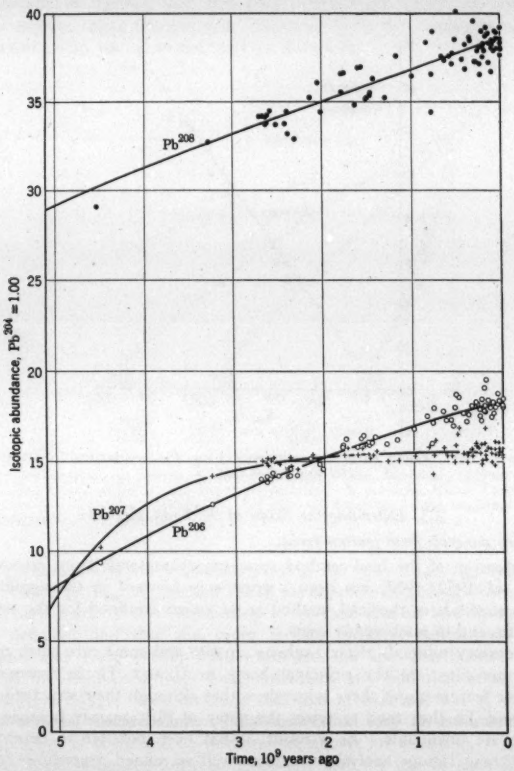

Figure 4. Variation of isotope composition of lead from galena of different ages. Roughly two-thirds of all known measurements have been used ; others are regarded as anomalous. [*After* Faul (1954). *With kind permission of John Wiley.*]

† It was once thought that such chemical ages tended to be over-estimates as allowance could not be made for the presence of common lead ; it now seems likely that they are often under-estimates (Ahrens 1955 b) because lead deficiency is common. As an extreme example, we have monazite from Antsirabe, Madagascar (for complete data, see Holmes and Cahen 1955), which has a chemical age of 700×10^6 years ; that is, only one-quarter of its likely age ($t_{convergent}$) of 2680×10^6 years (figure 2).

Precise measurements on individual parent–daughter ratios have been attempted (see, for example, Carnegie Institution 1954). Very few observations have been made, but it seems that in zircon also, the lead age distribution appears to be $t(\frac{207}{206}) > t(\frac{207}{235}) > t(\frac{208}{238}) > t(\frac{208}{232})$. For example, zircon separated from granite (Bagdad, Arizona) gave $t(\frac{207}{206})$ 1190×10^6 years; $t(\frac{207}{235})$ 750×10^6 years; and $t(\frac{208}{238})$ 630×10^6 years. Such disagreement may appear highly unsatisfactory, but it is quite possible that a precise convergent age estimate could be made provided several specimens were analysed.

As the accessory minerals are usually of low abundance, a considerable bulk of rock, often several pounds, is usually required. Concentration of zircons etc. may be achieved by the combined use of heavy liquids, magnetic separator and flotation cells (see, for example, Fairbairn 1955).

(ii) *Lead ores.*

The first isotope analyses of lead from several galena specimens (Nier 1938) indicated a tendency of the lead isotope constitution to vary regularly with age. Use has been made of this relationship for estimating the age of the earth (Gerling 1942, Koczy 1943, Holmes 1946, Holmes 1947, Houtermans 1947, Bullard and Stanley 1949, Vinogradov *et al.* 1952, Collins *et al.* 1953, and Allan, private communication, referred to by Ahrens 1955 c); Russell *et al.* (1954) have developed the idea that individual lead ores may be dated in this way. Figure 4 (after Faul 1954) shows the variation of lead isotope constitution with time and serves to provide some impression of the accuracy with which individual ages may be made. It should be emphasized, however, that only two-thirds of all published analyses have been employed in figure 4, the others being regarded as anomalous.

The use of galena would expand the scope of the lead method enormously. It is quite clear, however, that although single galena ages may serve as useful guides, too much reliance cannot be placed on them as precise estimates. In general, the validity of a galena age tends to improve with age and estimates less than about 800×10^6 years are not attempted (Bullard and Wilson 1954). If suites of specimens from the same area give the same age, it seems reasonable to assume that a reliable estimate has been achieved. Most published galena ages may be found in Bullard and Wilson (1954) and Wilson *et al.* (1954).

The relationship (figure 5, after Faul 1954) between ^{206}Pb, ^{207}Pb and ^{208}Pb in a suite of galenas and uranium ores from the Colorado plateau is most instructive. Although the galena constitutions concentrate toward the one end of the regularity, there is considerable overlap into the uranium ore range which is quite extensive. The location of the point for the Canyon Diablo meteorite (Patterson 1955 and earlier papers) is neatly placed at the end of the regularity; the isotope constitution of this lead is assumed to be that of true primary lead—that is, the constitution of lead when originally formed and not modified since by addition from the radioactivity of uranium and thorium. For further data in this respect see Patterson (1955).

2.4. *Use of the Ratio* $\frac{208}{210}$

It is theoretically possible to employ the ratio of any one of the members of a decay series to that of a stable daughter provided the series is in equilibrium;

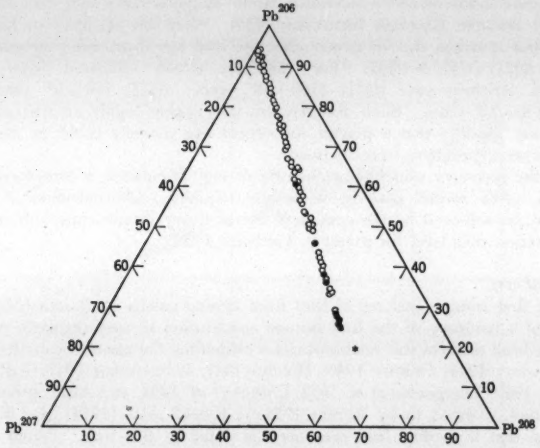

Figure 5. Variation of lead isotope constitution in uranium ores (o) and galena (•) from Colorado plateau. Note overlap and also the location of the point for lead from Canyon Diablo meteorite. [*After* Faul (1954). *With kind permission of John Wiley.*]

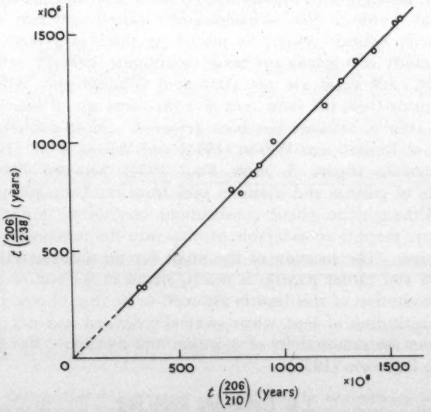

Figure 6. Relationship between $t\left(\frac{206}{238}\right)$ and $t\left(\frac{206}{210}\right)$ in fourteen specimens of pitchblende from the Lake Athabasca area. The relationship is very well developed. [*Data from* Eckelmann and Kulp (1956).]

hence ratios such as $^{206}Pb/^{226}Ra$, $^{206}Pb/^{214}Po$ and $^{206}Pb/^{210}Pb$ are possibilities in addition to those already discussed. Practical application is, however, only possible provided the half-life is not too short and chemical purification unduly difficult. Houtermans (1951) suggested the use of $^{206}Pb/^{210}Pb$ and a test on pitchblende from the Belgian Congo (Begemann *et al.* 1953) appeared successful. Subsequent large-scale investigations have been carried out by Kulp *et al.* (1953) and Eckelmann and Kulp (1956). Several details of analytical procedure are given by Kulp *et al.* (1953). Analytical manipulations are simplified by the fact that all measurements are confined to lead. Eckelmann and Kulp (1956) have made the significant observation that for a suite of Lake Athabasca pitchblendes $t(\frac{206}{210}) = t(\frac{206}{238})$ to within small limits; this is demonstrated graphically in figure 6. Eckelmann and Kulp conclude that this evidence shows equilibrium in the ^{238}U–^{206}Pb series.

Bullard and Wilson (1954) sum up the advantages of the $\frac{206}{210}$ age estimate as follows:

"(1) The ratio may be determined on any fraction of total lead in the mineral and hence it is unnecessary to carry out a quantitative chemical analysis. The proportion of ^{206}Pb present in a specimen of radiogenic lead is determined by a mass spectrometer.

(2) ^{210}Pb has a half-life of about 22 years and is easily measured by radioactive counting methods although the amount would be always too small to measure mass spectrometrically.

(3) The danger of contamination is slight since lead can be readily separated by chemical means from other members of the radioactive family. In addition, the $^{206}Pb/^{210}Pb$ ratio is unaffected by recent loss of uranium and only slightly affected by radon loss if the loss has been nearly uniform throughout the life of the mineral."

We should not overlook, however, that as $t(\frac{206}{210})$ is usually equal to $t(\frac{206}{238})$, individual estimates involving $t(\frac{206}{210})$ only are likely to be serious under-estimates of the age of the specimen.

§ 3. The Helium Method

A vast number of observations have been made during the investigation of the helium method and for a recent, full and authoritative review see Hurley (1954); this paper included many of the earliest observations and traces the development of the investigations until the present time. For reasons given in the introduction, the survey given here is very brief.

We have noted above that the central problem of the lead method is one of interpretation of lead age distributions and in the helium method a different major problem arises, namely, that of escape of helium; a second problem is one of occlusion of helium at the time of formation of the mineral.

Early observations of Strutt (1908 a, b) had indicated that helium leakage was likely to be particularly serious in highly radioactive minerals and this has been confirmed by later observations (see, for example, Hurley 1954). As a result minerals such as uraninite, commonly used in the lead method, cannot be used in the helium method. The development of methods of gas analysis having great sensitivity have made it possible to determine helium in minerals, rocks

and meteorites which contain very low concentrations of U + Th. Early observations on such rocks and minerals, though not wholly satisfactory because of some tendency to produce low ages were nevertheless encouraging (see Holmes 1937, for example, who gives a geological time scale based on He ages) but the large-scale investigations of Keevil (1938 a, b, 1942, 1943), Hurley and Goodman (1943), Hurley (1954) and others on a wide variety of minerals and rocks were far less encouraging. Helium age estimates of minerals from the same rock usually differed sharply among themselves and with an estimate of the age of the rock as a whole. Most such estimates appeared to be more or less serious under-estimates. The data (Keevil 1942) in table 2 serve as a typical example.

Table 2. Helium ' Ages ' of Minerals and the Whole Rock
(Cape Ann granite, Mass.)

	$\times 10^6$ years
Quartz	94
Feldspar	59
Ferromagnesians	159
Whole rock	89

The rock is Paleozoic and should presumably have an age of 200×10^6 years. Such differences were ascribed to varying helium retentivities by the structures of different minerals and Gerling (1939) suggested that close-packed minerals such as corundum, rutile, garnet, spinel and others were likely to retain a higher proportion of the helium. Whether serious escape of helium out of mineral structures does in fact take place has always been problematical as it is known (Hurley 1954) that the diffusion coefficients of helium in undisturbed crystals of some minerals (magnetite, zircon and sphene) are so small that measurable escape of helium is highly unlikely in a period of say 10^9 years.

The investigations of Curie (1946), Picciotto (1949, 1950, 1952), Hee (1948), Hee *et al.* (1951, 1954), Coppens (1951, 1952), Ford (1951)—for further references see Rankama (1954)—using photographic techniques, and Hurley (1950) using acid leaching experiments have shed much light on the cause of apparent helium escape and consequent under-estimation of age. The photographic plate was used to demonstrate the distribution of α-activity in minerals and rocks and showed that such activity was often localized and concentrated in cracks and fissures of minerals. Hurley (1950) observed that acid leaching removed a high proportion of activity from acid rocks and several minerals and concluded that the leachable U + Th had been concentrated on the surfaces of mineral grains and in the cracks and fissures. Helium would escape from such surficial concentrations and this apparently has been the cause of the low helium age estimates. Continued leaching fails to remove a significant proportion of the activity (Hurley 1950) and presumably such activity comes from U + Th structurally held within a mineral. Hurley (1954) has observed that acid treatment causes little change of activity in basic igneous rocks such as a basalt where U + Th are evidently much more uniformly distributed than in holocrystalline rocks such as granite.

The most satisfactory estimates of age have been made on magnetite and some sulphides (Hurley and Goodman 1943). Some of the estimates are obviously seriously in error and leaching experiments on two such specimens giving

excessively low ages have indicated (Hurley 1954) that a closer probable estimate is reached after leaching; surficial contamination was evidently the cause of the low age. Hurley (1952) and Hurley and Fairbairn (1953) have also carried out investigations on helium ages of minerals (zircon and sphene) containing a moderate concentration of uranium, most of which was considered to be held within the structure itself and not concentrated surficially. From observations on 42 specimens, it was concluded (Hurley 1954) that a major proportion of helium was retained in zircons of low activity and that helium escape was related to the total number of alpha particles per unit volume, that is, alpha activity multiplied by the age of the sample. Some specimens retained only about one-tenth of their helium. In a later investigation Hurley, Larsen and Gottfried (1956) compared the lead and helium ages of a suite of comparatively young non-metamict zircon crystals and found a systematic difference which expressed as a He/Pb age ratio was usually about 0·75. The authors were unable to suggest a likely mechanism for this difference from the available evidence and suggest further investigations.

The application of the helium method to the dating of meteorites, developed mainly by Paneth and co-workers (see, for example, Arrol, Jacobi and Paneth 1942) has been a specific application and we come to it again in the comparison of the ages of the oldest minerals with the ages of meteorites and other materials.

§ 4. Methods based on the Radioactivity of the Alkali Metals K and Rb

Although radioactivity was observed in K and Rb some fifty years ago, its application to the determination of geological age is a comparatively recent development. The simple nature of the decay

$$^{40}\mathrm{K} \begin{cases} \xrightarrow{\beta} {}^{40}\mathrm{Ca} \\ \xrightarrow{e} {}^{40}\mathrm{A} \end{cases} ; \qquad {}^{87}\mathrm{Rb} \xrightarrow{\beta} {}^{87}\mathrm{Sr}$$

in each case without significant recoil effect, is a particularly desirable feature; moreover, neither of the daughter elements Ca and Sr, or rather their cations Ca^{2+} and Sr^{2+}, are seriously foreign to the host mineral structures and are not likely to escape. From fundamental considerations, the alkali metal methods are superior to the lead and helium methods, but we shall see as we come to each in turn that progress has nevertheless been slowed by various other considerations, analytical accuracy and uncertainty of decay constants, for example. We will trace progress in the strontium method first, as it is the oldest of the alkali metal methods, then consider the argon method and finally survey the prospects of the potential calcium method together with other potential direct methods.

4.1. *The Strontium Method*

As in the case of ^{40}K (see below) the decay constant of ^{87}Rb has been the subject of much investigation. Emission of a soft β-particle has been a main cause of difficulty of accurate determination of half-life; various estimates, arranged in chronological order, are given in table 3.

The possibility that bound β-decay may be of some significance in this respect is mentioned by Kohman (1954).

The first strontium age determination (Hahn and Walling 1938) was described shortly after the discovery (Hahn *et al.* 1937) of radiogenic strontium in lepidolite, the mineral which has the highest rubidium content. In some of the first investigations, rubidium was determined by a flame photometric procedure, total strontium by a combined chemical enrichment–spectrochemical procedure (Hybbinette 1943) and the proportion of radiogenic strontium by a mass spectrographic analysis (photographic recording) of $SrBr_2$ (Mattauch 1947).

Ahrens (1947, 1949) sought to develop a rapid optical spectrochemical procedure for direct determination of Sr(total)/Rb ratios in lepidolite. Some thirty specimens have been examined this way and although the procedure serves very satisfactorily for reconnaissance and in this respect has revealed a second area containing uniquely old pegmatites (Ahrens and Macgregor 1951), accuracy is nevertheless unsatisfactory for many purposes. A marked step forward, as in

Table 3. Half-life Determinations of ^{87}Rb

Source	Half-life ($\times 10^{10}$ years)
Hahn and Rothenbach (1919)	7·5
Mühlhoff (1930)	12·0
Orbain (1931)	4·4
Strassmann and Walling† (1938)	6·3
Chaudhury (1942)	7·5
Eklund (1946)	5·8
Haxel, Houtermans and Kemmerich (1948)	6·0
Curran, Dixon and Wilson (1952)	6·15
Lewis (1952)	5·9
McGregor and Wiedenbeck (1952)	6·4
Bähnish, Huster and Walcher (1952)	4·8 (lower limit)
McGregor and Wiedenbeck (1954)	6·2
Flinta and Eklund (1954)	6·1

† Indirect. Based on Pb age of $1{\cdot}99 \times 10^9$ years for south-east Manitoba pegmatite; using a convergent Pb age value of 2680×10^6 years (Ahrens 1955 a) would increase this value.

many age methods, has been the introduction of isotope dilution–mass spectrometric procedures (Davis and Aldrich 1953, Tomlinson and Das Gupta 1953). For strontium, Aldrich and co-workers have used ^{84}Sr as the spike whereas Tomlinson and Das Gupta chose ^{90}Sr. Such procedures require only an extremely small quantity of specimen and accuracy is claimed to be high. A few of the first determinations are evidently in error but have since been revised (see discussion by Ahrens 1955 c). Most application of the strontium method has thus far been made in the pre-Cambrian (see, for example, Nicolaysen *et al.* 1953, Nicolaysen 1954), and it is here that this method evidently will find its greatest application.

Schreiner, Jamieson and Schonland (1955) report ages on three distinct varieties of mica (purple biaxial, $2{\cdot}69 \times 10^9$ years, green biaxial, $2{\cdot}82 \times 10^9$ years and purple uniaxial, $2{\cdot}57 \times 10^9$ years) from a single hand specimen from the Popes Claim pegmatite, Salisbury, S. Rhodesia. Although the three ages agree in magnitude, the difference is significant and greater than analytical error. This illustrates a source of error not heretofore observed, the cause of which, however,

is yet to be found. The magnitude of $2{\cdot}7 \times 10^9$ years (average of the above values) is somewhat lower than that reported by Nicolaysen *et al.* (1953) and Nicolaysen (1954) who used a similar analytical procedure and is very close to the convergent lead age (table 1) for Rhodesia pegmatites.

As in the lead method, there has been some progress towards expanding the strontium method. Lepidolite and other Rb-rich minerals are confined to pegmatites. Ahrens (1949), Whiting (1950) and Holyk (1952) have suggested and discussed the possibilities of using biotite, a common rock-forming mineral. Whereas more than 90% of the strontium from lepidolites and more than 40% of the strontium from pollucite, amazonite, hydrothermal microcline and some pegmatitic micas is usually radiogenic, the proportion in biotites from igneous rocks is much lower, usually 1 to 10% (Aldrich *et al.* 1953, Ahrens 1954). Nevertheless, this proportion of radiogenic strontium is significantly high, and it should be possible to determine strontium ages of quite a high proportion of pre-Cambrian biotites; Tomlinson and Das Gupta (1953) report one and Davis (see Carnegie Institution 1954) two biotite ages.

4.2. *The Argon Method*

No other method, perhaps, shows indications of greater promise than does the argon method. It is too early yet to attempt a definite prediction, but available data must be regarded as very encouraging when due allowance is given to the usual allotment of teething troubles associated with the development of a new method.

Shortly after Aldrich and Nier (1948) demonstrated the presence of appreciable quantities of radiogenic ^{40}A in some potassium minerals, Smits and Gentner (1950) attempted some age determinations of oligocene sylvite (Rhine Valley). Their paper describes the determination of total argon as well as its mass spectrometric analysis. Later papers (Gentner, Präg and Smits 1953, Gentner, Goebel and Präg 1954) discuss the dependence of argon diffusion on size of KCl crystals. Although these applications to salt deposits are indeed of use, it is in the dating of igneous rocks that the argon method seems to hold greatest promise; here it may be applied to the most ubiquitous of all minerals, mica and feldspar. Before surveying progress in this direction, it would be as well to recall that some uncertainty still exists about the precise value of the decay constants of ^{40}K, the rarest isotope of potassium (0·0119%, Nier 1950; 0·0118%, Reutersward 1952). The β-decay constant appears to be fairly accurately known ($\lambda_\beta = 0{\cdot}55 \times 10^9$ year^{-1}: Birch 1951, Burch 1953) but the value of the branching ratio is less certain and values based on direct laboratory measurements are usually higher than those based on the determination of radiogenic ^{40}A in minerals of assumed known age. Table 4 summarizes most of this information.

Most values claimed to be within approximately 10%, (1) to (16), based on direct observation, (17) and (18) on indirect (see above). Mousof (1952) and Russell *et al.* (1953) had previously reported a value of 0·06, but subsequent argon measurements caused an increase of this value to 0·085 to 0·09.

Although cognizance must be taken of some uncertainty in the decay constants of ^{40}K, it seems reasonable to assume that this difficulty is being resolved, and we now pass on to surveying progress of application of the argon method to dating

igneous rocks. The first such attempt is that of Gerling *et al.* (1952), who obtained nine argon ages (mainly on microcline) and who reported satisfactory agreement between argon ages and those of associated minerals determined by the lead and helium methods. Subsequent publications from two groups (Chicago: Wasserburg and Hayden 1955; Toronto: Russell *et al.* 1954) also indicate satisfactory agreement between lead and argon ages provided some adjustment is made to the observed branching ratio (table 4). The recent paper by Wasserburg and Hayden (1955) contains considerable analytical detail, and using the isotope dilution technique which they describe, it is apparently possible to determine ages as low as about 20×10^6 years. This is most satisfactory. The proportion of radiogenic ^{40}A is usually about 95% in feldspar: this high proportion reduces the magnitude of error which could have been caused by uncertainty

Table 4. Branching Ratio (β/e) for ^{40}K

Source	Ratio
(1) Kolhörster (1930)	0·061
(2) Mühlhoff (1930)	0·040
(3) Behounek (1931)	0·16
(4) Gray and Tarrant (1934)	0·02
(5) Ahrens and Evans (1948)	0·112
(6) Graf (1948)	0·115 ± 0·025
(7) Hess and Roll (1948)	0·109
(8) Hirzel and Waffler (1948)	0·087 ± 0·012
(9) Floyd and Borst (1949)	0·05 ± 0·01
(10) Sawyer and Wiedenbeck (1949)	0·098 ± 0·010
(11) Faust (1950)	0·122 ± 0·014
(12) Houtermans, Haxel and Heintz (1950)	0·105 ± 0·010
(13) Smaller, May and Freedman (1950)	0·05 ± 0·01
(14) Spiers (1950)	0·102
(15) Burch (1953)	0·119 ± 0·006
(16) Libby (see Kohman and Saito 1954)	0·10
(17) Shillibeer *et al.* (1954)	0·09
(18) Wasserburg and Hayden (1955)	0·085
(19) Suttle and Libby (referred to by Wasserburg and Hayden)	0·10

of isotope constitution of primary argon. The close relationships between lead and argon age have led Wasserburg and Hayden (1955) to conclude that argon diffusion is probably insignificant. On the other hand, Wetherill *et al.* (1955) find that the ratio $^{40}A/^{40}K$ in feldspar is systematically lower than the ratio in mica from the same rock. A significant proportion of argon evidently escapes from feldspar; nothing conclusive can, however, be drawn from the data as to whether mica retains virtually all of its argon.

The determination of potassium presents no serious problem unless present at low concentrations as in meteorites (see Ahrens, Pinson and Kearns 1952, Edwards and Urey 1955 in this respect) and Lawrence–Smith fusion or flame-photometric methods provide satisfactory accuracy.

Fleming and Thode (1953 a) draw attention to one possible cause of error in the argon method, namely, the great variation of $^{36}A/^{38}A$ ratios in highly active minerals. Age measurements usually involve $^{40}A/^{36}A$ measurements, and if the

mineral happened to be near a highly active one, the 'normal' ^{36}A abundance may be disturbed.

§ 5. Potential Methods

In addition to natural radioactivities already referred to, several others are known; table 5 lists most of these. (U, Th, K and Rb are included for the sake of completeness.) A few other radioactive elements have been reported, for example ^{50}V ($>10^{12}$ years)$\rightarrow{}^{50}Cr$?; ^{50}Ti?; ^{123}Sb (very long)$\rightarrow{}^{123}Te$; ^{129}I ($1{\cdot}72\times10^{7}$ years)$\rightarrow{}^{129}Xe$; ^{150}Nd (2×10^{15} years?)$\rightarrow{}^{150}Pm$. Natural fission (spontaneous and neutron induced) is discussed separately (see below). Each radioactivity represents a potential age method and prospects of their use in this respect will be surveyed briefly.

Table 5. Examples of Natural Radioactivity†

Decay	Half-life (years)
^{238}U (99·28%) $\xrightarrow{\text{complex}}$ ^{206}Pb	$4{\cdot}5\times10^{9}$
^{235}U (0·71%) $\xrightarrow{\text{complex}}$ ^{207}Pb	$7{\cdot}1\times10^{8}$
^{232}Th (100%) $\xrightarrow{\text{complex}}$ ^{208}Pb	$1{\cdot}39\times10^{10}$
^{40}K (0·012%) $\xrightarrow{e}{}^{40}A$; $\xrightarrow{\beta^-}{}^{40}Ca$	$1{\cdot}33\times10^{9}$ (see table 4)
^{87}Rb (27·85%) $\xrightarrow{\beta^-}{}^{87}Sr$	6×10^{10} (see table 3)
^{115}In (95·77%) $\xrightarrow{\beta^-}{}^{115}Sn$	6×10^{14}
^{130}Te (34·49%) $\xrightarrow{\text{double }\beta^-}{}^{130}Xe$	$\sim10^{21}$
^{138}La (0·089%) $\xrightarrow{e}{}^{138}Ba$; $\xrightarrow{\beta^-}{}^{138}Ce$	$\sim7\times10^{10}$
^{176}Lu (2·6%) $\xrightarrow{e}{}^{176}Yb$; $\xrightarrow{\beta^-}{}^{176}Hf$	$2{\cdot}4\times10^{10}$
^{187}Re (62·93%) $\xrightarrow{\beta^-}{}^{187}Os$	$\sim5\times10^{10}$
^{147}Sm (15·1%) $\xrightarrow{\alpha}{}^{143}Nd$	$1{\cdot}25\times10^{11}$
^{209}Bi (100%) $\xrightarrow{\alpha}{}^{205}Tl$	$2{\cdot}7\times10^{17}$

† Most values come from the *General Electric Chart of Nuclides* (4th Edition, 1952); ^{147}Sm (Beard and Wiedenbeck 1954); ^{187}Re (Herr, Hintenberger and Voshage 1954); ^{138}La (Mulholland and Kohman 1952). See Kohman and Saito (1954) for a discussion of these decays.

The first criterion which must be considered is that of half-life: if these are too long, the daughter concentration becomes so low that it becomes unmeasurable. What this lower limit is, is impossible to predict as the introduction of newer sensitive procedures keeps on lowering detection limits. For the sake of

this discussion we will set arbitrarily, as an approximate limit, a half-life greater than about $\times 100$ to 1000 the age of the early pre-Cambrian rocks (i.e. $\times 10^9$ years). This rules out ^{130}Te (10^{21} years), ^{209}Bi (10^{17} years), ^{115}In (6×10^{14} years) and ^{147}Sm (10^{16} years). Of the remaining decays, that of $^{40}\text{K} \rightarrow {}^{40}\text{Ca}$ will be considered first.

Radiogenic ^{40}Ca was discovered (Inghram *et al.* 1950) in sylvite and, as in the argon method, calcium ages of sylvite may presumably be determined. Whereas, however, the argon method appears capable of wide application for dating igneous rocks, the potential calcium method would be very restricted. This is due to swamping of small quantities of radiogenic calcium in almost all igneous minerals. The problem has been discussed by Ahrens (1951), who concludes that only lepidolites as well perhaps as some other late pegmatitic mica and feldspar, could be used. Most lepidolites contain about 10 to 500 parts per million total calcium (Ahrens 1951, Holyk 1952) and calculation based on the potassium and calcium (total) content of lepidolites of assumed known age indicate that up to approximately 30% of the calcium of pre-Cambrian lepidolites may be radiogenic. Potassium is easily determined in lepidolite by conventional methods and Holyk (1952) describes a spectrochemical procedure for determining total calcium; a mass spectrometric analysis may be made using the $^{40}\text{Ca}/^{44}\text{Ca}$ ratio. Despite several investigations which have been undertaken to detect radiogenic ^{40}Ca in lepidolite, none has yet apparently been successful.

Although the calcium method would be restricted in scope, a calcium age of strontium + argon dated lepidolite would be invaluable as it would serve as a triple age check and also a check on the branching ratio β/e of ^{40}K.

The next shortest half-life is probably that of ^{176}Lu. This is a fairly rare isotope (2·6%) and as lutetium is an extremely rare rare-earth, the amount of daughter produce is very small. A rare-earth mineral containing 1% Lu would produce about 0·1 part per million total daughter element in 10^9 years. Of this about two-thirds would be ^{176}Yb (this isotope is 12·73% of natural Yb). The abundance of ytterbium is usually far greater than lutetium in rare-earth minerals and this seems to make the determination of radiogenic ^{176}Yb virtually impossible. ^{176}Hf offers slightly better possibilities because the total hafnium concentration in a rare-earth mineral may be low enough to permit a determination of radiogenic ^{176}Hf: the operation would in any event be difficult. Similar concentration magnitudes have to be considered for the decay $^{138}\text{La} \rightarrow {}^{138}\text{Ce} + {}^{138}\text{Ba}$. As cerium is a common rare earth, this seems to rule out the possibility of using the ratio $^{138}\text{La}/^{138}\text{Ce}$. Saito *et al.* (unpublished, see Kohman and Saito 1954) have looked for ^{138}Ba in old rare-earth minerals but were unsuccessful.

Although rhenium and osmium do not show geochemical coherence, as compared with the rare-earth elements, for example, rhenium is unfortunately extremely rare and rarely reaches an effectively high concentration; a maximum of 0·3% is reached in some molybdenites. Libby (see Kohman and Saito 1954) has discussed the possibility of using this mineral and finds cause for some optimism. A generally favourable feature is that common osmium contains only 1·64% ^{187}Os. Hintenberger *et al.* (1954) have recently provided the necessary experimental evidence to indicate that an osmium method is a real possibility. They found 16 parts per million total Os (99·5% radiogenic) in a rhenium-rich (0·32%

Re) molybdenite. Two analytical methods were used for Os: one, an isotope dilution procedure involving the addition of cyclotron irradiated Os and the other a spectrophotometric procedure using thio-urea complex of Os. Total parent was determined by a colorimetric method (Beeston and Lewis 1953) and a neutron activation method. Further observations on $^{187}Re/^{187}Os$ ratios in molybdenite are awaited with much interest.

Natural fission is another possible age method. Its discovery goes back to 1940 (Flerov and Petrzhak 1940 a, b) and since then strong evidence (Khlopin, Gerling and Baranovskaya 1947, Macnamara and Thode 1950, Fleming and Thode 1953 b, Wetherill 1953) indicating two types of natural fission has been provided: spontaneous fission of ^{238}U [$t = 3{\cdot}1 \times 10^{15}$ years (Pose 1943), $8{\cdot}04 \times 10^{15}$ years (Segrè 1952), $1{\cdot}3 \times 10^{16}$ years (Perfilov 1947), $1{\cdot}9 \times 10^{15}$ years (Yagoda and Kaplan 1949)], and neutron induced fission in ^{235}U [$t_{1/2} = 1{\cdot}87 \times 10^{17}$ years (Seaborg 1951)]. It is evident that natural fission half-lives are extremely long and hence extremely small quantities of stable fission products are produced. Nevertheless, measurable amounts of fission product Xe and Kr have been quantitatively determined in highly active minerals (Macnamara and Thode 1950, Fleming and Thode 1953 b, Wetherill 1953), and from the point of view of use for age measurements, Fleming and Thode state: "A quantitative measure of the amount of fission gas present in ores per gramme of uranium and a knowledge of the proportion of spontaneous fission that has occurred should make age calculations possible" [see also Thode (1954) in this respect]. Marble (1952) has mentioned that trace quantities of rare earths might be produced by natural fission in U + Th minerals. Until such time as all known processes of natural fission (spontaneous and induced) are properly understood and more observations are at hand, it will not be possible to predict with confidence what likelihood there is of a successful application of natural fission for determining geological age. There is also the problem of possible unobserved fission processes. For example, Peppard *et al.* (1952) find $^{233}U/^{238}U$ ratios of $1{\cdot}3 \times 10^{-13}$ to 4×10^{-11} in pitchblende and monazite respectively, and the presence of ^{233}U could be attributed to the reaction

$$^{232}Th\ (n, \gamma)\ ^{233}Th\ ;\ ^{233}Th \xrightarrow{\beta^-} {}^{233}Pa \xrightarrow{\beta^-} {}^{233}U \dashrightarrow {}^{205}Tl.$$

There are other possibilities.

§ 6. A Comparison of the Ages of the Oldest Minerals with Estimates of the Age of the Earth, Meteorites, Solar System, Elements and Universe

The ages of the oldest minerals are of much interest to physicists, astrophysicists, geochemists, geologists and biologists. Despite considerable discordance in the data, particularly apparent when comparisons are made between age estimates by different methods, it is possible to arrive at fairly definite conclusions about (i) which of the pre-Cambrian minerals dated so far are the oldest, (ii) their absolute age, and (iii) the possibility of finding minerals of substantially greater age. This general topic has recently been reviewed by Ahrens (1955 c); this paper gives references to earlier relevant publications, particularly those by Holmes. It is concluded that evidence from the lead and strontium methods in

particular is sufficient to confirm fully the great antiquity of pegmatites from Rhodesia and south-eastern Manitoba; a lead age of 2680×10^6 years ($t_{\text{convergent}}$, figure 2) has been recommended (Ahrens 1955 a, b). This magnitude is somewhat lower than several strontium (isotope-dilution) age estimates (Davis and Aldrich 1953, Nicolaysen *et al.* 1953, Nicolaysen 1954, Schreiner *et al.* 1955). Recent strontium determinations (Schreiner *et al.* 1955) of Rhodesian lepidolite range from 2570 to 2820×10^6 years and are very similar in magnitude to the recommended lead age. It is instructive to observe how the lead age of Manitoban uraninite has been re-evaluated several times, as the Manitoba–Rhodesia age is often considered in discussions of the age of the earth, solar system and universe (see below). Before isotope data were available, the chemical lead age of 1700×10^6 years was recommended (Holmes 1937). Isotope data led at first to the recommendation of 1985×10^6 years (Holmes 1948), an age based on assumed radon loss. Collins *et al.* (1954), following Nier *et al.* (1941) have preferred a magnitude of 2500×10^6 years based on $t(\frac{207}{206})$, but even this value seems too low as the most likely lead age appears to be 2680×10^6 years; the increase is about 1000×10^6 years. There is evidence that the ages of minerals from other localities may be the same or very similar to those from Rhodesia–Manitoba (Ahrens 1955 c). There are indications also, however, that the ages of some minerals are slightly but distinctly greater than those from Rhodesia–Manitoba pegmatites. The most distinct evidence is that of a lead age of uraninite from Klerksdorp, Transvaal (Louw 1955), the convergent age of which has been estimated at 2930×10^6 years (Ahrens 1955 b). An estimate based on $t(\frac{207}{206})$ alone indicates a similar age for monazite from the Sula Mountains, Sierra Leone (Holmes and Cahen 1955); several galena 'ages' from this locality, Southern Rhodesia, Belgian Congo and Eastern Transvaal are of a similar general magnitude (Holmes and Cahen 1955). A statistical consideration of most of the available data has led to the prediction (Ahrens 1955 c) that there is little likelihood of finding a pegmatite *much* older, say $+500 \times 10^6$ years, than those from Rhodesia–Manitoba.

The ages of the oldest minerals provide a definite estimate of the minimum age of the earth, solar system and universe; they also make an interesting comparison with estimated ages of meteorites. Earlier attempts, mainly by Paneth and co-workers, to determine the ages of meteorites were based on the helium method (see, for example, Arrol, Jacobi and Paneth 1942). These observations were confined for the most part to metal meteorites and indicate a very wide age range. The recent observations of Paneth, Reasbeck and Mayne (1952, 1953) on $^3He/^4He$ ratios in meteorites has necessitated some re-evaluation. It is found, however (Paneth 1954, for example), that although these considerations do influence the helium age calculations, many estimates of the ages of iron meteorites remain comparatively young (most $100–200 \times 10^6$ years, a few down to 1×10^6 years), that is, when compared with the ages of the oldest rocks and the argon and lead ages (see below) of meteorites. For further discussions of these age variations see Urey (1955).

Gerling and Pavlova (1951) reported an argon age of 3×10^9 years for two chondrites (see also Gerling and Rik 1952). The potassium content which they reported was considerably higher than that typical of chondrites (Ahrens, Pinson

and Kearns 1952, Edwards and Urey 1955) and from this consideration their age is an under-estimate. Wasserburg and Hayden (1955) report argon ages of $4{\cdot}0$–$4{\cdot}5 \times 10^9$ years for two chondrites, using a value of 0·09 for the branching ratio β/e for ^{40}K. This magnitude is slightly less than that (2 at $3{\cdot}5 \times 10^9$ years) reported since by Thomson and Mayne (1955). These workers chose a branching ratio of 0·13 which if decreased to 0·09 would bring their age estimates closer to those of Wasserburg and Hayden. The magnitudes of 4–5×10^9 years are close to the lead age estimates of Patterson (1955). This paper gives several references to earlier observations. In contrast to these great ages of meteorites, the argon ages of tectites (Suess *et al.* 1951, Gerling and Yaschenko 1952) are only 10^6–10^7 years and Gerling and Yaschenko regard this as evidence against a cosmic origin of tectites.

Table 6. Comparison of the Ages of the Oldest Minerals with Estimated Ages of the Earth, Meteorites, Elements and Universe

		$\times 10^6$ years
The oldest minerals	Rhodesia–Manitoba Pb (t_{conv})	2680
	Sr	2500–3350
	Klerksdorp, Transvaal Pb (t_{conv})	(2930)†
The earth	(i) Pb isotopes in galena	4200
	(ii) Pb content of granite	~3500–4000
Elements and maximum age of earth		5300–5500
Stony meteorites	(i) lead	4400–4600
	(ii) argon	4600
		(4000)
Universe		~5000

† Based on one observation only.

Table 6 compares the ages of the oldest minerals with recent meteorite ages (as indicated above) and estimates of the age of the earth, elements and universe. The first value for the ' age of the earth '‡ is that given by Allan and Russell (private communication, referred to by Ahrens 1955 c), who used a method of calculation similar to that of other authors (Gerling 1942, Holmes 1946 and later papers, Houtermans 1947, Bullard and Stanley 1949, Vinogradov, Zadorozhnyi and Zykov 1952, and Collins, Russell and Farquhar 1953), but included additional recent information, particularly on young galena; the estimate of 4200×10^6 years ($\pm 10\%$) is greater than most earlier estimates, most of which ranged from 3200 to 3500×10^6 years. The second estimate of the age of the earth is actually a possible estimate of the age of granite using Pb and U contents respectively of 15 and 3·5–4 parts per million for average granite and $^{207}/^{204}$Pb and ^{206}Pb/^{204}Pb ratios of 15·55 and 18·4 respectively for tertiary lead. The estimated age of element formation, and maximum age of the earth, is based on the time required for ^{207}Pb, the daughter of the fastest decaying uranium isotope (^{235}U), to have been at zero (Alpher and Herman 1951, McCrady 1952, Collins, Russell and Farquhar 1953).

‡ Readers should consult original papers concerning the age of the actual event.

The astronomic estimate of the age of the universe is based on the rate of expansion and the present distance of the earth from certain outlying galaxies. Previous estimates were about 2000×10^6 years. The present value of 5000×10^6 years comes from a report by Baade (1952), who presented revised estimates of stellar brightness. This has caused a large increase in the calculated total time for expansion (general reference, Sharpless 1953).

A general impression left by table 6 is one of remarkably good agreement. Whereas this may be very satisfying in several respects, we should be strongly cautioned against accepting what we see without question. Much investigation is still required before it will be possible to establish firmly whether much of what appears to be in good agreement is indeed so or not. The remarks (Patterson 1954) concerning the reliability and accuracy of the lead ages of meteorites (table 6) are pertinent and salutary in this respect.

§ 7. Selected References on Methods and Techniques not discussed

7.1. *Dating of Ocean Sediments* (*Radium and Ionium Methods*)

Urry (1941, 1942, 1948 a, b, 1949), Piggot and Urry (1942), Kulp and Carr (1952), Volchok and Kulp (1952), Pettersson (1951, 1954), Kröll (1954), Picciotto and Wilgain (1954), Hough (1953), Holland and Kulp (1954 a, b), Isaac and Picciotto (1953).

7.2. *Use of Photographic Emulsion for Age Determinations*

(i) As applied to ^{210}Pb method : Söding (1951), Wilgain (1953) and Houtermans (1954).

(ii) As applied to pleochroic haloes : Hayase (1954), Houtermans (1954) and Deutsch, Hirschberg and Picciotto (1954).

The photographic emulsion has also been most effectively employed for obtaining information about the distribution of α-activity in rocks. This information is particularly instructive for the development of the lead method. Some recent significant contributions are : Curie (1946), Hee (1948), Hee *et al.* (1951, 1954), Picciotto (1949, 1950, 1952), Yagoda (1949), Coppens (1951, 1952), Coppens and Coppens (1950) and Ford (1951). For further references see Rankama (1954).

7.3. *Indirect Methods for determining Geological Age*

(i) Cube edge : Wasserstein (1951, 1954, 1955), Brooker and Nuffield (1952).

(ii) Radiation damage : Holland and Kulp (1950), Holland (1954), Hurley and Fairbairn (1952).

(iii) Thermoluminescence : Zeller (1954), Daniels (1951, 1954).

References

Adams, J. A. S., and Maeck, W. J., 1954, *Analyt. Chem.*, **26**, 1635.

Ahrens, L. H., 1947, *Trans. Geol. Soc. S. Afr.*, **50**, 24; 1949, *Bull. Geol. Soc. Amer.*, **60**, 217; 1951, *Geochim. et Cosmochim. Acta*, **1**, 312; 1954, *Nuclear Geology*, Ed. H. Faul (New York: John Wiley), p. 331; 1955 a, *Geochim. et Cosmochim. Acta*, **7**, 294; 1955 b, *Ibid.*, **8**, 1; 1955 c, *Geol. Soc. Amer. Special Paper No.* 62, 115.

Ahrens, L. H., and Evans, R. D., 1948, *Phys. Rev.*, **74**, 279.

Ahrens, L. H., and Macgregor, A. M., 1951, *Science*, **114**, 64.

Ahrens, L. H., Pinson, W. H., and Kearns, M. M., 1952, *Geochim. et Cosmochim. Acta*, **2**, 229.

Aldrich, L. T., Herzog, L. F., Holyk, W. K., Whiting, F. B., and Ahrens, L. H., 1953, *Phys. Rev.*, **89**, 631.

Aldrich, L. T., and Nier, A. O., 1948, *Phys. Rev.*, **74**, 876.

Alpher, R. A., and Herman, R. C., 1951, *Phys. Rev.*, **84**, 1111.

Arrol, W. J., Jacobi, R. B., and Paneth, F. A., 1942, *Nature, Lond.*, **149**, 235.

Baade, W., 1952, Internat. Astron. Union, Rome Meeting.

Bähnish, I., Huster, E., and Walcher, W., 1952, *Naturwissenschaften*, **39**, 379.

Beard, G., and Wiedenbeck, M. L., 1954, *Phys. Rev.*, **95**, 1245.

Beeston, J. M., and Lewis, J. R., 1953, *Analyt. Chem.*, **25**, 651.

Begemann, F., v. Buttlar, H., Houtermans, F. G., Isaac, N., and Picciotto, E., 1953, *Geochim. et Cosmochim. Acta*, **4**, 21.

Behounek, F., 1931, *Z. Phys.*, **69**, 654.

Birch, F., 1951, *J. Geophys. Res.*, **56**, 107.

Brooker, E. J., and Nuffield, E. W., 1952, *Amer. Min.*, **37**, 363.

Bullard, E. C., and Stanley, J. P., 1949, *Veröff. Finn. Geod. Inst.*, **36** (Bonsdorff Vol.), 33.

Bullard, E. C., and Wilson, J. T., 1954, International Union of Geodesy and Geophysics, Rome Meeting.

Burch, P. R. J., 1953, *Nature, Lond.*, **172**, 361.

Carnegie Institution, Washington, 1954, *Year Book*, **53**, 78–84.

Chaudhury, P. K., Sen., 1942, *Proc. Nat. Inst. Sci. India*, **8**, 45.

Collins, C. B., Farquhar, R. M., and Russell, R. D., 1952, *Phys. Rev.*, **88**, 1275; 1954, *Bull. Geol. Soc. Amer.*, **65**, 1.

Collins, C. B., Freeman, J. R., and Wilson, J. T., 1951, *Phys. Rev.*, **82**, 966.

Collins, C. B., Russell, R. D., and Farquhar, R. M., 1953, *Canad. J. Phys.*, **31**, 402.

Coppens, R., 1951, *C.R. Acad. Sci., Paris*, **232**, 1681; 1952, *Bull. Soc. Franç. Minér.*, **75**, 57.

Coppens, R., and Coppens, A., 1950, *Bull. Soc. Sci. Bretagne*, **25**, 17.

Curie, I., 1946, *J. Phys. Radium*, **7**, 313.

Curran, S. C., Dixon, D., and Wilson, H. W., 1952, *Phil. Mag.*, **43**, 82.

Dalton, J. C., Golden, J., Martin, G. R., Mercer, E. R., and Thomson, S. J., 1953, *Geochim. et Cosmochim. Acta*, **3**, 272.

Dalton, J. C., and Thomson, S. J., 1954, *Geochim. et Cosmochim. Acta*, **5**, 74.

Daniels, F., 1951, *Chem. Eng. News*, **29**, 1632; 1954, *Nuclear Geology*, Ed. H. Faul (New York: John Wiley), p. 188.

Davis, G. L., and Aldrich, L. T., 1953, *Bull. Geol. Soc. Amer.*, **64**, 379.

Deutch, S., Hirschberg, D., and Picciotto, E., 1954, International Union of Geodesy and Geophysics, Rome Meeting.

Dibeler, V. H., and Mohler, F. L., 1951, *J. Res. Nat. Bur. Stand.*, **47**, 337.

Eckelmann, W. R., and Kulp, T. L., 1956, *Bull. Geol. Soc. Amer.*, in the press.

Edwards, G., and Urey, H. C., 1955, *Geochim. et Cosmochim. Acta*, **7**, 154.

Eklund, S., 1946, *Ark. Mat. Ast. Fys.*, **33A**, No. 14.

Fairbairn, H. W., 1955, *Amer. Min.*, **40**, 458.

Farquhar, R. M., Palmer, G. H., and Aitken, K. L., 1953, *Nature, Lond.*, **172**, 860.

Faul, H. (Ed.), 1954, *Nuclear Geology* (New York: John Wiley).

Faust, W. R., 1950, *Phys. Rev.*, **78**, 624.

FLEMING, W. H., and THODE, H. G., 1953 a, *Phys. Rev.*, **90**, 857 ; 1953 b, *Ibid.*, **92**, 378.
FLEROV, G. N., and PETRZHAK, K. A., 1940 a, *J. Exp. Theor. Phys. U.S.S.R.*, **3**, 275 ; 1940 b, *Phys. Rev.*, **58**, 89.
FLINTA, J., and EKLUND, E., 1954, *Ark. Fys.*, **7**, 401.
FLOYD, J. J., and BORST, L. B., 1949, *Phys. Rev.*, **75**, 1106.
FORD, I. H., 1951, *Nature, Lond.*, **167**, 273.
FÖYN, E., 1938, *Skr. Norske Vidensk Akad.*, No. 4.
General Electric Chart of Nuclides, 4th Edn, 1952 (Knolls Atomic Power Laboratory).
GENTNER, W., GOEBEL, K., and PRÄG, R., 1954, *Geochim. et Cosmochim. Acta*, **5**, 124.
GENTNER, W., PRÄG, R., and SMITS, F., 1953, *Geochim. et Cosmochim. Acta*, **4**, 11.
GERLING, E. K., 1939, *C.R. Acad. Sci. U.R.S.S.*, **24**, 274 ; 1942, *Ibid.*, **24**, 274.
GERLING, E. K., ERMOLINE, G. M., BARANOVSKAYA, N. V., and TITOV, N. E., 1952, *Doklady Akad. Nauk S.S.S.R.*, **86**, 593.
GERLING, E. K., and PAVLOVA, T. G., 1951, *Doklady Akad. Nauk S.S.S.R.*, **76**, 825.
GERLING, E. K., and RIK, K. G., 1952, *Meteoritica*, **10**, 37.
GERLING, E. K., and YASCHENKO, M. L., 1952, *Doklady Akad. Nauk S.S.S.R.*, **83**, 901.
GILETTI, B. J., and KULP, J. L., 1955, *Amer. Min.*, **40**, 481.
GRAF, T., 1948, *Phys. Rev.*, **74**, 1199.
GRAY, L. H., and TARRANT, G. T. P., 1934, *Proc. Roy. Soc.* A, **143**, 681.
HAHN, O., and ROTHENBACH, M., 1919, *Phys. Z.*, **20**, 194.
HAHN, O., STRASSMANN, F., and WALLING, E., 1937, *Naturwissenschaften*, **25**, 189.
HAHN, O., and WALLING, E., 1938, *Chem. Z.*, **67**, 55.
HAXEL, O., HOUTERMANS, F. G., and KEMMERICH, M., 1948, *Phys. Rev.*, **74**, 1886.
HAYASE, I., 1954, *Amer. Min.*, **39**, 761.
HEE, A., 1948, *Ann. Géophys.*, **4**, 242.
HEE, A., DERVILLE, R. P., and JAROVY, M., 1954, *Amer. J. Sci.*, **252**, 736.
HEE, A., KLEIBER, J., FLESCH, L., and JAROVY, M., 1951, *Ann. Géophys.*, **7**, 245.
HERR, W., HINTENBERGER, H., and VOSHAGE, H., 1954, *Phys. Rev.*, **95**, 1691.
HESS, D. C., BROWN, H., INGHRAM, M. G., PATTERSON, C., and TILTON, G., 1953, *Circ. U.S. Bur. Stand.*, No. 522, p. 183.
HESS, V. F., and ROLL, J. D., 1948, *Phys. Rev.*, **73**, 916.
HINTENBERGER, H., HERR, W., and VOSHAGE, H., 1954, *Phys. Rev.*, **95**, 1690.
HIRZEL, O., and WÄFFLER, H., 1948, *Phys. Rev.*, **74**, 1553.
HOLLAND, H. D., 1954, *Nuclear Geology*, Ed. H. Faul (New York : John Wiley), p. 175.
HOLLAND, H. D., and KULP, J. L., 1950, *Science*, **111**, 312 ; 1954 a, *Geochim. et Cosmochim. Acta*, **5**, 197 ; 1954 b, *Ibid.*, **5**, 214.
HOLMES, A., 1937, *The Age of the Earth* (London : Thomas Nelson) ; 1946, *Nature, Lond.*, **157**, 680 ; 1947, *Ibid.*, **159**, 127 ; 1948, *Trans. Edinb. Geol. Soc.*, **15**, Part 2, 176 ; 1954, *Nature, Lond.*, **173**, 612.
HOLMES, A., and CAHEN, L., 1955, *Colon. Geol. Min. Resour.*, **5**, 3.
HOLMES, A., and SMALES, A. A., 1948, *Proc. Roy. Soc. Edinb.* B, **63**, Part 2, 115.
HOLYK, W., 1952, *Ph.D. Thesis*, Massachusetts Institute of Technology.
HORNE, J. E. T., and DAVIDSON, C. F., 1954, *U.K. Geological Survey and Museum, Atomic Energy Division, Report No.* 170.
HOUGH, J. L., 1953, *J. Geol.*, **61**, 252.
HOUTERMANS, F. G., 1947, *Z. Naturf.*, **2a**, 322 ; 1951, *S. B. Heidelberg Akad. Wiss., Math.-nat. Kl.*, No. 2, 123 ; 1954, *Supplemento Nuovo Cim.*, **11**, 390.
HOUTERMANS, F. G., HAXEL, O., and HEINTZ, J., 1950, *Z. Phys.*, **128**, 657.
HURLEY, P. M., 1950, *Bull. Geol. Soc. Amer.*, **61**, 1 ; 1952, *Trans. Amer. Geophys. Un.*, **33**, 174 ; 1954, *Nuclear Geology*, Ed. H. Faul (New York : John Wiley), p. 301.
HURLEY, P. M., and FAIRBAIRN, H. W., 1952, *J. Appl. Phys.*, **23**, 1408 ; 1953, *Bull. Geol. Soc. Amer.*, **64**, 659.
HURLEY, P. M., and GOODMAN, C., 1941, *Bull. Geol. Soc. Amer.*, **52**, 545 ; 1943, *Ibid.*, **54**, 305.
HURLEY, P. M., LARSEN, E. S., and GOTTFRIED, D., 1956, *Geochim. et Cosmochim. Acta*, in the press.
HYBBINETTE, A. G., 1943, *Svensk. Kem. Tidskr.*, **55**, 151.

INGHRAM, M. G., 1954, *Annual Review of Nuclear Science*, **4** (Stanford : Annual Reviews), p. 81.
INGHRAM, M. G., BROWN, H., PATTERSON, C., and HESS, D. C., 1950, *Phys. Rev.*, **80**, 916.
ISAAC, N., and PICCIOTTO, E., 1953, *Nature, Lond.*, **171**, 742.
JENKINS, E. N., 1954, *Atomic Energy Research Establishment Report*, C/R 1353.
KEEVIL, N. B., 1938 a, *Amer. J. Sci.*, **36**, 406 ; 1938 b, *Trans. Roy. Soc. Can.*, Sec. IV, **32**, 123 ; 1942, *Amer. J. Sci.*, **240**, 13 ; 1943, *Ibid.*, **247**, 277.
KHLOPIN, V. G., GERLING, E. K., and BARONOVSKAYA, N. V., 1947, *Bull. Acad. Sci. U.R.S.S., Classe. Sci. Chim.*, **599** (*Chem. Abs.*, **42**, 3664 (1948)).
KOCZY, F. F., 1943, *Nature, Lond.*, **151**, 24.
KOHMAN, T. P., 1954, *Proceedings of Conference on Nuclear Processes in Nature, Williams Bay, Wisconsin* (Sept. 1953).
KOHMAN, T. P., and SAITO, N., 1954, *Annual Review of Nuclear Science*, **4** (Stanford : Annual Reviews), p. 401.
KOLHÖRSTER, W., 1930, *Z. Geophys.*, **6**, 341.
KRÖLL, U. S., 1954, *Deep-sea Research*, **1**, 211.
KULP, J. L., BATE, G. L., and BROECKER, W. S., 1954, *Amer. J. Sci.*, **252**, 346.
KULP, J. L., BROECKER, W. S., and ECKELMANN, W. R., 1953, *Nucleonics*, **11**, 19.
KULP, J. L., and CARR, D. R., 1952, *J. Geol.*, **60**, 148.
LARSEN, E. S., Jun., KEEVIL, N. B., and HARRISON, H. C., 1952, *Bull. Geol. Soc. Amer.*, **63**, 1045.
LARSEN, E. S., Jun., WARING, C. L., and BERMAN, J., 1953, *Amer. Min.*, **38**, 1118.
LEWIS, G. M., 1952, *Phil. Mag.*, **43**, 1070.
LIBBY, W. F., 1955, *Radiocarbon Dating* (University of Chicago).
LOUW, J. D., 1955, *Trans. Geol. Soc. S. Afr.*, **57**, 1.
MCCRADY, E., 1952, *Trans. Amer. Geophys. Un.*, **33**, 156.
MCGREGOR, M. H., and WIEDENBECK, M. L., 1952, *Phys. Rev.*, **86**, 420 ; 1954, *Ibid.*, **94**, 138.
MACNAMARA, J., and THODE, H. G., 1950, *Phys. Rev.*, **80**, 471.
MARBLE, J. P., 1952, *Rep. Committee on the Meas. Geol. Time*, 1950–1 (Washington : National Research Council).
MATTAUCH, J., 1947, *Angew. Chem.*, A, No. 2, 37.
MOUSOF, A. K., 1952, *Phys. Rev.*, **88**, 150.
MÜHLHOFF, W., 1930, *Ann. Phys.*, **1**, 205.
MULHOLLAND, G. I., and KOHMAN, T. P., 1952, *Phys. Rev.*, **87**, 681.
NICOLAYSEN, L. O., 1954, *Ph.D. Thesis*, Princeton University.
NICOLAYSEN, L. O., ALDRICH, L. T., and DOAK, J. B., 1953, *Trans. Amer. Geophys. Un.*, **34**, 342.
NIER, A. O., 1938, *J. Amer. Chem. Soc.*, **60**, 1571 ; 1939, *Phys. Rev.*, **55**, 153 ; 1950, *Ibid.*, **77**, 789.
NIER, A. O., THOMPSON, R. W., and MURPHEY, B. F., 1941, *Phys. Rev.*, **60**, 112.
ORBAIN, G., 1931, *S. B. Akad. Wiss. Wien., Math.-Nat. Kl.* (IIa), **140**, 121.
PANETH, F., 1954, *Z. Elektrochem.*, **58**, 567.
PANETH, F., REASBECK, P., and MAYNE, K. I., 1952, *Geochim. et Cosmochim. Acta*, **2**, 300 ; 1953, *Nature, Lond.*, **172**, 200.
PATTERSON, C., 1954, *Nuclear Processes in Geologic Settings* (Williams Bay, Wisconsin, Conference, 1953) ; 1955, *Geochim. et Cosmochim. Acta*, **7**, 151.
PATTERSON, C., BROWN, H., TILTON, G., and INGHRAM, M., 1953, *Phys. Rev.*, **92**, 1234.
PEPPARD, D. F., MASON, G. W., GRAY, P. R., and MECH, J. F., 1952, *J. Amer. Chem. Soc.*, **74**, 6081.
PERFILOV, N. A., 1947, *J. Phys. U.S.S.R.*, **11**, No. 3.
PETTERSSON, H., 1951, *Nature, Lond.*, **167**, 942 ; 1954, *Nuclear Geology*, Ed. H. Faul (New York : John Wiley), p. 115.
PICCIOTTO, E. E., 1949, *Bull. Soc. Belge Geol. Pal. Hydr.*, **58**, 75 ; 1950, *Ibid.*, **59**, 170 ; 1952, *Ibid.*, **61**, 215.
PICCIOTTO, E., and WILGAIN, S., 1954, *Nature, Lond.*, **173**, 632.
PIGGOT, C. S., and URRY, W. D., 1942, *Bull. Geol. Soc. Amer.*, **53**, 1187.

Pose, H., 1943, *Z. Phys.*, **121**, 293.
Rankama, K., 1954, *Isotope Geology* (London : Pergamon Press).
Reutersward, C., 1952, *Ark. Fys.*, **4**, 203.
Russell, R. D., Farquhar, R. M., Cumming, G. L., and Wilson, J. T., 1954, *Trans. Amer. Geophys. Un.*, **35**, 301.
Russell, R. D., Shillibeer, H. A., Farquhar, R. M., and Mousof, A. K., 1953, *Phys. Rev.*, **91**, 1223.
Sawyer, G. A., and Wiedenbeck, M. L., 1949, *Phys. Rev.*, **76**, 1535.
Schreiner, G. D. L., Jamieson, R. T., and Schonland, B. F. J., 1955, *Nature, Lond.*, **175**, 464.
Seaborg, G. T., 1951, *Chem. Eng. News*, **29**, 3965.
Segrè, E., 1952, *Phys. Rev.*, **86**, 21.
Sharpless, S., 1953, Astronomical Society of the Pacific, *Leaflet No.* 290.
Shillibeer, H. A., Russell, R. D., Farquhar, R. M., and Jones, E. A. W., 1954, *Phys. Rev.*, **94**, 1793.
Smales, A. A., 1952, *Analyst*, **77**, 778.
Smaller, B., May, J., and Freedman, M., 1950, *Phys. Rev.*, **79**, 940.
Smits, F., and Gentner, W., 1950, *Geochim. et Cosmochim. Acta*, **1**, 22.
Söding, H., 1951, *Staatsexamenarbeit*, as referred to by Houtermans (1954).
Spiers, F. W., 1950, *Nature, Lond.*, **165**, 356.
Strassmann, F., and Walling, E., 1938, *Ber. Dtsch. Chem. Ges.* B, **71**, 1.
Strutt, R. J., 1908 a, *Proc. Roy. Soc.* A, **80**, 572 ; 1908 b, *Ibid.*, **81**, 272.
Suess, H., Hayden, R. J., and Inghram, M. G., 1951, *Nature, Lond.*, **168**, 432.
Thode, H. G., 1954, *Nuclear Geology*, Ed. H. Faul (New York : John Wiley), p. 143.
Thomson, S. J., and Mayne, K. I., 1955, *Geochim. et Cosmochim. Acta*, **7**, 169.
Tilton, G. R., 1954, *Nuclear Geology*, Ed. H. Faul (New York : John Wiley), p. 70.
Tilton, G. R., Patterson, C. C., and Inghram, M. G., 1952, *Bull. Geol. Soc. Amer.*, **63**, 1305.
Tomlinson, R. H., and Das Gupta, A. K., 1953, *Canad. J. Chem.*, **31**, 909.
Urey, H. C., 1955, *Nature, Lond.*, **175**, 321.
Urry, W. D., 1941, *Phys. Rev.*, **59**, 479 ; 1942, *Amer. J. Sci.*, **240**, 426 ; 1948 a, *Trans. N.Y. Acad. Sci.*, **10**, 63 ; 1948 b, *J. Mar. Res.*, **7**, 618 ; 1949, *Amer. J. Sci.*, **247**, 257.
Vinogradov, A. P., Zadorozhnyi, I. K., and Zykov, S. I., 1952, *Doklady Akad. Nauk S.S.S.R.*, **85**, 1107.
Volchok, H. L., and Kulp, J. L., 1952, *Bull. Geol. Soc. Amer.*, **63**, 1386.
Waring, C. L., and Worthing, H., 1953, *Amer. Min.*, **38**, 827.
Wasserburg, G. J., and Hayden, R. J., 1955, *Geochim. et Cosmochim. Acta*, **7**, 51.
Wasserstein, B., 1951, *Nature, Lond.*, **168**, 380 ; 1954, *Ibid.*, **174**, 1004 ; 1955, *Ibid.*, **176**, 159.
Wetherill, G. W., 1953, *Phys. Rev.*, **92**, 907.
Wetherill, G. W., Aldrich, L. T., and Davis, G. L., 1955, *Geochim. et Cosmochim. Acta*, **8**, 171.
Whiting, F. B., 1950, *Ph.D. Thesis*, Massachusetts Institute of Technology.
Wickman, F., 1942, *Geol. Fören. Stockh. Förh.*, **64**, 465.
Wilgain, S., 1953, *Petite Thèse, Université Libre de Bruxelles*, as referred to by Houtermans (1954).
Wilson, J. T., Farquhar, R. M., Gretener, P., Russell, R. D., and Shillibeer, H. A., 1954, *Nature, Lond.*, **174**, 1006.
Yagoda, H., 1949, *Radioactive Measurements with Nuclear Emulsions* (New York : John Wiley).
Yagoda, H., and Kaplan, N., 1949, *Phys. Rev.*, **76**, 702.
Zeller, E. J., 1954, *Nuclear Geology*, Ed. H. Faul (New York : John Wiley), p. 180.

INFRA-RED ABSORPTION IN SEMICONDUCTORS

By H. Y. FAN
Purdue University, Lafayette, Indiana

CONTENTS

	PAGE
§ 1. Introduction	108
§ 2. Theory	110
2.1. General discussion	110
2.2. The absorption edge	111
2.3. Pressure and temperature dependence of the absorption edge	115
2.4. Absorption by free carriers	117
2.5. Localized states	120
§ 3. Methods of measurement	121
§ 4. Germanium and silicon	123
4.1. Absorption edge	123
4.2. Carrier absorption in germanium	128
4.3. Carrier absorption in silicon	132
4.4. Impurities and lattice defects in germanium	132
4.5. Impurities and lattice defects in silicon	137
4.6. Lattice absorption	139
§ 5. Indium antimonide	141
5.1. Absorption edge	141
5.2. Long wavelength absorption	145
5.3. Lattice absorption	146
§ 6. Tellurium	148
6.1. Absorption edge	148
6.2. Carrier absorption	151
Acknowledgments	153
References	153

Abstract. Infra-red absorption in semiconductors is classified into four different types according to the mechanism: (i) intrinsic absorption associated with electron excitation across the energy gap; (ii) absorption due to the presence of free carriers; (iii) absorption associated with impurities or lattice defects; and (iv) absorption associated with lattice vibration. A general introduction is followed by some theoretical discussions. Electron excitation between different energy bands is discussed with emphasis on the intrinsic absorption edge. For the absorption by free carriers, the effects of electron scattering by lattice vibration and by impurity centres are considered. Absorption associated with localized electronic states is briefly discussed. Experimental results are discussed for four different semiconductors: germanium, silicon, indium antimonide, and tellurium. All four types of absorption have been investigated to some extent for germanium and silicon. The work done on these materials provides a pattern for infra-red studies on semiconductors. The absorption edge in indium antimonide is affected by the carrier concentration. Long wavelength absorption shows interesting behaviour, and the observed effects attributed to lattice vibration have provided information regarding the type of binding in the crystal. Tellurium, having an optical axis, is doubly refracting. Both the absorption edge and the absorption associated with free carriers depend on the direction of polarization of the radiation.

§ 1. Introduction

Important information about a semiconductor may be obtained by studying its infra-red properties. In turn, semiconducting materials facilitate the study by the fact that samples may be prepared with properties varying over a wide range, e.g. the conductivity can be controlled by adding a small amount of impurity or by varying the temperature. It is, therefore, possible to correlate the infra-red properties with other properties of the material by studying different samples under various conditions. The wide interest in semiconducting materials, stimulated in part by the practical application, has led to extensive research, and infra-red measurements have become an essential part of the investigation.

The optical properties can be understood by considering the electronic energy bands of the material. The wave functions of electrons in the periodic potential field of a crystal can be expressed, according to Bloch, by

$$\psi_{\mathbf{k}m} = e^{i\mathbf{k}\mathbf{r}} u_{\mathbf{k}m}(\mathbf{r}), \qquad \ldots\ldots(1.1)$$

which is a plane wave of wave number vector $\mathbf{k}$, modulated by a function $u_{\mathbf{k}m}$ having the periodicity of the crystal lattice. Each wave function corresponds to an energy $E_m(\mathbf{k})$. The subscript m indicates the various wave functions or energies which correspond to the same value of $\mathbf{k}$. The energy levels corresponding to different values of $\mathbf{k}$ and the same subscript m constitute the mth energy band. All distinct solutions can be obtained by varying $\mathbf{k}$ within the range

$$-\pi < \mathbf{k}.\mathbf{a}_i < \pi, \qquad \ldots\ldots(1.2)$$

where $\mathbf{a}_i$ $(i = 1, 2, 3)$ are the three primitive translations of the lattice. The values of $\mathbf{k}$ are discrete, and the number of different values within this range is equal to the number of primitive cells in the crystal. Taking into account the choice of two spins, the number of electrons in each energy band is limited to twice the number of cells, according to the Pauli principle.

There are just enough electrons in a semiconductor to fill up a certain number of the energy bands. The highest band that can be filled is called the valence band, since it is occupied by the valence electrons. The next highest band, the conduction band, is separated from the valence band by an energy gap E_G which is of fundamental importance for a semiconductor. There are some electrons in the conduction band, conduction electrons, due to thermal excitation. There are also some vacancies or holes in the valence band. Electrons in a completely filled band do not contribute to current conduction. The conduction properties of a semiconductor are determined only by the conduction electrons and holes which are generally called free carriers. The product of hole and electron concentrations at any temperature is determined by the energy gap. In an intrinsic semiconductor, where the effect of impurities and lattice imperfections is small, the number of conduction electrons is equal to the number of holes in the valence band.

The energy gap in a semiconductor is much larger than kT at ordinary temperatures. Consequently, the intrinsic concentration of carriers is very small. Therefore, the carrier concentrations are sensitive to small amounts of impurities or imperfections in the lattice structure. These disturbance centres in the

periodic field of the crystal give rise to localized electronic states, which correspond to discrete energy levels within the energy gap. The presence of such energy levels upsets the balance between the hole and electron concentrations. A level is called a donor level if it does not affect the balance when it is occupied by an electron. An acceptor level, on the other hand, does not affect the balance when it is unoccupied. A centre may be referred to as a donor or an acceptor depending on the type of energy levels it is associated with; however, cases are known where a centre gives donor as well as acceptor levels.

Infra-red absorption in a semiconductor may be divided into four types according to the mechanism: (i) intrinsic absorption, (ii) carrier absorption, (iii) absorption involving localized states, and (iv) lattice absorption.

(i) *Intrinsic absorption.* By this we refer to the absorption due to the excitation of valence electrons to the conduction band across the energy gap. It is responsible for semiconductors being opaque and having metallic reflection in the optical region. At sufficiently long wavelengths where the photon energy is insufficient to excite the electrons across the energy gap, the absorption becomes small and the radiation can be transmitted by bulk samples. The wavelength at which this occurs is in the infra-red for most semiconductors and may be used to estimate the width of the energy gap. However, optical transitions are subject to certain selection rules and excitations from the top levels of the valence band to the bottom level of the conduction band may be forbidden. Therefore, the estimation of the energy gap from the absorption edge may not be quite straightforward.

(ii) *Carrier absorption.* The absorption produced by the small amount of free carriers may be observed in the infra-red beyond the edge of the intrinsic absorption. Optical transitions between two energy levels of the same band are forbidden by the selection rules. Therefore, free electrons can only be excited to energy bands above the conduction band and holes can only give rise to excitations of electrons from energy bands below the valence band. Unless the separations are small for the energy bands concerned, such excitations will not be possible in the infra-red region. The absorption by carriers depends then on the disturbances in the periodic structure of the crystal, due to lattice vibrations or impurities and lattice defects. Since these factors are also responsible for the resistivity of the material, there should be a correlation between the electrical properties and the carrier absorption. The problem is the same as infra-red absorption in metals. In some crystals there are a number of overlapping energy bands in the conduction or/and the valence band. In such cases, infra-red absorption due to interband excitations of free carriers is observed which gives useful information on the structure of energy bands.

(iii) *Localized states.* Electrons may be excited to or from localized states to either the conduction or the valence band. Also, bound electrons and holes may be excited to a higher bound state. In the former case, the absorption is accompanied by photoconductivity, since free carriers are produced. Since localized states are associated with energy levels within the energy gap, such excitations take place in the infra-red beyond the edge of the intrinsic absorption. Photoconductivity at long wavelengths is of considerable interest, as it can

be utilized to detect infra-red radiation. In general, absorption studies are important for impurity and imperfection centres. Energy levels and other information of interest may be deduced from such observations.

(iv) *Lattice absorption.* The spectrum of infra-red absorption bands due to the lattice vibration is useful for deducing the frequencies of vibration. The absorption is strong in ionic crystals due to the polarization associated with the displacement of the ions. The intensity of the absorption can be therefore an indication of the degree of ionic binding. Weak lattice absorption has also been observed in crystals of homopolar binding. The mechanism of absorption in these cases presents an interesting problem.

§ 2. Theory

2.1. *General Discussion*

The optical properties of a material are characterized by the refractive index n and the extinction coefficient k. We shall consider only non-magnetic materials, and assume for simplicity that the dielectric constant ϵ and the conductivity σ are scalar quantities, which is true for cubic crystals. Then

$$n^2 - k^2 = \epsilon = 1 + 4\pi\chi, \qquad \ldots\ldots(2.1)$$

$$nk\nu = \sigma. \qquad \ldots\ldots(2.2)$$

The conductivity is associated with energy absorption, and the susceptibility is associated with polarization, being equal to the polarizability if there is no internal field correction. Both electronic transitions and atomic vibration contribute to the conductivity and the susceptibility χ. The electrons may be divided into four groups: free carriers, electrons or holes bound to centres of lattice imperfection, electrons in the valence band, and inner core electrons. At the frequencies we are concerned with, the inner core electrons contribute a small, constant polarizability but do not cause absorption and, therefore, do not contribute to the conductivity. The effect of the free carriers will be discussed later. Since the effect of a few holes in the valence band will be included in the effect of free carriers, we consider now the contributions due to a fully occupied valence band.

Electrons in the filled valence band may make transitions to the higher energy bands. The transition probability between initial state a and final state b is determined by the matrix element $(\mathbf{p}.\mathbf{A})_{ba}$, where $\mathbf{A}$ is the vector potential of the radiation field and $\mathbf{p}$ is the momentum of the electron. For electrons in a periodic potential field, it can be shown by using (1.1) that the matrix element vanishes except when the condition for the wave number vectors,

$$\mathbf{k}_a - \mathbf{k}_b = \pm\,\mathbf{k}_\lambda, \qquad \ldots\ldots(2.3)$$

is satisfied. This selection rule corresponds to the condition of conservation of momentum. The wave number vector $\mathbf{k}_\lambda$ of the radiation is small for the wavelengths of interest, therefore the selection rule is approximately

$$\mathbf{k}_a = \mathbf{k}_b. \qquad \ldots\ldots(2.4)$$

The contribution of the electrons in the valence band to the susceptibility and the conductivity are given by (see, for example, Fröhlich 1936)

$$\chi_v = \frac{e^2}{4\pi^2 m} \sum_j \sum_{\mathbf{k}} \frac{f_{j\nu\mathbf{k}}}{\nu_{j\nu\mathbf{k}}^2 - \nu^2} = \frac{e^2}{4\pi^2 m} \sum_j \frac{f_{j\nu\mathbf{k}}}{\nu_{j\nu\mathbf{k}}^2 - \nu^2} n_v(\nu_{j\nu\mathbf{k}})\, d\nu_{j\nu\mathbf{k}}, \quad \ldots\ldots(2.5)$$

$$\sigma_v = \frac{e^2}{4m} f_{j\nu}(\nu)\, n_v(\nu). \quad \ldots\ldots(2.6)$$

Here, $h\nu_{j\nu\mathbf{k}}$ is the energy difference between the state of $\mathbf{k}$ in the jth energy band and the state of $\mathbf{k}$ in the valence band. The oscillator strength for the transition between these two levels is

$$f_{j\nu\mathbf{k}} = \frac{2}{3mh\nu_{j\nu\mathbf{k}}} |\mathbf{p}_{j\nu\mathbf{k}}|^2. \quad \ldots\ldots(2.7)$$

$n_v(\nu_{j\nu\mathbf{k}})\, d\nu_{j\nu\mathbf{k}}$ gives the number of states in the valence band per unit volume, for which the transition frequency lies in the range between $\nu_{j\nu\mathbf{k}}$ and $\nu_{j\nu\mathbf{k}} + d\nu_{j\nu\mathbf{k}}$. In the absorption process, the electron is excited from the level of $\mathbf{k}$ in the valence band to the level of $\mathbf{k}$ in the jth band. The condition for the conservation of energy requires

$$\nu_{j\nu\mathbf{k}} = \nu.$$

Therefore the conductivity σ_v is determined only by the oscillator strength and density of electrons corresponding to the frequency of radiation. For the dispersion, the excited state of the electron is involved as an intermediate state in the process, for which the conservation of energy is not required. Hence, terms corresponding to all values of $\nu_{j\nu\mathbf{k}}$ enter into χ_v.

The lower limit of $h\nu_{j\nu\mathbf{k}}$ must be equal to or higher than the width of the energy gap E_G. For lower frequencies $\sigma_v = 0$. The concentrations of free carriers and imperfection centres are relatively small. The atomic vibrations give absorption only in certain frequency regions and the absorption is weak except for crystals of appreciable heteropolar binding. In general, the absorption in a semiconductor becomes very small when $\sigma_v = 0$. Regarding the susceptibility, the contribution of the valence electrons approaches a constant value χ_{v0} as the frequency becomes small compared with the lower limit of $\nu_{j\nu\mathbf{k}}$. The contributions of the free and the bound carriers are usually negligible in the infra-red region. When the effect of the lattice vibrations is small, as in homopolar crystals, the refractive index approaches a constant value at long wavelengths in the infra-red,

$$n^2 \simeq \epsilon = 1 + 4\pi(\chi_{v0} + \chi_c) \quad \ldots\ldots(2.8)$$

where χ_c is the contribution of the inner core electrons.

2.2. *The Absorption Edge*

On account of the selection rule (2.4), the low-frequency limit for electron transitions between the valence band and the conduction band corresponds to the width of the energy gap only when the lowest level of the conduction band and the highest level of the valence band have the same wave number vector $\mathbf{k}_0$.

Consider first this simple case. Assume for simplicity that $\mathbf{k}_0 = 0$ and that the energy can be expressed by

$$E(\mathbf{k}) = E_c + (\hbar^2/2m_e)\,k^2 \qquad \ldots\ldots(2.9)$$

near the bottom E_c of the conduction band and by

$$E(\mathbf{k}) = E_v - (\hbar^2/2m_h)\,k^2 \qquad \ldots\ldots(2.10)$$

near the top E_v of the valence band. m_e and m_h are the effective masses of conduction electrons and holes, respectively. Then we have near the absorption edge

$$h\nu_{cv\mathbf{k}} = E_G + [\hbar^2(m_e+m_h)/2m_e m_h]\,k^2 = E_G + (\hbar^2/2m_r)\,k^2. \qquad \ldots\ldots(2.11)$$

We get from this expression the number of $\mathbf{k}$ vectors corresponding to the frequency range $h\nu$ to $h(\nu+d\nu)$. Multiplying by 2 to take into account both spins, we get

$$n_v(\nu)\,d\nu = \frac{(2m_r)^{3/2}}{\pi\hbar^2}\,(h\nu - E_G)^{1/2}\,d\nu. \qquad \ldots\ldots(2.12)$$

Using wave functions (1.1) with $u(\mathbf{r})$ normalized for unit cell, the matrix element in (2.7) can be shown to be

$$\mathbf{p}_{cv\mathbf{k}} = \frac{\hbar}{i}\left[\int u_{\mathbf{k}v}^{*}\,\mathrm{grad}\,u_{\mathbf{k}c}\,d\tau - i\mathbf{k}\int u_{\mathbf{k}c}^{*}\,u_{\mathbf{k}v}\,d\tau\right] \qquad \ldots\ldots(2.13)$$

where the integrations are over the volume of a unit cell. The second term vanishes on account of the orthogonality of the wave functions $\psi_{\mathbf{k}c}$ and $\psi_{\mathbf{k}v}$, which is the same as the orthogonality of $u_{\mathbf{k}c}$ and $u_{\mathbf{k}v}$. In so far as the initial and final wave numbers actually differ by $\mathbf{k}_\lambda$, we should get a small contribution from the second term. Using (2.11), (2.12), and (2.7), we get from (2.6)

$$\sigma = \frac{e^2}{6\pi m^2}\,\frac{(2m_r)^{3/2}}{\hbar^2}\,|\,\mathbf{p}_{cv}(\nu)\,|^2\,\frac{(h\nu - E_G)^{1/2}}{h\nu} \qquad \ldots\ldots(2.14)$$

where $|\,\mathbf{p}_{cv}(\nu)\,|^2$ is the average of $|\,\mathbf{p}_{cv\mathbf{k}}\,|^2$ over the values of $\mathbf{k}$ which correspond to the transition frequency ν. Normally the first term in (2.13) should be the dominant term and would not be expected to vary very rapidly with ν. Near the absorption edge, the frequency dependence of $\sigma\nu$ should be controlled by $(h\nu - E_G)^{1/2}$. If plane waves instead of (1.1) were used as an approximation for the electron wave functions, the first term in (2.14) would vanish and the matrix element would be simply $\hbar\mathbf{k}$, giving

$$\sigma = \frac{e^2}{6\pi m^2}\,\frac{(2m_r)^{3/2}}{\hbar^2}\,\frac{(h\nu - E_G)^{3/2}}{h\nu}. \qquad \ldots\ldots(2.15)$$

The discussion regarding (2.13) shows that the use of plane waves may not be a good approximation for this calculation.

Indirect transitions. Even with the lowest level of the conduction band and the highest level of the valence band at different values of $\mathbf{k}$, fairly strong absorption may begin at $h\nu = E_G$ due to violation of the selection rule which applies strictly only to perfect crystals. The effect of perturbation due to lattice vibration was treated by Cheeseman (1952), and by Hall, Bardeen and Blatt (1954)

with regard to germanium and silicon. The absorption process is accompanied by the emission or absorption of a phonon or a quantum of lattice vibration. The condition for the conservation of momentum is

$$\mathbf{k}_a = \mathbf{k}_b \pm \mathbf{q}, \qquad \ldots\ldots(2.16)$$

instead of (2.4). $\mathbf{q}$ is the wave number vector of the phonon. The plus and minus signs apply, respectively, to the emission and the absorption of a phonon. The condition for the conservation of energy is

$$\hbar\omega = E_b - E_a \mp \hbar\omega_q. \qquad \ldots\ldots(2.17)$$

Consider, for example, the energy band structure of germanium shown in figure 1 (or that of silicon in figure 2). The top of valence band E_v is at $\mathbf{k} = 0$,

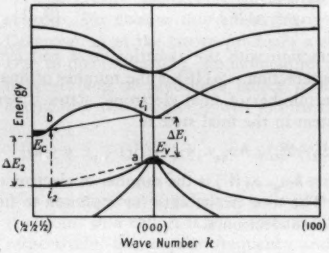

Figure 1. Schematic diagram of energy band contours in germanium along [111] and [100] axes in $\mathbf{k}$ space. E_c is the lowest energy of the conduction band. E_v is the highest energy of the valence band. (*After* Herman 1954.)

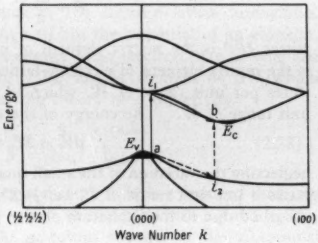

Figure 2. Schematic diagram of energy band contours in silicon along [111] and [100] axes in $\mathbf{k}$ space. E_c is the lowest energy of the conduction band. E_v is the highest energy of the valence band. (*After* Herman 1954.)

whereas the lowest energy E_c of the conduction band corresponds to eight equivalent wave vectors along the $\langle 111 \rangle$ directions. We shall denote by δ the number of minima in the conduction band. Let the energy near E_v in the valence band be expressed by (2.10) and the energy in the conduction band be given by

$$E = E_c + \frac{\hbar^2}{2}\left[\frac{(\Delta k_1)^2}{m_1} + \frac{(\Delta k_2)^2}{m_2} + \frac{(\Delta k_3)^2}{m_3}\right]. \qquad \ldots\ldots(2.18)$$

The corresponding numbers of states (for either spin) per unit energy range are

$$\rho_c(E) = \frac{V}{4\pi^2}\left(\frac{2m_c}{\hbar^2}\right)^{3/2}(E - E_c)^{1/2}$$
$$\rho_v(E) = \frac{V}{4\pi^2}\left(\frac{2m_v}{\hbar^2}\right)^{3/2}(E_v - E)^{1/2}, \qquad \ldots\ldots(2.19)$$

where $m_c = \delta^{2/3}(m_1 m_2 m_3)^{1/3}$ and V is the volume of the crystal.

Absorption at $\hbar\omega \sim E_G$ corresponds to the excitation of valence electrons with $E_a \sim E_v$ to energy levels $E_b \sim E_c$. The absorption may be accomplished by two processes: A. The electron is optically excited from a to i_1, followed by the

transition from i_1 to b with phonon interaction. B. An electron is excited from i_2 to b, followed by the transition of the electron at a to the hole at i_2. The energy W of the system, the crystal and radiation field, is not conserved in the intermediate state

$$(W_1 - W_0)_A = (E_{i_1} - E_a) - \hbar\omega \sim \Delta E_1 - \hbar\omega$$
$$(W_1 - W_0)_B = (E_b - E_{i_2}) - \hbar\omega \sim \Delta E_2 - \hbar\omega. \qquad \ldots\ldots(2.20)$$

Each of the processes A and B may involve either the absorption or the emission of a phonon. There are thus essentially four different processes leading to the excitation of an electron from a to b. Therefore the probability for a photon to be absorbed by the excitation is

$$P = \frac{2\pi}{\hbar} \sum_1^4 \frac{H^{(1)} H^{(\nu)2}}{(W_1 - W_0)^2} \rho_f(W) \qquad \ldots\ldots(2.21)$$

where $H^{(\nu)}$ is the matrix element of interaction with the radiation field and $H^{(1)}$ is the matrix element of electron–lattice interaction. $\rho_f(W)$ is the number of final states per unit range of W, which is the number of final electronic states b per unit range of W. The energy of the system in the final state is

$$W_f = W_0 + (E_b - E_a) \pm \hbar\omega_q$$

neglecting the variation of the small quantity $\hbar\omega_q$, $\rho_f(W)$ is the number of electronic states b per unit range of E, i.e. $\rho_c(E)$. The total probability for a photon to be absorbed due to the excitation of any valence electron is

$$P_a = 2\int_0^{\hbar\omega - E_G} P \rho_v(E)\, d(E_v - E). \qquad \ldots\ldots(2.22)$$

For $\hbar\omega \sim E_G$, the phonon wave numbers involved are close to the electron wave number corresponding to E_c, according to (2.16). Therefore $H^{(1)}$ given by (2.28) can be taken as a constant and written in the form

$$|H^{(1)}|^2 = M^2_{\mathbf{q}-\mathbf{k}_c} \Big|_{n_q+1}^{n_q}. \qquad \ldots\ldots(2.23)$$

The process A involves M_c^2 for the conduction band, and the process B involves M_v^2 for the valence band; the two quantities may have different values.

The quantity $H^{(\nu)}$ is determined by the matrix element (2.13). If the electron wave functions are approximated by plane waves, $\mathbf{p}_{cvk} = \hbar\mathbf{k}$ and $H^{(\nu)}$ is given by (2.39) with m in place of m^*. Using (2.19), (2.20) and (2.23), we get from (2.22)

$$P_a = \frac{K}{\hbar\omega}\left[\frac{M_c^2}{(\Delta E_1 - \hbar\omega)^2} m_v (\hbar\omega \pm \hbar\omega_q - E_G)^3 + \frac{M_v^2}{(\Delta E_2 - \hbar\omega)^2} (\hbar k_c)^2 (\hbar\omega \pm \hbar\omega_q - E_G)^2\right]_{n_q}^{n_q+1}. \qquad \ldots\ldots(2.24)$$

The plus sign and $n_q + 1$ correspond to phonon emission, while the minus and n_q correspond to phonon absorption. The expression is the sum of four terms. It reduces to the form obtained by Hall, Bardeen and Blatt originally, if $M_c^2 = M_v^2$ and $\Delta E_1 = \Delta E_2$ are assumed and $\hbar\omega_q$ is neglected. The constant K is

$$K = \frac{1}{\epsilon} \frac{\delta}{48\pi} \frac{e^2\hbar}{m^2} \left(\frac{2m_v}{\hbar^2}\right)^{3/2} \left(\frac{2m_c}{\hbar^2}\right)^{3/2}. \qquad \ldots\ldots(2.25)$$

We have pointed out in connection with (2.15) that free electron approximation is not satisfactory for such calculation. Putting $\mathbf{p}_k = \mathbf{p}_0$ for the process A and $\mathbf{p}_k = \mathbf{p}_{k_c}$ for the process B, we get

$$P_a = \frac{K}{\hbar\omega}\left[\frac{M_c^2 |\mathbf{p}_0|^2}{(\Delta E_1 - \hbar\omega)^2} + \frac{M_v^2 |\mathbf{p}_{k_c}|^2}{(\Delta E_2 - \hbar\omega)^2}\right](\hbar\omega \pm \hbar\omega_q - E_G)^2 \begin{Bmatrix} n_q + 1 \\ n_q \end{Bmatrix}. \quad \ldots\ldots(2.26)$$

The conductivity is related to P_a by

$$\sigma = (\epsilon/4\pi) P_a. \quad \ldots\ldots(2.27)$$

2.3. *Pressure and Temperature Dependence of the Absorption Edge*

The energy gap may change with the pressure or the temperature of the crystal. To discuss this effect, let us consider the electron–lattice interaction. Deformation of the lattice produces a change ΔU in the potential of an electron. Due to this interaction, the momentum and energy of an electron may be changed by absorbing or exciting a lattice phonon. The matrix element of ΔU which determines the process is well known from the theory of conductivity

$$[(\mathbf{k} \pm \mathbf{q}, n_q \mp 1)|\Delta U|(\mathbf{k}, n_q)] = \mp i(MN)^{-1/2}\frac{2}{3}Cq\left(\frac{\hbar}{2\omega_q}\right)^{1/2}\begin{Bmatrix} n_q^{1/2} \\ (n_q+1)^{1/2} \end{Bmatrix}. \quad \ldots\ldots(2.28)$$

N is the number of primitive cells in the crystal lattice, M is a reduced mass for the atoms in a cell, $\mathbf{q}$ is the wave number vector of the phonon. ω_q and n_q are, respectively, the angular frequency and the quantum number of the vibrational mode. The upper signs and $n_q^{1/2}$ apply to phonon absorption while the lower signs and $(n_q+1)^{1/2}$ apply to phonon emission. C is an integral, the evaluation of which requires the knowledge of ΔU and the electronic wave functions. The change of momentum or scattering of the carriers due to the interaction with lattice vibration contributes to the resistivity of the crystal. For a classical gas of carriers, the mobility as determined by the lattice vibration is

$$\mu = 3(\pi/2)^{1/2} e\hbar^4 s\rho[(kT)^{3/2} m^{*5/2} C^2]^{-1} \quad \ldots\ldots(2.29)$$

where s is the velocity of elastic waves and ρ is the density of the crystal.

Lattice dilatation. The energy levels in a crystal are naturally functions of the interatomic distance. For small dilatations Δ of the lattice, an energy level may be assumed to vary linearly with Δ:

$$E = E_0 + E_1\Delta; \quad \ldots\ldots(2.30)$$

the coefficient E_1 may be different for different levels. Let E_{1c} and E_{1v} be the coefficients for the levels close to the bottom of the conduction band and the top of the valence band, respectively. In non-polar crystals, carrier scattering is produced mainly by the acoustical modes of lattice vibration. Furthermore, the vibrational modes effective in the scattering of an electron have wave numbers of the same order of magnitude as the wave number of the electron. For carriers of thermal energy, the effective vibrational modes have very long wavelengths compared with the dimension of a unit cell. Bardeen and Shockley (1950) pointed out that such vibrations produce lattice deformations uniform in many cells,

therefore the perturbation potential Δu is the same as $E_1\Delta$. They showed that E_1 is related to the parameter C in (2.29) by

$$E_1 = \tfrac{2}{3}C. \qquad \ldots\ldots(2.31)$$

Thus the magnitude of E_1 can be deduced from the experimental value of mobility which involves E_1^2. The effect of lattice dilatation on the energy gap is

$$\Delta E_G = (E_{1c} - E_{1v})\Delta. \qquad \ldots\ldots(2.32)$$

This relation provides a check between the carrier mobilities and ΔE_G although neither the magnitude nor the sign of ΔE_G can be determined from the mobilities, on account of the uncertainty about the signs of E_{1c} and E_{1v}.

Lattice vibration. Lattice dilatation should be mainly responsible for any pressure effect on the energy gap. When the temperature is varied, however, not only the lattice dimension but also the intensity of lattice vibration is changed, which may affect the energy levels and give an additional effect of temperature on the absorption edge. Theoretical treatment of this effect, in which energy level broadening was calculated, gave estimates of the right order of magnitude for ionic crystals but too small for non-polar materials. Fan (1950) treated the problem by calculating the shift of energy levels and obtained reasonable estimates of the effect for germanium and silicon. A similar treatment was given independently by Muto and Oyama (1950).

Energy levels and wave functions for a lattice of fixed atoms are changed when the atoms are in vibration. The perturbed wave functions change the transition probability between two levels. This effect has been treated above as indirect transitions. In fact, such transitions can be calculated as direct transitions in the perturbed lattice, if the perturbed wave functions were determined. In the present problem we are interested in the change of energy which will be calculated by the perturbation method. The matrix element of the perturbation potential is given by (2.28). The diagonal elements are equal to zero, giving zero perturbation energy in the first-order approximation. In the second-order approximation, the electron–lattice interaction energy of the crystal is

$$W_1 = \sum_{\mathbf{k},m} \sum_{\mathbf{q},m'} \frac{[(\mathbf{k}\pm\mathbf{q}, m';\ n_\mathbf{q} \mp 1)\,|\Delta U|\,(\mathbf{k}, m;\ n_\mathbf{q})]^2}{E(\mathbf{k}, m) - [E(\mathbf{k}+\mathbf{q}, m') \mp h\omega_\mathbf{q}]} \qquad \ldots\ldots(2.33)$$

where the index m indicates the energy band. The summation over $\mathbf{k}$ and m covers all states occupied by an electron, whereas the summation over $\mathbf{q}$ and m' is limited by the requirement that $(\mathbf{k}\pm\mathbf{q}, m')$ must be an unoccupied state. When an additional electron is introduced in the lowest level of the conduction band and an additional hole is introduced in the top level of the valence band at the same time, there is a change in W_1, with the quantum numbers $n_\mathbf{q}$ of lattice vibration remaining the same. Due to this change of interaction energy, which we shall denote by E_{1G}, the threshold energy for optical transitions is

$$E_t = E_G + E_{1G}, \qquad \ldots\ldots(2.34)$$

E_G being the energy gap in the lattice with atoms fixed at their equilibrium positions.

The calculations were made under the following assumptions: (i) Both the conduction band and the valence band have spherical constant energy surfaces in $\mathbf{k}$ space. (ii) Only terms with $m' = m$ in (2.33) are taken, assuming that the

denominator is large for $m' \neq m$. This may not be a good approximation when there are overlapping bands near the edges of the energy gap. (iii) Only acoustical modes of vibration are taken into account. With these assumptions we get

$$E_{iG} = -\frac{1}{(2\pi)^3}\frac{4}{9}\frac{1}{\rho\hbar s}(m_c C_c^2 + m_v C_v^2)\left(\frac{kT}{\hbar s}8\pi q_m + 2\pi q_m^2\right) = E_{iG0} + E_{iG1}T \qquad \ldots\ldots(2.35)$$

for temperature $kT > \hbar s q_m$, where q_m is the maximum reduced wave number of the lattice. For temperature $kT < \hbar s q_m$, E_{iG} no longer varies linearly with T but approaches E_{iG0} more rapidly with decreasing temperature. Thus for sufficiently high temperatures, the effective energy gap may be expressed by

$$E_t = E_0 + (\partial E_t/\partial P)_T P + [(\partial E_t/\partial T)_v - (\beta/\chi)(\partial E_t/\partial P)_T]\,T \qquad \ldots\ldots(2.36)$$

with $\quad E_0 = E_{G0} + E_{iG0}, \qquad (\partial E_t/\partial P)_T = \chi(E_{1c} - E_{1v}), \qquad (\partial E_t/\partial T)_v = E_{iG1},$

where χ is the compressibility and β is the thermal coefficient of volume expansion.

It should be pointed out that each of the effective masses, m_c and m_v, which determine E_{iG1} characterizes the entire band. On the other hand, the effective mass of carriers is determined only by the band edge. The assumption (i) used in deriving (2.35) implies that the effective mass is a constant of the band and inversely proportional to the band width. With an effective mass equal to the free electron mass, this assumption would give about 10 ev for the width of the band. This assumption is a poor approximation in some cases, where the carrier effective mass is small and the width of the band is estimated to be small also. Each of the effective masses in E_{iG1} is actually a measure of $1/E$ averaged over all states in the band, and in such cases the values of m_c and m_v to be used for calculating E_{iG1} should be much higher than the effective masses of carriers.

It is important to note that, in thermal equilibrium, the energy associated with a hole–electron pair due to the existence of the energy gap is not E_t. Because of the electron–lattice interaction E_{iG}, the energy per hole–electron is not the same as the energy required to produce the pair without changes in the lattice quantum numbers n_q. It has been shown by James (1954) that E_t is equal to F_G, the free energy associated with a hole–electron pair due to the energy gap. F_G determines the carrier concentrations and may be called the intrinsic activation energy. In an intrinsic semiconductor the concentration n_i of hole–electron pairs is given by

$$n_i^2 = N_c N_v \exp(-F_G/kT) \qquad \ldots\ldots(2.37)$$

where N_c and N_v are the densities of states in the conduction band and the valence band, respectively.

2.4. *Absorption by Free Carriers*

The effect of carriers with a relatively small concentration can be observed only beyond the edge of intrinsic absorption for $\hbar\omega < E_t$. In the absorption process, the carriers either remain in the same energy band or make transitions to another band. In the latter case, the separation between the two bands must be smaller than E_t. Such absorption has been found in germanium due to the overlapping of energy bands in the valence band. The absorption due to interband transitions has been considered in § 2.1 and the specific considerations

involved in dealing with carriers will be discussed in connection with the absorption in germanium. We shall consider now the absorption in which the carriers remain in the same band and shall refer to it as the free carrier effect.

In an unperturbed periodic lattice, electrons cannot absorb radiation energy and remain in the same energy band on account of the selection rule (2.4). Absorption arises through the interaction of electrons with the lattice perturbed by vibrations or imperfections, just as the indirect interband transitions discussed previously. Optical phenomena associated with conduction electrons have been treated quantum-mechanically by Kronig (1931). The free electron effect corresponds to a resonance frequency equal to zero. The absorption is obtained by introducing a broadening of the resonance, which is equivalent to the introduction of a damping factor for electron oscillation in the classical Drude theory. The same formula for conductivity is obtained

$$\sigma = \frac{n_e e^2}{m^*} \frac{1/\tau}{\omega^2 + (1/\tau)^2} = \frac{\sigma_0}{\tau^2\omega^2 + 1} \simeq \frac{\sigma_0}{\tau^2\omega^2} \qquad \ldots\ldots(2.38)$$

with effective mass m^* replacing the free electron mass. n_e is concentration of free electrons. The quantity $1/\tau$ is estimated by assuming that σ_0 is the d.c. conductivity; usually $\tau^2\omega^2 \gg 1$. The use of a constant $1/\tau$ for all electrons is a rough approximation. Furthermore, the electron–lattice interaction in an absorption process cannot be inferred directly from the d.c. conductivity which is concerned with electrons of thermal energy. Therefore the essentially classical expression (2.38) is not satisfactory. More rigorous treatment depends on the mechanism of interaction, of which lattice vibration and impurity atoms are usually the most important. Theory has been worked out for each of these effects (Fan and Becker 1951), the theory for the effect of lattice vibration being due to H. Fröhlich.

Lattice vibration. The effect of lattice vibration can be treated in the same way as the indirect interband transition, using second-order time dependent perturbation method. The matrix element for the perturbation due to radiation field is

$$H^{(r)} = -(V\epsilon)^{-1/2}(e\hbar^2/m^*)(2\pi/\hbar\omega)^{1/2} k \cos(\mathbf{p}_\lambda, \mathbf{k}) \qquad \ldots\ldots(2.39)$$

where $\mathbf{p}_\lambda$ is the direction of polarization, and the radiation field is normalized for one photon in the volume V of the crystal.

As discussed previously, there are four processes of absorption corresponding to photon absorption followed by phonon emission or absorption and photon absorption preceded by the two alternatives of phonon interaction. Let subscripts 0, i and f refer to the initial, intermediate and final states respectively. For the two processes with photon absorbed first, the conditions for the wave vectors and the energies are

$$\mathbf{k}_i = \mathbf{k}_0, \mathbf{k}_f = \mathbf{k}_0 \mp \mathbf{q}, \quad W_i - W_0 = -\hbar\omega. \qquad \ldots\ldots(2.40)$$

For phonon interaction preceding, the conditions are

$$\mathbf{k}_i = \mathbf{k}_0 \mp \mathbf{q}, \quad \mathbf{k}_f = \mathbf{k}_i, \quad W_i - W_0 = \frac{\hbar^2}{2m^*}(k_i^2 - k_0^2) \pm \hbar\omega\mathbf{q}. \qquad \ldots\ldots(2.41)$$

The upper sign in these equations corresponds to phonon emission whereas the lower sign corresponds to phonon absorption; $\mathbf{q}$ is the wave number vector of the phonon involved. The energy of the final state is

$$W_f = W_0 + \frac{\hbar^2}{2m^*}(k_f^2 - k_0^2) \pm \hbar\omega_q - \hbar\omega. \qquad \ldots\ldots(2.42)$$

The number of $\mathbf{q}$ values in a volume $d\Omega_q$ in $\mathbf{q}$ space is $Vd\Omega_q/(2\pi)^3$, therefore the number of final states per unit energy range is

$$\rho_f(W) = \frac{V}{(2\pi)^3}\frac{d\Omega_q}{dW_f} = \frac{V}{(2\pi)^3}\frac{m^* q}{\hbar^2 k_0}\,dq\,d\phi. \qquad \ldots\ldots(2.43)$$

The matrix element for the perturbation by lattice vibration $H^{(1)}$ is given by (2.28). The quantum number of a lattice vibrational mode is

$$n_q = [\exp(\hbar\omega_q/kT) - 1]^{-1}. \qquad \ldots\ldots(2.44)$$

Considering only acoustical modes, we have $\hbar\omega_q = \hbar sq$. The maximum of q in the absorption process is determined by (2.42). Under normal conditions $\hbar\omega_q \ll kT$, and the approximation $n_q = kT/\hbar sq$ can be used.

Substituting the various expressions in (2.21) and integrating over dq and $d\phi$, we get the absorption probability for a photon due to the excitation of an electron of initial energy E_k. The result is averaged over the energy distribution of the electrons and multiplied by the total number of electrons. Thus we get the total absorption probability of a photon

$$P_a = \frac{16}{27} n_e \frac{e^2 C^2 (2m^*)^{1/2}}{\epsilon\rho\hbar^2 s^2} \frac{kT}{(\hbar\omega)^{3/2}} \left\langle \left(1 + \frac{2E_k}{\hbar\omega}\right)\left(1 + \frac{E_k}{\hbar\omega}\right)^{1/2} \right\rangle, \qquad \ldots\ldots(2.45)$$

which gives the conductivity according to (2.27). Using the expression (2.29) for the mobility $\mu = \sigma_0/en_e$, we get

$$\sigma = \frac{4}{9\pi^{1/2}} \frac{\sigma_0}{\tau^2\omega^2} \left(\frac{\hbar\omega}{kT}\right)^{1/2} \left\langle \left(1 + \frac{2E_k}{\hbar\omega}\right)\left(1 + \frac{E_k}{\hbar\omega}\right)^{1/2} \right\rangle, \qquad \ldots\ldots(2.46)$$

where the relaxation time τ is defined as $\mu m^*/e$. The electron energy E_k is of the order of kT for classical distribution. For $\hbar\omega > kT$, this equation gives a conductivity proportional to $\omega^{-1.5}$ instead of ω^{-2} according to (2.38).

Impurity scattering. Impurity atoms and lattice defects act as scattering centres for the conduction electrons, thereby enabling them to give absorption. We shall consider electrically charged centres, since they give much stronger scattering. These will be treated as point charges in a medium having the dielectric constant of the crystal. The problem could be treated in the same manner as for the preceding case. We can simplify the calculation by noting that such absorption is essentially the inverse process of bremsstrahlung which Sommerfeld (1931) has treated by first-order perturbation method, using wave functions of electrons scattered by a Coulomb potential. The matrix elements of the dipole moment averaged over the directions of the electron wave vector is given by

$$M_{0f}^2 = \frac{e^2}{V}\frac{2(4\pi)^2}{3}\left(\frac{Ze}{\epsilon}\right)^2 \left(\frac{\hbar^2}{2m^*}\right)^2 \frac{1}{(\hbar\omega)^4}\frac{1}{k_0 k_f} \ln\left(\frac{k_f + k_0}{k_f - k_0}\right). \qquad \ldots\ldots(2.47)$$

Using this expression, the absorption probability of a photon due to a conduction electron in the potential field of a single scattering centre can be readily calculated. Ordinarily the scattering centres are separated far enough to be considered independently. Multiplying the result by the number of scattering centres and integrating over the distribution of electrons, we get

$$P_a = \frac{N_i n_e}{\epsilon} \frac{16\pi^2}{3} \left(\frac{Ze}{\epsilon}\right)^2 \frac{e^4\hbar}{m^*(\hbar\omega)^3} \left\langle \frac{1}{k_0} \ln\left(\frac{k_f + k_0}{k_f - k_0}\right) \right\rangle, \qquad \ldots\ldots(2.48)$$

in which the wave numbers of the electron before and after absorption are related by

$$(\hbar^2/2m^*)\, k_f^2 = (\hbar^2/2m^*)\, k_0^2 + \hbar\omega. \qquad \ldots\ldots(2.49)$$

For electrons obeying classical distribution,

$$\left\langle \frac{1}{k_0} \ln\left(\frac{k_f + k_0}{k_f - k_0}\right) \right\rangle = 2\hbar(2\pi m^* kT)^{-1/2} \exp(\hbar\omega/2kT)\, K_0(\hbar\omega/2kT) \qquad \ldots\ldots(2.50)$$

where K_0 is the modified Bessel function of order zero. This result gives a stronger frequency dependence of absorption than either the effect of lattice vibration or the semi-classical expression (2.38). For $\hbar\omega > kT$,

$$P_a \simeq \frac{N_i n_e}{\epsilon} \frac{16\sqrt{2\pi^2}}{3} \left(\frac{Ze}{\epsilon}\right)^2 \frac{e^4\hbar^2}{m^{*3/2}(\hbar\omega)^{3.5}}. \qquad \ldots\ldots(2.51)$$

More recently, the same result has been obtained by Wolfe (1954). An expression was also obtained, using a screened Coulomb potential to take into account the screening of charged centres by the conduction electrons. The expression is in the form of an integral which is difficult to evaluate. The screening should be weak for the electron concentrations normally found in semiconductors.

2.5. *Localized States*

The general problem of localized states associated with lattice imperfections is difficult to treat theoretically. There is one type of localized states which can be treated approximately, i.e. levels very close to the edge of either the conduction band or the valence band. Substitutional impurity atoms, which are close to the regular atoms in valency, usually give rise to such levels. The wave function of the impurity state can be approximated by the crystal wave function for the band edge, modulated by a function which is the solution of the Schrödinger equation for the perturbing potential of the impurity atom. The effective mass of the carriers is used in the equation instead of the free electron mass. With small binding energy, the radius orbit of the impurity state is many times the interatomic distance and the perturbation potential can be taken as the Coulomb potential of a charged centre in a medium having the dielectric constant of the crystal. When the effective mass is a scalar quantity the problem reduces to that of a hydrogenic atom with an ionization energy

$$E_i = (m^*/m)\, E_H/\epsilon^2 \qquad \ldots\ldots(2.52)$$

E_H being the ionization energy of hydrogen. Neglecting the effect of the periodic variation of the crystal wave function given by $u_k(\mathbf{r})$ in (1.1), the absorption is

the same as for the hydrogenic atom. For photo-ionization, the cross section for absorption can be written (see, for example, Hall 1936)

$$\frac{\alpha}{N} = \frac{1}{n}\frac{2^{10}\pi^2}{3}\frac{\hbar e^2}{m^* c E_1}\left(\frac{\nu_1}{\nu}\right)^4 f\left(\frac{\nu-\nu_1}{\nu}\right) \qquad \ldots\ldots(2.53)$$

$$f(x) = \exp(-4x\tan^{-1}x)/[1-\exp(-2\pi x)]$$

where α is the absorption coefficient, N is the concentration of impurity atoms, n is the refractive index of the crystal, E_1 is the ionization energy of the impurity state and ν_1 is the corresponding frequency. Near the threshold frequency ν_1

$$\frac{\alpha}{N} = \frac{6.31\times10^{-18}}{n}\frac{m}{m^*}\frac{E_H}{E_1}\left(\frac{\nu_1}{\nu}\right)^{8/3}. \qquad \ldots\ldots(2.54)$$

For $\nu \gg \nu_1$,

$$\frac{\alpha}{N} = \frac{5.26\times10^{-17}}{n}\frac{m}{m^*}\frac{E_H}{E_1}\left(\frac{\nu_1}{\nu}\right)^{3.5}. \qquad \ldots\ldots(2.55)$$

The effective mass is not a scalar quantity in the conduction band of silicon and germanium. Furthermore, there are several states with different wave numbers which correspond to the lowest energy of the band. Also, the top of the valence band at $\mathbf{k} = 0$ is degenerate. The solution of the effective-mass wave equation is therefore more complicated. The problem has been treated recently by a number of authors (Kittel and Mitchell 1954, Lampert 1955, Luttinger and Kohn 1955, Kohn and Luttinger 1955). The wave functions obtained from these solutions can be used to calculate the absorption (Kohn 1955). Kohn and Luttinger have also examined the effect of the fact that the effective mass treatment breaks down in the immediate neighbourhood of the impurity.

For localized states far removed from either band edge, the effective mass formalism is not applicable. Koster and Slater (1954) have discussed general methods for treating impurity levels. Calculations have to be made for each kind of impurity or lattice imperfection.

§ 3. Methods of Measurement

In most cases, the interest is in the absorption edge and the absorption at long wavelengths. The absorption is usually weak enough to be determined by the measurement of transmission through bulk samples (Fan and Becker 1951). The measurement gives the absorption coefficient α which is related to the extinction coefficient k by

$$\alpha = \frac{4\pi k}{\lambda} = \frac{4\pi\sigma}{cn}. \qquad \ldots\ldots(3.1)$$

For some crystals, slabs of several microns in thickness can be readily prepared and absorption coefficient over 10^3 cm^{-1} can be measured. The quantity measured is the ratio of incident and transmitted intensities I/I_0. For monochromatic radiation

$$\frac{I}{I_0} = \frac{(1-R)^2+4R\sin^2\psi}{e^{\alpha d}+R^2e^{-\alpha d}-2R\cos 2(\phi+\psi)} \qquad \ldots\ldots(3.2)$$

where d is the sample thickness, R is the reflectivity, and

$$\phi = \frac{4\pi nd}{\lambda}, \quad \psi = \tan^{-1}\frac{2k}{n^2+k^2-1}. \qquad \ldots\ldots(3.3)$$

The term $2R\cos 2(\phi+\psi)$ gives a variation of I/I_0 with wavelength which is the interference effect. It can be avoided for a given thickness of the sample by using a sufficiently broad band of radiation. It can be readily shown that under such conditions

$$\frac{I}{I_0}=\frac{(1-R)^2+4R\sin^2\psi}{e^{\alpha d}-R^2e^{-\alpha d}}. \qquad \ldots\ldots(3.4)$$

The value of ψ is small, since for $\alpha<10^3$ cm^{-1} the value of k is much smaller than one. Therefore the term $4R\sin^2\psi$ can usually be neglected.

The reflectivity of the material is determined by

$$R=\frac{(n-1)^2+k^2}{(n+1)^2+k^2}. \qquad \ldots\ldots(3.5)$$

Actually the reflectivity depends on the surface condition. Usually sample surfaces are polished. It has been found for a number of materials that with a good polish the reflectivity can be made to be close to the value given by this expression, corresponding to the optical constants of the crystal. For the purpose of determining the absorption coefficient, it is only necessary that sample surfaces can be prepared with reproducible reflectivity. Then the absorption coefficient and the surface reflectivity can be determined by varying the thickness of the sample. High values of I/I_0, corresponding to small αd, approach $(1-R)/(1+R)$, whereas low values of I/I_0 vary almost exponentially with αd and extrapolate to $(1-R)^2$ at $d=0$.

The refractive index can be obtained from reflectivity; usually the extinction coefficient is small and can be neglected in (3.5). The reflectivity can be determined more accurately from reflection measurements. Lark-Horovitz and Meissner (1949) made first reflection measurements on germanium and silicon crystals, to 150 microns in the case of germanium. For crystals of low conductivity, a constant reflectivity was found beyond 2 microns, from which the low frequency dielectric constant was determined for the two elements. Germanium crystals of high conductivity gave higher reflectivities at long wavelengths, indicating the effect of free carriers.

It was mentioned that the reflectivity is more or less affected by the surface condition. Where the absorption is small enough, measurements of the deflection of a beam, transmitted through a prism prepared of the material, give more accurate determination of the refractive index, and the value obtained is truly characteristic of the bulk material. Another method that has been used is to observe the interference shown in the variation of transmission with wavelength, using thin samples and a narrow band width. Table 1 gives the values of refractive index determined by the different methods for several semiconductors.

We shall discuss the experimental results for four semiconductors on which a large amount of work has been done: germanium, silicon, indium antimonide, and tellurium. Germanium and silicon have been studied intensively in recent years and the knowledge obtained on these crystals has led to better understanding of semiconductors in general. Lately, binary compounds of group III and group V elements have begun to receive increasing attention, beginning with the work of Welker and his associates, the work of whom has been reviewed

recently by Welker (1954). Of these, indium antimonide has been studied the most. Finally, tellurium is one of the few elementary semiconductors and has a hexagonal structure, in contrast to the other three crystals having structures of cubic symmetry. It illustrates additional aspects associated with the presence of an optical axis. There is another group of semiconductors, the lead compounds PbS, PbSe and PbTe, the optical and photoconductive properties of which have been investigated in some detail in recent years. The properties of these materials have been reviewed before and will not, therefore, be included in the present discussion.

Table 1. Refractive Indices of Germanium, Silicon, Indium Antimonide and Tellurium

The wavelength in microns is given in the brackets.

	Method of measurement		
	Reflectivity	Prism	Interference
Ge	4 (2–150)[1]	4·143–4·068[2] (1·80) (2·60)	3·96 (1·8–3)[3] 3·92 (8–12)[4]
Si	3·5 (2–10)[1]	3·565–3·443[2] (1·05) (2·60)	—
InSb	4 (40–150)[5]	3·98 (~7)[6]	3·5 (7–15)[7]
Te	—	$E \parallel c$ axis: 6·34–6·20[8]; 6·26–6·23[9] (3·6) (8·0) (8·0) (14·0)	—
		$E \perp c$ axis: 4·97–4·85[8]; 4·81–4·79[9] (3·9) (8·0) (8·0) (14·0)	

[1] Lark-Horovitz and Meissner (1949), Fan and Becker (1951); [2] Briggs (1950 a); [3] Rank and Cronemeyer (1953); [4] Collins (1953); [5] except in the neighbourhood of 50 microns, Spitzer and Fan (1955); [6] Briggs, Cummings, Hrostowski and Tanenbaum (1954); [7] Breckenridge, Blunt, Hosler, Frederikse, Becker and Oshinsky (1954); [8] Hartig and Loferski (1954); [9] R. S. Caldwell (unpublished).

§ 4. Germanium and Silicon

4.1. *Absorption Edge*

It was found (Becker and Fan 1949 a, b, Fan and Becker 1951) that the absorption edge in germanium and silicon shifts to shorter wavelengths with decreasing temperature but agrees approximately with the energy gap determined by conductivity and Hall coefficient measurements. Recent experiments on cyclotron resonance of conduction electrons showed that the bottom of the conduction band in the two crystals does not correspond to electron wave number $\mathbf{k} = 0$. There are eight or four equivalent values of $\mathbf{k}$ along $\langle 111 \rangle$ directions in germanium and six equivalent values of $\mathbf{k}$ along $\langle 100 \rangle$ directions in silicon, which correspond to the lowest energy of the conduction band. A constant energy surface in $\mathbf{k}$ space consists of a corresponding number of prolate ellipsoids with major axes along $\langle 111 \rangle$ directions in germanium and along $\langle 100 \rangle$ directions in silicon. The longitudinal effective mass m_l along the direction of the major axis is much larger than the transverse effective mass m_t. In germanium $m_l = 1{\cdot}58m$ and $m_t = 0{\cdot}082m$, and in silicon $m_l = 0{\cdot}97m$ and $m_t = 0{\cdot}19m$. On the other hand, cyclotron resonance of free holes showed two separate effective masses, each having a small anisotropy. The values are approximately $m_1 = 0{\cdot}34m$, $m_2 = 0{\cdot}042m$ in germanium and $m_1 = 0{\cdot}52m$, $m_2 = 0{\cdot}16m$ in silicon. These experiments were carried

out at the University of California and the Lincoln Laboratory, M.I.T., and the results have been summarized by Dresselhaus, Kip and Kittel (1955). These results and the theoretical calculations made by Herman (1954) lead to the energy

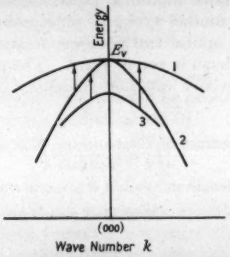

Figure 3. Schematic diagram of energy band contours near the top of the valence band in germanium or silicon.

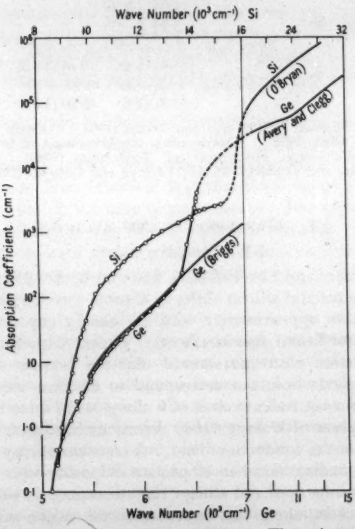

Figure 4. Absorption spectra of germanium and silicon. The points give the results of Fan, Shepherd and Spitzer (1954), obtained from transmission measurements, using single crystal samples. Briggs' curve (1952) for germanium was obtained by measuring transmission through evaporated films. O'Bryan's result (1936) for silicon was obtained by measuring reflection, using polarized light; the result of Avery and Clegg (1953) for germanium was obtained by the same method, single crystal sample with a natural surface was used. (*After* Fan, Shepherd and Spitzer 1954.)

band structures shown in figures 1 and 2. There are three bands meeting at the top of the valence band corresponding to $\mathbf{k} = 0$. More accurately, there are two bands joining at $\mathbf{k} = 0$ with a third band lying lower, split off by spin–orbit interaction. The picture near the top of the valence band is shown in figure 3. With the bottom of the conduction band and the top of the valence band corresponding to different values of $\mathbf{k}$, the agreement between the absorption edge and the energy gap suggests that the absorption arises from indirect transitions (Hall, Bardeen and Blatt 1954).

Figure 4 shows the absorption spectra of germanium and silicon. The points give results obtained from transmission measurements made on single crystal

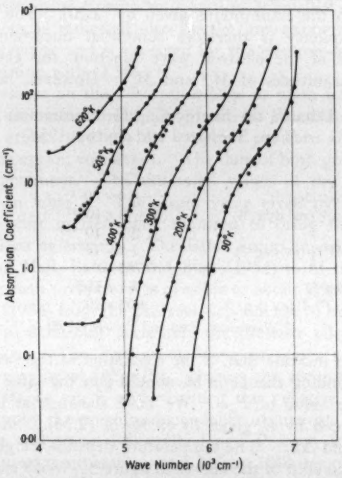

Fig. 5. Absorption edge in germanium at various temperatures. (*After* Fan, Shepherd and Spitzer 1954.)

samples of high purity, with resistivity over 20 ohm cm. The absorption threshold is estimated to be 5000 cm^{-1} (0·62 ev) for germanium and 8450 cm^{-1} (1·05 ev) for silicon. Log–log plots of absorption coefficient against $\nu - \nu_t$ show that the absorption coefficient increases approximately as $(\nu - \nu_t)^{2\cdot5}$ and $(\nu - \nu_t)^2$ for germanium and silicon respectively. The dependence is stronger than is expected for direct transitions, according to (2.14) or (2.15). The germanium curve shows a sharp turn at about 6400 cm^{-1} (0·82 ev) which may correspond to the beginning of direct transitions. This behaviour was observed also by Dash, Newman and Taft (1955). Furthermore, Haynes (1955) observed recently a second peak in the radiation emitted by the recombination of excess electrons and holes, at about the same wavelength. In the case of silicon, we expect a sharp rise of absorption around 15 000 cm^{-1} (1·85 ev) by combining the transmission measurements

and O'Bryan's (1936) data. Likewise, this rise may correspond to the onset of direct transitions.

Figure 5 shows the effect of temperature variation for germanium. The curves for different temperatures appear to be parallel to each other but shifted in frequency. The high temperature curves flatten out towards longer wavelengths due to the increasing intrinsic concentration of carriers which give absorption at long wavelengths. We are not concerned with this absorption in the present discussion. The curves for different temperatures can be brought to coincidence by a horizontal and a vertical shift relative to each other.

Theoretically, absorption arising from indirect transitions is given by either (2.24) or (2.26), depending on the assumption. Furthermore, both expressions were obtained with the assumptions given by (2.20). The exact dependence of absorption on frequency is therefore somewhat uncertain in the absence of detailed knowledge of the electron wave function, the energy band structure, and the relative magnitudes of M_c^2 and M_v^2. However, both (2.24) and (2.26)

Table 2. Data on the Energy Gap for Germanium and Silicon (Fan, Shepherd and Spitzer 1954)

	Ge	Si
E_0 (ev)	0·77	1·19
$(\partial E_t/\partial T)_P$ (ev deg^{-1})	$-4{\cdot}4\times10^{-4}$	-4×10^{-4}
$(\partial E_t/\partial P)_T$ (ev cm^3 dyn^{-1})	$(8\pm1)\times10^{-12}$	$\sim5\times10^{-12}$
	$5{\cdot}5\times10^{-12}$†	-2×10^{-12}†
$(\beta/\chi)(\partial E_t/\partial P)_T$ (ev deg^{-1})	$-1{\cdot}5\times10^{-4}$	$\sim-0{\cdot}5\times10^{-4}$
E (ev)	0·785	1·21
A (cm^{-6} deg^{-3})	$3{\cdot}1\times10^{33}$	$1{\cdot}5\times10^{33}$
$k\ln(N_cN_v/T^3A)$ (ev deg^{-1})	$-4{\cdot}03\times10^{-4}$	$-4{\cdot}19\times10^{-4}$

† Warshauer, Paul and Brooks (1955).

and their derivation indicate that, if the separation of the two energy bands were changed, a corresponding change in $\hbar\omega$ should give the same value of P_a, or more precisely, the same value of $P_a\omega$. We have shown that in optical transitions E_G should be replaced by E_t given by (2.34) or (2.36). Similar changes should be made for ΔE_1 and ΔE_2. The temperature dependence given by (2.36) would lead to the horizontal shift of the curves in figure 5. With change of temperature, the quantum numbers n_q change according to (2.44). The resulting variation of the absorption would correspond to the vertical shift of the curves in figure 4, which is approximately given by $1+2n_q$. The experimental data were replotted in the form of $\ln(\alpha\tilde{\nu})$ versus $\tilde{\nu}$. The curves differ in shape only slightly from those shown in figure 5. The relative horizontal shift of the curves varies approximately linearly with temperature. The value of the temperature coefficient $(\partial E_t/\partial T)_P$ obtained is given in table 2. The low temperature curves in figure 3 have been measured to very low values of α, where they become very steep. There the values of E_t can be estimated. The estimated value of E_0, the constant term in E_t, is also given in the table. The relative vertical shift of the curves can be fitted with a value $\hbar\omega_q = k\,(400°\text{K})$.

The results for silicon are similar. The values of $(\partial E_t/\partial T)_P$ and E_0, determined in the same way as for germanium, are given in table 2. It is difficult to estimate in this case the relative vertical shift of the curves.

Similar measurements have been reported by Macfarlane and Roberts for germanium (1955a) and for silicon (1955b). The data covered a temperature range from 4·2°K to room temperature and were limited to values of α below 64 cm^{-1}. An expression

$$\alpha = A\left[\frac{(\hbar\omega - E_t - k\theta)^2}{1-e^{\theta/T}} + \frac{(\hbar\omega - E_t + k\theta)^2}{e^{\theta/T}-1}\right] \qquad \ldots\ldots(4.1)$$

was used to fit the curves obtained at each temperature. For each material, a value of θ is chosen for best fitting. The values of E_t obtained are somewhat different from the values according to table 2. The values for 4·2°K and 20°K indicate that the variation of E_t with temperature is smaller at the low temperatures. This behaviour is indicated also by the low temperature measurements made at Purdue University and is expected for the electron–lattice interaction, as pointed out in connection with (2.35).

The effect of pressure on the absorption edge at room temperature has been reported by Spitzer, Bennett and Fan (1955) and by Warshauer, Paul and Brooks (1955). The latter group used a wider range of pressure and measured within a smaller range of absorption coefficient. The data of both groups for germanium are in substantial agreement. The estimated values of the pressure coefficient $(\partial E_t/\partial P)_T$ are given in table 2. The larger value given by the first group was estimated from the shift in frequency required to bring the curves of $\alpha\tilde{\omega}$ for different pressures into agreement. The latter group found that, by using the original expression of Hall, Bardeen and Blatt (1954) to fit the absorption curve and determine E_t for each pressure, it is possible to obtain the lower value deduced by Paul and Brooks (1954) from the pressure dependence of intrinsic conductivity. It is more difficult to determine accurately the pressure effect from the experimental data for silicon. The first group using pressures up to 1000 kg cm^{-2} obtained the positive value of $(\partial E_t/\partial P)_T$, whereas the second group used higher pressures, up to 8000 kg cm^{-2}, and obtained the negative value. A negative value is indicated also by the pressure dependence of intrinsic resistivity at sufficiently high pressures and above 120°c (Paul and Pearson 1955); there are no data pertaining to room temperature and below 1000 kg cm^{-2}. According to (2.36), $(\beta/\chi)(\partial E_t/\partial P)_T$ gives the temperature coefficient of E_t arising from the effect of lattice expansion. Table 2 shows that the major part of the temperature coefficient $(\partial E_t/\partial T)_P$ corresponds to the term $(\partial E_t/\partial T)_V$ given by the electron–lattice interaction.

The intrinsic carrier concentration is determined by $F_G = E_t$, according to (2.37). For the energy band structure of germanium and silicon

$$N_c N_v = 4(2\pi kT/h^2)^3\,\delta(m_t m_t^2)^{1/2}(m_1^{3/2} + m_2^{3/2}), \qquad \ldots\ldots(4.2)$$

where m_t and m_t are the longitudinal and transverse effective masses of conduction electrons, δ is the number of minima in the conduction band, and m_1 and m_2 are the effective masses of holes in the two energy bands joining at the top of the valence band. The equation for intrinsic carrier concentration can be written

$$n_i^2 = N_c N_v \exp\left[-(\partial E_t/\partial T)_P/k\right]\exp\left(-E_0/kT\right). \qquad \ldots\ldots(4.3)$$

The intrinsic carrier concentration determined experimentally by measuring the conductivity and Hall coefficient at various temperatures can be expressed by

$$n_i^2 = AT^3 \exp(-E/kT). \qquad \ldots\ldots(4.4)$$

Thus the values of E_0 and $(\partial E_i/\partial T)_P$ are to be compared with E and $\mathbf{k} \ln (N_c N_v/T^3 A)$, respectively. The values of the various quantities are listed in table 2. The value of $N_c N_v$ was calculated using the effective masses given by the cyclotron resonance measurements, and the experimental values of E and A were determined by Morin and Maita (1954 a, b). The comparison shows satisfactory agreement.

4.2. *Carrier Absorption in Germanium*

4.2.1. *Absorption by conduction electrons.*

Absorption by conduction electrons can be observed in n-type samples with a sufficiently large carrier concentration. Following the early work of Becker (Fan and Becker 1951), Collins (1953) made measurements on samples of various electron concentrations in the temperature range 78° to 450°K, covering a wavelength region 2 to 35 microns. Some measurements at room temperature were extended to 150 microns by Collins and by Johnson and Spitzer (1954). The absorption increases smoothly with increasing wavelength as expected for carrier absorption. Originally, Johnson and Spitzer observed a drop of reflectivity at 152 microns which was later found to be due to scattered light of short wavelengths. Extensive measurements and comparison of the result with theory have been made by Spitzer, Collins and Fan (1955) for three temperatures, 78°K, 291°K and 450°K.

Since the effect of lattice scattering increases with temperature, the theory predicts that it should be the dominant mechanism of absorption at the high temperature, 450°K. The absorption should be proportional to the carrier concentration and the shape of the spectral absorption curve should be the same for all samples. The experimental results are in agreement with these predictions. The solid points in figure 6 give the absorption per unit carrier concentration obtained on a number of samples with various carrier concentrations. Curve 1 is the theoretical curve calculated according to (2.45) using $m^* = 0{\cdot}1m$.

With decreasing temperature, the effect of impurity scattering becomes more important, and at 78°K it should be the major effect in samples of high impurity concentrations. The absorption is expected then to depend on the impurity concentration as well as the density of carriers. Experimentally, the absorption was found to increase more rapidly than the carrier concentration, in accordance with the fact that higher carrier concentrations correspond to higher impurity contents. Also, samples with compensating impurities gave higher absorption than the samples of the same carrier concentration but having no added acceptor impurity and therefore a smaller total impurity content. For the different samples used, the absorption per unit carrier concentration was found to consist of a constant part and a part proportional to the impurity concentration. The constant part is to be attributed to the effect of lattice scattering. Calculations using $m^* = 0{\cdot}11m$ in (2.46) and $m^* = 0{\cdot}083m$ in (2.48) give the best over all fit for the results obtained for the various samples. The open circles in figure 6 give the

experimental results for one of the samples showing the good agreement with the calculated curve 2. Due to the stronger frequency dependence of absorption with impurity scattering, the curve for 78°K is seen to be much steeper than the curve for 450°K. Similar agreements between the theory and the experimental results were obtained also at the intermediate temperature. The value of the electron effective mass, $m^* \sim 0{\cdot}1m$, is reasonable in the light of the cyclotron resonance measurements.

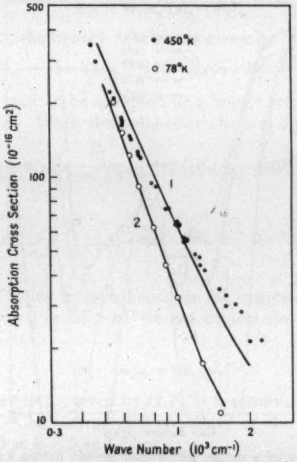

Figure 6. Absorption cross section of conduction electrons in n-type germanium. The solid points for 450°K represent combined data obtained on samples of various carrier concentrations. Curve 1 is calculated for the effect of lattice scattering. The open circles give results for a sample of 10^{18} cm^{-3} impurity (Sb) concentration, at 78°K. Curve 2 is calculated for this sample, taking into account both lattice and impurity scatterings.

4.2.2. *Absorption by free holes.*

Absorption by free holes can be observed in p-type samples. The absorption cross section of holes is much higher than that of electrons and does not vary smoothly with wavelength. Two weak bands at about 2200 cm^{-1} and 3500 cm^{-1} were reported by Briggs and Fletcher (1952), and Kaiser, Collins and Fan (1953 a) reported a steep rise of absorption to a high level at long wavelengths, beginning at about 10 microns. The absorption is proportional to the hole concentration. Figure 7 shows the absorption for a p-type sample as function of wave number for different temperatures. Extending the measurements to 152 microns, Johnson and Spitzer (1954) found that the absorption rises again beyond 80 microns. This rise may be the free carrier effect, but the absorption at shorter wavelengths with the structures as shown in figure 7 is not understandable on that basis. Both groups, Kaiser, Collins and Fan (1953 b) and Briggs and Fletcher (1953),

proposed that the absorption corresponds to transitions between overlapping bands within the valence band. Such a mechanism was first considered by Fan and Becker (1950) in connection with absorption by holes in silicon.

Theoretical calculations by Herman and Callaway (1953) suggested that the top of the valence band at $\mathbf{k} = 0$ is threefold degenerate. On the other hand, cyclotron resonance measurements gave only two effective masses for holes.

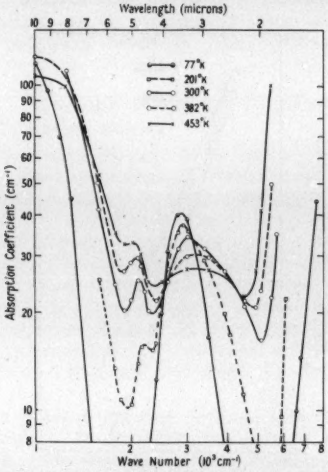

Figure 7. Absorption spectra of a p-type germanium sample having a resistivity of 0·04 ohm cm at room temperature. (*After* Kaiser, Collins and Fan 1953 b.)

Dresselhaus, Kip and Kittel (1954) suggested that, due to the spin–orbit interaction, the top of the valence band is twofold degenerate with a third band at lower energy, as shown in figure 3. Kahn (1955) made calculations using this model and was able to obtain agreement with the experimental results shown in figure 7. The absorption bands at 3500 cm^{-1} and 2200 cm^{-1} and the band beginning at 1800 cm^{-1} correspond to transitions between the energy bands 3 and 1, 3 and 2, and 2 and 1, respectively. These transitions occur in consequence of the presence of holes. The expression (2.6) of σ for interband transitions is for the case where the lower band is completely filled and the upper band is vacant. In general, for a lower band j and a higher band i, the conductivity associated with interband transitions is given by

$$\sigma_{ij} = \frac{e^2}{4m} f_{ij}(\nu)\, n_{ij}(\nu)\, [f_j^{(e)} f_i^{(h)} - f_i^{(e)} f_j^{(h)}], \qquad \ldots\ldots(4.5)$$

where $f^{(e)}$ is the probability for a state to be occupied by an electron and $f^{(h)}$ is the probability for a state to be vacant or occupied by a hole. The negative term corresponds to induced emission.

We assume that the energy in the three bands can be expressed by

$$E_i(\mathbf{k}) = E_i(0) - (\hbar^2/2m_i)\,k^2 \qquad \ldots\ldots(4.6)$$

with the top of each band at $\mathbf{k} = 0$. For the two bands, 1 and 2, $E(0)$ is the same and equal to E_v, the top of the valence band. For band 3, $E(0) = E_v - \Delta E$. For (ij) interband transition

$$h\nu_{ij} = E_i(\mathbf{k}) - E_j(\mathbf{k}) = E_i(0) - E_j(0) + (\hbar^2/2m_{ij})\,k^2, \qquad \ldots\ldots(4.7)$$

where

$$m_{ij} = m_i m_j/(m_i - m_j). \qquad \ldots\ldots(4.8)$$

By analogy with (2.12), the density function is given by

$$n_{ij}(\nu_{ij} = \nu) = (2m_{ij})^{3/2}\,[h\nu - E_i(0) + E_j(0)]^{1/2}/\pi\hbar^3. \qquad \ldots\ldots(4.9)$$

The probability for a state to be occupied by a hole is related to the concentration of holes n_h in the band. When the holes obey classical distribution, $f^{(e)} \sim 1$ and

$$f_i^{(h)}(E_k) = n_{hi}\frac{h^3}{2(2\pi m_i kT)^{3/2}}\exp\{[E_i(k) - E_i(0)]/kT\}. \qquad \ldots\ldots(4.10)$$

It follows that

$$f_i^{(h)}(\nu_{ij} = \nu) = n_{hi}\frac{h^3}{2(2\pi m_i kT)^{3/2}}\exp\{-(m_{ij}/m_i)\,[h\nu - E_i(0) + E_j(0)]/kT\}. \qquad \ldots\ldots(4.11)$$

The concentration of holes in each band can be expressed in terms of the total concentration of holes. For $\Delta E \gg kT$ we can neglect the holes in band 3, getting $n_h = (n_h)_1 + (n_h)_2$ with

$$(n_h)_1/(n_h)_2 = (m_1/m_2)^{3/2}. \qquad \ldots\ldots(4.12)$$

The oscillator strength f_{ij}, given by (2.7), is determined by the matrix elements p_{ij}, given by (2.13). Considering the symmetry of the crystal structure, Kahn concludes that $p_{ij} = 0$ at $\mathbf{k} = 0$ and takes

$$|\mathbf{p}_{ij}|^2 \propto k^2 = [h\nu - E_i(0) - E_j(0)]\,2m_{ij}/\hbar^2. \qquad \ldots\ldots(4.13)$$

Substituting the expressions for the various quantities in (4.5) we get

$$\sigma_{13} \propto n_h \frac{|h\nu - \Delta E|^{3/2}}{\nu(kT)^{3/2}}\exp\left(\frac{m_3}{m_3 - m_1}\frac{h\nu - \Delta E}{kT}\right) \qquad \ldots\ldots(4.14a)$$

$$\sigma_{23} \propto n_h \frac{|h\nu - \Delta E|^{3/2}}{\nu(kT)^{3/2}}\exp\left(\frac{m_3}{m_3 - m_2}\frac{h\nu - \Delta E}{kT}\right) \qquad \ldots\ldots(4.14b)$$

$$\sigma_{12} \propto n_h \frac{\nu^{1/2}}{(kT)^{3/2}}\left[\exp\left(\frac{m_2}{m_2 - m_1}\frac{h\nu}{kT}\right) - \exp\left(\frac{m_1}{m_2 - m_1}\frac{h\nu}{kT}\right)\right]. \qquad \ldots\ldots(4.14c)$$

The term corresponding to induced emission is neglected in σ_{13} and σ_{23} since the hole concentration in band 3 is negligible. Cyclotron resonance experiments give $m_1 = 0{\cdot}3m$ and $m_2 = 0{\cdot}04m$. The expressions are in qualitative agreement with the experimental results, if $\Delta E = 0{\cdot}3$ ev $= 2400$ cm^{-1} and $m_3 = 0{\cdot}1m$ are used. It should be mentioned that with m_3 less than m_1 the absorption σ_{13} is at $h\nu$ greater than ΔE, and with m_3 greater than m_2 the absorption σ_{23} takes place at $h\nu$ less than ΔE. Thus σ_{13} and σ_{23} account for the two weak absorption bands.

The expression σ_{12} gives absorption extending to $\nu = 0$. It accounts for the strong absorption at long wavelengths, beginning around 1800 cm^{-1}. However, using the values of m_1 and m_2 given above, the calculated absorption extends too far towards short wavelengths and overlaps the other two bands. On the whole, the absorption by free holes seems to have a correct interpretation and provides an experimental evidence for the existence of band 3.

4.3. *Carrier Absorption in Silicon*

Absorption by free carriers has not yet been investigated carefully for silicon. Some measurements have been reported for the absorption by holes in p-type samples (Becker and Fan 1949 b, Briggs 1950 b, Fan and Becker 1950). The absorption seems to be proportional to the concentration of holes and increases approximately as the wavelength squared, in the measurements made up to about 10 microns. The magnitude of the absorption is about ten times higher than that given by the classical expression with $m^* = m$. This discrepancy might be explained by the small values of the effective mass given by the cyclotron resonance experiment. However, a sample measured by Becker and Fan showed an absorption increasing steadily as the temperature is raised from 77°K to 663°K, whereas the variation of d.c. conductivity and hole concentration predicts according to (2.38) a quite different temperature dependence for the absorption. Here again we have an evidence that the classical expression is not applicable.

Recently, measurements on p-type samples have been extended to 35 microns by Spitzer. Over the entire wavelength range, the absorption varied smoothly, approximately as λ^2. This behaviour indicates the absorption is a free carrier effect, in contrast to the case of p-type germanium, where the absorption is primarily produced by transitions between the three bands within the valence band and the free carrier effect comes in only at very long wavelengths. An estimate of the splitting due to spin–orbit interaction (Dresselhaus, Kip and Kittel 1955) indicates that band 3 (see figure 3) should be about 0·04 ev below the top of the valance band. Thus an absorption band is expected at around 30 microns. Measurements made at Purdue by Spitzer showed no indication of a band up to 40 microns. It is possible that the band is masked by the strong free carrier effect.

4.4. *Impurities and Lattice Defects in Germanium*

To observe the absorption associated with the excitation and ionization of impurities, measurements must be made at sufficiently low temperatures so that the impurities are not thermally ionized. A table of ionization energies of various impurities, with references to the original works, has been compiled by Burton (1954). The impurities commonly added to germanium and silicon are group III and group V elements which act as acceptors and donors respectively. These impurities have small ionization energies, around 0·01 ev in germanium, due to the relatively large dielectric constant of the crystal, which reduces the binding of an electron to a charged centre. Therefore, absorption by bound electrons or holes can be observed only at very low temperatures, below 20°K. The absorption threshold should be at wavelengths over 100 microns. So far, low temperature measurements have not yet been carried to such wavelengths.

The absorption in p-type germanium containing indium, measured at liquid helium temperature, is shown in figure 8. The resistivity of the specimen at 5°K was several orders of magnitude higher than at 77°K, indicating that practically all the holes were in the impurity states at the lower temperature. Thus, the absorption at 5°K is to be attributed to the bound holes. This is verified by the presence of photoconductivity which showed a spectral response curve (broken curve in figure 8) similar in shape as the absorption curve. Such a photo-response

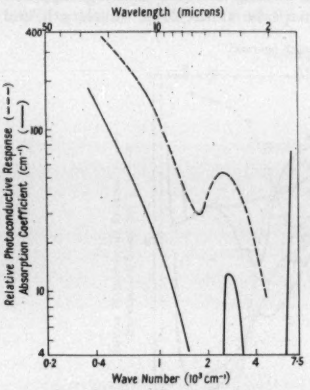

Figure 8. Absorption coefficient (solid curve, *after* Kaiser, Collins and Fan 1953 b) and photoconductivity (broken curve, measured by W. Kaiser) of a p-type, indium-doped germanium crystal as functions of frequency, at 5°K.

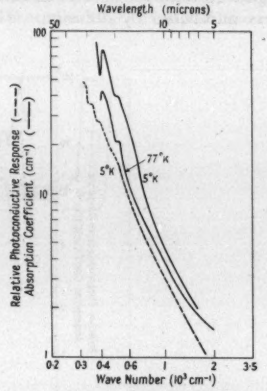

Figure 9. Absorption coefficient (solid curves) and relative photoconductive response (broken curve) of an n-type, antimony-doped germanium crystal as function of frequency. (*After* Collins 1953.)

curve has been observed also by Burstein, Davisson, Bell, Turner and Lipson (1954). The similarity between the absorption by free holes at 77°K and the absorption by the bound holes at 5°K can be explained in the following way (Kahn 1955). From the ionization energy and the effective mass of holes, the orbit radius of the impurity state can be estimated to be about $13a_0$, a_0 being the hydrogen Bohr radius. The wave function of the impurity state, when analysed into plane waves, will contain wave numbers ranging up to $0{\cdot}2a_0^{-1}$. This range is of the same order of magnitude as the range of wave numbers of free holes in band 1 (see figure 3) at 77°K. Hence the absorption produced by the excitation of electrons from the lower bands 2 and 3 may be similar for free holes in band 1 and for bound holes in the impurity states. It is clear that, in the case of bound holes, there is additional excitation from band 1.

The absorption in n-type germanium containing antimony is shown in figure 9. For comparison, the absorption by free carriers at 77°K is also shown for the same sample. The two small peaks are the lattice absorption bands. At 5°K, the absorption is associated with photoconductivity, shown by the broken curve,

indicating ionization of bound electrons. The dependence on frequency is somewhat less, but close to $(1/\nu)^{3\cdot5}$ according to (2.55). To fit the observed curve by (2.55) a value of $m/m^* \sim 30$ is required, which is too high to be compatible with the values of the effective mass. However, the approximate expression can only be expected to give an order of magnitude.

Absorption measurements have also been made for two impurity elements outside group III and group V, i.e. copper and gold. The solid curves in figure 10 show the absorption coefficient for a specimen containing copper which was introduced by diffusion. The two peaks at the long wavelength end are

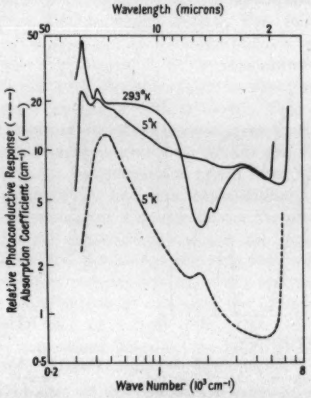

Figure 10. Absorption coefficient (solid curves) and relative photoconductive response (broken curve) of a p-type, copper-doped germanium crystal as functions of frequency. (*After* Kaiser and Fan 1954 a.)

lattice absorption bands. The curve for room temperature shows typical absorption by free holes. At 5°K, the resistivity is about 10^7 ohm cm and photoconductivity, shown by the broken curve, extended to long wavelengths beyond the main absorption edge, indicating that most of the holes are in the impurity states. Similar photoconductivity curve was found also by Burstein *et al.* (1954). Both the low temperature absorption and photoconductivity curves show a long wavelength threshold which agrees with the ionization energy, 0·04 ev (31 microns), determined from the temperature variation of conductivity and Hall coefficient. There is no pronounced absorption peak corresponding to the 2700 cm^{-1} band in the free carrier absorption and in the absorption by indium impurity. Thus, the excitation from the valence band 3 to the copper level must be weak. Analysis of the absorption curve suggests that there is a component in the absorption with a long wavelength threshold near 5 microns or 0·25 ev (see also Burstein, Davisson, Bell, Turner and Lipson 1954). The photoconductivity curve also shows a hump at about this wavelength. The existence of an acceptor level for copper with such ionization energy has been deduced from electrical measurements.

The magnitude of the maximum absorption near the long wavelength threshold gives an absorption cross section $\alpha/N \simeq (10^{-17}/n)(E_H/E_i)$, taking the refractive index $n = 4$ for germanium, the ionization energy $E_i = 0{\cdot}04$ ev and the concentration of copper atoms $N = 2 \times 10^{17}$ cm^3 given by the room temperature Hall coefficient. The value 10^{-17} is reasonable compared with $0{\cdot}63 \times 10^{-17} m/m^*$ of (2.54).

Figure 11 shows the absorption curves of p-type germanium containing gold. The room temperature curve is characteristic of absorption by free holes, except that it shows higher absorption near the main absorption edge, as in the case of

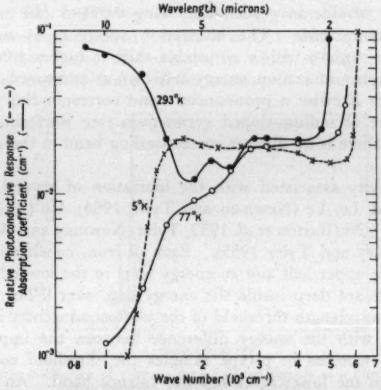

Figure 11. Absorption coefficient (solid curves, measured by W. Kaiser) and relative photoconductive response (broken curve, *after* Kaiser and Fan 1954 a) of a p-type, gold-doped germanium crystal, as function of frequency.

copper impurity. It has been found that gold gives an energy level at about 0·2 ev below the conduction band. In n-type crystals, this level is not occupied by electrons and excitation of electrons from the valence band to this level can be responsible for an additional absorption at wave numbers within 1600 cm^{-1} of the absorption edge. The absorption curve at 77°K is quite different. At this temperature most of the holes became bound in impurity states, the concentration of free holes having decreased to about 10^9 cm^{-3} from a value of around 10^{15} cm^{-3} at room temperature. The crystal was very photosensitive. The broken curve in figure 11 shows the photoconductivity curve at 5°K. It is known from conductivity and Hall coefficient measurements that gold gives an acceptor level 0·18 ev from the valence band. The long wavelength threshold of the photoconductivity curve is in agreement with an ionization energy of this value. The absorption rises near the threshold of the photoconductivity. It shows distinctly another rise to nearly constant values above 3000 cm^{-1}. The second rise corresponds apparently to the 2700 cm^{-1} band in the free hole absorption which can be seen in the room temperature curve. It is thus the excitation of electrons

from valence band 3 to the acceptor levels. In contrast to the case of copper impurity where this absorption is unobserved, the excitation from band 3 seems to be actually more efficient than the excitations from bands 1 and 2 which begin at the threshold of ionization. Investigation of absorption by impurities should provide useful information for the understanding of impurity states, particularly those with large ionization energy.

Absorption (Burstein, Henvis and Sclar 1954) and photoconductivity (Burstein, Davisson, Bell, Turner and Lipson 1954) have been measured for zinc-doped germanium at liquid helium temperature. The measurements were limited to wavelengths below 38 microns and a threshold was not reached, the thermal ionization energy of zinc in germanium being 0·031 ev (40 microns) according to electrical measurements. The absorption spectrum is similar to that of indium-doped germanium with a noticeable shift to higher frequency, in agreement with the higher ionization energy 0·031 ev as compared with 0·011 ev for indium. There is likewise a pronounced band corresponding to the 2700 cm^{-1} band in the curve of indium-doped germanium (see Burstein, Picus and Sclar 1954); however, there is no distinct corresponding band in the photoconductivity curve.

Photoconductivity associated with the ionization of several other impurities has been observed, i.e. Fe (Newman and Tyler 1954), Co (Tyler, Newman and Woodbury 1955 a), Ni (Burton *et al.* 1953, Tyler, Newman and Woodbury 1955 b), and Mn (Woodbury and Tyler 1955). Each of iron, cobalt and nickel gives an energy level in the upper half and an energy level in the lower half of the energy gap. These levels are deep inside the energy gap, over 0·2 ev from the nearest edge. The long wavelength threshold of the photoconductivity in n-type samples can be identified with the energy difference between the upper level and the conduction band, whereas in p-type samples the threshold corresponds to the separation between the lower level and the valence band. An interesting point about the spectral response is the fact that in p-type samples the curves seem to have a flat region like the broken curve in figure 11 whereas in n-type samples the curves rise more gradually. In this respect, we note that photoconductivity in n-type germanium containing gold, measured by Newman (1954) and by Morton, Hahn and Schultz (1954), also does not show the broad flat region as does the response in p-type crystals, given in figure 11. The difference between the spectral response in n- and p-type samples was explained by the authors on the assumption that in n-type samples excitations from more than one level to the conduction band were observed. No absorption measurements have yet been reported for these impurities.

Photoconductivity associated with the ionization of electrons and holes in localized states of lattice defects was observed in germanium irradiated with fast electrons (Fan, Kaiser, Klontz, Lark-Horovitz and Pepper 1954, Stoeckmann, Klontz, Fan and Lark-Horovitz 1955). Atoms are displaced from regular lattice sites by elastic collisions with the fast 4·5 Mev electrons. The bombardment produces photoconductivity on the long wavelength side of the main absorption edge, which after falling to a minimum rises again to a peak at 0·35 ev. Similar effect has been observed (Longo and Kleitman, unpublished) in germanium irradiated by 10 Mev deuterons. These results show the similarity in the effect

of irradiation by electrons and by the heavier particles, and they are used to determine the energy levels of the lattice defects.

A shift of the absorption edge to longer wavelengths has been observed by Lipson, Burstein and Smith (1955) in plastically deformed germanium. The effect is attributed by the authors to local changes of density as discussed by Dexter (1954) for edge dislocations. There is also an extended tail of weak absorption which may be attributed to transitions to an acceptor level introduced by the defects. A long wavelength absorption tail was also observed in samples irradiated by neutrons.

4.5. *Impurities and Lattice Defects in Silicon*

Absorption involving impurity states was observed in silicon by Fan and Becker (1950). They found that samples in which a large part of the carriers became bound in impurity states, upon cooling to a low temperature, showed

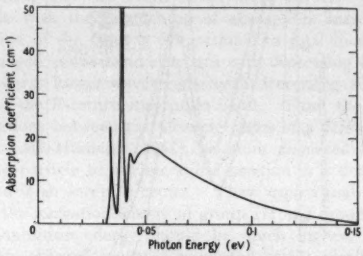

Figure 12. Absorption coefficient of a boron-doped silicon sample as a function of photon energy. (*After* Burstein, Picus and Sclar 1954.)

increased absorption, whereas samples in which the carriers remained free showed decreased absorption. Absorption has now been measured at low temperatures for a number of group III and group V impurities, including B, Al, Ga, In, As and P, by the group at the U.S. Naval Research Laboratory (Burstein, Oberly, Davisson and Henvis 1951, Burstein, Bell, Davisson and Lax 1953, Burstein, Picus and Sclar 1954, Burstein, Picus, Henvis and Lax 1955). Photoconductivity associated with the photo-ionization has also been observed by this group (Burstein, Oberly and Davisson 1953) and by Rollin and Simmons (1952, 1953). For impurities outside the group III and group V elements, only photoconductivity for gold-doped silicon was observed (Newman 1954), the long wavelength threshold of which was found to agree with the thermal ionization energy.

Figure 12 shows the absorption spectrum for silicon containing boron. The broad peak can be identified with the onset of photo-ionization. The three sharper peaks on the long wavelength side correspond to excitations of the bound holes. These bands become broader with increasing temperature, their widths being of the order of magnitude of estimated broadening of absorption lines, resulting from the lattice vibration (Lax 1954). The frequencies of the three peaks are related to each other as the 1s–2p, 1s–3p and 1s–4p excitation energies

according to the hydrogenic model of impurity centre. Using the dielectric constant of silicon, these energies correspond to a hole effective mass of $0{\cdot}45m$, according to (2.52). Since the broad peak does not yield an accurate value of the ionization energy a value of 0·046 ev was estimated using the hydrogenic model, which agrees with the thermal ionization energy, 0·045 ev, determined by electrical measurements. However, the integrated absorption cross sections for these excitation bands differ considerably from those for the hydrogenic model. For the other impurities of group III the ionization energy was estimated using the observed excitation band of highest energy : 0·067 ev for Al, 0·071 ev for Ga, and 0·16 ev for In. The values for Al and Ga are somewhat higher than the available data for thermal ionization energy which are 0·057 ev

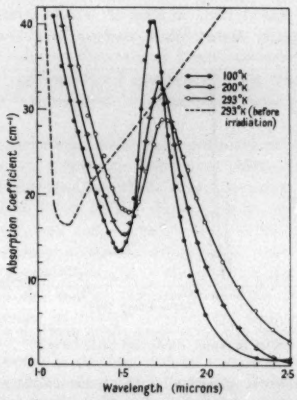

Figure 13. Absorption coefficient of a p-type silicon sample as a function of wavelength, showing the effect of neutron irradiation. The broken curve was measured before the irradiation. The solid curves were measured after irradiation by neutrons in the Oak Ridge pile. (*After* Becker 1951.)

for Al, 0·065 ev for Ga, and 0·16 ev for In. The large variation of the ionization energy among these impurities shows that the simple hydrogenic model is inadequate. Analysis of the data indicated that the energies of the excited p-states remain approximately unchanged with respect to the valence band. It seems that the breakdown of the effective mass approach in the neighbourhood of the impurity is an important factor. The effect should be more important for the 1s ground state than for large p-orbits.

Recently Kleiner (1955) and Kohn (1955) calculated the energy levels of donor impurity in silicon using the effective-mass wave equation and taking into account the anisotropy of the effective mass of conduction electrons. The results were compared with the experimental absorption spectra of arsenic and phosphorus in silicon. The experimentally observed excitation bands were attributed to $1s \rightarrow (2p, m = 0)$, $1s \rightarrow (2p, m = \pm 1)$, $1s \rightarrow (3p, m = \pm 1)$, and $1s \rightarrow (4p, f, m = \pm 1)$

transitions. Kohn showed that the spacings of the observed bands are in agreement with the theoretically calculated spacings. This result constitutes a justification of the effective mass formalism for the excited p-states.

Absorption effects associated with the lattice defects produced by high energy neutron and deuteron irradiations were observed by Becker (Becker, Fan and Lark-Horovitz 1952, Fan 1952). Both donor type and acceptor type centres are produced by the irradiation and the carrier concentration in both n- and p-type samples decreases upon irradiation, approaching the intrinsic value. The broken curve in figure 13 shows the absorption before irradiation, the free carriers being responsible for the absorption increasing with wavelength. The absorption after the neutron irradiation is given by the solid curves measured at three different temperatures. There is no more carrier absorption but two additional effects have appeared; a sharp band has developed with peak at 1·8 microns (0·7 ev) and the absorption edge seems to have shifted towards longer wavelengths as can be seen by comparing the two room temperature curves. The width of the band is compatible with the broadening of absorption lines in crystals. The integrated absorption of the band is proportional to total flux of the irradiation and remains unchanged as the band sharpens with decreasing temperature. The peak also shifts towards longer wavelengths with decreasing temperature, similar to the behaviour of the F-centre absorption band. Thus, the band seems to be produced by transitions between two discrete states of a defect centre. According to James and Lark-Horovitz (1951), an atom displaced by elastic collision with a bombarding particle to an interstitial position is a donor centre and the vacancy left behind is an acceptor centre. They argued that the first ionization energy is small as the ionization energy of group III and group V impurities, and that the second ionization energy should be much higher, since the stronger binding of a doubly charged centre is associated with a small electron orbit for which the potential is not effectively reduced by the dielectric constant of the crystal. The observed absorption band at the relatively large energy of 0·7 ev should then correspond to the excitation of an ionized centre.

The apparent shift of the absorption edge extends to the limit of the measurements, 0·82 micron. The effect is proportional to the flux of bombarding particles, about -2×10^{-18} ev per particle/cm^2, with a tendency to saturate for irradiations over 5×10^{16} particle/cm^2. We have seen that the absorption in the region of the absorption edge corresponds to indirect transitions. It is not certain whether this effect of the lattice defects is an enhancement of the indirect transition or an effective reduction of the energy gap. The data obtained so far seem to favour the second interpretation.

4.6. *Lattice Absorption*

Several absorption bands in the region between 9 and 35 microns were observed in germanium and silicon by various groups (Burstein and Oberly 1950, Lord 1952, Briggs 1952, Collins and Fan 1952, 1954, Lax and Burstein 1955), which were attributed to lattice vibrations. Collins and Fan determined the absorption coefficient over this region for n- and p-type samples of various carrier concentrations and found that the absorption bands are present in the same strength in all samples, in addition to the carrier absorption which varies among

the samples. This result shows that the absorption bands are truly an effect of the lattice. Figure 14 gives the absorption curves for germanium and silicon. There are a number of bands in each case corresponding apparently to combination modes. Hsieh (1954) has calculated the vibration spectrum for germanium and silicon, following the calculations of Smith (1948–49) for diamond, but selection rules for combination modes have not yet been determined. A relation between the elastic constants and the limiting frequency of

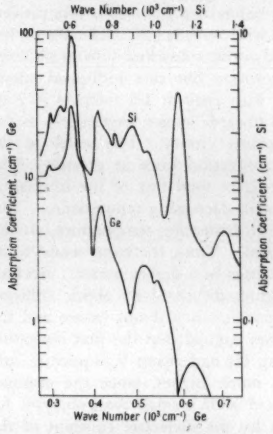

Figure 14. Lattice absorption bands in germanium and silicon crystals at room temperature. (*After* Collins and Fan 1954.)

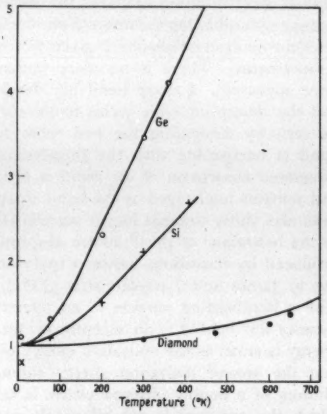

Figure 15. Calculated curves of mean-square displacement of atoms as a function of temperature for germanium, silicon, and diamond. The points give the relative magnitudes of the 340 cm^{-1} band in germanium, the 610 cm^{-1} band in silicon, and the 2175 cm^{-1} band in diamond.

optical mode of vibration was derived by Born and revised subsequently by Nagendra Nath (see Born 1946). Using the known values of the elastic constants we get a frequency of 400 cm^{-1} for germanium and 845 cm^{-1} for silicon. These values fall within the region of the absorption bands.

For these crystals of diamond type lattice the optical mode of vibration should be infra-red inactive. As is well known, diamond shows a number of infra-red absorption bands, one group of which is present in Type I and Type II diamonds, whereas an additional group is found only in Type I diamonds. It has been suggested (Blackwell and Sutherland 1949) that the latter group is caused by lattice imperfections of chemical or physical nature. Collins and Fan found that the lattice bands in germanium are not sensitive to added impurities with concentrations up to 10^{18} cm^{-3}. These bands are affected neither by plastic deformation produced by a 5° bend nor by thermal quenching from near the

melting point. In the case of silicon, a sample with 3×10^{18} cm^{-3} of chemical impurity and with about the same concentration of lattice defects produced by nucleon irradiation showed the same absorption as purer and unirradiated samples. The bands in both materials were about the same in all samples measured, although some variation of two of the bands, at 606 cm^{-1} and 1110 cm^{-1}, among different silicon samples have been reported later by Lax and Burstein. Therefore, most of the bands, like the group of bands in Type II diamond, do not seem to be caused by lattice imperfections.

More significant is the variation of the bands with temperature. Collins and Fan observed that the absorption is temperature dependent and is proportional to the mean square thermal displacement of the atoms. Measurements were made also on diamond, which showed that the absorption bands in Type II diamonds varied with temperature in the same manner, whereas the additional band in Type I diamonds is temperature insensitive. The correlation between the absorption and the mean square displacement can be seen in figure 15. The only exception is the 1110 cm^{-1} band in silicon which sharpens with decreasing temperature but does not decrease in magnitude at the peak. This band, which has been also found by Lax and Burstein to vary among different samples, seems to be caused by some lattice imperfection. These results show that, with the exception of the silicon 1110 cm^{-1} band, the absorption in germanium and silicon as well as in Type II diamond is intrinsic to the lattice. Vibration of the diamond lattice could give rise to electric moment, and therefore to absorption if charge deformation around the atoms is produced. Apparently the charge deformation associated with optically excited vibrations is proportional to the root mean square of the atomic displacement. Lax and Burstein discussed the problem theoretically by considering the optical excitation of a combination of two modes. As usual, the excitation depends on the quantum numbers or the degree of thermal excitation of the two modes, giving thus a temperature dependence of the absorption. The selection rules for the excitation of two modes have yet to be worked out.

§ 5. Indium Antimonide

5.1. *Absorption Edge*

Measurements of the absorption edge were reported first by Tanenbaum and Briggs (1953). In the purer samples, the edge was found to be in the vicinity of 7 microns (0·18 ev) at room temperature. It shifted to a shorter wavelength at 77°K. From the two measurements, a shift of $-4{\cdot}0 \times 10^{-4}$ ev deg^{-1} was deduced. Later measurements of Kaiser and Fan (1954 a, 1955) in the temperature range 5°K to 520°K gave a value of 0·175 ev for the edge at room temperature and a value of $-2{\cdot}8 \times 10^{-4}$ ev deg^{-1} for the temperature shift. The smaller value of the temperature shift was confirmed by Austin and McClymont (1954). The constant term of the threshold energy is thus $E_0 = 0{\cdot}26$ ev for this temperature range. From intrinsic carrier concentration, determined by Hall coefficient and conductivity measurements, Madelung and Weiss (1954) and Austin and McClymont (1954) deduced an E_0 close to this value. Similar measurements by Breckenridge, Blunt, Hosler, Frederikse, Becker and Oshinsky (1954) gave somewhat smaller, scattered values of E_0; the temperature shift of the absorption edge measured was also smaller and showed some scattering.

Moss (1954) estimated that the effect of electron–lattice interaction, given by (2.35), is small compared with the observed temperature shift of the energy gap, and that the lattice dilatation effect could account largely for the shift. Recently, Long and Miller (1955) and Keyes (1955) determined the variation of the energy gap with pressure by measuring the change of intrinsic conductivity. They obtained $(\partial E_i/\partial P)_T \sim 1{\cdot}5 \times 10^{-5}$ ev/atm, about three times larger than in germanium. This would account for the observed temperature shift, if the ratio of thermal coefficient of volume expansion to compressibility had a value of 20 kg cm^{-2} deg^{-1}. This value is not unreasonable, e.g. the value for germanium is 18·5 kg cm^{-2} deg^{-1}. Thus, it seems possible that the temperature shift of the energy gap is largely due to the thermal expansion of the lattice.

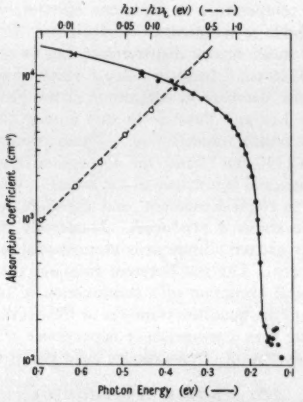

Figure 16. Absorption coefficient (solid curve) as a function of photon energy for a p-type InSb sample of high purity. The threshold energy is estimated to be $h\nu_t = 0{\cdot}175$ ev. The broken curve shows the absorption coefficient plotted against $h\nu - h\nu_t$. (Measured by G. W. Gobeli.)

By studying the magneto-resistance effect as a function of the angle between the current and the magnetic field, Pearson and Tanenbaum (1953) concluded that in the conduction band the surfaces of constant energy are spherical in **k** space. Recently, Dresselhaus, Kip, Kittel and Wagoner (1955) observed cyclotron resonance at 2·2°K corresponding to a small, 0·013m, isotropic effective mass, which was attributed to conduction electrons. In view of these results, we may assume that the bottom of the conduction band is at the centre of the Brillouin zone, $\mathbf{k} = 0$. On the other hand, the behaviour of the magneto-resistance effect in p-type samples, measured by Hatton and Rollin (1954), indicates that the valence band is more complicated. On the basis of theoretical considerations, Dresselhaus (1955) suggested that constant energy surfaces near the top of the valence band may be spheroids on ⟨111⟩ axes and that the peaks of the valence band may be close to the centre of the Brillouin zone. Thus, we may expect to have direct

transitions near the absorption edge, in contrast to germanium and silicon where the top of the valence band is at $\mathbf{k} = 0$, but the bottom of the conduction band corresponds to $\mathbf{k}$ values far away from the origin. The solid curve in figure 16 gives the absorption coefficient as a function of the photon energy obtained by Gobeli (unpublished) from transmission measurements on a sample which was intrinsic at room temperature. The two points indicated by crosses are taken from the results obtained by Moss (1954) from reflection measurements for a high conductivity n-type sample. As we shall see presently, the absorption edge is quite different in such samples, but the absorption should be the same at high levels, sufficiently away from the threshold. Assuming the steep edge to correspond to the threshold energy, we get $h\nu_t = 0{\cdot}175$ ev. The broken curve is the absorption coefficient as a function of $h\nu - h\nu_t$ in a log–log plot. It shows that the absorption coefficient is proportional to $(\nu - \nu_t)^{0{\cdot}6}$. This relationship is much closer to (2.14) for direct transitions than to (2.26) for indirect transitions. It should be noted that these results pertain to the range of absorption coefficient above 100 cm^{-1}. The tail end of absorption edge at small absorption levels, $< 100\ cm^{-1}$, has not yet been carefully investigated.

Assuming spherical energy surfaces in both the conduction and the valence bands, the expression for the product of densities of states (4.2) reduces to

$$N_c N_v = 4(2\pi kT/h^2)^3 (m_e m_h)^{3/2} \qquad \ldots\ldots(5.1)$$

where m_e and m_h are the effective masses of electrons and holes respectively. From the intrinsic carrier concentration, Tanenbaum and Maita (1953) found, by using (4.3), that a value of $(m_e m_h)^{1/2}/m = 0{\cdot}083$ corresponds to an energy gap of 0·18 ev at room temperature, with a variation of -3×10^{-4} ev deg^{-1}; these values are in close agreement with the results of optical measurements. Electrical measurements show that the electron mobility is one to two orders of magnitude higher than the hole mobility, indicating that the holes have a much larger effective mass. Thus m_e/m must be very small.

Tanenbaum and Briggs (1953) observed that the absorption edge in n-type samples with large amount of impurity lies at considerably shorter wavelengths than in purer samples. Burstein (1954) was first to suggest that the effect is due to the filling of the energy levels near the bottom of the conduction band. With a small effective mass, the electron gas becomes degenerate at high concentrations and fills up levels over an appreciable energy range. Transitions of electrons from the valence band take place only to unoccupied levels higher above, resulting in a shift of the absorption edge to higher energy. Comparing the absorption edges of two samples with different carrier concentrations, Burstein found that the effect is compatible with an electron effective mass of $0{\cdot}03m$.

Figure 17 shows the results obtained by three groups of investigators. The solid points are the results of Kaiser and Fan (1955). The values of $h\nu$ were taken corresponding to an absorption coefficient of 300 cm^{-1}. The points are to be compared with the curve calculated theoretically in the following way. Constant energy surfaces are assumed to be spherical in both bands with centre at $\mathbf{k} = 0$. The photon energy corresponding to the excitation of electrons with wave number $\mathbf{k}$ is the difference between the energy $\hbar^2 k^2/2m_e$ in the conduction band and the energy $-E_G - \hbar^2 k^2/2m_h$ in the valence band, the energies being

referred to the bottom of the conduction band. Thus

$$h\nu = E_G + \frac{m_e + m_h}{m_h}\frac{\hbar^2}{2m_e}k^2. \qquad \ldots\ldots(5.2)$$

The absorption coefficient is proportional to the probability of the level in the conduction band being unoccupied by electrons,

$$\frac{\alpha(\nu)}{\alpha_0(\nu)} = 1 - \frac{1}{\exp\left[(\hbar^2k^2/2m_e - \zeta)/kT\right] - 1} \qquad \ldots\ldots(5.3)$$

where α_0 is the absorption coefficient for the case of an empty conduction band and ζ is the Fermi level. Combining the two equations, we get

$$h\nu(\alpha) = E_G + \left(1 + \frac{m_e}{m_h}\right)\left[\zeta - kT\ln\left(\frac{\alpha_0 - \alpha}{\alpha}\right)\right]. \qquad \ldots\ldots(5.4)$$

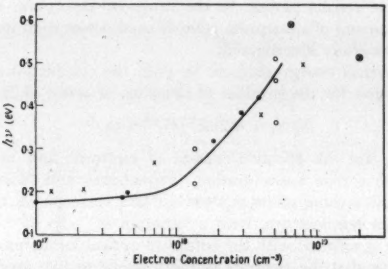

Figure 17. Photon energy corresponding to the absorption edge in n-type indium antimonide as a function of carrier concentration. The solid points and the curve are the experimental results and the calculated curve of Kaiser and Fan (1955). The crosses are the results of Hrostowski, Wheatley and Flood (1954). The circumscribed crosses were taken from polycrystalline samples. The open circles are the results of Breckenridge, Blunt, Hosler, Frederikse, Becker and Oshinsky (1954).

The curve was calculated according to this expression, taking $m_e = 0{\cdot}03m$ in the calculation of ζ. A value of 0·15 was taken for m_e/m_h. The values of $\alpha_0(\nu)$ can be taken from figure 16. The calculated curve is seen to agree fairly well with the solid points. The cross points were measured by Hrostowski, Wheatley and Flood (1954). The three points for small electron concentrations are higher than the calculated curve and led the authors to suggest that the electron effective mass varies linearly with ζ. The values of $h\nu$ taken correspond to 0·1% transmission and the thicknesses of the various samples were not specified. More extensive data seem to be required to verify this point.

The cyclotron resonance, observed by Dresselhaus *et al.* and attributed to the conduction electrons, also corresponds to a mass of $0{\cdot}012m$ instead of $0{\cdot}03m$. The observation was made at 2·2°K on a pure sample of small carrier concentration. It should be pointed out that the existence of degenerate semiconductors presents an interesting problem. It was first noted by Johnson and Lark-Horovitz (1947) that germanium samples with large impurity concentrations

become a degenerate semiconductor at sufficiently low temperatures. If the impurity levels are inside the energy gap, then the electrons or holes on becoming a degenerate gas would all be in the impurity states leaving no carriers in the conduction or the valence band. As the impurity concentration increases, the impurity states may form an energy band capable of giving conduction (Hung 1950, James and Ginzbarg 1953, Aigrain 1954). At high concentrations, separate impurity states may no longer exist, but the effect of the impurity centres will influence the states in the conduction band and affect the density of levels. Thus, it is possible that an effective mass used to characterize the density of states depends upon the impurity concentration. Recently Stern and Talley (unpublished)† made an estimate of this effect using a simple model of impurity atoms arranged in a regular lattice. To fit the observed shifts of the absorption edge in indium antimonide, an effective mass of 0·03m had to be assumed for the pure crystal.

5.2. *Long Wavelength Absorption*

Kaiser and Fan investigated the absorption at long wavelengths beyond the edge. In the intrinsic range, the absorption increases with wavelength and with temperature. The absorption can, therefore, be attributed to the free carriers.

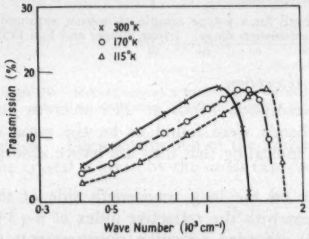

Figure 18 (*a*). Transmission as a function of frequency for an n-type sample of indium antimonide. (*After* Kaiser and Fan 1955.)

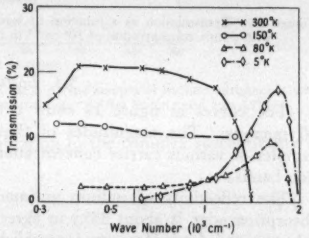

Figure 18 (*b*). Transmission as a function of frequency for a p-type sample of indium antimonide. (*After* Kaiser and Fan 1955.)

In the extrinsic range, the absorption increases with wavelength in n-type samples, whereas it remains practically constant, up to 25 microns, in p-type samples. Thus the absorption in intrinsic samples seems to be largely caused by the conduction electrons. Figures 18 (*a*), (*b*) show the transmission curves measured at different temperatures for an n-type and a p-type sample respectively. The interesting point to note is the decrease of transmission or increase of absorption with decreasing temperature. The conductivity and Hall coefficient in these samples did not show large variations over the temperature range. The behaviour is also shown by the curves in figure 19 for a p-type sample of much smaller carrier concentration, being near intrinsic at room temperature. The transmission at wavelengths below 25 microns decreased as the temperature was lowered from 210°K.

† The author is indebted to Dr. Stern for allowing him to see the manuscript of this paper.

The shape of the absorption spectrum in p-type samples and the variation with temperature cannot be readily explained on the basis of free carrier effect. Furthermore, in the samples studied by Kaiser and Fan the absorption did not vary as much as the carrier concentration. The long wavelength absorption in indium antimonide presents an interesting problem for future investigation.

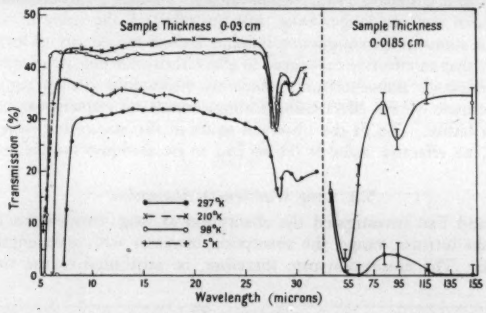

Figure 19. Transmission as a function of wavelength for a p-type sample of indium antimonide with a hole concentration of 10^{15} cm^{-3} in the exhaustion range. (*After* Spitzer and Fan 1955.)

5.3. *Lattice Absorption*

The curves in figure 19 show two absorption bands at 28·2 microns and 30 microns. The magnitudes of these bands were found to be the same in samples of various carrier concentrations, indicating that they are lattice absorption bands.

The reflectivity of indium antimonide on the long wavelength side of the absorption edge is about 35% in agreement with the refractive index of $n \sim 3{\cdot}9$. Johnson and Lark-Horovitz (unpublished) extended reflection measurements to 150 microns using residual rays. The study was continued by Spitzer and Fan (1955). The solid curves in figure 20 show the reflectivity for a p-type sample at two different temperatures. There is a strong reflection band at 52 microns. In addition, the room temperature curve shows high reflection above 100 microns which is not present in the low temperature curve. These effects show up correspondingly in the transmission curves. A strong absorption band is seen at 52 microns. At 78° K the absorption is small beyond this band, while at room temperature the absorption becomes very high above 100 microns.

Consider first the high reflection beyond 100 microns. The sample has a hole concentration of 10^{15} cm^{-3} at low temperatures and is intrinsic at room temperature with approximately 2×10^{16} cm^{-3} of holes and electrons. Another sample with a higher hole concentration, 10^{17} cm^{-3} at low temperatures, had at room temperature a small electron concentration, approximately 4×10^{15} cm^{-3}. The room temperature reflectivity in this sample did not rise beyond 100 microns, remaining about 35%. On the other hand, the reflectivity observed in an n-type sample of 10^{17} cm^{-3} electron concentration rose beyond 100 microns to an even

higher value than is shown by the room temperature curve in figure 20. These results lead to the conclusion that the high reflectivity at very long wavelengths is due to the absorption by conduction electrons, which increases with wavelength as discussed in the previous section.

The reflection band at 52 microns is the same in all samples. It is therefore a lattice band. The large effect indicates some degree of ionic binding in the

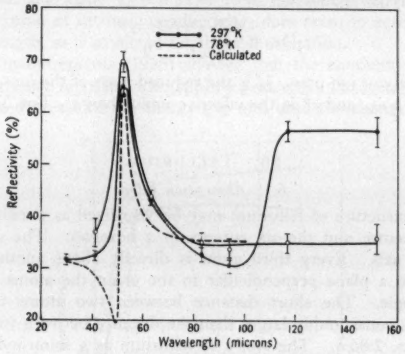

Figure 20. Reflectivity as a function of wavelength for a p-type sample of indium antimonide with a hole concentration of 10^5 cm^{-3} in the exhaustion range. (*After* Spitzer and Fan 1955.)

lattice. The contribution of the lattice vibration to the complex susceptibility of the crystal is given by the usual expression

$$\alpha_c = \frac{\Delta\epsilon_s}{4\pi} \frac{\omega_0^2}{(\omega_0^2 - \omega^2) + i\gamma\omega} \qquad \ldots\ldots(5.5)$$

where $\Delta\epsilon_s$ is the contribution to the static dielectric constant $\omega_0/2\pi$ is the vibration frequency, and γ is the broadening giving an absorption. When the free carrier effect is small, the dielectric constant at $\omega \ll \omega_0$ is higher than at $\omega \gg \omega_0$ by $\Delta\epsilon_s$, as in insulating crystals. The corresponding difference in reflectivity is

$$\Delta R = \left[\frac{(\epsilon + \Delta\epsilon_s)^{1/2} - 1}{(\epsilon + \Delta\epsilon_s)^{1/2} + 1}\right]^2 - \left[\frac{\epsilon^{1/2} - 1}{\epsilon^{1/2} + 1}\right]^2. \qquad \ldots\ldots(5.6)$$

Experimentally, where the electron concentration and carrier absorption are small, the reflectivity at long wavelengths is, within the experimental error, the same, 35%, as on the short wavelength side of the band. This fact can be seen in the low temperature curve in figure 20. It is estimated that $\Delta\epsilon_s = 1{\cdot}5$ as a limiting value. The broken curve in figure 20 is calculated using this value and $\gamma = 1{\cdot}3 \times 10^{12}\,\text{sec}^{-1}$. To get the observed high reflectivity at 52 microns, it is necessary to use a small value of γ which gives a very narrow band. The difference between the calculated curve and the experimental curves seems to be due to the fact that the band width of the residual rays used for the measurement is too wide. This explanation is supported by the following observation. The

peak reflectivity was determined by using the residual ray obtained with three NaCl crystals and an InSb crystal as the reflection plates. Using four NaCl plates, the measured peak reflectivity was considerably smaller, being 50% at 78°K instead of the 65% shown in figure 20. This result proves the narrowness of the band in InSb and shows the inadequacy of residual rays for determining its true shape.

Szigeti (1949) has shown that

$$\Delta\epsilon_s = \frac{4\pi N e^{*2}}{M\omega_0^2}\frac{(n^2+2)^2}{9} \qquad \ldots\ldots(5.7)$$

where N is density of ion pairs, M is the reduced mass of the ions, n is the refractive index for $\omega \gg \omega_0$, and e^* is the effective ionic charge. For $\Delta\epsilon_s = 1{\cdot}5$, we get $e^* = 0{\cdot}34e$.

§ 6. Tellurium

6.1. *Absorption Edge*

The crystal structure of tellurium may be visualized as parallel, spiral chains located at the centre and the six corners of a hexagon. The direction of the chains is the c axis. Every third atom is directly above another atom in the chain, so that in a plane perpendicular to the chain the atoms project into an equilateral triangle. The short distance between two atoms in neighbouring chains, 3·45 Å, is considerably larger than the distance between two neighbouring atoms in a chain, 2·86 Å. The study of tellurium as a semiconductor has been carried on by Lark-Horovitz and his associates at Purdue University during the last decade; extensive measurements on single crystals were made by Bottom (1949 a, b, 1952). The electrical conductivity reflects the anisotropy of the crystal structure, conductivity parallel to the c axis being about 1·9 times higher than that in a perpendicular direction. The temperature variation of intrinsic conductivity and Hall coefficient yields a value $E_0 = 0{\cdot}33 \pm 0{\cdot}01$ ev for the energy gap. A value of $0{\cdot}343 \pm 0{\cdot}005$ ev has been reported by Fukuroi (1951). So far, all tellurium crystals prepared at Purdue and in other laboratories are p-type in the extrinsic range. Doping with various impurities (Bottom 1949 a) has not succeeded in producing n-type samples. Another interesting point is the reversal of sign of the intrinsic Hall effect (Bottom 1949 b). The Hall effect being positive in the extrinsic range becomes negative as the sample becomes intrinsic, indicating that the electron mobility is higher than hole mobility. However, it changes again to positive sign above 230°C. The temperature at which the sample becomes intrinsic and the first sign reversal of Hall effect occurs can be changed by varying the impurity concentration. The second reversal, on the other hand, occurs always at the same temperature. Samples which have a very large impurity concentration and become intrinsic only above 230°C maintain positive Hall coefficient throughout the temperature range.

Moss (1949) observed photoconductivity in evaporated tellurium films and found that the long wavelength threshold is in the range 3·2 microns to 3·5 microns in approximate agreement with the value of E_0 given above. Infra-red transmission through bulk samples was reported by Loferski and Miller (1951, 1952). The observed absorption edge seemed to be shifted to shorter wavelengths for

radiation polarized with E vector parallel to the c axis as compared with the edge for radiation polarized perpendicular to the c axis, as shown by the transmission curves in figure 21 (Loferski 1954). Accurate determination of the threshold energy E_t from the absorption edge is always a problem. In the absence of a theory, a close estimate can not be obtained when the edge is not very steep, which seems to be the case for radiation polarized parallel to the c axis. However, we see that the value $E_0 = 0{\cdot}33$ ev (3·65 microns), determined from the temperature variation of intrinsic conductivity, does seem to agree with the edge of longer wavelength, as is expected for thermal excitation.

Bridgman's measurements (1925) showed that the conductivity of tellurium at a given temperature increases with applied pressure. Bardeen (1949) attributed this effect to the decrease of the energy gap and used the change of conductivity

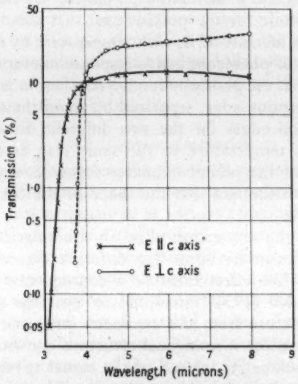

Figure 21. Transmission versus wavelength for a typical tellurium crystal, showing the effect of the direction of polarization of the radiation.

between two temperatures to calculate the intrinsic activation energy for different pressures. The results give an average value of $\partial E_t/\partial P = -1{\cdot}1 \times 10^{-5}$ ev cm^2 kg^{-1} in the pressure range 10 000 to 30 000 kg cm^{-2}; Bridgman's sample was not intrinsic at lower pressures. Using the mobilities and effective masses of electrons and holes, estimated from the analysis of conductivity and Hall effect, Bardeen and Shockley (1950) and Fukuroi (1951) calculated a value of about 4 ev for the lattice dilatation coefficient of the energy gap, $E_{1c} - E_{1v}$ in (2.32). Multiplied by the compressibility, this gives $\partial E_t/\partial P \sim -2 \times 10^{-5}$ ev cm^2 kg^{-1}. Of the two methods of estimating $\partial E_t/\partial P$ the first is more straightforward and should give the more reliable result, but the result was obtained for high pressures. The value of $\partial E_t/\partial P$ may be larger at low pressures. Recently Neuringer (1955) measured the shift of the absorption edge with pressure and obtained $\partial E_t/\partial P = -1{\cdot}9 \times 10^{-5}$ ev cm^2 kg^{-1} for radiation polarized parallel to the c axis. The edge for radiation polarized perpendicular to the c axis was observed to

shift also to smaller energy with increasing pressure, but a quantitative result has not yet been obtained. The shift of this edge is to be compared with the pressure effect on thermal activation energy.

The ratio of thermal expansion coefficient to compressibility for tellurium is $\beta/\chi \sim 10{\cdot}6$ kg cm^{-2} deg^{-1}. The variation of E_t resulting from the thermal expansion of the lattice is thus 1×10^{-4} to 2×10^{-4} ev deg^{-1}. Loferski (1954) observed that both edges shift by about $-0{\cdot}3\times10^{-4}$ ev deg^{-1}, in the temperature range 100°K to 400°K. Thus E_t actually decreases with increasing temperature although the effect of lattice dilatation is to increase it. A net of $-1{\cdot}3\times10^{-4}$ to $-2{\cdot}3\times10^{-4}$ ev deg^{-1} is to be attributed then to the effect of electron–lattice interaction. Using the theoretical expression (2.35) Fukuroi (1951) calculated a value of $-0{\cdot}68$ ev deg^{-1} for this effect. The expression is based on the simple model of spherical energy surfaces and a diamond type lattice. It can only be expected to give an order of magnitude for the present case. It should be pointed out that Moss (1950) obtained an increase of E_t with temperature by estimating E_t from the 'threshold' wavelength of photoconductive response in evaporated tellurium films. Loferski (1954) found that the photoconductive response in tellurium crystals shows two peaks near the absorption edge, separated by about the same difference in frequency as the absorption edges for the two different directions of polarization. These peaks shift with temperature in the same way as the absorption edges, while the 'threshold' of the photoconductive response appeared to shift in the opposite direction due to the fact that the shape of the curve near the threshold changes with temperature.

The dependence of the absorption edge on the polarization of the radiation shows that different transitions occur for different directions of the E vector relative to the c axis. The effect must be a consequence of selection rules for optical transitions. Callen (1954) attempted to treat the problem by deducing the electronic band structure from the symmetry properties of the crystal. He considered, for simplification, a tetragonal structure consisting of straight chains arranged with square symmetry, instead of the actual tellurium structure having spiral chains arranged with hexagonal symmetry. The assumed structure serves to indicate the effect of a large spacing between chains as compared with the interatomic distance within a chain, although the discussion cannot be entirely valid for tellurium. According to this work, the valence band is derived from the two atomic 4p states, the wave functions of which are each elongated along a direction perpendicular to the c axis. Because of the large spacing between chains, these wave functions do not overlap strongly, therefore the energy level is not broadened too much and the resulting band remains separated by an energy gap from the bands derived from higher atomic states. The valence band is filled by the four 4p valence electrons. The conduction band is derived from atomic 4d states. The energy level corresponding to the wave function elongated along the c axis is broadened into a wide band, the lowest level of which is the bottom of the conduction band. The energy levels corresponding to the wave functions elongated in a plane perpendicular to the c axis give narrow bands overlapped by the broad d band. With E vector perpendicular to the c axis, transitions are possible from the valence band to the bottom of the broad d band. On the other hand, for E vector parallel to the c axis, transitions from the valence

band are allowed only to the narrower d band within the broad band, giving thus a higher threshold energy.

Callen uses the structure of the conduction band discussed above to explain also the sign reversal of the intrinsic Hall effect. It is assumed that electrons near the bottom of the conduction band have a higher mobility than the holes, whereas electrons in the narrower band above have a lower mobility than the holes. The fraction of conduction electrons which is in the narrow band increases with increasing temperature. Thus the Hall effect becomes positive at sufficiently high temperatures as the mean-squared mobility of the electrons in the two bands becomes smaller than the hole mobility squared. Such explanation had been assumed previously by Fukuroi and Tanuma (1952).

From the crystal structure, tellurium might be expected to be doubly refracting. The refractive index, measured by Hartig and Loferski (1954) and given in table 1, is in fact quite different for radiations polarized parallel and perpendicular to the *c* axis. The birefringence should be mainly the consequence of the fact that the transitions between the valence band and the conduction band are different for different directions of polarization. According to (2.5), these transitions are important in determining the polarizability.

6.2. *Carrier Absorption*

The absorption at long wavelengths, up to 25 microns, has been investigated by Caldwell and Fan (1954) using single crystals and polarized radiation. Figure 22 shows the absorption curves measured at various temperatures. The solid curves were obtained on one sample and the broken curves were measured on another similar sample. The spectra for the two directions of polarization are quite different. With *E* vector perpendicular to the *c* axis, the absorption increases smoothly with wavelength, as may be expected for the free-carrier effect. On the other hand, the spectrum for *E* parallel to the *c* axis shows a pronounced band with a peak at about 11 microns. The absorption is higher for *E* parallel to the *c* axis due to the presence of this band. The band is present at low temperatures where the samples are extrinsic and p-type, as shown by the 200°K and 90°K curves; measurements on samples of different hole concentrations showed that the magnitude of the band is proportional to the hole concentration. Furthermore, in a given sample, this band increases with increasing temperature in the intrinsic range, indicating again that it is related to the concentration of free carriers. We conclude, therefore, that the absorption is associated with free holes. This suggests that there is another band about 0·1 ev below the top of the valence band. The presence of holes at the top of the valence band gives rise to optical transitions from the lower band, similar to the transitions from band 3 to band 1 in the valence band of germanium. The absence of this band for *E* perpendicular to the *c* axis implies that the transitions are forbidden by selection rules, and provides a useful information for the understanding of the band structure.

In the band structure proposed by Callen there is a band lying above the bottom of the conduction band. One might expect then to find an absorption band associated with transitions of conduction electrons between these two energy bands. Although optical transitions between the atomic d states, from which

the two energy bands are derived, is forbidden, the selection rule applies only for $\mathbf{k} = 0$. Experimentally, beside the 11 micron band associated with holes, no additional absorption band has been observed in the intrinsic range where the number of conduction electrons is about equal to the number of holes. However, the energy difference between the edges of the two energy bands may be as small as 0·05 ev, judging by the relative shift of the two absorption edges shown in figure 21. Absorption corresponding to electron transitions between these two bands may be beyond the limit of the measurements, 25 microns or 0·05 ev.

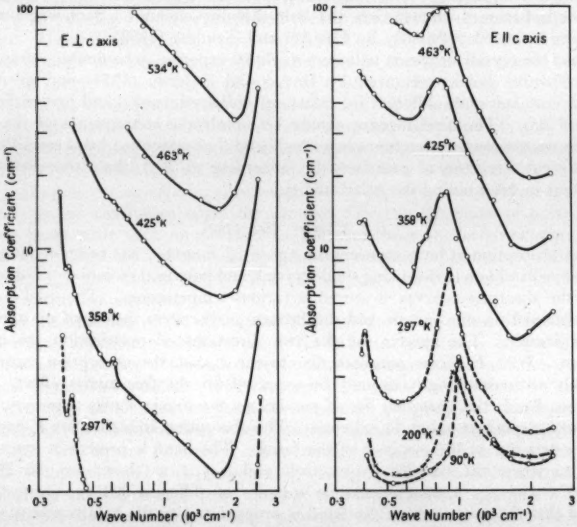

Figure 22. Absorption coefficient of single crystal samples of tellurium. The solid curves were measured on one sample and the broken curves were measured on another similar sample, by R. S. Caldwell (unpublished).

It seems possible that the overlapping energy bands in the valence band, revealed by the 11 micron absorption band, are actually responsible for the dependence of the absorption edge on the polarization of the radiation. Furthermore, by using (4.14*a*) to fit the shape of the absorption band the effective mass for the lower energy band is estimated to be about one third of the effective mass at the top of the valence band. The holes of sufficient energy to be in this energy band will have a much higher mobility. Calculations show that instead of assuming overlapping conduction bands to give lower mobility for high energy conduction electrons, the higher mobility of high energy holes is sufficient to give the sign reversal of Hall effect above 500°K. Conclusive experimental evidence is needed to decide between the two alternative interpretations.

There are two weak absorption bands at 24·4 microns and 14·8 microns respectively. Both can be seen in figure 22 on the 358°K curve for E perpendicular to the c axis. These bands are unrelated to the carrier concentration and are observed with radiation polarized in either direction, provided they are not masked by a high carrier absorption. They are, therefore, lattice absorption bands. The 14·8 micron band varies among different samples, e.g. it was not observed in the sample on which the 297°K curve for E parallel to the c axis was measured. It is probably associated with the presence of impurities.

Acknowledgments

I am indebted to Professor K. Lark-Horovitz for reading the manuscript and giving helpful criticism. I also wish to thank Mr. W. Spitzer for his assistance in preparing some of the figures.

References

Aigrain, P., 1954, *Physica*, **20**, 978.
Austin, I. G., and McClymont, D. R., 1954, *Physica*, **20**, 1077.
Avery, D. G., and Clegg, P. L., 1953, *Proc. Phys. Soc.* B, **66**, 512.
Bardeen, J., 1949, *Phys. Rev.*, **75**, 1777.
Bardeen, J., and Shockley, W., 1950, *Phys. Rev.*, **80**, 72.
Becker, M., 1951, *Ph.D. Thesis*, Purdue University.
Becker, M., and Fan, H. Y., 1949 a, *Phys. Rev.*, **76**, 1530; 1949 b, *Ibid.*, **76**, 1531.
Becker, M., Fan, H. Y., and Lark-Horovitz, K., 1952, *Phys. Rev.*, **85**, 730.
Blackwell, D. C., and Sutherland, G. B. B. M., 1949, *J. Chim. Phys.*, **46**, 9.
Born, M., 1946, *Nature, Lond.*, **157**, 582.
Bottom, V. E., 1949 a, *Ph.D. Thesis*, Purdue University; 1949 b, *Phys. Rev.*, **75**, 1310; 1952, *Science*, **115**, 570.
Breckenridge, R. G., Blunt, R. F., Hosler, W. R., Frederikse, H. P. R., Becker, J. H., and Oshinsky, W., 1954, *Phys. Rev.*, **96**, 571.
Bridgman, P. W., 1925, *Proc. Amer. Acad. Sci.*, **60**, 366.
Briggs, H. B., 1950 a, *Phys. Rev.*, **77**, 287; 1950 b, *Ibid.*, **77**, 727; 1952, *J. Opt. Soc. Amer.*, **42**, 686.
Briggs, H. B., Cummings, R. F., Hrostowski, H. J., and Tanenbaum, M., 1954, *Phys. Rev.*, **93**, 912.
Briggs, H. B., and Fletcher, R. C., 1952, *Phys. Rev.*, **87**, 1130; 1953, *Ibid.*, **91**, 1342.
Burstein, E., 1954, *Phys. Rev.*, **93**, 632.
Burstein, E., Bell, E. E., Davisson, J. W., and Lax, M., 1953, *J. Phys. Chem.*, **57**, 849.
Burstein, E., Davisson, J. W., Bell, E. E., Turner, W. J., and Lipson, A. H., 1954, *Phys. Rev.*, **93**, 65.
Burstein, E., Henvis, B. W., and Sclar, N., 1954, *Phys. Rev.*, **94**, 750.
Burstein, E., and Oberly, J. J., 1950, *Phys. Rev.*, **78**, 642.
Burstein, E., Oberly, J. J., and Davisson, J. W., 1953, *Phys. Rev.*, **89**, 331.
Burstein, E., Oberly, J. J., Davisson, J. W., and Henvis, B. W., 1951, *Phys. Rev.*, **82**, 764.
Burstein, E., Picus, G., Henvis, B., and Lax, M., 1955, *Phys. Rev.*, **98**, 1536.
Burstein, E., Picus, G. S., and Sclar, N., 1954, presented at Conference on Photoconductivity, Atlantic City, will appear in the Proceedings of the Conference.
Burton, J. A., 1954, *Physica*, **20**, 845.
Burton, J. A., Hull, G. W., Morin, F. J., and Severiens, J. C., 1953, *J. Phys. Chem.*, **57**, 853.
Caldwell, R. S., and Fan, H. Y., 1954, *Phys. Rev.*, **94**, 1427.
Callen, H. B., 1954, *J. Chem. Phys.*, **22**, 518.
Cheeseman, I. C., 1952, *Proc. Phys. Soc.* A, **65**, 25.
Collins, R. J., 1953, *Thesis*, Purdue University.
Collins, R. J., and Fan, H. Y., 1952, *Phys. Rev.*, **86**, 648; 1954, *Ibid.*, **93**, 674.

DASH, W. C., NEWMAN, R., and TAFT, E. A., 1955, *Phys. Rev.*, **98**, 1192.
DEXTER, D. L., 1954, *Proceedings of Photoconductivity Conference, Atlantic City*.
DRESSELHAUS, G., 1955, *Phys. Rev.*, **100**, 580.
DRESSELHAUS, G., KIP, A. F., and KITTEL, C., 1954, *Phys. Rev.*, **95**, 568; 1955, *Ibid.*, **98**, 368.
DRESSELHAUS, G., KIP, A. F., KITTEL, C., and WAGONER, G., 1955, *Phys. Rev.*, **98**, 556.
FAN, H. Y., 1950, *Phys. Rev.*, **78**, 808; 1951, *Ibid.*, **82**, 900; 1952, *Ibid.*, **85**, 730.
FAN, H. Y., and BECKER, M., 1950, *Phys. Rev.*, **78**, 178; 1951, *Semiconducting Materials* (*Reading Conference*), Ed. H. K. Henisch, pp. 132–147 (London: Butterworths Scientific Publications).
FAN, H. Y., KAISER, W., KLONTZ, E., LARK-HOROVITZ, K., and PEPPER, R. R., 1954, *Phys. Rev.*, **95**, 1087.
FAN, H. Y., SHEPHERD, M., and SPITZER, W., 1954, Paper presented at the Photoconductivity Conference, Atlantic City, to be published in the Conference Proceedings.
FRÖHLICH, H., 1936, *Elektronentheorie der Metalle* (Berlin: Springer).
FUKUROI, T., 1951, *Sci. Rep. Res. Insts, Tôhoku Univ.*, **A3**, 175.
FUKUROI, T., and TANUMA, S., 1952, *Sci. Rep. Res. Insts, Tôhoku Univ.*, **A4**, 353.
HALL, H., 1936, *Rev. Mod. Phys.*, **8**, 359.
HALL, L. H., BARDEEN, J., and BLATT, F. J., 1954, *Phys. Rev.*, **95**, 559; see also the Paper by the same authors presented at the Photoconductivity Conference, Atlantic City, 1954, to be published in the Conference Proceedings.
HARTIG, P. A., and LOFERSKI, J. J., 1954, *J. Opt. Soc. Amer.*, **44**, 17.
HATTON, J., and ROLLIN, B. V., 1954, *Proc. Phys. Soc.* A, **67**, 385.
HAYNES, J. R., 1955, *Phys. Rev.*, **98**, 1866.
HERMAN, F., 1954, *Phys. Rev.*, **95**, 847.
HERMAN, F., and CALLAWAY, J., 1953, *Phys. Rev.*, **89**, 518.
HROSTOWSKI, H. J., WHEATLEY, G. H., and FLOOD, W. F., 1954, *Phys. Rev.*, **95**, 1683.
HSIEH, Y. C., 1954, *J. Chem. Phys.*, **22**, 306.
HUNG, C. S., 1950, *Phys. Rev.*, **79**, 727.
JAMES, H. M., 1954, Paper presented at the Photoconductivity Conference, Atlantic City, to be published in the Conference Proceedings.
JAMES, H. M., and GINZBARG, A. S., 1953, *J. Phys. Chem.*, **57**, 840.
JAMES, H. M., and LARK-HOROVITZ, K., 1951, *Z. Phys. Chem.*, **198**, 107.
JOHNSON, E. J., and SPITZER, W. G., 1954, *Phys. Rev.*, **94**, 1415.
JOHNSON, V. A., and LARK-HOROVITZ, K., 1947, *Phys. Rev.*, **71**, 374.
KAHN, A. H., 1955, *Phys. Rev.*, **97**, 1647.
KAISER, W., COLLINS, R. J., and FAN, H. Y., 1953 a, *Phys. Rev.*, **91**, 230; 1953 b, *Ibid.*, **91**, 1380.
KAISER, W., and FAN, H. Y., 1954 a, *Phys. Rev.*, **93**, 977; 1954 b, *Ibid.*, **94**, 1431; 1955, *Ibid.*, **98**, 966.
KEYES, R. W., 1955, *Phys. Rev.*, **99**, 626.
KITTEL, C., and MITCHELL, A. H., 1954, *Phys. Rev.*, **96**, 1488.
KLEINER, W. H., 1955, *Phys. Rev.*, **97**, 1722.
KOHN, W., 1955, *Phys. Rev.*, **98**, 1856.
KOHN, W., and LUTTINGER, J. M., 1955, *Phys. Rev.*, **98**, 915.
KOSTER, G. F., and SLATER, J. C., 1954, *Phys. Rev.*, **96**, 1208.
KRONIG, R. DE L., 1931, *Proc. Roy. Soc.* A, **133**, 245.
LAMPERT, M. A., 1955, *Phys. Rev.*, **97**, 352.
LARK-HOROVITZ, K., and MEISSNER, K. W., 1949, *Phys. Rev.*, **76**, 1530.
LAX, M., 1954, presented at the Photoconductivity Conference, Atlantic City, to be published in the Conference Proceedings.
LAX, M., and BURSTEIN, E., 1955, *Phys. Rev.*, **97**, 39.
LIPSON, H. G., BURSTEIN, E., and SMITH, L., 1955, *Phys. Rev.*, **99**, 444.
LOFERSKI, J. J., 1954, *Phys. Rev.*, **93**, 707.
LOFERSKI, J. J., and MILLER, P. H., 1951, *Phys. Rev.*, **83**, 876; 1952, *Ibid.*, **86**, 652.
LONG, D., and MILLER, P. H., 1955, *Phys. Rev.*, **98**, 1192.
LORD, R. C., 1952, *Phys. Rev.*, **85**, 140.

LUTTINGER, J. M., and KOHN, W., 1955, *Phys. Rev.*, **97**, 869.
MACFARLANE, G. G., and ROBERTS, V., 1955 a, *Phys. Rev.*, **97**, 1714 ; 1955 b, *Ibid.*, **98**, 1865.
MADELUNG, O., and WEISS, H., 1954, *Z. Naturf.*, **9a**, 527.
MORIN, F. J., and MAITA, J. P., 1954 a, *Phys. Rev.*, **94**, 1525 ; 1954 b, *Ibid.*, **96**, 28.
MORTON, J. A., HAHN, E. E., and SCHULTZ, M. L., 1954, *Proceedings of the Photoconductivity Conference, Atlantic City.*
MOSS, T. S., 1949, *Proc. Phys. Soc.* A, **62**, 264 ; 1950, *Phys. Rev.*, **79**, 1011 ; 1954, Paper presented at the Conference on Photoconductivity, Atlantic City, to be published in the Conference Proceedings.
MUTO, T., and OYAMA, S., 1950, *Progr. Theor. Phys., Osaka*, **5**, 833.
NEURINGER, L. J., 1955, *Phys. Rev.*, **98**, 1193.
NEWMAN, R., 1954, *Phys. Rev.*, **94**, 278.
NEWMAN, R., and TYLER, W. W., 1954, *Phys. Rev.*, **96**, 882.
O'BRYAN, H. M., 1936, *J. Opt. Soc. Amer.*, **26**, 122.
PAUL, W., and BROOKS, H., 1954, *Phys. Rev.*, **94**, 1128.
PAUL, W., and PEARSON, G. L., 1955, *Phys. Rev.*, **98**, 1755.
PEARSON, G. L., and TANENBAUM, M., 1953, *Phys. Rev.*, **90**, 153.
RANK, D. H., and CRONEMEYER, D. C., 1953, *Phys. Rev.*, **90**, 202.
ROLLIN, B. V., and SIMMONS, E. L., 1952, *Proc. Phys. Soc.* B, **65**, 995 ; 1953, *Ibid.*, **66**, 161.
SMITH, H., 1948–49, *Phil. Trans. Roy. Soc.* A, **241**, 105.
SOMMERFELD, A., 1931, *Ann. Phys., Lpz.*, **11**, 257.
SPITZER, W., BENNETT, C. O., and FAN, H. Y., 1955, *Phys. Rev.*, **98**, 228.
SPITZER, W. G., COLLINS, R. J., and FAN, H. Y., 1955, *Phys. Rev.*, **98**, 1536.
SPITZER, W., and FAN, H. Y., 1955, *Phys. Rev.*, **99**, 1891.
STOECKMANN, F., KLONTZ, E., FAN, H. Y., and LARK-HOROVITZ, K., 1955, *Phys. Rev.*, **98**, 1535.
SZIGETI, B., 1949, *Trans. Faraday Soc.*, **45**, 155.
TANENBAUM, M., and BRIGGS, H. B., 1953, *Phys. Rev.*, **91**, 1561.
TANENBAUM, M., and MAITA, J. P., 1953, *Phys. Rev.*, **91**, 1009.
TYLER, W. W., NEWMAN, R., and WOODBURY, H. H., 1955 a, *Phys. Rev.*, **97**, 669 ; 1955 b, *Ibid.*, **98**, 461.
WARSHAUER, D. M., PAUL, W., and BROOKS, H., 1955, *Phys. Rev.*, **98**, 1193.
WELKER, H., 1954, *Physica*, **20**, 893.
WOLFE, R., 1954, *Proc. Phys. Soc.* A, **67**, 74.
WOODBURY, H. H., and TYLER, W. W., 1955, *Phys. Rev.*, **98**, 1534.

AERO-THERMOACOUSTICS

(THE GENERATION OF SOUND BY TURBULENCE AND BY HEAT PROCESSES)

By O. K. MAWARDI†

Massachusetts Institute of Technology, Cambridge, Massachusetts

CONTENTS

	PAGE
§ 1. Introduction	156
§ 2. Sounds of aerodynamic origin	157
2.1. The mechanism of interaction	157
2.2. Turbulence and sound	160
2.2.1. The sound sources	161
2.2.2. Sound production and moving frame of reference	164
2.2.3. The effect of shear on the sound production	165
2.2.4. Dimensional analysis of sound production	166
2.2.5. Experimental findings	167
2.3. Effect of solid boundaries on sound production	170
2.3.1. Sound generation in a boundary layer	171
2.4. The scattering of sound by turbulence	175
§ 3. The interaction of heat with sound	178
3.1. Thermally induced sound fields	178
3.2. The Rijke phenomenon	179
3.2.1. Experimental results	182
3.3. Flame-driven acoustic oscillations	184
§ 4. Conclusion	186
References	186

Abstract. An analysis of the general equations of motion of a viscous compressible fluid leads to the identification of three modes (vorticity, compression and entropy modes) of energy associated with the fluid. Interaction between these modes gives rise to acoustical phenomena, of which some are of great interest to the study of aircraft noises.

The first part of this report deals with acoustical effects resulting from the interaction of a vorticity and a compression mode. It considers in detail the generation of sound from turbulence as encountered in a jet and in a boundary layer, and the scattering of sound from turbulence.

In the remaining part the interaction of the entropy mode with the compression mode is discussed. Special emphasis has been placed on the study of heat-maintained vibrations as encountered in Rijke's phenomenon and in flame-driven oscillations.

The article concludes with a speculative discussion of acoustical phenomena in which the couplings between the three modes are equally important.

§ 1. Introduction

The subject matter of this report is aero-thermoacoustics, the phase of acoustics dealing with sounds generated aerodynamically and/or with heat-maintained sounds. The mechanism of these sounds, by-products of airflows, is quite distinct from that of sound production by the vibration of solids.

† John Simon Guggenheim Fellow, 1954–1955.

The interest in aero-thermoacoustics has been instigated in part by the need for an understanding of acoustical phenomena associated with aircraft sounds. These, however, are special cases of a wide variety of sounds associated with fluctuating airflows. The fluctuations may be the result of an instability of some sort which in the absence of heat sources in the airflow give rise, at low Reynolds number, to a regular eddy pattern responsible for the maintenance of sound in wind instruments. On the other hand, at high Reynolds number these fluctuations cause the flow to assume a turbulent pattern and the associated sound has a broad band spectrum.

The presence of heat sources in the airflow completely alters the physics of the situation. A fluctuating transfer of heat can under certain conditions introduce an instability into the flow and can be responsible for the maintenance of oscillations similar to those encountered in the Rijke phenomenon.

There has been in the past a number of investigations dealing with these sounds of aero-thermoacoustic origin. The emphasis, however, was placed on an estimation of the frequency of the sounds emitted with no attempt at finding the intensity of the sound produced. The studies often started from the premise that the problem was essentially concerned with unstable flows, little attention if any being given to the allied acoustical effects. No attempt, furthermore, was made at establishing a generalized theory of this class of phenomena.

The present report has been divided in two parts. The first of these deals with acoustic effects associated with the turbulent flow of a fluid. Prime importance is given to the sounds associated with turbulence because of the current desire to understand the mechanism of sound production by means of jets, and because of the almost invariable occurrence of turbulence in fast-moving fluids. The second part of the report will be concerned with acoustic effects resulting from heat sources in the flow.

§ 2. Sounds of Aerodynamic Origin

2.1. *The Mechanism of Interaction*

The equations governing the flow of viscous fluids cannot be readily derived from a Lagrangian or Hamiltonian formulation. Although several attempts have been made to formulate a variation principle from which these flow relations can be deduced, the Navier–Stokes relation is still best interpreted as the energy–momentum conservation criterion of conventional field theory. The Lagrangian concept, however, leads to a very powerful technique for the generalized discussion of interaction between systems. That the explanation of the mechanisms of the phenomena described in this report is closely linked with interaction processes is readily predicted on the basis of physical intuition.

By a careful analysis of the kinematics of turbulence of a compressible fluid Moyal (1952) was able to prove the existence of a coupling between the vorticity, dilatation, entropy and pressure fields associated with the flow. A more interesting presentation of these same concepts has recently been given by Kováznay (1953). The starting point of his discussion is the relations for the conservation of momentum, energy and mass together with the equation of state.

These well-known relations for a Stokesian gas are respectively

$$\rho\frac{\partial \mathbf{V}}{\partial t} = -\nabla p - \tfrac{1}{2}\rho\nabla(\mathbf{V}.\mathbf{V}) + \rho(\mathbf{V}\times\nabla\times\mathbf{V}) + \mu(\nabla^2\mathbf{V} + \tfrac{1}{3}\nabla\nabla.\mathbf{V}), \quad \ldots\ldots(1)$$

$$\rho C_p\frac{\partial T}{\partial t} = k\nabla^2 T + \frac{\partial p}{\partial t} + \mathbf{V}.\nabla p - \rho C_p\mathbf{V}.\nabla T + \phi, \quad \ldots\ldots(2)$$

$$\frac{\partial \rho}{\partial t} + \nabla.(\rho\mathbf{V}) = 0, \quad \ldots\ldots(3)$$

and finally,

$$\frac{p}{\rho} = \frac{\gamma-1}{\gamma}C_p T. \quad \ldots\ldots(4)$$

In the above relations ρ stands for the density of the fluid, p for its pressure, $\mathbf{V}$ for its velocity, C_p for its specific heat at constant pressure, γ for the ratio of specific heats, μ for the coefficient of viscosity, k for the coefficient of thermal conductivity and ϕ for the dissipation function. In vector notation the latter function is

$$\phi = \mu[(\nabla\times\mathbf{V}).(\nabla\times\mathbf{V}) + \nabla^2(\mathbf{V}.\mathbf{V}) - \tfrac{2}{3}(\nabla.\mathbf{V})^2 - 2\nabla.(\mathbf{V}\times\nabla\times\mathbf{V}) - 2\mathbf{V}.(\nabla\nabla.\mathbf{V})]. \quad \ldots\ldots(5)$$

To simplify the discussion Kováznay considers the case of a fluid flow in which the turbulence is restricted to a finite domain G. A moving system of coordinates is now chosen so that the average value of the fluctuating velocity reckoned with respect to this moving frame of reference vanishes inside G. When the fluctuations of the parameters describing the flow are much smaller than their average values, and furthermore when the fluctuations of the velocity are negligible in comparison with the sound velocity, equations (1) to (4) can be solved by a perturbation method. The additional restrictive assumption of the exclusion of solid boundaries in G and at its boundaries extends the range of validity of the solution to the entire domain of G.

Introducing fluctuating quantities by means of the notation $T = T_0 + \theta$, $p = P_0 + \Delta p$; $\rho = \rho_0 + \Delta\rho$ where quantities with a subscript denote averaged values, Kováznay finds by manipulation of equations (1) to (4) that to a first order these same relations yield a new set which is

$$\frac{\partial \boldsymbol{\omega}}{\partial t} - \nu\nabla^2\boldsymbol{\omega} = 0 \quad \ldots\ldots(6)$$

$$\frac{\partial \mathscr{S}}{\partial t} - \frac{4\nu}{3}\nabla^2\mathscr{S} = -\frac{4(\gamma-1)\nu}{3C^2}\nabla^2\mathscr{P} \quad \ldots\ldots(7)$$

$$\frac{1}{C^2}\frac{\partial^2\mathscr{P}}{\partial t^2} - \nabla^2\mathscr{P} - \frac{4\gamma\nu}{3C^2}\frac{\partial\nabla^2\mathscr{P}}{\partial t} = 0. \quad \ldots\ldots(8)$$

The $\boldsymbol{\omega}$ occurring in the above equations is $\nabla\times\mathbf{V}$, $\mathscr{P} = \Delta p/\gamma P_0$ is a non-dimensional pressure, $\nu = \mu/\rho$ is the kinematic viscosity and $\mathscr{S}$ is a non-dimensional entropy defined by means of $\mathscr{S} = \theta/T_0 - (\gamma-1)\mathscr{P}$.

By inspection of equations (6) to (8) it is possible to identify three modes associated with the motion of the fluid. These correspond to modes of vorticity, equation (6), entropy, equation (7), and compression, equation (8). The first two modes obey a diffusion equation, the third a wave equation. For small perturbations there is consequently no interaction inside G between the vorticity and the entropy or compression. When non-interacting modes, however, pass through a region of strong gradient they may interact with the strong field and conversion from one mode to the other is possible. This question will be discussed at great length in following sections.

When the magnitudes of the fluctuations are not small enough to warrant the use of a first-order approximation but at the same time are not too large completely to destroy the picture of modes, it is possible to work out a theory of weak interaction. Under these conditions the three relations (6), (7) and (8) can be formally represented by

$$\frac{\partial \boldsymbol{\omega}}{\partial t} - \nu \nabla^2 \boldsymbol{\omega} = f_1(\boldsymbol{\omega}, \mathscr{P}, \mathscr{S}) \qquad \ldots\ldots(9)$$

$$\frac{\partial \mathscr{S}}{\partial t} - \frac{4\nu}{3} \nabla^2 \mathscr{S} = f_2(\boldsymbol{\omega}, \mathscr{P}, \mathscr{S}) \qquad \ldots\ldots(10)$$

$$\frac{1}{c^2} \frac{\partial^2 \mathscr{P}}{\partial t^2} - \nabla^2 \mathscr{P} - \frac{4\gamma\nu}{3c^2} \frac{\partial \nabla^2 \mathscr{P}}{\partial t^2} = f_3(\boldsymbol{\omega}, \mathscr{P}, \mathscr{P}). \qquad \ldots\ldots(11)$$

The functions f_1, f_2 and f_3 can functionally be considered as sources. Physically f_1 can be visualized as the rate of vorticity created by the combined action of the three modes, and similarly f_2 and f_3 are the rates of entropy and pressure fluctuations caused by the weak interaction between the fields.

In a second-order interaction each one of the functions f_1, f_2 and f_3 can be considered to be the sum of six terms each of which has a well-defined physical interpretation. The function of special interest to the subject matter of this report is f_3. For this reason it will be considered in some detail. We expect to find for this function an expression of the form

$$f_3(\boldsymbol{\omega}, \mathscr{P}, \mathscr{S}) = f_{3,1}(\boldsymbol{\omega}, \boldsymbol{\omega}) + f_{3,2}(\mathscr{P}, \mathscr{P}) + f_{3,3}(\mathscr{S}, \mathscr{S}) + f_{3,4}(\boldsymbol{\omega}, \mathscr{P}) + f_{3,5}(\boldsymbol{\omega}, \mathscr{S}) + f_{3,6}(\mathscr{S}, \mathscr{P}). \qquad \ldots\ldots(12)$$

The term $f_{3,1}(\boldsymbol{\omega}, \boldsymbol{\omega})$ represents the strength of the source of sound generated by the vorticity in the flow, $f_{3,3}(\mathscr{S}, \mathscr{S})$ the strength of the source of sound caused by temperature irregularities in the flow, and $f_{3,5}(\boldsymbol{\omega}, \mathscr{S})$ that of the source of sound due to vorticity mixing of the temperature irregularities. The remaining terms are not true sources. Thus, $f_{3,2}(\mathscr{P}, \mathscr{P})$ is closely associated with the non-linear term usually responsible for the steepening of the sound waves during their propagation, while $f_{3,4}(\boldsymbol{\omega}, \mathscr{P})$ and $f_{3,6}(\mathscr{S}, \mathscr{P})$ are linked with the scattering of the sound wave by the vorticity and the temperature fluctuations respectively.

The mechanisms underlying the terms of equation (12) have been far from completely understood. It is only recently that progress has been made toward clarifying some of the aspects of aero-thermoacoustics which are represented by the f functions. Actually the content of this report will in great part consist in theoretical and experimental findings related to these functions.

2.2. *Turbulence and Sound*

The general theory for the generation of sound waves from turbulence was explained for the first time by Lighthill (1952). The case he first considered is that of the generation of sound from a turbulent field restricted in a finite domain G of volume V. No solid boundaries are assumed to be present in G or at its boundaries. The restrictions of solid boundaries do not invalidate the generality of Lighthill's theory and an extension of his work to include solid boundaries is considered in a later section. It is first assumed that the turbulence is immersed in a medium at rest. The result of the discussion can readily be adapted to moving reference axes. This mathematical extension will be shown later.

The starting point of the discussion is the equations (1) and (3) for the conservation of momentum and of matter. The former relation (1) is first rewritten in Reynolds' form

$$\frac{\partial}{\partial t}(\rho v_i)+\frac{\partial}{\partial x_j}(\rho v_i v_j+p_{ij})=0 \qquad \ldots\ldots(13)$$

in which tensor notation has been introduced and where p_{ij} is the compressive stress tensor. The latter includes all the viscous stresses. Combining (13) with (3) and subtracting $c_0^2\nabla^2\rho$ from both sides of the equation, there follows

$$c_0^2\nabla^2\rho-\frac{\partial^2\rho}{\partial t^2}=-\frac{\partial^2 T_{ij}}{\partial x_i\partial x_j}. \qquad \ldots\ldots(14)$$

In the above relation the tensor T_{ij} stands for $\rho v_i v_j+p_{ij}-c_0^2\nabla^2\rho\delta_{ij}$ and c_0 denotes the velocity of propagation of sound waves outside G where the medium is assumed to be at *rest*.

It can be argued now that equation (14) describes the differential relation of the sound aerodynamically generated and for which the equivalent external stress field is expressed by the right-hand side of (14). Furthermore, the formulation of (14) is done in such a manner as to incorporate in the terms of the right-hand side effects such as the convection and scattering of sound by the turbulent flow. Whereas equation (11) is an approximate derivation obtained by a perturbation method, equation (14) is rigorously exact. Thus, although the physical interpretation of the analysis is complicated by the fact that the equivalent sources [i.e. the right-hand side of (14)] are treated as uniform and stationary, Lighthill's method of investigation is quite general and thus is very powerful.

The density fluctuations outside the turbulence in the domain G will propagate with a sound velocity c_0 and are formally found by means of

$$\rho(\mathbf{x},t)-\rho_0=\frac{1}{4\pi c_0^2}\int\delta\left(t'-t+\frac{|\mathbf{x}+\mathbf{x}'|}{c_0}\right)\Big/|\mathbf{x}-\mathbf{x}'|\frac{\partial^2 T_{ij}(\mathbf{x}',t')}{\partial x_i\partial x_j}\,d\mathbf{x}'\,dt', \qquad \ldots\ldots(15)$$

where the integration is carried only over the volume of the turbulence, since by hypothesis the applied stress field represented by T_{ij} vanishes outside G. When the viscous stresses and the heat conduction effects are small, so that the expression for the conservation of energy, equation (2), can be approximated to that for an isentropic process, the tensor $T_{ij}\simeq\rho v_i v_j+\Delta p-c_0^2\Delta\rho$. It is now noticed (Kraichnan

1953) that equation (15) becomes in fact an integral equation for the unknown density ρ. This integral equation, however, can be solved by a method of successive approximation. Indeed, the use of two successive iterations leads to the approximation $T_{ij} \sim \rho_0 v_i v_j$. The order of magnitude of the error committed in the true value of T_{ij} when the number of iterations is limited to two, is readily evaluated to be proportional to the square of the Mach number M.

The substitution of $\rho_0 v_i v_j$ for T_{ij} inside G is equivalent to considering the density ρ to be a constant equal to ρ_0. But this implies that the turbulence field is simulated to a first approximation by that of an *incompressible* fluid flow localized inside G. The equation (14) with the new form of T_{ij} reduces to a form similar to that of equation (11), with the f_3 function becoming a term which involves only the vorticity of the fluid. This is tantamount to defining a relation for the mechanism of sound production in which the energy of shear (turbulence) is transformed in part to an energy of compression in the form of acoustic radiation.

2.2.1. *The sound sources.*

An old theorem due to Lamb (1879) states that the effect of a fluctuating force concentrated at *a point* is equivalent to an acoustic dipole localized at this point. This theorem was used by Lighthill as the starting point of a demonstration in which he showed that the equivalent stress field is in fact a quadrupole field whose strength per unit volume is the tensor T_{ij}. The proof is readily found by inspection of equation (13). The Reynolds stresses T_{ij} produce a force per unit volume which by (13) is actually $-\partial T_{ij}/\partial x_j$. But the right-hand side of (14), i.e. the effective sources, are in fact $-\partial^2 T_{ij}/\partial x_i \partial x_j$. Consequently, the source field is identified by a quantity which is the gradient of a dipole field. But this latter distribution corresponds to that of a quadrupole field, as is made apparent from the construction of any one of the components of the gradient by means of the limiting process

$$\lim_{\Delta x_3 \to 0} \left[\left(\frac{\partial T_{ij}}{\partial x_i}(x_1, x_2, x_3 + \Delta x_3) - \frac{\partial T_{ij}}{\partial x_i}(x_1, x_2, x_3) \right) \Big/ \Delta x_3 \right].$$

This relation describes the addition of two dipoles of *opposite* sign and by definition is, in the limit of a vanishing Δx_3, a quadrupole point source, thus proving the proposition.

The sound intensity is the quantity which is of special interest to workers in acoustics since all discussions pertaining to noise evaluations are based on intensity measurements. It is well known that there is a simple relation between the intensity and the density fluctuation: the intensity is c_0^3 times the square of the density fluctuation $\Delta\rho$. When the flow is turbulent it is expected that the whole field contributes in an ergodic manner to the sound production. Accordingly, it is the variance of the condensation which has to be taken instead of the condensation itself. The intensity at a point outside the domain G is therefore obtained directly by using the result of equation (15) together with the simple formula giving the dependence of the intensity on the square of the condensation. In view of the symmetrical appearance of time and distance in the argument of T_{ij} when the retarded potential effect is introduced, the space derivative in the integrand can be substituted for a time derivative with a constant factor $1/c_0$.

Accordingly, the intensity is given by

$$I(\mathbf{x}) = \frac{1}{16\pi^2\rho_0 c_0^5}\iint\frac{(x_i-y_i)(x_j-y_j)(x_k-z_k)(x_l-z_l)}{|\mathbf{x}-\mathbf{y}|^3\,|\mathbf{x}-\mathbf{z}|^3} \times\left[\frac{\partial^2}{\partial t^2}T_{ij}\left(\mathbf{y},t-\frac{|\mathbf{x}-\mathbf{y}|}{c_0}\right)\frac{\partial^2}{\partial t^2}T_{kl}\left(\mathbf{z},t-\frac{|\mathbf{x}-\mathbf{z}|}{c_0}\right)\right]_{\text{av}}d\mathbf{y}\,d\mathbf{z}. \qquad \ldots\ldots(16)$$

The domain of integration is extended over that of G.

The concept of the quadrupole sources is very useful in deriving several characteristics of sound due to the turbulence. First it is observed that if the strength of two quadrupoles are uncorrelated then the intensity of the field due to both together is the sum of the intensity of the fields of each one taken separately. But the statistical behaviour of the velocities in the turbulent field is such that there is no correlation between the values of the velocities at points distant by an amount greater than a typical dimension L. Accordingly, if one divides the field into an imaginary set of non-overlapping regions which completely fills the domain G each with a volume of the order of L^3, then the intensity as derived by equation (16) can be considered as the contribution of the intensity due to the field produced by a distribution of point quadrupoles localized in these non-overlapping regions. Actually each one of these elementary regions is really made up in its turn of a distribution of quadrupoles whose strength distribution is described by the correlation curve for T_{ij}. If as a first approximation this correlation curve is replaced by one of square shape, then all the quadrupoles in the elementary volume are in phase, and are of equal strength. The problem of the evaluation of the sound field produced by the turbulence thus reduces to the consideration of the radiation field from this array of quadrupoles.

The total power radiated from any one volume L^3 is readily determined by integrating the value of the intensity given by equation (16) over a sphere of radius x very large compared with the scale of the volume V of the turbulence field. This power is readily found to be

$$P = \frac{1}{60\pi\rho_0 c_0^5}\iint\left[\frac{\partial^2}{\partial t^2}T_{ij}\left(\mathbf{y},t\frac{|\mathbf{x}-\mathbf{y}|}{c_0}\right)\frac{\partial^2}{\partial t^2}T_{kl}\left(\mathbf{z},t\frac{|\mathbf{x}-\mathbf{z}|}{c_0}\right)\right]_{\text{av}}\epsilon_{ijkl}\,d\mathbf{y}\,d\mathbf{z}$$

where
$$\epsilon_{ijkl} = 1 \text{ for } i=j;\ k=l \qquad \ldots\ldots(17)$$
$$= 2 \text{ for } i=k;\ j=l.$$

When the turbulence is isotropic the expression (17) is independent of the direction of the reference axes and the calculations are considerably simplified. The power radiated from an elementary eddy volume was evaluated for this special case by Proudman (1952). Although the radiation field described by equation (15) for the fluctuation of the density is formally expressed by that due to the radiation from a combination of quadrupoles, both lateral and longitudinal, yet the resultant field actually reduces to a configuration of simple sources alone. This result is not surprising since the isotropy of the turbulence implies a random distribution of the direction of the axes of the quadrupoles.

In writing down the correlation between the values of T_{ij} Proudman takes into account the fact that the turbulence is decaying. This means that the time derivatives in the integrand may have a non-vanishing value for their mean in

view of the gradual reduction of the energy of the turbulence. On the basis of dimensional consideration it is concluded that the latter effect is quite small, of the order of 1% of the whole strength of the acoustic sources, and can be consequently neglected. Accordingly, the expression for the intensity becomes

$$I(\mathbf{x}) = \frac{\rho_0}{16\pi^2 c_0^2 x^2} \int \left[\frac{\partial^2}{\partial t^2} \left(\frac{x_i v_i}{x}(0,t) \right)^2 \frac{\partial^2}{\partial t^2} \left(\frac{x_i v_i}{x}(\mathbf{z},t) \right)^2 \right]_{\text{av}} d\mathbf{z}. \qquad \ldots\ldots(18)$$

The intensity is thus independent of the direction of x in view of the isotropy of the turbulence, showing that the directional distribution degenerates to that of simple sources whose power output per unit volume p_a is

$$p_a = \frac{\rho_0}{4\pi c_0^5} \int \left[\frac{\partial^2}{\partial t^2} v_i^2(0,t) \frac{\partial}{\partial t^2} v_i^2(\mathbf{z},t) \right]_{\text{av}} d\mathbf{z}, \qquad \ldots\ldots(19)$$

where v_i stands for an arbitrary component of $\mathbf{v}$.

The correlation of the velocities occurring in equation (16) is of the fourth order and would be quite difficult to evaluate in general. To overcome this difficulty Proudman substitutes for it the correlation of second order obtained by assuming that the values of v_i and its first two derivatives at 0 and z have a normal joint probability distribution. This idea had been previously used by Batchelor (1950). If we introduce now a suggestion originally due to Heisenberg (1949) that the form of the correlation function for the velocity in the isotropic case is gaussian and if we use once more the approximate form for the correlation, the integral of equation (19) finally reduces to the form

$$p_a = \frac{38\rho_0 \overline{v_i^2}}{c_0^2} \epsilon \qquad \ldots\ldots(20)$$

where ϵ is the mean rate of dissipation of energy per unit mass.

The general discussion which has been used in the study of the power radiated from an eddy volume can also be extended to an evaluation of the sound spectrum due to turbulence. Any one of the non-overlapping regions mentioned above will be considered to be approximately spheres of radius L. This choice, which simplifies the analysis, is also consistent with the isotropy of the situation.

From the point of view of spherical harmonic analysis it is well known that the field due to a longitudinal quadrupole can be analysed into terms corresponding to a spherical harmonic of second order and a harmonic of zero order. On the other hand, the field due to a transverse quadrupole is described by a harmonic of second order. The sound sources can then be combined together to form a mixture of simple sources and of transverse quadrupoles. The spectral density of the strength of the source can be estimated (Mawardi 1955) by means of an artifice which will visualize the acoustic power as radiated from an assembly of transverse quadrupoles and simple sources concentrated in a volume of order L^3. With the supposition that eddies of wave number $|\mathbf{k}| = \omega/c$ will contribute only noise of frequency ω, it is plausible to assume that, at low Mach numbers, the extent of this contribution will be such that the strength of the source at a frequency ω will be proportional to the spatial spectrum density of $u_i u_j$ of corresponding wave number k. The ratio of the strength of the simple sources to that of the transverse quadrupoles is readily deduced from some of the results of

Proudman's analysis. Accordingly, making use of the four-dimensional Fourier transform of the velocity and introducing the condition of isotropy on a Fourier expansion for this transform we can find the transform of the correlation function. The statistical addition of the contribution from all wave numbers $|\mathbf{k}|$ leads to an expression for the power spectrum of the noise radiated from an eddy volume. This spectrum is found to be

$$P \sim \left[\frac{1}{(kL)^2[D_0'(kL)]^2} + \frac{5/4}{(kL)^2[D_2'(kL)]}\right]\overline{v_i^2} \qquad \ldots\ldots(21)$$

in which it is observed that at low frequencies the spectrum is approximately of the order $(kL)^2$ and at high frequencies asymptotically approaches $1/(kL)^3$. D_0' and D_2' are the derivatives respectively of the zero-order and second-order spherical Bessel function. Actually at high frequencies the influence of the accession to inertia on the radiation (Stokes effect) is negligible and the spectrum character is completely governed by the behaviour of T_{ij}.

2.2.2. *Sound production and moving frame of reference.*

When the turbulence is superimposed on a mean flow, the radiation of the sound is expected to be modified so that the quadrupoles will radiate far more sound in the direction of convection than against it when the Mach number of the mean flow is smaller than unity. The necessary alterations in the calculated expressions for the sound field are readily obtained by means of a transformation for the translation of the coordinate systems. The underlying reason behind the transformation is that the rate of distortion of the local eddies is least when viewed in a frame moving with a certain average velocity.

To fix the ideas, two reference systems are defined: one is fixed with respect to the undisturbed medium and the other has its origin convected down the flow with a velocity $c_0 M$, where M is the mean Mach number of the flow. Let it now be assumed that the moving axes coincide with the fixed ones at time t. The symbol T_{ij}, used with the same meaning as before, has a retarded value measured with respect to the fixed axes given by

$$T_{ij} \sim T_{ij}(\mathbf{z}, t - |\mathbf{x}-\mathbf{y}|/c_0), \qquad \ldots\ldots(22)$$

where $\mathbf{z} = \mathbf{y} + \mathbf{M}|\mathbf{x}-\mathbf{y}|$. The previous relation now contains all the basic information required to make the necessary transformation. Since the Jacobian for the transformation is found from

$$\frac{\partial(z_1, z_2, z_3)}{\partial(y_1, y_2, y_3)} = 1 - \frac{\mathbf{M}.(\mathbf{x}-\mathbf{y})}{|\mathbf{x}-\mathbf{y}|} \qquad \ldots\ldots(23)$$

it is not too difficult to derive the altered form of the relation (16) with the retarded expression for T_{ij} given by (22). Performing an integration over a surface of a large sphere yields as before an expression for the total acoustic power radiated which has to be corrected to take into account the motion of the quadrupoles. Lighthill finds that the result of (17) has to be changed by $(1-M^2)^{-3}$ when neither of the quadrupole axes is in the direction of $\mathbf{M}$, by $(1+5M^2)/(1-M^2)^4$ when one of their axes coincides with $\mathbf{M}$ and by $(1+10M^2+5M^4)/(1-M^2)^5$ when both axes coincide with $\mathbf{M}$.

Another direct illustration of this theory, given by Lighthill, is the polar distribution of the intensity radiated from a moving quadrupole. Figure 1 shows the plot of the distribution for the case of three mutually orthogonal quadrupoles translated with a velocity $c_0\mathbf{M}$. Figure 2 shows, on the other hand, the corresponding distribution from a lateral quadrupole moving with a translation velocity $c_0\mathbf{M}$.

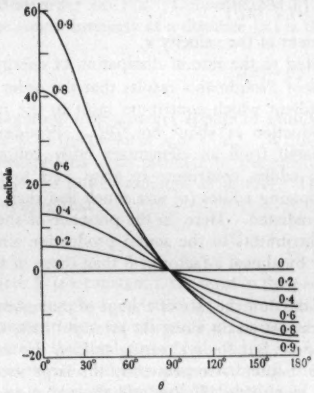

Figure 1. Effect of convection on the directional response of three equal orthogonal longitudinal quadrupoles as a function of the angle θ measured from the direction of mean flow. The Mach number is indicated on the curves. (*After* Lighthill 1952.)

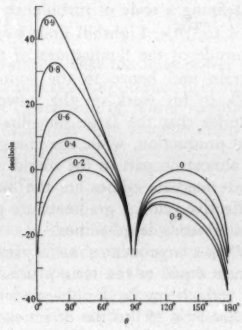

Figure 2. Effect of convection on the directional response of a lateral quadrupole as a function of the angle θ measured from the direction of the mean flow. The Mach number is indicated on the curves. (*After* Lighthill 1952.)

(*Reproduced by permission of the Royal Society.*)

2.2.3. *The effect of shear on the sound production.*

The mechanism for the generation of sound by turbulence becomes considerably more efficient in the presence of a mean shear. This increase in efficiency can be explained by the fact that momentum flux is considerably increased when it takes place in the direction of a large velocity gradient. A quantitative demonstration of this statement is found from the rate of change of the momentum flux $\partial(\rho v_i v_j)/\partial t$. Repeated use of the equations of motion leads to the result that

$$\frac{\partial}{\partial t}(\rho v_i v_j) = p_{ik}\frac{\partial v_j}{\partial x_k} + p_{jk}\frac{\partial v_i}{\partial x_k} - \frac{\partial}{\partial x_k}(\rho v_i v_j v_k + p_{ik} v_j + p_{jk} v_i). \quad \ldots\ldots(24)$$

The last term can be neglected in the analysis because of the presence of the gradient which will lead to a higher order field than that of the quadrupoles. Hence the last term contributes very little to the sound production.

The last equation emphasizes the effect of the gradient of the velocity in the sense that the contribution to the rate of change of momentum due to pressure fluctuations is amplified by the presence of the shear. When no solid boundaries

are present, viscous effects are negligible, $p_{ij} = p\delta_{ij}$ and the rate of change of the momentum flux is expressed by $p(\partial v_i/\partial x_j + \partial v_i/\partial x_i)$. The term in parentheses is the rate of strain and consequently the expression corresponding to equation (19) for the case of isotropic turbulence with no mean flow becomes (Lighthill 1954) in the presence of shear

$$p_a = \frac{1}{\pi\rho_0 c^5}\sigma^2\left\{\frac{\partial}{\partial t}\left(p\,\frac{\partial v_i}{\partial x_i}\right)\right\}, \qquad \ldots\ldots(25)$$

where v_i is as before an arbitrary component of the velocity $\mathbf{v}$.

Defining a scale of turbulence L related to the rate of dissipation of energy ϵ as $L = (\overline{v_i^2})^{3/2}/\epsilon$, Lighthill finds by means of Proudman's results that the order of magnitude of the fluctuations of the gradient which contribute most to the rate of strain and hence to the sound production is about $8(\overline{v_i^2})^{1/2}/L$. Proudman (1952), in his work on the power radiated from an elementary eddy volume, concludes that the large non-dissipating eddies contribute in great part to the sound production, while the energy dissipating eddies (of size much less than L) have almost no part in the sound power radiated. Here, in the presence of shear the intermediate eddies are the main contributors to the sound production since the effective velocity gradients are greater by almost a factor of 8 than those of the non-dissipating large eddies.

When a large mean shear is present in the flow the rate of change of momentum is almost equal to the term p times the rate of strain along its principal axis, the latter term being by far the dominant one. But for a shearing motion the axis is inclined by 45° to the direction of the motion. Consequently the large mean shear will tend to align the quadrupoles along this 45° line and the radiation of sound will be expected to be a maximum in this direction.

To take into account the effect of the moving system of reference the expression for the power has to be altered by a factor mentioned in § 2.2.2, viz., $A = (1+5M^2)/(1-M^2)^4$. The power radiated is thus

$$p_a = \frac{1}{15\pi\rho_0 c_0^5}\int\left[\frac{\partial}{\partial t}\left(p\,\frac{\partial v_i}{\partial x}(0,t)\right)\frac{\partial}{\partial t}\left(p\,\frac{\partial v_i}{\partial x}(\mathbf{z},t)\right)\right]_{\mathrm{av}} d\mathbf{z}. \qquad \ldots\ldots(26)$$

Evaluation of the integrand is difficult because data are not available in the literature. Several approximate forms have been suggested, but none seems so far to have been successful and more accurate estimation of p must await further information on such parameters as $(\partial p/\partial t)^2$, $\{\partial p(0)/\partial t\}\{\partial p(\mathbf{z})/\partial t\}$, etc.

2.2.4. *Dimensional analysis of sound production.*

Several attempts have been made (Lighthill 1952, Westley and Lilley 1952, Mawardi and Dyer 1953) to estimate several characteristics of the noise production by means of dimensional analysis arguments.

The case considered by Lighthill is a direct deduction from the expression (17) when applied to geometrically similar mechanisms of flow production. Actually, his analysis was aimed at discussing the sound generation from the turbulence in a jet. The argument makes use of a typical velocity of flow V, a typical linear dimension d, a typical frequency f, and the usual physical properties for the fluid, ρ_0, c_0 and ν.

The non-dimensional quantities which may be important in determining the sound production are then the Reynolds number $R = Vd/\nu$, the Mach number $M = V/c_0$ and the non-dimensional frequency fd/V. The fluctuations in a flow at low Mach number are such that the corresponding Strouhal number fd/V is independent of the Reynolds number. Actually fd/V rises very slowly with R. To obtain a rough idea of the sound production, frequencies will be taken to be of the order of V/d. Consequently $\partial^2 T_{ij}/\partial t^2$ will be of the order $(V/l)^2\rho_0 V^2$. The sound intensity at a distance $|\mathbf{x}|$ is then by (16)

$$I(\mathbf{x}) \sim \rho_0 \frac{V^8}{c_0^5}\left(\frac{d}{|\mathbf{x}|}\right)^2. \qquad \ldots\ldots(27)$$

Integration over a larger sphere of radius $|\mathbf{x}|$ indicates that the total power radiated is of the order of $\rho_0 d^2 V^8/c_0^5$. A quantity of practical importance to acoustical investigations is an estimate of the efficiency of conversion of power supplied to the jet to power radiated as sound. This is estimated very roughly from (27) by noting that

$$P = K\frac{V^5}{c_0^5}\left(\frac{\rho_0 V^3}{2} d^2\right), \qquad \ldots\ldots(28)$$

where K is a constant ; the term in the parentheses is identified with the mechanical power supplied. Hence for geometrically similar flow producing systems one expects to find an efficiency proportional to the fifth power of the Mach number, whereas the total power radiated is expected to follow an eighth power law for a characteristic velocity associated with the system. The coefficient K is expected to be a very slowly varying function of the Reynolds number for a flow of low Mach number.

2.2.5. *Experimental findings.*

A great deal of information on several characteristics of aircraft noise is now available. Typical data of this type have recently been reported in the proceedings of two symposia on aircraft noise sponsored by acoustical societies in America (Symposium 1953) and Great Britain (Symposium 1954). The difficulty in this sort of information, however, is that the noise measurements found from engine noise are actually due to composite effects of various factors such as combustion noise, boundary layer noise together with the free turbulence noise which is the subject of this section. Accordingly, the engine type of noise measurement, valuable as it is to the designer of noise-abatement systems, is of little direct use to the unravelling of the mechanism of true aerodynamic sound.

A more specialized type of experiment, however, has been reported by Fitzpatrick and Lee (1952), Lassiter and Hubbard (1952, 1953, 1954, 1955), Powell (1952) and Westley and Lilley (1952). In this sort of measurement, compressed air from a reservoir is allowed to escape from a nozzle. The procedure used in the evaluation of the total power radiated has been performed in one of two ways. The jet was allowed to radiate sound in free space and the total power consequently obtained from a direct integration of the polar distribution for the intensity, or the radiation took place in a highly reverberant enclosure, so that the enclosure itself performed the integration. The disadvantage of the

latter procedure is that the character of the spectral density of the noise produced is altered by the resonances of the enclosure. The total power radiated, however, is not affected. This is true as long as the interaction between the sound and the turbulence is weak and there is no back reaction of the sound on the turbulence.

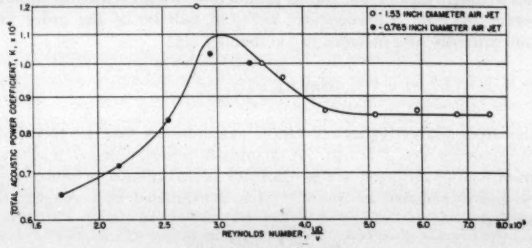

Figure 3. Dependence of the efficiency coefficient K on the Reynolds number R. (*After* Fitzpatrick and Lee 1952.)

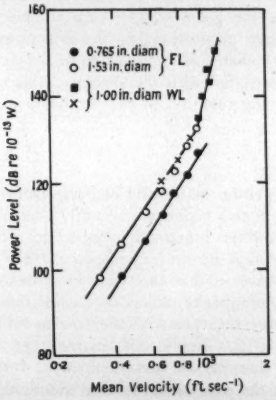

Figure 4. Total acoustic power radiated from a cold air jet as a function of the mean flow velocity. For low Mach numbers of the flow, the power radiated follows an eighth power dependence, for high Mach number the power varies as a much higher index. (FL, Fitzpatrick and Lee 1952; WL, Westley and Lilley 1952.)

The results of these experiments, especially at low Mach numbers, are in substantial agreement with the theoretical predictions. The main features of these results are that :

(i) The efficiency of conversion of mechanical to acoustical energy is a slowly varying function of the Reynolds number (figure 3) at low Mach numbers and

seems to follow the predicted value of M^{-5} fairly well. Typical values obtained for the constant K of equation (28) vary from $0{\cdot}3$ to $1{\cdot}0 \times 10^{-4}$. At high values of the Mach number, however, the efficiency undergoes an abrupt change and the power radiated shows a dependence on the velocity to an exponent considerably higher than 8 (figure 4). Obviously the mechanism of sound production is then quite different and the theoretical aspects of it are still not very well understood.

(ii) The sound spectrum is very broad (figure 5) and has an ill-defined peak. There is still not enough conclusive evidence to show that the peak frequency varies as $V/2d$, where d is the diameter of the jet. The peak frequency seems, however, to be less sensitive to velocity variation than it is to the size of the jet

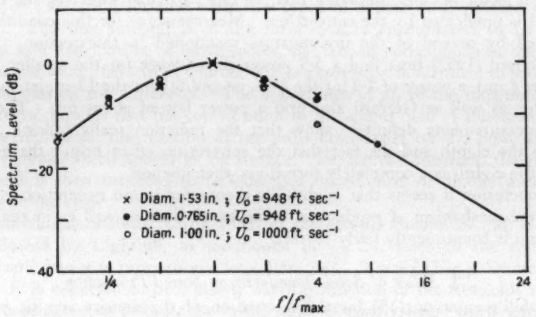

Figure 5. Typical normalized sound spectrum for a cold air jet. The data are from octave band measurements. (*After* Fitzpatrick and Lee 1952, Westley and Lilley 1952.)

diameter. In all measurements obtained so far the spectral density falls on both sides of the peak in the range of the available spectra which extend over six to seven octaves.

(iii) The polar distribution for the intensity of the sound radiated follows a ' butterfly ' type of configuration in which almost all the sound radiated is encompassed in an acute angle with the jet. The angle for the directional maximum is apparently a function of the frequency and of the Mach number. Defining a Strouhal number fd/V, Lassiter and Hubbard (1952) state that this angle varies from 30° to 40° for fd/V values of $0{\cdot}4$ to $1{\cdot}5$.

For lower values of this ratio the angle slowly decreases to 15° for a corresponding ratio of $0{\cdot}2$. Information on the case of supersonic flow is scanty. Westley and Lilley, however, find that the angle for directional maximum is 40° for a Mach number of unity and for Strouhal numbers greater than $0{\cdot}7$. For lower values of the frequency they find that the maximum angle recedes to 30°. For supersonic jets it seems that Gerrard (quoted by Lighthill 1954) still finds a maximum at an angle of 40° for the higher frequencies (Strouhal number = $0{\cdot}6$) and an angle of 30° for the lower frequencies (Strouhal number = $0{\cdot}3$). The intermediate frequencies have their maxima at intervening angles.

(iv) The dependence of the total acoustic power on the eighth power law of the velocity predicted by (28) seems to be corroborated by the experiments for subsonic flow. This fact is very surprising and is indeed very hard to explain since the expression (28) does not take into account the effect of convection on the radiation from the quadrupoles. Indeed, the mean flow should increase the radiated power and a dependence on a higher power of the velocity is expected. But this apparently is not the case. A possible explanation for this dilemma can be seen by examining in more detail the angle dependence of the intensity of the sound. In the calculations of the previous sections we derived correction factors which will take into account the effect of the convection. One such factor was of the form $(1-M\cos\theta)^{-6}$. An interesting fact is that at an angle of 90° the correction factor is unity, implying that for this particular direction the radiation of sound is unaffected by the convection. Measurements for this condition were performed by several of the investigators mentioned in this section. Lassiter and Hubbard (1952) thus find a 5·5 power dependence for the smaller jet used (diameter $\frac{3}{4}$ in.), a power of 7·0 for the 3-in. jet and 6·3 for the 12-in. jet. Westley and Lilley as well as Gerrard also find a power law of about 6·3. These consistent measurements definitely show that the radiation really follows a power *less* than the eighth and the fact that the convection effect brings the exponent back to the eighth is a completely fortuitous phenomenon.

In conclusion it seems that Lighthill's theory for sound generation is able to explain the mechanism of production in its broad lines as well as in some of its details and is consequently fairly correct.

2.3. *Effect of Solid Boundaries on Sound Production*

Lighthill's equation (15) for the fluctuation of the density can be extended without difficulty to the case of the domain G containing solid boundaries. This new formulation, given by Curle (1955), is based on a well-known relation in boundary value problems which follows directly from Green's second identity. In the notation of the previous sections this relation is (Morse and Feshbach 1953)

$$\rho(\mathbf{x},t)-\rho_0=\frac{1}{4\pi c_0^2}\int_V\frac{\partial^2 T_{ij}}{\partial y_i\partial y_j}\frac{d\mathbf{y}}{|\mathbf{x}-\mathbf{y}|}$$

$$+\frac{1}{4\pi}\int_S\int_0^t\{G(\mathbf{x},t\,;\,\mathbf{y},t')\,\partial_n\rho(\mathbf{y}t')-\partial_n G(\mathbf{x},t\,;\,\mathbf{y},t')\,\rho(\mathbf{y},t')\}\,d\mathbf{y}\,dt'$$

$$+\frac{1}{4\pi c_0^2}\int_V\left\{\frac{\partial G}{\partial t'}\rho(\mathbf{y},t')-G\frac{d\rho}{\partial t'}(\mathbf{y},t')\right\}_{t'=0}d\mathbf{y} \qquad \ldots\ldots(29)$$

where $G(\mathbf{x},t;\mathbf{y},t')$ is the Green's function for the domain bounded by the surface S and where $\partial_n(\,.\,)$ stands for the derivative along the outward normal to S. Just as in the previous section, the sound field is first evaluated on the assumption that the mean flow velocity of the turbulence vanishes. The effect of the convection is later taken into account by a transformation similar to that of § 2.2.2. By manipulation of (29) and several straightforward transformations, together with the assumption of a vanishing normal component of the velocities at the solid boundaries, Curle finds for the density fluctuation due to the turbulence

without mean motion,

$$\rho(\mathbf{x},t)-\rho_0=\frac{1}{4\pi c_0^2}\left\{\frac{\partial^2}{\partial x_i\partial x_j}\int_V\frac{T_{ij}(\mathbf{y},t-|\mathbf{x}-\mathbf{y}|/c_0)}{|\mathbf{x}-\mathbf{y}|}\,d\mathbf{y}\right.$$
$$\left.-\frac{\partial}{\partial x_i}\int_S\frac{l_jp_{ij}(\mathbf{y},t-|\mathbf{x}-\mathbf{y}|/c_0)}{|\mathbf{x}-\mathbf{y}|}\,dS(\mathbf{y})\right\} \qquad \ldots\ldots(30)$$

in which the l_i's ($i=1,2,3$) are the direction cosines of the normal to the surface S. The relation (30) is derived from an exact analysis and contains as in Lighthill's equation (15) the essential features of sound production. But it is a difficult relation to evaluate for the general case in view of the scanty information on the form of T_{ij} and p_{ij} in the vicinity of the solid boundaries. The two integrals of (30) are associated with two types of source with definite physical meaning. The first integral is of the form usually encountered so far and is identified as a distribution of quadrupoles, the second corresponds to the contribution to the sound field from sources whose expression is identical to a distribution of dipoles on the surface S. The appearance of p_{ij} in the integrand of the latter integral implies that the contribution to the sound field of this second type of source represents the reaction of the solid boundaries on the flow, as manifested by *forces* which appear at its surface. By Lamb's theorem, the resultant sound field is then expected to be due to a distribution of dipoles and this is found to be the case.

A dimensional analysis (Curle 1955) of the second integral of (30) along the lines followed by Lighthill, as mentioned in § 2.2.4, leads to the result that total acoustic power is proportional to $\rho_0V^6c_0^{-3}d^2$. Then $K(V/c_0)^3$, where the the constant K is expected to be a slowly varying function of the Reynolds number, may be considered as defining an ' efficiency ' of conversion. Curle applied his derivations to the discussion of the sound generated from the shedding of vortices in a flow past a cylinder and came to the conclusion that the corresponding sound field is that of a dipole field with the direction of the dipole at right angles to the flow.

This particular case seems to have received some attention by acoustics workers in Russia, and Blokhintzev (1946 a) derives by means of dimensional analysis an expression similar to that of Curle and shows that the intensity at a large distance $|\mathbf{x}|$ is expressed by

$$I(\mathbf{x})=\alpha\frac{\cos^2\theta}{|\mathbf{x}|^2}ld\rho_0\frac{V^6}{c_0^3} \qquad \ldots\ldots(31)$$

where α is a slowly varying function of the Reynolds number, θ is measured from the diameter normal to the flow, d is the diameter of the cylinder and l is a function of the angular coordinates (θ,ϕ); l, however, is taken to a first approximation as the length of the cylinder.

2.3.1. *Sound generation in a boundary layer.*

The explanation of the mechanism of sound production associated with the surface stresses of the second integral of (30) can readily be given in terms of the reaction of the fluid forces on an obstacle. A quantitative estimate of this contribution to the sound generated in a turbulent flow has recently been obtained

by Phillips (1956 a, b). His discussion is based on the fact that turbulent fluctuations of pressure and velocity near a rigid boundary are responsible for the appearance of a fluctuating stress distribution over its surface, which balances at the surface equal and opposite stresses in the fluid. The normal component of these stresses is the fluctuating pressure while the tangential components are the fluctuating shear stresses. By a line of argument analogous to those leading to equation (18) it is found that

$$I(\mathbf{x}) = \frac{x_i x_j}{8\pi^2 \rho_0 c_0^3 |\mathbf{x}|^4} \int_S \left[\frac{\partial F_i(0,t)}{\partial t} \frac{\partial F_j(\mathbf{z},t)}{\partial t} \right]_{\text{av}} d\mathbf{z} \qquad \ldots\ldots(32)$$

where $I(\mathbf{x})$ is as usual the intensity of the sound at a large distance from S and F_i is the component of stress in the α_i direction. In estimating the surface stress distribution, the effects of compressibility in the boundary layer are neglected. The justification for this approximation is that at low Mach numbers the compressibility is not expected appreciably to alter the stress distribution computed on the basis of an incompressible viscous flow in the vicinity of the boundary. This simplification is actually consistent with the order of approximation which has been used in deriving a theory of weak interaction as discussed in § 2.1.

Phillips considers the case of a plane boundary layer. The stresses F_i are then identified with $\mu(\partial v_1/\partial x_2)_0$, p_0 and $\mu(\partial v_3/\partial x_2)_0$ when the boundary is taken as the plane $x_2 = 0$ and where the subscript zero denotes the values of the quantities at $x_2 = 0$. In the notation of this paper v_1, v_2 and v_3 are the components of $\mathbf{V}$ in the x_1, x_2 and x_3 directions respectively. Expression (32) includes terms of the form given above and the sound radiated can be considered to be the resulting effect of pressure fluctuations only, of stresses due to shear fluctuations alone, and finally a term whose integrand is a mixture of pressure and shear fluctuations. Because of the randomly fluctuating property of the fluid Phillips shows that the last term does not contribute to the sound radiation. He is also able to prove the very important result that over a *rigid* plane boundary the pressure fluctuations play no part in the production of surface noise.

The expression (32) does not take into account the effect of convection. In accordance with the general method developed by Lighthill and discussed in the previous sections, the latter effect can be accounted for by choosing a plane of reference moving with a fluid with a local eddy convection velocity in which the frequency scale of the fluctuation is least. In a boundary layer, it is the motion in the region of fully developed turbulence *outside* the viscous sublayer which sets up a distribution of velocity gradients responsible for the shear stresses at the walls (Townsend 1951, Laufer 1950, 1953). Now, in the fully turbulent region there is a whole assembly of eddies which move with different convection velocities and with different corresponding frequencies. It is consequently pertinent to find the eddies which influence most the stresses at the boundaries and accordingly define the local eddy convection velocity. Since the motion in the region outside the viscous sublayer is mainly governed by inertia forces, the frequency scale is then found to be

$$f^2 \sim \frac{\overline{v_2^2}}{\overline{v_1^2}} \left(\frac{\partial V}{\partial x_2} \right)^2 \qquad \ldots\ldots(33)$$

where V is the mean flow. The value of the gradient is that for the position of maximum influence which Phillips shows to be of the order of $d/10$, where d the usual thickness of the layer is defined, following Clauser (1954), by

$$d = 0{\cdot}3\int_0^\infty \frac{U_\infty - U(x_2)}{V_\tau}\,dx_2, \qquad \ldots\ldots(34)$$

U_∞, $U(y)$ and V_τ have the conventional meaning for the velocities outside the boundary layer, in the boundary layer and for $\{\nu(\partial V/\partial x_2)_0\}^{1/2}$ respectively.

Making use of an experimental observation due to Townsend (1951) that $\overline{v_1^2} \sim \overline{v_2^2}$, Phillips finds for the expression (32) when referred to a moving frame of reference of mean Mach number M_c

$$I(\mathbf{x}) \sim \frac{x_1^2 + x_3^2}{(|\mathbf{x}| - M_c.\mathbf{x})^4}\,\frac{[\partial\tau/\partial t]_{av}^2\mu^2}{16\pi^2\rho_0 c^3}$$
$$\int\left\{\left[\frac{\partial}{\partial t}\left(\frac{\partial v_1(0,t)}{\partial x_2}\right)\frac{\partial}{\partial t}\left(\frac{\partial v_1(\mathbf{z},t)}{\partial x_2}\right)\right]_{av} + \left[\frac{\partial}{\partial t}\left(\frac{\partial v_3(0,t)}{\partial x_2}\right)\frac{\partial}{\partial t}\left(\frac{\partial v_3(\mathbf{z},t)}{\partial x_2}\right)\right]_{av}\right\}d\mathbf{z}\Big/\left[\left(\frac{\partial\tau}{\partial t}\right)^2\right]_{av}$$
$\ldots\ldots(35)$

where τ is the fluctuating shear stress and x_1 is the direction of mean flow. The integral of (35) can be identified with integral length scales associated with the region of high shear by introducing the frequency (33) together with an appeal to the experimental observations of Laufer (1950). But Townsend (1951) had given some relation of the dependence of these scales on the thickness d. Phillips thus arrives at an expression for the power radiated per unit area

$$P \sim \frac{120}{(1-M_c^2)^2\rho_0 c^3}\left[\mu\left(\frac{\partial V}{\partial y}\right)_0\right]^3 \qquad \ldots\ldots(36)$$

which he further approximates to

$$P \sim \frac{K}{(1-M_c^2)^2}\,\frac{\rho_0 V^6}{c^3} \qquad \ldots\ldots(37)$$

where K is a slowly varying function of the Reynolds number and is of the order of 10^{-7}.

It is very unfortunate that very little information is available on boundary layer noise. As in the case of experiments on sounds of aerodynamic origin several of the observations which have been reported in the technological literature are not truly representative of boundary layer noise, but are the result of several other factors as well: panel vibrations, aerodynamic sounds, engine noise, etc. A few specialized types of experiments, however, have been described (Lubin 1952, Mawardi and Dyer 1953) in the scientific literature and some information can be gleaned from these observations.

In this sort of measurement, compressed air from a reservoir is allowed to escape into a conduit whose walls are sufficiently rigid for panel resonance to be excluded. In Lubin's experiment a diverging conduit of very small angle was used. At the opening the escaping air velocity was so low that it contributed very little to the sound production once it left the conduit. The sound was detected at a large distance from the conduit. The walls of the conduit were so rigid that almost all of the sound was radiated from the opening of the conduit.

The power radiated was measured from the angular distribution of the intensity. In Mawardi and Dyer's experiment the measurements were performed outside the conduit and the sound detected was that transmitted through its walls. The power radiated was estimated from the angular dependence around the conduit and at very large distance from it.

An inherent difficulty in these experiments is that sound is generated by the turbulence *in the fluid* (i.e. by the distribution of equivalent quadrupoles) as well as by the stress distribution at the walls. The latter was found to be akin to a dipole-like type of field. The relative importance of these two mechanisms of sound production was considered by Phillips (1956 b), who found a criterion for the predominance of the dipole field contribution over that of the quadrupole field. His calculations, which do not take into account convection effects and are thus valid for very low Mach numbers, lead to the condition that the dipole field will be dominant whenever

$$M^2 < \frac{15}{12}\frac{\overline{\tau}^2}{\overline{p}^2}\frac{S}{S'}, \qquad \ldots\ldots(38)$$

where S and S' are average eddy areas defined in terms of shear and pressure fluctuations respectively. For Reynolds number of the order 10^7 to 10^9, $\overline{\tau}^2/\overline{p}^2$ is about $\frac{1}{6}$ and S/S' is nearly 4 for a plane boundary. Accordingly M^2 should be less than $\frac{5}{6}$. This criterion seems to imply that the dipole field will almost always be far more important than the quadrupole field.

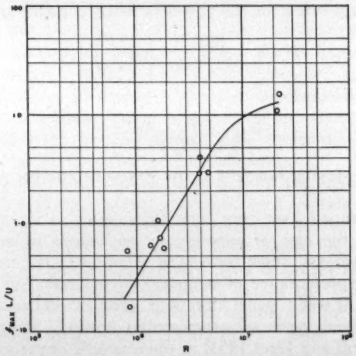

Figure 6. Dependence of the frequency of the maximum on the Reynolds number for boundary layer noise. (*After* Mawardi and Dyer 1953.) (*Reproduced by permission of the American Institute of Physics.*)

The other difficulty is in connection with the sound field due to the pressure distribution at the walls. It was seen that in the case of the rigid plane boundary it is the shear stresses only which contribute to the sound field. The validity of this condition when the surface is curved or when the surface is not rigid is doubtful. The results of the second experiment mentioned above are consequently open to

question, as it is not easy to separate the individual contributions of the several stress distributions to the total sound generated.

The main features of the experimental results are that :

(i) The value of the acoustic efficiency for the conversion of available mechanical power to acoustical power is of the order of 10^{-4}. This is of the same order of magnitude as the efficiency observed from vortex-producing flows.

(ii) The acoustic power follows a 5·4–5·8 power law of the velocity. The dimensional analysis, on the other hand, indicates a sixth-power law for a stationary flow and the effect of the convection would lead one to expect an increase in sound radiation. Additional theoretical and experimental information is needed to clarify this question.

(iii) The spectrum of the sound produced is fairly broad and extends over several octaves. The frequency of the maximum intensity cannot be easily predicted and the data seem to indicate that this frequency $f_{\max}$ is given by $f_{\max} L/V = f(R)$ where L is a dimension of the duct cross section and R is the Reynolds number based on the mean flow V and L (figure 6).

2.4. *The Scattering of Sound by Turbulence*

The general question of the scattering of sound waves in a medium with random variations in its index of refraction has received a great deal of attention from workers in acoustics (Obukhov 1943, Blokhintzev 1945, 1946 a, b, Bergmann 1946, Ellison 1951, Lax 1951, Mintzer 1953 a, b). The general method followed in the work of these investigators generally falls into one of two categories. In the first procedure used, the scattered sound is evaluated by means of an approximate solution of a wave equation with a variable velocity of propagation. A typical method of solution is one obtained by a Born approximation (Mintzer, Ellison, Lax). The other line of attack which has successively been used is that of a ray technique (Bergmann) in which the eikonal relation is the starting point of the discussion. In the Russian work (Blokhintzev 1945, 1946 a, b) the assumption underlying the theory is not too clear, although the arguments used by Blokhintzev (1946 b) are essentially of the first category mentioned above, viz. that of a wave equation with a randomly varying velocity of propagation. The conventional method used in treating the propagation of waves in an inhomogeneous medium can be adapted to take into consideration the case of scattering by turbulence and indeed this was attempted by Villars and Weisskopf (1954) in considering the scattering of an electromagnetic wave by a turbulent atmosphere. The procedure, however, becomes very cumbersome with the result that generalized predictions are difficult to obtain.

The formulation of the generation of sound from turbulence as discussed in the previous sections lends itself very well also to an investigation of the mechanism of scattering of the sound waves by turbulence. In order to extend to the scattering problem the concept of the quadrupole point sources encountered in a turbulent field, a flow velocity field v_i is defined. A sound velocity field V_i is now supposed to be superimposed on the turbulent field. For small magnitudes of v_i and V_i (compared with c_0) the combined field velocity is to a first approximation $v_i + V_i$.

The fluctuation in the density due to the above-mentioned quadrupole is, by virtue of the arguments of § 2.1, determined from the quadrupole point source

distribution (Lighthill 1953):

$$\rho_0(v_i+V_i)(v_j+V_j)=\rho_0 v_i v_j+\rho_0 V_i V_j+\rho_0(v_i V_j+v_j V_i). \quad \ldots\ldots(39)$$

The terms on the right-hand side of (39) can be associated with well-defined physical processes. The first term $\rho_0 v_i v_j$ is of the form encountered in the previous discussion and is readily identified with the usual sound of aerodynamic origin. The term $\rho_0 V_i V_j$ is connected with a second-order effect in a sound wave and represents the non-linear type of distortion of the sound due to its finite amplitude. The last term $\rho_0(v_i V_j+v_j V_i)$ containing a mixture of velocities of the two types of fields describes the sound produced through the interaction of the turbulence and the sound fields and is thus truly representative of the scattering quadrupoles. When the turbulent flow velocity v_i consists of a mean flow $\overline{v_i}$ and a fluctuating component v_i', the scattering quadrupole can in its turn be divided in two parts. The first of these, $\rho_0(\overline{v_i}V_j+\overline{v_j}V_i)$, is obviously correlated with the sound field and is indicative of an ordered refraction of the sound by the mean flow. The remaining term, $\rho_0(v_i' V_j+v_j' V_i)$, is then the scattering quadrupole due to the turbulence proper. This is the part of special interest to the subject matter of this report and in what follows the prime will be dropped, for the sake of convenience, but it is the fluctuating component of v_i which will be referred to in the text.

The energy scattered from a plane wave incident on a turbulence field restricted in a finite domain G can be obtained by following a procedure analogous to that used in evaluating the sound radiated from a volume distribution of quadrupoles of strength $\rho_0(v_i V_j+v_j V_i)$. Here the component $V_i=A\cos\{k(x_1-c_0 t)\}\,\delta_{i1}$ in which the wavelength of the sound is $2\pi/k$ and the incident plane wave is propagated in the direction x_1. By means of the method outlined above Lighthill (1953) evaluated the intensity of the scattered wave to be

$$I_S=\frac{2\pi k^4 I}{{c_0}^2}\frac{x_i x_j x_1^2}{x^6}\left[\frac{1}{8\pi^3}\int\int\overline{v_i(\mathbf{y})v_j(\mathbf{z})}\cos\{\mathbf{k}.(\mathbf{y}-\mathbf{z})\}\,d\mathbf{y}\,d\mathbf{z}\right] \quad \ldots\ldots(40)$$

where I is the intensity of the incident sound wave and where

$$\mathbf{k}=k(x_i/x-\delta_{i1})=2k\sin\tfrac{1}{2}\theta.$$

But the quantity between brackets is the Fourier transform of $\int v_i(\mathbf{y})\,v_j(\mathbf{y})\,d\mathbf{y}$ taken over the domain G, and can be interpreted as its spectrum with respect to $\mathbf{k}$.

In the special case of homogeneous isotropic turbulence the expression (40) can be evaluated accurately. First the Fourier transform mentioned above can be related to turbulent energy $E(k)$ per unit mass. Indeed, the spectral density given (Batchelor 1949) by

$$\Gamma_{ij}(\mathbf{k})=\frac{1}{8\pi^3}\int R_{ij}(\mathbf{y})\exp(-i\mathbf{k}.\mathbf{y})\,d\mathbf{y} \quad \ldots\ldots(41)$$

is such that the quantity between brackets in equation (40) corresponds to its real part. Since $\Gamma_{ij}(\mathbf{k})=[E(k)/4\pi k^4](k^2\delta_{ij}-k_i k_j)$ it is shown that

$$I_S=\frac{Ik^2\cos^2\theta\cot^2\frac{1}{2}\theta}{8c^2}\frac{}{x^2}E(2k\sin\tfrac{1}{2}\theta). \quad \ldots\ldots(42)$$

The form of (42) indicates that when $2k$ is considerably smaller than the wave number of the energy-bearing eddies there is little scattering. On the other hand, in the extreme case when k is much greater than those wave numbers the scattered energy will be included in a cone of small angle θ. When k is smaller than Taylor's correlation radius L Lighthill shows that the expected attenuation due to the scattering of a plane wave is $8\pi^2(L_1/\lambda)^2\overline{v_i^2}/c^2$ per unit distance where λ is the wavelength of the incident sound wave.

A similar method to that of Lighthill was used by Kraichnan (1953) to arrive at an expression for the differential scattering cross section of the turbulence. Kraichnan's starting point for his discussion is the four-dimensional Fourier transform of (15). In accordance with the arguments of § 2.1, the Reynolds stresses $\rho v_i v_j$ are approximated to $\rho_0 v_i v_j$. The transform to (15) is obtained in two intermediate steps to allow certain simplifications. The time–frequency transform is

$$\Delta\rho(\mathbf{x},\omega) = \frac{1}{4\pi c^2}\int \frac{\exp(-i\omega|\mathbf{x}-\mathbf{x}'|/c)}{|\mathbf{x}-\mathbf{x}'|}\mathcal{T}(\mathbf{x}',\omega)\,d\mathbf{x}' \qquad \ldots\ldots(43)$$

where $\mathcal{T}(\mathbf{x}',\omega)$ stands for

$$(2\pi)^{-\frac{1}{2}}\int_{-\infty}^{\infty} v_i(\mathbf{x},t)\,v_j(x,t)\,dx.$$

At large distances from the turbulence, i.e. for $|\mathbf{x}| \gg |\mathbf{x}'|$, the denominator of the integrand becomes $|\mathbf{x}-\mathbf{x}'| \sim |\mathbf{x}|$ and $\exp(-i\omega|\mathbf{x}-\mathbf{x}'|/c)$ is approximated to $\exp(-i\omega|\mathbf{x}|/c)\exp(-i\omega|\mathbf{x}|^{-1}x_i x_i'/c)$. These steps reduce the above integral to

$$\Delta\rho(\mathbf{x},\omega) = \frac{1}{4\pi c^2|\mathbf{x}|}\exp\left(-i\frac{\omega}{c}|\mathbf{x}|\right)\int\exp\left(-i\frac{\omega}{c}|\mathbf{x}|^{-1}x_i x_i'\right)\mathcal{T}(\mathbf{x}',\omega)\,d\mathbf{x}' \qquad \ldots\ldots(44)$$

where the integral is identified as that which yields the spatial Fourier transform of $\mathcal{T}(\mathbf{x}',\omega)$ to within a factor of $(2\pi)^{-3/2}$. Denoting the Fourier transform of $\mathcal{T}(\mathbf{x}',\omega)$ by $\mathcal{T}^*(\omega x_i/c|\mathbf{x}|,\omega)$, equation (44) shows that at large distances from the domain G when the turbulence is restricted,

$$4\pi c^2|\mathbf{x}|\Delta\rho(\mathbf{x},\omega) = (2\pi)^{3/2}\exp\left(-i\frac{\omega}{c}|\mathbf{x}|\right)\mathcal{T}^*\left(\frac{\omega}{c}\frac{x_i}{|\mathbf{x}|},\omega\right). \qquad \ldots\ldots(45)$$

Define a unit vector $\mathbf{n}$ of components $n_i = x_i/|\mathbf{x}|$; it is now reasonable to introduce as a measure for the power spectrum in the direction $\mathbf{n}$ the quantity

$$P(\mathbf{n},\omega) = |\mathbf{x}|^2\left|\frac{\rho}{\rho_0}(\mathbf{x},\omega)\right|^2. \qquad \ldots\ldots(46)$$

This leads directly to the differential cross section which is found to be

$$\sigma(\mathbf{n}) = \frac{c_0^2}{\tau}\int_{-\infty}^{\infty} P(\mathbf{n},\omega)\,d\omega \qquad \ldots\ldots(47)$$

where the cross section has been averaged over the period τ in terms of which the Fourier integrals have been defined. In view of the positive character of

$P(\mathbf{n}, \omega)$ the average of the right-hand side of expression (47) can be interchanged with the integral, whence

$$\langle \sigma(\mathbf{n}) \rangle = \frac{c^2}{\tau} \int_{-\infty}^{\infty} \langle P(\mathbf{n}, \omega) \rangle \, d\omega. \qquad \ldots\ldots(48)$$

The evaluation of (48) in the general case is a difficult question, in view of the complicated analytical form of the turbulence field. Kraichnan has obtained an estimate for the hypothetical case in which the turbulent energy per unit mass is independent of the wave number. This case, however, is of little practical interest.

There are hardly any experimental data on the scattering of sound from turbulence which are worth mentioning. A few experiments have been performed on the scattering of sound from the wakes of moving obstacles in water, but the complications introduced by the presence of water bubbles in the wake makes the interpretation of the data extremely difficult, and there is a very great need for careful experiments on the scattering of sound from well-defined turbulent fields.

§3. The Interaction of Heat with Sound

3.1. *Thermally Induced Sound Fields*

It is evident that the release of heat in the body of a mass of gas at rest gives rise to a compressive wave which is propagated in the gas. The acoustic wave will be produced even though the release is unaccompanied by a transfer of mass and/or momentum. The generation of this wave is a typical consequence of the direct interaction of a compression and an entropy mode.

We first consider the case of a release of heat without mass transport. It is unfortunate that the mathematical description of this process is quite complex so that very few cases are amenable to tractable solutions. These solutions usually refer to conditions in which the geometry of the situation is very simple. One such instance considered by Trilling (1955) is concerned with the investigation of the sonic wave which accompanies the instantaneous temperature rise of an infinite plane wall. The complication of Trilling's solution is mainly due to the retention of the viscous terms of the set of equations (1) to (3).

Trilling first discusses the disturbance, produced by the temperature rise of a wall, as it is propagated in the semi-infinite space in front of the wall. For a relative temperature rise of $\Delta T_0/T_0$, it is found that the one-dimensional pressure wave propagated in the x direction is given by

$$\frac{\Delta p}{P_0}(x, t) = \frac{\Delta T}{T_0} \frac{\Gamma(1/4)}{2\pi} \left(\frac{2\nu}{3\gamma c_0 x} \right)^{1/4} \int \exp\{-(c_0 t - x)^2 / \tfrac{16}{3} \gamma \nu t\}. \qquad \ldots\ldots(49)$$

A one centigrade degree rise in the temperature of the wall originally at room temperature produces at a distance of 1 cm an instantaneous peak pressure rise of 94 dynes, i.e. roughly 113 dB with respect to 2×10^{-4} dyn cm^{-2}. As the predicted width of the pressure pulse is $4(\pi\gamma\nu t/3)^{1/2}$, it is found that at a distance of one metre the pulse peak value has dropped to 102 dB and its width is about 1 mm. To a fixed observer at that distance the passage of the pulse width occurs in 3·08 microseconds.

Of course, it is not possible to produce an instantaneous temperature rise over an area large enough to send out a plane wave. It is, consequently, of interest to discuss the case of a sphere instantaneously raised by an incremental temperature ΔT. Trilling discusses this case also and finds that the pressure pulse, for a sphere of radius r_0, is expressed by

$$\frac{\Delta p}{P_0} = \frac{\Delta T_0}{T_0}\frac{\Gamma(1/4)}{4\pi}\left(\frac{2\nu}{3\gamma c_0 r_0}\right)^{1/4}\left(\frac{r_0}{r}\right)^{5/4}\exp\left(-c_0 t - x\right)^2/\tfrac{16}{3}\gamma\nu t). \qquad \ldots\ldots(50)$$

The above result indicates that the 1° rise above room temperature for a sphere of radius 1 mm produces a peak pressure of 35 dB at a distance of 1 metre from the sphere.

The two examples considered by Trilling clearly show that appreciable pulses can be produced as a result of a sudden temperature rise. These problems, however, do not lend themselves easily to an evaluation of the order of magnitude of the efficiency of conversion of the thermal energy into acoustic energy, since the power is assumed infinite by hypothesis (the energy supplied from the source, however, is not). As the interest in aero-thermoacoustics is relatively recent, experimental information on this phase of the topic is scanty. Some attempts have been made to study the sound pulse accompanying a thermal wave, but quite often the boundaries move at the same time as their temperature is raised. The boundary conditions are then more appropriate for the representation of a detonation wave than a thermally induced wave.

The interaction of an entropy mode with a compression mode when accompanied by a transport of mass is a case of very great interest which has received a great deal of attention from workers in fluid dynamics. The reason for the interest in this interaction is due to the fact that under certain conditions it can introduce an instability in the flow. These instabilities of which the singing flames (Rayleigh 1878) and the Rijke phenomenon (Rijke 1859) are representative instances, have been known for a long time and lengthy descriptive accounts of these can be found in the scientific literature (for a review, see Richardson 1929). It is only recently, however, that systematic quantitative studies of these thermoacoustic processes have been attempted.

The general class of thermoacoustic phenomena discussed in this report is concerned with sounds maintained by heat sources immersed in a moving fluid. Two broad types of mechanism of sound production have been considered. In the first type (Rijke's experiment) the heat source is not accompanied by combustion, while in the other the heat source is a flame. The explanation of essentially all these heat-maintained oscillations leans heavily on the understanding of the process of interaction of the entropy mode with the compression mode in the fluid and the detail of this interaction is discussed in the following section.

3.2. *The Rijke Phenomenon*

In this phenomenon discovered by Rijke in 1859, a vertical open-ended tube is made to sing by the presence of a heated grid in the lower half of the tube. The experimental arrangement is shown in schematic form in figure 7. The convection flow set up by the heater is essential to the phenomenon. Furthermore, the maintenance of the oscillations depends on the position of the grid.

It is observed that the strongest oscillations occur when the grid is approximately one-quarter of the way up from the bottom end of the tube. For heater positions in the upper half of the tube, damping instead of driving results. By supplying heat to the grid from a source of electric power, the oscillations can be maintained indefinitely.

Rayleigh (1878) appears to have presented for the first time a reasonable explanation for the Rijke phenomenon. His explanation is given in an interesting memoir on the general theory of maintenance of oscillations. Rayleigh's discussion, which is completely qualitative, is based on the observation that the forces which act on an oscillatory system connected to a source of energy affect the system in one or both of two ways: the forces may affect the natural period of the system, or may sustain or damp the oscillations.

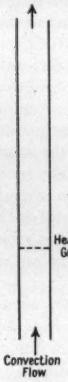

Figure 7. Schematic arrangement for the Rijke experiment.

For the case of a heat source connected to a system capable of acoustical oscillations, the oscillations will be sustained whenever heat is communicated to the system at the moment of maximum condensation. The period of the system is, however, practically unaffected. If, on the other hand, the timing of the heat communication is altered so that heat is added at the instant of maximum rarefaction then the oscillations cannot be maintained.

These arguments are now extended to the case of the Rijke phenomenon. Without any drift velocity present in the tube, the particles of gas in the vicinity of the heater oscillate about the heater position. Heat is added during both parts of the cycle and the oscillations are unaffected. When an upward drift velocity is superimposed on the fluctuating motion, it is noticed that during the condensation part of the cycle, the motions combine in the lower half of the tube while they oppose each other in the upper half. When the heater is placed in the lower half of the tube the drift velocity conveys the particles through the heater in the condensation cycle. The oscillations are subsequently sustained.

Rayleigh's explanation has been given in some detail because of its frequent use by several investigators as the starting point of their discussions. Lehman (1937), using Rayleigh's criterion for the maintenance of oscillations, evaluates the energy absorbed by a cold layer of air as it crosses the heater and from it estimates an incremental drift velocity. He also deduces that the intensity of the fundamental note of the tube increases linearly with the drift velocity, a fact which is not borne out by experimental evidence.

Several other unsuccessful attempts have been made to formulate the mechanism of the Rijke phenomenon by means of one-dimensional perturbation techniques (Neuringer and Hudson 1952, Putnam and Dennis 1953 a, b, Kerwin 1954). The shortcomings of these attempts are due to the fact that a complete theory needs to answer satisfactorily two distinct questions. The theory has to explain first the mechanism of thermoacoustic transduction and only then can it predict the conditions for the maintenance of oscillations expressed as a function of the parameter of flow.

An approach following this line of argument was made by Carrier (1955) who first discussed the fluctuating release of heat from a heated strip immersed in a pulsating flow. The object of Carrier's discussion was to arrive at an estimate of the interaction between the entropy and the compression mode in the vicinity of the heater. It was mentioned in § 2.1 that in the presence of a strong gradient the interaction between any two modes can be strong. Carrier determines this interaction by means of the heat released. This latter quantity is estimated from expression (2) which is simplified to

$$\rho C_p\left(\frac{\partial T}{\partial t}+\alpha V\frac{\partial T}{\partial x}\right)-k\nabla^2 T=0. \qquad \ldots\ldots(51)$$

The above equation is similar in form to the equation of conservation of energy for an incompressible fluid with the exception of the term $\alpha V(\partial t/\partial x)$ which replaces $\mathbf{v}.\nabla T$. The coefficient α is a positive number smaller than unity and V is the free stream velocity. This approximation, permissible because of the low Reynolds number of the flow, has been shown to hold by Lewis and Carrier (1949). Introducing a perturbation technique to solve equation (51), Carrier finds that the fluctuating heat released to the moving fluid per unit length of heater is given by

$$q=-\frac{2ia^{3/2}kT}{\beta}\left(\frac{u}{V_0}\right)(\xi)^{1/2}\operatorname{erf}(\xi d)^{1/2}+(\pi d)^{1/2}(e^{-\xi d}-1), \qquad \ldots\ldots(52)$$

where a stands for $\rho C_p V_0/k$, β is $\rho C_p\omega/k$, $V_0+u=c_0V$, where V is the stream velocity in the x direction, V_0 is the mean value of the velocity and u the fluctuating component. The width of the heater is d and ξ is that root of $z^2-az-i\beta=0$ which tends to zero when β vanishes.

In order to find the effect of the heat source on the sound wave, the requirements for the conservation of mass, momentum and energy for a flow across the heater are written down. Assuming the heater to be inverted in a tube of cross section A, Carrier finds for the ratio of acoustic particle velocities at large distances upstream u_2 and downstream u_1 of the heaters

$$u_1/u_2=1+x \qquad \ldots\ldots(53)$$

where x, related to the heat released per unit area, is found by Carrier to be $[(\gamma-1)/\gamma P_0]\,ql/A$ in which l is the equivalent length of the heater. This relation indicates that the sound velocity is 'amplified' as the wave front traverses the heater, the additional energy being of course provided by the heater.

The disadvantage of Carrier's approach is that it does not clearly demonstrate the mechanism of interaction between the entropy and the compressive modes. If the fluid is assumed inviscid, the interaction between the two modes takes place only in the temperature wake. This is clearly shown by separating the two equations for mean and fluctuating values associated with equation (2). These relations are readily found to be

$$\nabla^2 T_0-a\frac{\partial T_0}{\partial x}=0$$

and

$$\nabla^2\theta-a\frac{\partial\theta}{\partial x}-\beta\theta=\frac{a}{V_0}u\frac{\partial T_0}{\partial x}. \qquad \ldots\ldots(54)$$

It is now apparent by inspection of the second relation of (54) that the appearance of the fluctuation velocity u implies an interaction between the θ and u fields. Another point of interest is that the right-hand side also contains the quantity $\partial T_0/\partial x$, thus proving the statement that strong gradients will tend to increase the interaction.

To find the criterion for the maintenance of the oscillations it is now necessary to take into account the conditions at both ends of the pipe. This question now

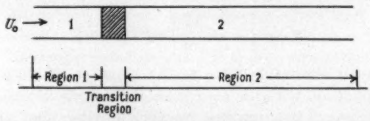

Figure 8. Flow regions indicated in the text. The hatched region corresponds to the heater position.

reduces to a typical boundary value problem. The pressure and particle velocity in region 1 (figure 8) are denoted by subscript one, and those in region 2 by subscript two. Accordingly, it is possible to write

$$p_1 = Ap_1^+ + Bp_1^-, \quad u_1 = Cu_1^+ + Du_1^- \qquad \ldots\ldots(55)$$

with similar relations for region 2. The positive and negative superscripts denote the waves travelling in the opposite directions. The C and D coefficients are expressed in terms of A and B by means of the conditions at the ends as described by a reflection coefficient. Carrier states without proof that this coefficient is $R(1-M)/(1+M)$ where M is the Mach number for the mean flow V_0/c_0 and R is the reflection coefficient for an open-ended pipe obtained for the case of a medium at rest.

The matching of the solutions of region 1 with those of region 2 leads to a complicated characteristic equation by means of which the frequency of oscillation is obtained. This frequency, which turns out to be the root of the characteristic equation, is in general a complex number of the form $\alpha+i\omega$, if the time dependence of (55) had been taken as $\exp(\rho t)$. The criterion for the maintenance of the oscillation is that $\alpha \leqslant 0$.

3.2.1. *Experimental results.*

An essential feature of the excitation of the Rijke phenomenon is the provision for an adequate release of heat to the moving gas. Rayleigh suggests the use of a couple of layers of gauze in order to increase the heat transfer between the grid and the surrounding gas. Lehman also noticed that the maintenance of the oscillations can be considerably improved if a fine meshed screen is introduced in the vicinity of the electrical heater. Since the efficiency of transduction from heat into sound is very small, a negligible amount of loss in the resonant tube is sufficient to prevent the onset of the oscillations. Accordingly, there are two phases of the phenomenon which it is of interest to consider: one is directly connected with the thermoacoustic transduction and the other refers to the Rayleigh criterion for the maintenance of the oscillations.

Kerwin was able experimentally to determine the magnitude of the coefficient σ which appears in Carrier's calculation. The method he used was in essence as follows. An electric heater which could be moved along the axis of the tube was provided with sufficient electrical power input to drive the oscillations. Its position then was in the lower half of the tube (figure 7). Additional losses were then successively introduced in the tube until the oscillations just stopped. An evaluation of these losses leads to an estimate of the value of σ. When the position of the heater is such that the tube cannot be driven into self oscillations, i.e. for heater positions for which the timing of the heat addition is such that the oscillations are not sustained, the value of σ was obtained by Kerwin from a measurement of the width of the resonance curve of the tube with the heater in operation.

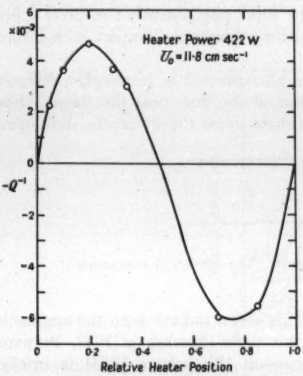

Figure 9. Driving power (or damping) denoted by the Q for the resonant tube as a function of the relative position of the heater. The direction of the mean flow is also that of increasing abscissa. (*After* Kerwin 1954.)

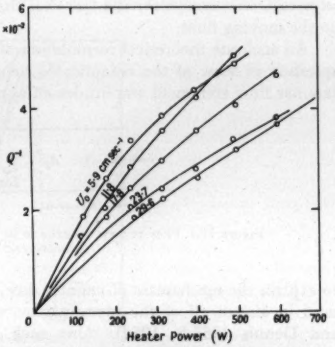

Figure 10. Dependence of the driving power as a function of the heater power input. (*After* Kerwin 1954.)

It is not too difficult to show that the reciprocal of the Q for the resonant tube is twice the ratio of σ to the resonance frequency ω. In this manner Kerwin was able to obtain the dependence of σ on the position of the heater. His results are shown in figure 9.

The acoustic power generated does not increase linearly with the added heat. There is an optimum heat input beyond which the acoustic power starts to diminish as more heat is added to the moving gas. Actually this effect, which could not have been predicted by means of a perturbation theory, is closely related to non-linear effects.

Typical behaviour for the dependence of the power generated on the heat input is shown in figure 10, which is taken from Kerwin's work. A similar result is also quoted by Lehman.

Although the discussion of Carrier is essentially correct in its broad lines, his method of estimating the fluctuating release of heat to the body of gas needs

to be improved. Predictions determined by means of Carrier's theory cannot be experimentally checked. It is felt, however, that the main features of the Rijke phenomenon are essentially understood. A more complete prediction of the maintenance of oscillation will eventually be obtained as a better understanding of the details of the interaction processes is developed.

3.3. *Flame Driven Acoustic Oscillations*

Under certain conditions, the presence of a flame in a moving stream of gas can excite the tube inside which the flow takes place into resonance. Representative examples of this class of phenomenon are the singing flames mentioned in the previous section. For low Mach numbers for the mean value of the flow velocity there is a great similarity between the Rijke phenomenon and these types of oscillations except for the fact that the burning flames also impart momentum to the moving fluid.

An accurate theoretical formulation of the phenomenon is, however, a difficult question in view of the complicated behaviour of the flow near the flame. For laminar flow and small amplitudes an approximate linear theory can be developed

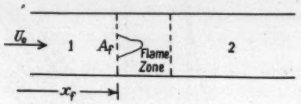

Figure 11. Flow regions referred to in the text. The distance x_f is measured from the end of the tube.

to explain the mechanism of maintenance. This seems to have been the approach used in almost all of the investigations on this topic (Blackshear 1953, Putnam and Dennis 1953 b, 1954). One such discussion (Blackshear 1953) is briefly presented below. The tube in which the oscillations takes place is divided in three zones (figure 11). A flame area is now defined by means of the usual perturbation convention as $A_f = A_0 + a$, where A_0 is the average flame area and a is the fluctuation superimposed on the mean value.

By means of the usual conservation relations (momentum, mass and energy) applied to the different regions of the tube, Blackshear shows that the fluctuating velocities on two sides of the transition zone are related by means of

$$u_2 = u_1 + a\frac{V_0}{A_0}\left(\frac{\rho_1}{\rho_2} - 1\right). \qquad \ldots\ldots(56)$$

The quantity $a(V_0/A_0)(\rho_1/\rho_2 - 1) = a^*$ which is the additional velocity introduced by the flame can be directly related to the fluctuating momentum imparted to the flow by the burning gases. Actually, substitution of (56) in the appropriate relation for the conservation of momentum leads to

$$P_1 - P_2 = \rho_1\left(\frac{\rho_1}{\rho_2} - 1\right) V_0^2 + 2\rho_1 V_0\left[a\frac{V_0}{A_0}\left(\frac{\rho_1}{\rho_2} - 1\right)\right] \qquad \ldots\ldots(57)$$

which proves the above statement.

To find the criterion for the maintenance of oscillations, Blackshear tries to formulate the problem in a manner which can be reconciled with Rayleigh's criterion mentioned in § 3.2.1. Accordingly, Blackshear breaks all quantities into waves travelling to the left and writes v_1^+, v_1^-, v_2^+, v_2^-, etc.; he considers the criterion for oscillation as the condition for a^{*+} to be in phase with v_1^+, v_2^+, and a^{*-} in phase with v_1^-, v_2^-, but it can be readily checked that this is equivalent to stating that the phasing of a^* is such that heat is released at the time of maximum condensation. This crude one-dimensional theory can predict only the main features of flame-driven oscillations. Experimental evidence thus shows that: (i) The position of the flame is very important to the excitation of the oscillations (Blackshear, Putnam and Dennis). The oscillations are most easily excited when the flame holder (and flame) is in the region of the standing wave where maximum condensation occurs. (ii) It is possible to excite the higher harmonics of the pipe.

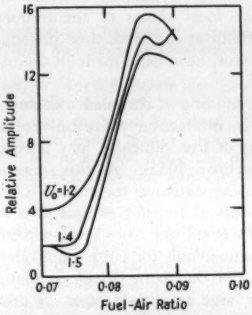

Figure 12. Dependence of the amplitude of the sound produced as a function of the fuel–air ratio. The values for the mean flow velocity are indicated on the curves and are in ft sec^{-1}. (*After* Blackshear 1953.)

The sound intensity of the harmonics, however, is less than that of the fundamental, and the harmonic frequency excited is such that the flame position corresponds to the location of a condensation maximum in the accompanying standing wave (Blackshear, Putnam and Dennis). (iii) The theory completely breaks down when the amplitude of the sound oscillations becomes very large. The flame then may burn upstream of the flame holder and away from it or even flash back. The excitation of the fundamental becomes then sporadic and difficult to maintain (Blackshear). At higher values of the Mach number and for large amplitudes of oscillation only higher order peripheral (i.e. those with angular dependence) modes can be excited. Not all the modes corresponding to those with plane wave fronts can be maintained (Moore and Maslen 1954). (iv) The fuel to air ratio as well as the flame holder geometry seem to have a marked effect (figure 12) on the intensity of the sound excited (Blackshear). The amplitude of the sound obtained seems to be greatest for a fuel–air ratio of 0·07. Studies on flame speed (Gerstein *et al.* 1950, Dugger and Heimel 1952) do not indicate a radical change in speed

with value of the ratio and it is perhaps the flame area change which has a strong flame speed dependence. Little information, however, is available on this dependence.

§ 4. Conclusion

The discussions of this report have shown that aero-thermoacoustics deals with a large number of phenomena which are just beginning to be understood. The difficulties encountered in the study of these acoustical phenomena is of both a theoretical and an experimental nature. The non-linearity of the basic differential equations for the motion of a fluid has compelled the majority of investigators to use perturbation techniques in the attempted solutions. These, as is expected, are of very limited scope and completely fail once the order of magnitude of the perturbations invalidates the premise of a small-signal hypothesis. The experimental difficulties are caused by the lack of simple methods for the direct measurement of the local values of the important parameters (such as density, velocity, etc.) without at the same time introducing a disturbance in the field. Great strides, however, have been made in the improvement of the experimental methods.

The lack of our understanding of turbulence theory makes an exact treatment of the general problem of interaction of turbulence and sound appear to be intractable. The way out of this difficulty may perhaps be by the methods of statistical mechanics (Kraichnan 1955). At this stage in the state of our knowledge, the advisability of using statistical techniques is still questionable.

The details of the process of transfer of heat in a boundary layer and in the presence of a pulsating flow is still far from being solved. Accordingly, a general treatment of the Rijke phenomenon for large amplitudes of motion still awaits a solution. The mechanism of the flame-driven oscillations also are not too well understood, especially the large amplitude case. A great deal of theoretical and experimental evidence is still needed to clarify the process of maintenance.

Finally, very little if anything is known of the case of strong interaction between the three modes. Certain attempts have been made to discuss the instability of flames (Markstein 1953, Markstein and Squire 1955) as representative instances of such interactions, but little success has been encountered toward establishing a reliable theory of strong interaction.

References

Batchelor, G. K., 1949, *Proc. Roy. Soc.* A, **195**, 513; 1950, *Proc. Camb. Phil. Soc.*, **47**, 359.

Bergmann, P. G., 1946, *Phys. Rev.*, **70**, 486.

Blackshear, P. L., 1953, *Fourth Symposium on Combustion*, p. 553 (Baltimore: Williams and Wilkins Co.).

Blokhintzev, D. I., 1945, *C.R. Acad. Sci., U.R.S.S.*, **46**, 136; 1946 a, *The Acoustics of an Inhomogeneous Moving Medium* (Research Analysis Group, Brown University, Providence); 1946 b, *J. Acoust. Soc. Amer.*, **18**, 329.

Carrier, G. F., 1955, *Quart. Appl. Math.*, **12**, 383.

Clauser, F. H., 1954, *J. Aero. Sci.*, **21**, 91.

Curle, N., 1955, *Proc. Roy. Soc.* A, **231**, 505.

Dugger, G. L., and Heimel, S., 1952, *Tech. Notes Nat. Adv. Comm. Aero., Wash.*, 2624.

Ellison, R. H., 1951, *J. Atmos. Terr. Phys.*, **2**, 14.

FITZPATRICK, H. M., and LEE, R., 1952, David W. Taylor Model Basin Report 835.
GERSTEIN, M., LEVINE, O., and WONG, E. L., 1950, *Res. Memor. Nat. Adv. Comm. Aero., Wash.*, E50G24.
HEISENBERG, W., 1949, *Proc. Roy. Soc.* A, **195**, 402.
KERWIN, E. M., 1954, *Doctoral Thesis*, Massachusetts Institute of Technology.
KOVÁZNAY, L. S. G., 1953, *J. Aero. Sci.*, **20**, 657.
KRAICHNAN, R. H., 1953, *J. Acoust. Soc. Amer.*, **25**, 1096 ; 1955, *Ibid.*, **27**, 438.
LAMB, H., 1879, as quoted in *Textbook of Hydrodynamics*, 1945, p. 502 (New York : Dover Publications).
LASSITER, L. W., and HUBBARD, H. H., 1952, *Tech. Notes Nat. Adv. Comm. Aero., Wash.*, 2757 ; 1953, *J. Acoust. Soc. Amer.*, **25**, 381 ; 1954, *Tech. Notes Nat. Adv. Comm. Aero., Wash.*, 3187 ; 1955, *J. Acoust. Soc. Amer.*, **27**, 431.
LAUFER, J., 1950, *Tech. Notes Nat. Adv. Comm. Aero., Wash.*, 2123 ; 1953, *Ibid.*, 2954.
LAX, M., 1951, *Rev. Mod. Phys.*, **23**, 287.
LEHMAN, K. O., 1937, *Ann. Phys., Lpz.*, **29**, 527.
LEWIS, J. A., and CARRIER, G. F., 1949, *Quart. Appl. Math.*, **7**, 228.
LIGHTHILL, M. J., 1952, *Proc. Roy. Soc.* A, **211**, 564 ; 1953, *Proc. Camb. Phil. Soc.*, **49**, 531 ; 1954, *Proc. Roy. Soc.* A, **222**, 1.
LUBIN, M. J., 1952, *Thesis*, Massachusetts Institute of Technology.
MARKSTEIN, G. H., 1953, *Fourth Symposium on Combustion*, p. 44 (Baltimore : Williams and Wilkins Co.).
MARKSTEIN, G. H., and SQUIRE, W., 1955, *J. Acoust. Soc. Amer.*, **27**, 416.
MAWARDI, O. K., 1955, *J. Acoust. Soc. Amer.*, **27**, 442.
MAWARDI, O. K., and DYER, I., 1953, *J. Acoust. Soc. Amer.*, **25**, 389.
MINTZER, D., 1953 a, *J. Acoust. Soc. Amer.*, **25**, 922 ; 1953 b, *Ibid.*, **25**, 1107.
MOORE, F. K., and MASLEN, S. H., 1954, *Tech. Notes Nat. Adv. Comm. Aero., Wash.*, 3152.
MORSE, P. M., and FESHBACH, H., 1953, *Methods of Theoretical Physics* (New York : McGraw Hill Book Co.).
MOYAL, P., 1952, *Proc. Camb. Phil. Soc.*, **48**, 329.
NEURINGER, J. L., and HUDSON, G. E., 1952, *J. Acoust. Soc. Amer.*, **24**, 667.
OBUKHOV, A. M., 1943, *C.R. Acad. Sci., U.R.S.S.*, **39**, 46.
PHILLIPS, O. M., 1956 a, *Proc. Roy. Soc.* A, **234**, 327 ; 1956 b, *Brit. Aero. Res. Ccl*, FM 2099.
POWELL, A., 1952, *Rep. Aero. Res. Comm., Lond.*, 15333.
PROUDMAN, I., 1952, *Proc. Roy. Soc.* A, **214**, 119.
PUTNAM, A. A., and DENNIS, W. R., 1953 a, *Trans. Amer. Soc. Mech. Engrs*, 45 ; 1953 b, *Fourth Symposium on Combustion*, p. 566 (Baltimore : Williams and Wilkins Co.) ; 1954, *J. Acoust. Soc. Amer.*, **26**, 716.
RAYLEIGH, Lord, 1878, *Nature, Lond.*, **18**, 319.
RICHARDSON, E. G., 1929, *Sound* (London : Arnold Press).
RIJKE, P. L., 1859, *Phil. Mag.*, **17**, 419.
SYMPOSIA ON AIRCRAFT NOISE, 1953, *J. Acoust. Soc. Amer.*, **25**, 363 ; 1954, *J. Roy. Aeronaut. Soc.*, **58**, 221.
TOWNSEND, A. A., 1951, *Proc. Camb. Phil. Soc.*, **47**, 375.
TRILLING, L. J., 1955, *J. Acoust. Soc. Amer.*, **27**, 425.
VILLARS, F., and WEISSKOPF, V. F., 1954, *Phys. Rev.*, **94**, 232.
WESTLEY, R. M., and LILLEY, G. M., 1952, *Rep. Coll. Aero. Cranfield*, 53.

SOME ASPECTS OF DIFFRACTION THEORY AND THEIR APPLICATION TO THE IONOSPHERE

By J. A. RATCLIFFE
Cavendish Laboratory, Cambridge

CONTENTS

PART I. SOME ASPECTS OF DIFFRACTION THEORY PAGE

§ 1. Introduction ... 190
§ 2. The angular spectrum and the Fraunhofer diffraction pattern ... 191
2.1. Introduction ... 191
2.2. The angular spectrum ... 191
2.3. A cosine diffracting screen ... 193
2.4. Evanescent waves ... 195
§ 3. Some examples of angular spectra ... 196
3.1. Complementary examples ... 196
3.2. A Gaussian distribution of amplitude ... 196
3.3. Amplitude-modulated diffracting screen ... 196
3.4. Phase-modulated diffracting screen ... 198
3.5. A medium which alters both amplitude and phase ... 200
3.6. Two-dimensional diffracting screens ... 201
3.7. Diffraction in three dimensions ... 204
§ 4. Fresnel diffraction ... 206
4.1. Relation to angular spectrum ... 206
4.2. A cosinusoidal amplitude screen ... 208
4.3. A cosinusoidal phase-changing screen ... 208
§ 5. The auto-correlation function and the Wiener–Khintchine theorem ... 210
5.1. The Wiener–Khintchine theorem ... 210
5.2. Applications to angular spectra and Fraunhofer diffraction ... 212
5.3. Application to Fresnel diffraction ... 213
§ 6. The angular spectra from random diffracting screens ... 214
6.1. Random functions and correlation functions ... 214
6.2. Other forms of correlation function ... 215
6.2.1. The correlation function of $\mathbf{f}(x)$ when $[\mathbf{f}(x)]_{av} \neq 0$ ... 215
6.2.2. The correlation function $r(\xi)$ ... 215
6.2.3. The difference correlation function $\Delta_A(\xi)$ (the 'after-effect' function) ... 216
6.3. The angular power spectra from random screens ... 217
6.4. 'Blobby' random screens ... 217
6.5. A medium which produces random changes of both amplitude and phase ... 218
6.6. A thick medium with weak three-dimensional irregularities ... 220
6.7. Non-uniform illumination ... 222
6.8. The production of a 'randomly phased spectrum' ... 224
§ 7. Incoherent sources ... 224
7.1. An incoherent source considered as a completely rough diffracting screen ... 224
7.2. The visibility of 'Young's double slit' interference fringes ... 225
7.3. The Michelson radio-stellar interferometer ... 227

PAGE

§ 8. Fresnel diffraction by random screens 227
8.1. The ' size ' of the irregularities 227
8.2. Distribution of amplitude and phase produced by a ' randomly phased ' spectrum 228
8.3. The correlation of amplitude 232
8.4. The correlation of phase 232
8.5. Correlation interferometers 233
8.6. Fresnel diffraction of waves from a point source 234
§ 9. Time-varying diffraction patterns 235
9.1. Description of time-varying patterns 235
9.2. Analysis of a pattern which drifts and changes 236
9.3. Time-varying diffraction 238
9.4. Time variations as the result of Doppler shifts 239

PART II. APPLICATIONS OF DIFFRACTION THEORY TO THE IONOSPHERE

§ 10. Introduction 239
§ 11. Scintillations of radio stars 240
11.1. The phenomenon 240
11.2. The Michelson radio-stellar interferometer 240
11.3. The method of the drifting pattern 242
11.4. The results 242
11.5. Deductions about the ionosphere 243
11.6. Diffraction by the solar corona 245
§ 12. Waves reflected from the ionosphere at steep incidence 246
12.1. The angular power spectrum 247
12.2. Observations on frequencies between 2 and 7 Mc/s 248
12.2.1. Methods 248
12.2.2. Observed amplitude distribution 249
12.2.3. Observed angular power spectra 249
12.3. Observations on frequencies less than 1 Mc/s 250
(*a*) 70–150 kc/s 250
(*b*) 16 kc/s 250
§ 13. Deductions from observations of reflected waves 251
13.1. The thin slab model 251
13.2. Diffraction at levels where $\mu \neq 1$ 252
13.3. Conclusions from experiments 253
§ 14. Some miscellaneous points 255
14.1. Reflection from randomly moving irregularities 255
14.2. Diffraction from meteor trails 256
14.3. Quick methods of analysis 257
14.4. Spaced-aerial direction finders 257
Appendices 257
1. The convolution theorem 257
2. Parseval's theorem 258
3. The Wiener–Khintchine theorem 258
4. Relations between correlation functions 258
5. The difference correlation function 259
6. A medium which produces changes of both amplitude and phase 259
7. The visibility of Young's double-slit interference fringes 260
8. Probability distributions 261
9. Diffraction of the radiation from a point source 262
10. Average distance between maxima 262
Bibliography 263

Abstract. In Part I the ' Fourier ' approach to diffraction theory is outlined in such a way as to emphasize its physical significance. Particular attention is paid to diffraction phenomena of the Fresnel type, and to diffraction from screens which alter both the phase and the amplitude of the incident wave. The ' Fourier ' approach is extended to deal with problems of ' random ' diffraction, for which purpose the use of auto-correlation functions is introduced and explained in physical terms.

In Part II measurements made on radio waves reflected from, or transmitted through, the ionosphere are discussed. The nature of the radio diffraction pattern observed at the ground is first summarized and deductions are then made about the ionosphere which has given rise to this diffraction.

There are few references in the text, but the bibliography provides brief abstracts of the more important papers on the subject.

PART I. SOME ASPECTS OF DIFFRACTION THEORY

§ 1. Introduction

The purpose of this report is to give an account of how the mathematical methods of Fourier transforms, and of autocorrelation functions, have been applied to the solution of problems of diffraction. When these methods are used in their most general form, and with all mathematical rigour, they appear somewhat formidable in spite of the fact that the physical ideas involved are quite simple. The aim will be to show, in physical terms, and with the minimum of mathematics, how these concepts arise and how they can be simply applied to a wide range of problems.

The sort of diffraction theory discussed here is related to a full theory based on Maxwell's equations and precise boundary conditions, much as Huygens' theory is, and it appears that, like Huygens' theory, it is quite adequate for most practical purposes. The arguments used will probably satisfy most physicists ; they are considerably elaborated in papers which will be referred to, and these should be consulted by those who desire a more rigorous treatment.

One advantage of considering diffraction in terms of Fourier transforms is that profitable analogies can then be drawn with other phenomena, and in particular with phenomena in electrical circuits. In this report diffraction theory will be extended to deal with the case when the diffracting medium is ' random ' so that it has to be described in statistical terms. It will then prove profitable to draw analogies with random ' noise ' in electrical circuits and to adopt, for this purpose, many of the conclusions of Rice's (1944, 1945) classical papers on the subject.

Some of the methods of analysis which are here described have been developed especially for dealing with problems concerning the diffraction of radio waves by an ionosphere which is random and is constantly changing. In this part of the report they will be described in general terms applicable to all diffraction phenomena. In Part II their particular application to the ionosphere will be considered.

The bibliography contains a list of papers, together with a note on the important points in each which bear on the subject of this report. Only in special cases will they be referred to in the body of the report.

§ 2. The Angular Spectrum and the Fraunhofer Diffraction Pattern

2.1. *Introduction*

Consider first the problem of a monochromatic electromagnetic wave travelling in the Z direction and incident normally on a thin diffracting sheet of material which modifies its amplitude A and its phase ϕ in different ways at different places, so that when it emerges A and ϕ are both functions of position (X, Y)† over the wave front, and the complex amplitude $\mathbf{f}(X, Y)$ is given by

$$\mathbf{f}(X, Y) = A(X, Y)\exp\{i\phi(X, Y)\}.$$

It is convenient to consider this wave as made up of a series of uniform infinite plane waves travelling in different directions. We will call this assembly of plane waves the angular spectrum of the wave-field and will show that it is related to the distribution $\mathbf{f}(X, Y)$ by a Fourier transform.

Each of the component plane waves in the angular spectrum travels in its own direction like an ordinary plane wave. At any plane other than the diffracting plane each will arrive with a phase depending on its direction, and the assembly of waves will build up a distribution of complex amplitude which, in general, is different from that over the diffracting plane. These distributions over planes parallel to the diffracting plane and at finite distances from it, constitute the Fresnel diffraction patterns at the different distances.

If the illumination over the diffracting screen is limited in lateral extent it can be shown (Booker and Clemmow 1950) that over a parallel plane at a sufficiently great distance the distribution of complex amplitude corresponds to the distribution with angle in the angular spectrum. Over planes more distant than this the distribution will remain the same; we shall call it the Fraunhofer diffraction pattern. It may be thought of as the (Fresnel) diffraction pattern formed on a plane at a great distance, and is often approximated to in optics by the diffraction pattern seen in the focal plane of a viewing lens.

2.2. *The Angular Spectrum*

Consider first a two-dimensional problem, in which there is no variation in the Y direction of a rectangular system of axes. Let a system of uniform plane waves, of frequency n, travelling in directions making angles θ with the Z axis, constitute an angular spectrum of plane waves, as in figure 1. Assume that the waves are polarized with either their electric or their magnetic vectors in the XZ plane,‡ and that the resultant complex amplitude§ of those whose wave-normals are at angles between θ and $\theta+d\theta$ is $\mathbf{A}(\theta)\,d\theta$, so that the corresponding elementary wave-bundle is given by

$$\mathbf{A}(\theta)\,d\theta\exp\left[2\pi i\{(X\sin\theta+Z\cos\theta)/\lambda-nt\}\right].$$

† We shall use capital letters such as X, Y, Z to represent distances measured in terms of the unit of length, and small letters, such as x, y, z, to represent distances measured in terms of the wavelength of the radiation as a unit.

‡ A case of more general polarization can be considered as a sum of these two special cases.

§ Complex numbers will be rendered throughout in heavy type.

The X-component of the resultant vector $\mathbf{A}$ from all the waves can now be written $\mathbf{f}(x, z)\exp(-2\pi int)$, where, if $X/\lambda = x$ and $Z/\lambda = z$,

$$\mathbf{f}(x, z) = \int_{-\pi/2}^{+\pi/2} \mathbf{A}(\theta)\cos\theta \exp[2\pi i(x\sin\theta + z\cos\theta)]\, d\theta. \qquad \ldots\ldots(1)$$

Now let the angle be expressed in terms of $\sin\theta(\equiv S)$ and write

$$\mathbf{A}(\theta) \equiv \mathbf{F}(\sin\theta) \equiv \mathbf{F}(S)$$

and $$\cos\theta = C,$$

so that equation (1) becomes

$$\mathbf{f}(x, z) = \int_{-1}^{+1} \mathbf{F}(S)\exp\{2\pi i(Sx + Cz)\}\, dS. \qquad \ldots\ldots(2)$$

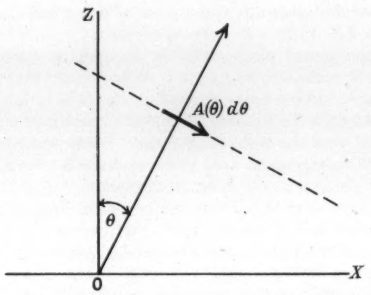

Figure 1. One component wave of an angular spectrum.

This equation represents a wave-field, varying over the two dimensions X and Z, in terms of an angular spectrum $\mathbf{F}(S)$ of plane waves. Over the plane $z = 0$ the wave-field is given by

$$\mathbf{f}(x) = \int_{-1}^{+1} \mathbf{F}(S)\exp(2\pi iSx)\, dS, \qquad \ldots\ldots(3)$$

and if the limits of the integral had been $\pm\infty$ this would show that $\mathbf{f}(x)$ and $\mathbf{F}(S)$ form a Fourier transform pair. We shall write the limits $\pm\infty$ for the present and shall justify the procedure later. We then have

$$\mathbf{f}(x) = \int_{-\infty}^{+\infty} \mathbf{F}(S)\exp(2\pi iSx)\, dS \qquad \ldots\ldots(4)$$

and by the inversion theorem of Fourier transforms it is also true that

$$\mathbf{F}(S) = \int_{-\infty}^{+\infty} \mathbf{f}(x)\exp(-2\pi iSx)\, dx. \qquad \ldots\ldots(5)$$

The two equations are similar except that the sign of the exponent is different. We shall use the negative sign when the integration is with respect to x. It is

convenient to indicate that $\mathbf{f}(x)$ and $\mathbf{F}(S)$ form a Fourier transform pair which obeys equations (4) and (5) by writing

$$\mathbf{f}(x) \longleftrightarrow \mathbf{F}(S). \qquad \ldots\ldots(6)$$

The above analysis has shown that an angular spectrum $\mathbf{F}(S)$ will produce, over the plane $z = 0$, a field component along the X direction given by $\mathbf{f}(x)$, where $\mathbf{f}(x) \longleftrightarrow \mathbf{F}(S)$. But this implies that if the field distribution $\mathbf{f}(x)$ is experimentally produced, by any means, it is equivalent to the angular spectrum $\mathbf{F}(S)$. It is thus possible to state the following general theorem :

> When a one-dimensional diffracting screen is illuminated by a wave of length λ, the angular spectrum produced, expressed in terms of $S(\equiv \sin\theta)$ is the Fourier transform of the distribution of complex amplitude over the wave front just as it leaves the screen, expressed in terms of λ as a unit.

This theorem will be much used in what follows, but before considering its application some important subsidiary points will be discussed.

2.3. *A Cosine Diffracting Screen*

It is helpful to consider first a simple case in which the angular spectrum consists only of two components of complex amplitude $\mathbf{F}(+S_0)\,\delta S$ and $\mathbf{F}(-S_0)\,\delta S$ at angles $\pm S_0$, and to suppose that

$$\mathbf{F}(+S_0)\,\delta S = \tfrac{1}{2}a\,e^{i\phi},$$
$$\mathbf{F}(-S_0)\,\delta S = \tfrac{1}{2}a\,e^{-i\phi}.$$

This spectrum is shown in figure 2 (*a*). The resultant disturbance is then given by

$$\begin{aligned}\mathbf{f}(x,z)\exp(-2\pi int) &= \tfrac{1}{2}a[\exp\{2\pi i(S_0x + C_0z) + i\phi\} \\ &\qquad + \exp\{2\pi i(-S_0x + C_0z) - i\phi\}]\exp(-2\pi int) \\ &= a\cos(2\pi S_0x + \phi)\exp\{2\pi i(C_0z - nt)\}. \qquad \ldots\ldots(7)\end{aligned}$$

This represents a wave-motion travelling along the positive Z direction and having an amplitude $\mathbf{f}$ which varies cosinusoidally over the wave front as given by $a\cos(2\pi S_0x + \phi)$ and as represented in figure 2 (*b*). It might be described as a wave with a striated wave front. The spatial periodicity of the striations is given by d where

$$d = 1/S_0. \qquad \ldots\ldots(8)$$

Here d is, as usual, measured in terms of the wavelength as a unit.

The composite wave of equation (7) travels only along the Z direction and with a velocity† given by $v = n/C_0$. If we write $n = v_0$, the velocity of a uniform plane wave, and substitute $C_0 = (1 - S_0^2)^{1/2} = (1 - 1/d^2)^{1/2}$, then

$$v = v_0(1 - 1/d^2)^{-1/2}. \qquad \ldots\ldots(9)$$

The velocity is thus greater than the velocity of a uniform plane wave and depends on the spatial period. The wave is like one of those which could be propagated in a waveguide with metallic boundaries situated in any two of the nodal planes.

† Velocity is here measured in units of one wavelength in unit time.

On the plane $z = 0$ the disturbance of equation (7) is represented by

$$\mathbf{f}(x) = a\cos\{2\pi S_0 x + \phi\} \qquad \ldots\ldots(10)$$

and it could have been produced by allowing a uniform plane wave, travelling in the direction OZ, to pass through a diffracting screen which impressed this amplitude upon it.† The resulting disturbance is the same as that produced by the two original uniform plane waves of figure 2 (*a*) travelling in the directions

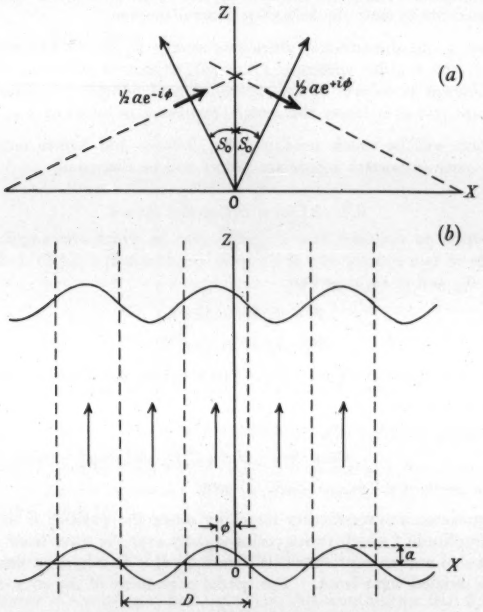

Figure 2. (*a*) A pair of crossing plane waves.
(*b*) The wave with a ' striated ' wave front, with amplitude $a\cos(2\pi S_0 x + \phi)$, which results from the superposition of the two waves in (*a*).

$\pm S_0$, and they therefore represent the angular spectrum corresponding to diffraction by this screen.

The relation between the *cosine diffracting screen* and the *angular spectrum* to which it gives rise, is illustrated in figure 3, in which, as usual, distances are measured in terms of the wavelength as a unit. It will be noticed that the two

† This diffracting screen would be such that it transmitted an amplitude which was a cosinusoidal function of distance x, and to do this it would have to be provided with phase-reversing sections to produce the negative parts of the amplitude distribution.

spectra occur at angles given by $dS_0 = 1$, or $D \sin\theta = \lambda$, as we should expect from the ordinary expression for a diffraction grating of periodicity D, that there is no zero-order spectrum with $S = 0$, because of the mutual interference of the portions of the screen with positive and negative amplitudes, and that the position of the screen with respect to the origin of X affects only the temporal phases $\pm\phi$ of the spectra, and not their positions. Indeed, a cosine diffracting screen which moved parallel to itself would produce spectra constant in amplitude and position.

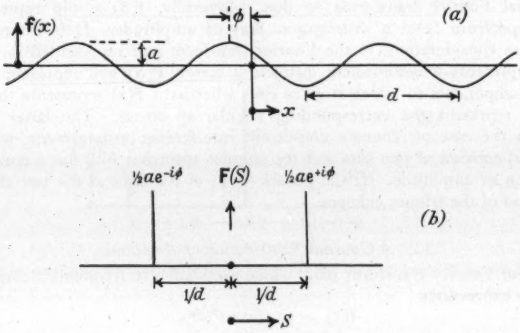

Figure 3. A cosine diffracting screen $\mathbf{f}(x)$, and its angular spectrum $\mathbf{F}(S)$. $\mathbf{f}(x)$ and $\mathbf{F}(S)$ form a Fourier transform pair.

2.4. *Evanescent Waves*

Consider next the fact that in the synthesis from a series of travelling waves the limits in the integral were ± 1 whereas in the Fourier transform of the distribution $\mathbf{f}(x)$ the limits were $\pm\infty$. For this purpose it is necessary to consider the meaning to be attached to values of $|S| > 1$. When $|S| > 1, \cos\theta = (1 - S^2)^{1/2}$ will be an imaginary quantity; let us write it $i\gamma$. Then a small bundle of waves in the angular spectrum represented by equation (2) will become

$$\begin{aligned} &\mathbf{F}(S)\, dS \exp\{2\pi i(Sx + i\gamma z)\} \exp(-2\pi i n t) \\ &= \mathbf{F}(S)\, dS \exp(-2\pi\gamma z) \exp\{2\pi i(Sx - nt)\} \qquad \ldots\ldots(11) \end{aligned}$$

which has a spatial periodicity $1/S$ (or λ/S in unit measure) along the X direction and is attenuated in the Z direction. A disturbance of this kind is called an evanescent wave. Since $|S| > 1$ the spatial period in the X direction is less than λ.

If the wave-field $\mathbf{f}(x)$ at the diffracting screen has Fourier components of spatial period less than λ they will correspond to evanescent waves, which are rapidly attenuated as they leave the screen. At a distance of more than about one wavelength only the travelling waves will remain in the angular spectrum, and if only these are to be included the limits to the integral of equation (4) must be $S = \pm 1$. If, however, all the waves, including the evanescent ones, are to be included, the limits will be $S = \pm\infty$. The fact that only the travelling waves in

the angular spectrum are appreciable at a distance corresponds to the fact that light of wavelength λ cannot reveal structure in the diffracting screen of magnitude less than λ.

§ 3. Some Examples of Angular Spectra

3.1. *Complementary Examples*

The angular spectrum $\mathbf{F}(S)$ and the distribution of complex amplitude $\mathbf{f}(x)$ are mutual Fourier transforms so that, conversely, $\mathbf{f}(S)$ would represent the angular spectrum from a distribution $\mathbf{F}(x)$ of amplitude. It is interesting to apply these considerations to the Fourier transform pair represented in figure 3. If $\mathbf{f}(x)$ represents a cosinusoidal diffracting screen $\mathbf{F}(S)$ will represent the two spectral components to which it gives rise, whereas if $\mathbf{F}(x)$ represents the screen $\mathbf{f}(S)$ will represent the corresponding angular spectrum. The latter example represents the case of Young's double-slit interference arrangement, where the screen $\mathbf{F}(x)$ consists of two slits and the angular spectrum $\mathbf{f}(S)$ has a cosinusoidal distribution of amplitude. If the phases ($\pm\phi$) of the light at the two slits alter, the position of the fringes changes.

3.2. *A Gaussian Distribution of Amplitude*

A useful Fourier transform pair, which we shall use frequently, corresponds to the two expressions

$$\mathbf{f}(x) = \exp(-\pi x^2/d^2), \qquad \ldots\ldots(12)$$

$$\mathbf{F}(S) = \exp(-\pi S^2 d^2). \qquad \ldots\ldots(13)$$

This is one of a large number of expressions which, apart from a scale factor, transform into themselves.

3.3. *Amplitude-modulated Diffracting Screen*

We have previously considered a diffracting screen which transmits an amplitude $\mathbf{f}(x) = A\cos(2\pi x/d)$, which changes sign every half (spatial) period. Let us now consider a screen in which the amplitude is always positive and is given by

$$\mathbf{f}(x) = 1 + m\cos(2\pi x/d) \qquad \ldots\ldots(14)$$

where $m \leqslant 1$. It is represented in figure 4 (*a*) and is said to be amplitude modulated, by analogy with the corresponding time-varying amplitude

$$\mathbf{f}(t) = 1 + m\cos(2\pi t/T) \qquad \ldots\ldots(15)$$

of an amplitude-modulated oscillation. $\mathbf{f}(x)$ can be split into a uniform distribution of unit amplitude to which is added a cosine distribution of amplitude m. The uniform distribution corresponds to a uniform plane wave of unit amplitude travelling along the Z direction, and the cosine distribution corresponds to two waves of amplitude $\frac{1}{2}m$ travelling in directions $S = \pm 1/d$ and in phase with the main wave at the origin. The angular spectrum thus consists of a zero order component of unit amplitude, and two side components of amplitude $\frac{1}{2}m$ as shown in figure 4 (*b*). The three components correspond to the ' carrier ' and the two ' side bands ' of a cosinusoidal amplitude-modulated oscillation.

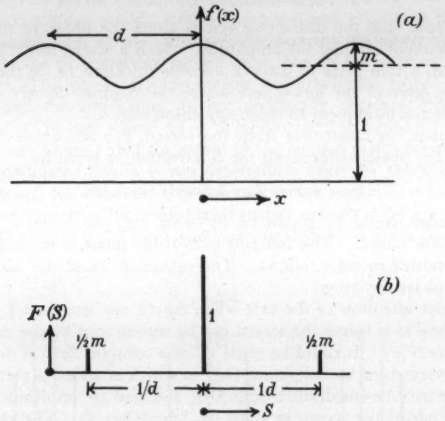

Figure 4. An amplitude-modulated diffracting screen (*a*), and the corresponding angular spectrum (*b*).

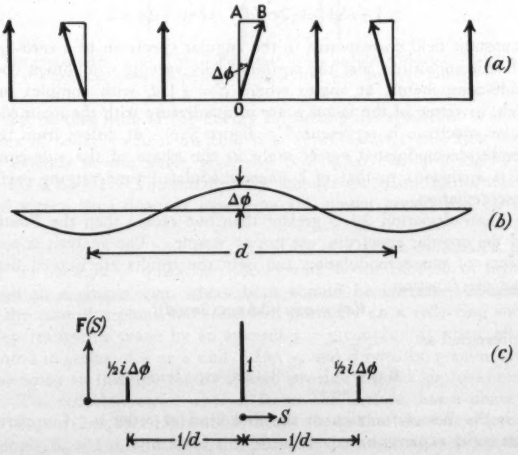

Figure 5. A cosinusoidally phase-modulated screen of small phase deviation : (*a*) represents the emerging field as time-rotating vectors, (*b*) represents the *x*-variation of the quadrature component AB, (*c*) represents the angular spectrum.

3.4. *Phase-modulated Diffracting Screen*

Next suppose that the diffracting screen alters the phase of the wave which traverses it, without altering the amplitude. Such a screen might be, in the case of visible light, a thin piece of glass of variable thickness or, in the case of radio waves, a thin layer of the ionosphere where the electron density varied but the collisions were too infrequent to cause any absorption.

Suppose that, on emergence from the screen, the amplitude of the wave is constant but the phase varies along the X direction as given by

$$\phi(x) = \phi_0 + \Delta\phi \cos(2\pi x/d). \qquad \ldots\ldots(16)$$

This distribution could be produced by what may be called a cosinusoidally modulated phase screen. The constant part of the phase is of no special interest and will be omitted in what follows. The excursion $\Delta\phi$ of the variable part will be called the phase deviation.

Next restrict attention to the case when $\Delta\phi \ll 1$ say less than $\frac{1}{8}$ radian. The field in the wave as it leaves the screen can be represented by the rotating vectors shown in figure 5 (*a*). It could be made up of a constant field of unit magnitude, represented everywhere by the vector OA, to which is added a vector AB, which is everywhere in time-quadrature with OA, and has an amplitude which varies cosinusoidally across the screen as given by $\Delta\phi \cos(2\pi x/d)$. The variation of this part is shown at (*b*). This decomposition of the field could equally well be achieved by writing

$$\mathbf{f}(x) = \exp\{i\Delta\phi \cos(2\pi x/d)\}, \qquad \ldots\ldots(17\,a)$$

$$\simeq 1 + i\Delta\phi \cos(2\pi x/d) \quad \text{when} \quad \Delta\phi \ll 1. \qquad \ldots\ldots(17\,b)$$

The constant field corresponds in the angular spectrum to a zero-order component of unit amplitude, and the cosinusoidally varying component corresponds to two side-components, at angles where $S = \pm 1/d$, with complex amplitudes $\frac{1}{2}i\Delta\phi$ which, in virtue of the factor i, are in quadrature with the main component. The angular spectrum is represented in figure 5 (*c*). It differs from that of the cosine amplitude-modulated screen only in the phase of the side-components. The case is analogous to that of a phase-modulated time-varying oscillation of small phase-deviation.

If the phase-deviation $\Delta\phi$ is greater than one radian then the Fourier transform, and the angular spectrum, are not so simple. The analysis is well known in the theory of phase modulation and only the results are quoted here. It is known that the function

$$\mathbf{f}(x) = \exp\{i\Delta\phi \cos(2\pi x/d)\} \qquad \ldots\ldots(18)$$

can be represented as

$$\mathbf{f}(x) = \sum_{n=-\infty}^{+\infty} (i)^n \mathrm{J}_n(\Delta\phi) \exp(2\pi i n x/d) \qquad \ldots\ldots(19)$$

where J_n is the Bessel function of the first kind of order n. Comparison with the Fourier series expansion

$$\mathbf{f}(x) = \sum_{n=-\infty}^{+\infty} F(S_n) \exp(2\pi i S_n x) \qquad \ldots\ldots(20)$$

shows that the Fourier transform $\mathbf{F}(S)$ of $\mathbf{f}(x)$ has components at values of S given by $0, \pm 1/d, \pm 2/d, \ldots \pm n/d \ldots$ and not just at 0 and $\pm 1/d$ as is the case when $\Delta\phi \ll 1$. The amplitudes of the successive components are given by $J_n(\Delta\phi)$ and their phases change progressively by $\pi/2$ from one to the next as indicated by the factor $(i)^n$. The zero-order component has amplitude $J_0(\Delta\phi)$ which is no longer unity, and the amplitudes do not necessarily decrease regularly as the order increases. The case where $\Delta\phi = 10$ is illustrated in figure 6.

It is clear from figure 6 that the extent of the angular spectrum produced by a cosine phase-modulated screen is not determined solely by the spatial period d of the modulation, for although this determines the angle $S_0 = 1/d$ of the first side component there may be many higher orders present if $\Delta\phi > 1$. The amplitude of the nth order is $J_n(\Delta\phi)$ and it so happens that, for a given $\Delta\phi$, this is small

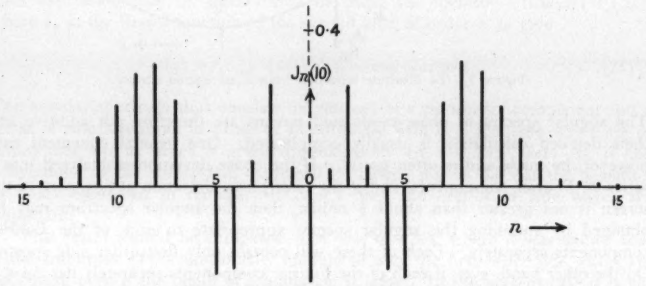

Figure 6. The magnitudes $J_n(10)$ of the components in the angular spectrum of a wave front over which the phase varies like $\Delta\phi\cos(2\pi x/d)$ with $\Delta\phi = 10$ radians.

when $n > \Delta\phi$, so that little of the energy in the angular spectrum is contained in components of order $n > \Delta\phi$. Indeed, it is approximately true that the angular spectrum extends to the angle given by $S = S_0\Delta\phi = \Delta\phi/d$ if $\Delta\phi > 1$, and by $S = S_0 = 1/d$ if $\Delta\phi < 1$. The extent of the angular spectrum from a cosine phase-modulated screen thus depends jointly on the spatial period and on the phase deviation.

It is interesting to see how the treatments of a phase-modulated diffracting screen by the method of diffraction theory and by the method of rays give the same result in a simple case where both should be correct. Consider, as in figure 7, the case of a plane wave incident normally on a reflecting sheet whose surface departs from a plane by an amount $y = y_0\cos(2\pi x/d)$ where all distances are measured in terms of λ as a unit. Let y_0 and d both be greater than one or two wavelengths so that ray theory should provide a good approximation to the solution. The reflected wave, when it leaves the surface, has a phase given by $\phi(x) = 2\pi . 2y_0\cos(2\pi x/d)$. Diffraction theory shows that the first side component is at an angle $S_0 = 1/d$, and since the phase deviation is $\Delta\phi = 4\pi y_0$, the angular spread of the radiation is $S_0\Delta\phi = 4\pi y_0/d$. On a ray picture different parts of the surface act as plane reflectors and the greatest deviation by reflection is from the

parts of greatest slope, where $(dy/dx)_{max} = 2\pi y_0/d = \theta_m$. The greatest angular deviation is then $2\theta_m = 4\pi y_0/d$ in agreement with the result of diffraction theory.

If a phase-modulated screen contains components with two spatial periods, so that, for example,

$$\Delta\phi = \Delta\phi_1 \cos(2\pi x/d_1) + \Delta\phi_2 \cos(2\pi x/d_2),$$

then, in general, the Fourier transform, and the angular spectrum, will contain components not only where $S = m/d_1$ and n/d_2, but also where $S = m/d_1 \pm n/d_2$.

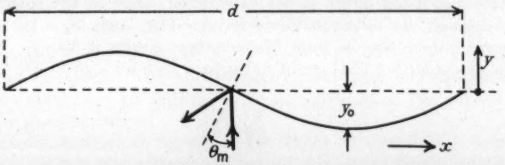

Figure 7. To illustrate reflection from a corrugated surface.

The angular spectra of phase-modulated screens are therefore not additive and their detailed calculation is usually complicated. One general statement can, however, be made and is often useful. If the phase deviation is analysed into a series of Fourier components, and if the *total* phase deviation at any part of the screen is not greater than about $\frac{1}{4}$ radian, then the angular spectrum may be obtained by summing the angular spectra appropriate to each of the Fourier components separately. Each of these will contain only first order side spectra. On the other hand, even if each of the Fourier components separately has $\Delta\phi \ll 1$, the resulting spectrum will not be the sum of the individual spectra if, at any point on the screen, the total phase deviation is greater than one radian.

3.5. *A Medium which alters both Amplitude and Phase*

Most media alter both the amplitude and the velocity of a wave traversing them, and the result is conveniently expressed in terms of a complex refractive index $\boldsymbol{\mu}$. If a uniform plane wave, originally of unit amplitude, passes normally through a thin slab of the medium, of thickness Δz, it will emerge with a complex amplitude which may be written

$$\begin{aligned} \mathbf{f} &= \exp\{2\pi i \boldsymbol{\mu} \Delta z\} \\ &= \exp\{i\boldsymbol{\varphi}\}, \qquad \ldots\ldots(21) \end{aligned}$$

where $\boldsymbol{\varphi}$ is a complex phase which describes both the absorbing and the refracting effects of the slab. If now the density N of the medium changes across the slab in the X direction, and with it the complex refractive index, then $\mathbf{f}$ and $\boldsymbol{\varphi}$ become functions of x, and we may write

$$\mathbf{f}(x) = \exp\{i\boldsymbol{\varphi}(x)\}.$$

The case where the medium was non-absorbing and $\boldsymbol{\varphi}(x)$ was purely real and equal to $\Delta\phi \cos(2\pi x/d)$ was considered in the last section. If absorption alone is important, and the variations of velocity are negligible, $\boldsymbol{\varphi}(x)$ is purely imaginary

and may be written $i\kappa(x)$ where $\kappa(x)$ is the absorption in nepers produced by the slab. It is of interest to consider the case when

$$\kappa(x) = \kappa_0 + \Delta\kappa \cos(2\pi x/d) \qquad \ldots\ldots(22)$$

which corresponds to a cosine variation of density superposed on a mean. Then

$$f(x) = f_0 \exp\{-\Delta\kappa \cos(2\pi x/d)\} \qquad \ldots\ldots(23)$$

where $f_0 = \exp(-\kappa_0)$. The variable factor in equation (23) is like that of the phase-modulated case of equation (17 *a*) if $i\Delta\kappa$ is written for $\Delta\phi$, so that the angular spectrum is obtained by substituting $\Delta\phi = i\Delta\kappa$ into equation (19) to give

$$f(x) = f_0 \sum_{n=-\infty}^{+\infty} i^n \mathrm{J}_n(i\Delta\kappa) \exp(2\pi i n x/d). \qquad \ldots\ldots(24)$$

This expression may be transformed by using the identity $\mathrm{J}_n(i\Delta\kappa) \equiv i^n \mathrm{I}_n(\Delta\kappa)$, where I_n is the Bessel function of the second kind of order n, to give

$$f(x) = f_0 \sum_{n=-\infty}^{+\infty} (-1)^n \mathrm{I}_n(\Delta\kappa) \exp(2\pi i n x/d). \qquad \ldots\ldots(25)$$

The angular spectrum thus consists, in general, of a zero-order component and a series of side waves, all in phase or in antiphase with it. The side waves are of importance up to order n given approximately by $n = \Delta\kappa$. Here $\Delta\kappa$ is the 'deviation' of the absorption, expressed in nepers, just as $\Delta\phi$ was the deviation of phase expressed in radians. If $\Delta\kappa \ll 1$ only the first-order side waves are important.

This result should be compared with that of § 3.3, where it was shown that if the amplitude $|\mathbf{f}|$ is sinusoidally modulated only the first-order side waves are produced, even if the depth of modulation is large. In the present case it is not the amplitude, but the logarithm of the amplitude, which is sinusoidally modulated, and that is why higher-order side waves are produced. There is thus a difference according as the Fourier analysis is performed on the density of the diffracting medium, which determines the logarithm of the amplitude, or on the amplitude itself. It is usually more satisfactory to analyse the medium, since then both amplitude and phase are treated in the same way.

3.6. *Two-dimensional Diffracting Screens*

A straightforward extension of the foregoing analysis to the case where the transmission properties of the thin diffracting screen vary in both X and Y directions can be made as follows. In place of the one-dimensional Fourier transform we have the two-dimensional one

$$\mathbf{f}(x, y) = \int_{-\infty}^{+\infty}\int_{-\infty}^{+\infty} \mathbf{F}(S_1, S_2) \exp\{2\pi i(S_1 x + S_2 y)\}\, dS_1\, dS_2 \qquad \ldots\ldots(26)$$

and

$$\mathbf{F}(S_1, S_2) = \int_{-\infty}^{+\infty}\int_{-\infty}^{+\infty} \mathbf{f}(x, y) \exp\{-2\pi i(S_1 x + S_2 y)\}\, dx\, dy \qquad \ldots\ldots(27)$$

and this can be interpreted as the sum of a set of uniform plane waves travelling in directions with direction cosines S_1, S_2 and with complex amplitudes $\mathbf{F}(S_1, S_2)$. If $S_1^2 + S_2^2 > 1$ the wave is evanescent.

If $\mathbf{f}(x,y)$ is such that it depends only on $r=(x^2+y^2)^{1/2}$ it is convenient to introduce two-dimensional polar coordinates r and $\phi=\tan^{-1}(y/x)$ in the x,y plane and $S=(S_1^2+S_2^2)^{1/2}$ and $\psi=\tan^{-1}(S_2/S_1)$ in the S_1,S_2 plane. Equation (27) may then be written as

$$\mathbf{F}(S,\psi)=\int_0^{+\infty}\int_{-\pi}^{+\pi}\mathbf{f}(r)\exp\{-2\pi irS\cos(\psi-\phi)\}\,r\,dr\,d\phi. \qquad \ldots\ldots(28)$$

The integral with respect to ϕ is the Bessel function $J_0(2\pi rS)$ so that

$$\mathbf{F}(S)=2\pi\int_0^{\infty}\mathbf{f}(r)\,J_0(2\pi rS)\,r\,dr. \qquad \ldots\ldots(29)$$

The inverse relation

$$\mathbf{f}(r)=2\pi\int_0^{\infty}\mathbf{F}(S)\,J_0(2\pi rS)\,S\,dS \qquad \ldots\ldots(30)$$

is derived in a similar way from equation (26).

As an example of the use of this form of the expression let us calculate the angular spectrum from a circular aperture of radius r_1. This case corresponds to

$$f(r)=1 \quad \text{for} \quad r<r_1$$

$$f(r)=0 \quad \text{for} \quad r>r_1$$

and, from equation (29)

$$\mathbf{F}(S)=2\pi\int_0^{r_1}J_0(2\pi rS)\,r\,dr$$

$$=\frac{r_1J_1(2\pi Sr_1)}{S}. \qquad \ldots\ldots(31)$$

This gives the form of the angular spectrum, and for small angles S its magnitude becomes $\frac{1}{2}r_1^2$. It can be normalized so that $\mathbf{F}(S)=1$ when $S=0$ by dividing by $\frac{1}{2}r_1^2$ to give

$$F(S)=\frac{2J_1(2\pi Sr_1)}{Sr_1}$$

and this is the well-known form derived by Airey.

It is interesting to consider the case where the symmetrical two-dimensional angular spectrum is given by $F(S)=(1-S^2)^n$ or $F(\theta)=(\cos\theta)^{2n}$. This is of particular interest because, when n is large, $(\cos\theta)^{2n}$ is a good approximation to $\exp(-\theta^2/S_0^2)$ if $n=1/S_0^2$. Equation (30) shows that

$$f(r)=\int_0^1 S(1-S^2)^n\,J_0(2\pi rS)\,dS$$

$$=\int_0^{\frac{1}{2}\pi}\sin\theta(\cos\theta)^{2n+1}\,J_0(2\pi r\sin\theta)\,d\theta \qquad \ldots\ldots(32)$$

which is a special case of Sonine's first integral and gives

$$f(r)=\Gamma(n+2)\,2^{n+1}(2\pi r)^{-(n+1)}\,J_{n+1}(2\pi r). \qquad \ldots\ldots(33)$$

It is thus possible to calculate the approximate two-dimensional distributions $f(r)$ which would correspond to two-dimensional angular spectra $F(\theta)=\exp(-\theta^2/S_0^2)$ for different values of S_0. Equation (33) is not a very convenient one for calculation when n is large, but values calculated for $n=11$ ($S_0=0{\cdot}3$) are shown by

the crosses in figure 8. Curves for other values of n calculated by Briggs and Phillips (1950), who used a different method, are also shown in the figure labelled with values of S_0. It can be seen that their curve for $n = 12{\cdot}5$ ($S_0 = 0{\cdot}28$) is close to the crosses calculated for $n = 11$ ($S_0 = 3$) from equation (33).†

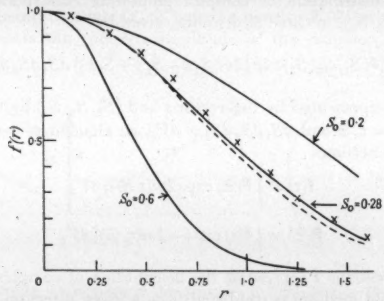

Figure 8. The two-dimensional distributions $f(r)$ corresponding to two-dimensional angular spectra $F(\theta) = \exp(-\theta^2/S_0^2)$ for different values of S_0. The continuous curves were calculated by Briggs and Phillips (1950), the crosses were calculated from equation (33) with $S_0 = 0{\cdot}3$ and the broken curve from equation (34) with $S_0 = 0{\cdot}3$. This curve corresponds to a one-dimensional variation.

In equation (33) $f(r)$ represents the two-dimensional distribution which would correspond to a two-dimensional angular spectrum $F(\theta) = \exp(-\theta^2/S_0^2)$ or, for small angles $F(S) = \exp(-S^2/S_0^2)$. If this angular spectrum had been a one-dimensional one it would have corresponded to a one-dimensional distribution of amplitude given by

$$f(x) = \exp(-\pi^2 x^2 S_0^2). \qquad \ldots\ldots(34)$$

It is interesting to compare the two-dimensional distribution of equation (33) with the one-dimensional one of equation (34) which would give the same angular spectrum. The curve which represents equation (34) when $S_0 = 0{\cdot}3$ is shown in figure 8 as a broken line. It is seen that it approximates closely to the continuous curve which represents $f(r)$, so that in this particular case the two-dimensional diffraction pattern is well represented by the simpler expression appropriate to the one-dimensional case. In what follows we shall assume that this equivalence is true in general, although it has only been demonstrated for the special case where $S_0 = 0{\cdot}3$.

It is well known that when the one-dimensional diffraction pattern of a slit is compared with the two-dimensional pattern of a circular aperture, of diameter equal to the slit width, the distances to the first zero are in the ratio 1 : 22. From what has just been stated it does not seem that there is any corresponding difference between the one- and two-dimensional diffraction patterns represented by the normal distribution functions here considered.

† It should be noticed that the curves shown in figure 5 of the paper by Briggs and Phillips are labelled with values of n which are four times those used here. The reasons for this are indicated in their figure 3(*b*) and are related to their assumption of a point-source radiator (see our § 8.6).

3.7. *Diffraction in Three Dimensions*

Suppose a three-dimensional medium contains irregularities and is irradiated by a plane wave. Then the irregularities cause a change in the wave-field which can be represented by a complex amplitude $\mathbf{f}(x, y, z)$ which varies throughout the medium. This distribution of complex amplitude corresponds to an angular spectrum $\mathbf{F}(S_1, S_2, S_3)$, in three dimensions, given by

$$\mathbf{f}(x, y, z) = \iiint \mathbf{F}(S_1, S_2, S_3) \exp\{2\pi i(S_1 x + S_2 y + S_3 z)\}\, dS_1 dS_2 dS_3. \quad \ldots\ldots(35)$$

If (x, y, z) is represented by the vector $\mathfrak{r}$ and (S_1, S_2, S_3) by the vector $\mathfrak{S}$, then $S_1 x + S_2 y + S_3 z = \mathfrak{r}.\mathfrak{S}$ and $dS_1 dS_2 dS_3 = dV_{\mathfrak{S}}$ an element of volume in $\mathfrak{S}$-space, and the equation becomes

$$\mathbf{f}(\mathfrak{r}) = \int \mathbf{F}(\mathfrak{S}) \exp\{2\pi i(\mathfrak{r}.\mathfrak{S})\}\, dV_{\mathfrak{S}} \quad \ldots\ldots(36)$$

and inversely

$$\mathbf{F}(\mathfrak{S}) = \int \mathbf{f}(\mathfrak{r}) \exp\{-2\pi i(\mathfrak{r}.\mathfrak{S})\}\, dV_{\mathfrak{r}}. \quad \ldots\ldots(37)$$

In these expressions $\mathbf{f}$ represents the distribution of complex wave amplitude produced when the medium is irradiated from a given direction. The phase of $\mathbf{f}$ depends on the direction of the irradiation, and its magnitude $|\mathbf{f}|$ depends on the structure of the medium and on the intensity of the incident wave. If it can be assumed that the amount of scattering is small, so that the intensity of the incident wave is not appreciably altered as it traverses the medium, and re-diffraction of the once-diffracted waves can be neglected, then $|\mathbf{f}|$ depends only on the structure of the medium. Born was the first to discuss these conditions in problems of wave mechanics and the approximation is called the Born approximation. It is often valid in problems of x-ray scattering and in the scattering of radio waves from weak irregularities in the ionosphere. The calculation of the angular spectrum is then well known to those who are concerned with x-ray diffraction and is given in detail, for example, in James (1948). The results are usually expressed as follows.

In equations (36) and (37) $\mathbf{f}(\mathfrak{r})$ represents the complex wave amplitude at each point, its magnitude $|\mathbf{f}(\mathfrak{r})|$ is proportional to the density of scattering material. Let

$$|\mathbf{f}(\mathfrak{r})| \longleftrightarrow \mathbf{F}_1(\mathfrak{S}) \quad \ldots\ldots(38)$$

then $\mathbf{F}_1(\mathfrak{S})$ is determined solely by the medium and not at all by the incident radiation. Let $\mathbf{F}_1(\mathfrak{S})$ be represented by a density distribution in three dimensions such that the density at the point $\mathfrak{S}$ is equal to $\mathbf{F}_1(\mathfrak{S})$. This distribution is called the distribution in reciprocal space. If $|\mathbf{f}(\mathfrak{r})|$ represents the density of scattering material in a crystal lattice $\mathbf{F}_1(\mathfrak{S})$ will have finite density only at certain points and it is called the reciprocal lattice.

It is then shown in the standard treatment that when a plane wave is incident along any direction AB (see figure 9) the wave diffracted (or scattered) in a direction BC is given by

$$\mathrm{A}(\theta) = \int |\mathbf{f}(\mathfrak{r})| \exp(2\pi i \mathfrak{r}.\mathfrak{R})\, dV_{\mathfrak{r}} \quad \ldots\ldots(39)$$

where

$$\mathfrak{R} = 2\mathrm{u} \sin \tfrac{1}{2}\theta \quad \ldots\ldots(40)$$

and u is a vector of magnitude $1/\lambda$ in the direction bisecting the angle ABC. It can then be shown that $A(\theta)$ is obtainable by the following geometrical construction involving reciprocal space.

From the origin O of reciprocal space draw a line OA (figure 10) of length $1/\lambda$ in the direction opposite to the incident radiation. With its far end A as centre draw a sphere passing through O. Then the density $\mathbf{F}_1(\mathfrak{S})$ at each point B on the sphere represents the complex amplitude of the radiation scattered in the direction AB.

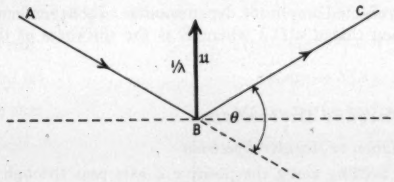

Figure 9. To illustrate the meaning of the quantities in equation (40).

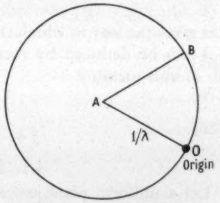

Figure 10. The geometrical construction in reciprocal space for determining the amplitude of the diffracted wave in the direction BC in figure 9.

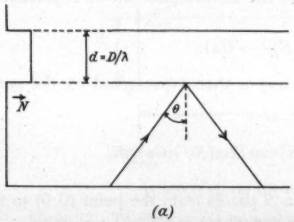

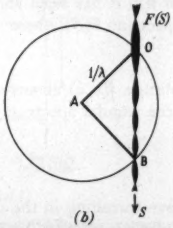

Figure 11. (*a*) represents the reflection of a wave from a uniform slab in which the refractive index is a little greater than normal ; (*b*) represents the construction made in reciprocal space for the purpose of determining how the reflection coefficient varies with θ and λ.

The procedure can be illustrated by a simple example appropriate to the ionosphere. Suppose waves are incident at any angle on a uniform slab of the ionosphere of thickness d (measured in wavelengths) in which the electron density is a little greater than in the surroundings [see figure 11 (*a*)], and let us find how the reflected amplitude changes with angle of incidence and wavelength. Because the difference of electron density is small the Born approximation can be used. In the problem

$$\begin{aligned} |\mathbf{f}(x)| &= a \quad \text{when} \quad -\tfrac{1}{2}d < x < \tfrac{1}{2}d \\ &= 0 \quad \text{when} \quad |x| > \tfrac{1}{2}d, \end{aligned}$$

hence

$$\mathbf{F}_1(S) = \{a \sin(\pi S_1/d)\}/\{\pi S_1/d\}, \qquad \ldots\ldots(41)$$

and represents a density distribution along a *line* in the S_1 direction as shown in figure 11 (*b*). Let a wave be incident at angle θ and draw OA of unit length in the direction opposite to θ, and then construct a sphere with A as centre. The only place where this sphere cuts any finite density of $\mathbf{F}_1$ is at B, and it follows that the only scattering is in the direction appropriate to specular reflection. The magnitude of $\mathbf{F}_1$ at B is

$$\mathbf{F}_1(2\cos\theta) = \frac{a\sin\{(2\pi\cos\theta)/d\}}{(2\pi\cos\theta)/d}. \qquad \ldots\ldots(42)$$

This gives the way in which the reflected amplitude depends on θ. Its dependence on λ can be deduced by recalling that $d = D/\lambda$ where D is the thickness of the slab in unit measure.

§ 4. Fresnel Diffraction

4.1. *Relation to Angular Spectrum*

Let a uniform plane wave travelling along the positive Z axis pass through a thin diffracting screen in the plane $z = 0$ and then travel on to a parallel plane at a distance z_0 where it produces a diffraction pattern. This will be called a Fresnel diffraction pattern and it is the purpose of this section to investigate its nature.

If the diffracting screen at $z = 0$ produces a one-dimensional variation of amplitude $\mathbf{f}(x)$ it has been shown that the disturbance can be represented by an angular spectrum $\mathbf{F}(S)$ where

$$\mathbf{F}(S) \longleftrightarrow \mathbf{f}(x).$$

The amplitude $\mathbf{f}(x, z)$ at any point (x, z) is then represented by the sum of the waves in the angular spectrum and

$$\mathbf{f}(x,z) = \int_{-\infty}^{+\infty} \mathbf{F}(S)\exp\{2\pi i(Sx + Cz)\}\,dS. \qquad \ldots\ldots(43)$$

As the wave travelling in the direction S passes from the point $(0, 0)$ to the point $(0, z_0)$ its phase is retarded by an amount ϕ where

$$\begin{aligned}\phi &= 2\pi C z_0 \\ &= 2\pi z_0(1 - S^2)^{1/2} \\ &\simeq 2\pi z_0 - \pi z_0 S^2. \qquad \ldots\ldots(44)\end{aligned}$$

The part $2\pi z_0$ represents the phase delay of the undiffracted wave in travelling the distance z_0, and $-\pi z_0 S^2$ represents an additional phase gain suffered by the component of the angular spectrum travelling in the direction S. If attention is restricted to diffraction through small angles (say $S < \frac{1}{6}$ or $\theta < 10°$) the approximation of equation (44) is reasonably accurate.

Let $\mathbf{g}(x)$ represent the distribution of complex amplitude in the Fresnel diffraction pattern at the distance z_0 with its phase referred to the point $(0, z_0)$ as origin. Then $\mathbf{g}(x)$ is synthesized from the same angular spectrum as that which makes up $\mathbf{f}(x)$ on the diffracting screen, but the temporal phase of each component in the

spectrum has been advanced by an amount $\pi z_0 S^2$. This state of affairs is expressed in symbols as follows

$$\mathbf{f}(x) \longleftrightarrow \mathbf{F}(S)$$

$$\mathbf{g}(x) \longleftrightarrow \mathbf{F}(S) \exp(-i\pi z_0 S^2) = \mathbf{G}(S) \quad (\text{with } S < \tfrac{1}{6}) \qquad \ldots\ldots(45)$$

where $\mathbf{G}(S)$ represents the angular spectrum referred to the point $(0, z_0)$ as origin. The application of this relationship to some special cases is considered in the following sections.

It is first interesting to apply the convolution theorem (see Appendix 1) to equation (45) as follows.

Write $$\exp(-i\pi z_0 S^2) = \mathbf{Y}(S) \qquad \ldots\ldots(46)$$

and let $$\mathbf{y}(x) \longleftrightarrow \mathbf{Y}(S) \qquad \ldots\ldots(47)$$

so that $$\mathbf{y}(x) = \exp(+i\pi x^2/z_0). \qquad \ldots\ldots(48)$$

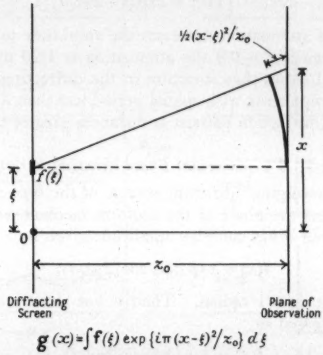

Figure 12. To illustrate the calculation of a Fresnel diffraction pattern by the usual method.

Then from equations (45) and (46)

$$\mathbf{g}(x) \longleftrightarrow \mathbf{F}(S)\mathbf{Y}(S) \qquad \ldots\ldots(49)$$

whence, by application of the convolution theorem,

$$\mathbf{g}(x) = \int_{-\infty}^{+\infty} \mathbf{f}(\xi) . \mathbf{y}(x-\xi)\, d\xi. \qquad \ldots\ldots(50)$$

But this is just the Fresnel expression for $\mathbf{g}(x)$ obtained in the usual way as indicated in figure 12.

It is thus possible to express the diffraction pattern $\mathbf{g}(x)$ in terms of the complex amplitude distribution $\mathbf{f}(x)$ by equation (50); or alternatively to express the angular spectrum $\mathbf{G}(S)$, referred to the point z_0, in terms of the angular spectrum $\mathbf{F}(S)$, referred to the point $z = 0$, by equation (45).

4.2. *A Cosinusoidal Amplitude Screen*

As a first example of Fresnel diffraction consider a diffracting screen which produces a cosinusoidal variation of amplitude $\mathbf{f}(x) = \cos(2\pi x/d)$ on the emerging wave front. It has already been shown [see equation (9) and figure 2 (*b*)] that a disturbance of this kind will travel in a direction perpendicular to the screen with a velocity which depends on d, and that the distribution of amplitude in the X direction is the same on all planes. The Fresnel diffraction pattern at all distances is hence the same as the distribution over the diffracting screen.

This result is immediately obvious from another point of view. The angular spectrum consists only of the two waves at angles $S = \pm 1/d$ (see figure 3), and whatever the phase shift caused by their travel they still add together at all distances z_0 to produce the original cosine distribution of amplitude.

If $d < 1$ (i.e. $D < \lambda$) then $S > 1$ and the disturbance is evanescent. It is attenuated in the Z direction like

$$\exp\{-2\pi z(S^2-1)^{1/2}\} = \exp\{(-2\pi z/d)(1-d^2)^{1/2}\}. \qquad \ldots\ldots(51)$$

If $d^2 \ll 1$ ($D^2 \ll \lambda^2$) this attenuation decreases the amplitude to $\exp(-\pi) \simeq 1/20$ in a distance $z = \frac{1}{2}d$. Even if $d = 0{\cdot}9$ the attenuation is 1/20 in a distance of about one wavelength. It follows that structure in the diffracting screen which corresponds to Fourier components with spatial period less than λ will fail to be reproduced in the Fresnel diffraction pattern at distances greater than λ.

4.3. *A Cosinusoidal Phase-changing Screen*

Consider a phase-changing diffracting screen, of the type discussed in § 3.4 and figure 5, which changes the phase of the uniform incident wave by $\Delta\phi\cos(2\pi x/d)$ so that the wave leaving it has complex amplitude given by

$$\mathbf{f}(x) = \exp\{i\Delta\phi\cos(2\pi x/d)\} \qquad \ldots\ldots(52)$$

and suppose first that $\Delta\phi < 1$ radian. Then it has already been seen that equation (52) may be expressed as

$$\mathbf{f}(x) = 1 + i\Delta\phi\cos(2\pi x/d) \qquad \ldots\ldots(53)$$

which represents the addition, to a uniform plane wave of amplitude 1, of a wave in time quadrature, which has a cosinusoidal distribution of amplitude across the wave front. The propagation of the 'striated' wave, with the cosinusoidal amplitude distribution, was discussed in the previous section and it was shown that it travels with a velocity different from that of the uniform wave and that the 'striations' are maintained as it travels. At a certain distance, therefore, the striated wave and the plane wave, which started in quadrature, will be in antiphase and will add up together to produce an amplitude-modulated distribution given by

$$\mathbf{f}(x) = 1 - \Delta\phi\cos(2\pi x/d). \qquad \ldots\ldots(54)$$

At twice this distance the two waves will again be in quadrature and will produce phase modulation, and on successive planes separated by the same distance the distribution will be alternately one of amplitude and one of phase, as shown in figure 13 (*a*).

The same phenomena can be discussed slightly differently by expressing the complex amplitude distribution of equation (53) as

$$\mathbf{f}(x) = 1 + \tfrac{1}{2}i\Delta\phi \exp(2\pi ix/d) + \tfrac{1}{2}i\Delta\phi \exp(-2\pi ix/d).$$

This is equivalent, at the screen, to two side spectra at $S = \pm 1/d$ which are in quadrature with the main wave. In their travel to a plane at a distance z_0 they gain in phase by $\pi z_0 S^2$ compared with the main wave [see equation (44)] so that, when $z_0 = 1/2S^2 = \frac{1}{2}d^2$ they are in antiphase with it and the wave front is amplitude modulated. At successive distances of $\frac{1}{2}d^2$ they gain $\pi/2$ in phase, as shown in figure 13 (*b*). When they are in phase or in antiphase the amplitude varies, when they are in quadrature the phase varies.

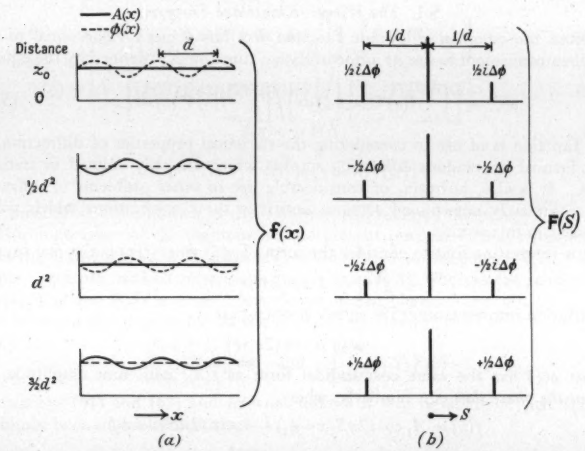

Figure 13. (*a*) Amplitude and phase distributions, and (*b*) corresponding angular spectra, at planes distant 0, $\frac{1}{2}d^2$, d^2, $\frac{3}{2}d^2$ from a plane in which there are cosinusoidal phase variations of small deviation.

Suppose next that the cosine phase screen produces a phase deviation $\Delta\phi > 1$ radian. The angular spectrum then contains side waves not only at angles $S = 1/d$ but also at multiples of S, up to about nS where $n \simeq \Delta\phi$ and the phase of each side wave is advanced by $\pi/2$ on that of the previous one. The amplitudes in the spectrum are represented in figure 6 for $\Delta\phi = 10$ radians. If now the resulting disturbance is observed at a series of planes parallel to the diffracting screen, and at increasing distances z from it, then the phase of each side wave will catch up on that of the main wave. The side wave which travels in the direction nS will gain in phase by $\pi/2$ when it reaches a plane at a distance $z_0 = 1/(2n^2S^2)$ and will then combine with the main wave to produce amplitude modulation of spatial period $1/nS = d/n$. As the wave advances, therefore, the successive side waves

produce their own components of amplitude modulation in succession, the higher order side waves, corresponding to the smaller spatial periods, producing their full effects nearer to the screen, and the lower order ones, corresponding to the longer spatial periods, producing their effects at the greater distances. It is especially to be noticed that the Fresnel diffraction pattern at all distances contains Fourier components with spatial periods smaller than the spatial period of the phase in the diffracting screen, and these will give rise to variations of amplitude which show structure smaller than any structure in the screen itself.

§ 5. The Auto-correlation Function and the Wiener–Khintchine Theorem

5.1. *The Wiener–Khintchine Theorem*

Often the complex amplitude function $\mathbf{f}(x)$ has a mean value equal to zero. It is then convenient to use its autocorrelation function $\rho(\xi)$ defined by the equation

$$\rho(\xi) = \left[\int_{-\infty}^{+\infty} \mathbf{f}(x)\,\mathbf{f}^*(x+\xi)\,dx\right] \Big/ \left[\int_{-\infty}^{+\infty} \mathbf{f}(x)\,\mathbf{f}^*(x)\,dx\right]. \qquad \ldots\ldots(55)$$

This function is of use in considering the statistical properties of diffraction patterns formed by random diffracting screens which are only defined in statistical terms. It is also, however, of considerable use in other problems of diffraction from completely determined screens, and it is these applications which will be discussed in this section.

It is interesting first to consider the form of $\rho(\xi)$ when $f(x)$ is the real function

$$f(x) = A\cos(2\pi Sx + \phi). \qquad \ldots\ldots(56)$$

Substitution into equation (55) shows at once that

$$\rho(\xi) = \cos(2\pi S\xi) \qquad \ldots\ldots(57)$$

so that $\rho(\xi)$ has the same cosinusoidal form as $f(x)$, with unit amplitude, *and without the phase shift* ϕ. Similarly, when

$$f(x) = A_1\cos(2\pi S_1 x + \phi_1) + A_2\cos(2\pi S_2 x + \phi_2) \qquad \ldots\ldots(58)$$

it is a simple matter to show that

$$\rho(\xi) = \frac{A_1^2}{A_1^2 + A_2^2}\cos 2\pi S_1\xi + \frac{A_2^2}{A_1^2 + A_2^2}\cos 2\pi S_2\xi. \qquad \ldots\ldots(59)$$

Equation (58) indicates that $f(x)$ has a ' spectrum ' with components of frequencies S_1 and S_2 which have amplitude A_1 and A_2 and phases ϕ_1 and ϕ_2, and equation (59) shows that $\rho(\xi)$ has a spectrum with components of the *same frequencies* S_1 and S_2, each with *zero phase*, and with amplitudes $A_1^2/(A_1^2+A_2^2)$ and $A_2^2/(A_1^2+A_2^2)$. If now A_1^2 and A_2^2 are thought of as the ' powers ' of the two components in the original spectrum, by analogy with the frequency spectrum of a time-varying quantity, then the two quantities $A_1^2/(A_1^2+A_2^2)$ and $A_2^2/(A_1^2+A_2^2)$ can be called the normalized powers. It follows, from equation (59) that the spectrum of $\rho(\xi)$ corresponds to the ' normalized power spectrum ' of the original function $f(x)$. This result, proved here for a simple case, holds generally and may be stated as follows.

The auto-correlation function $\rho(\xi)$ of a function $f(x)$ is formed by making a Fourier analysis of $f(x)$, squaring all the amplitudes and removing all the phase differences so as to represent the powers in the different components, then reconstituting the Fourier synthesis and dividing by the total power to normalize the result.

A simple proof of this general result could be given by a straightforward extension of the one which has already been given ; a more formal and neater one is given in Appendix 3. The theorem in its general form holds for complex functions, and may be stated thus :

If $$\mathbf{f}(x) = \int_{-\infty}^{+\infty} \mathbf{F}(S) \exp(2\pi i S x)\, dS \qquad \ldots\ldots(60)$$

and $$\rho(\xi) = \left[\int_{-\infty}^{+\infty} \mathbf{f}(x)\, \mathbf{f}^*(x+\xi)\, dx\right] \Big/ \left[\int_{-\infty}^{+\infty} \mathbf{f}(x)\, \mathbf{f}^*(x)\, dx\right] \qquad \ldots\ldots(61)$$

then $$\rho(\xi) = \left[\int_{-\infty}^{+\infty} |\, \mathbf{F}(S)\,|^2 \exp(2\pi i S\xi)\, dS\right] \Big/ \left[\int_{-\infty}^{+\infty} |\, \mathbf{F}(S)\,|^2\, dS\right] \qquad \ldots\ldots(62)$$

or if $$\mathbf{f}(x) \longleftrightarrow \mathbf{F}(S) \qquad \ldots\ldots(63)$$

then $$\left\{\int_{-\infty}^{+\infty} |\, \mathbf{F}(S)\,|^2\, dS\right\} \rho(\xi) \longleftrightarrow |\, \mathbf{F}(S)\,|^2. \qquad \ldots\ldots(64)$$

This theorem is often known as the ' Wiener–Khintchine ' theorem.

The importance of the theorem for the present purpose is that equation (64) shows the auto-correlation function $\rho(\xi)$ to be related to the power $|\, \mathbf{F}(S)\,|^2$ in the angular spectrum, *without reference to the phase of* $\mathbf{F}(S)$, whereas the relation (63) between $\mathbf{f}(x)$ and $\mathbf{F}(S)$ involves a knowledge of that phase.

It is inconvenient to divide by the normalizing factors

$$\int_{-\infty}^{+\infty} |\, \mathbf{f}(x)\,|^2\, dx \quad \text{and} \quad \int_{-\infty}^{+\infty} |\, \mathbf{F}(S)\,|^2\, dS$$

in equations (61) and (62) and in what follows it will be assumed that $\mathbf{f}(x)$ has previously been normalized so that

$$\int_{-\infty}^{+\infty} |\, \mathbf{f}(x)\,|^2\, dx = 1.$$

It follows that $$\int_{-\infty}^{+\infty} |\, \mathbf{F}(S)\,|^2\, dS = 1,$$

as shown in Appendix 2, or as may be seen by considering a time-varying quantity in which x represents time, when it is clear that both the integrals represent the total energy in the disturbance, one obtained by integrating the instantaneous power with respect to time, and the other obtained by integrating the power spectrum with respect to frequency. When $\mathbf{f}(x)$ is normalized in this way the Wiener–Khintchine theorem may be written

if $$\mathbf{f}(x) \longleftrightarrow \mathbf{F}(S) \qquad \ldots\ldots(65)$$

then $$\rho(\xi) \longleftrightarrow |\, \mathbf{F}(S)\,|^2 \qquad \ldots\ldots(66)$$

and this is the form in which it will be used here.

In general $\rho(\xi)$ is a complex quantity, but in the cases to be considered in this Report the angular power spectrum $|\mathbf{F}(S)|^2$ will be symmetrical about $S = 0$ so that $\rho(\xi)$ will be a real function. This limitation is not necessary but will be made to keep the analysis simple.

The theorem can be extended in a straightforward way to functions in two or three dimensions. The normalized three-dimensional form is as follows:

If

$$\mathbf{f}(x, y, z) = \int_{-\infty}^{+\infty}\int_{-\infty}^{+\infty}\int_{-\infty}^{+\infty} \mathbf{F}(S_1, S_2, S_3) \exp\{2\pi i(S_1 x + S_2 y + S_3 z)\}\, dS_1\, dS_2\, dS_3$$

and ……(67)

$$\rho(\xi, \eta, \zeta) = \int_{-\infty}^{+\infty}\int_{-\infty}^{+\infty}\int_{-\infty}^{+\infty} \mathbf{f}(x, y, z)\ \mathbf{f}^*\{(x+\xi), (y+\eta), (z+\zeta)\}\, dx\, dy\, dz$$

then ……(68)

$$\rho(\xi, \eta, \zeta) = \int_{-\infty}^{+\infty}\int_{-\infty}^{+\infty}\int_{-\infty}^{+\infty} |\mathbf{F}(S_1, S_2, S_3)|^2 \exp\{2\pi i(S_1 \xi + S_2 \eta + S_3 \zeta)\}\, dS_1\, dS_2\, dS_3$$

……(69)

or if $$\mathbf{f}(x, y, z) \longleftrightarrow \mathbf{F}(S_1, S_2, S_3)$$ ……(70)

then $$\rho(x, y, z) \longleftrightarrow |\mathbf{F}(S_1, S_2, S_3)|^2.$$ ……(71)

5.2. *Applications to Angular Spectra and Fraunhofer Diffraction*

In most diffraction phenomena it is comparatively easy to measure the power in the angular spectrum, or in the Fraunhofer diffraction pattern, but it is difficult to measure the phase. When there is information only about the power in the angular spectrum it is interesting to ask what can be determined about the nature of the diffracting screen. The Wiener–Khintchine theorem shows at once that, given the normalized angular power spectrum $|\mathbf{F}(S)|^2$, the auto-correlation function of the diffracting screen is known, since $\rho(\xi) \longleftrightarrow |\mathbf{F}(S)|^2$. Some examples of this result are as follows.

(*a*) If a diffraction grating is moved parallel to itself in its own plane its auto-correlation function is not altered, and therefore its angular power spectrum does not alter either. For example, in a well-known method of measuring the wavelength of an ultrasonic wave travelling through a liquid, light is passed through the liquid and is diffracted by the wave. The diffracted spectra remain stationary although the ultrasonic wave is moving.

(*b*) If a radio antenna is required to produce a given 'polar diagram' of radiation it is the 'power polar diagram' which is specified. The antenna must therefore be designed so that it has a given auto-correlation function $\rho(\xi)$. There are, in general, an infinite number of possible functions $\mathbf{f}(x)$ which will lead to the required $\rho(\xi)$, and hence to the required polar diagram.†

(*c*) In X-ray analysis the three-dimensional power spectrum of the scattered X-rays is measured. It is therefore possible to deduce the three-dimensional auto-correlation function $\rho(\xi, \eta, \zeta)$ of the scattering density. This is often called the Patterson function.

† It will be shown later that the possible distributions $\mathbf{f}(x)$ may be considered as Fresnel diffraction patterns formed at different distances from any one of the distributions acting as a diffracting screen.

5.3. *Application to Fresnel Diffraction*

It was shown in § 4.1 that the Fresnel diffraction patterns formed at different distances from a diffracting screen were all made up from the same angular spectrum of waves, and that in successive diffraction patterns only the relative phases altered so that the power spectrum remained the same. The Wiener–Khintchine theorem then shows that the auto-correlation function of the complex wave-amplitude over each plane is the same. It can thus be stated that:

> The auto-correlation function of the complex amplitude $\mathbf{g}(x)$ over all observing planes parallel to the diffracting screen is the same, and is the same as the auto-correlation function of the complex amplitude distribution $\mathbf{f}(x)$ over the diffracting screen itself.

This deduction can be made symbolically as follows.

If the distribution of complex amplitude over the diffracting screen and over a parallel observing plane at a distance z_0 are $\mathbf{f}(x)$ and $\mathbf{g}(x)$ respectively, then

$$\mathbf{f}(x) \longleftrightarrow \mathbf{F}(S)$$

therefore $$\rho_f(\xi) \longleftrightarrow |\mathbf{F}(S)|^2 \qquad \ldots\ldots(72)$$

also from equation (45) $$\mathbf{g}(x) \longleftrightarrow \mathbf{F}(S)\exp(-i\pi z_0 S^2)$$

therefore $$\rho_g(\xi) \longleftrightarrow |\mathbf{F}(S)\exp(-i\pi z_0 S^2)|^2$$

$$\longleftrightarrow |\mathbf{F}(S)|^2.$$

Hence from (72) $$\rho_g(\xi) = \rho_f(\xi). \qquad \ldots\ldots(73)$$

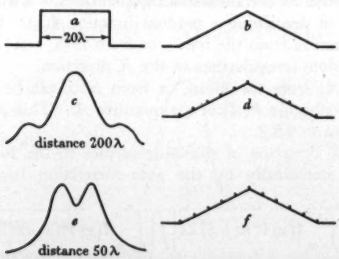

Figure 14. Generalized auto-correlation functions of Fresnel diffraction patterns produced by a slit. *a* represents the distribution of amplitude over a slit 20λ wide; *b* represents the auto-correlation function of this distribution; *c* and *e* represent the distributions of amplitude in the Fresnel diffraction patterns at distances of 200 and 50λ; in *d* and *f* the auto-correlation functions calculated for the diffraction patterns of *c* and *e* respectively are shown as dots. The continuous lines repeat the auto-correlation function shown at *b*. (*After* Booker, Ratcliffe and Shinn.) (*Reproduced by permission of the Royal Society.*)

This result is illustrated in figure 14 by reference to the Fresnel diffraction patterns of a slit. The function $f(x)$, representing the distribution of amplitude over the slit is represented at *a* and $\rho_f(\xi)$ is shown at *b*. At *c* and *e* are shown the distributions of amplitude over planes at different distances from the slit,

calculated from tables of the Fresnel integral. The dotted curves at *d* and *f* represent $\rho_g(\xi)$ at these different distances. They are seen to be quite closely the same as $\rho_f(\xi)$, which is represented by the continuous line.

§ 6. The Angular Spectra from Random Diffracting Screens

6.1. *Random Functions and Correlation Functions*

The results of previous sections apply to any completely known diffracting screen however irregular the distribution $\mathbf{f}(x)$ of amplitude may be. Sometimes, however, the precise form of $\mathbf{f}(x)$ is not known, and it can only be described in statistical terms. The statistics may partially describe it in terms of the value of some quantity averaged over the whole of the screen. This description is useful only if the same average value is obtained from different sections of the screen taken separately, and then the screen may be said to be statistically uniform. The statistics may, however, refer not to one screen, but to an assembly of screens all of which have similar characteristics, and then the quantity concerned may be averaged over different specimens in the assembly. The members of an assembly of this kind can be said to be statistically similar.

When it is desirable to distinguish between averages taken over one screen, and averages taken over an assembly of screens, the former will be denoted by a suffix ' av ' written after the quantity concerned, and the latter by a suffix ' ass. av '.

The word ' irregular ' will be used to describe a function which, although not represented by any simple smooth curve is yet completely known, and the word ' random ' to describe irregular functions which are not fully known, but which can be partially described by certain statistical quantities. Two different statistical quantities are useful in describing a random function $\mathbf{f}(x)$. One tells about the magnitude of its departure from the mean, or from zero, and the other tells about the ' size ' of the random irregularities in the X direction.

The departures (A) from the mean, or from zero, can be described in terms of the probability distribution $P(A)$ of the quantity A. This probability distribution will be considered in § 8.2.

The size in the X direction of the irregularities in the function $\mathbf{f}(x)$ is conveniently described statistically by the auto-correlation function $\rho(\xi)$ already defined as

$$\rho(\xi) = \left[\int_{-\infty}^{+\infty} \mathbf{f}(x)\,\mathbf{f}^*(x+\xi)\,dx\right] \Big/ \left[\int_{-\infty}^{+\infty} \mathbf{f}(x)\,\mathbf{f}^*(x)\,dx\right]. \qquad \ldots\ldots(74)$$

It is often useful to express this definition differently and write

$$\rho(\xi) = [\mathbf{f}(x)\ \mathbf{f}^*(x+\xi)]_{\text{av}} / [\mathbf{f}\mathbf{f}^*]_{\text{av}} \qquad \ldots\ldots(75)$$

where the mean is taken either over all values of x from one sample, if the sample is statistically uniform, or over all members of an assembly if they are statistically similar.

The significance of the auto-correlation function is seen most simply if $f(x)$ is a random real quantity which has positive and negative values and mean value zero. $f(x)$ and $f(x+\xi)$ will then both have the same sign everywhere if ξ is small, but if ξ is large they will sometimes have opposite signs. When the mean

product $[f(x)f^*(x+\xi)]_{av}$ of equation (75) is calculated the value will be greater when ξ is small than when it is large. If ξ is larger than (roughly) the 'size' of one irregularity in $f(x)$ the product is equally likely to be positive or negative and the mean will be zero. $\rho(\xi)$ will thus be equal to unity when $\xi = 0$ and will decrease to zero when ξ approximates to the 'size of one irregularity'.† Of course it is not satisfactory to talk of the 'size of an irregularity' and the purpose of the auto-correlation function is to provide a quantitative measure of what this means. It will be shown in § 8.1 that the auto-correlation function also provides some measure of what might be called 'the shape of an average irregularity'.

6.2. *Other Forms of Correlation Function*

6.2.1. *The correlation function of* $\mathbf{f}(x)$ *when* $[\mathbf{f}(x)]_{av} \neq 0$.

When $[\mathbf{f}(x)]_{av} \neq 0$ the correlation function $\rho(\xi)$ is defined slightly differently, as follows:

$$\rho_f(\xi) = \frac{[\mathbf{f}(x)\,\mathbf{f}^*(x+\xi)]_{av} - \{[\mathbf{f}(x)]_{av}\}^2}{[\mathbf{f}(x)\,\mathbf{f}^*(x)]_{av} - \{[\mathbf{f}(x)]_{av}\}^2}. \qquad \ldots\ldots(76)$$

If $\mathbf{f}(x)$ is written

$$\mathbf{f}(x) = \mathbf{a} + \mathbf{g}(x) \qquad \ldots\ldots(77)$$

where $[\mathbf{f}(x)]_{av} = \mathbf{a}$ and $\mathbf{g}(x)$ is a random function with mean equal to zero it is shown in Appendix 4 (*a*) that

$$\rho_f(\xi) = \rho_g(\xi). \qquad \ldots\ldots(78)$$

6.2.2. *The correlation function* $r(\xi)$.

It is sometimes convenient to use a slightly different form of auto-correlation function, calculated without removing the mean, defined as follows:

$$r_f(\xi) = [\mathbf{f}(x)\,\mathbf{f}^*(x+\xi)]_{av} / [\mathbf{f}(x)\,\mathbf{f}^*(x)]_{av}. \qquad \ldots\ldots(79)$$

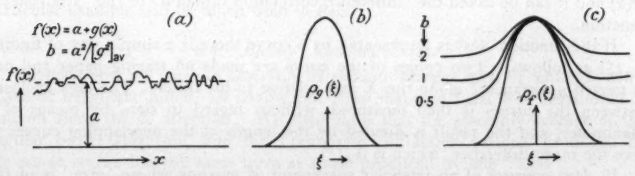

Figure 15. Auto-correlation functions when $f(x)$ consists of a random part superimposed on a constant part.

It is shown in Appendix 4 (*b*) that, if $\mathbf{f}(x)$ is given by equation (77) then

$$r_f(\xi) = \frac{b + \rho_g(\xi)}{b+1} \qquad \ldots\ldots(80)$$

where $b = |\mathbf{a}|^2/|\mathbf{g}|^2$. If, as often happens with random functions, $\rho_g(\xi)$ becomes zero for large values of ξ, as indicated, for example, in figure 15 (*b*), then $r_f(\xi)$ has a form indicated by figure 15 (*c*) which falls to the value $b/(b+1)$ for large values of ξ.

† The fact that $\rho(\xi)$ measures the 'size of one irregularity' is only true when $f(x)$ is real. See, for example, § 6.5.

The quantity b measures the ratio of the ' power ' $|\mathbf{a}|^2$ of the constant part to the ' power ' $|\mathbf{g}|^2$ of the random part. In a corresponding problem with time-varying quantities the constant part might represent a sinusoidal signal oscillation of constant amplitude and the random part might represent random ' noise '. In that case b would be called the ' signal-to-noise ' ratio, and it will be given this same name in the present context.

6.2.3. *The difference correlation function* $\Delta_A(\xi)$ (*the ' after-effect ' function*).

It is sometimes useful to define a quantity $\Delta_A(\xi)$ derived from a real function $A(x)$, by the following relations: $\delta_A(\xi) = A(x) - A(x+\xi)$ and $\Delta_A(\xi) = [|\delta_A(\xi)|]_{av}$ so that $\Delta_A(\xi)$ is the mean value of the difference of values of A at points separated by ξ taken without regard to sign. The mean can be taken over a single sample if it is statistically uniform, or over an assembly of samples which are statistically

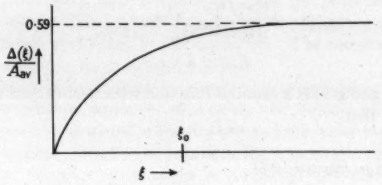

Figure 16. To illustrate the form of the difference correlation function $\Delta(\xi)$ of a random function with ' irregularities ' of average size ξ_0.

similar. The quantity $\Delta_A(\xi)$ provides another measure of the auto-correlation of $A(x)$ and it can be called the ' difference correlation function ' or the ' after-effect ' function.

If the function $A(x)$ is represented by a curve there is a simple way of finding $\Delta_A(\xi)$ as follows. Two copies of the curve are made on tracing paper and one is moved a distance ξ along the X axis relative to the other. The area enclosed between the curves is then measured, without regard to sign, by means of a planimeter, and the result is divided by the length of the overlapping curves to give the mean difference, which is $\Delta_A(\xi)$.

If $A(x)$ consists of an irregular succession of maxima whose ' size ' is of the order ξ_0 then $\Delta_A(\xi)$ plotted against ξ will have a form something like figure 16.

It often happens that $\delta_A(\xi)$ can be shown, either from experiment or from theory, to have a Gaussian probability distribution. Under these conditions it can be shown (see Appendix 5) that

$$[\Delta_A(\xi)]^2 = (4/\pi)(A_{av})^2\{1 - r_A(\xi)\}. \qquad \ldots\ldots(81)$$

If, in addition, it is known that A has a Rayleigh probability distribution, then

$$[\Delta_A(\xi)]^2 = \frac{4(4-\pi)}{\pi^2}(A_{av})^2\{1 - \rho_A(\xi)\}. \qquad \ldots\ldots(82)$$

These relations between $\Delta_A(\xi)$, $\rho_A(\xi)$ and $r_A(\xi)$ are often useful.

6.3. *The Angular Power Spectra from Random Screens*

Consider an assembly of random screens which are statistically similar, and suppose the distributions $\mathbf{f}(x)$ of the wave-fields emerging from them are described in terms of their mean auto-correlation function $[\rho_f(\xi)]_{\text{ass. av}}$. Then the mean angular power spectrum is given by

$$[|F(S)|^2]_{\text{ass. av}} \longleftrightarrow [\rho_f(\xi)]_{\text{ass. av}} \qquad \ldots\ldots(83)$$

and is known if $[\rho_f(\xi)]_{\text{ass. av}}$ is known. Take as an example the case where

$$[\rho_f(\xi)]_{\text{ass. av}} = \exp(-\pi^2\xi^2/l^2) \qquad \ldots\ldots(84)$$

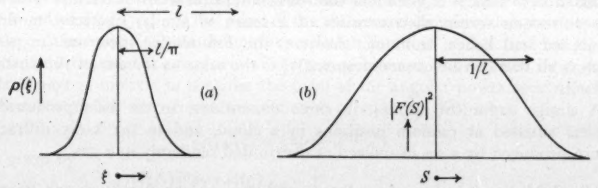

Figure 17. The angular power spectrum $|F(S)|^2$ from a random screen with a Gaussian correlation function.

as illustrated in figure 17 (*a*). The correlation falls to e^{-1} when $\xi = l/\pi$ and corresponds to a random screen in which the ' size ' of the individual irregularities is of the order l/π wavelengths. The mean angular power spectrum would then be given by

$$[|F(S)|^2]_{\text{ass. av}} = \exp(-l^2S^2) \qquad \ldots\ldots(85)$$

so that the power would decrease to e^{-1} when $S = 1/l$. The spread of the angular spectrum thus depends on the fineness of structure in the random screen. This particular example will be much used in Part II.

6.4. ' *Blobby* ' *Random Screens*

Suppose now we have an assembly of random screens each of which is composed of irregular ' blobs ' all having the same shape and size but distributed at random along the X direction. We shall show that the assembly average of the angular power spectrum, and the Fraunhofer diffraction pattern, produced by the whole screen has the same form as those produced by one ' blob '.

To prove this consider one ' blob ' situated with its centre at the origin of coordinates and let it produce an angular spectrum $\mathbf{F}_1(S)$. Now let it move a distance x; then the angular spectrum is changed only in phase and becomes $\mathbf{F}_1(S)\exp(2\pi iSx)$. Now add to this a series of n other equal blobs, situated at other distances x_k, so that the resulting angular spectrum becomes

$$\mathbf{F}(S) = \sum_{k=1}^{n} \mathbf{F}_1(S)\exp(2\pi iSx_k). \qquad \ldots\ldots(86)$$

If the distances x_k are randomly distributed the phases in this summation are also random so that, as always with the addition of equal vectors making random angles with each other, the ' powers ' add and

$$[|\mathbf{F}(S)|^2]_{\text{ass. av}} = n\,|\mathbf{F}_1(S)|^2. \qquad \ldots\ldots(87)$$

The assembly average of the power spectrum has thus the same form as the power spectrum of one ' blob '.

A simple extension of this proof shows that if the sizes of the individual ' blobs ' are themselves normally distributed the result still holds. It can also be shown that the theorem stated at the start of this section is true for two- or three-dimensional ' blobs ' and their corresponding angular spectra.

The result is frequently of use in problems of optical or x-ray diffraction. An example in two dimensions is Young's method for determining the diameters of dust particles of approximately the same size. In this method the dust is sprinkled over a sheet of glass and the Fraunhofer diffraction pattern is measured. The diffracting screen then consists of a series of similar obstacles randomly distributed and hence, from our theorem, the Fraunhofer spectrum (in power, which is all that can be observed optically) is the same as for one of the obstacles by itself.

A similar argument applies, in three dimensions, to the halo produced by droplets situated at random positions in a cloud, and to the x-ray diffraction pattern produced by a set of molecules distributed randomly in a gas.

6.5. *A Medium which produces Random Changes of both Amplitude and Phase*

Suppose a wave, travelling along the Z direction, traverses, at normal incidence, a thin slab of a medium in which the molecular (or electronic) number-density N departs from its mean value by an amount $\Delta N(x)$ which varies along the X direction. Suppose also that the medium alters both the amplitude and the phase of the wave. Then it is shown in Appendix 6 that the complex amplitude in the emerging wave front varies along the X direction as given by

$$\mathbf{f}(x) = \exp\{i\Delta\boldsymbol{\varphi}(x)\} \qquad \ldots\ldots(88)$$

where

$$\Delta\boldsymbol{\varphi}(x) = C\exp(i\psi)\,\Delta N(x), \qquad \ldots\ldots(89)$$

C and ψ being real constants characteristic of the medium.

If now $\Delta N(x)$ is a random function, with a normal distribution of standard deviation N_{m}, and with auto-correlation function $\rho_{\Delta N}(\xi)$, then it can be shown (Bramley 1955, § 6.3) that the auto-correlation function† $r_f(\xi)$ of $\mathbf{f}(x)$ is given by

$$r_f(\xi) = \exp[-\phi_{\mathrm{m}}^2\{1-\rho_{\Delta N}(\xi)\}] \qquad \ldots\ldots(90)$$

where ϕ_{m} is the standard deviation of $|\Delta\boldsymbol{\varphi}(x)|$ and is given, from equation (89) by

$$\phi_{\mathrm{m}} = CN_{\mathrm{m}}. \qquad \ldots\ldots(91)$$

This expression leads to interesting results when $\phi_{\mathrm{m}}^2 \ll$ or $\gg 1$.

When $\phi_{\mathrm{m}}^2 \ll 1$ equation (90) can be written

$$r_f(\xi) \simeq 1-\phi_{\mathrm{m}}^2\{1-\rho_{\Delta N}(\xi)\}. \qquad \ldots\ldots(92)$$

The fact that r_f is not small when $\rho_{\Delta N}$ is small implies (see § 6.2) that $\mathbf{f}(x)$ consists of a random part superimposed on a greater steady mean. If the ' signal-to-noise ' ratio is b and the auto-correlation function of the random part is $\rho_\varrho(\xi)$, then comparison of equation (92) with equation (80) shows that

$$b = 1/\phi_{\mathrm{m}}^2 \quad \text{and} \quad \rho_\varrho(\xi) = \rho_{\Delta N}(\xi) \qquad \ldots\ldots(93)$$

† $r_f(\xi)$ is defined by equation (79) of § 6.2.

when $\phi_m^2 \ll 1$. In this case the ' scale ' of the structure in $\mathbf{f}(x)$ is the same as the ' scale ' of the structure in ΔN.

When $\phi_m^2 \gg 1$ it is interesting to inquire into the form of $r_f(\xi)$ when

$$\rho_{\Delta N}(\xi) = \exp(-\xi^2/\xi_0^2).$$

Equation (90) then shows that for all except the smallest values of $r_f(\xi)$ we shall be concerned only with $\xi^2 \ll \xi_0^2$ so that it may be re-written

$$r_f(\xi) = \exp\{-\phi_m^2 \xi^2/\xi_0^2\}. \qquad \ldots\ldots(94)$$

The auto-correlation function of $\mathbf{f}$ is thus similar in shape to that of ΔN, but its scale is reduced by $1/\phi_m$. The ' size ' of the auto-correlation function thus depends jointly on the ' size ' (ξ_0) of the auto-correlation function of ΔN, and on ϕ_m, the standard deviation of the modulus of the complex phase, and is given by ξ_0/ϕ_m.

It is next of interest to consider the form of the angular power spectrum $\mathbf{F}(S)$ associated with the auto-correlation function of equation (90) when

$$\rho_{\Delta N}(\xi) = \exp(-\xi^2/\xi_0^2).$$

It is given by

$$|\mathbf{F}(S)|^2 \longleftrightarrow r_f(\xi)$$
$$\longleftrightarrow \exp[-\phi_m^2\{1-\exp(-\xi^2/\xi_0^2)\}] \qquad \ldots\ldots(95)$$

and Bramley (1955, eqn. (30)) has shown that this gives

$$|\mathbf{F}(S)|^2 = \exp(-\phi_m^2)\left[\delta(S)+\pi^{1/2}\xi_0\sum_{n=1}^{\infty}\frac{\phi_m^{2n}}{n!}\frac{\exp(-\pi^2\xi_0^2S^2/n)}{n^{1/2}}\right]. \qquad \ldots\ldots(96)$$

The delta-function in this expression represents a ' zero-order ' undeviated wave, and the other terms represent side waves. If $\phi_m^2 \ll 1$ the undeviated wave is reduced from unity by a negligibly small amount and the side waves are represented quite accurately by the term with $n = 1$, i.e. by

$$\pi^{1/2}\xi_0\phi_m^2\exp(-\pi^2\xi_0^2S^2). \qquad \ldots\ldots(97)$$

This part of the angular spectrum thus has a shape given by the Fourier transform of $\rho_{\Delta N}(\xi)$, and an amplitude proportional to ϕ_m^2, the square of the standard deviation of the modulus of the complex phase, and to ξ_0 the ' width ' of the irregularities of density. All this might have been expected from the simple considerations previously given in § 3.5 for the cosinusoidal cases where only the phase altered (φ purely real) and where only the amplitude altered (φ purely imaginary).

The undeviated component in equation (96) contains power equal to $\exp(-\phi_m^2)$ and the side waves contain the rest of the power equal to

$$\{1-\exp(-\phi_m^2)\}.$$

The ' signal-to-noise ' ratio b is thus given by

$$b = \{\exp(-\phi_m^2)\}/\{1-\exp(-\phi_m^2)\}$$
$$= 1/\{\exp(\phi_m^2)-1\}. \qquad \ldots\ldots(98)$$

When ϕ_m^2 is less than about 0·5 this reduces to

$$b \simeq 1/\phi_m^2. \qquad \ldots\ldots(99)$$

The continuous distribution of side waves, given by the terms under the summation sign, can be shown to represent a spread of power out to an angle which is determined by ϕ_m/ξ_0.

Summary.

The results of this section are especially useful for application to the ionosphere. They may be summarized as follows. Let a wave pass normally through a thin slab of a medium in which the complex refractive index is related to the number density N of molecules (or electrons) by the expression

$$\mu^2 - 1 = AN$$

and let N depart from its mean value by $\Delta N(x)$. Then on emergence the complex wave amplitude varies across the wave front in a manner determined both by the auto-correlation function $\rho_{\Delta N}(\xi)$ of ΔN and by the standard deviation ϕ_m of the modulus of the complex phase variation introduced by the slab. ϕ_m is itself proportional to the standard deviation N_m of the number density. The relations between these quantities are given in equations (90) and (91). The resulting angular spectrum is given in equation (96). Two important cases arise when $\phi_m^2 \ll$ or $\gg 1$.

(*a*) If $\phi_m^2 \ll 1$, i.e. the variations of amplitude do not exceed one neper and the variations of phase do not exceed one radian. The angular spectrum then contains a large undeviated component (a 'specularly' reflected component in the case of diffractive reflection) and weaker side components. The 'signal-to-noise' ratio is approximately $1/\phi_m^2$ and the auto-correlation function $r_f(\xi)$ of the wave-field does not fall to zero when ξ is large. The side components have the spread which they would have if the irregularities of ΔN constituted an 'amplitude' diffracting screen, and $\rho_f(\xi) = \rho_{\Delta N}(\xi)$ so that the scale of the structure in $\mathbf{f}(x)$ is the same as that in ΔN.

(*b*) If $\phi_m^2 \gg 1$, i.e. the variations of amplitude exceed one neper, and/or the variations of phase exceed one radian. Then the undeviated component of the angular spectrum is small and the side waves extend to angles determined both by the auto-correlation function $\rho_{\Delta N}(\xi)$ and also by ϕ_m. If $\rho_{\Delta N}(\xi) = \exp(-\xi^2/\xi_0^2)$ the angular extent is determined by ϕ_m/ξ_0 and is ϕ_m times larger than it would be for the case where $\phi_m^2 \ll 1$. The auto-correlation function $\rho_f(\xi)$ of the wave-field has a scale which is $1/\phi_m$ times that of the distribution of number density.

6.6. *A Thick Medium with Weak Three-dimensional Irregularities*

Suppose that a wave travels a considerable distance Z through a medium in which there are irregularities of refractive index distributed randomly in three dimensions, and it is required to find the distribution $\mathbf{f}(x, y)$ of complex amplitude over the wave front. The investigation has been made in two different ways by Bramley (1954) and by Fejer (1953). Both supposed in effect that the refractive index μ had an auto-correlation function given by $\exp(-R^2/L^2)$ and a standard deviation μ_m. It was further supposed that the deviations of refractive index were small compared with the mean, so that $\mu_m \ll \mu_{av}$.

The method used by Bramley can be expressed in simple terms as follows: Consider the irregular medium to be made up of a series of superposed 'blobs',

each with the auto-correlation function $\exp(-R^2/L^2)$, with 'size' of the order L, and situated an average distance L apart. Then a straight line drawn through a thickness Z of the medium will pass, on the average, through a number n of blobs given by $n = Z/L$. The optical distance along this line, represented by $\int_0^Z \mu dZ$ will be increased by some of the 'blobs', which have $\mu > 1$ and will be decreased by others; the mean square total change will be proportional to n, and to the mean square change introduced by one blob, which is of the order $(L\mu_m)^2$. It is now assumed that the distribution of phase over the emerging wave front is proportional to the distribution of 'optical path', calculated as above, divided by the wavelength. The mean square phase deviation ϕ_m^2 is thus proportional to $(Z/L)(L\mu_m)^2/\lambda^2$ or $\phi_m \propto \mu_m(LZ)^{1/2}/\lambda \propto \mu_m(lz)^{1/2}$ if l and z are measured in terms of λ as a unit. The auto-correlation of ϕ in the (x, y) plane is the same as that of the refractive index and is given by

$$\rho_\phi(\xi, \eta) = \exp\{-(\xi^2+\eta^2)/l^2\}. \qquad \ldots\ldots(100)$$

In the emerging wave front the phase is thus randomly distributed in such a way that the departure $\Delta\phi$ from the mean is normally distributed with standard deviation

$$\phi_m \propto \mu_m(lz)^{1/2} \qquad \ldots\ldots(101)$$

and with auto-correlation given by equation (100). A distribution of phase of this kind produced by passage of a wave through a thin screen was discussed in § 6.5 and the results were summarized at the end of that section.

Using a different method of approach Fejer (1953) supposed the thick medium to be divided into a series of superimposed thin slabs and considered the successive diffraction effects they would produce. If unit power is incident the first slab transmits a power Q without deviation and diffracts a power Q_1. Of the undeviated power Q the second slab transmits Q^2 still without deviation and diffracts QQ_1, and of the power Q_1 diffracted by the first slab the second one transmits QQ_1 without deviation and diffracts Q_1^2 a second time. On the whole Q^2 remains undeviated, $2QQ_1$ has been diffracted once, and Q_1^2 has been diffracted twice. By continuing this kind of argument it is possible to calculate the powers remaining at the end in the undeviated and in the once, twice, ..., etc. diffracted waves, and if the angular power spectrum produced by one slab is known the final angular power spectrum can be determined. It is expressed, in Fejer's equation (41) as the sum of the $1, 2, \ldots, n, \ldots$, times diffracted powers.

Bramley showed that Fejer's expression was the same as the one he had deduced, and that the terms which were summed were the same as those in equation (96). This agreement provides some justification for Bramley's assumption that the optical path through the thick diffracting medium can be calculated by integrating along a straight line, even when diffractive effects are known to occur.

For application to specific problems it is now convenient to express the results of the calculations as follows. From Bramley's equation (11) it can be shown that, for the case of the ionosphere, ϕ_m of our equation (96) is given by

$$\phi_m = \left(\frac{\pi^{-3/4}e^2}{\epsilon_0 mc}\right)\frac{1}{f}(LZ)^{1/2}N_m \qquad \ldots\ldots(102)$$

where f is the wave frequency, and it is assumed that the effects of electron collisions are small. Here L and Z are measured in terms of unit distance.

6.7. *Non-uniform Illumination*

Up to here it has been supposed that the average illumination over the random diffracting screen was constant and that the screen had infinite extent sideways. Let us now examine what will happen if the illumination varies, on the average, across the screen. The non-uniformity might arise in different ways. For example it might be caused by a non-uniform illumination from the source, or by the screen itself which might transmit less well in some places, while continuing to have the same small-scale statistical structure over its whole surface. A particular example would be one in which a screen with smooth regular transmission

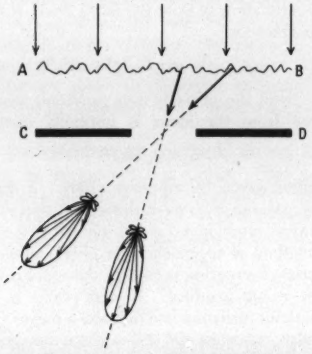

Figure 18. A random screen AB produces an incoherent angular spectrum of plane waves, each of which is afterwards spread into a coherent ' polar diagram ' by diffraction at a slit CD.

characteristics was placed in contact with one which had small-scale random characteristics ; an important special case would be that in which the former screen represents a slit in front of the random screen.

It is convenient first to consider the special case of an assembly of random screens placed in succession in front of a given slit. The state of affairs is represented in figure 18. Suppose that each screen of the random assembly extends to infinity with the illumination uniform across it, and that the structure in the screen is narrow so that the angular spectrum is wide. Each component plane wave in the angular spectrum passes, after it leaves the random screen, through the slit and is diffracted in the process so that its contribution is spread out through a range of angles as indicated in the figure by the ' polar diagrams '. If the diffraction pattern of the slit is narrow compared with the diffraction pattern of the original random screen (i.e. if the slit is wide compared with the extent of one of the irregularities in the screen) the distribution of power in the angular spectrum is not altered appreciably but coherence has been introduced into the spectrum as follows.

Suppose that in the angular spectrum, $\mathbf{F}(S)$, appropriate to any one sample of the (original) infinite random screen the amplitude and phase changed irregularly from one angle S to the next $S+\sigma$, and that the normalized auto-correlation function $\rho_F(\sigma)$ defined by

$$\rho_F(\sigma) = [\mathbf{F}(S)\,\mathbf{F}^*(S+\sigma)]_{\text{av}} \qquad \ldots\ldots(103)$$

was zero for all finite values of σ, however small. When the second screen with the slit was inserted in front, each component of the angular spectrum would itself be spread out into a *coherent* angular spectrum by diffraction at the slit, so that coherence would be introduced between the total radiation travelling in the direction S and that travelling in the direction $S+\sigma$. It appears reasonable to suppose that the correlation in the resulting spectrum might be represented by the function which describes the diffraction pattern of the slit itself, and that, in fact, proves to be the case. A general proof of this statement is given in the next paragraph.

Let the normalized complex amplitude in the wave front emerging from the random screen be $\mathbf{f}(x)$, and let its auto-correlation function be $\rho_f(\xi)$. Suppose also that the distribution of power over the emerging wave front, when averaged over the assembly, is given by $[|\mathbf{f}(x)|^2]_{\text{ass. av}}$ and is limited in extent, but that it extends over a distance considerably greater than that over which $\rho_f(\xi)$ has appreciable magnitude. Then if $\mathbf{F}(S)$ is the angular spectrum of $\mathbf{f}(x)$, equation (6) shows that

$$\mathbf{f}(x) \longleftrightarrow \mathbf{F}(S) \qquad \ldots\ldots(104)$$

and, from equation (66)

$$\rho_f(\xi) \longleftrightarrow |\mathbf{F}(S)|^2. \qquad \ldots\ldots(105)$$

But equation (104) represents a symmetrical Fourier transform so that the inverse of equation (105) is true and

$$\rho_F(\sigma) \longleftrightarrow |\mathbf{f}(x)|^2 \qquad \ldots\ldots(106)$$

where

$$\rho_F(\sigma) = [\mathbf{F}(S)\,\mathbf{F}^*(S+\sigma)]_{\text{av}} \qquad \ldots\ldots(107)$$

by analogy with

$$\rho_f(\xi) = [\mathbf{f}(x)\,\mathbf{f}^*(x+\xi)]_{\text{av}}. \qquad \ldots\ldots(108)$$

This result is of importance in the discussion of the interference effects produced by Young's double slits, and by Michelson's stellar interferometer, as will be shown in the next section.

It is first interesting to use the results of this section to consider what sort of variations could be detected in an angular spectrum by the use of a phase-sensitive observing instrument which accepted only the radiation falling inside a narrow range ΔS of angles. If σ_1 represents an angular separation in the spectrum for which $\rho_F(\sigma_1)$ is small, then the observing apparatus would receive effectively n independent values of $\mathbf{F}(S)$ simultaneously, where $n = \Delta S/\sigma_1$, and would record their average. This average would fluctuate from sample to sample, or as the angle S of observation was altered for one sample, by an amount which depended on $\sqrt{n}$. If $\Delta S \gg \sigma_1$ there would be little fluctuation, and if $\Delta S \ll \sigma_1$ there would be marked fluctuations. It is especially worthy of notice that when σ_1 is very small (very wide source) the angular spectrum fluctuates rapidly from one angle to the next, but any practical observing instrument would show only inappreciable fluctuations.

6.8. *The Production of a 'Randomly phased Spectrum'*

In later sections some special results will be proved for angular spectra which are made up of a large number of components having independent, and randomly distributed, phases. Whether or not a spectrum is of this kind will depend largely on the nature of the irregularities in the diffracting screen which produces it, but it will also depend on the mean distribution of power across it. Here the effect of this mean distribution will alone be discussed, the effect of the nature of the irregularities will be considered in § 8.2.

Suppose the irregularities in the screen are such that, if the mean distribution of power across it were uniform, it would produce a spectrum, spread over an angle S_1, in which the phase varied randomly from angle to angle, so that the auto-correlation function $\rho_F(\sigma)$ was small even when σ was infinitesimal. Next suppose that the mean distribution of power becomes non-uniform so that, according to equation (106) there is finite correlation in the spectrum over angles of the order σ_1. Then in making a traverse over the whole spectrum the number of independent phases encountered will be of the order S_1/σ_1. If this number is large it can be assumed that, in adding up the effects of all the spectral contributions, we are concerned with a large number of randomly phased vectors. A spectrum of this type will be called a 'randomly phased' spectrum.

Equation (105) implies that the extent S_1 of the angular spectrum is inversely proportional to the extent ξ_1 of $\rho_f(\xi)$, and equation (106) implies that σ_1 is inversely proportional to the 'extent' x_1 of the mean power distribution. The condition $S_1/\sigma_1 \gg 1$ is thus satisfied if $x_1/\xi_1 \gg 1$, i.e. if the mean power is effectively constant over a distance which contains a large number of irregularities. This condition must be satisfied if the spectrum is to be 'randomly phased'. The other conditions to be satisfied are discussed in § 8.2.

§ 7. Incoherent Sources

7.1. *An Incoherent Source considered as a Completely Rough Diffracting Screen*

Suppose that when a wave emerges from a diffracting screen its complex amplitude $\mathbf{f}(x)$ contains equal numbers of irregularities of all sizes down to much less than one wavelength so that in the Fourier analysis $\mathbf{F}(S)$ of $\mathbf{f}(x)$, and in the angular spectrum, there are components of equal magnitude at all values of S up to and greater than 1. At a distance† the angular spectrum is limited to $-1 < S < 1$, i.e. to $-\frac{1}{2}\pi < \theta < \frac{1}{2}\pi$, but inside this range of angles the power is equally distributed through all values of S. A diffracting screen of this kind might be called completely rough and it would have such a fine structure that it scattered equally all round.

It is often useful to think of an incoherent source of radiation as though it were a completely rough diffracting screen. For example, in a natural source of monochromatic light the radiating atoms are, at each instant, distributed randomly in position and are radiating with phases which are randomly related. At a later instant the positions and the phases have altered.‡ Within the sort of time

† The components with $|S| > 1$ represent evanescent waves which die away rapidly as the distance from the screen is increased.

‡ The effective source is completely reconstituted in a time of the order 10^{-9} sec.

for which observations can be made there are presented a very large number of statistically independent samples of the random distribution, and the time-average which is recorded by an observer represents the assembly-average over these sources. Since the size of the individual atomic radiators is much less than one wavelength the auto-correlation function over the source is narrow and the angular spectrum extends with constant power out to $\theta = \pm \frac{1}{2}\pi$. The radiation emerging from the source is similar to that produced when a series of ' completely rough ' diffracting screens are placed in rapid succession in a uniform beam of radiation. This concept of an incoherent source will be used in § 7.2.

7.2. *The Visibility of ' Young's Double Slit ' Interference Fringes*

It is well known that if, as in figure 19, a uniform plane wave of light coming from a very narrow slit P at some distance is incident on two narrow slits A and B behind which a lens is placed, then cosinusoidal interference fringes are

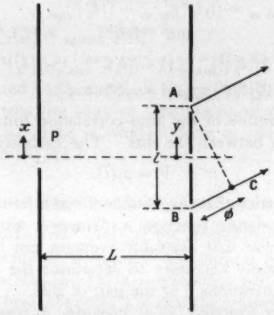

Figure 19. Young's double-slit interference arrangement.

produced in the focal plane of the lens. The distribution of intensity (or power) in these fringes is proportional to $1+\cos\phi$, where ϕ is the phase difference corresponding to BC in the figure. If now the slit P is made wider, the fringes become less clear and the distribution of intensity takes the form $1+V\cos\phi$, where the quantity V, called the visibility, is less than unity.

This result is usually demonstrated in textbooks by considering the addition of fringes formed by all the independent point sources in the slit P. This approach is used in Appendix 7, where it is shown that, if the distribution of power over P is given by $|\mathbf{f}(x)|^2$ then, with the nomenclature of figure 19

$$V = \int_{-\infty}^{+\infty} |\mathbf{f}(x)|^2 \cos(2\pi lx/L)\, dx, \qquad \ldots\ldots(109)$$

i.e. V is the normalized cosine Fourier transform of the power distribution over P.

The problem will now be approached another way and it will be shown how it can be considered in terms of the correlation between the wave amplitudes at the two slits A and B. Suppose these (complex) amplitudes are $\mathbf{f}_1$ and $\mathbf{f}_2$ and

suppose the (Fraunhofer) interference pattern is viewed in a direction which introduces a phase difference ϕ between the two beams. The resulting amplitude $\mathbf{f}$ in this direction is then given by

$$\mathbf{f} = \mathbf{f}_1 + \mathbf{f}_2 e^{i\phi} \qquad \ldots\ldots(110)$$

and the power, or the intensity, is

$$|\mathbf{f}|^2 = \{\mathbf{f}_1 + \mathbf{f}_2 e^{i\phi}\}\{\mathbf{f}_1^* + \mathbf{f}_2^* e^{-i\phi}\}. \qquad \ldots\ldots(111)$$

In many actual cases, and in particular if the wave is a light wave, $\mathbf{f}_1$ and $\mathbf{f}_2$ are always changing rapidly and the mean power is got by averaging over the assembly presented in time sequence to give

$$[|\mathbf{f}|^2]_{\text{ass. av}} = [\mathbf{f}_1\mathbf{f}_1^*]_{\text{ass. av}} + [\mathbf{f}_2\mathbf{f}_2^*]_{\text{ass. av}} + [\mathbf{f}_1\mathbf{f}_2^*]_{\text{ass. av}} e^{-i\phi} + [\mathbf{f}_2\mathbf{f}_1^*]_{\text{ass. av}} e^{i\phi}. \qquad \ldots\ldots(112)$$

Now if the illumination is, on the average, uniform over the wave front

$$[\mathbf{f}_1\mathbf{f}_1^*]_{\text{ass. av}} = [\mathbf{f}_2\mathbf{f}_2^*]_{\text{ass. av}} = [|\mathbf{f}_1|^2]_{\text{ass. av}}$$
$$\text{and} \quad [\mathbf{f}_1\mathbf{f}_2^*]_{\text{ass. av}} = [\mathbf{f}_2\mathbf{f}_1^*]_{\text{ass. av}}, \qquad \ldots\ldots(113)$$

so that
$$[|\mathbf{f}|^2]_{\text{ass. av}} = 2[|\mathbf{f}_1|^2]_{\text{ass. av}}\{1 + ([\mathbf{f}_1\mathbf{f}_2^*]_{\text{ass. av}}/[|\mathbf{f}_1|^2]_{\text{ass. av}})\cos\phi\}$$
$$= 2[|\mathbf{f}_1|^2]_{\text{ass. av}}\{1 + \rho_f(l)\cos\phi\} \qquad \ldots\ldots(114)$$

where $\rho_f(l)$ is the magnitude of the auto-correlation function of the wave amplitude $\mathbf{f}$ for the distance l between the slits. The visibility V is thus given by

$$V = \rho_f(l). \qquad \ldots\ldots(115)$$

It is interesting to notice that the double-slit interferometer provides a method of finding the auto-correlation function $\rho_f(\xi)$ over a wave front which is known to be random in the sense that assembly averages can be determined by taking time averages. It is simply necessary to determine the visibility of the Young's fringes for a series of separations ξ of the pair of slits.

The auto-correlation function $\rho_f(\xi)$ provides a measure of the amount of ' coherence ' in the wave. If $\rho_f(\xi)$ is unity for all values of ξ the wave is a coherent plane wave and $V = 1$. If $\rho_f(\xi)$ falls to a small value for $\xi < l$, then V is small and no interference fringes are produced. Zernike (1938) was the first to express the coherence properties of a wave front in this way.

It has been shown how the auto-correlation function over a wave front determines the visibility of the Young's fringes which can be produced from it. It will next be shown how the auto-correlation function depends on the slit P producing the wave front. If the source is a natural one, consisting of a very large number of independently radiating point sources, each of which is very small, then, as shown in § 6.7, it will radiate a wide angular spectrum $F(S)$ in which the correlation $\rho_F(\sigma)$ is known if the distribution $|\mathbf{f}(x)|^2$ of power across the slit P is known. At a sufficient distance L from the slit the distribution of amplitude with distance y over a plane will correspond to the Fraunhofer spectrum, and will be given in terms of the angular spectrum $F(S)$ by $F(y/L)$ (see figure 19). The correlation $\rho_f(l)$ between the amplitudes at two points separated by a distance l in the y-plane is thus obtained from $\rho_F(\sigma)$ by writing $\sigma = l/L$ and is given by

$$\rho_f(l) = \rho_F(l/L). \qquad \ldots\ldots(116)$$

If the two points separated by the distance l now correspond to the two slits A and B, then the visibility $V(l)$ of the fringes is given, from equations (115) and (116), by

$$V(l) = \rho_F(l/L) \qquad \ldots\ldots(117)$$

and since

$$\rho_F(\sigma) = \int_{-\infty}^{+\infty} |\mathbf{f}(x)|^2 \exp(-2\pi i\sigma x)\, dx \qquad \ldots\ldots(118)$$

we have

$$V(l) = \int_{-\infty}^{+\infty} |\mathbf{f}(x)|^2 \exp(-2\pi i l x/L)\, dx \qquad \ldots\ldots(119)$$

which is the exponential form of the result already obtained in equation (109) by the usual textbook treatment.

7.3. *The Michelson Radio-stellar Interferometer*

Let us develop the equations of the previous section somewhat differently as follows :

$$\rho_F(\sigma) \longleftrightarrow |\mathbf{f}(x)|^2$$

and

$$L\sigma = l$$

so that

$$V(l) = \rho_F(l) = \rho_F(L\sigma) \longleftrightarrow |\mathbf{f}(x/L)|^2. \qquad \ldots\ldots(120)$$

Thus if $V(l)$ is measured for a series of values of l it is possible to calculate $|\mathbf{f}(x/L)|^2$, which represents the angular distribution of power over the slit P, as seen from the plane AB. This is what is done in the Michelson radio-stellar interferometer described in § 11.2.

§ 8. Fresnel Diffraction by Random Screens

8.1. *The ' Size ' of the Irregularities*

If the normalized complex wave-field distribution across a plane diffracting screen is $\mathbf{f}(x)$ and that across the Fresnel diffraction pattern on a parallel plane is $\mathbf{g}(x)$, then it has already been shown (§ 5.3) that the auto-correlation functions $\rho_f(\xi)$ and $\rho_g(\xi)$ are equal, provided Fourier components of $\mathbf{f}(x)$ and $\mathbf{g}(x)$ shorter than the wavelength of the radiation are excluded. In the case of radio waves we are concerned with observing the field $\mathbf{g}(x)$ at the ground and trying to deduce the statistics of the electron distribution in the ionosphere.

It has been shown in § 6.5 that the ' size ' of the ionospheric irregularities, as given by $\rho_{\Delta N}(\xi)$, is related to the ' size ' of the irregularities in the emerging wave front, as given by $\rho_f(\xi)$, in a way which depends on the standard deviation, ϕ_m, of the modulus of the complex phase in the wave. It is convenient to express ϕ_m in terms of the standard deviation A_0 of the amplitude measured in nepers, and ϕ_0 of the phase measured in radians so that $\phi_m = (A_0^2 + \phi_0^2)^{1/2}$. The results of § 6.5 can then be applied as follows :

(*a*) If $(A_0^2 + \phi_0^2)^{1/2} < 1$, then $\rho_{\Delta N}(\xi) \simeq \rho_f(\xi) \simeq \rho_g(\xi)$. Hence the size of the ionospheric irregularities is of the same order as the size of the irregularities in the wave-field observed at the ground.

(*b*) If $(A_0^2 + \phi_0^2)^{1/2} > 1$, then the ' size ' of $\rho_{\Delta N}(\xi)$ is approximately $(A_0^2 + \phi_0^2)^{1/2}$ times the ' size ' of $\rho_f(\xi) = \rho_g(\xi)$. In this case the size of the irregularities observed on the ground can be much smaller than the size of the ionospheric irregularities.

These results, demonstrated in § 6.5 for a thin slab, are shown, in § 6.6, to be equally true for transmission through a thick ionosphere. They represent what can be deduced if both the amplitude and phase of the wave at the ground can be measured.

Often, however, it is inconvenient to measure the phase of the wave at the ground, and only the amplitude is observed. Under these circumstances it is still possible to make useful deductions if it can be assumed that the angular spectrum is randomly phased. Spectra of this type are considered in the following sections.

8.2. *Distribution of Amplitude and Phase produced by a 'Randomly phased' Spectrum*

Suppose that in the angular spectrum $\mathbf{F}(S)$ there are a large number of independent components, all of the same amplitude $|\mathbf{F}(S)|$, but with phases $(\arg \mathbf{F}(S))$ which differ from each other in a random manner. The form of the resulting

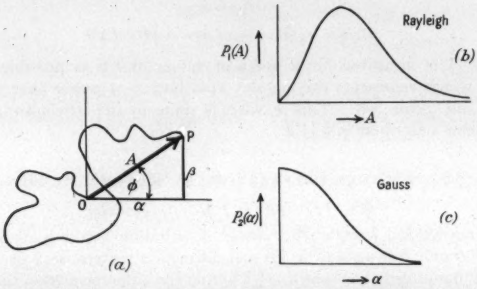

Figure 20. The resultant of a series of randomly distributed vectors is represented in (*a*) by OP, of magnitude A and phase ϕ; (*b*) represents the Rayleigh function $P_1(A)$ of equation (121) which gives the probability distribution of A; (*c*) represents the Gaussian function $P_2(\alpha)$ of equation (122) which represents the probability distribution of $\alpha = A\cos\phi$ or $\beta = A\sin\phi$.

disturbance over the plane $z = 0$ will depend on whether or not there is one component in $\mathbf{F}(S)$ which is considerably greater than all the others. It will first be supposed that there is no unique component in this sense. Then at a point x all the components in the angular spectrum will add together as a series of vectors $\mathbf{F}(S)\exp(2\pi iSx)$ whose magnitudes $|\mathbf{F}(S)|$ are known, but whose phases are random. The addition is illustrated in figure 20 (*a*). At one point the resultant vector will be $\mathbf{f}(x) = A(x)\exp\{i\phi(x)\}$. At another point the values of $\mathbf{f}$, A and ϕ will be different because the relative phases of the component vectors $\mathbf{F}(S)\exp(2\pi iSx)$ will be different. Over a range of different values of x there will be a range of values of $\mathbf{f}$, A and ϕ and it is possible to calculate their probability distributions. This is just what was done by Rayleigh in his solution of 'the problem of the drunkard's walk'. He showed that the probability $P_1(A)dA$ of finding A within the range A to $A+dA$ was

$$P_1(A)\,dA = \{2A/A_m^2\}\exp\{-A^2/A_m^2\}\,dA \qquad \ldots\ldots(121)$$

where A_m^2 is the mean square value of A. This function is represented in figure 20 (*b*). We shall call it a ' Rayleigh distribution '. He also showed that all values of ϕ between $-\pi$ and $+\pi$ were equally probable.

If, instead of considering the amplitude A, which is the same as the magnitude of $\mathbf{f}$, the real part α of $\mathbf{f} = \alpha + i\beta$ had been considered, a different result would have been obtained. Since the component random vectors take all possible phases at different positions x, and since the real part α corresponds to projection on to the real Oα axis of figure 20 (*a*) the sign of α will take positive and negative values equally frequently. Rayleigh showed that the probability of obtaining a value between α and $\alpha + d\alpha$ was given by

$$P_2(\alpha)\,d\alpha = \{1/(2\pi)^{1/2}\alpha_m\}\exp(-\alpha^2/2\alpha_m^2)\,d\alpha \qquad \ldots\ldots(122)$$

where α_m^2 is the mean square value of α. This function is represented in figure 20 (*c*) and is called a ' Gaussian distribution '. By arguments from symmetry it is seen that the imaginary part β, of $\mathbf{f}$, has the same Gaussian distribution.

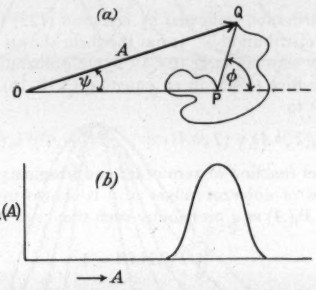

Figure 21. A steady wave vector OP with a randomly varying one PQ of considerably smaller r.m.s. magnitude gives a resultant of magnitude A which has the ' displaced-Gauss ' probability distribution shown at (*b*).

Next suppose that there is one component in the angular spectrum which has a power greater than that of all the side waves put together. The field at each point x is then made up of a series of component vectors of the kind just described, arising from the side waves, together with a larger vector of constant phase and amplitude, arising from the main wave. The situation is shown in figure 21 (*a*) where OP represents the main wave, PQ the resultant of the side waves, and OQ the total resultant of magnitude A. It has already been shown that over all positions x the magnitude of PQ has a Rayleigh distribution and its phase takes all values equally. In general the resultant OQ will have a complicated probability distribution, but if the r.m.s. magnitude of PQ is sufficiently less than the magnitude of OP the distribution is more simple. Let the amplitude of the steady component OP be normalized to unity, and let A_1 the r.m.s. amplitude of the variable component be less than about $\frac{1}{3}$. Then the amplitude A of the resultant is given approximately by $A = 1 + A_1\cos\phi$, where ϕ is the phase difference between OP and PQ. Now $A_1\cos\phi = \alpha$ is the in-phase component of

the random Rayleigh-distributed vector PQ, and it has already been shown that it has a Gaussian probability distribution $P_2(\alpha)$ so that the probability that the amplitude A will depart from unity by an amount between α and $\alpha + d\alpha$ is given by $P_2(\alpha)\,d\alpha$. Another way of expressing the result is to say that the probability $P_3(A)\,dA$ of obtaining a resultant between A and $A + dA$ is

$$P_3(A)\,dA = \{1/(2\pi)^{1/2}\alpha_m\}\exp\{-(A-1)^2/2\alpha_m^2\}\,dA. \quad \ldots\ldots(123)$$

In this expression α_m^2 is the mean value of α^2 and is given by

$$\alpha_m^2 = [A_1^2\cos^2\phi]_{av} = \tfrac{1}{2}A_1^2 \quad \ldots\ldots(124)$$

when all values of ϕ are equally likely. Now $\frac{1}{2}A_1^2$ represents the mean power in the side waves which go to make up the random part of the disturbance and hence $1/2\alpha_m^2$ represents the ratio of steady power to random power in the wave. If this ratio is denoted by b, equation (123) takes the form

$$P_3(A)\,dA = \{b/\pi\}^{1/2}\exp\{-b(A-1)^2\}\,dA. \quad \ldots\ldots(125)$$

The probability distribution indicated by equation (125) is what might be called a ' displaced Gauss distribution '. It has the form shown in figure 21 (b).

When b is neither zero nor large ($0 < b < 3$) the probability distribution function has a form given by Rice (1945) in an equation (3.10–16) which, in our nomenclature, is equivalent to

$$P_4(2\sqrt{b}A) = (2\sqrt{b}A)\exp\{-2b(1+A^2)\}\,I_0(4bA) \quad \ldots\ldots(126)$$

where I_0 is the Bessel function of zero order and imaginary argument. The form of $P_4(A)$ for a series of different values of b is shown in figures 22 (a) and (b). Figure 22 (a) shows $P_4(A)$ as a probability such that

$$\int_0^\infty P_4(A)\,dA = 1$$

and figure 22 (b) shows $P_4(A)$ normalized so that the probability of A's having a value unity is equal to unity. If the value of b is known the curves of figure 22 (a) are the more useful, but if only experimental results are available the results will be plotted as in figure 22 (b) and the value of b will have to be deduced from the shape of the resulting curve.

Let us now return to the case where $b > 3$, represented by figure 21 (b), and consider the probability distribution of the phase ψ of the resultant. With the approximations we have already made, $\psi = A_1\sin\phi = \beta$. Now the statistics of α and β are the same, and if ψ_m^2 represents the mean square magnitude of ψ we have

$$\psi_m^2 = \beta_m^2 = \alpha_m^2 = 1/2b. \quad \ldots\ldots(127)$$

Moreover, since the probability distribution of α (or β) is given by equation (122), it follows that

$$P_2(\psi) = \{1/(2\pi)^{1/2}\psi_m\}\exp\{-\psi^2/2\psi_m^2\} \quad \ldots\ldots(127\,a)$$

and the distribution of ψ is Gaussian.

Rayleigh and Gauss distributions will be encountered frequently in what follows. Some important quantities related to them are listed in Appendix 8.

Up to here it has been supposed that the angular spectrum was known to be ' randomly phased '. In practice it is the distribution $\mathbf{f}(x)$ of the complex amplitude over a plane which is observed, and the nature of the angular spectrum has to be inferred. If the statistics of the amplitude and phase of $\mathbf{f}(x)$ are both of the type described above, then the phases in the angular spectrum are random, but

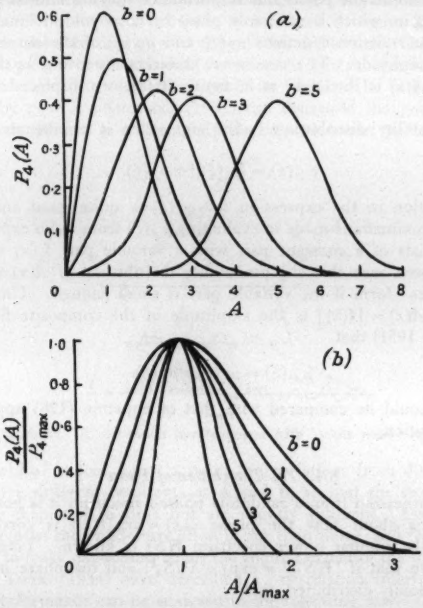

Figure 22. (*a*) Probability distribution $P_A(A)$ of the resultant amplitude when a random wave of unit mean power is added to a constant wave of power b.
(*b*) Shows the same curves normalized by dividing by P_{max} = the maximum value of P, and A_{max} = the value of A which gives P_{max}. (*After* McNicol (1949).)
The numbers attached to the curves are values of $2\sqrt{b}$ and not of b.

otherwise they are not. The angular spectrum would *not* be randomly phased, for example, at a plane where $\mathbf{f}(x)$ was random, but entirely real, corresponding to a diffracting screen which modifies only the amplitude, or where it had constant modulus but random phase, corresponding to a screen which modifies only the phase.

In much of the work on the ionosphere it has been assumed without sufficient proof that the angular spectrum was randomly phased. There are no established methods for testing this assumption, without examining in detail the distribution of amplitude and phase in $\mathbf{f}(x)$, and that is often prohibitively difficult. It is

important that methods should be devised for determining when a spectrum is randomly phased.

8.3. *The Correlation of Amplitude*

The auto-correlation function $\rho_f(\xi)$ of a complex field $\mathbf{f}(x)$ can in general be evaluated only if both the phase and amplitude of $\mathbf{f}(x)$ are known. If, however, $\mathbf{f}(x)$ has a spectrum which is randomly phased it is possible to make deductions about the auto-correlation functions $\rho_A(\xi)$ and $\rho_{A^2}(\xi)$ of the amplitude and the square of the amplitude. The results are different according as the probability distribution of $A(x)$ is Rayleigh, as in figure 20 (*b*), or ' displaced Gauss ', as in figure 20 (*c*).

If the probability distribution is Rayleigh, then it can be shown (Bramley 1951) that

$$\rho_{A^2}(\xi) = [\rho_f(\xi)]^2 \simeq \rho_A(\xi). \qquad \ldots\ldots(128)$$

The approximation in the expression for $\rho_A(\xi)$ is quite good and is certainly better than approximations made in evaluating $\rho_A(\xi)$ from radio experiments.

If $\mathbf{f}(x)$ consists of a constant part with a variable part $\mathbf{f}_1(x)$ superimposed, it has already been seen that the probability distribution of $A(x)$ will be of the ' displaced Gauss ' form if the variable part is small enough. Under these circumstances, if $A(x) = |\mathbf{f}(x)|$ is the amplitude of the composite field it can be shown (Bramley 1951) that

$$\rho_{A^2}(\xi) = \rho_{f_1}(\xi) \simeq \rho_A(\xi). \qquad \ldots\ldots(129)$$

This relation should be compared with that of equation (128) appropriate to a Rayleigh distribution.

8.4. *The Correlation of Phase*

If $\mathbf{f}(x)$ is synthesized from a randomly phased spectrum it is possible to draw some conclusions about how the phase $\phi(x) = \arg\{\mathbf{f}(x)\}$ is correlated in the X direction if the angular power spectrum $\mathbf{F}(S)$ is known. Thus MacDonald (1949) has shown that if $|\mathbf{F}(S)|^2 = \exp(-S^2/S_0^2)$ and the phase in the angular spectrum is randomly distributed, then

$$\Delta_\phi(\xi) = [|\phi(x) - \phi(x+\xi)|]_{\mathrm{av}} = \sqrt{2\pi} S_0 \xi. \qquad \ldots\ldots(130)$$

Here $\Delta_\phi(\xi)$ is the ' difference auto-correlation function ' of the phase in the distribution $\mathbf{f}(x)$ and is seen to be simply related to the spread S_0 in the angular spectrum.

Sometimes it is known that $\mathbf{f}(x)$ is everywhere of unit amplitude and only the phase varies with x so that

$$\mathbf{f}(x) = \exp\{i\phi(x)\}. \qquad \ldots\ldots(131)$$

Under these circumstances it can be shown (Bramley 1954) that $\rho_f(\xi)$ and $\rho_\phi(\xi)$ are related through the expression

$$\rho_f(\xi) = \exp[-\phi_{\mathrm{m}}^2\{1 - \rho_\phi(\xi)\}] \qquad \ldots\ldots(132)$$

where ϕ_{m}^2 is the mean square variation of the phase.

8.5. *Correlation Interferometers*

A Michelson stellar interferometer, or a spaced aerial direction finder, provides information by comparing the phases of a quasi-periodic wave as received at two points. If, instead of being periodic, the incident wave came from a point source and had an irregular time variation appropriate to ' white noise ', then the output of the two receivers would both be similar, and irregular, but would in general be displaced in time, as indicated in figure 23, and from the time difference the direction of arrival could be deduced.† This would best be done by finding the cross-correlation‡ between the two records for different time-displacements τ, and the correlation would be found to be unity for a displacement given by $c\tau = d$. Nodtvedt (1951) has discussed the possibility of using this type of arrangement as a direction finder in underwater acoustics.

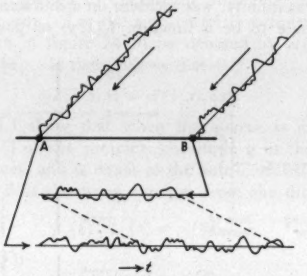

Figure 23. A correlation interferometer with ' white noise ' incident.

If the ' white ' source is not a point the radiations from different parts of it add up to give different resultants at A and B, so that the two recorded traces are not only displaced in time but are slightly different. Even with the best time-displacement the cross-correlation is not then unity, and from its magnitude it is possible to make deductions about the angular extent of the source. Hanbury-Brown and Twiss (1954) have described a ' correlation interferometer ' of this kind. Its performance can be analysed in the following way.

Suppose, as is always the case in practice, that the random ' noise-like ' radiation is received only over a narrow band-width, so that it is quasi-periodic. Then the ordinary Michelson stellar interferometer, which takes account of phase, produces an output proportional to $1+\rho_f(l)\cos\phi$ [see equation (117)] which corresponds to cosinusoidal interference fringes of visibility equal to $\rho_f(l)$, the correlation of the complex amplitude $\mathbf{f}$ as observed at the two receivers separated by the distance l. Now if the incident angular spectrum is randomly phased it is known that the correlation of real amplitude A is related to the correlation of complex amplitude $\mathbf{f}$ by equations (128) or (129) which state that $[\rho_f(\xi)]^2 = \rho_{A^2}(\xi)$ if the signal-to-noise ratio $b<1$ or $\rho_f(\xi) = \rho_{A^2}(\xi)$ if $b>1$. It is therefore

† Interesting points about the ' pulse theory ' of white light suggest themselves and it is clear that it would be best developed in terms of the theory of ' white noise '.

‡ If $\mathbf{f}_1(t)$ and $\mathbf{f}_2(t)$ are two functions each with zero mean value, and for which $[|\mathbf{f}_1(t)|^2]_{\mathrm{AV}} = [|\mathbf{f}_2(t)|^2]_{\mathrm{AV}} = 1$ then the cross-correlation with time displacement τ is defined to be $[\mathbf{f}_1(t)\mathbf{f}_2^*(t+\tau)]_{\mathrm{AV}}$.

useful to determine the squared amplitudes A^2 at the two receivers and to find their auto-correlation, instead of finding the auto-correlation of the complex field $\mathbf{f}$. This is precisely what is done in the correlation interferometer of Hanbury-Brown and Twiss. The advantage of an arrangement of this kind is that there is no need to preserve the radio-frequency phases of the outputs from the two receivers before performing the operation which determines their correlation. Only the squared amplitudes are needed, and since these are more easily transmitted to a distance the arrangement can be used with quite large separation of the receivers and large resolving powers are possible.

8.6. *Fresnel Diffraction of Waves from a Point Source*

In previous paragraphs it has been supposed that an infinite plane wave, coming from a point at infinity, was incident on a diffracting screen which caused the emerging amplitude to be a function $\mathbf{f}_1(x, y)$ of position. If the incident

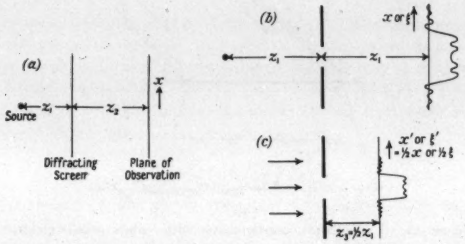

Figure 24. To illustrate Fresnel diffraction patterns formed when the source is at different distances from the diffracting screen. (*a*) explains the nomenclature. In (*b*) and (*c*) the shape of the patterns is the same, but the scale is changed.

wave had come, instead, from a point or line source at a finite distance its complex amplitude would have varied over the diffracting screen as given by a function $\mathbf{f}_2(x, y)$ which could be determined. The emerging complex amplitude would then have been given by $\mathbf{f}(x, y) = \mathbf{f}_1(x, y)\,\mathbf{f}_2(x, y)$, and the diffraction pattern would be the same as that produced by an infinite plane wave incident on a screen $\mathbf{f}(x, y)$. In principle, therefore, the Fresnel diffraction pattern formed by light originating in a point source at a finite distance is solved. In practice, however, it does not seem easy to use this general method to demonstrate clearly the relation between Fresnel diffraction patterns formed by point sources at different distances from the diffracting screen, and for that purpose another approach will be used.

Let a line source of light (figure 24 (*a*)) at a distance z_1 from a diffracting screen produce a Fresnel diffraction pattern on a parallel observing plane at a distance z_2. Then ordinary diffraction theory (see Appendix 9) can be used to show that the distribution of complex amplitude varies with distance x across the diffraction pattern, as given by a function of the two quantities

$$x\left(\frac{z_1}{z_1+z_2}\right) \quad \text{and} \quad z_2\left(\frac{z_1}{z_1+z_2}\right).$$

Suppose now we first use an arrangement with a point source of light distant z_1, and an observing plane distant z_2, and next an arrangement in which the point source is removed to infinity, and the observing plane is at z_3; then if $z_3 = z_2 z_1/(z_1+z_2)$ the shape of the diffraction pattern will be unchanged but its scale, in the X direction, will be altered in the ratio $z_1/(z_1+z_2)$.

This result is of importance in considering the diffractive reflection of waves incident normally on the ionosphere, for then the problem can often be considered as analogous to one of diffractive transmission with $z_1 = z_2 = z$. The theorem which has just been proved is illustrated in figure 24 (*b*) and (*c*), which show that the diffraction pattern on the ground is similar in shape to, but twice as large as, that which would be produced at a distance $\frac{1}{2}z$ if the incident radiation came from an infinitely distant point source.

These results can be applied to discuss the auto-correlation of a diffraction pattern in the following way. Let the auto-correlation function of any quantity in the diffraction pattern of figure 24 (*b*) be denoted by $\rho(\xi)\{z, z\}$, and that of figure 24 (*c*) by $\rho(\xi)\{\infty, \frac{1}{2}z\}$. It then follows that

$$\rho(2\xi)\{z, z\} = \rho(\xi)\{\infty, \tfrac{1}{2}z\}. \qquad \ldots\ldots(133)$$

Now the results of § 5.3 show that when the source is at infinity the auto-correlation function $\rho_g(\xi)$ of the complex amplitude $\mathbf{g}$ in the diffraction pattern is the same at all distances, and is equal to the auto-correlation function $\rho_f(\xi)$ of the complex amplitude $\mathbf{f}$ as the wave emerges from the diffracting screen. In particular

$$\rho_g(\xi)\{\infty, \tfrac{1}{2}z\} = \rho_f(\xi). \qquad \ldots\ldots(134)$$

Hence from equation (133)

$$\rho_g(2\xi)\{z, z\} = \rho_f(\xi) \qquad \ldots\ldots(135)$$

and $\rho_f(\xi)$ could be deduced from observations of $\rho_g(2\xi)\{z, z\}$ made with point source illumination. It should be noted that the scale of the variations of $\mathbf{f}$ deduced by means of equation (135) from observed values of ρ_g is half as large as it would have been if it had been assumed that the diffracting screen was illuminated by a plane wave.

If the angular spectrum is randomly phased it is possible to use correlation functions of amplitude A, as in § 8.3, and to show that

$$\rho_A(2\xi)\{z, z\} = [\rho_f(\xi)]^2 \quad \text{if} \quad b<1 \qquad \ldots\ldots(136)$$

or

$$\rho_A(2\xi)\{z, z\} = \rho_f(\xi) \quad \text{if} \quad b>1. \qquad \ldots\ldots(137)$$

§ 9. Time-varying Diffraction Patterns

9.1. *Description of Time-varying Patterns*

In radio-wave phenomena which will be considered in Part II, the diffracting medium is not stationary and correspondingly the diffraction pattern is constantly changing. Up to now this fact has only been taken into account in so far as it allowed an average to be taken over different samples of an ' assembly ' by taking an average over time. The analysis of the time variations will now be considered more fully. The treatment here is quite general and could be applied, for example, to the moving patches of dark and light illumination observed when

light shines through a rising stream of hot air, or to the optical scintillation of stars. Details of the radio applications are given later.

First consider the simplified problem of a normalized field distribution $\mathbf{f}(x,t)$ which changes with distance x along a line and with time t. Consider now simply the *description* of $\mathbf{f}(x,t)$ without any reference to the fact that it might be caused by a process of diffraction. It can be synthesized from a double Fourier spectrum $\mathbf{F}(S,p)$ by writing

$$\mathbf{f}(x,t) = \int_{-\infty}^{+\infty}\int_{-\infty}^{+\infty} \mathbf{F}(S,p)\exp\{2\pi i(Sx+pt)\}\,dS\,dp. \qquad \ldots\ldots(138)$$

This synthesis is equivalent to building up $\mathbf{f}(x,t)$ by adding a series of travelling F-waves, with amplitude distribution $\mathbf{F}(S,p)$, each having spatial period $1/S$, time period $1/p$, and velocity $-p/S$. These waves are to be clearly distinguished from any radiation waves which may be considered later.

Next define a spatial and temporal auto-correlation function $\rho(\xi,\tau)$ by the expression

$$\rho_f(\xi,\tau) = [\mathbf{f}\{x,t\}\,\mathbf{f}^*\{(x+\xi),(t+\tau)\}]_{\mathrm{av}}. \qquad \ldots\ldots(139)$$

This measures the correlation between values of $\mathbf{f}$ taken at distances ξ apart and at times separated by τ. It follows immediately from the analysis for two spatial variables already sketched in § 5.1 that

$$\rho_f(\xi,\tau) \longleftrightarrow |\mathbf{F}(S,p)|^2. \qquad \ldots\ldots(140)$$

The value of $\rho_f(\xi,\tau)$ is thus related to the power $|\mathbf{F}(S,p)|^2$ in the travelling F-wave of corresponding $S = 1/\xi$ and $p = 1/\tau$. It is a straightforward matter to extend the discussion to a two-dimensional time-varying function $f(x,y,t)$ and its auto-correlation function $\rho(\xi,\eta,\tau)$.

9.2. *Analysis of a Pattern which Drifts and Changes*

When an irregular radio diffraction-pattern is observed at the ground it is found to be constantly changing. The change is, in general, made up of a steady drift of the pattern as a whole, combined with a changing of the pattern as it moves. If observations of the complex amplitude were made only at one point it would not be possible to decide how much each of these two mechanisms contributed to the changes, but if observations are made simultaneously at two or more points it is possible to separate the two phenomena and to measure each statistically. We shall now consider how the velocity of steady drift, and the rate of change of the pattern as it moves, can be deduced from the observations. At this stage we are concerned only with the geometry of an irregular pattern, and not with any problem of diffraction.

Let us simplify the problem by considering a special case where quantities change only along the X direction, and let $\mathbf{f}(x,t)$ represent the normalized complex amplitude in the pattern. Suppose first that it has no organized drift movement, but that at one point it changes irregularly with time, as described by a temporal auto-correlation function $\rho_f{}^{(1)}(\tau)$. Suppose also that the distribution along the X direction is random and, at a fixed time, can be described in terms of a spatial auto-correlation function $\rho_f{}^{(2)}(\xi)$. It will be assumed that, if τ and ξ are not too large, $\rho^{(1)}$ and $\rho^{(2)}$ have the same form, and the combined auto-correlation function $\rho(\xi,\tau)$ which represents the correlation at two points separated

by a distance ξ, at two times separated by τ, will be assumed† to be a function of the quantity $\xi^2+V_c^2\tau^2$. V_c then has the dimensions of a velocity, it is the ratio of the distance ξ_1, which provides a given auto-correlation at a given instant, to the time-lag τ_1, which produces the same correlation at a given place, so that

when $$\rho(\xi_1, 0) = \rho(0, \tau_1) \qquad \ldots\ldots(141)$$

then $$V_c = \xi_1/\tau_1. \qquad \ldots\ldots(142)$$

The velocity V_c will be called the ' characteristic random velocity ' of the pattern.

Contours of constant $\rho(\xi, \tau)$ plotted in the ξ, τ plane will be similar ellipses, as represented in figure 25 (*a*). If, however, the contours of constant ρ are plotted as functions of ξ and of $V_c\tau$ they will be circles as indicated in figure 25 (*b*).

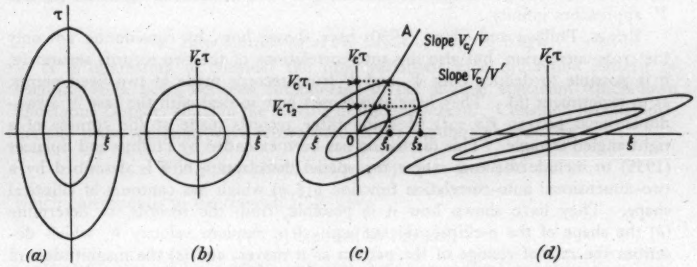

Figure 25. To illustrate the auto-correlation function $\rho(\tau, \xi)$ of a one-dimensional pattern which changes with time; (*a*) represents contours of ρ, (*b*) shows these with the scale altered so that they are circular, (*c*) shows the form which (*b*) takes if the observer, or the pattern, moves with a constant velocity V, (*d*) shows the form of (*c*) if V is large.

Now suppose that the time-varying pattern has a drift, of velocity V, imposed on it along the X direction. An equivalent effect could be produced by leaving the pattern stationary and causing the observer to move with velocity $-V$. The effect of this can be described by replacing ξ by $\xi - V\tau$ [or $\xi-(V/V_c)(V_c\tau)$] in the previous argument. The contours of figure 25 (*b*) would then be sheared into the ellipses of figure 25 (*c*) in which the line OA has the slope V_c/V.

Next suppose that two different experiments (*a*) and (*b*) are made as follows:

Experiment (*a*). Let the time-variations $\mathbf{f}\{x, t\}$ and $\mathbf{f}\{(x+\xi_1), t\}$ be recorded at two points separated by a distance ξ_1. Let the cross-correlation $\rho_f(\xi_1, \tau_1)$ between the records be determined for a *fixed time-difference* τ_1, and then let ξ_1 be altered until the correlation is a maximum. The quantities $V_c\tau_1$ and ξ_1 will then be related as shown in figure 25 (*c*), and the ratio $V_c\tau_1/\xi_1$ will be the same as the slope of the line OA and will represent the ratio V_c/V. If, therefore, V_c were known, V could be determined. This experiment would involve the use of movable recorders so that ξ_1 could be altered, and it would not be easy.

Experiment (*b*). Let the cross-correlation $\rho_f(\xi_2, \tau_2)$ between the two records be determined *for a fixed separation* ξ_2, and let the time-difference τ_2 be altered

† Since at $\xi = 0$ and $\tau = 0$, ρ has a maximum value, with respect both to variations of ξ and of τ, any variation with ξ and τ must have this form for small values of ξ and τ.

until the correlation is a maximum. The quantities $V_c\tau_2$ and ξ_2 will then be related as shown in figure 25 (*c*) and their ratio will NOT be the same as the slope of OA and will NOT represent the ratio V/V_c. This experiment would be simpler than experiment (*a*), because it involves only two stationary recorders, but it cannot be used to provide a direct measure of V.

If, in the result of the simpler experiment (*b*), we write $\xi_2/V_c\tau_2 = V'/V_c$ then V' is the 'effective' velocity which would be determined by taking records at two fixed points and finding the time difference which gave best correlation between them. It is clear from figure 25 (*c*) that $V' > V$, the true velocity of drift. If $V \gg V_c$ then the sloping ellipses become narrow and degenerate into straight lines as in figure 25 (*d*), and there is little difference between V' and V. If, however, $V \ll V_c$ the ellipse approximates to the circle of figure 25 (*b*) and V' approaches infinity.

Briggs, Phillips and Shinn (1950) have shown how, by considering not only the cross-correlation, but also the auto-correlations of the two records separately, it is possible to deduce both V_c and V from records made at two fixed points, as in experiment (*b*). They have also shown how to deal with the case of a two-dimensional pattern $\mathbf{f}(x, y, t)$ by using three records made at the corners of a right-angled triangle. This discussion has been extended by Phillips and Spencer (1955) to include the case where the spatial distribution of $\mathbf{f}$ is described by a two-dimensional auto-correlation function $\rho(\xi, \eta)$ which has contours of elliptical shape. They have shown how it is possible, from the records, to determine (*a*) the shape of the ρ-ellipse, (*b*) the equivalent random velocity V_c which describes the rate of change of the pattern as it moves, and (*c*) the magnitude and direction of the velocity V with which the pattern drifts as a whole.

9.3. *Time-varying Diffraction*

Suppose that $\mathbf{f}(x, t)$ represents the distribution of complex amplitude along the X direction in a time-varying diffraction pattern formed by an electromagnetic wave of frequency n and wavelength λ, and that distances are measured in terms of λ as a unit.

Then it has been shown in § 9.1 that $\mathbf{f}(x, t)$ can be synthesized from a set of 'F-waves', travelling back and forth along the X direction, such that

$$\mathbf{f}(x,t) = \int_{-\infty}^{+\infty}\int_{-\infty}^{+\infty} \mathbf{F}(S,p)\exp\{2\pi i(Sx+pt)\}\,dS\,dp. \qquad \ldots\ldots(143)$$

Now each component 'F-wave' corresponds, in the angular spectrum of the electromagnetic waves of frequency n, to a wave

$$\mathbf{F}(S,p)\exp\{2\pi i(Sx+Cz+pt)\}\exp(-2\pi int)\,dS\,dp$$

with a time-varying amplitude. The complete electromagnetic disturbance is the sum of all these components and has a complex amplitude given by

$$\mathbf{f}(x,z,t) = \int_{-\infty}^{+\infty}\int_{-\infty}^{+\infty} \mathbf{F}(S,p)\exp\{2\pi i(Sx+Cz+pt)\}\,dS\,dp. \qquad \ldots\ldots(144)$$

Equation (144) represents the complex amplitude in the angular spectrum which makes up the original disturbance of equation (143) over the plane $z = 0$, and is

similar to that discussed elsewhere in this paper. The only difference is that, in equation (144), the amplitudes of the component waves are not constant.

The angular spectrum of equation (144) is common to the wave distributions **f** and **g** over two parallel planes in the diffraction pattern, and since the auto-correlation functions depend only on the angular spectrum the argument of § 5.3 can be used to show that

$$\rho_f(\xi,\tau) = \rho_g(\xi,\tau). \qquad \ldots\ldots(145)$$

This relation implies that $\rho_f(\xi,0) = \rho_g(\xi,0)$ so that the instantaneous spatial auto-correlation functions over the diffracting screen and over the diffraction pattern are equal, and also that $\rho_f(0,\tau) = \rho_g(0,\tau)$, so that at fixed points the temporal auto-correlation functions in the two planes are the same.

9.4. *Time Variations as the Result of Doppler Shifts*

It is interesting to consider the time variations in a diffraction pattern as resulting from beats between components in the angular spectrum which have undergone Doppler shifts in the moving diffracting screen. Consider, for example, the one plane radiation-wave represented in the angular spectrum by

$$\mathbf{F}(S,p)\exp\{2\pi i(Sx+Cz+pt)\}\exp\{-2\pi int\}\,dS$$

which corresponds to the travelling ' F-wave '

$$\mathbf{F}(S,p)\exp\{2\pi i(Sx+pt)\}\,dS$$

in the diffracting screen. If this radiation wave is re-written

$$\mathbf{F}(S,p)\exp\{2\pi i(Sx+Cz)\}\exp\{-2\pi i(n-p)\,t\} \qquad \ldots\ldots(146)$$

it is seen that it corresponds to a wave which has had its frequency altered from n to $n-p$. Now the velocity of the ' F-wave ' along the X direction is $-p/S$ so that the radiation wave which it diffracts in the direction S has its frequency altered by $-S(p/S) = -p$, and this is the Doppler shift included in expression (146). Thus in general all the radiation waves have their frequencies altered by all the travelling ' F-waves ', and it is the beating together of these waves of different frequency which produces the time variations in the diffraction pattern.

PART II. APPLICATIONS OF DIFFRACTION THEORY TO THE IONOSPHERE

§ 10. Introduction

When radio waves, emitted by a radio star, or by a sender on the earth, are received at the earth after transmission through, or reflection from, the ionosphere they are often found to exhibit properties which can be attributed to the effect of diffraction in the ionosphere. From observations of the waves when they are received at the ground it should be possible to make some deductions about the ionosphere through which they have passed. The application of diffraction theory for this purpose will be considered in this Part of the Report.

The problem is usually broken up into subsidiary ones in which the aim is to determine, as far as possible,

(*a*) the spatial statistics of the wave-field at the ground on a series of different radio frequencies, and the description of that field in terms of an angular spectrum ;

(*b*) the temporal statistics (fading or scintillation) of the wave-field at the ground on a series of different frequencies.

From these statistics an attempt is next made to determine

(*c*) the spatial and temporal statistics of the wave-field as it emerges from the ionosphere ;

(*d*) the size and location of ionospheric structure which could produce the wave-field of (*c*) ;

(*e*) the regular (drift) and irregular motions of the ionospheric structure.

It will appear, as the account progresses, that in many cases it is not possible to draw firm conclusions about some of these points. This is particularly true of those listed under (*d*). The results based on the radio-astronomical observations are less ambiguous than those based on observations of reflected pulses, and will be dealt with first.

§ 11. Scintillations of Radio Stars

11.1. *The Phenomenon*

In some of the earliest work on radio astronomy it was observed that when a narrow-beam aerial was directed towards an area in the neighbourhood of the constellation Cassiopeia the intensity of the received wave sometimes varied markedly, particularly at night. Later work has shown that these variations take place in the radiation coming from an intense radio star†, and the variations are imposed on the waves as they traverse the terrestrial ionosphere. The details of the phenomenon have been elucidated with the help of a radio interferometer analogous to the stellar interferometer of Michelson.

11.2. *The Michelson Radio-stellar Interferometer*

In the Michelson radio-stellar interferometer two aerial arrays, situated some distance apart, are connected to a receiver whose output indicates the total power in the combined input. As the earth rotates and carries the aerials round with it the difference of the paths from a radio star to the two aerials changes and the output exhibits sinusoidal fluctuations analogous to the fringes in the optical instrument of Michelson. A special phase-switching arrangement, due to Ryle (1952), ensures that the mean of the trace is automatically in the centre of the chart, so that a symmetrical sinusoidal trace is all that appears if a radio star is recorded against a general background of radiation. An example is shown in figure 26 (*a*). The analogy between this device and Young's double-slit interference arrangement has been discussed in § 7.3 together with its application to the determination of the distribution of radio emission over the source.

† Astronomical regions of intense radio radiation which subtend small angles at the earth are called radio stars.

The recorded trace from a radio-stellar interferometer repeats regularly from day to day in the same form, and in the day time it is smooth and constant. It is deduced that the radiations from the sources are constant over considerable times. Often, at night, the sinusoidal trace is irregular, as shown in figure 26 (*b*, *c*). By analogy with the variation of the intensity of visible stars these irregularities are called ' scintillations '. The random variation of amplitude is measured by the departure of the trace from a smooth sine-curve. Experiments have shown that

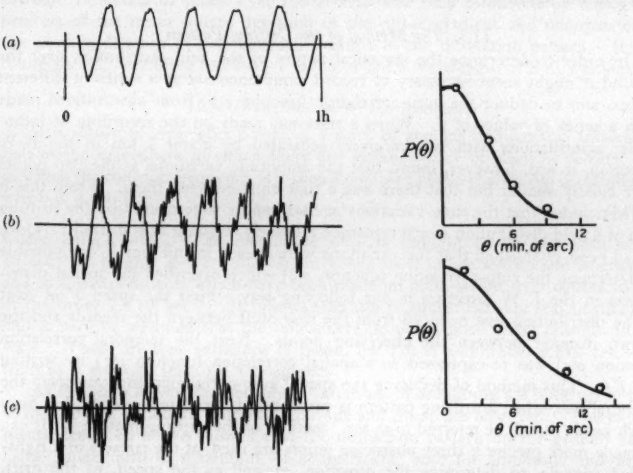

Figure 26. Records of radiation from a radio star received on a phase-switched interferometer when the ionosphere was (*a*) smooth, (*b*) irregular, and (*c*) very irregular. The corresponding probability distributions $P(\theta)$ of the ' angle flicker ' θ are shown. (*After* Hewish (1952).)

the scintillations are quite different at places 100 km apart and that there is considerable correlation at places 5 km apart. It appears that they are caused by some irregularities which occur in the ionosphere at night.

Detailed observations of radio-stellar scintillations have been made, and the variations of both amplitude and phase have been studied. The fluctuation ΔA of the amplitude A has been observed and used to find (*a*) the probability distribution function $P(A)$ of A, (*b*) the ratio $\{[\,|\Delta A|\,]_{\mathrm{av}}\}/A_{\mathrm{av}}$ of the mean fluctuation to the mean amplitude, (*c*) the time-variation of A as represented by the auto-correlation function $\rho_A(\tau)$, (*d*) the space-variation of A as represented by the auto-correlation function $\rho_A(\xi)$.

The phase was investigated by determining the difference ψ between the phases received on two aerials. This was found from records, of the type shown in figure 26, obtained with a phase-switched interferometer of large spacing. In this type of record the trace crosses the zero line whenever the fields at the two

aerials are in quadrature (see Ryle 1952). In the trace at (*a*), which represents results obtained during day time, the crossings repeat with regular time-intervals determined by the rotation of the earth. In the traces at (*b*) and (*c*) which were obtained at night, the times of crossing are irregular and it is possible to use them to deduce the fluctuations $\Delta\psi$ of the phase difference ψ. If desired these fluctuations of phase can be interpreted as a fluctuation in the angle θ of arrival of the waves (see § 14.5). The statistical distribution of the angle flicker $\Delta\theta$ is indicated in the figure for the traces (*b*) and (*c*).

11.3. *The Method of the Drifting Pattern*

In order to determine the statistical nature of the field distribution over the ground it might seem necessary to record simultaneously at a series of different places, and to deduce the auto-correlation function $\rho(\xi)$ from observations made with a series of values of ξ. When a start was made on the recording of radio-stellar scintillations with two receivers separated by about 1 km in the E–W direction, it was, however, found that the amplitude variations at the two points were closely similar but that there was a time-shift between them. From this it was concluded that the time-variations at both points were caused by the drifting past of a field distribution which remained relatively constant as it drifted.† Once it had been established that the variations were caused in this way it was possible to determine the auto-correlation function $\rho(\xi)$ which described the spatial distribution in the E–W direction in the following way. First the speed V of drift of the distribution was deduced from the time-shift between the records and the known distance between the observing points. Next the temporal correlation function $\rho(\tau)$ was re-expressed as a spatial correlation function $\rho(\xi)$ by writing $\xi = V\tau$. This method of deducing the spatial auto-correlation function from the temporal one, when a drifting pattern is present with measured velocity, has been much used; it will be referred to as the ' method of the drifting pattern '. It can be made more precise if three observing points are used, at the corners of a right-angled triangle, to determine the direction, as well as the speed, of the drift. Applications of the method will be mentioned again in other connections.

11.4. *The Results*

Hewish (1952) observing at night on wavelengths of 6·7 and 8 m determined the fluctuations ΔA of amplitude as recorded at two points separated by about one kilometre in the E–W direction, and used the method of the drifting pattern to determine the spatial distribution of A. He did not evaluate the full auto-correlation function, but showed, instead, that the average distance between maxima was about 5 km. If it is supposed that the auto-correlation function of the amplitude distribution over the ground is given by $\rho_A(\xi) = \exp(-\xi^2/\xi_0^2)$, then it is shown in Appendix 10 that the experimental value of 5 km for the average distance between maxima corresponds to $\xi_0 = 5/2{\cdot}6 \simeq 2$ km.

Hewish next used the method already described to determine the difference ψ of phase between the two aerials of an interferometer, of spacing 400 m. He found that ψ fluctuated in a random manner with a quasi-period about the same

† The fact that the pattern did not change much as it moved was usually obvious from the close similarity of the records made at the two points. When they were not obviously very similar an analysis of the type described in § 9.2 was necessary before the velocity V of drift could be deduced.

as that of the amplitude A. Since variations in both A and ψ were caused by the steady drift of a pattern this implied that the lateral extents of the phase-variations and the amplitude-variations were the same. The difference ψ of the phases recorded at the two aerials was then related to the variations of the phase ϕ of the wave over the ground, as follows. The mean square value $[(d\phi/dx)^2]_{\text{av}}$ of the phase-gradient over the ground was given by $[\psi^2]_{\text{av}}/d^2$, where d was the distance between the two aerials, and the mean square magnitude ϕ_{m}^2 of the extreme variations of phase over the ground was then estimated by taking the product of the mean square deviation of the phase gradient and one-quarter of the average distance (5 km) between maxima in the diffraction pattern. It was found that ϕ_{m} was often less than 1 radian when a wavelength of 8 m was used.

11.5. *Deductions about the Ionosphere*

It is shown in Appendix 6 that, if a wave of angular frequency ω traverses a slab of the ionosphere in which there are variations ΔN of electron density, and in which the collision frequency is ν, then a complex phase-change $\Delta\varphi$ is introduced which is given by

$$\Delta\varphi = C\exp(i\psi)\,\Delta N \qquad \ldots\ldots(147)$$

where $\tan\psi = -\nu/\omega$. The magnitude of ν is thought to be less than about $10^7\,\text{sec}^{-1}$ at heights above about 80 km where most of the ionosphere is situated, and in the experiments which have been made on radio-stellar scintillations ω was of the order $2\times10^8\,\text{sec}^{-1}$. It follows that $\Delta\varphi$ is almost entirely real in this case and it may be assumed that the ionosphere produces pure phase changes in the wave. There are thus variations of phase, but not of amplitude, across the wave front as it emerges from the ionosphere.

As the wave leaves the ionosphere variations of amplitude are built up so that, at the ground, variations both of amplitude and phase are observed. The experiments described above showed that the diffraction pattern on the ground had a 'size', maximum to maximum, of about 5 km, both for amplitude and phase. Moreover, the phase deviation was less than one radian, and the amplitude deviation less than one neper, so that, for reasons given in § 6.5, it could be concluded that the 'size' of the ionospheric irregularities was of the same order as the 'size' of the irregularities in the wave-field at the ground, i.e. about 5 km from maximum to maximum in the E–W direction.

In the above results, because $\phi_{\text{m}}<1$ it would be expected that the relative amplitude variations would be small [see § 8.2 and figure 21 with ϕ written for ψ], and the signal-to-noise ratio would be greater than unity. If the components of the angular spectrum had completely random phases, equation (127) should apply with $\Delta A_{\text{rms}}/A_{\text{av}}$ written for α_{m}, so that

$$1/\sqrt{(2b)} = \Delta A_{\text{rms}}/A_{\text{av}} = \phi_{\text{m}}/\sqrt{2}. \qquad \ldots\ldots(148)$$

Observations on a wavelength of 8 m showed, in fact, that $\Delta A_{\text{rms}}/A_{\text{av}}\simeq0{\cdot}03$, while $\phi_{\text{m}}\simeq0{\cdot}2$, so that the amplitude variation was smaller than it would be if the phases in the angular spectrum were completely random. It is, indeed, more like that which the wave would have on emergence from the ionosphere, where all the variations would be in phase and none in amplitude. It seems that the wave had not travelled far enough for the full amplitude variation to establish itself (see § 4.3).

Hewish (1952) has considered in detail how a wave, which starts with only a phase-variation across its wave front, will develop an amplitude-variation as it travels. He showed how $\Delta A_{rms}/A_{av}$ would change with the distance Z of travel, for different values of ϕ_m, and the results are shown by the line in figure 27. Some simultaneous measurements of $\Delta A_{rms}/A_{av}$ and ϕ_m made on different occasions are shown in the figure. It is noticeable that those made when the star was more

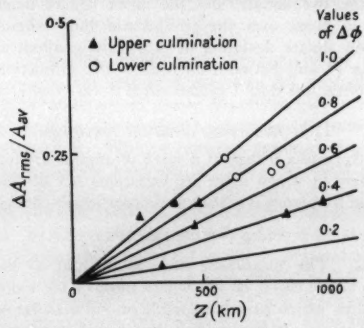

Figure 27. Values of $\Delta A_{rms}/A_{av}$ and $\Delta\phi$ observed simultaneously on a wavelength of 8 m and compared with the values expected at different distances Z from a phase-changing screen with irregularities of size 5 km. (*After* Hewish (1952).)

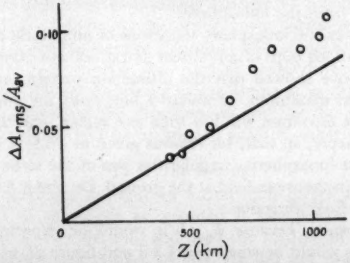

Figure 28. Increase in the amplitude $\Delta A_{rms}/A_{av}$ of the scintillations as a function of the distance Z from a thin diffracting layer assumed to be at a height of 400 km and to produce a r.m.s. phase deviation $\Delta\phi = 0{\cdot}2$ radian. The straight line represents the result of theory and the points the result of experiments made on a given radio star at different angles of elevation. (*After* Hewish (1952).)

nearly overhead (upper culmination) correspond, on the whole, to distances Z which are less than those which correspond to the oblique reception of the radiation when the star was at lower culmination. It appears that the observations could be explained, at least in outline, on the hypothesis that the diffracting layer was relatively thin and that the magnitude of $\Delta A_{rms}/A_{av}$ changed with the inclination of the radiation because the distance between the ground and the layer changed. The results obtained on a wavelength of 6·7 m for a source whose

inclination varied markedly through the day are shown in figure 28. Here the distance Z was calculated on the assumption that the (thin) diffracting layer was at a height of 400 km and the results are seen to agree fairly well with the theoretical curve appropriate to the observed value $\phi_m = 0{\cdot}2$.

In continuation of the work of Hewish, Spencer (1955) used three recorders working on a frequency of 38 Mc/s ($\lambda = 7{\cdot}9$ m) at the corners of a right-angled triangle with one side of length about 700 m (98λ) and the other about 1200 m (167λ). Phase-switching arrangements were used at each recorder to isolate the radiation from one of the intense radio stars, and the excursion of the trace was taken as a measure of the received intensity.

The experiments showed that, when scintillations were present at night, the diffraction pattern produced at the ground had a roughly elliptical correlation function $\rho(\xi, \eta)$ with ratio of axes 5 : 1 or greater. The orientation of the ellipse was found to change as the radio star moved across the sky and was shown to be consistent with the supposition that the ionospheric irregularities causing the diffraction were oriented along the direction of the earth's magnetic field.

With an elongated diffraction pattern of this kind it is only possible, with the available experimental accuracy, to determine the component of the drift velocity perpendicular to the long axis of the pattern. This circumstance seems to explain some of the results which have been reported, especially those which suggested a rather sudden reversal of the drift near midnight. The size of the irregularities, measured across their shortest dimension, was about 3 km, in rough accord with Hewish's value of 5 km.

11.6. *Diffraction by the Solar Corona*

Hewish (1955) has shown that the electron density in the solar corona is irregularly distributed so that the radiation from a radio star is diffracted after passing through it. An interferometer was used to record this radiation on a succession of days and it was found that the ' visibility ' of the fringes was less when the radiation passed nearer to the sun, as shown by the records of figure 29. Now, as shown in § 7.2, the ' visibility ' measures the correlation between the wave-fields at the two aerials of the interferometer and it may be related to the size of the irregularities of electron density in the corona. The analysis which follows is equivalent to that of Hewish, but differs from it in detail.

Suppose a uniform plane wave from a distant radio star passes through a thickness Z of the solar corona in which there are irregularities of electron density with standard deviation N_m and with a spherically symmetrical auto-correlation function $\rho_N(r) = \exp(-r^2/L^2)$. Then the argument of § 6.6 shows that, when the wave emerges, the auto-correlation function of the complex field $\mathbf{f}$ over its wave front is given by

$$\rho_f(\xi) = \exp(-\xi^2/\xi_0^2) \qquad \ldots\ldots(149)$$

where ξ_0 depends on the magnitude of ϕ_m defined by

$$\phi_m = \left(\frac{\pi^{-3/4}\, e^2}{16\epsilon_0 mc}\right) \frac{1}{f} (LZ)^{1/2} N_m. \qquad \ldots\ldots(150)$$

If $$\phi_m < 1, \quad \xi_0 = L \qquad \ldots\ldots(151)$$

and if $$\phi_m > 1, \quad \xi_0 = L/\phi_m. \qquad \ldots\ldots(152)$$

It is also known that the auto-correlation function $\rho_g(\xi)$ of the complex wave-field at the earth is the same as that $\rho_f(\xi)$ of the field as it leaves the corona so that the equations (149), (151) and (152) also determine $\rho_g(\xi)$ and hence the visibility of the recorded fringes.

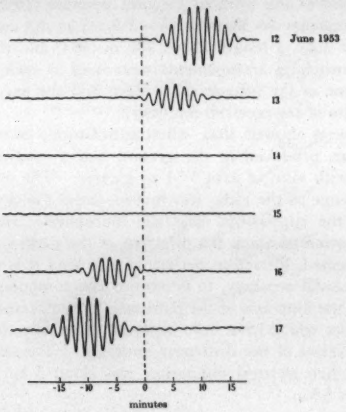

Figure 29. Records of radiation of wavelength 3·7 m from a radio star made with a phase-switched interferometer on successive days as the radiation passed through the solar corona. Zero time represents solar transit. (*After* Hewish (1955).) (*Reproduced by permission of the Royal Society.*)

From the experiments it was possible to estimate ξ_0. The relation of ξ_0 to L, the size of the coronal irregularities, is given by equations (151) and (152) and depends on the magnitude of ϕ_m, which is not known. If, however, experiments are made on more than one frequency, ϕ_m will alter as given by equation (150), and if $\phi_m > 1$ then ξ_0 will also change with frequency, whereas if $\phi_m < 1$, $\xi_0 = L$ at all frequencies. By using different frequencies Hewish was able to show that $\phi_m > 1$ so that the measured ξ_0 was given by

$$\xi_0 = L/\phi_m = \left(\frac{16\epsilon_0 mc}{\pi^{-3/4}e^2}\right)\frac{f}{N_m}\left(\frac{L}{Z}\right)^{1/2}.$$

He then assumed that Z was equal to the radial distance from the centre of the sun, and from his experimental results he obtained a series of possible magnitudes for N_m and for L at different radial distances.

§ 12. Waves reflected from the Ionosphere at Steep Incidence

Experiments have been made, on frequencies near 16, 70, 85, 150, 2000, 4000 and 6000 kc/s, to study the nature of the wave-field received near the ground after reflection from the ionosphere at steep incidence. In these experiments precautions were taken to ensure that only a singly reflected wave was

observed. When it was convenient to use pulses the singly reflected wave was isolated with a ' time-gate ', but even then it was sometimes necessary to guard against the simultaneous reception of two magneto-ionic components by using a circularly polarized aerial. When it was not possible to use pulses existing c.w. or morse transmissions were used, the ground-wave was removed by special aerial arrangements, and observations were made under conditions when the reflection coefficient of the ionosphere was so small that doubly reflected waves were negligible.

For the frequencies which are reflected from the ionosphere, as distinct from those which are transmitted through it, it is not always easy to decide whether the ionosphere impresses mainly a variation of phase or of amplitude, or of both, and there is a corresponding uncertainty in the interpretation of the results. Further difficulties are introduced by the fact that reflection occurs near a level where the refractive index is zero. These, and other, points in the interpretation of the results will be discussed in § 13. First, however, some account will be given of the angular power spectrum and of the auto-correlation function which might be expected at the ground.

12.1. *The Angular Power Spectrum*

The angular power spectrum of the waves returned from the ionosphere can be deduced from the distance correlation observed at the ground. In making this deduction the following points are of importance.

(1) Observations have usually been made only of the amplitude; useful deductions can then be made only if the angular spectrum is assumed to be ' randomly phased ' in the sense of § 8.2.

(2) The relation between $\rho_A(\xi)$ and $\rho_g(\xi)$ observed at the ground depends on the observed magnitude of the ' signal-to-noise ' ratio b [see § 8.3, equations (128) and (129)].

(3) The angular spectrum deduced from given observations will depend on whether it is supposed to be one-dimensional or two-dimensional. It has been shown in § 3.6 that, for narrow angular spectra of the type with which we shall be concerned, the difference is slight.

Once the angular spectrum at the ground is known deductions can be made about the ionospheric irregularities which gave rise to it. These deductions will depend on whether it is supposed that the incident radiation was a plane wave or was spreading from a point. The results of § 8.6 show that, if the distance correlation at the ground is observed to be $\rho_g(\xi)\{z,z\}$ when the wave is returned at vertical incidence from a sender on the ground, then $\rho_f(\xi)$ in the wave on emergence from the ionosphere will be given by $\rho_f(\xi) = \rho_g(2\xi)\{z,z\}$ [see equation (135)] and the size of the structure on the ground will be twice that in the wave at the ionosphere. If, now, the two auto-correlation functions are expressed in terms of corresponding angular spectra so that

$$|\mathbf{F}(S)|^2 \longleftrightarrow \rho_f(\xi) \qquad \ldots\ldots(153)$$

and

$$|\mathbf{G}(S)|^2 \longleftrightarrow \rho_g(\xi)\{z,z\} \qquad \ldots\ldots(154)$$

then

$$|\mathbf{F}(S)|^2 = |\mathbf{G}(\tfrac{1}{2}S)|^2. \qquad \ldots\ldots(155)$$

$|\mathbf{F}(S)|^2$ will then represent the angular spectrum which would be produced if the ionosphere were irradiated by a uniform plane wave. It is this angular spectrum, and not that, $|\mathbf{G}(S)|^2$, observed at the ground, which is directly related to the size of the ionospheric structure, as given by equation (153).

It appears that this point has been missed by all workers on the subject except Briggs and Phillips (1950), and although they emphasized the point they expressed it differently. They considered that if a single scattering centre would return power to the ground according to a law $F(\theta)$ if the layer was irradiated with a plane wave, then if it was irradiated by a point source the scattering law would be $F(2\theta)$. From measurements which they made on $\rho_p(\xi)\{z, z\}$ they deduced the angular spectrum received at the ground with a sender on the ground and specified it by a parameter θ_0. In deducing the size of the ionospheric irregularities from this angular spectrum they made the proper correction for point-source illumination. This explains why the relations between their values of l and θ_0 do not seem to be the same as those of others. In what follows we will make the proper corrections to the results of all workers, and will express them in terms of an angular spectrum of the form

$$|F(\theta)|^2 = \exp(-\theta^2/S_0^2) \qquad \ldots\ldots(156)$$

which would be produced if the layer was irradiated by a plane wave. S_0 will then represent the angle at which the power in the spectrum falls to e^{-1} (0·37) or the amplitude to $e^{-0.5}$ (0·67). With point-source illumination the corresponding diffraction pattern at the ground would be given by $\exp(-\xi^2/l^2)$ with $l = 2/\pi S_0$.

12.2. *Observations on Frequencies between 2 and 7 Mc/s*

12.2.1. *Methods.*

In the frequency range between 2 and 7 Mc/s experiments have been made by Bramley (1951), Briggs and Phillips (1950) and McNicol (1949).

Bramley used a pulsed sender and, at a distance of about 10 km, three receivers at the corners of a right-angled triangle with short sides about 100 m long. He recorded amplitudes A at the three receivers and phase differences ψ between pairs of receivers. The experiments were made by day and were concerned with reflections from the F and E_s layers. From the amplitude measurements he evaluated the magnitude of the quantity $[|\Delta A|]_{av}/A_{av}$ and the magnitude of $\rho_A(\xi)$ for the fixed values of ξ appropriate to the aerial positions (he did not use the method of the drifting pattern). The phase difference between any two aerials varied slowly as though the wave was reflected from an ionosphere of varying tilt, but superimposed on these gradual changes there were more rapid ones caused, presumably, by diffraction processes. Attention was concentrated on the more rapid deviations $\Delta\psi$ from the slower smooth variation.

Briggs and Phillips used three receivers at the corners of a right-angled triangle of short side about 130 m and recorded amplitude alone. They used frequencies of 2·4 and 4·8 Mc/s. Their results for reflection from the F layer were obtained entirely by night on the frequency of 2·4 Mc/s and mainly by night on 4·8 Mc/s. The results for the E layer were obtained entirely by day.

McNicol used a single receiver to record amplitude in the frequency range 2–6 Mc/s.

12.2.2. *Observed amplitude distribution.*

The probability distribution of amplitude in the fading wave was discussed fully by McNicol. He showed that both Rayleigh and displaced Gauss distributions occurred from time to time. Amongst 152 samples investigated he found that the ratio b of specularly reflected to diffusely reflected power was between 0 and 0·25 on 61% of occasions, between 1 and 4 on 25%, and greater than 6 on 14%. Briggs and Phillips found that on most occasions the amplitude distribution was approximately Rayleigh (i.e. $b < 1$). Bramley, who worked mainly by day, found values of b of the order of 4. These different results may be partly accounted for by real differences between night and day.

12.2.3. *Observed angular power spectra.*

Bramley analysed his results in terms of a one-dimensional power spectrum and made allowance for the presence of a specular component corresponding to $b = 2$. For frequencies between 4 and 5 Mc/s he then deduced results which

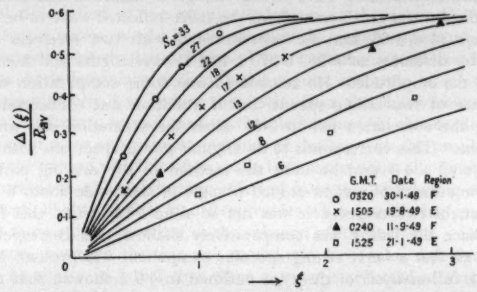

Figure 30. Normalized difference correlation functions expected for two-dimensional auto-correlation functions $\exp(-S^2/S_0^2)$ for different values of S_0, measured in degrees, together with experimental points for four occasions, when S_0 had values approximately 6°, 13°, 17° and 27°. (*After* Briggs and Phillips (1950).)

would correspond to $S_0 = 3{\cdot}6°$ for plane-wave illumination. For frequencies greater than 5 Mc/s the angular spread was smaller, but was difficult to measure.

Briggs and Phillips used the method of the drifting pattern to evaluate the difference auto-correlation function $\Delta(\xi)$, confining their attention to those occasions, which they found to be a majority, when the probability distribution of amplitude was Rayleigh. They compared the observed values of $\Delta(\xi)$ with values calculated for different widths of a two-dimensional angular power spectrum given by $(\cos\theta)^n$. They showed that, for the large values of n which were found to occur in practice, this kind of variation was closely the same as $\exp(-\theta^2/S_0^2)$. Their theoretical curves, labelled in terms of our parameter S_0, are shown for the case of plane-wave illumination in figure 30, together with their experimental results for four occasions. It is clear that the experimental results agree well with the form of the theoretical curve but that the angular spread changes considerably from time to time.

The full analysis by the method of the drifting pattern was performed sufficiently often to show that the assumed form of the angular spectrum was satisfactory. After that it was sufficient to determine the correlation between e.m.f.'s received at two aerials separated by a fixed distance and to use this to estimate the value of S_0. This was done on several occasions and it was found that for the F layer the most probable value of S_0 for plane-wave illumination at night was 8° on a frequency of 2·4 Mc/s, and 4° on 4·8 Mc/s. For the E layer by day the value was 8° for a frequency of 2·4 Mc/s, about the same as for the F layer, but the values for the E_s layer were more variable, and were sometimes quite large.

12.3. *Observations on Frequencies less than* 1 *Mc/s*

(*a*) 70–150 *kc/s*.

Bowhill (1956) used the c.w. radiation from the senders of the Decca radio-navigation system and received at angles of incidence of about 30° on frequencies of 85 and 70 kc/s. He used special aerials to balance out the ground wave. Only at night was the downcoming wave strong enough to measure, and even then the reflection coefficient was small enough for the twice-reflected wave to be neglected.

On 85 kc/s ($\lambda = 3{\cdot}53$ km) he experimented with two receivers separated, successively, by distances of 0·28, 0·57, 1·4, 4·1 wavelengths and measured the correlation of the amplitude. He considered that some complication was caused by the presence of two fading speeds, but if attention was concentrated on the slower fading the correlation fell to 0·61 when the separation was increased to 1·3 wavelengths. This corresponds to an angular power spectrum with $S_0 = 20°$.

On 70 kc/s ($\lambda = 4{\cdot}3$ km) he used the method of the drifting pattern, with receivers at the corners of a right-angled triangle of short side about 6 km ($1{\cdot}4\lambda$) but found that, in two respects, it was not so simple to use on this frequency. In the first place the fading was comparatively shallow, and corresponded to a value of $b \simeq 4$ so that a fairly strong specular component was present, and in the second place a full analysis of the type outlined in § 9.2 showed that the fading was only partially attributable to a steady drift velocity V, and depended to a considerable extent on a component V_c of random velocity. It was, however, possible to deduce V and to apply the method of the drifting pattern, and to allow for the presence of the specularly reflected component. It was found that $\rho(\xi)$ had fallen to 0·61 when $\xi \simeq 1{\cdot}4\lambda$ so that, allowing for point-source illumination, we find $S_0 = 18°$.

Millman (1952) used pulses on 150 kc/s ($\lambda = 2$ km) and received at night at nearly vertical incidence on three aerials at the corners of a triangle of short side about 1·8 km ($0{\cdot}9\lambda$). He recorded both the amplitude and the phase. The amplitude was found to have a Rayleigh probability distribution and the phase excursion was of the order of one radian. The method of the drifting pattern was used to deduce the spatial auto-correlation function $\rho_A(\xi)$ of the amplitude and from this the spread of the angular power spectrum appropriate to plane-wave illumination was found to have a mean value of $S_0 = 14°$.

(*b*) 16 *kc/s*.

Harwood (1954) used the morse transmissions from the 16 kc/s ($\lambda = 18{\cdot}8$ km) sender GBR, received at an angle of incidence of about 30°. He used two receivers

which were placed at different distances apart. Each was connected to an aerial arrangement which balanced out the ground wave, and reasons were given for supposing that the twice-reflected downcoming wave was unimportant.

Although an appreciable downcoming wave was present both by day and by night, the fluctuations were only appreciable at night, and the following results apply only to them. An important specularly reflected component was present in the downcoming wave, and the mean value of b was found to be about 12. The auto-correlation function $\rho_A(\xi)$ of the total amplitude A fell to 0·6 at a distance of 1·5 wavelengths. Since the auto-correlation function $\rho_{\Delta A}(\xi)$ of the variable part of the amplitude is the same as $\rho_A(\xi)$ (see § 6.2) we deduce that $\xi_0 = 2{\cdot}1$ and for plane-wave illumination $S_0 = 17°$.

§ 13. Deductions from Observations of Reflected Waves

13.1. *The Thin Slab Model*

The observations made on the ground would, if they were complete, provide a statistical description of the angular spectrum at the ground, and this, apart from evanescent waves, would be the same as the angular spectrum of the waves as they emerged from the ionosphere. We are often more interested in the sizes of the ionospheric irregularities than in the angular spectrum which they produce, and the main difficulty is to deduce those sizes from the observations. At present there is no satisfactory way of making this deduction ; in this section an account will be given of some approximate methods of dealing with the problem.

An approximation which is often made is to assume that the ionospheric effects are concentrated in a thin slab often referred to as the ' diffracting screen '. It is not, of course, likely that this model represents what actually happens, but its use allows one more step to be taken in the solution of the problem. In the following circumstances, however, the thin slab model may have some real significance.

It will be shown in § 13.2 that when a wave is reflected at vertical incidence the diffraction probably occurs near the level of reflection, where the refractive index is small. This limited region might well be equivalent to a thin slab in the sense here discussed. If the wavelength is sufficiently great the approximation is likely to be more accurate.

If the wave had been returned by sharp reflection at an irregular wrinkled surface the assumption of the thin slab model would be satisfied. This case occurs in the ionosphere when a wave is reflected from the irregular boundary of an ionized meteor trail. It also occurs when a wave is reflected from the irregular surface of the ground or the sea and is important in considering the behaviour of waves returned to the earth after being reflected twice by the ionosphere and once by the ground.

If a thin irregular slab in the ionosphere has variations of electron density across its surface given by $N(x)$, and if it introduces variations in complex amplitude $\mathbf{f}(x)$, then the auto-correlation function $\rho_f(\xi)$ of the complex amplitude is the same as that $\rho_{\Delta N}(\xi)$ of the electron density, provided the amplitude variation ΔA does not exceed one neper, nor the phase variation $\Delta\phi$ one radian (see the summary of § 6.5). The auto-correlation function $\rho_I(\xi)$ is the same as that observed at the ground so that a measurement of the latter will lead to information

about the auto-correlation function $\rho_{\Delta N}(\xi)$ of the electron density. At the ground the condition that $\Delta A < 1$ neper and $\Delta\phi < 1$ radian will still hold. If, conversely, it is found at the ground that $\Delta A < 1$ neper and $\Delta\phi < 1$ radian, then it can be assumed that $\rho_f(\xi)$ as determined at the ground will be the same as $\rho_{\Delta N}(\xi)$ in the thin-slab model ionosphere.

If, however, it is found at the ground that either $\Delta A > 1$ neper or $\Delta\phi > 1$ radian, then it cannot be deduced that $\rho_f(\xi)$ is the same as $\rho_{\Delta N}(\xi)$.

13.2. *Diffraction at Levels where* $\mu \neq 1$

In the examples drawn from the subject of radio astronomy the frequency is so great compared with the plasma frequency of the ionosphere that it may be assumed that the refractive index μ is everywhere nearly unity, and it is possible

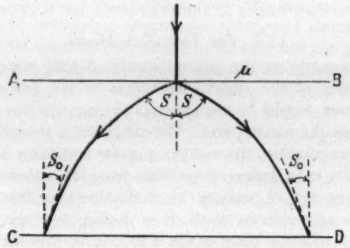

Figure 31. Diffraction occurs at a level AB, where the refractive index is μ, and the diffracted waves emerge into free space at CD.

to neglect refraction of the waves after they have been diffracted. On the contrary, in the case of a wave reflected from the ionosphere at vertical incidence, μ takes all values between 1 and 0 at different parts of the trajectory, and if diffraction occurs at any level where $\mu \neq 1$ the diffracted waves will suffer refraction on their journey to the ground.

To elucidate the main features of the phenomenon consider the case of a plane wave passing through a stratified ionosphere in a direction perpendicular to the planes of stratification and suppose, as indicated in figure 31, that diffraction is caused by irregularities in a thin slab situated in a plane AB where the mean refractive index is μ, and that the waves then pass on to a distant plane CD where $\mu = 1$. Now suppose that the ionospheric irregularities produce a cosinusoidal variation of amplitude $f(X) = \cos(2\pi X/D)$ over the plane AB. Simple theory shows that this variation corresponds to diffracted waves at angles $\pm S$ ($S \equiv \sin\theta$), where $DS = \lambda$ (§ 2.3). But λ is the wavelength in the medium, and is equal to λ_0/μ, where λ_0 is the free-space wavelength, so that

$$DS\mu = \lambda_0. \qquad \ldots\ldots(157)$$

The diffracted waves are now refracted as they pass to the plane CD where $\mu = 1$, and if they arrive there making an angle S_0 then Snell's law, combined with equation (157), shows that

$$S_0 = S\mu = \lambda_0/D. \qquad \ldots\ldots(158)$$

But S_0 is then just the angle at which the diffracted wave would travel if the variation of amplitude, of periodicity D, had been imposed in free space. The same is true of each of the cosinusoidal components of variation across AB which go to make up the Fourier synthesis of a general distribution. We may conclude that if diffraction takes place near any localized plane of stratification in the medium the distribution of amplitude over the plane can be correctly deduced by observing the angular spectrum at the ground and assuming that the diffracting slab is situated in free space, where $\mu = 1$.

It is interesting to consider what would happen if the variations $\mathbf{f}(x)$ of amplitude imposed on the wave in the plane AB had all sizes down to a minimum D_1, in such a way that the Fourier transform $\mathbf{F}(S)$ of $\mathbf{f}(x)$ had components of all spatial periods greater than D_1 with equal power, but that none was present with spatial period less than D_1. Then the angular spectrum in the slab would extend to $S = \pm \lambda_0/\mu D_1$ and if $\mu D_1 < \lambda_0$ would include values of $S > 1$, corresponding to evanescent waves. Only those with $S \leqslant 1$ would contribute to the spectrum of travelling waves, and as this spectrum travels from the slab into free space the limiting waves are refracted so that, on emergence into free space, the limit is $S_0 = \mu$. In this case the limit S_0 to the angular spectrum would provide a measure of the refractive index μ at the level where diffraction occurred. If, on the other hand, $\mu D_1 > \lambda_0$, then the limit to the angular spectrum at the plane AB would be given by $S = \pm \lambda_0/\mu D_1$ and this would correspond, on emergence into free space, to an angle $S_0 = \mu S = \lambda_0/D_1$ and a measurement of S_0 would then provide a value for D_1.

If the problem is one of reflection from a point-source on the ground, instead of refraction of a parallel beam of radiation, a factor 2 must be inserted into the above expressions as explained in § 12.1.

13.3. *Conclusions from Experiments*

The results of the experiments described in § 12 are summarized in the table. It should be emphasized that these results do not refer to comparable conditions in the ionosphere. Some refer to the F layer and some to the E layer, and in the

Reference	H	B	B	M	B & P	B & P	Br
Frequency (kc/s)	16	70	85	150	2400	4800	4000 } 5000 }
Wavelength (m)	18700	4300	3500	2000	125	62·5	67
S_0 (radians)	0·30	0·31	0·35	0·25	0·14	0·07	0·063
S_0 (degrees)	17	18	20	14	8	4	3·6
S/N ratio b	12	4	—	<1	<1	<1	4
ξ_0	2·1	1·0	0·91	1·3	2·3	4·6	5
L (m)	20500	4300	3700	2600	290	290	340

H = Harwood ; B = Bowhill ; M = Millman ; B & P = Briggs and Phillips ; Br = Bramley.

E layer the lower frequencies were reflected from lower down. Most of the results refer to night, but some of those on the higher frequencies refer to day. The information is too scrappy to permit the making of deductions about what happens at different levels in the ionosphere, and in what follows an attempt will be made to see whether it can all be explained in terms of ionospheric irregularities which

are similar at all heights. Some recent work of Bowhill (1956) suggests that the overall result may be more complicated than is apparent from the table and that there may be two different mechanisms producing fading, one on the lower frequencies and the other on the higher frequencies, and that in the neighbourhood of 80 kc/s the two phenomena occur together in varying degree. In what follows these new suggestions will not be considered and the implications of the table will be discussed in their simplest terms. When more work has been done along the lines suggested by Bowhill the conclusions may need modification in detail.

The most striking point about the results in the table is that the angular spread appears to be roughly constant from the lowest frequencies up to somewhere between 150 and 2400 kc/s and then to decrease as the frequency is increased. For the greater frequencies the angular spread is approximately inversely proportional to frequency as is shown by the approximate constancy of the quantity

$$L = \lambda_0 \xi_0 = \lambda_0 / \pi S_0.$$

Booker (1955) has suggested that this may come about in the following way. Suppose that most of the diffraction occurs in a localized slab at a level where the refractive index is μ, and that the variations $\mathbf{f}(X)$ of amplitude imposed on the wave have all sizes down to a minimum D_1, in the sense discussed in § 13.1. Then, as shown in that section, the angular spectrum observed at the ground would extend to $\pm S_1$ where

$$S_1 = \mu \quad \text{if} \quad \lambda_0 > \mu D_1 \qquad \ldots\ldots(159)$$

and

$$S_1 = \lambda_0 / D_1 \quad \text{if} \quad \lambda_0 < \mu D_1. \qquad \ldots\ldots(160)$$

Booker supposed that, for those frequencies for which $S_0 \simeq 0{\cdot}3$ radian, equation (159) is appropriate and shows that $\mu = 0{\cdot}3$, and that the other results, which roughly fit the law $S_1 \propto \lambda_0$, correspond to equation (160).

If this over-simplified picture were taken to be strictly accurate the distance D_1 could be estimated by noting that the transition from S_0 independent of frequency to S_0 dependent on frequency should occur when $\lambda_0 = \mu D_1$. The table shows that the corresponding value of λ_0 lies between 125 and 2000 m, so that D_1 lies between 400 and 6700 m.

The experiments do not suggest that there is any sharp cut-off in the angular spectrum, and it is probably more satisfactory to make estimates of the size of the structure in the diffracting slab by assuming that, for the higher frequencies, $\lambda_0 < \mu D_1$. The discussion of § 13.1 then shows that, for these frequencies, the structure of the slab is related to the angular spectrum at the ground as though propagation were in free space throughout, and the auto-correlation function of the wave-amplitude in the diffracting slab would be the same as that over the ground. If, in accord with the results of Briggs and Phillips (1950), the auto-correlation function is assumed to have the form $\rho(\xi) = \exp(-\xi^2/\xi_0^2)$ with ξ and ξ_0 measured in terms of λ as a unit, the observed magnitudes of ξ_0 are shown in the table, together with the magnitudes of $L = \lambda_0 \xi_0$. The mean value of L determined from the results on wavelength less than 200 m, where S_0 is proportional to wavelength, is about 300 m. This implies that the auto-correlation of the irregularities in the emerging wave would drop to e^{-1} in a distance of 300 m. If it could be assumed that $\phi_m < 1$ (see summary of § 6.5) then this length would represent the 'size' of the ionospheric

irregularities. Unfortunately this assumption cannot, at present, be properly justified and there is a possibility that $\phi_m > 1$ and that the ' size ' of the ionospheric irregularities is 300 ϕ_m.

In the model here discussed it is supposed that the important contributions to diffraction occur at a level where $\mu \simeq 0{\cdot}3$. Booker (1955) has suggested that this is because, near the level where $\mu = 0$, scattering from ionospheric irregularities is likely to be enhanced by a process of resonance first mentioned by Herlofson (1951).

If the explanation in terms of resonant scattering is accepted it appears that the following deductions can be made about the ionospheric irregularities.

(*a*) The irregularities measured in any experiment are situated near the level at which the waves are reflected.

(*b*) The regular and irregular drift movements which are deduced from the measurements apply to this level.

(*c*) The magnitude of L is of the order 300 m both for F and E regions, but, as pointed out above, this only sets a lower limit to the size of the ionospheric irregularities.

The irregular drift velocities, of the order of V_c, are small compared with the regular drift velocities (V) at the higher frequencies, but V_c and V become comparable at frequencies in the neighbourhood of 70 kc/s. At 16 kc/s V_c is so much greater than V that the regular drift velocity cannot be determined. The regular drift movements have been fully discussed by Briggs and Spencer (1955).

§ 14. Some Miscellaneous Points

14.1. *Reflection from Randomly Moving Irregularities*

It is not easy to understand precisely how a wave is reflected at vertical incidence from a horizontally stratified ionosphere which contains random irregularities of electron density. In most work on the subject, and in this report, it is assumed that diffractive effects occur independently of the process of reflection and lead to diffracted waves travelling in the same direction as the main wave. It is, however, possible that, near the level where $\mu = 0$, irregularities of electron density scatter radiation *backwards* out of the up-going wave. In an early discussion of ionospheric diffraction (Ratcliffe 1948) it was assumed that these irregularities might be moving randomly in all directions, so that their velocities in the line-of-sight were distributed with a probability

$$p(V) \propto \exp(-V^2/2V_0^2). \qquad \ldots\ldots(161)$$

It was then possible to determine the Doppler shifts at each reflection and to show that the back-scattered wave would have a (temporal) power spectrum given by

$$|F(n)|^2 \propto \exp\{-c^2(n-n_0)^2/8n_0^2V_0^2\}, \qquad \ldots\ldots(162)$$

where n = frequency, n_0 = frequency of incident wave, c = velocity of light.

From this power spectrum the characteristics of the fading could be deduced. Several workers have used this analysis in the examination of experimental results and have derived values for the quantity V_0 which represents the root-mean-square velocity of the randomly moving scattering irregularities. The order of magnitude of this quantity has usually been found to be 5 m sec^{-1}.

Unfortunately there is an error in this suggested mechanism for fading, as follows. If an irregularity moving in the line of sight with velocity V is situated in a place where the mean refractive index is μ the Doppler shift of the wave scattered backwards is $2\mu V/c$ and not $2V/c$ as was assumed in the original analysis. The quantity which is determined from analysis of fading is then μV_0. Now irregularities in the medium which correspond to changes in the refractive index will scatter an energy backwards proportional to $\Delta\mu/\mu$ and this is only likely to be great near where $\mu = 0$. It follows that the values quoted for V_0 in the literature may be considerably too small, and it does not seem easy to decide how much too small. Probably μ should be taken to be 0·1 or smaller, in which case the correct result for the root mean square line-of-sight velocity would be more nearly 50 m sec^{-1}.

If the irregularities had random velocities of the same mean square magnitude *across* the line of sight they would constitute an irregular diffractive reflector of the kind previously considered in this report, and if its random changes were described in terms of the 'characteristic random velocity' V_c introduced in § 9.2 then $V_c \simeq V_0$. Moreover it has been shown in § 13.2 that, even if such a reflector were situated at a level where the refractive index was different from unity, the velocity V_c would still be measured correctly at the ground.

The present position is probably best summarized as follows. Fading on the higher frequencies (> 1 Mc/s) is predominantly caused by the drift of an irregular ionosphere, and not much by the random changing of its form. On lower frequencies V and V_c are of the same order and V_c represents either (*a*) the random components of the velocity in the horizontal plane or (*b*) μ times the random components of velocity in the line of sight (i.e. nearly vertically), where $\mu \leqslant 0{\cdot}1$. If random components were equally distributed in all directions the horizontal ones would alone be noticed. It appears best, therefore, to abandon the original idea of velocities in the line of sight, and to suppose that V_c represents the random component of velocity in the horizontal plane.

14.2. *Diffraction from Meteor Trails*

A meteor travelling through the ionosphere leaves behind it a straight line of ionized gas, which may subsequently drift, or become distorted. Immediately after it is formed the trail behaves like a one-dimensional straight reflector, and as its head passes the foot of the perpendicular drawn to it from a radar station the recorded echo exhibits Fresnel straight-edge diffraction maxima and minima. The amplitude of the echo then decreases without fluctuating for a short time until the random movements have rendered the ionization 'rough' in the sense that its boundary is irregular to a depth of the order of $\frac{1}{4}\lambda$, and from then onwards the echo is returned as if from an irregular reflector, so that it shows fading with a Rayleigh distribution.

The rate of fading in this case can probably be correctly explained in terms of the irregular velocities in the line of sight, as discussed in § 14.1, and the root-mean-square velocity is found to be about 15 m sec^{-1}. With velocities of this order it would take a straight trail a time of about 0·2 sec to become 'rough' if the wavelength were 8 m. This prediction agrees with the experimental results which also confirm that the time elapsing before the start of fading is proportional to the wavelength.

There is evidence that, at a later stage, the trail often breaks up into comparatively large pieces, each of which is irregular, and which drift apart, so as to produce quasi-periodic fading superimposed on the random fading.

14.3. *Quick Methods of Analysis*

In many experiments the aim has been to deduce the mean horizontal velocity of drift of the ionosphere, without determining either the size of the random structure or the 'equivalent random velocity'. For this purpose special circuits have been used to record the time-intervals τ_x and τ_y between the maxima on pairs of records made at two points separated along the X- and Y-axes. It is then possible to find average values of these two time intervals quickly, and to deduce the drift.

In experiments of this kind there are always considerable variations of τ about their mean values, and it has been shown (Ratcliffe 1954) that this is just what would be expected with a diffraction pattern which had a random shape, even if it did not also change as it moved. If, in addition, the pattern changes as it moves it is not easy to deduce the 'equivalent random velocity' from observed values of τ_x and τ_y but it has been shown in principle how it could be done. It is more satisfactory for this purpose to record the wave-amplitude and to use the full analysis of Briggs, Phillips and Shinn (1950), and the extension of this analysis to an anisometric pattern by Phillips and Spencer (1955).

14.4. *Spaced-Aerial Direction Finders*

In spaced-aerial direction finders measurements of the difference $[\phi(x)-\phi(x+d)]$ of phase between two aerials a distance d apart are used to determine the direction θ of arrival of the wave. In the case where the waves arrive in a direction nearly normal to the line joining the two aerials,

$$2\pi\theta d = \phi(x)-\phi(x+d). \qquad \ldots\ldots(163)$$

If the wave is returned from an irregular ionosphere of such a type that there is no specular component and the fading has a Rayleigh distribution, then it has been shown in § 8.4 that

$$[\,|\,\phi(x)-\phi(x+d)\,|\,]_{\text{av}} = \sqrt{2}\pi S_0 d \qquad \ldots\ldots(164)$$

where S_0 is defined by equation (156). It follows that

$$[\,|\,\theta\,|\,]_{\text{av}} = S_0/\sqrt{2} \qquad \ldots\ldots(165)$$

so that a measure of S_0 gives a measure of the mean deviation (without regard to sign) of the observed direction of arrival. This relation no longer holds if there is an appreciable component of specularly reflected wave.

APPENDICES

1. *The Convolution Theorem*

Let $$\mathbf{F}(S) \longleftrightarrow \mathbf{f}(x) \qquad \ldots\ldots(A1.1)$$

and $$\mathbf{G}(S) \longleftrightarrow \mathbf{g}(x) \qquad \ldots\ldots(A1.2)$$

so that $$\mathbf{F}(S) = \int_{-\infty}^{+\infty} \mathbf{f}(x) \exp(-2\pi i S x)\, dx \qquad \ldots\ldots(A1.3)$$

and $$\mathbf{g}(x) = \int_{-\infty}^{+\infty} \mathbf{G}(S) \exp(2\pi i S x)\, dS. \qquad \ldots\ldots(A1.4)$$

Then $$\int_{-\infty}^{+\infty} \mathbf{f}(\xi)\,\mathbf{g}(x-\xi)\,d\xi = \int_{-\infty}^{+\infty}\int_{-\infty}^{+\infty} \mathbf{f}(\xi)\{\mathbf{G}(S)\exp[2\pi i S(x-\xi)]\,dS\}\,d\xi$$

$$= \int_{-\infty}^{+\infty} \mathbf{F}(S)\,\mathbf{G}(S)\exp(2\pi i S x)\,dS. \qquad \ldots\ldots(A1.5)$$

This may be written $$\int_{-\infty}^{+\infty} \mathbf{f}(\xi).\mathbf{g}(x-\xi)\,d\xi \longleftrightarrow \mathbf{F}(S).\mathbf{G}(S). \qquad \ldots\ldots(A1.6)$$

The expression on the left-hand side of the equation is a function of x which is called the 'convolution' of $\mathbf{f}(x)$ and $\mathbf{g}(x)$. Equation (A1.6) is called the 'convolution theorem'. It may be stated in words as follows:

"The Fourier transform of the product of two functions is the convolution of their Fourier transforms."

2. *Parseval's Theorem*

In equation (A1.5) replace ξ by y, and let $\mathbf{g}(y) = \mathbf{f}^*(-y)$, so that $\mathbf{G}(S) = \mathbf{F}^*(S)$ and we obtain

$$\int_{-\infty}^{+\infty} \mathbf{f}(y)\,\mathbf{f}^*(y-x)\,dy = \int_{-\infty}^{+\infty} \mathbf{F}(S)\,\mathbf{F}^*(S)\exp(2\pi i S x)\,dS. \qquad \ldots\ldots(A2.1)$$

If, in (A2.1), x is written equal to zero there results

$$\int_{-\infty}^{+\infty} |\,\mathbf{f}(y)\,|^2\,dy = \int_{-\infty}^{+\infty} |\,\mathbf{F}(S)\,|^2\,dS. \qquad \ldots\ldots(A2.2)$$

This is Parseval's theorem.

3. *The Wiener–Khintchine Theorem*

In equation (A2.1) write $y-x=w$ so that

$$\int_{-\infty}^{+\infty} \mathbf{f}(w+x)\,\mathbf{f}^*(w)\,dw = \int_{-\infty}^{+\infty} |\,\mathbf{F}(S)\,|^2\exp(2\pi i S x)\,dS. \qquad \ldots\ldots(A3.1)$$

But, by definition, the left-hand side of this equation is $\rho_f(x)$, the auto-correlation function of $\mathbf{f}(w)$, so that, from (A3.1)

$$\rho_f(x) \longleftrightarrow |\,\mathbf{F}(S)\,|^2. \qquad \ldots\ldots(A3.2)$$

This is the Wiener–Khintchine theorem.

4. *Relations between Correlation Functions*

(*a*) Let $$\mathbf{f}(x) = \mathbf{a}+\mathbf{g}(x), \quad [\mathbf{g}(x)]_{av} = 0$$

$$\mathbf{f}_1 = \mathbf{f}(x) \qquad \mathbf{g}_1 = \mathbf{g}(x)$$

$$\mathbf{f}_2 = \mathbf{f}(x+\xi) \qquad \mathbf{g}_2 = \mathbf{g}(x+\xi)$$

$$\rho_f(\xi) = \frac{[\mathbf{f}_1\mathbf{f}_2^*]_{av} - |\,\mathbf{f}_{av}\,|^2}{[\mathbf{f}\mathbf{f}^*]_{av} - |\,\mathbf{f}_{av}\,|^2} \qquad \rho_g(\xi) = \frac{[\mathbf{g}_1\mathbf{g}_2^*]_{av}}{[\mathbf{g}\mathbf{g}^*]_{av}}.$$

Then $$\rho_f(\xi) = \frac{[(\mathbf{a}+\mathbf{g}_1)(\mathbf{a}^*+\mathbf{g}_2^*)]_{av} - |\,\mathbf{a}\,|^2}{[(\mathbf{a}+\mathbf{g})(\mathbf{a}^*+\mathbf{g}^*)]_{av} - |\,\mathbf{a}\,|^2}$$

$$= [\mathbf{g}_1\mathbf{g}_2^*]_{av}/[\mathbf{g}\mathbf{g}^*]_{av} = \rho_g(\xi).$$

Hence $$\rho_f(\xi) = \rho_g(\xi). \qquad \ldots\ldots(A4.1)$$

(*b*) Let $$r_f(\xi) = [\mathbf{f}_1\mathbf{f}_2^*]_{av}/[\mathbf{ff}^*]_{av},$$

Then $$r_f(\xi) = \frac{|\mathbf{a}|^2 + [\mathbf{g}_1\mathbf{g}_2^*]_{av}}{|\mathbf{a}|^2 + [\mathbf{gg}^*]_{av}}$$

$$= \frac{|\mathbf{a}|^2/[|\mathbf{g}|^2]_{av} + [\mathbf{g}_1\mathbf{g}_2^*]_{av}/[|\mathbf{g}|^2]_{av}}{|\mathbf{a}|^2/[|\mathbf{g}|^2]_{av} + 1}$$

$$= \frac{b + \rho_g(\xi)}{b+1} \qquad \text{.....(A4.2)}$$

where $$b = |\mathbf{a}|^2/[|\mathbf{g}|^2]_{av}. \qquad \text{.....(A4.3)}$$

Also, from equations (A4.1) and (A4.2)

$$r_f(\xi) = \frac{b + \rho_f(\xi)}{b+1}. \qquad \text{.....(A4.4)}$$

5. *The Difference Correlation Function*

Let $A(x) = A_1$ and $A(x+\xi) = A_2$ and write $\delta = |A_1 - A_2|$, and $\delta_{av} = \Delta_A(\xi)$. Then $\Delta_A(\xi)$ is called the difference correlation function of the quantity A. Sometimes δ has a (half) Gaussian distribution so that $[\delta^2]_{av} = \frac{1}{2}\pi\delta_{av}{}^2$.

Then $$[(A_1 - A_2)^2]_{av} = [A_1^2]_{av} + [A_2^2]_{av} - [2A_1A_2]_{av}$$

or $$[A_1A_2]_{av} = [A^2]_{av} - \tfrac{1}{2}[\delta^2]_{av}$$

$$= [A^2]_{av} - \tfrac{1}{4}\pi(\delta_{av})^2$$

$$= [A^2]_{av} - \tfrac{1}{4}\pi[\Delta_A(\xi)]^2. \qquad \text{.....(A5.1)}$$

Hence $$r_A(\xi) = [A_1A_2]_{av}/[A^2]_{av}$$

$$= 1 - \tfrac{1}{4}\pi[\Delta_A(\xi)]^2/[A^2]_{av}$$

or $$[\Delta_A(\xi)]^2 = (4/\pi)[A^2]_{av}\{1 - r_A(\xi)\}. \qquad \text{.....(A5.2)}$$

Also $$\rho_A(\xi) = \frac{[A_1A_2]_{av} - (A_{av})^2}{[A^2]_{av} - (A_{av})^2}. \qquad \text{.....(A5.3)}$$

If A has a Rayleigh distribution, so that

$$[A^2]_{av} = \frac{4}{\pi}(A_{av})^2 \qquad \text{.....(A5.4)}$$

then from (A5.1), (A5.2), (A5.3) and (A5.4) it can be shown that

$$[\Delta_A(\xi)]^2 = \frac{4(4-\pi)}{\pi^2}\{1 - \rho_A(\xi)\}. \qquad \text{.....(A5.5)}$$

6. *A Medium which produces Changes of Amplitude and Phase*

Let a wave of length λ pass normally through a slab of thickness ΔZ so that it emerges with a distribution of complex amplitude given by

$$\mathbf{f}(x) = \exp\{i\boldsymbol{\varphi}(x)\}$$

where $$\boldsymbol{\varphi}(x) = 2\pi(\Delta Z/\lambda)\,\boldsymbol{\mu}(x)$$

and $\mu(x)$ is a complex refractive index, as discussed in § 3.5. For most media

$$[\mu(x)]^2 = 1 + AN\exp(i\psi) \qquad \ldots\ldots(A6.1)$$

where A and ψ are real constants characteristic of the medium and N is the molecular (or the electronic) number density. For the case of the ionosphere, with the earth's magnetic field neglected,

$$\tan\psi = -\nu/\omega \qquad \ldots\ldots(A6.2)$$

where ν is the electron collision frequency and ω is the angular frequency of the wave.

If the density in the slab varies with distance x along it, so that its departure from the mean is given by $\Delta N(x)$, then $\mu(x)$ departs from its mean value by an amount

$$\Delta\mu(x) = (A/2\mu)\exp(i\psi).\Delta N(x)$$

and the phase φ varies from its mean value by

$$\Delta\varphi(x) = (\pi A\Delta Z/\mu\lambda)\exp(i\psi).\Delta N(x). \qquad \ldots\ldots(A6.3)$$

In cases of practical interest, where the absorption is not too great, $\mu \simeq \mathscr{R}(\mu)$ and $\mu\lambda \simeq \lambda_0$, the free-space wavelength. With Δz written for $\Delta Z/\lambda_0$ equation (A6.3) then becomes

$$\Delta\varphi(x) \simeq (\pi A\Delta z)\exp(i\psi).\Delta N(x) \qquad \ldots\ldots(A6.4)$$

$$\simeq C\exp(i\psi).\Delta N(x) \qquad \ldots\ldots(A6.5)$$

where

$$C = \pi A\Delta z. \qquad \ldots\ldots(A6.6)$$

7. *The Visibility of Young's Double-slit Interference Fringes*

In figure 32 let an incoherent source in the plane OX illuminate two slits at A and B and let the resulting Fraunhofer diffraction fringes be observed in the

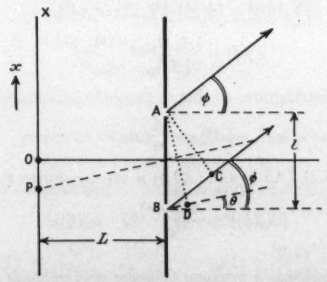

Figure 32. To illustrate a calculation of the visibility of Young's interference fringes.

direction BC. Then if all the angles are small the path difference for light coming from the point P on the source is

$$\mathrm{BC} - \mathrm{BD} = l(\phi - \theta).$$

If the element of the source at P emits power $|\mathbf{f}(x)|^2\,dx$ the power in the corresponding fringes is given by

$$|\mathbf{f}(x)|^2\,dx\{1+\cos 2\pi l(\phi-\theta)\}$$

if l is measured in wavelengths. Each element in the source will produce its own set of fringes in which, because the source is incoherent, the powers will add, so that the total power $P(\phi)$ is given by

$$P(\phi)=\int_{-\infty}^{+\infty}|\mathbf{f}(x)|^2\{1+\cos 2\pi l(\phi-x/L)\}\,dx$$

where x/L is written for θ and it is assumed that the source does not extend far enough to invalidate this approximation. If now the source is assumed to be symmetrical we obtain

$$P(\phi)=\int_{-\infty}^{+\infty}|\mathbf{f}(x)|^2\,dx\left[1+\frac{\int_{-\infty}^{+\infty}|\mathbf{f}(x)|^2\cos(-2\pi lx/L)\,dx}{\int_{-\infty}^{+\infty}|\mathbf{f}(x)|^2\,dx}\cos 2\pi l\phi\right]$$

which represents a set of fringes with visibility V given by

$$V=\left\{\int_{-\infty}^{+\infty}|\mathbf{f}(x)|^2\cos(-2\pi lx/L)\,dx\right\}\Big/\left\{\int_{-\infty}^{+\infty}|\mathbf{f}(x)|^2\,dx\right\}.$$

This is the normalized Fourier transform of the distribution $|\mathbf{f}(x)|^2$ of power over the source.

8. *Probability Distributions*

(*a*) *Rayleigh distribution.*

The Rayleigh distribution is given by

$$P_1(x)=(2x/x_m^2)\exp(-x^2/x_m^2).$$

In this distribution

$[x^2]_{av}=x_m^2$	(mean square value)
$x_{av}=\frac{1}{2}\pi^{1/2}x_m$	(mean value)
$x_p=x_m/\sqrt{2}$	(most probable value)

(*b*) *Gauss distribution, or normal distribution.*

The Gauss distribution is given by

$$P_2(x)=[1/(2\pi)^{1/2}x_m]\exp(-x^2/2x_m^2).$$

In this distribution

$[x^2]_{av}=x_m^2$	(mean square value)
$[\,|x|\,]_{av}=\sqrt{(2/\pi)}\,x_m$	(mean magnitude)
$x_p=0$	(most probable value)
$x_{av}=0$	(algebraic mean value)

9. *Diffraction of the Radiation from a Point Source*

In figure 33 let radiation from a point source at P reach a diffracting screen XX′ at the point A and then be re-radiated to a point Q on a plane of observation YY′. The path difference PAQ − PBQ is then given approximately by

$$\mathrm{PAQ}-\mathrm{PBQ}\simeq\tfrac{1}{2}(\mathrm{AC})^2\left(\frac{1}{\mathrm{PC}}+\frac{1}{\mathrm{CQ}}\right)$$

$$\simeq\tfrac{1}{2}\left\{x-\left(\frac{z_1}{z_1+z_2}\right)\xi\right\}^2\left(\frac{1}{z_1}+\frac{1}{z_2}\right)\simeq\tfrac{1}{2}\{x-\alpha\xi\}^2\frac{1}{\alpha z_2}$$

where $\alpha = z_1/(z_1+z_2)$.

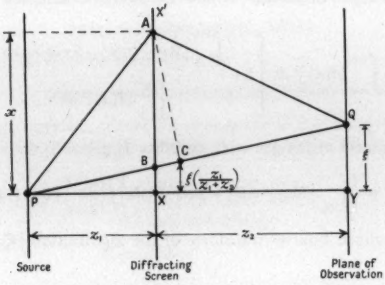

Figure 33. To illustrate diffraction of radiation from a point source.

If, at the point A, the screen transmits an amplitude $f(x)\,dx$ then the resultant amplitude $g(\xi)$ at Q is given by

$$\int_{-\infty}^{+\infty}\exp\left\{\frac{i\pi(x-\alpha\xi)^2}{\alpha z_2}\right\}f(x)\,dx$$

and may be written $g(\alpha\xi, \alpha z_2)$, a function of $\alpha\xi$ and αz_2. Now suppose that the geometry of the situation is altered, but that $\alpha\xi$ and αz_2 are kept constant, then the diffraction pattern on the observing screen will still be represented by $g(\alpha\xi, \alpha z_2)$ and will have the same shape as before, but the scale will have changed because α has changed.

10. *Average Distance between Maxima*

Rice (1944, equation (3.6-6)) has shown that, if a function $f(x)$ has an auto-correlation function $\rho(\xi)$, then the average distance X between maxima of $f(x)$ is given by

$$X = 2\pi\left[-\frac{(\partial^2\rho/\partial\xi^2)_0}{(\partial^4\rho/\partial\xi^4)_0}\right]^{1/2}.$$

If $\rho(\xi) = \exp(-\xi^2/\xi_0^2)$ this gives $X = 2\pi[\xi_0^2/6]^{1/2} = 2{\cdot}6\xi_0$.

Bibliography

Ament, W. S., 1953, *Proc. Inst. Radio Engrs, N.Y.*, **41**, 142.
Toward a theory of reflection by a rough surface.

Banerji, R. B., 1953, *Proc. Phys. Soc.* B, **66**, 105.
Some studies on random fading characteristics.
Shows that the probability distribution of $\delta_A(\xi)$ (see § 6.2.3 of this report) for a fading wave is not closely related to the probability distribution of line-of-sight velocities, and that it is not seriously altered by the presence of a specularly reflected component.

Berg, H., 1955, *The Physics of the Ionosphere* (London : Physical Society), p. 104.
Zur Deutung der Wanderung von Feldstärkeschwankungen als Ionosphärenwinde.
Concerns the analysis of records made at three points simultaneously.

Bergman, P. G., 1946, *Phys. Rev.*, **70**, 486.
Propagation of radiation in a medium with random inhomogeneities.
A somewhat complicated treatment restricted to methods of ray optics.

Booker, H. G., 1955, *J. Atmos. Terr. Phys.*, **7**, 343.
On the level at which fading is imposed on waves reflected vertically from the ionosphere.
Points out that scattering by irregularities in and near the classical reflecting stratum is nearly as important a mechanism for returning energy as classical internal reflection itself.

Booker, H. G., and Clemmow, P. C., 1950, *Proc. Instn Elect. Engrs*, Pt. III, **97**, 11.
The concept of an angular spectrum of plane waves, and its relation to that of polar diagram and aperture distribution.

Booker, H. G., and Gordon, W. E., 1950, *Proc. Inst. Radio Engrs, N.Y.*, **38**, 401.
A theory of radio scattering in the troposphere.
Many of the ideas in this paper can be taken over in the consideration of ionospheric scattering at oblique incidence.

Booker, H. G., Ratcliffe, J. A., and Shinn, D. H., 1950, *Phil. Trans. Roy. Soc.* A, **242**, 579.
Diffraction from an irregular screen with applications to ionospheric problems.
A combination of the ideas of the angular spectrum and the statistics of ' noise ' to deal with the problem of diffraction by a random screen, and an outline of how the analysis can be applied to ionospheric problems. No detailed consideration of experimental results. No discussion of phase-changing screens.

Bowhill, S. A., 1956, *J. Atmos. Terr. Phys.*, **8**, 129.
The fading of radio waves of frequencies between 16 and 2400 kc/s.
Experiments made at vertical incidence on 85 and 70 kc/s gave the angular spread of the downcoming wave. There was evidence of different diffracting mechanisms at work on frequencies above and below 80 kc/s.

Bramley, E. N., 1951, *Proc. Instn Elect. Engrs*, Pt. I, **98**, 19.
Diversity effects in spaced-aerial reception of ionospheric waves.
Develops the theory of a random ' cone ' of downcoming waves from first principles, taking over many of the methods introduced by Rice for the analogous problem of time-varying ' noise '. Stresses in particular the effect of a steady ' specularly reflected ' component in the spectrum. Derives expressions particularly appropriate in direction-finding work. The paper contains most of the fundamental mathematics of diffraction by random media.

Bramley, E. N., 1954, *Proc. Roy. Soc.* A, **225**, 515.
The diffraction of waves by an irregular refracting medium.
Shows how the results of Bramley (1955) lead to the same conclusion as that of Fejer (1953) concerning the passage of a wave through a thick irregular medium.

Bramley, E. N., 1955, *Proc. Instn Elect. Engrs*, B, **102**, 533 (paper 1713 R).
Some aspects of the rapid directional fluctuations of short radio waves reflected at the ionosphere.
In the appendix the theory is developed for an ionosphere in which the electron density varies irregularly and in which the collision frequency cannot be neglected.

The passage of waves through a thick medium of this type is considered. Experiments are described which deal with the rapid 'angle flicker' of short waves reflected at vertical and at oblique incidence and evidence is presented to show that the angle flicker of waves reflected from the F region is caused by their passage through the E region.

BRIGGS, B. H., 1951, *Proc. Phys. Soc.* B, **64**, 255.
An investigation of certain properties of the ionosphere by means of a rapid frequency-change experiment.

BRIGGS, B. H., and PAGE, E. S., 1955, *The Physics of the Ionosphere*, 1954 (London : Physical Society), p. 119.
An empirical study of random functions which arise in the interpretation of ionospheric movements.

BRIGGS, B. H., and PHILLIPS, G. J., 1950, *Proc. Phys. Soc.* B, **63**, 907.
A study of the horizontal irregularities of the ionosphere.
Diffraction from a thin reflecting screen irregular in two dimensions is considered by taking the case of irregularities which scatter power like $(\cos\theta)^n$. The results are related to those for an auto-correlation coefficient which falls to 0·5 in a distance l.
Experiments are described from which the spread of the angular spectrum and the magnitude of l are deduced, for waves of frequencies 2·4 and 4·8 Mc/s, reflected from E and F regions.

BRIGGS, B. H., PHILLIPS, G. J., and SHINN, D. H., 1950, *Proc. Phys. Soc.* B, **63**, 106.
The analysis of observations on spaced receivers of the fading of radio signals.
Shows how it is possible to analyse records of the time variation of a function $f(x, y, t)$ made at three places $0, 0$; $x, 0$; and $0, y$ so as to find (*a*) the velocity V of drift of the pattern of f, (*b*) the 'characteristic random velocity' V_c with which the pattern alters, and (*c*) the correlation function $\rho(\xi)$ of the pattern, assumed isometric.

BRIGGS, B. H., and SPENCER, M., 1954, *Rep. Progr. Phys.*, **17**, 245 (London : Physical Society).
Horizontal movements in the ionosphere. A survey of experimental results.

BRIGGS, B. H., and SPENCER, M., 1955, *The Physics of the Ionosphere* (London : Physical Society), p. 123.
The variability of time shifts in measurements of ionospheric movements.
This paper and that by Briggs and Page (1955) discuss the analysis of records from three receivers when only the time differences between maxima are recorded.

BROWN, R. H., and TWISS, R. Q., 1954, *Phil. Mag.*, **45**, 663.
A new type of interferometer for use in radio astronomy.
The instantaneous amplitudes of narrow-band radio noise received at two places from a radio star are considered and it is shown that the correlation between them contains information about the angular size of the radio star.

CHANDRASEKHAR, S., 1952, *Mon. Not. R. Astr. Soc.*, **112**, 475.
A statistical basis for the theory of stellar scintillation.
Develops the statistics of rays refracted in a thick medium with random variations of refractive index. Does not consider diffraction.

DISCUSSION ON STELLAR SCINTILLATIONS, 1954, *Quart. J. Roy. Met. Soc.*, **80**, 241.
Deals with the scintillation of stars observed in visible light.
Contains several important experimental points and some discussion of the application of the theories which have been developed particularly for radio waves.

ELLISON, T. H., 1952, *J. Atmos. Terr. Phys.*, **2**, 14.
The propagation of sound waves through a medium with very small random variations in refractive index.
Develops a first-order diffraction theory without any consideration of multiple diffraction. Fejer's (1953) paper extends the consideration to include multiple diffraction.

ELLYETT, C. D., 1950, *Phil. Mag.*, **41**, 694.
The influence of high altitude winds on meteor trail ionization.

FEINSTEIN, J., 1954, *Trans. Inst. Radio Engrs, N.Y.*, Vol. AP **2**, 23, 63.
Some stochastic problems in wave propagation. Parts I and II.

Reflection from a surface with small random irregularities and transmission through a medium with small random deviations of refractive index. Results similar to those of Fejer (1953) and Bramley (1955) but with rather different nomenclature.

FEJER, J. A., 1953, *Proc. Roy. Soc.* A, **220**, 455.
The diffraction of waves in passing through an irregular refracting medium.

Deduces the angular spectrum produced when a wave passes through a thick medium containing weak irregularities of electron density having a three-dimensional auto-correlation function $\exp(-r^3/r_0^3)$. The deduction is in terms of successive diffraction by elementary slabs of the medium.

FÜRTH, R., 1955, *The Physics of the Ionosphere*, 1954 (London: Physical Society), p. 140.
Statistical analysis of star scintillations as a means of investigating atmospheric disturbances.

Discussion of the 'after-effect function' ('difference correlation function') and its application to the analysis of visible stellar scintillations.

FÜRTH, R., and MACDONALD, D. K. C., 1947, *Proc. Phys. Soc.*, **59**, 375.
Statistical analysis of spontaneous electrical fluctuations.

Introduces the 'difference correlation function', or the 'after-effect function' $\Delta(\xi)$ in their equation (16) and discusses some of its properties.

GREENHOW, J. S., 1952, *Proc. Phys. Soc.* B, **65**, 169.
Characteristics of radio echoes from meteor trails: III. The behaviour of the electron trails after formation.

HARWOOD, J., 1954, *Proc. Instn Elect. Engrs*, Pt. IV, **101**, 183 (Monograph No. 86).
Spaced-receiver experiments on radio waves of 19 km wavelength.

HERLOFSON, N., 1951, *Ark. Fys.*, **3**, 247.

HEWISH, A., 1951, *Proc. Roy. Soc.* A, **209**, 81.
The diffraction of radio waves in passing through a phase-changing ionosphere.

Detailed discussion of a thin diffracting screen which imposes phase variations on a wave traversing it. The phase variations considered vary either sinusoidally or randomly across the screen. The results are applied to observations of the scintillations of radio stars.

HEWISH, A., 1952, *Proc. Roy. Soc.* A, **214**, 494.
The diffraction of galactic radio waves as a method of investigating the irregular structure of the ionosphere.

Experiments on radio-stellar scintillation are described and the results used to determine the steady drift motion and the size of the ionospheric irregularities producing them. Theory is developed and used for determining the height of the irregularities from observations of the amplitude and phase of the received wave.

HEWISH, A., 1955, *Proc. Roy. Soc.* A, **228**, 238.
The irregular structure of the outer regions of the solar corona.

Uses the theory of Fejer (1953) for a thick diffracting region to consider the phenomena observed when waves from a radio star pass through the solar corona and makes deductions about the irregularities in the corona.

JAMES, R. W., 1948, *The Optical Principles of the Diffraction of X-rays* (London: Bell), Chap. 1.

JONES, R. E., MILLMAN, G. H., and NERTNEY, R. J., 1953, *J. Atmos. Terr. Phys.*, **3**, 79.
The heights of ionospheric winds as measured at long radio wavelengths.

Contains an analysis of diffraction by a screen which produces a sinusoidal variation of both amplitude and phase.

KELLER, G., 1953, *Astr. J.*, **58**, 113.
Astronomical seeing, and its relation to atmospheric turbulence.

LITTLE, C. G., 1951, *Mon. Not. R. Astr. Soc.*, **111**, 289.
A diffraction theory of the scintillation of stars on optical and radio wavelengths.

Stresses particularly the importance of the relation between the sizes of the first 'Fresnel zone' and of the 'blobs' which make up the irregular refracting medium.

LITTLE, C. G., and MAXWELL, A., 1951, *Phil. Mag.*, **41**, 267.
Fluctuations in the intensity of radio waves from galactic sources.
Experimental results concerning radio-stellar scintillation and deduction that the ' size ' of the corresponding ionospheric irregularities is about 4 km.

MACDONALD, D. K. C., 1949, *Proc. Camb. Phil. Soc.*, **45**, 368.
Some statistical properties of random noise.
Considers the statistics of the phase in random noise.

MCNICOL, R. W. E., 1949, *Proc. Instn Elect. Engrs*, Pt. III, **96**, 517.
The fading of radio waves of medium and high frequencies.
Experimental fading curves were obtained on short wave pulses returned at vertical incidence and medium-wave c.w. returned at oblique incidence. They were analysed to give the amplitude probability distribution and the temporal auto-correlation function. The relation between the difference correlation function and the product correlation function is derived (eqn (7)).

MILLMAN, G. H., 1952, *Ann. Geophys.*, **8**, 365.
A study of ionospheric winds and turbulence utilizing long radio waves.
Recorded the amplitudes of 150 kc/s pulses received at vertical incidence on three receivers and also the variations of phase at one receiver. Discusses drifts, depth of fading, and size of irregularity in the equivalent ' thin screen ' ionosphere.

MITRA, S. N., 1949, *Proc. Instn Elect. Engrs*, Pt. III, **96**, 505.
Statistical analysis of fading of a single downcoming wave from the ionosphere.

NEWSTEAD, G., 1954, *J. Atmos. Terr. Phys.*, **5**, 173.
The analysis of fading records from spaced receivers.
Discusses the analysis of results when only the time intervals between corresponding maxima are recorded (see Ratcliffe 1954).

NODTVEDT, H., 1951, *Phil. Mag.*, **42**, 1022.
The correlation function in the analysis of directive wave propagation.

PAWSEY, J. L., 1935, *Proc. Camb. Phil. Soc.*, **31**, 125.
Further investigations of the amplitude variations of downcoming wireless waves.
Experiments with spaced receivers. First determination of ionosphere drift velocities.

PHILLIPS, G. J., 1955, *The Physics of the Ionosphere* (London : Physical Society), p. 174.
Diffuse ionospheric reflection of medium waves at night.
Determined the spread of the angular power spectrum reflected from the E layer when waves of frequency 863 kc/s were incident at an angle of 58° from the vertical.

PHILLIPS, G. J., and SPENCER, M., 1955, *Proc. Phys. Soc.* B, **68**, 481.
Effects of anisometric amplitude patterns in the measurement of ionospheric drifts.
Shows how to use observations at three recording points to determine the statistical departure from symmetry of the diffraction pattern on the ground, and to allow for this departure in the calculation of regular and irregular movements. Experiments showed that the pattern produced by reflection of 2·4 Mc/s waves from the E or the F layer was often such that the correlation ellipse on the ground had axes with ratio about 2, but with no preferred orientation.

PÜTTER, P., 1955, *The Physics of the Ionosphere* (London : Physical Society), p. 191.
Messung des Ionosphärenwindes aus der Wanderungsgeschwindigkeit eines Zustandes längs der Erdoberfläche.
A companion paper to that of Berg (1955).

RATCLIFFE, J. A., 1948, *Nature, Lond.*, **152**, 9.
Diffraction from the ionosphere and the fading of radio waves.
Suggests that diffraction effects from an irregular ionosphere can explain fading and that the analysis can be carried over from the analogous phenomenon of random noise. Stresses the effects of back scattering from randomly moving irregularities.

RATCLIFFE, J. A., 1954, *J. Atmos. Terr. Phys.*, **5**, 173.
The determination of the velocity of winds from spaced-receiver experiments.
Discusses the analysis of results when only the time intervals between corresponding maxima are recorded (see Newstead 1954).

RATCLIFFE, J. A., and PAWSEY, J. L., 1933, *Proc. Camb. Phil. Soc.*, **29**, 301.
A study of the intensity of downcoming wireless waves.
Experiments with spaced receivers suggested that fading is produced by a diffraction mechanism.

RICE, S. O., 1944, *Bell Syst. Tech. J.*, **23**, 282; 1945, *Ibid.*, **24**, 46.
Mathematical analysis of random noise.
The classical papers on which the theory of diffraction by random screens is based.

ROY, R., and VERMA, J. K. D., 1953, *J. Geophys. Res.*, **58**, 473.
Irregularities in the ionosphere.

RYLE, M., 1952, *Proc. Roy. Soc.* A, **211**, 351.
A new radio interferometer and its application to the observation of weak radio stars.
A description of the phase-switched Michelson radio-stellar interferometer.

SPENCER, M., 1955, *Proc. Phys. Soc.* B, **68**, 493.
The shape of irregularities in the upper ionosphere.
Uses observations of radio-stellar scintillations made at three points to deduce the statistical shape of the diffraction pattern at the ground and finds that it can be explained by elongated irregularities in the F2 region with ratio of axes 5 or greater, and situated with their long axes along the earth's magnetic field.

ZERNIKE, F., 1938, *Physica*, **5**, 785.
The concept of degree of coherence and its application to optical problems.
Shows that a quantity which is the same as the auto-correlation function represents the degree of coherence between two points in a wave front, and that it is transmitted without change through an optical system. Shows how it is related to the distribution of intensity (power) over the source, and to the visibility of $\cos^2$ interference fringes.

SOME TOPICS IN NEUTRON DIFFUSION THEORY

By J. H. TAIT

Atomic Energy Research Establishment, Harwell, Didcot, Berks.

CONTENTS

	PAGE
§ 1. Introduction	268
§ 2. Calculations of the spectrum of neutrons in an infinite moderating medium with a homogeneous distribution of sources	273
2.1. The spectrum of neutrons in a monatomic gas at zero temperature	273
2.2. The spectrum in monatomic hydrogen gas at a non-zero temperature	274
2.3. The spectrum in heavy moderating gases at a non-zero temperature	276
2.4. The determination of the neutron spectrum by a time-of-flight method	277
2.5. The determination of the average neutron velocities in various media	278
§ 3. Calculations of the spatial distribution of slowed-down neutrons	280
3.1. Holte's method	280
3.2. The moment method	286
§ 4. Calculations of critical size	289
4.1. One-velocity-group theory	289
4.2. Multi-velocity-group diffusion theory	292
4.3. The solution of the energy-dependent transport equation	294
Acknowledgment	297
References	297

Abstract. This paper is divided into four sections. In the first section the integro-differential neutron transport equation is given in its most general form. The form of the scattering law for elastic collisions with moderating nuclei, at rest or in motion, is discussed. The second section deals with the spectrum of neutrons in an infinite moderating medium, including the case when the medium is at a non-zero temperature. The determination of the spectrum is useful in the elucidation of various problems in the physics of thermal reactors, as the presence of large amounts of capturing material prevents the neutrons from reaching thermal equilibrium with the moderating atoms. A comparison of the calculations with experimental determinations of the neutron spectrum is given. In the third section methods of calculating the spatial distribution at large distances from the neutron source are described. The fourth section is devoted to calculations of critical size. An indication is given of the accuracy of the diffusion approximation when it is used for calculating the critical size of small systems.

§ 1. Introduction

Numerous articles dealing with the solution of problems in neutron transport theory have appeared recently. However, before discussing the contents of some of these articles, it will be convenient to consider the general equation of neutron transport theory.

The following notations will be used :

v is the velocity of a neutron ;
E is its energy ;

u is the lethargy of a neutron with respect to some energy E_0, i.e. $u = \log(E_0/E)$;

$\boldsymbol{\Omega}$ is a unit vector which specifies the direction of motion of a neutron;

$\mathbf{r}$ is a vector which specifies the position of a point P;

$N(\mathbf{r}, v\boldsymbol{\Omega}, t)\, dv\, d\Omega$ is the number of neutrons per unit volume at the point P, with velocities in the range v to $v+dv$ and directions lying in the elementary cone $d\Omega$ about $\boldsymbol{\Omega}$, at time t;

$G_s(\mathbf{r};\ v\boldsymbol{\Omega} \to v'\boldsymbol{\Omega}';\ t)$ is the scattering rate per neutron from velocity $v\boldsymbol{\Omega}$ to velocity $v'\boldsymbol{\Omega}'$;

$\gamma(\mathbf{r}, v\boldsymbol{\Omega}, t)$ is the absorption rate per neutron at velocity v;

$S(\mathbf{r}, v\boldsymbol{\Omega}, t)$ is the source strength.

If, in a volume element at $\mathbf{r}$, we determine the change in the neutron density due to the leakage of neutrons, the scattering rate both into and out of the velocity interval dv and cone $d\Omega$, the absorption rate and the sources, then it can be shown that the following Boltzmann equation (or transport equation) is satisfied by $N(\mathbf{r}, v\boldsymbol{\Omega}, t)$. It is a linear equation, since the neutron density is small compared with the density of scattering nuclei.

$$\partial N(\mathbf{r}, v\boldsymbol{\Omega}, t)/\partial t + v\boldsymbol{\Omega}.\mathbf{grad}\, N(\mathbf{r}, v\boldsymbol{\Omega}, t)$$
$$+ \gamma(\mathbf{r}, v\boldsymbol{\Omega}, t)\, N(\mathbf{r}, v\boldsymbol{\Omega}, t) + \iiint G_s(\mathbf{r};\ v\boldsymbol{\Omega} \to v'\boldsymbol{\Omega}';\ t)\, N(\mathbf{r}, v\boldsymbol{\Omega}, t)\, dv'\, d\Omega'$$
$$= S(\mathbf{r}, v\boldsymbol{\Omega}, t) + \iiint G_s(\mathbf{r};\ v'\boldsymbol{\Omega}' \to v\boldsymbol{\Omega};\ t)\, N(\mathbf{r}, v'\boldsymbol{\Omega}', t)\, dv' d\Omega'. \quad \ldots\ldots(1.1)$$

This equation is valid whether or not the scattering and capturing nuclei are at rest. They may have, for example, a Maxwellian distribution of velocities.

When the scattering nuclei are at rest, equation (1.1) simplifies to

$$\partial N(\mathbf{r}, v\boldsymbol{\Omega}, t)/\partial t + v\boldsymbol{\Omega}.\mathbf{grad}\, N(\mathbf{r}, v\boldsymbol{\Omega}, t) + v\alpha N(\mathbf{r}, v\boldsymbol{\Omega}, t)$$
$$= \iiint \beta v' N(\mathbf{r}, v'\boldsymbol{\Omega}', t) f(v'\boldsymbol{\Omega}' \to v\boldsymbol{\Omega})\, dv' d\Omega' + S(\mathbf{r}, v\boldsymbol{\Omega}, t). \quad \ldots\ldots(1.2)$$

Here

α is the inverse of the total neutron mean free path l;

β is the mean number of secondaries per unit path, i.e. $\beta = \alpha c$, where c is the mean number of secondary neutrons per collision;

$cf(v'\boldsymbol{\Omega}' \to v\boldsymbol{\Omega})\, dv d\Omega$ is the mean number of neutrons produced in the velocity range dv and cone $d\Omega$ when a neutron of velocity v' and direction $\boldsymbol{\Omega}'$ undergoes a collision with a stationary nucleus.

f is normalized to unity, i.e. $\iiint f(v'\boldsymbol{\Omega}' \to v\boldsymbol{\Omega})\, dv d\Omega = 1$.

We shall consider the second equation in more detail. It can be seen that we have used a single term on the right-hand side of the equation to represent all processes by which a neutron can be produced in the velocity range dv and cone $d\Omega$, i.e. fission, and elastic and inelastic scattering.

Let us consider the various types of collision which a neutron can undergo, in order to determine expressions for l, c and f. A neutron can be scattered elastically or inelastically, cause fission or be captured. Let $\sigma_e, \sigma_{in}, \sigma_f$ and σ_c denote the cross sections for these processes. If there are n nuclei per unit volume, then

$$\alpha = l^{-1} = n(\sigma_e + \sigma_{in} + \sigma_f + \sigma_c), \qquad \ldots\ldots(1.3)$$

$$\beta = c\alpha = n(\sigma_e + \sigma_{in} + \nu\sigma_f), \qquad \ldots\ldots(1.4)$$

where ν is the probable number of neutrons emitted per fission.

The expression for $cf(v'\mathbf{\Omega}' \to v\mathbf{\Omega})$ is

$$cf(v'\mathbf{\Omega}' \to v\mathbf{\Omega}) = \nu p_f f_f + p_{in} f_{in} + p_e f_e, \qquad \ldots\ldots(1.5)$$

where p_f, p_{in} and p_e are the probabilities for fission, inelastic scattering and elastic scattering in a collision.

$\nu f_f(v'\mathbf{\Omega}' \to v\mathbf{\Omega})\, dv d\Omega$ is the probable number of neutrons produced in the velocity interval dv and cone $d\Omega$ from the fission of a nucleus by a neutron of velocity v' travelling in the direction $\mathbf{\Omega}'$. In fission, the neutrons are emitted isotropically. ν and the fission spectrum $F(v)$ are assumed to be independent of v', and therefore

$$\nu f_f(v'\mathbf{\Omega}' \to v\mathbf{\Omega}) = \nu F(v)/4\pi. \qquad \ldots\ldots(1.6)$$

$f_{in}(v'\mathbf{\Omega}' \to v\mathbf{\Omega})\, dv d\Omega$ is the probable number of neutrons produced in the velocity interval dv and cone $d\Omega$ when a neutron of velocity v' and direction $\mathbf{\Omega}'$ is scattered inelastically by a nucleus. In an inelastic nuclear collision, the neutron is absorbed by the scattering nucleus. It is then emitted isotropically at a lower energy, leaving the scattering nucleus in an excited state ; thus

$$f_{in}(v'\mathbf{\Omega}' \to v\mathbf{\Omega}) = g(v' \to v)/4\pi, \qquad \ldots\ldots(1.7)$$

where $g(v' \to v)\, dv$ is the probability that the neutron is scattered into the velocity interval dv.

There is another form of inelastic scattering for neutrons of low energy (~ 1 ev), namely inelastic molecular scattering and interactions of the neutrons with a crystal lattice. Various models have been considered by different authors to obtain the scattering function f, but we shall not give details of these calculations here.

All other scattering processes, i.e. those in which the scattering nucleus can be considered free and is left in its original nuclear state, we shall call elastic. Let us consider the form which f_e takes for this type of collision, sometimes called a billiard-ball collision.

Let the velocity and the direction of the neutron before the collision be v' and $\mathbf{\Omega}'$, and after the collision v and $\mathbf{\Omega}$. Let v_M and $\mathbf{\Omega}_M$ be the velocity and direction of the scattering nucleus (of atomic mass M), which is considered to be at rest before the collision.

From the conservation of momentum,

$$v'\mathbf{\Omega}' = v\mathbf{\Omega} + v_M \mathbf{\Omega}_M M, \qquad \ldots\ldots(1.8)$$

and from the conservation of energy,

$$v'^2 = v^2 + v_M{}^2 M. \qquad \ldots\ldots(1.9)$$

On elimination of v_M between these two equations

$$\mathbf{\Omega}.\mathbf{\Omega}' = \tfrac{1}{2}[(M+1)\, v/v' - (M-1)\, v'/v]. \qquad \ldots\ldots(1.10)$$

The maximum energy loss occurs when†

$$\boldsymbol{\Omega}.\boldsymbol{\Omega}' = -1, \quad \text{i.e.} \quad (v/v')^2 = [(M-1)/(M+1)]^2.$$

To determine the scattering function completely, an assumption must be made about the scattering in the centre-of-mass system. Let us denote the various velocities and directions in the centre-of-mass system by the subscript cm. Then

$$v_{\text{cm}}'\boldsymbol{\Omega}_{\text{cm}}' = \frac{M}{M+1}v'\boldsymbol{\Omega}',$$

$$v_{\text{cm}}\boldsymbol{\Omega}_{\text{cm}} = v\boldsymbol{\Omega} - \frac{1}{M+1}v'\boldsymbol{\Omega}'.$$

Let Θ be the angle between $\boldsymbol{\Omega}_{\text{cm}}'$ and $\boldsymbol{\Omega}_{\text{cm}}$; then

$$\begin{aligned}\cos\Theta &= \frac{v_{\text{cm}}'\boldsymbol{\Omega}_{\text{cm}}'.v_{\text{cm}}\boldsymbol{\Omega}_{\text{cm}}}{v_{\text{cm}}'v_{\text{cm}}} \\ &= \frac{vv'\boldsymbol{\Omega}.\boldsymbol{\Omega}' - v'^2/(M+1)}{v'[v^2 - \{2vv'/(M+1)\}\boldsymbol{\Omega}.\boldsymbol{\Omega}' + v'^2/(M+1)^2]^{1/2}} \\ &= \frac{\frac{1}{2}(M+1)v^2 - \frac{1}{2}v'^2(M^2+1)/(M+1)}{v'^2M/(M+1)}. \qquad \ldots\ldots(1.11)\end{aligned}$$

If the scattering is isotropic in the centre-of-mass system, then all values of $\cos\Theta$ are equally probable. From equation (1.11) we see that all permissible values of v^2 are equally likely. The function f_s takes the following form:

$$f_s(v'\boldsymbol{\Omega}' \to v\boldsymbol{\Omega}) = \frac{(M+1)^2v}{4\pi Mv'^2}\,\delta\left(\boldsymbol{\Omega}.\boldsymbol{\Omega}' - \tfrac{1}{2}(M+1)\frac{v}{v'} + \tfrac{1}{2}(M-1)\frac{v'}{v}\right), \qquad \ldots\ldots(1.12)$$

if $[(M-1)/(M+1)]\,v' \leqslant v \leqslant v'$, and zero otherwise; $\delta(x)$ is Dirac's δ-function, and $(M+1)^2/4\pi M$ is a normalization factor such that the integral of f_s over all v and $\boldsymbol{\Omega}$ is unity. Let E' be the energy of the incident neutron. The neutron is scattered with uniform probability to any energy in the range E' to $[(M-1)/(M+1)]^2E'$. The average energy loss is $2ME'/(M+1)^2$.

If we wish to calculate the scattering rates G_s in equation (1.1), we must consider the form which the scattering law takes when the scattering nucleus has an incident velocity v_M' and is travelling in the direction $\boldsymbol{\Omega}_M'$. The scattering law is

$$f_s(v'\boldsymbol{\Omega}' \to v\boldsymbol{\Omega}) = \frac{(M+1)^2}{4\pi M^2}\frac{w}{v_r^2}\,\delta\left(\mathbf{s}.\mathbf{s}' - \frac{M+1}{2M}\frac{w}{v_r}\right)dw\,d\Omega^0, \qquad \ldots\ldots(1.13)$$

where

$$v_r\mathbf{s}' = v_M'\boldsymbol{\Omega}_M' - v'\boldsymbol{\Omega}',$$

$$w\mathbf{s} = v\boldsymbol{\Omega} - v'\boldsymbol{\Omega}',$$

and $\mathbf{s}, \mathbf{s}'$ are unit vectors; v_r is the initial velocity of the scattering nucleus relative to the neutron, and w the velocity of the neutron after the collision relative to its motion before the collision; $d\Omega^0$ is an element of solid angle in a coordinate system in which the neutron was originally at rest.

In some problems, however, it is convenient to write the scattering law in another form. Let $P(v' \to v;\, v_M')\,dv$ be the probability that a neutron of velocity v' is

† Except for hydrogen ($M = 1$), in which it occurs when $\boldsymbol{\Omega}.\boldsymbol{\Omega}' = 0$.

scattered into the velocity interval dv on collision with a nucleus of mass M and velocity v_M', and $\cos^{-1}\mu_0$ the angle between the initial directions of the nucleus and the neutron in the laboratory system. Then

$$\begin{aligned} P(v'\to v;\, v_M')\,dv &= 0 \quad (v<v_1) \\ &= \frac{2v\,dv}{v_2^2-v_1^2} \quad (v_1\leqslant v\leqslant v_2) \\ &= 0 \quad (v_2<v) \end{aligned} \qquad \ldots\ldots(1.14)$$

where v_1 and v_2 are the minimum and the maximum velocities attainable by a neutron in a collision, and are given by

$$v_1 = V_c - Mv_r/(M+1), \quad v_2 = V_c + Mv_r/(M+1),$$

where v_r is as before the initial relative velocity of the neutron and the nucleus, and V_c is the velocity of the centre of mass :

$$v_r = [v'^2 + v_M'^2 - 2v'v_M'\mu_0]^{1/2},$$

$$V_c = [v'^2 + 2Mv'v_M'\mu(v', v_M') + M^2 v_M'^2]/(M+1), \text{ with an obvious notation.}$$

These relations can easily be obtained by writing down the equations for the conservation of momentum and energy. The scattering is assumed to be isotropic in the centre-of-mass system, i.e. the cosine of the angle between the velocity (in the centre-of-mass system) of the neutron after the collision and any fixed direction is uniformly distributed. By suitably choosing this fixed direction (1.13) can easily be proved. We shall later consider expressions for $P(v'\to v;\, v_M')$ integrated over a distribution of nuclear velocities v_M', e.g. a Maxwellian distribution.

We have assumed hitherto that the scattering is isotropic in the centre-of-mass system. This is true only if the de Broglie wavelength of the neutron is greater than the dimensions of the scattering nucleus. For light nuclei, the energy must be less than several MeV, and for heavy nuclei less than several hundred keV. However, even for low energies the scattering may not be isotropic in the centre-of-mass system, owing to resonances in the scattering cross section. Often the experimental information about the angular distribution in the centre-of-mass system for scattering from such a resonance is scanty. When the scattering nucleus is very heavy, the energy loss is small and can often be neglected. We are then interested only in the angular distribution of the scattered neutrons in the laboratory system. In many calculations we do not consider the detailed angular distribution $f_e(\mu)$; instead, we assume that the scattering is isotropic and replace the scattering cross section σ_s by σ_s', where

$$\sigma_s' = \sigma_s\left[1 - \int_{-1}^{1}\mu f_e(\mu)\,d\mu\right]; \qquad \ldots\ldots(1.15)$$

μ is the cosine of the angle between the initial and final directions of the neutron. The quantity

$$\int_{-1}^{1}\mu f_e(\mu)\,d\mu$$

is provided by experimental measurement.

In developing some neutron diffusion theories, it is sometimes convenient to use the lethargy variable u. Equation (1.2) then becomes

$$\partial N'(\mathbf{r}, u, \boldsymbol{\Omega}, t)/\partial t + v\boldsymbol{\Omega}.\mathbf{grad}\, N'(\mathbf{r}, u, \boldsymbol{\Omega}, t) + vN'(\mathbf{r}, u, \boldsymbol{\Omega}, t)/l(u)$$
$$= \iiint \beta(u')\, v' N'(\mathbf{r}, u', \boldsymbol{\Omega}', t)\, f'(u', \boldsymbol{\Omega}' \to u, \boldsymbol{\Omega})\, du'\, d\Omega' + \text{source terms}, \quad \ldots\ldots(1.16)$$

where $N'(\mathbf{r}, u, \boldsymbol{\Omega}, t)\, du\, d\Omega$ is the number of neutrons per unit volume, in the lethargy interval du and cone $d\Omega$, at time t; v is given by $v = (2E_0)^{1/2} \exp(-\frac{1}{2}u)$.

$f_e'(u', \boldsymbol{\Omega}' \to u, \boldsymbol{\Omega})\, du\, d\Omega$ is the probability that a neutron of lethargy u' travelling in the direction $\boldsymbol{\Omega}'$ is scattered into the lethargy interval du and cone $d\Omega$. It takes the following form:

$$f_e'(u', \boldsymbol{\Omega}' \to u, \boldsymbol{\Omega}) = \frac{(M+1)^2}{8\pi M} \exp(u'-u)\, \delta[\boldsymbol{\Omega}.\boldsymbol{\Omega}' - \tfrac{1}{2}(M+1) \exp\{\tfrac{1}{2}(u'-u)\} + \tfrac{1}{2}(M-1) \exp\{\tfrac{1}{2}(u-u')\}]. \quad \ldots\ldots(1.17)$$

The probability that a neutron of lethargy u' is scattered into the lethargy interval du can be obtained by integrating (1.17) over $\boldsymbol{\Omega}$:

$$\iint f_e'\, d\Omega = \frac{(M+1)^2}{4M} \exp(u'-u) \quad \text{for} \quad u' - 2\log\frac{M+1}{M-1} \leqslant u \leqslant u'$$
$$= 0 \quad \text{otherwise.}$$

We denote $2\log[(M+1)/(M-1)]$ by q_M.

§ 2. Calculations of the Spectrum of Neutrons in an Infinite Moderating Medium with a Homogeneous Distribution of Sources

2.1. *The Spectrum of Neutrons in a Monatomic Gas at Zero Temperature*

In this class of problem the leakage term $v\boldsymbol{\Omega}.\mathbf{grad}\, N$ in equation (1.1) vanishes, since N is independent of $\mathbf{r}$. Placzek (1946) and Marshak (1947) have considered such problems in some detail. They assume that the scattering nuclei are stationary, that the slowing down is due to elastic collisions, and that the scattering is isotropic in the centre-of-mass system.

Let $\psi_0(v)$ be the average number of collisions occurring per unit volume per unit time per unit velocity interval due to sources emitting one neutron of velocity v_0 per unit time per unit volume. If we restrict ourselves to the time-independent case, $\psi_0(v)$ is given by

$$\psi_0(v) = \frac{v}{l(v)} \iint N(v\boldsymbol{\Omega})\, d\Omega. \quad \ldots\ldots(2.1)$$

For slowing down in a hydrogen medium the expression for $\psi_0(v)$ is

$$\psi_0(v) = \frac{2l(v_0)}{vl_s(v_0)} \exp\left[-\int_v^{v_0} \frac{2l(v')}{v'l_c(v')}\, dv'\right], \quad \ldots\ldots(2.2)$$

where $l(v)$, $l_c(v)$ and $l_s(v)$ are the total, capture and scattering mean free paths at velocity v. For zero capture $\psi_0(v) = 2/v$.

For moderators heavier than hydrogen, no simple relation exists. However, for the case of zero capture, $\psi_0(v)$ tends to an asymptotic value

$$2/\xi v, \qquad \ldots\ldots(2.3)$$

where ξ is the mean logarithmic energy loss per collision and is given by

$$1-\{(M+1)^2/4M\}\, q_M \exp(-q_M).$$

The solution for $\psi_0(v)$ contains, in addition to (2.3), various transient terms which die away rapidly.

When capture is present, a simple solution for $\psi_0(v)$ can be obtained for slowing down in hydrogen, if the scattering mean free path is assumed constant and the capture mean free path is proportional to the velocity v. Then

$$\psi_0(v) = \frac{2v(v_0+v_c)}{v_0(v+v_c)^2}, \qquad \ldots\ldots(2.4)$$

where v_c is the velocity at which the mean free paths for scattering and capture are equal.

For slowing down in other moderators whose atomic weight M is small, $\psi_0(v)/v$ can be conveniently expressed as a power series in v_c/v. For large values of M it is more convenient to write $\log[\psi_0(v)/v]$ as a power series in v_c/v.

For other variations of the capture cross section approximate solutions can be obtained; these cases are discussed in detail by Marshak (1947).

2.2. *The Spectrum in Monatomic Hydrogen Gas at a Non-zero Temperature*

The solution of the slowing-down problem in moderators, taking into account the thermal motion of the scattering nuclei, is of considerable interest when one wishes to elucidate various problems in the physics of thermal reactors. The presence of a large amount of capturing material prevents the neutrons from reaching thermal equilibrium with the scattering atoms of the moderator, and the spectrum of thermal neutrons may be different from a Maxwellian distribution.

The scattering law is known exactly only in the case of moderation by a monatomic gas, and we shall describe some of the calculations of the spectrum in such gases, and attempt to compare these with some experimental measurements which are available.

The law giving the probability that a neutron of velocity v' is scattered into the velocity interval from v to $v+dv$, on colliding with an atom of velocity v_M', has been given in equation (1.14). If the moderator atoms have a Maxwellian distribution $F(v_M')$, then

$$F(v_M')\, dv_M' = \frac{4}{\sqrt{\pi}}\left(\frac{M}{2kT}\right)^{3/2} v_M'^2 \exp(-Mv_M'^2/2kT)\, dv_M', \qquad \ldots\ldots(2.5)$$

T being the temperature of the moderator; k is Boltzmann's constant, equal to $8{\cdot}61\times10^{-5}$ ev per degree. The equation satisfied by the neutron density $N(v)$ [$=\iint N(v\boldsymbol{\Omega})\, d\Omega$] is obtained from (1.1) by integrating over all $\boldsymbol{\Omega}$:

$$\{V(v)+\gamma(v)\}\, N(v) = \int G(v'\to v)\, N(v')\, dv' + S(v), \qquad \ldots\ldots(2.6)$$

where $\gamma(v)$ is the absorption rate at velocity v;

$$V(v) = \int G(v \to v')\, dv';$$

$$G(v \to v')\, dv' = \tfrac{1}{2} dv' \int_0^\infty \int_{-1}^{1} v_r \sigma_s(v_r)\, F(v_M')\, P(v \to v';\, v_M')\, d\mu\, dv_M';$$

$P(v' \to v;\, v_M')$ is given by (1.14);

v_r is the relative velocity of the neutron and the moderator atom.

It is possible to solve equation (2.6) analytically in a few special cases. The first calculation of this type was carried out by Wigner and Wilkins (1948), for slowing down in monatomic hydrogen gas. A similar calculation has been carried out by Davison (1953). However, in the latter calculation Davison represented the spectrum by a power series in ϵ, the ratio of the capture and scattering cross sections at the velocity corresponding to the peak of the Maxwellian distribution. The solution is therefore restricted to the case of small capture.

The Wigner–Wilkins solution is valid also for large values of the capture, corresponding to the case where material which absorbs neutrons is mixed with the hydrogen. We have therefore restricted ourselves to this calculation.

The scattering cross section is assumed to be constant. If we neglect the source term $S(v)$ in (2.6) we can divide that equation by σ_s. The variables v and v' are replaced by x and x', where $x = \beta v, x' = \beta v'$, and $\beta^2 = 1/2kT$. $G(x' \to x)$ is then given by the formulae

$$\left.\begin{aligned} G(x' \to x) &= \frac{2x}{x'} \operatorname{erf} x \quad \text{for} \quad x < x' \\ &= \frac{2x}{x'} \exp(x'^2 - x^2) \operatorname{erf} x \quad \text{for} \quad x' < x, \end{aligned}\right\} \qquad \ldots\ldots(2.7)$$

and

$$V(x) = \frac{2x^2+1}{2x} \operatorname{erf} x + \frac{\exp(-x^2)}{\sqrt{\pi}}.$$

In equation (2.6), $N(x)$ and $G(x' \to x)$ are replaced by $\nu(x)$ and $S(x, x')$, defined as follows:

$$S(x, x') = \sqrt{\left(\frac{F(x)}{F(x')}\right)}\, G(x \to x') = S(x', x), \qquad \ldots\ldots(2.8)$$

i.e. $S(x', x)$ is symmetrical in x and x';

$$\nu(x) = N(x)/\sqrt{F(x)}. \qquad \ldots\ldots(2.9)$$

Equation (2.6) then becomes

$$\exp(-\tfrac{1}{2}x^2) \int_0^x \exp(\tfrac{1}{2}u^2) \operatorname{erf} u \,.\, \nu(u)\, du + \exp(\tfrac{1}{2}x^2) \operatorname{erf} x \int_x^\infty \exp(-\tfrac{1}{2}u^2)\, \nu(u)\, du$$
$$= \tfrac{1}{2}[V(x) + \beta\gamma]\, \nu(x). \qquad \ldots\ldots(2.10)$$

By operating on equation (2.10) with the operator

$$L(x) = \frac{d}{dx} p(x) \frac{d}{dx} + r(x),$$

where $$1/p(x) = \exp(-x^2) + (\pi x)^{1/2} \operatorname{erf} x$$

and $$r(x) = p(x)\,[p(x)\exp(-x^2) - x^2], \qquad \ldots\ldots(2.11)$$

equation (2.10) is converted into a differential equation,

$$\frac{d}{dx}\left[p(x)\frac{d}{dx}(V+\beta\gamma)\,\nu(x)\right] + \left[r(x)(V+\beta\gamma) + \frac{4}{\sqrt{\pi}}\right]\nu(x) = 0. \qquad \ldots\ldots(2.12)$$

This second-order homogeneous linear differential equation can be reduced to a Riccati equation by the substitutions

$$\mu(x) = [V(x)+\beta\gamma]\,\nu(x), \quad y(x) = p(x)\,\mu'(x)/\mu(x). \qquad \ldots\ldots(2.13)$$

Equation (2.12) then becomes

$$py' = -y^2 - p\{r(x) + 4[V(x)+\beta\gamma]^{-1}/\sqrt{\pi}\}. \qquad \ldots\ldots(2.14)$$

The solution of equation (2.14) can be obtained as a series of ascending odd powers of x, beginning with x^{-1}. Then $\mu(x)$ is obtained from (2.13), utilizing the appropriate boundary conditions on μ. The series for $y(x)$ was used up to $x = \frac{1}{2}$; beyond that point, $y(x)$ was determined by numerical integration.

2.3. *The Spectrum in Heavy Moderating Gases at a Non-zero Temperature*

Cohen (1955) has reported some unpublished calculations by Wilkins and by Hurwitz on slowing down in a heavy moderator with constant cross sections. Wilkins transforms the integral equation (2.6) into a second-order differential equation, which is accurate to order $1/M$. He has shown that

$$\int_0^\infty S(x,y)\,\nu(y)\,dy = x\nu(x) + \frac{1}{2M}[(4-x^2)\,x\nu(x) + \nu'(x) + x\nu''(x)] + \ldots, \qquad \ldots\ldots(2.15)$$

where $\nu(x) = N(x)/\sqrt{F(x)}$ as in (2.9), and

$$\left.\begin{aligned} S(x,y) = \theta^2[&\exp\{\tfrac{1}{2}(x^2-y^2)\}\{\operatorname{erf}(\theta x - \xi y) \pm \operatorname{erf}(\theta x + \xi y)\} \\ &+ \exp\{\tfrac{1}{2}(y^2-x^2)\}\{\operatorname{erf}(\theta y - \xi x) \mp \operatorname{erf}(\theta y + \xi x)\}]\,; \\ \theta = (M+1)/2\sqrt{M}, &\quad \xi = (M-1)/2\sqrt{M}. \end{aligned}\right\} \qquad \ldots\ldots(2.16)$$

On substituting into equation (2.6) and noting that $V(x) \sim x + 1/2Mx$, the integral equation becomes

$$x\nu'' + \nu' + (4x - x^3 - 2M\beta\gamma)\,\nu = 0,$$

and the equation for N is

$$xN'' + (2x^2-1)\,N' + (4x - 2M\beta\gamma)\,N = 0. \qquad \ldots\ldots(2.17)$$

Wilkins has developed this equation, with the restriction that $x^2 \gg 4/M$. Hurwitz also has derived this equation. From his derivation the solution appears to be valid with the restriction that $x^2 \ll M/4$. It would seem, therefore, that the equation is valid for the entire range of x, for sufficiently large M.

Equation (2.17) is solved by writing $N(x) = \mu(x)\,x^2\exp(-x^2)$, i.e. $\mu(x)$ is a measure of the deviation from the Maxwellian distribution. The solution for $\mu(x)$ can be determined as a series $\Sigma a_n x^n$, where

$$\left.\begin{aligned} a_n &= [a_{n-1}\Delta + 2(n-2)\,a_{n-2}]/n(n+2), \\ a_0 &= 1, \quad a_1 = \tfrac{1}{3}\Delta, \quad \Delta = 2M\beta\gamma. \end{aligned}\right\} \qquad \ldots\ldots(2.18)$$

An asymptotic solution can be found for large x:

$$N(x) \sim \frac{C \exp(-\Delta/2x)}{x^2 - 2}. \qquad \ldots\ldots(2.19)$$

The exponential term is equivalent to the usual ' resonance escape probability ' $\exp\{-\int(2\sigma_a/\xi v\sigma_s)\,dv\}$ for an absorption cross section which varies inversely with the velocity.

Cohen also reports some numerical calculations carried out by Brown and St. John (unpublished) at the Savannah River Laboratory. In these calculations, equation (2.6) was solved numerically. It is necessary to replace the right-hand side of (2.6) by

$$S^* + \int_0^{v^*} G(v' \to v)\, N(v')\, dv',$$

where

$$S^*(x) = S(v) + \int_{v^*}^{\infty} G(v' \to v)\, N(v')\, dv'.$$

v^* is taken so large that we can substitute for $N(v')$ the solution for the neutron density in a stationary moderator; this determines $S^*(v)$. The remaining integral in (2.6) is replaced by a sum: $\Sigma G_{ij} \Delta v_j N_j$. A set of linear equations is obtained, which are then solved on a high-speed computing machine. The calculations have been carried out for a variable scattering cross section.

A different numerical approach has been followed by Coveyou, Bate and Osborne (1955). They have determined the spectrum in various moderators, using the Monte Carlo method and assuming a constant scattering cross section. The results obtained for hydrogen were identical with the results of the calculations by Wigner and Wilkins.

2.4. *The Determination of the Neutron Spectrum by a Time-of-Flight Method*

Poole (1955) has measured the spectrum in a pure water moderator and that in boric acid solutions by a time-of-flight method, using a pulsed neutron source. The linear electron accelerator is used to produce pulses at the centre of a tank about 46 cm cube. A ' probe tube ' of diameter 1 to 2 cm penetrates the system, ending at the point where a measurement of the spectrum is desired. Outside the tank, a collimator is arranged so that only neutrons originating from the end of the probe are transmitted. The energy spectrum of these neutrons is then determined by the usual time-of-flight method. Sykes (1954) has shown that this method can be used in suitable cases to measure the energy spectrum, provided that the pulse of neutrons when slowed down to thermal energies is not too long, and that the neutron flight path is long enough to give the necessary resolution.

It is not easy to make a direct comparison between the results obtained by Poole and the calculations which we have previously described. It should be stressed that the calculations were carried out for monatomic hydrogen gas. Poole has obtained the spectrum in pure water at three distances from the source: 2, 5 and 10 cm. He showed that, between the energies of 0·01 ev and 1 ev, the spectrum has a fairly accurately Maxwellian portion. The result would therefore be the same in an infinite medium, and this result agrees with the calculations. The interesting comparison is with the measurements in boric acid. The spectrum

has been determined at one distance only, namely 10 cm from the source. Poole gives the temperatures of the Maxwellian parts of the spectra as a function of the effective capture cross section per hydrogen atom. These are shown in table 1. The temperature of the moderator was 15°C.

Table 1

σ_c per H atom (barns)	2·5	5	7·5
Excess over moderator temperature (°c)	19	37	57

In the calculations an effective temperature was determined by a least-squares fit of a Maxwellian to the computed flux in the range $0 \leqslant E \leqslant 3{\cdot}6kT$.

The results of the calculations by Coveyou *et al.* give the temperature as a function of the ratio of the capture to the scattering cross section σ_c/σ_s, at 2200 m sec^{-1}, viz. for $\sigma_c/\sigma_s = 0{\cdot}22$, $T = 69$°c and for $\sigma_c/\sigma_s = 0{\cdot}44$, $T = 121$°c. If we take for σ_s a value of 50 barns, as being the mean of 20 barns (the value of the hydrogen cross section at approximately 2 ev) and 80 barns (its value at 0·025 ev), then the temperature corresponding to $\sigma_c = 50 \times 0{\cdot}22 = 11$ barns is about equal to the experimental value for $\sigma_c = 7{\cdot}5$ barns. This comparison is not very significant, however.

2.5. *The Determination of the Average Neutron Velocities in Various Media*

Tolstov, Shapiro and Shtranikh (1955) have measured the average neutron velocities in various media. They made the following measurements: (i) a determination of the mean neutron velocity $\bar{v}$ and the value of $1/\overline{v^{-1}}$ (which they call $\langle v \rangle$); (ii) a measurement of the diffusion length and diffusion coefficient of the neutrons at various temperatures; (iii) a determination of the temperature dependence of the transport mean free path from albedo measurements.

The experiments were performed both with homogeneous moderators (graphite, paraffin and water), including conditions where substances absorbing neutrons by the $1/v$ law were placed in the moderator, and in heterogeneous systems with graphite and water as moderators. Experiments were also done to compare the spectra and energy of the neutrons inside the moderators and those emerging from the surfaces.

It has been shown that the energy of thermal neutrons is practically the same at all distances from the fast neutron source (Guzhevskii 1955, Troyan 1955). In graphite, the measurements were made for source distances varying from 20 to 60 cm, and it was found that, within the limits of the statistical errors (2%), the values of $\bar{v}$ and $\langle v \rangle$ measured in the experiments are independent of the source distance.

In the experiments with the paraffin moderator, the latter had dimensions 20 cm × 60 cm × 60 cm, and the source was placed at distances of 20 and 40 cm from a channel of diameter 56 mm, in which the measurements were made. In water, the experiments were performed in a tank of diameter 32 cm and height 80 cm, with a measurement channel of diameter 45 mm. The lifetime of the neutrons in water was diminished by the introduction of boron. The source was placed at a distance of 15 to 20 cm from the channel. Table 2 gives the results of the measurements.

The paper by Tolstov *et al.* is also interesting for its treatment of the mean velocity of the neutrons emerging from a moderator surface. Although this is really out of place in this section, we shall briefly mention the results. Experiments by Fermi *et al.* (1947) and Anderson *et al.* (1946) have shown that neutrons emitted by a cavity in graphite have a temperature of 300°K. The temperature of the neutrons from a graphite surface is 200°K (Zinn 1947). Tolstov *et al.* considered two limiting cases.

(i) The first limiting case is when there is only a slight change of energy after a collision of a neutron with an atom of the medium. Neutrons of various velocities form separate groups, and the extrapolated boundary is different for each group. The neutrons whose extrapolated boundary is more distant will have a higher density at and near the actual boundary.

Table 2

Medium	$\bar{v}/\bar{v}_{gr}$	$\langle v\rangle/\langle v\rangle_{gr}$	Ratio of macroscopic cross section to its value in water
Paraffin	$1{\cdot}0 \pm 0{\cdot}3$	$0{\cdot}97 \pm 0{\cdot}03$	0·9
Water	$1{\cdot}02 \pm 0{\cdot}02$	$1{\cdot}03 \pm 0{\cdot}04$	1
Water + boron	$1{\cdot}2 \pm 0{\cdot}04$	$1{\cdot}10 \pm 0{\cdot}07$	5·2

The suffix gr denotes the value for graphite.

The current of neutrons emerging with velocity v is proportional to the diffusion coefficient $D(v)$. $D(v)$ is given by $CN(v)v\lambda_{tr}(v)$, where $N(v)$ is the spectrum of neutrons in the medium, C is a constant, and $\lambda_{tr}(v)$ is the transport mean free path. The velocity distribution of emergent neutrons $\Phi_1(v)$ is then $D(v)/v = CN(v)\lambda_{tr}(v)$.

(ii) The second limiting case is when there is a considerable energy change. In the limit, suppose that, in consequence of the energy exchange, the emergence of neutrons from the medium does not alter their velocity distribution within it. Then the total number of neutrons emerging per unit time is given by

$$D(v) = \frac{1}{2}\int_0^{\pi/2} \sin\theta\, d\theta \int_0^{\infty} \rho(v,z)\frac{v}{\lambda_s(v)} \exp\{-z/\lambda_t(v)\cos\theta\}\, dz. \qquad \ldots\ldots(2.20)$$

According to Mark (1947), the density near a surface is given by

$$\rho(z) = \rho_0\{z + 0{\cdot}71\lambda_{tr} - 0{\cdot}133\lambda_{tr}\exp(-3{\cdot}7z/\lambda_{tr})\}.$$

If this is substituted into the integral (2.20), the spectrum $D(v)/v = \Phi_2(v)$ of the neutrons can be obtained.

The spectrum of neutrons emerging lies between these two limiting cases. The closeness of the spectrometric measurements to $\Phi_1(v)$ indicates that in paraffin only a slight exchange of energy with the paraffin molecules occurs after the average number of collisions which a neutron undergoes near the paraffin surface.

It can be seen that the spectrum of neutrons emitted by the surface of a medium is determined by their spectrum inside the medium and by the energy dependence of the neutron transport mean free path λ_{tr}.

Tolstov *et al.* showed that, in a heterogeneous system, the neutron spectrum is not Maxwellian, and the values of $\bar{v}$ and $\langle v\rangle$ are less than in a homogeneous system with the same ratio of numbers of absorber and moderator atoms.

We have hitherto considered calculations for a free monatomic gas. Cohen states that the approximation of a free gas tends to be better for heavier elements, whose Einstein and Debye temperatures are lower. It is not a good approximation for graphite and beryllium, and it may be necessary either to carry out a detailed quantum-mechanical analysis of the scattering process, or to determine experimentally the differential inelastic scattering cross section for slow neutrons as a function of neutron energy and angle of scattering, if accurate calculations of the thermal spectrum of neutrons in these moderators are to be made.

§3. Calculations of the Spatial Distribution of Slowed-down Neutrons

3.1. *Holte's Method*

In this section we shall consider first the solution of the idealized problem of a plane source in an infinite moderating medium, assuming that the neutrons are slowed down by elastic collisions. The solution of these problems is of considerable interest in the theory of neutron shielding. We are able to determine the form of the expression for the neutron flux at various distances from the source. Marshak (1947) has discussed this problem in considerable detail. He has calculated the slowing-down length for a single element and for various mixtures of elements. [If $\phi_0(z, E)$ is the flux of neutrons of energy E at a distance z from a plane source of neutrons of energy E_0, the slowing-down length L_s from E_0 to E is defined by

$$L_s^2(E) = \frac{1}{2}\int z^2 \phi_0(z, E)\, dz \Big/ \int \phi_0(z, E)\, dz. \qquad \ldots\ldots(3.1)]$$

He also calculates the higher spatial moments of the neutron density.

Marshak derives what is known as ' age theory ' from the transport equation by assuming that the neutron angular distribution is nearly isotropic and that the neutron spectrum as a function of lethargy can be written as two terms of a Taylor series. Improvements on age theory for the case of a constant mean free path are discussed by Marshak to illustrate the range of its applicability. Wick's solution (1949) for the asymptotic density at very large distances is also described.

We shall now give an account of a calculation by Holte (1951, 1952), which attempts to bridge the gap between the region over which age theory is valid and that where Wick's asymptotic solution is correct. These two latter theories are obtained from Holte's as special cases.

The starting point is equation (1.16), for the case of a plane geometry and slowing down by a single non-capturing element, i.e. $\beta = \alpha$. Let

$$\psi(z, \mu, u) = vN'(z, \mu, u)/l(u) \equiv vN'(\mathbf{r}, \boldsymbol{\Omega}, u)/l(u), \qquad \ldots\ldots(3.2)$$

where z is the spatial coordinate and $\cos^{-1}\mu$ the angle between the direction $\boldsymbol{\Omega}$ and the z axis. In the time-independent case, equation (1.16) becomes

$$\mu l(u)\frac{\partial}{\partial z}\psi(z, \mu, u) + \psi(z, \mu, u)$$

$$= \iiint \psi(z, \mu', u') f_e'(u', \boldsymbol{\Omega}' \to u, \boldsymbol{\Omega})\, du'\, d\Omega' + S\delta(z)\,\delta(u)/E_0. \qquad \ldots\ldots(3.3)$$

For elastic collisions with nuclei of mass M and scattering isotropic in the centre-of-mass system, f_e' is given by (1.17). Following Marshak, (1.17) can be expanded as a Legendre series :

$$f_e'(u', \boldsymbol{\Omega}' \to u, \boldsymbol{\Omega}) = \frac{(M+1)^2}{16\pi M} \exp(u'-u) \sum_{n=0}^{\infty} (2n+1) \mathrm{P}_n(\boldsymbol{\Omega}.\boldsymbol{\Omega}')$$

$$\times \mathrm{P}_n[\tfrac{1}{2}(M+1) \exp\{\tfrac{1}{2}(u'-u)\} - \tfrac{1}{2}(M-1) \exp\{\tfrac{1}{2}(u-u')\}]. \quad \ldots\ldots(3.4)$$

If $\psi(z, \mu', u')$ is expanded as a Legendre series in $\mathrm{P}_n(\mu')$ (μ' being the cosine of the angle between $\boldsymbol{\Omega}'$ and the z axis), i.e.

$$\psi(z, \mu', u') = \frac{1}{4\pi} \sum_{n=0}^{\infty} (2n+1) \psi_n(z, u') \mathrm{P}_n(\mu'),$$

then the right-hand side of equation (3.3) becomes

$$\frac{(M+1)^2}{16\pi M} \sum_{n=0}^{\infty} (2n+1) \mathrm{P}_n(\mu) \int_{u-q_M}^{u} \psi_n(z, u')$$
$$\times \mathrm{P}_n[\tfrac{1}{2}(M+1) \exp\{\tfrac{1}{2}(u'-u)\} - \tfrac{1}{2}(M-1) \exp\{\tfrac{1}{2}(u-u')\}]$$
$$\times \exp(u'-u)\, du' + S\delta(z)\, \delta(u)/E_0. \quad \ldots\ldots(3.5)$$

We take the Laplace transform of (3.3) with respect to u and the Fourier transform with respect to z. We assume that the variation of the mean free path $l(u)$ with lethargy is given by

$$l(u) = \sum_{\nu=0} l_\nu \exp(-d_\nu u). \quad \ldots\ldots(3.5a)$$

Let
$$\Pi(p, \mu, \eta) = \int_0^{\infty} \mathrm{e}^{-\eta u}\, du \int_{-\infty}^{\infty} \mathrm{e}^{-ipz} \psi(z, \mu, u)\, dz, \quad \ldots\ldots(3.6)$$

i.e.
$$\psi(z, \mu, u) = \frac{1}{4\pi^2 i} \int_{\eta_1 - i\infty}^{\eta_1 + i\infty} \mathrm{e}^{\eta u}\, d\eta \int_{-\infty}^{\infty} \mathrm{e}^{ipz} \Pi(p, \mu, \eta)\, dp, \quad \ldots\ldots(3.7)$$

where η_1 lies to the right of every pole of Π. We expand $\Pi(p, \mu, \eta)$ in Legendre polynomials $\mathrm{P}_n(\mu)$:

$$\Pi(p, \mu, \eta) = \frac{1}{4\pi} \sum_{n=0}^{\infty} (2n+1) \mathrm{P}_n(\mu)\ \Pi_n(p, \eta). \quad \ldots\ldots(3.8)$$

We multiply the doubly transformed equation (3.3) by $\mathrm{P}_n(\mu)$ and integrate over μ, which gives

$$ip \sum_{\nu} l_\nu [(n+1)\Pi_{n+1}(p, \eta + d_\nu) + n\Pi_{n-1}(p, \eta + d_\nu)]$$
$$+ (2n+1) h_n(\eta)\, \Pi_n(p, \eta) = S\delta_{0n}/E_0. \quad \ldots\ldots(3.9)$$

The solution for the collision density due to a point source can easily be obtained from the solution

$$\psi_0(z, u) = \iint \psi(z, \mu, u)\, d\Omega$$

for a plane source, by using the relations

$$\psi_{0,\,pl} = -\frac{1}{2\pi r} \left[\frac{\partial \psi_0(z, u)}{\partial z}\right]_{z=r} = -\frac{1}{8\pi^3 r} \int_{\eta_1 - i\infty}^{\eta_1 + i\infty} \mathrm{e}^{\eta u}\, d\eta \int_{-\infty}^{\infty} p \mathrm{e}^{ipr}\, \Pi_0(p, \eta)\, dp.$$

In order to illustrate Holte's method, we consider first the case of constant mean free path. In the set of equations (3.9), η then appears only as a parameter, and equations (3.9) become

$$ipl_0[(n+1)\,\Pi_{n+1}(p,\eta)+n\Pi_{n-1}(p,\eta)] + (2n+1)\,h_n(\eta)\,\Pi_n(p,\eta) = S\delta_{0n}/E_0. \quad \ldots\ldots(3.10)$$

The $h_n(\eta)$ are given by the formula

$$h_n(\eta) = 1-\frac{(M+1)^2}{2M}\int_\delta^1 \mathrm{P}_n(\mu)\frac{[G(\mu)]^{2\eta}}{(M^2-1+\mu^2)^{1/2}}\,d\mu,$$

where $\delta = 0$ or -1 according as $M = 1$ or $M > 1$,

and $$G(\mu) = [\mu+(\mu^2+M^2-1)^{1/2}]/(M+1). \quad \ldots\ldots(3.11)$$

The solution of equations (3.10) for $\Pi_0(p,\eta)$ is given by the continued fraction

$$\Pi_0(p,\eta) = \cfrac{S/E_0}{h_0(\eta)+\cfrac{p^2l_0^2}{3h_1(\eta)+\cfrac{4p^2l_0^2}{5h_2(\eta)+\ldots}}}, \quad \ldots\ldots(3.12)$$

which was first obtained by Waller (1947).

It can be shown that, if $\lim_{n\to\infty} h_n(\eta) = 1$, the continued fraction converges, except at isolated poles, in the complex plane cut from $p = -i\infty$ to $p = -i/l_0$ and from $p = i/l_0$ to $p = i\infty$.

The transform $\Pi_0(p,\eta)$ is inverted by approximating the integral over p by the contribution at a pole of $\Pi_0(p,\eta)$ and evaluating the integral over η by the saddle-point method. It follows from (3.12) that small values of the poles p of the continued fraction $\Pi_0(p,\eta)$, which yield a large residue because of the small exponent in e^{-ipx}, occur when $h_n(\eta)\simeq 0$. The main pole † $p_0 = i/L(\eta)$ is small when $h_0(\eta) = 0$, i.e. when $\eta = 1$. Holte therefore considers p_0 as a function of $\theta = \eta - 1$. When $\theta\to\infty$ we are considering neutrons of the initial energy, and $p_0(\theta)\to 1$. In a small circle round the point $\theta = 0$, $\omega_0(\theta)$ can be expanded as a series :

$$[\omega_0(\theta)]^2 = c^2\theta(1-b_1\theta-b_2\theta^2-\ldots) = c^2\theta(1-\beta_1\theta-\beta_2\theta^2-\ldots)^2. \quad \ldots\ldots(3.13)$$

It follows from (3.12) that the leading term in the expansion of $\omega_0^2(\theta)$ is θ. The constants $c^2, b_1, b_2, \ldots$ depend on $h_n(\eta)$ and its derivatives at the point $\theta = 0$.

In order that the solution should not be too restricted, it is necessary to know $\omega_0(\theta)$ for much larger values of θ. This is achieved by the analytic continuation of the function $\omega_0(\theta)$. This is the essential step in Holte's analysis. It can be shown that the analytic continuation of $p_0(\theta) = i\omega_0(\theta)/l_0$ satisfies the equation $\Pi_0^{-1}[p_0(\theta),\theta] = 0$. If we calculate the residue of Π_0 at the main pole, we obtain

$$[\text{res } \Pi_0]_{p=p_0(\theta)} = \frac{S.3h_1(\theta).A(\theta)}{E_0.2\omega_0(\theta).l_0^2 i}. \quad \ldots\ldots(3.14)$$

This defines a new function $A(\theta)$, such that $A(0) = 1$. For small values of θ, $A(\theta)$ can be expanded as a power series :

$$A(\theta) = 1+\alpha_1\theta+\alpha_2\theta^2+\ldots. \quad \ldots\ldots(3.15)$$

† It will be convenient to write $p_0(\eta) = i\omega_0(\eta)/l_0$.

$A(\theta)$ may be calculated for points outside the radius of convergence of the series, again by analytic continuation.

The solution for $\psi_{0,\,pl}(R,u)$ (where $R = r/l_0$) is therefore given by

$$\psi_{0,\,pl}(R,u) = \frac{S.3h_1}{8\pi^2 Ri}\int_{L_\theta} d\theta.\exp\{u\theta - R\omega_0(\theta)\}.A(\theta), \qquad \ldots\ldots(3.16)$$

taking only the contribution from the pole at $p_0(\theta)$. Here the path of integration L_θ is a straight line in the right half-plane, parallel to the imaginary axis. To carry out these calculations, we must start with a thorough knowledge of $\omega_0(\theta)$ and $A(\theta)$ in the neighbourhood of the origin. The coefficients b_r and a_r depend on the derivatives $h_n^{(i)}$ of h_n with respect to η. The finding of these is an extremely laborious procedure. Holte, however, has determined two recurrence systems of equations for the calculation of b_r and a_r; β_r is then calculated from (3.13). We shall not go into the details of these calculations, but merely mention some of the results. Holte shows that the coefficients b_r, β_r and α_r are all of the order of magnitude of $1/M^r$. Thus the radius of convergence ρ_θ of the power series is roughly proportional to M. From numerical results it seems that the equation $\rho_\theta = \frac{1}{2}M$ is approximately valid for all values of M, for both the power series $\omega_0(\theta)$ and $A(\theta)$. Ten terms of the series for $A(\theta)$ and $\omega_0(\theta)$ give accurate results when $|\theta| \leqslant 0{\cdot}4M$.

The analytic continuation of the expansions (3.15) and (3.13) is performed by taking $1/\theta$ as the variable instead of θ, and putting

$$y = 1/\theta, \quad H(y) = \omega_0(1/y), \quad L(y) = A(1/y).$$

A real positive value y_0 is taken so that $\theta_0 = 1/y_0 < 0{\cdot}3\rho_\theta$. We calculate the values of $H(y)$ and $L(y)$ and their derivatives at $y = y_0$, and form new Taylor expansions at this point. Another point y_1 is taken on the positive real axis, with $\theta_0 < 1/y_1 = \theta_1 < \rho_\theta$. The coefficients of the Taylor series at y_1 are calculated from those at y_0. The reason for taking $\theta_1 < \rho_\theta$ is to facilitate the numerical calculation. The accuracy of the procedure depends on how many coefficients b_r, β_r and α_r are initially computed. For large θ we are considering neutrons of the initial energy, and $\omega_0(\theta) \to 1$. Hence, for $y = 0$, $H(0)$ and $L(0) = 0$, and Holte therefore performs an analytic continuation to $y = 0$, calculating $H(0), H'(0), \ldots, L(0), L'(0), \ldots$. The series is somewhat arbitrarily adjusted so that $H(0) = 1$ and $L(0) = 0$ exactly; this involves only a slight correction.

Holte investigates some simple approximate formulae for $\omega_0(\theta)$, which we denote by $\omega_s(\theta)$. For small θ,

$$\omega_s(\theta) = C\sqrt{\theta}(1 - \beta_1\theta), \qquad \ldots\ldots(3.17)$$

while for any real and positive θ

$$\omega_s(\theta) = a - b/(c + \theta), \qquad \ldots\ldots(3.18)$$

where a, b, c are constants to be determined numerically.

The above method differs from Wick's (1949) in that the latter merely outlines a numerical method for determining the values of $A(\theta)$ point by point for intermediate values of θ.

Having obtained expressions for $A(\theta)$ and $\omega_0(\theta)$, we can now perform the integration in (3.16). The path of integration L_θ is deformed to pass through a

saddle-point along a 'path of steepest descent'. Instead of the exponential function in (3.16), we take as the rapidly varying function the exponential with $\omega_0(\theta)$ replaced by $\omega_s(\theta)$; the difference is so small that, even when it is multiplied by R in the exponent, its exponential can be considered to vary as slowly as $A(\theta)$. To obtain the saddle-point, we differentiate the exponent with $\omega_s(\theta)$ in place of $\omega_0(\theta)$, obtaining

$$u - R\omega_s'(\theta) = 0. \qquad \ldots\ldots(3.19)$$

Let the root of (3.19) be $\theta = \theta_s$. For different ranges of θ, we have different formulae for ω_s and different formulae for θ_s. The standard procedure for evaluating the integral has to be modified slightly, since $\omega_0(\theta) \sim \theta^{3/2}$. It is necessary to transform the integral by putting $\theta = \phi^2$.

The results can be stated as follows.† The collision density is given by

$$\psi_0(r, u) = \frac{\mu_M(R/u)}{l_0^3 u^{3/2}} \exp\{-\nu_M(R/u)\, R\}, \qquad \ldots\ldots(3.20)$$

where $R = r/l_0$, and μ_M and ν_M are functions of R/u to the first approximation, taking different forms for different ranges of R/u. The most important quantity is $\nu_M(R/u)$, which varies monotonically from 0 to 1 as R/u goes from 0 to ∞.

(i) The lowest range of R/u is given by $0 < R/u \ll A$, where A is a constant depending on M. In this region

$$\nu_M = RC^2/4u, \qquad \ldots\ldots(3.21)$$

where

$$\begin{aligned} C &\simeq 6/M \quad \text{for} \quad M \gg 1 \\ &\simeq 1{\cdot}2 \quad \text{for} \quad M = 2 \\ &\simeq 1 \quad \text{for} \quad M = 1 \end{aligned} \qquad \ldots\ldots(3.22)$$

and

$$\begin{aligned} A &\simeq M/6 \quad \text{for} \quad M \gg 1 \\ &\simeq 0{\cdot}6 \quad \text{for} \quad M = 2 \\ &\simeq 1{\cdot}0 \quad \text{for} \quad M = 1. \end{aligned} \qquad \ldots\ldots(3.23)$$

Thus, for $M \gg 1$, $\nu_M \simeq 3R/2Mu$ for $0 < R/u \ll M/6$. $\ldots\ldots(3.24)$

This corresponds to the well-known result of age theory.

(ii) As R/u increases ν_M varies more slowly, becoming

$$\nu_M = \frac{RC^2}{4u}\left[1 - B\frac{R^2}{u^2}\right], \qquad \ldots\ldots(3.25)$$

where

$$\begin{aligned} B &\simeq 6/M^2 \quad \text{for} \quad M \gg 1 \\ &\simeq 1/6 \quad \text{for} \quad M = 1. \end{aligned} \qquad \ldots\ldots(3.26)$$

This holds for R/u increasing past A up to

$$R/u \simeq D,$$

where

$$\begin{aligned} D &\simeq \tfrac{1}{2}M \quad \text{for} \quad M \gg 1 \\ &\simeq 2{\cdot}8 \quad \text{for} \quad M = 1. \end{aligned}$$

† A summary of the results of Holte's method has been given by Spinney (1953).

(iii) As R/u increases further, ν_M becomes

$$\nu_M = a - 2\sqrt{(bu/R)} + cu/R, \qquad \ldots\ldots(3.27)$$

where a, b, c can be regarded as constants, for a given M, over fairly large ranges of R/u. They are of the order of unity.

(iv) As $R/u \to \infty$, ν_M retains the form (3.27). The last set of values of a, b, c giving the asymptotic form of ν_M, is $a = 1, b = k_1, c = c_\infty$, where c_∞ and k_1 have been determined by Wick (1949).

The function $\mu_M(R/u)$ in (3.20) takes the following forms. Let

$$H = \frac{3 - 2/M}{(2\sqrt{\pi})^3}. \qquad \ldots\ldots(3.28)$$

In the region (i), $\mu_M \simeq HC$, where C is given by (3.22). In the region (ii)

$$\mu_M \simeq HC(1 - 3BR^2/u^2),$$

and decreases more rapidly as R/u increases. In the region (iii), i.e. $R/u \geqslant D$, we have

$$\mu_M \simeq Hb^{1/4}(u/R)^{3/4}\left[1 - \frac{4}{M}\left(\sqrt{\frac{bR}{u}} - c\right)\right]. \qquad \ldots\ldots(3.29)$$

In region (iv), as $R/u \to \infty$, μ_M approaches the asymptotic form

$$\mu_M = Hm_1 k_1^{-1/4}(u/R)^{3/4}, \qquad \ldots\ldots(3.30)$$

where m_1 is another constant, depending on M, of the order of unity.

There are certain limitations on R and u. For high neutron energies, i.e. $u < 10$, there is a domain round the source where the formulae do not apply. This is not a serious limitation in shielding problems.

The values of the constants, a, b and c for various elements can be obtained from Holte's paper.

Let us now consider the case of variable mean free path. Holte uses the same technique of analytic continuation to determine $\psi_0(r, u)$. The problem is, however, more complicated, and we shall not reproduce any of the analysis here. Holte assumes that the mean free path varies in accordance with the formula (3.5*a*) and makes the further assumption that $l(u)$ decreases monotonically as u increases. According to (3.5*a*), l_0 is the mean free path as $u \to \infty$, i.e. the mean free path for thermal neutrons, while $l_m = \Sigma l_r$ is the mean free path for $u = 0$, i.e. at the initial energy.

For small values of $r, \psi_0(r, u)$ varies with r according to a gaussian curve, i.e. as in case (i) for a constant mean free path. This soon changes to an exponential decay, with a relaxation length decreasing to l_m as r/u tends to infinity.

The asymptotic form can be written

$$\psi_0(r, u) = \frac{\mu_M \exp(u\theta_m - r/l_m)}{4\pi l_m^3 (r/l_m)^\rho}. \qquad \ldots\ldots(3.31)$$

The shape of the limiting spectrum is determined by the constant θ_m, which decreases as l_m/l_0 increases but increases with M; ρ is a quantity first derived by Wick: it depends on the form of $l(u)$ near $u = 0$, and varies slowly with M; μ_M increases with M (approximately as M for large M), and with l_m/l_0.

There is a marked difference between the asymptotic formulae for constant and variable mean free paths. In the latter case, the shape of the energy spectrum of ψ_0 is independent of r as $r \to \infty$, whilst in the former case the exponent is

$$-R + 2\sqrt{(k_1 uR)} - c_\infty u.$$

Spinney (1953) has shown that there is good agreement between calculations, using Holte's method, of the indium resonance energy neutrons (1·44 ev) from a source of energy 0·9 Mev and some experimental results given by O'Neal (1946).

3.2. *The Moment Method*

This method was first used by Spencer and Fano (1951) to calculate the propagation of x-rays through a medium. The fundamental idea is as follows. Consider a distribution $f(z)$ over a single space variable z, which varies from $-\infty$ to ∞; f is assumed to vanish sufficiently rapidly at both ends of this range. To obtain a polynomial expansion of f, a suitable weight function $w(z)$, vanishing at $\pm\infty$, is chosen. A series of polynomials $p_0, p_1, \ldots, p_n$, with an adjoint series $p_0^+, p_1^+, \ldots$, satisfying the orthogonality condition

$$\int_{-\infty}^{\infty} w(z) p_{n'}{}^{+}(z)\, p_n(z)\, dz = \delta_{nn'}, \qquad \ldots\ldots(3.32)$$

can be used to expand the function $f(z)$:

$$f(z) = w(z) \sum_n a_n p_n(z). \qquad \ldots\ldots(3.33)$$

The coefficients a_n are given by

$$a_n = \int_{-\infty}^{\infty} p_n{}^{+}(z) f(z)\, dz. \qquad \ldots\ldots(3.34)$$

If all the moments

$$\int_{-\infty}^{\infty} z^m f(z)\, dz$$

of the function f are known, the a_n can be calculated and the expansion (3.33) determined.

For the problem of x-ray diffusion, a weight factor $e^{-\alpha z}$ was taken. The corresponding series of polynomials is formed by the Laguerre polynomials

$$L_n(\alpha z) = \sum_\nu \frac{n!}{(n-\nu)!} \frac{(-\alpha z)^\nu}{(\nu!)^2}.$$

It is not necessary to compute the moments, since recurrence relations are found to hold between the coefficients a_n when the series is substituted for the neutron density in the transport equation.

However, in neutron diffusion problems the weight factor $e^{-\alpha z}$ would not necessarily give good convergence of (3.33), except for slowing down in hydrogen.

The moments

$$\int_{-\infty}^{\infty} z^m f(z)\, dz$$

are calculated and the function $f(z)$ is constructed from them. We shall give here some results due to Certaine (1955). Unfortunately, no details are given of the method by which the function f was constructed from the moments. However,

the method is very powerful, and it is worth while to indicate how the moments are calculated, and to give some idea of the complexity of the calculation.†

We start from equation (1.16) for the case of plane geometry and no time dependence :

$$\mu\frac{\partial\phi(z,\mu,u)}{\partial z}+\alpha(u)\,\phi(z,\mu,u)$$

$$=\int\beta(u')\,du'\iint\phi(z,\mu',u')f'(u',\boldsymbol{\Omega}'\rightarrow u,\boldsymbol{\Omega})\,d\Omega'+S(z,\mu,u), \qquad \ldots\ldots(3.35)$$

where ϕ denotes vN and μ is the cosine of the angle between the neutron direction and the z axis.

Let ϕ be expanded as a Legendre series :

$$\phi(z,\mu,u)=\frac{1}{4\pi}\Sigma(2n+1)\,\phi_n(z,u)\,\mathrm{P}_n(\mu). \qquad \ldots\ldots(3.36)$$

Equation (3.35) is multiplied by $\mathrm{P}_n(\mu)$ and integrated over μ, yielding

$$\frac{n+1}{2n+1}\frac{\partial\phi_{n+1}(z,u)}{\partial z}+\frac{n}{2n+1}\frac{\partial\phi_{n-1}(z,u)}{\partial z}+\alpha(u)\,\phi_n(z,u)$$

$$=\int\beta(u')\,du'\iint\phi(z,\mu',u')\,d\Omega'\int f'(u',\boldsymbol{\Omega}'\rightarrow u,\boldsymbol{\Omega})\,\mathrm{P}_n(\mu)\,d\mu+S_n(z,u), \qquad \ldots\ldots(3.37)$$

where S_n is the appropriate moment of S.

Equation (1.17) shows the form of the scattering function f' for scattering isotropic in the centre-of-mass system. When the scattering is not isotropic, but is given by some function $p(u',\cos\Theta)$, the form of the function f' is similar ; it is still a function of the angle $\cos^{-1}\mu_0$ between the initial and final directions of the neutron in the laboratory system, and of the lethargies u and u' ; Θ is the angle between the directions in the centre-of-mass system.

Let f' be expanded in a series of Legendre polynomials $\mathrm{P}_n(\mu_0)$, i.e.

$$f'=\frac{1}{4\pi}\sum_{n=0}^{\infty}(2n+1)f_n(u,u')\,\mathrm{P}_n(\mu_0). \qquad \ldots\ldots(3.38)$$

It can then be shown that the first term on the right-hand side of equation (3.37) reduces to

$$\int\beta(u')\,\phi_n(z,u')f_n(u,u')\,du'. \qquad \ldots\ldots(3.39)$$

We have shown previously [cf. (1.11)] that $\cos\Theta$ is related to u' by

$$\cos\Theta=1-\frac{(M+1)^2}{2M}\,[1-\exp\{-(u-u')\}]. \qquad \ldots\ldots(3.40)$$

If we substitute for u' from (3.40) in (3.39), the latter becomes

$$\int_{-1}^{1}\beta(u')\,p(u',\cos\Theta)\,\mathrm{P}_n(\mu_0)\,\phi_n(z,u')\,d\cos\Theta \qquad \ldots\ldots(3.41)$$

† The calculation is similar to that described for the determination of the spectrum in an infinite medium. However, it is a little more complicated because the scattering is not assumed isotropic in the centre-of-mass system.

(μ_0 is a one-valued function of $\cos\Theta$; cf. § 1). This is a convenient form of the integral, since the function $p(u', \cos\Theta)$ is determined experimentally.

Let the moment ϕ_{mn} be defined by the equation

$$\phi_{mn}(u) = \int_{-\infty}^{\infty} \frac{z^m}{m!}\, dz \iint_{4\pi} \mathrm{P}_n(\mu)\phi\,(z, \mu, u)\, d\Omega. \qquad \ldots\ldots(3.42)$$

If equation (3.37) is multiplied by z^m and integrated over all z, we have

$$-\frac{n+1}{2n+1}\,\phi_{m-1,\,n+1}(u) - \frac{n}{2n+1}\,\phi_{m-1,\,n-1}(u) + \alpha(u)\,\phi_{mn}(u)$$

$$= \int_{-1}^{1} \beta(u')\, p(u', \cos\Theta)\, \mathrm{P}_n(\mu_0)\, \phi_{mn}(u')\, d\cos\Theta + S_{mn}(u), \qquad \ldots\ldots(3.43)$$

where

$$S_{mn}(u) = \int_{-\infty}^{\infty} \frac{z^m\, S_n(z, u)\, dz}{m!}.$$

The function $p(u', \cos\Theta)$ is determined by graphs of the coefficients

$$p_l(u') = \iint_{4\pi} p(u', \cos\Theta)\, \mathrm{P}_l(\cos\Theta)\, d\Omega' \qquad \ldots\ldots(3.44)$$

i.e.

$$p(u', \cos\Theta) = \frac{1}{4\pi}\, \Sigma(2l+1)\, p_l(u')\, \mathrm{P}_l(\cos\Theta). \qquad \ldots\ldots(3.45)$$

The chief problem is therefore to determine expressions for integrals of the type

$$\frac{2l+1}{2} \int_{-1}^{1} \beta(u')\, p_l(u')\, \mathrm{P}_l(\cos\Theta)\, \mathrm{P}_n(\mu_0)\, \phi_{mn}(u')\, d\cos\Theta. \qquad \ldots\ldots(3.46)$$

These integrals are evaluated numerically. Let $H(u')$ be defined by

$$H(u') = \beta(u')\, p_l(u')\, \phi_{mn}(u').$$

The variable u' ranges from u up to u_0, where $u_0 - u$ is the maximum lethargy change possible in a collision. We divide the range into a number of equal intervals h. It is assumed that H is linear in each interval. The integral (3.46) can now be evaluated, and is given by the sum

$$\sum_{k=0}^{N+1} H_k \mathrm{e}^{-kh}\, \psi_{lkn}, \qquad \ldots\ldots(3.47)$$

where H_k is the value of H for $u_k' = u + kh$, and $\mu_0 = \mu + (N+1)h$. The expressions for ψ_{lkn} contain integrals of the type

$$\int_{\cos\Theta_{k+1}}^{\cos\Theta_k} \log \frac{M^2 + 2M\cos\Theta + 1}{M^2 + 2M\cos\Theta_{k+1} + 1}\, \mathrm{P}_l(\cos\Theta)\, \mathrm{P}_n(\mu_0)\, d\cos\Theta. \qquad \ldots\ldots(3.48)$$

We shall not, however, write out these expressions in detail.

It is evident that the integral in equation (3.43) can also be expressed as a sum of the form

$$\sum_{k=0}^{N+1} a_k \phi^{j+k}{}_{mn},$$

where $\phi^{j+k}{}_{mn} = \phi_{mn}(u + kh) = \phi_{mn}(jh + kh)$, i.e. $u = jh$.

The coefficient a_k is the sum of integrals of the type (3.48). Equation (3.43) can now be replaced by

$$-\frac{n+1}{2n+1}\phi^j_{m-1,\,n+1}-\frac{n}{2n+1}\phi^j_{m-1,\,n-1}+\alpha^j\phi^j_{mn}=\sum_{k=0}^{n+1}\phi^{j+k}_{mn}+S^j_{mn}, \quad \ldots\ldots(3.49)$$

where $\alpha^j=\alpha(jh)$ and $S^j_{mn}=S_{mn}(jh)$. When $m=0$, the terms $\phi^j_{m-1,\,n+1}$ are absent from the left-hand side of (3.49). We can then determine ϕ^j_{0n} for each j and each particular value of n, by solving the recurrence relations (3.49). We then proceed to $m=1$; the first two terms on the left-hand side of (3.49) are now known, and we can calculate ϕ^j_{1n}, and so on.

Certaine (1954) has also reported calculations for hydrogen and compounds of hydrogen with a heavier element. Use is made of the fact that, for large atomic masses M, the integral term can be expanded as a power series in $1/M$. In the calculations, the first two terms of this expansion were used. The calculation which we have described involves no such approximation, and can be carried out to any desired accuracy.

Aronson, Certaine and Goldstein (1954) have reported calculations of doses and differential neutron flux spectra at distances of up to 120 cm from various isotropic sources, most of which emitted nearly monoenergetic neutrons at 2, 4, 6, 8, 10 and 14 MeV.

§ 4. Calculations of Critical Size

4.1. *One-velocity-group Theory*

In one-velocity-group theory, we assume that the cross sections are constant. Equation (1.2) can then be integrated over all velocities, and if scattering is isotropic in the laboratory system we have the equation

$$\boldsymbol{\Omega}\,.\,\mathbf{grad}\,\phi(\mathbf{r},\boldsymbol{\Omega})+\alpha\phi(\mathbf{r},\boldsymbol{\Omega})=\frac{\beta}{4\pi}\int\!\!\int\phi(\mathbf{r},\boldsymbol{\Omega}')\,d\Omega', \quad \ldots\ldots(4.1)$$

where

$$\phi(\mathbf{r},\boldsymbol{\Omega})=\int vN(\mathbf{r},v\boldsymbol{\Omega})\,dv$$

is the angular distribution of the neutron flux $\phi_0(\mathbf{r})$. Davison (1947) has shown that equation (4.1) can be integrated, and the following integral equation is obtained for the neutron flux $\phi_0(\mathbf{r})$ in a homogeneous medium:

$$\phi_0(\mathbf{r})=\beta\int\!\!\int\!\!\int\phi_0(\mathbf{r}')\,K(\mathbf{r},\mathbf{r}')\,dV', \quad \ldots\ldots(4.2)$$

where the kernel $K(\mathbf{r},\mathbf{r}')$ is defined by

$$K(\mathbf{r},\mathbf{r}')=\mathrm{e}^{-\alpha R}/4\pi R^2, \quad \ldots\ldots(4.3)$$

with

$$R=|\mathbf{r}-\mathbf{r}'|.$$

The integration is extended over the reacting medium. Solutions $\phi_0(\mathbf{r})$ exist if β is one of the eigenvalues of the equation (4.2), and we are interested in the solution corresponding to the smallest eigenvalue. The equation can easily be modified so as to be applicable to a system consisting of a core and a reflector (Davison 1947, Fuchs 1943).

Let us now consider solutions of the integral equation (4.2) when the integration is extended over all space. Using Cartesian coordinates, we expand $\phi_0(\mathbf{r}')$ as a Taylor series about the point $\mathbf{r}$, i.e.

$$\phi_0(\mathbf{r}') = \phi_0(\mathbf{r}) + \left\{(x'-x)\frac{\partial\phi_0}{\partial x} + (y'-y)\frac{\partial\phi_0}{\partial y} + (z'-z)\frac{\partial\phi_0}{\partial z}\right\} + \ldots\ldots\ldots\ldots (4.4)$$

This series is substituted in the right-hand side of equation (4.2), and the following equation is obtained for ϕ_0:

$$\phi_0(\mathbf{r}) = \frac{\beta}{\alpha}\left[\phi_0(\mathbf{r}) + \frac{\nabla^2\phi_0(\mathbf{r})}{3\alpha^2} + \frac{\nabla^4\phi_0(\mathbf{r})}{5\alpha^4} + \ldots\right]. \qquad \ldots\ldots (4.5)$$

A solution of the equation $\nabla^2\phi_0 + \kappa^2\phi_0 = 0$ ……(4.6)

will also be a solution of (4.5), provided that κ satisfies

$$\kappa/\beta = \kappa/\alpha - \tfrac{1}{3}(\kappa/\alpha)^3 + \tfrac{1}{5}(\kappa/\alpha)^5 - \ldots \qquad \ldots\ldots (4.7)$$

$$= \tan^{-1}(\kappa/\alpha), \qquad \ldots\ldots (4.8)$$

or $\kappa/\alpha = \tan(\kappa/\beta)$.

This procedure is justifiable only if $\kappa < \alpha$.

Thus, for an infinite medium, the integral equation (4.2) will be satisfied by solutions of (4.6), with κ given by (4.8). If $\beta < \alpha$, κ is imaginary, and equals $i\mu$ (say). Then μ is given by the equation

$$\mu/\alpha = \tanh(\mu/\beta). \qquad \ldots\ldots (4.9)$$

If β/α is nearly unity, κ/α is small, and we can neglect the terms after the second on the right of (4.7):

$$\kappa^2 = 3\alpha^2(\beta-\alpha)/\beta \simeq 3\alpha(\beta-\alpha). \qquad \ldots\ldots (4.10)$$

Davison (1947) has shown that the neutron current vector $\mathbf{j}$, defined as

$$\mathbf{j} = \iint \boldsymbol{\Omega}\phi(\mathbf{r}, \boldsymbol{\Omega})\, d\Omega, \qquad \ldots\ldots (4.11)$$

is given by $\mathbf{j}(\mathbf{r}) = -D\,\mathbf{grad}\,\phi_0(\mathbf{r})$, ……(4.12)

where $D = (\beta-\alpha)/\kappa^2$. ……(4.13)

The scalar product of $\mathbf{j}$ with any unit vector $\mathbf{n}$ gives the number of neutrons passing per unit time through unit area perpendicular to $\mathbf{n}$.

If $\beta \simeq \alpha$, then

$$D \simeq 1/3\alpha. \qquad \ldots\ldots (4.14)$$

The solutions of (4.6) which are exact for an infinite medium can also be used with considerable success to predict the critical size and neutron distribution for finite systems large compared with the neutron mean free path, provided that a one-group solution is adequate. Equation (4.6) is solved for each region of the reactor, and solutions are chosen which are regular and possess the requisite symmetry. The solutions are matched at common boundaries by imposing suitable boundary conditions on the neutron flux and the normal component of the current vector. These conditions may be summarized as follows.

Suppose that we wish to match the solutions of $(\nabla^2+\kappa^2)\phi_{0c}=0$ in the core and $(\nabla^2-\mu^2)\phi_{0r}$ in a capturing reflector, the suffixes c and r denoting core and reflector respectively. Then

$$j_c = j_r, \qquad \ldots\ldots(4.15)$$

where j is the normal component of the current vector at the boundary, and

$$\alpha_c \frac{\beta_c-\alpha_c}{\kappa^2}\phi_{0c} = \alpha_r \frac{\alpha_r-\beta_r}{\mu^2}\phi_{0r} \qquad \ldots\ldots(4.16)$$

if the boundary is plane, or in spherical systems where the mean free paths are equal in the two media; this formula is due to Davison (1944, 1947). There is a discontinuity in the solution for ϕ at the boundary. The true solution of the integral equation would not possess such a discontinuity, which is a measure of the inadequacy of equation (4.6) near the boundary.

If $\alpha_c \simeq \beta_c$ and $\alpha_r \simeq \beta_r$, it can be seen from (4.10) that the condition (4.16) reduces to the continuity of the flux.

At a free surface in a plane geometry, we have a boundary condition

$$\phi_0/(d\phi_0/dx) = \lambda, \qquad \ldots\ldots(4.17)$$

where the reacting region is to the right of the boundary. λ is called the linear extrapolation length. Case, de Hoffmann and Placzek (1953) have tabulated λ as a function of α and β. For a purely scattering medium it is equal to $0{\cdot}71/\alpha$.

The boundary condition at a spherical boundary is

$$r\phi_0(r)\,[d(r\phi_0)/dr] = -\lambda. \qquad \ldots\ldots(4.18)$$

Alternatively, we may use the boundary condition that the flux vanishes at a distance x_0 beyond the free surface of the medium (at radius $r = a+x_0$ for a spherical medium of radius a). The value of x_0 also has been tabulated (Case *et al.* 1953) as a function of β/α. The application of this boundary condition is sometimes called the end-point method.

Davison (1951) has calculated the extrapolation lengths λ at the surfaces of black (i.e. completely absorbing) spheres and cylinders as a function of their radii. These calculations were done by a perturbation method. Recently, calculations have been reported of the boundary conditions to be used at the surfaces of grey bodies (the word 'grey' meaning that the body does not completely absorb the neutrons incident on it). Kushneriuk and McKay (1954) have described a calculation of the linear extrapolation length at the interface between a cylinder and a homogeneous isotropically and elastically scattering medium of infinite extent, with neutron sources far from the cylinder. λ was calculated by means of the variational method, perturbation theory, and the Wiener–Hopf method for cylinders of infinitely large radius. The calculations were carried out for a homogeneous cylinder surrounded by an air gap or a thin slightly absorbing sheath, or both.

Zaretsky (1955) has also described a calculation of the effective boundary conditions for grey bodies. He neglects scattering in the body in comparison with capture. Royston (1955) has also made a similar calculation for cylinders, but the work of Kushneriuk is the most comprehensive.

If κ is calculated from (4.8), and if the end-point boundary condition is applied for a bare sphere, we obtain a relation between κ and the critical radius a which yields surprisingly accurate results for the value of a, even in systems whose radii are of the order of one mean free path, i.e. spheres of pure fissile material.

The equation (4.6), with κ calculated from (4.8), forms the basis of what is called modified diffusion theory, or asymptotic theory. This theory (Codd, Shepherd and Tait 1956) is often adequate for the analysis of flux distributions and perturbation experiments in zero-energy fast assemblies such as 'Zephyr', 'Godiva' and 'Topsy'†. The first of these has a core of plutonium and uranium and a uranium reflector, the second is an enriched uranium sphere and the third has this as a core with a uranium reflector.

There are methods for the exact solution of (4.1), without the restriction that the system should be large. One of the most powerful is the spherical harmonics method, in which the angular distribution is expanded in spherical harmonics. A complete description of the method has been given by Mark (1944), whose reports tabulate the various functions used in applying the method. We shall not give details here, since the interest in neutron diffusion theory lies in calculations where the neutron mean free path cannot be assumed independent of energy.

4.2. *Multi-velocity-group Diffusion Theory*

The one-velocity-group asymptotic theory which we have outlined can easily be extended to take account of two velocity groups. Let ϕ_{01}, ϕ_{02} be the fluxes and α_1, α_2 the inverse mean free paths in the two groups. Let β_{11} and β_{21} be the number of secondaries per unit path produced in the first and second group respectively by a neutron in the first group. β_{22} and β_{12} are similar quantities for the second group.

By a calculation similar to what we outlined for the one-velocity-group case, if f is a solution of

$$\nabla^2 f + \kappa^2 f = 0, \qquad \ldots\ldots(4.19)$$

then

$$\phi_{01} = f, \quad \phi_{02} = \xi f,$$

provided that κ and ξ satisfy the relations

$$[\kappa - \beta_{11}\tan^{-1}(\kappa/\alpha_1)]\,[\kappa - \beta_{22}\tan^{-1}(\kappa/\alpha_2)] = \beta_{12}\beta_{21}\tan^{-1}(\kappa/\alpha_1)\tan^{-1}(\kappa/\alpha_2) \qquad \ldots\ldots(4.20)$$

and

$$\xi = \{[\kappa/\tan^{-1}(\kappa/\alpha_1)] - \beta_{11}\}/\beta_{12}. \qquad \ldots\ldots(4.21)$$

The derivation of these equations is valid only if $\kappa < \alpha_1, \alpha_2$. Certain combinations of values of the constants have the result that the roots of (4.20) do not meet this condition, and these roots are therefore unusable.

When $\alpha_1 \simeq \beta_{11}, \alpha_2 \simeq \beta_{22}$, equation (4.20) reduces to

$$[\kappa^2 + 3\alpha_1(\beta_{11} - \alpha_1)]\,[\kappa^2 + 3\alpha_2(\beta_{22} - \alpha_2)] = 9\beta_{12}\beta_{21}\alpha_1\alpha_2. \qquad \ldots\ldots(4.22)$$

The current vectors $\mathbf{j}_1$ and $\mathbf{j}_2$ in the two groups are given by

$$\mathbf{j}_1 = -\frac{1}{3\alpha_1}\,\mathbf{grad}\,\phi_{01}, \quad \mathbf{j}_2 = -\frac{1}{3\alpha_2}\,\mathbf{grad}\,\phi_{02}. \qquad \ldots\ldots(4.23)$$

A theory in which this approximation is used is called simple diffusion theory.

† 'Godiva' and 'Topsy' are American zero-energy assemblies.

Let us now consider the form of the simple diffusion equations in multi-velocity-group theory (with any number of groups). Most calculations have been carried out for spherically symmetric systems. The flux is then a function of only one spatial coordinate, the distance of a point from the centre of the system.

Let ϕ_{0g} be the neutron flux in a particular group g. Then ϕ_{0g} satisfies the equation

$$-\frac{1}{3\alpha_g}\frac{d^2(r\phi_{0g})}{dr^2}+r\alpha_g\phi_{0g}=r\sum_{g'}\beta_{gg'}\phi_{0g'}+rf_g, \qquad \ldots\ldots(4.24)$$

where α_g is the inverse mean free path; $\beta_{gg'}$ is the appropriate cross section per unit volume for transfer from group g' to group g by processes other than fission (β_{gg} being the corresponding cross section for neutrons to remain in group g after scattering). f_g is the number of fission neutrons emitted in group g, i.e.

$$f_g=F_g\sum_{g'}\phi_{0g'}\alpha_{fg'}, \qquad \ldots\ldots(4.25)$$

where α_{fg} is the cross section per unit volume for fission in group g, and F_g is the number of fission neutrons emitted in group g. In principle, an analytic solution of equations (4.24) can be written down for a system consisting of a core and any number of layers of reflector. However, a numerical procedure is preferable when the number of groups is large.

Equations (4.24) are solved by a source iteration procedure. That is, we assume a given distribution of fissions, determine the fluxes in each group, and then calculate a new fission source distribution f_g. The process is repeated until the ratio of $f_g(r)$ for two consecutive iterations is independent of r and equal to m (say). Then m is the multiplication rate per generation of neutrons. If the constants of the system are fixed, we desire to know the value of the core radius for which m is unity. This involves a calculation of m for several values of the radius, and the radius for which m is unity is found by interpolation.

Let $\Phi_g(r)=r\phi_{0g}(r)$. In a numerical solution, we divide the range of integration over r into equal intervals Δr in the core, and equal (but possibly different from Δr) intervals $\Delta' r$ in the reflector. Let the space points be denoted by r_n, and $\Phi_g(r_n)=\Phi_{gn}$. Then

$$\left[\frac{d^2\Phi_g(r)}{dr^2}\right]_{r=r_n}=\frac{\Phi_{g,n+1}+\Phi_{g,n-1}-2\Phi_{gn}}{(\Delta r)^2}. \qquad \ldots\ldots(4.26)$$

On substituting into equation (4.24), we have an equation of the form

$$\Phi_{g,n+1}=k_g\Phi_{gn}-\Phi_{g,n-1}-I_{gn}, \qquad \ldots\ldots(4.27)$$

where

$$k_g=2+3\alpha_g(\alpha_g-\beta_{gg})(\Delta r)^2,$$

$$I_{gn}=3\alpha_g(\Delta r)^2\sum_{g'\neq g}\beta_{gg'}\Phi_{gn}+3r_n\alpha_g f_{gn}(\Delta r)^2.$$

The manipulation thus far is straightforward. Ehrlich and Hurwitz (1954) have reported an ingenious method (due to Stark) of solving equations (4.27).

Let the homogeneous form of (4.27) be

$$A_{n+1}=k_gA_n-A_{n-1}, \qquad \ldots\ldots(4.28)$$

and put

$$\alpha_{n+1}=A_{n+1}/A_n. \qquad \ldots\ldots(4.29)$$

Then

$$\alpha_{n+1}=k_g-1/\alpha_n. \qquad \ldots\ldots(4.30)$$

Let $$\beta_n = \sum_{j=0}^{n} A_j I_{gj}/A_n. \qquad \ldots\ldots(4.31)$$

Then
$$\begin{aligned}\beta_n &= I_{gn} + \sum_{j=0}^{n-1} A_j I_{gj}/A_n \\ &= I_{gn} + \frac{A_{n-1}}{A_n} \sum_{j=0}^{n-1} A_j I_{gj}/A_{n-1} \\ &= I_{gn} + \beta_{n-1}/\alpha_n. \qquad \ldots\ldots(4.32)\end{aligned}$$

The solution for the α_n and β_n is started with $\alpha_2 = k_g$ and $\beta_1 = I_1$. Then it can be shown by induction that

$$\Phi_{gn} = (\Phi_{g,n+1} + \beta_n)/\alpha_{n+1}.$$

This equation is solved for the Φ_{gn}, starting from the outside of the system with Φ_{gn} zero at the extrapolated end-point. The technique of solving the equations is to take a complementary solution and a particular solution of equations (4.27), combined in such a way as to satisfy the external boundary condition. Unless this procedure is used, the two solutions might increase outwards.

Okrent, Avery and Hummel (1955) have given a comparison of the result of calculations by simple diffusion theory with three and ten energy groups (the number of energy groups does not greatly affect the results) and those obtained from an accurate numerical solution of the transport equation (to be described below). The ratio of the critical radii given by the two methods is shown in the figure as a function of the radius of the core (in mean free paths).

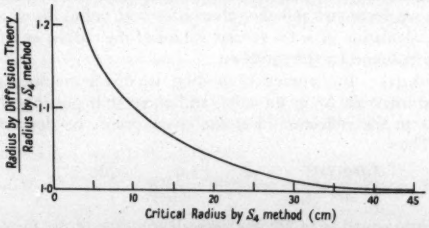

The ratio of critical radii (diffusion theory to S_4 method) as a function of S_4 critical radius for two-velocity-group theory.

This figure does not give an estimate of the accuracy of modified diffusion theory, which is more accurate than the simple theory.

Reacting systems are, of course, not always spherical in shape. However, by replacing a cylindrical system by an equivalent spherical one, the critical mass can be determined with accuracy to 10%. To obtain greater accuracy, the diffusion equations must be solved in more than one spatial dimension (Wachspress 1955).

4.3. *The Solution of the Energy-dependent Transport Equation*

Several methods have been described for the solution of equation (1.2). The spherical harmonics method in the multi-velocity-group form (Mandl 1953) is

extremely complicated. Davison (1952) and Elliott (1953, 1954) have developed a polynomial method, in which the moments of the angular distribution $N(\mathbf{r}, v\boldsymbol{\Omega})$ are expanded as polynomials in the velocity. This necessitates the expansion of the cross sections as polynomials in the velocity, which is a serious drawback to the method when the cross sections are rapidly varying.

The most powerful method seems to be the S_N method of Carlson (1955). This is a numerical method of solving problems in plane, spherical and cylindrical geometry, and is intended for use with high-speed computing machines. Time-dependent problems can also be treated by this method.

We divide the energy range into a series of intervals and integrate equation (1.2) over the range of energy in each interval, assuming that the cross sections are constant in that interval. For the case of spherical symmetry and isotropic scattering, we then have for each energy group g

$$\left[\mu D_r + \frac{1-\mu^2}{r} D_\mu + \alpha_g(r)\right] \phi_g(r, \mu) = S_g(r), \qquad \ldots\ldots(4.33)$$

where $D_r = \partial/\partial r$, $D_\mu = \partial/\partial\mu$, $\phi_g(r, \mu)$ is the angular distribution of flux in group g, r is the distance from the centre of the system, $\cos^{-1}\mu$ is the angle between $\boldsymbol{\Omega}$ and the radius vector $\mathbf{r}$. The source term $S_g(r)$ in equation (4.33) takes the form

$$\sum_{g'} \beta_{gg'} \phi_{0g'}(r) + f_g,$$

where f_g is given by (4.25), and

$$\phi_{0g'}(r) = \frac{1}{2}\int_{-1}^{1} \phi_{g'}(r, \mu)\, d\mu. \qquad \ldots\ldots(4.34)$$

Carlson divides the range of integration over μ into N (usually equal) sub-intervals. Let the points defining these sub-intervals be $\mu_j (j = 0, 1, \ldots, N)$, so that $\mu_0 = -1$, $\mu_N = 1$. The number of intervals N defines the order of the approximation.

In the sub-interval between μ_{j-1} and μ_j, we assume that $\phi_g(r, \mu)$ is linear in μ, i.e.

$$\phi_g(r, \mu) = \frac{\mu - \mu_{j-1}}{\mu_j - \mu_{j-1}} \phi_g(r, \mu_j) + \frac{\mu_j - \mu}{\mu_j - \mu_{j-1}} \phi_g(r, \mu_{j-1}). \qquad \ldots\ldots(4.35)$$

Equation (4.33) is integrated over μ from μ_{j-1} to μ_j; assuming that $\phi_g(r, \mu)$ is given by (4.35), we have

$$[a_j D_r + b_j/r + \alpha_g(r)]\, \phi_g(r, \mu_j) + [\bar{a}_j D_r - b_j/r + \alpha_g(r)]\, \phi_g(r, \mu_{j-1}) = 2S_g(r), \qquad \ldots\ldots(4.36)$$

where

$$a_j = \tfrac{1}{3}(2\mu_j + \mu_{j-1}),$$

$$\bar{a}_j = \tfrac{1}{3}(\mu_j + 2\mu_{j-1}),$$

$$b_j = 2(3 - \mu_j^2 - \mu_j\mu_{j-1} - \mu_{j-1}^2)/3(\mu_j - \mu_{j-1}).$$

The $\phi_{0g'}$ occurring in $S_g(r)$ are easily calculated from (4.34). We thus have N differential equations to calculate the $N+1$ functions $\phi_g(r, \mu_j)$. These are supplemented by an additional equation obtained by putting $\mu = -1$ in equation (4.33), giving

$$[-D_r + \alpha_g(r)]\, \phi_g(r, -1) = S_g(r). \qquad \ldots\ldots(4.37)$$

The technique of solving equations (4.36) and (4.37) is to assume some source function $S_g(r)$ for each energy group g, and then to integrate equation (4.37) over r numerically from the outer boundary to the centre of the system, using the boundary condition of no inward neutron flux at the outer surface $r = b$, viz. $\phi_g(b, \mu) = 0$ for $\mu < 0$. The integration over r is done similarly to that over μ. The r range is divided into intervals (r_{i-1}, r_i), and $\phi_g(r, \mu_j)$ is assumed linear in each interval. Equation (4.37) is integrated over the range, taking an average value of $\alpha_g(r)$ in each interval and replacing $1/r$ by $2/(r_i + r_{i-1})$.

Having calculated $\phi_g(r, -1) = \phi_g(r, \mu_0)$, we substitute into (4.36) for $j = 1$ and solve for $\phi_g(r, \mu_1)$, again integrating inwards, and we continue in this manner until $\phi_g(r, 0)$ is obtained. To determine $\phi_g(r, \mu_j)$ for $\mu_j > 0$, we start from the centre and integrate outwards, using the central condition of symmetry :

$$\phi_g(0, -\mu) = \phi_g(0, \mu). \qquad \ldots\ldots(4.38)$$

Having computed the $\phi_g(r, \mu)$ from a guessed S_g in each group, new values of S_g are calculated from

$$S_g = \sum_{g'} \beta_{gg'} \phi_{0g'}(r) + f_g.$$

This process is repeated until a desired agreement is reached on comparing two successive iterations point by point. The ratio of $S_g(r)$ for successive iterations will then be equal to a factor m (the multiplication), independent of g and r. The calculation is repeated with various values of the core radius, and the critical radius is determined as that for which m is unity.

The fundamental idea in Carlson's method is the manner in which equations (4.36) and (4.37) are solved in order to ensure the stability of the numerical process. The following physical arguments can be advanced in favour of the methods described above. Consider a thin layer of material containing a source distribution T. Let Q_1 be the flux of neutrons incident on one of its surfaces, and Q_2 the emergent flux. Then

$$Q_2 = qQ_1 + tT,$$

where q is the attenuation factor for the incident neutrons and t is the fraction of source neutrons escaping.

If Q_2 is determined from Q_1, any error in Q_1 will be reduced in Q_2, since q is less than unity, whereas if Q_1 is determined from Q_2 (as by integrating against the direction of the neutron flow) the errors will accumulate.

In the case of a spherical system, negative values of μ correspond to directions towards the centre, and positive values to directions away from the centre. If we consider a particular neutron path approaching the centre (but not passing through it), the value of $\mu (= \mathbf{r}.\boldsymbol{\Omega}/r)$ will increase as we approach the centre. In order to integrate along the direction of the neutron flow, the integration over r must be performed towards the centre for negative μ and away from the centre for positive μ.

In some problems, up to fifty iterations may be necessary for the source function S_g to converge. The r intervals must be taken small, so that the variation of the flux in a given interval is smooth. The accuracy of the method increases with the number N of μ intervals : S_2 is better than diffusion theory, and S_4 is very accurate. In general, for reflected spheres the error of the critical radius by the S_4 method is about 1% (Okrent *et al.* 1955), and the value is under-estimated.

ACKNOWLEDGMENT

I am indebted to Dr. J. B. Sykes for his invaluable help in the preparation of the manuscript.

REFERENCES

ANDERSON, H. L., FERMI, E., and MARSHALL, L., 1946, *Phys. Rev.*, **70**, 815.

ARONSON, R., CERTAINE, J., and GOLDSTEIN, H., 1954, *U.S. Atomic Energy Commission Report*, NYO 6269.

CARLSON, B. G., 1955, *Los Alamos Report*, LA 1891.

CASE, K. M., DE HOFFMANN, F., and PLACZEK, G., 1953, Introduction to the theory of neutron diffusion, I (Los Alamos : U.S. Atomic Energy Commission).

CERTAINE, J., 1954, *U.S. Atomic Energy Commission Report*, NYO 3081 ; 1955, *Nuclear Development Associates Report*, NYO 6268.

CODD, J., SHEPHERD, L. R., and TAIT, J. H., 1956, *Progress in Nuclear Energy, Series I, Physics and Mathematics*, Vol. I, p. 251 (London : Pergamon Press).

COHEN, E. R., 1955, *International Conference on the Peaceful Uses of Atomic Energy, Geneva*, P/611.

COVEYOU, R. R., BATE, R. R., and OSBORNE, R. K., 1955, *Oak Ridge Report*, ORNL 1958.

DAVISON, B., 1944, *Ministry of Supply Report*, MS 82A ; 1947, *Chalk River Lecture Notes*, LT 18 ; 1951, *Proc. Phys. Soc.* A, **64**, 881 ; 1952, *Harwell Report*, AERE T/R 826 ; 1953, *Harwell Memorandum*, AERE T/M 82.

EHRLICH, R., and HURWITZ, H., Jr., 1954, *Nucleonics*, **12**, No. 2, 23.

ELLIOTT, J. P., 1953, *Harwell Report*, AERE T/R 1174 ; 1954, *Ibid.*, AERE T/R 1429.

FERMI, E., MARSHALL, J., and MARSHALL, L., 1947, *Phys. Rev.*, **72**, 193.

FUCHS, K., 1943, *Ministry of Supply Report*, MS 85.

GUZHEVSKII, B., 1955, *Diploma Thesis*, USSR Academy of Sciences (quoted in Tolstov *et al.*, 1955).

HOLTE, G., 1951, *Ark. Fys.*, **2**, 523 ; 1952, *Ibid.*, **3**, 209.

KUSHNERIUK, S. A., and MCKAY, C., 1954, *Chalk River Report*, CRT 566.

MANDL, M. E., 1953, *Harwell Report*, AERE T/R 1295.

MARK, C., 1944, *Montreal Reports*, MT 92, 97 ; 1947, *Phys. Rev.*, **72**, 558.

MARSHAK, R. E., 1947, *Rev. Mod. Phys.*, **19**, 185.

OKRENT, D., AVERY, R., and HUMMEL, H. H., 1955, *International Conference on the Peaceful Uses of Atomic Energy, Geneva*, P/609.

O'NEAL, R. D., 1946, *Phys. Rev.*, **70**, 1.

PLACZEK, G., 1946, *Phys. Rev.*, **69**, 423.

POOLE, M. J., 1955, *Harwell Memorandum*, AERE NP/M 77.

ROYSTON, R. J., 1955, *J. Nuclear Energy*, **1**, 194.

SPENCER, L. V., and FANO, U., 1951, *J. Res. Nat. Bur. Stand.*, **46**, 446.

SPINNEY, K. T., 1953, *Harwell Report*, AERE T/R 1221.

SYKES, J. B., 1954, *Harwell Report*, AERE T/R 1367.

TOLSTOV, K. D., SHAPIRO, F. L., and SHTRANIKH, I. V., 1955, *Conference on the Peaceful Uses of Atomic Energy, Moscow, Division of Physical and Mathematical Sciences* (New York : Consultants Bureau), pp. 95–108.

TROYAN, YU., 1955, *Diploma Thesis*, USSR Academy of Sciences (quoted in Tolstov *et al.*, 1955).

WACHSPRESS, E. L., 1955, *Knolls Laboratory Report*, KAPL 1333.

WALLER, I., 1947, *Ark. Mat. Astr. Fys.*, **A34**, Nos. 3 to 5.

WICK, G. C., 1949, *Phys. Rev.*, **75**, 738.

WIGNER, E. P., and WILKINS, J. E., Jr., 1948, *U.S. Atomic Energy Commission Report*, AECD 2275.

ZARETSKY, D. F., 1955, *International Conference on the Peaceful Uses of Atomic Energy, Geneva*, P/667.

ZINN, W. H., 1947, *Phys. Rev.*, **71**, 752.

NEW LENS SYSTEMS

By C. G. WYNNE
Wray (Optical Works) Ltd., Bromley, Kent

CONTENTS

	PAGE
§ 1. Introduction	298
1.1. Primary aberration theory and corrected lens forms	299
1.2. Higher order aberrations	302
1.3. The literature	304
§ 2. New optical materials and processes	304
2.1. New optical glasses	304
2.2. Synthetic crystals	306
2.3. Plastics	307
2.4. Reduction of surface reflection	307
§ 3. Lens systems with spherical surfaces	308
3.1. Triplet derivatives	308
3.2. Wide-aperture double-Gauss lenses	310
3.3. Lower aperture double-Gauss lenses and related forms	311
3.4. Wide-angle lenses	313
3.5. Telephoto lenses	315
3.6. Petzval lenses	316
3.7. Other wide-aperture lenses	316
3.8. Zoom lenses	317
§ 4. Lens systems with aspheric surfaces	317
§ 5. Reflecting systems	319
References	322
Patents	323

Abstract. After an introductory discussion of the elementary aberration theory of corrected optical systems, and some consideration of new optical materials and processes, recent forms of optical imaging systems are described; most of these are systems of spherical refracting surfaces; aspheric and reflecting systems are also included.

§ 1. Introduction

This report is concerned with progress in the design of optical systems giving well-defined images of more or less extended objects; such systems find their main application for normal photographic purposes (and for optical projection, for which similar lenses are commonly used), for astronomical photography, and for microscopy. No account will be given of particular techniques of use.

Optical systems are normally required to give an image of an object in a plane normal to the lens axis, the image being well defined, geometrically similar to the object and on a parallel plane; even if these two latter conditions (freedom from distortion and field curvature) are not required, all optical systems suffer to a greater or less extent from aberrations, i.e. spherical wave fronts from different points of the object, after passing through the system, do not conform to spherical surfaces centred on the corresponding image points. The aberrations of the wave front for different object points and different wavelengths of light are not, except in the

simplest systems, amenable to a fully analytic treatment in terms of the shapes of lens or mirror surfaces, their separations, and the optical constants of the various media.

The aberrations of an optical system are a function of the aperture and field angles, and if they be considered as expanded in a power series of these variables, then for systems having rotational symmetry the terms involving the lowest powers may be simply evaluated numerically in terms of the constructional parameters of the system ; these are the five Seidel aberrations for monochromatic light, and two chromatic aberrations. For the aperture and field angles of useful systems these seven primary aberrations generally give an inadequate description of the optical performance, a considerable number of terms involving higher powers being significant, but generally having too great algebraic complexity to be calculated ; but the primary aberrations give a correct description of the performance for small apertures and fields and their reduction to zero or a small value for the complete system is therefore a necessary, though not a sufficient condition for good imagery.

For a system of thin lenses, i.e. one in which the thickness of all the media of different refractive index from that of the object and image space is assumed to be negligibly small, the expressions for the primary aberrations are simplified, with a corresponding extension of the possible range of analysis. In fact the effect of the finite lens thicknesses which are necessary for a physical realization of the system is rarely negligible, and the method breaks down for example in the case of a thick lens of zero power whose aberrational effect may be considerable ; but thin lens analysis is often of value in the early stages of a design, and in giving a qualitative indication of the effect of changes in the constructional parameters of a system of lenses of finite thickness.

A typical procedure for the design of a corrected optical system is therefore as follows. A system is found, using thin lens theory or more empirical methods, giving small total values for the seven primary aberrations by balancing larger terms of opposite sign arising at individual surfaces, and a representative set of rays from different points on the object is traced numerically through the system, the results giving an estimate of the total aberration for each object point. The system is then modified in an attempt to reduce the higher order aberrations while maintaining the primary aberrations at appropriate small values ; methods of achieving this may be suggested by experience, by heuristic considerations of the form of higher order aberrations, or by calculated differential coefficients of the total aberration with respect to the various design parameters, derived from calculation of the ray-paths. Rays are then traced through the modified system, and these processes are repeated until an acceptable design is achieved.

1.1. *Primary Aberration Theory and Corrected Lens Forms*

For the case of a system of separated thin lenses, consideration of three only of the primary aberrations leads to certain general conclusions of the types of lens that may give corrected systems. If the powers of the separate lenses be denoted by k_1, k_2, etc., the incidence heights on these lenses of a paraxial ray from the axial point of the object be y_1, y_2, etc. and of a ray through the centre of the aperture stop (which is normally placed approximately centrally) be $\bar{y}_1, \bar{y}_2$, etc., then if the

unit of length be chosen so that the equivalent focal length of the complete system be unity

$$\sum \frac{yk}{y_0} = 1 \qquad \ldots\ldots(1)$$

where y_0 is the incidence height of the axial ray on the unit plane of the complete system, and the summation is for the whole system.

For the primary field curvature (Petzval sum) to be zero

$$\sum \frac{k}{n} = 0 \qquad \ldots\ldots(2)$$

where n denotes the refractive index of the individual lens element.

For the axial focus to be achromatized

$$\sum \frac{y^2 k}{\nu} = 0 \qquad \ldots\ldots(3)$$

and for the magnification of an extended object to be achromatized,

$$\sum \frac{y^2 k}{\nu} \frac{\bar{y}}{y} = 0 \qquad \ldots\ldots(4)$$

where ν is the Abbe number, defining the dispersion of the material of any lens element.

Since the dispersion of all optical materials has the same sign, it follows from equation (3) that achromatism can only be achieved by a combination of positive and negative lenses; for a convergent system the positive lenses must have larger ν values than the negative ones. The total range of refractive indices of usable optical materials for the visible spectrum is fairly small (about 1·50 to 1·75 for yellow light), the higher indices being associated with moderately or very large dispersions (small ν values) and the lower indices with lower dispersions; hence, if individual lenses of high power are to be avoided, equation (2) requires that the sum of the individual lens powers is small, and equation (1) can therefore only be satisfied by arranging for the converging elements to have higher values of y than the diverging ones. This may be most simply achieved in a system of a front lens of positive power which converges the incident light on to a diverging lens separated from it, and hence having a lower value of y, the powers and separations being chosen so as to satisfy equations (1) and (2), or by the reverse of this arrangement. Such a system of two single lenses can be made, by a suitable choice of ν values, to satisfy equation (3) but cannot satisfy equation (4). It follows from elementary considerations that the effect of a change of stop position is to add a term to $\bar{y}/y$ which is constant for each lens of the system, to the order of approximation considered in primary aberration theory, and hence if equation (3) is satisfied, equation (4) is satisfied for all stop positions. If therefore in the simple two-lens combination the stop is taken on one of the lenses, its contribution to the sum of equation (4) is zero, and that of the other lens is finite. Equation (4) can be satisfied if, instead of single convergent and divergent thin lenses, a pair of thin lenses in contact is used, giving together in each case an achromatized system satisfying equation (3). This gives the simplest form of telephoto lens when the front doublet is convergent and inverted telephoto lens in the reverse case.

Alternatively a system may be constructed to satisfy all four conditions, consisting of two outer converging simple lenses separated from a central divergent lens, having a symmetry about the centre such that for the two outer lenses $\bar{y}yk/\nu$ has equal and opposite values ; this gives the Cooke triplet form of lens (figure 1) ; the inverse construction of two outer negative lenses separated from a central positive one also affords a solution. Such forms, having a measure of symmetry about a central stop, have additional advantages. For an exactly symmetrical system working at unit magnification, the oblique aberrations of all orders depending on odd powers of the object size are absent, by virtue of the symmetry : for a lens which

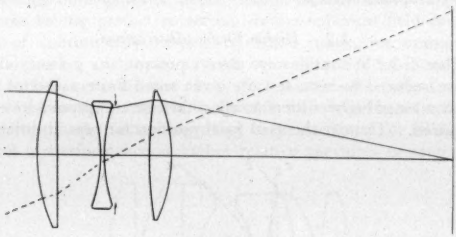

Figure 1.

is not working at unit magnification, no such simple relationship exists, but these aberration terms are in general of opposite sign and similar magnitude for lenses similarly placed before and behind the stop, so that their correction is facilitated by such construction ; and in fact almost all lenses designed for at all large field angles are of an approximately symmetrical form.

The general discussion given above of thin lens theory has been restricted to the three primary aberrations which depend only on power and position of the lenses : the remaining four Seidel aberrations, corresponding to spherical aberration, coma, astigmatism and distortion, depend on the distribution of power between the two lens surfaces ; the analysis of these is more complicated, but in general it can be shown that, for the simple lens forms discussed above, forms exist satisfying all the conditions for absence of primary aberrations ; but in each case higher order aberrations are present which restrict the size of aperture and field over which good definition is obtainable.

If systems of finite thickness are considered, additional terms are introduced in equations (2), (3) and (4), but similar general conclusions emerge, namely that in order to correct primary field curvature, a lens system must comprise converging lenses or surfaces and diverging ones, the former having higher incidence heights for a ray from the axial object point than the latter ; and that unless the front and back parts are separately achromatized, chromatic correction of magnification requires a form of symmetry about the centre, such symmetry being also desirable for the correction of a number of other aberration terms of oblique imagery.

So far only lenses with corrected field curvature have been considered. For some purposes where only a small angle of field has to be covered, field curvature

may be neglected, since it introduces aberrations depending on the second and higher even powers of the field angle. For such lenses, since equation (2) need not be satisfied, the diverging lens elements need not be separated from the converging ones. The Petzval lens is the most common form with this type of correction, consisting in its simplest form of two cemented doublets, separated by a considerable air-space so that a suitable primary astigmatism can be introduced to reduce the effect of the uncorrected field curvature. Such lenses can give good axial correction over considerable apertures, and have been widely used for narrow-angle projection.

A general treatment of aberration theory and its application to lens design has been given by Hopkins (1950).

1.2. *Higher Order Aberrations*

Since higher order aberrations are always present, the primary aberrations are not in practice reduced to zero, but are given small finite values of opposite sign to that of the combined higher orders, to effect the best compromise over the aperture and field required. Thus, if the axial focal position for rays at different apertures

Figure 2.

be plotted as abscissae against the aperture as ordinates, the paraxial focus being taken as zero, then for a lens having zero primary spherical aberration, the curve will normally be of the form of curve *a* in figure 2 : the introduction of a small primary spherical aberration of appropriate sign gives the form of correction shown by curve *b*, which is that normally achieved. Such curves are also typical of the form of other aberrations ; for example, if the separation between the sagittal or tangential focus and the paraxial focal plane be plotted as abscissae against field angle as ordinate, then curve *b* in figure 2 represents the normal form of correction, and similarly for other aberrations. A particular aberration is normally described as ' corrected ' if it is zero for two values of the appropriate parameter. For most forms of lens, improvement of performance takes the form of a reduction of the combined higher order aberrations, without change of sign, so that correction is achieved with a smaller value of the primary aberration, and the curve is flattened : in some forms of lens for particular aberrations the designer may be able to control the value and sign of the second order aberration, thereby making possible a second order correction of the form shown by curve *c* in figure 2, for three values of the

parameter, giving in general much lower residual aberrations ; but this is unusual. In some special cases, perfect correction of some aberrations for all values of the parameter is possible ; for example, if an aspheric surface is used, as in a Schmidt camera, the profile may be chosen to give perfect correction of all orders of axial spherical aberration, but this is not maintained for oblique imagery ; again, a system of concentric surfaces has complete correction, over a spherical field, of all aberrations depending on field angle, but the spherical aberration can only be given the form of correction shown in figure 2, *b*. Perfect correction of all aberrations simultaneously does not appear to be possible in a system of a finite number of surfaces separating homogeneous media, though no formal proof of this has been given ; systems having perfect correction over a spherical field can be designed using media of continuously varying refractive index, for example Maxwell's ' fish-eye ' ; and other such systems have been described by Toraldo di Francia (1955) ; but such systems are not physically realizable for optical wavelengths.

A number of known procedures is available to reduce higher order aberrations in a lens system, thereby either improving its performance, or allowing it to have the same level of performance at higher relative apertures or larger field angles.

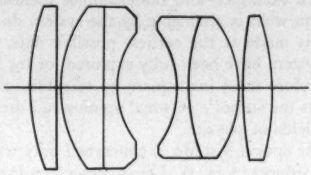

Figure 3.

Both the primary and higher order aberrations may be reduced by replacing a single lens by two lenses giving together the same power : the use of higher refractive index glasses for converging lens elements generally reduces both the primary and higher order aberrations, as also does the use of more dispersive glasses for the diverging elements. A more sophisticated approach is the deliberate introduction of lenses or surfaces having large higher order aberrations of the correct sign to give an improved overall performance, as is done by the convergent cemented surface of high curvature in the Tessar form of lens, and its derivatives. A number of examples of the recent use of these procedures will be given below.

A large proportion of lens systems may be considered as derived from the triplet, telephoto and Petzval forms by one or more of the above devices. The most important other form is the double-Gauss lens, in which the central diverging part of the lens, with relatively low incidence heights for an axial ray, instead of the biconcave lens of the triplet, is formed by the concave inner surfaces of two meniscus lenses, one on either side of the central stop ; the front and back converging parts of the lens each consist of an odd number of surfaces (in the simplest form, three), and to ensure chromatic correction at large apertures the meniscus lenses are generally compounded (figure 3). This form of lens, with its derivatives, provides most of the wide aperture lens designs covering at all large angles of field.

1.3. *The Literature*

The fact that fully analytic methods are only possible for the simplest forms of optical system is reflected in the literature. A number of papers has been published giving mathematical analyses of the aberrations of very simple systems—for example Schmidt cameras, two-mirror systems, systems of concentric surfaces; for such systems the possibility of improved design is inherently limited. The majority of the more complicated systems are described only in patent specifications,† which makes the task of reviewing a difficult one. Patent specifications are written to comply with legal, rather than scientific standards; all inventions are described as improvements, often with no further indication of the character of the improvement, or one only in very general qualitative terms—the improvement may be simply the evasion of an earlier patent; since the applicant for a patent is concerned to secure as wide a monopoly as possible, the claims may cover a much wider range of systems than that within which good correction occurs, and the form of the claims often bears no relation to the way in which improvements, if any, have been achieved. Numerical examples are frequently given, but generally without any details of performance so that extensive calculation is required to determine the aberrations of such examples, and the examples themselves commonly have a performance inferior to what is attainable by the system described, either because a patent application is made at the earliest possible date, rather than when the potentialities of the system have been fully explored, or for less creditable reasons. The literature is therefore most inadequate by scientific standards, and a review of it necessarily reflects the author's personal opinion to a greater extent than would be the case in most fields of physics.

This review of new optical systems is concerned only with developments since the last report on this subject by H. W. Lee in *Reports on Progress in Physics* (1940). No attempt is made to make reference to all publications; the patent literature is extremely voluminous, and apart from much which is trivial, substantially the same developments have frequently been described by a number of different authors. Some sections of the subject which have been effectively reviewed recently in other publications are not dealt with in detail here, reference being made to such reviews.

§2. New Optical Materials and Processes

2.1. *New Optical Glasses*

Since 1940 the range of optical glass has been considerably extended. If the refractive indices n (for the d-line) of glasses be represented by ordinates and the dispersions $\nu[=(n_d-1)/(n_F-n_c)]$ by abscissae, then the older optical glasses almost all lie within the closed contour shown in figure 4, indices above about 1·66 being only available associated with high dispersions, rising rapidly with index; moreover the older glasses much above 1·66 in index were yellow in colour, making the more extreme high index glasses unusable for most purposes. The use of rare-earth oxides has led to the development of high index glasses of lower dispersion, some of which are shown as dots in figure 4. These new glasses have some

† Patents are commonly taken out in a number of countries; only one such patent is quoted, and English Language ones have been chosen where possible; the date of the original application, and of acceptance or publication, are given in the references, together with the country of the original application if this is not that of the patent cited.

limitations: some of the more extreme ones have a rather high absorption at the violet end of the spectrum; there are difficulties in some cases in making large pieces of optical quality; a tendency to devitrification restricts moulding operations;

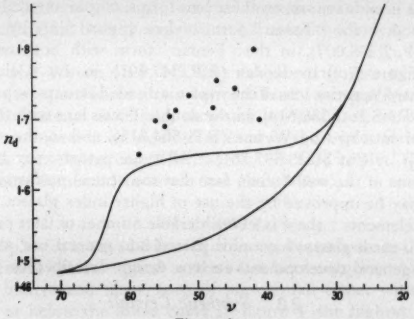

Figure 4.

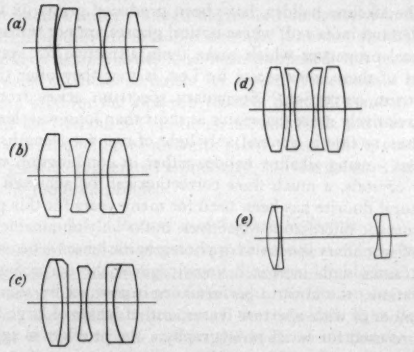

Figure 5.

and the cost is high. But these glasses have very considerably extended the possibilities of lens design. A further important development is that closer control of the production process and of the purity of raw materials has reduced the absorption of the denser flint glasses, increasing the useful range of these older glasses.

The first publications on rare-earth glasses suggested that considerably higher refractive indices were attainable than has since proved to be practicable in pieces of useful size. Some of the earlier lens patents, taken out before any rare-earth glasses were available, accordingly employ glasses which have not yet been realized;

Warmisham used such glasses in the triplet (B.P. 523,062) to give an aperture of f/2·25 ; in the triplet whose front element is divided into two lenses each of about half the power (figure 5(*a*), B.P. 523,218) corrected over a narrow angle at f/1·8, and in the double-Gauss form (figure 3) at f/1·4 (B.P. 523,061). A number of later patents has been taken out on these lens forms, employing real glasses. These glasses were used in the ' Tessar ' form of lens (figure 5(*b*)) by Herzberger and Hoadley (U.S.P. 2,308,007), in the ' Pentac ' form with both convergent lenses compounded (figure 5(*c*)) by Kodak (B.P. 547,691), in the ' Celor ' (figure 5(*d*)) in which the central negative lens of the triplet is divided into two separated biconcave lenses by Aklin (U.S.P. 2,338,614), in the double-Gauss lens with the back converging lens divided into two by Wynne (B.P. 564,815), and in the simple telephoto lens (figure 5(*e*)) by Cox (B.P. 587,761). All these patents may be considered as direct applications of the well-known fact that the optical performance of all these forms of lens may be improved by the use of higher index glasses, particularly for the converging elements : there is a considerable number of later patents on similar lines. The rare-earth glasses have now passed into general use, and are used in a number of the general developments in lens design described in § 3.

2.2. *Synthetic Crystals*

Since Lee's earlier report (1940) the range and size of synthetic isotropic crystals available have been considerably increased. These crystals, of which the most important are the alkaline halides, have been produced primarily for spectroscopy in the ultra-violet and infra-red, where optical glasses are not transparent, but they have other optical properties which make them attractive for systems for visible light. The first of these, mentioned by Lee, is that they offer the possibility of secondary spectrum correction. Secondary spectrum arises from the fact that flint glasses are relatively more dispersive at short than long wavelengths, compared with crown glasses, so that in general only light of two wavelengths can be brought to the same focus ; using alkaline halides either in combination with appropriate glasses or other crystals, a much finer correction can be achieved over the whole spectrum. Natural fluorite has been used for many years for this purpose, in high aperture apochromatic microscope objectives, but is only obtainable in small pieces. The correction of secondary spectrum in photographic lenses is becoming of increasing importance, since with increased knowledge of the correction of the monochromatic aberrations, the limit to performance is now set by secondary colour in the case of a number of wide aperture lenses, and of lenses of large focal length and moderate aperture used for aerial photography : the problem is aggravated by the fact that the highest degree of monochromatic correction of such lenses often requires the use of very highly dispersive materials, and for the highly dispersive flint glasses the secondary spectrum errors are greater than with flints of lower dispersion.

Apart from the correction of secondary spectrum, synthetic crystals are also attractive since they offer refractive indices and dispersions outside the range of existing glasses ; in particular the alkaline halides have a wide range of refractive indices with dispersions much larger than can be reached with glasses of the same index, i.e. they lie below the lower curve of figure 4. Magnesium oxide (n_d 1·738, ν 53·5) lies away from the range of glasses in the opposite direction, but has lost some

of its interest since the development of the rare-earth glasses, which approach it in high index combined with low dispersion.

Despite these optical advantages, synthetic crystals have been little used for instruments for the visible spectrum on account of their numerous physical failings : they are soft and liable to cleavage, many of them are soluble in water, and their temperature coefficients, both of expansion and refractive index, are much larger than those of glasses.

Warmisham and Wynne (B.P. 547,666) described the use of alkaline halides to correct secondary spectrum in a number of different forms of lens, and they have a number of other patents describing particular applications ; in B.P. 559,699 and 559,864 potassium bromide or an alum is used in the triplet form of lens where one of the outer converging components is a cemented triplet, the crystal being protected by being cemented between two glass lenses.

2.3. *Plastics*

Transparent plastics are available with differing dispersions, so that achromatism is possible, and their use for optical systems has been suggested by many authors. The refractive indices and dispersions of plastics fall either within the range of optical glasses, or below the lower curve in figure 4, the highest refractive index being about 1·60. The physical characteristics of the plastics are most unfavourable for optical work ; they are all relatively soft, and have high thermal expansion and change of refractive index ; a high degree of homogeneity is difficult to attain, and in varying degrees they are unstable with age, humidity and high temperatures. Some optical designs using plastics have been published, but no serious use seems to have been made of these materials for optical instruments of normal types. Plastics have been used for the aspheric plates of Schmidt cameras ; Starkie (1947) has described the use of moulded plastic plates, and Rinia and van Alphen (1947–8) have described the production of aspheric plates of gelatine moulded on glass, the mould having a greatly exaggerated asphericity, and the gelatine being subsequently shrunk to give the required profile.

2.4. *Reduction of Surface Reflection*

The introduction of methods of reducing the reflection of light from lens surfaces, generally referred to as ' blooming ', has had a considerable indirect effect on the trend of lens design. A proportion of the light incident on any refracting surface suffers reflection, the relative intensity of the reflected light depending on the refractive indices at the surface, and on the angle of incidence. As the number of surfaces in a lens system increases, the intensity of the refracted, image-forming light is reduced by successive reflection losses : moreover, at each surface after the first a proportion of the back-reflected light is again reflected from surfaces in front ; some of the light undergoing an even number of reflections will finally fall on the image plane, where it will in general form a more or less uniform illumination superimposed on the image, and therefore degrade its contrast ; in particular designs of lens, some multiple reflections may form ' ghost ' images focused near to the primary image plane. The latter effect can be avoided by appropriate design of lens system, but the former effect is always present, and makes desirable the reduction of the number of surfaces, particularly air–glass surfaces, to a minimum in any

optical design. The introduction of ' blooming ' to reduce the intensity of reflected light has led lens designers to produce systems of greater complexity than would previously have been considered tolerable.

The process of ' blooming ' in its simplest form consists ideally in applying to the surface a layer of transparent material of refractive index which is the geometric mean of that of the two original media, and of a thickness to give a phase difference of π between the light reflected from its front and rear surfaces. Complete suppression of reflected light results when these conditions are met. In practice, for a number of reasons, the suppression is not complete : the above conditions can only be fulfilled for one wavelength and one direction of incidence of light, and optical systems normally use an extended wavelength range and light falling on the surfaces over a considerable range of directions ; materials are not available of sufficiently low refractive index to comply with the required conditions except on the surfaces of the higher index glasses. By the use of multilayer films, the variation of reflection with wavelength may be reduced, and materials exist giving good reflection reduction on low index glasses ; but the change of efficiency with angle of incidence is greater for multilayer systems (see Heavens 1955). Actual measurements of the reduction of ' veiling glaze ' by ' blooming ' (e.g. Guild 1951) show that the actual efficiency is still lower than the above considerations would suggest. Even with bloomed surfaces, therefore, some veiling glaze is present and increases with the number of air–glass surfaces. For some purposes when the object contrast tends to be low, for example aerial photography, the maintenance of image contrast is of great importance, and it appears probable that in some lenses developed for these purposes, some of which are described below, the reduction of aberrations achieved by great complexity of design may be more than offset by the contrast loss.

§ 3. Lens Systems with Spherical Surfaces

The vast majority of optical systems fall in this category ; most of them can conveniently be considered as derived from one or other of the basic types discussed in § 1.

3.1. *Triplet Derivatives*

The simple Cooke triplet has a degree of correction which for most purposes will not allow a relative aperture greater than about f/3·5, or a field angle greater than about 50° to 55°. A very large number of modifications had already been made before the period covered by this review, by the substitution of two or more separate lenses for one of the simple triplet, the use of higher index glasses, and the introduction of cemented convergent surfaces to give higher order aberrations of the sign required, such lenses having in common the characteristic that the central divergent part consists of one or more biconcave lenses ; such modifications continue to be made. In general this form does not appear to be correctable for large field angles, and as the relative aperture is increased in the more complex forms, the correction of oblique imagery deteriorates, such lenses being therefore designed for narrower angles of field. Among such lenses may be mentioned that shown in figure 6(*a*), due to Durand (U.S.P. 2,260,368) with an aperture of f/1·8, Schade's f/1·5 lens (figure 6(*b*)) covering a 20° field (U.S.P. 2,259,004), and an

f/1·13 lens designed by Berek, Zimmermann and Kleineberg (U.S.P. 2,297,452). Second order axial correction has been achieved by Glancy (1945), at apertures approaching f/2, using a thin meniscus of very low power, steeply convex to the centre of the lens (figure 6(*c*)) and by Lotmar at f/1·4 using a deep converging cemented surface in the central negative lens (figure 6(*d*)), a device originally due to Leitz (B.P. 381,135); in both cases the degree of correction falls rapidly away from the axis. By correcting over a curved field, so that the Petzval condition may be relaxed and the power of the central negative lens decreased, Schade has achieved an aperture of f/1·1 (U.S.P. 2,586,866, figure 6(*e*)), and in a more complicated form f/0·75 (U.S.P. 2,604,013).

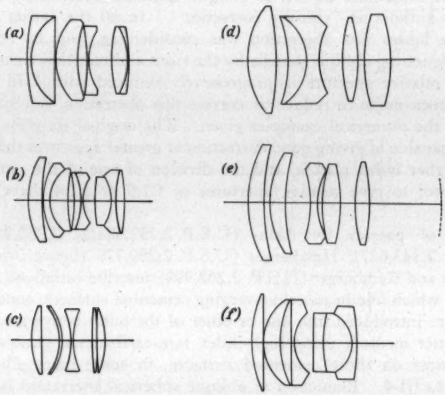

Figure 6.

If the second air space of the form of lens shown in figure 5(*a*) be replaced by a low index glass, the reflection losses are reduced, and this form of lens is correctable over moderate field angles, though the distortion is generally rather large; the correction can be improved, and hence the aperture increased, by introducing one or more cemented surfaces in the back. A high index difference is desirable at the contact surfaces of the second, triplet, component, and the new high-index glasses are therefore particularly useful for this form of lens. Earlier lenses of this type were described by Lee (1940); a number of recent modifications has been made by Bertele, of which figure 6(*f*), f/1·4 (B.P. 681,456) may be taken as typical.

For correction over larger angles of field at lower apertures, Altman (B.P. 563,206) has shown that both the axial and oblique correction of the triplet may be considerably improved by inserting, in one of the triplet air-spaces, a meniscus lens of low power concave to the centre; a somewhat similar modification to the Tessar lens form had previously been made by Tronnier (B.P. 476,349). Wynne, using an air-space with small difference of curvature in place of the cemented surface of the Tessar, has designed an f/4·5 lens covering a 65° field (B.P. 577,763).

3.2. *Wide-aperture Double-Gauss Lenses*

The first lens of relative aperture f/2 giving good correction over a reasonably large field (about 50°) was designed by Lee in 1920 (B.P. 157,040) and was of the double-Gauss form (figure 3); the vast majority of wide aperture lenses covering moderately large field angles has been derived from this lens, and since Lee's original over 100 patents have been published describing various modifications, some of these being included in Lee's earlier review (1940). Such lenses can give a very good correction of most aberrations, the main defect of the earlier lenses being a higher order aberration, arising at the inner concave surfaces, which gives over-correction of spherical aberration for oblique pencils, increasing with field angle; this is sometimes known as oblique spherical aberration, and sometimes by American authors as 'rim-ray correction'. In all the earlier wide-aperture double-Gauss lenses this aberration was considerable, and its effect has been reduced by vignetting oblique pencils by the front and rear lens mountings, so that the effective relative aperture is progressively reduced with field angle; many claims have been made to reduce or correct this aberration, not all of which are borne out by the numerical examples given. The original six-glass double-Gauss lens was not capable of giving good correction at greater apertures than f/2 or f/1·9; the use of higher index glasses, and the division of one of the outer convergent lenses into two, to give relative apertures of f/1·5 or f/1·4, have already been mentioned.

A series of patents by Aklin (U.S.P. 2,252,681/2, 2,262,985, 2,336,207 (figure 7(*a*)), 2,343,627), Herzberger (U.S.P. 2,289,779 (figure 7(*b*)), 2,350,035) and Frederick and Herzberger (U.S.P. 2,262,998) describe variations of the double-Gauss lens in which one or more converging cemented surfaces, concave or convex to the stop, are introduced into one or other of the outer converging lenses, or in one of the inner menisci, using high-index rare-earth oxide glasses to give large index differences on these cemented surfaces, in some cases allowing relative apertures up to f/1·4. Reduction of oblique spherical aberration is claimed, and in some cases achieved, by these converging cemented surfaces, which can be made to give oblique spherical aberration of the opposite sign to that arising in the rest of the lens. Disadvantages of this method of correction are that the cemented surfaces also introduce considerable higher order coma and astigmatism, with a consequent deterioration of the lens in these respects, and that, since to be effective such surfaces must be rather highly curved, the diameter that can be given to the cemented member is restricted, so that vignetting of oblique pencils cannot be avoided. Warmisham (B.P. 556,401, figure 7(*c*)) attempted to reduce the oblique spherical aberration by inserting a central biconcave lens, thus distributing over four surfaces the diverging power normally carried by two, and consequently reducing curvatures. A number of later variants of both these methods has been published.

Wynne (B.P. 575,075, figure 7(*d*)) has shown that one of the cemented surfaces of the original f/2 double-Gauss form may be dispensed with; correction of transverse chromatic aberration then requires that the single meniscus be thinner than the doublet one, giving lenses of abnormally long back focus, or short back focus and overall length, according as the front or rear meniscus is the single one; a similar single-meniscus construction is used, with a divided front converging lens,

to give a relative aperture of f/1·0 (B.P. 604,883, figure 7(*e*)). The over-correction of oblique spherical aberration in the double-Gauss lens arises from the fact that the angles of incidence at the two inner concave surfaces for rays at large apertures, which are already rather large for an axial pencil, increase to very large values as

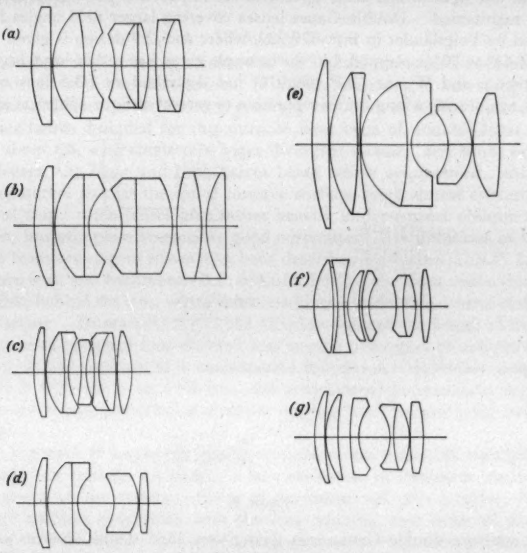

Figure 7.

the obliquity increases; this effect is reduced if the central air-space be increased in length, and in this way Wynne has designed an f/2 lens with the oblique spherical aberration corrected in the sense used above, i.e. it changes sign at an intermediate field angle (B.P. 575,076). Baker has followed the same course, using a slightly longer central separation still (U.S.P. 2,532,751/2), and Schade (U.S.P. 2,611,295) has used a long centre separation in an f/1·4 lens, with a triple-cemented rear meniscus. Central separations longer than were formerly used in f/2 double-Gauss lenses, but shorter than those claimed by Wynne and Baker, are used by Kleineberg and Zimmermann (U.S.P. 2,622,478, figure 7(*f*)) and Tronnier (U.S.P. 2,627,204/5, figure 7(*g*)) in forms with additional air spaces, and a corresponding increase in the number of air–glass surfaces.

3.3. *Lower Aperture Double-Gauss Lenses and Related Forms*

Lenses of relative aperture of f/2 or greater can give a degree of aberration correction which is acceptable for fairly short focal lengths over a field angle of

about 50°. The conditions for good axial correction (which is necessary for large apertures) conflict with those for good correction of oblique imagery, so that if larger angles of field are required, some reduction of aperture is necessary: and again for lenses of larger focal length such as are used, for example, for aerial photography at low light levels, lower apertures are required if photographic resolution is to be maintained. Double-Gauss lenses covering larger field angles have been described by Voigtländer in B.P. 677,202, where an f/2·9 design is given for which a field of 63° to 70° is claimed, but the example given has rather large higher-order astigmatism; and Wynne (B.P. 689,916) has described an f/3·5 lens covering a 60° field, again using a long centre separation to correct oblique spherical aberration.

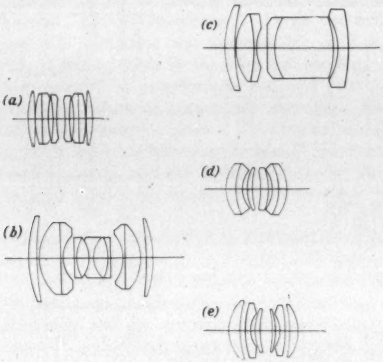

Figure 8.

A lower aperture double-Gauss lens giving very high definition over small field angles has been described by Herzberger (U.S.P. 2,466,424, f/4·5, 30° field); Cook (B.P. 707,943), following Warmisham's earlier patent 556,402 mentioned above, claims a high performance over 46° for an f/3·5 lens in which two biconcave elements have been inserted in the central air-space of the double-Gauss form (giving twelve air–glass surfaces) (figure 8(*a*)) and Baker (U.S.P. 2,628,532) at the same aperture has inserted a central cemented combination of five glasses, with very deep curvatures, to give correction of secondary spectrum (figure 8(*b*)); Baker suggests that this design is suitable for a lens of 24 inches focal length. A rather simpler design by Baker for the same purpose but without secondary spectrum correction is described in U.S.P. 2,671,380.

Two other forms of lens have been used to give lenses of lower aperture than f/2 with moderately wide angle, or a high degree of correction over smaller angles. The Zeiss Biogon discussed by Lee, with a Gauss form of front but with the third component convergent and the fourth divergent, has been modified by Bertele (B.P. 696,925, figure 8(*c*)) to give an f/2·8 lens covering a field of 62°, and more complicated modifications, at about the same aperture and field, have been described by Schade (U.S.P. 2,461,182) and Zeiss–Opton (B.P. 723,544). A form of lens,

also originally due to Zeiss (B.P. 278,338) using two inner converging meniscus lenses between two outer compound divergent lenses has been modified by Cook in a series of patents (B.P. 690,402–5) using high index glasses and additional air spaces, to give apertures from f/4 to f/3·5 covering field angles from 50° to 70° (figures 8(*d*), (*e*)).

3.4. *Wide-angle Lenses*

Wide-angle lenses, covering a field of 90° or slightly more, have become increasingly important with the development of photogrammetry in surveying; a very high degree of distortion correction is generally required, as well as high resolution. The earlier lenses designed for this purpose have been of double-Gauss form, of aperture about f/6, with single thin inner divergent menisci, and single outer convergent lenses, the front and back halves being nearly symmetrical, with a large central separation so that the inner concave surfaces were almost concentric with the central stop; such lenses give rather heavily under-correct oblique spherical aberration, but otherwise reasonably good correction. Modifications of this form using two front convergent lenses have been described by Rayton (U.S.P. 2,325,275, f/6·3, figure 9(*a*)) and Richmond (B.P. 656,011, f/5·5); the latter uses a thick plane-parallel plate behind the lens, whose thickness gives a useful fine control of distortion in manufacture. Durand (U.S.P. 2,383,115) has reduced the length of the central separation in the original four-element lens to give correction of oblique spherical aberration, at the expense of a considerable increase in high-order astigmatism. Wynne (B.P. 689,916) in an f/5·6 lens with a cemented rear meniscus (figure 9(*b*)) has corrected oblique spherical aberration, together with second order astigmatism correction.

Since a system of concentric spherical surfaces has rotational symmetry about any straight line through the centre, a lens consisting of concentric surfaces, with a stop centred on the common centre of curvature, will give imagery, for object and image surfaces concentric with the lens surfaces, free from all aberrations depending on field angle. Concentric lens systems can be corrected for spherical aberration and colour, for example by a combination of a central low index low dispersion sphere cemented between two high index high dispersion spherical shells; the use of concentric surfaces only greatly simplifies the aberration theory, which has recently been investigated by Hekker (1947); such lenses have frequently been considered for wide-angle applications, but the practical inconvenience of a curved image surface has prevented their general use. Russinov and Kosyrew (1939) have described an f/11 lens covering a field of 100° which appears to have been suggested by the concentric lens, with modifications to the outer curves and the addition of outer negative lenses to give a flat field (figure 9(*c*)); Cook (B.P. 730,411) has described a somewhat similar lens where the outer lenses are thick menisci of low power.

For any lens corrected for distortion and field curvature, the illumination in the focal plane can be shown to fall off as $\cos^4\theta$, where θ is the angle of obliquity from the axis, assuming that there is no vignetting of the aperture for oblique pencils of light by lens mountings, and that there is no aberration of the entrance pupil. For wide-angle lenses this represents a serious light loss—for a lens covering a full field of 90° the illumination at the edge of the field is one quarter that at the

centre, and the types of wide-angle lenses discussed above have aberrations which make some vignetting of the oblique aperture necessary, so that the illumination is in fact always rather lower than this. The fact that the $\cos^4$ law is only true if the entrance pupil is free from certain types of aberration was first pointed out by Slussareff (1941); this assumption is approximately correct for the earlier types of wide-angle lens, but Slussareff showed that the possibility exists of increasing the oblique illumination by introducing heavy coma of the entrance pupil, which can be done without introducing aberrations of the normal image. The first

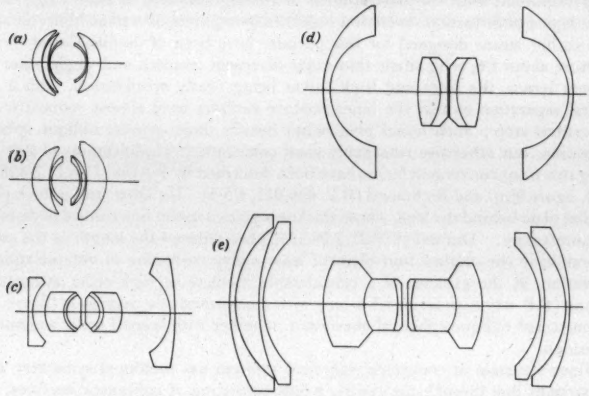

Figure 9.

application of this principle was made by Roossinov (B.P. 640,232), who described lenses of relative aperture f/8 covering up to 133° field, for which an illumination proportional to $\cos^3 \theta$ is claimed, consisting of a central convergent part, with outer divergent meniscus lenses (figure 9(*d*)); the same principle has been used by Wild (B.P. 680,185) to give an f/5 lens covering a field of 90°, using two divergent menisci on each side of a more complex central convergent part (figure 9(*e*)); and later modifications have been made by Wild (B.P. 708,797) and Bertele (B.P. 719,162). In all these lenses the required coma of the entrance pupil is produced mainly by the front diverging lenses; large pupil coma can only be produced, using lenses of reasonably low power, if they are located rather far from the physical stop, so that these diverging lenses are necessarily of large diameter in order to transmit light pencils at large field angles; similar diverging lenses are used at the rear to give distortion correction. Apart from introducing coma of the stop, these outer diverging lenses have another important function; in the forms of wide-angle lens described earlier, with convergent outer lenses, a principal ray through the stop centre is much more steeply inclined to the axis at the centre of the lens than in the object or image spaces, making a high degree of correction at wide angles more difficult to achieve, since very high order aberrations are introduced; the diverging

outer lenses of the Roossinov type of system have the opposite effect, so that a high degree of correction is attainable which allows vignetting of the oblique aperture to be reduced or eliminated, and the full advantage of the reduction of the $\cos^4$ effect to be realized.

3.5. *Telephoto Lenses*

The telephoto lens, consisting of a front convergent part rather widely separated from a back divergent part (figure 5(*e*)), was developed in order to provide lenses of long focal length and narrow field angle whose overall length to the focal plane was small compared with more symmetrical lens forms. The optical performance is generally inferior to that of other forms of the same complexity, so that, with the trend in normal photography to the use of smaller film sizes which reduces the importance of relatively short overall length, interest in telephoto lenses tended to decline. More recently, however, a new impetus has been given to the design

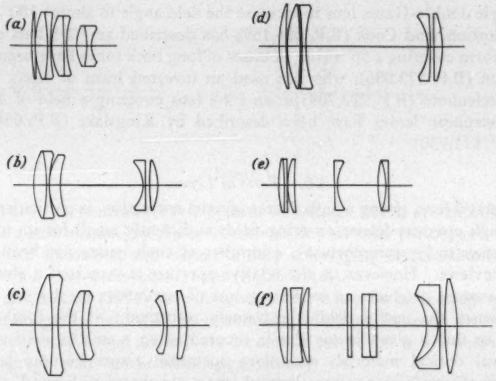

Figure 10.

of telephoto lenses by the growing use of aerial photography, with lenses of focal length of the order of a metre, a very high degree of correction being required at moderate apertures (f/8 to f/4).

For the shorter focal lengths Cox has used a form in which the rear negative component of the conventional telephoto is reversed, so that it is convex towards the front, using a variety of more or less complex front components and giving apertures up to f/2·5 : B.P. 552,024 and 565,411 (figure 10(*a*)) are typical. This form of telephoto has an improved axial correction, at the expense of some deterioration of oblique imagery : the primary aberration theory has been discussed by T. Smith (1945). Voigtländer (B.P. 709,659) has described an f/5·4 lens with abnormally large telephoto effect.

The longer focal length designs have generally followed Lee's earlier patent (B.P. 222,709, figure 10(*b*)) in introducing additional lenses at the front, and dividing the back doublet, thus making distortion correction possible, which could not

be achieved in the original telephoto ; variants of this form have been described by Aklin (f/5·6, U.S.P. 2,378,170), Schade and van Graafeiland (f/5·6, U.S.P. 2,541,485, figure 10(*c*)) and Cook (f/4, B.P. 697,336, figure 10(*d*)). Some advantage would appear to be gained by a change of shape of the rear divergent element, so that the aberrations are more equally distributed between its two surfaces ; such lenses have been described by Cox (f/6·3, B.P. 609,408, figure 8(*e*)), Baker (f/6·3, U.S.P. 2,576,436), Wreathall (f/6·3, B.P. 641,069) and Wynne (f/4, B.P. 697,910). A more complex telephoto lens still, due to Baker (U.S.P. 2,629,285) is shown in figure 10(*f*).

The inverted telephoto lens, with a divergent front, has been used both to give an increase of field angle and an unusually long back focus in relation to focal length. For the former purpose, a large divergent lens of low power may be placed rather far in front of some normal form of lens, whose design requires small modification since the aberrations of the divergent lens are small apart from distortion, which is uncorrected ; Richter (U.S.P. 2,247,068) has used a divergent lens in front of a wide-angle double-Gauss lens to increase the field angle to almost 180°, with very heavy distortion, and Cook (B.P. 696,159) has described an f/2·5 lens of inverted telephoto form covering a 56° field. Lenses of long back focus have been described by Langton (B.P. 572,086), who has used an inverted form of Lee's distortion-corrected telephoto (B.P. 222,709) in an f/2·8 lens covering a field of 45° : other inverted telephoto lenses have been described by Kingslake (B.P. 658,501) and Tolle (B.P. 671,730).

3.6. *Petzval Lenses*

The Petzval lens, giving a high degree of axial correction, is particularly suitable for very high aperture lenses covering fields sufficiently small for its uncorrected field curvature to be unimportant ; a number of such lenses has been described in earlier reviews. However, as the relative aperture is increased a given amount of field curvature produces an increasing loss of resolution, so that for very wide aperture lenses the useful field is extremely restricted ; if the focal length be increased, so that a given image size is secured using a smaller field angle, then with normal optical materials secondary spectrum errors become large. The applications of very high aperture Petzval lenses are therefore limited. Kaprelian (U.S.P. 2,424,827) claims to have designed lenses of relative aperture up to f/0·6 (figure 11(*a*)) using a single lens and a cemented doublet in place of each of the two cemented doublets of the simple Petzval lens—no numerical example is given in the patent specification ; and Back and Lowen (U.S.P. 2,578,624) have used a separated doublet and two triple-cemented combinations to give an f/1·15 lens. The primary field curvature of the Petzval lens may be removed by a diverging lens close to the focal plane, giving some increase in field angle ; such negative field lenses have been used, behind Petzval lenses of varying degrees of complexity, by Schade (U.S.P. 2,541,484) and Angenieux (B.P. 673,353, figure 11(*b*)).

3.7. *Other Wide-aperture Lenses*

A form of wide-aperture lens falling into none of the above categories has been described by Warmisham (B.P. 641,626), having a series of doublet lenses in contact, of a form giving correction of coma and astigmatism with respect to a stop at some distance from them ; the spherical aberration which is inherent in such a system

is removed by a thick meniscus lens whose surfaces are concentric with the stop; field curvature is not corrected; apertures up to f/1·0 (figure 11(*c*)) are claimed, with a level of performance which is said to be adequate in short focal lengths.

Another unusual form of wide-aperture lens (f/0·71), covering a flat field of about 20°, has been described by Wynne (1951 and B.P. 696,902); a front system of lenses in contact corrected for spherical aberration and coma has its field curvature

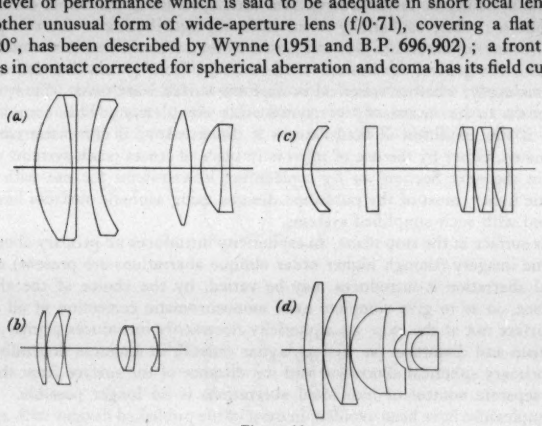

Figure 11.

and astigmatism corrected by a rear system of surfaces which are approximately in the aplanatic and normal-incidence conditions for an axial pencil, and hence free from spherical aberration and coma; a deep converging cemented surface at the back controls higher-order aberrations (figure 11(*d*)).

Offner and Decker (1951) have designed an f/1·0 lens for a spectrograph camera, giving a flat tangential field of 7°, by introducing additional lenses in the symmetrical ball lens mentioned above; complete chromatic correction is not necessary, since the spectrograph plate can be tilted appropriately.

3.8. '*Zoom*' *Lenses*

Lenses of variable focal length, sometimes known as 'zoom' lenses, in which a relative movement of the parts of the system changes the total power while maintaining aberration correction, will not be dealt with here; a general review of the subject has been given by Hopkins (1950).

§4. Lens Systems with Aspheric Surfaces

The great difficulty of making and testing non-spherical surfaces to optical accuracy very largely precludes their use in normal optical imaging systems, though they are commonly used for condensers in illuminating systems, where a lower standard of precision is required, and for a few special imaging systems, for example astronomical telescopes, where their special advantages justify the high cost.

The use of non-spherical surfaces gives the lens designer additional degrees of freedom, but some aspects of the design problem are unaffected. The primary

aberrations of an axially symmetrical system of aspheric lenses may be considered as made up of those of a system of spherical surfaces having the axial curvatures of the actual system plus terms arising from the departure of the actual curves from these spheres; these asphericity terms make no contribution to the two primary chromatic aberrations and to field curvature, so that, for achromatic systems having a flat field, the general conclusions reached in § 1 from a consideration of these conditions apply, whether spherical or aspheric surfaces are used. Such systems were shown to be necessarily of considerable complexity. This complexity is avoided if the condition of field-flatness is discarded, or if chromatic correction is eliminated, either by the use of mirrors in place of lenses (such systems are discussed in the next Section) or by considering lens systems for use with monochromatic light; most of the published designs using aspheric surfaces have been concerned with such simplified systems.

For a surface at the stop plane, an asphericity introduces no primary aberrations of oblique imagery (though higher order oblique aberrations are present) and the spherical aberration it introduces may be varied, by the choice of the shape of the surface, so as to give complete axial monochromatic correction of all orders. For a surface not at the stop, an asphericity necessarily introduces primary coma, astigmatism and distortion (as well as higher orders), in amounts depending only on the primary spherical aberration and the distance of the surface from the stop, so that separate control of individual aberrations is no longer possible. Again, these complexities have been avoided, in most of the published designs with aspheric surfaces, by considering only aspheric surfaces at the stop.

Investigations of the use of aspheric surfaces have been restricted to special simple cases in the various ways mentioned above on account of the greater mathematical complexity of the general problem, and the fact that manufacturing difficulties at present rule out the use of aspheric surfaces for most purposes. A further limitation often imposed, on account of somewhat less difficult manufacture, is that the aspheric surfaces shall have an axial curvature which is small, or zero, as in the figured plate of the Schmidt camera. It has frequently been suggested that better lenses for normal purposes could be produced if surfaces of any required non-spherical form could be used throughout; this appears plausible, but has not yet been demonstrated. It is probably true to say that no optical system with aspheric surfaces has yet been designed giving a higher degree of correction than can be achieved by a system of spherical surfaces of slightly greater complexity; the relative simplicity of the aspheric systems is however sometimes of overriding importance, particularly in the case of instruments of large size for astronomy, discussed in the next Section.

A number of papers has appeared on methods of calculating aspheric surface shapes to fulfil various conditions, but without reference to particular optical systems; such papers will not be considered here. Comparatively few actual aspheric lens systems have been described recently. Warmisham has suggested that the performance of a double-Gauss lens might be improved by designing with a figured plate in the stop plane (B.P. 577,123). Bouwers (U.S.P. 2,492,461), using an aspheric surface at the central stop plane of concentric or near-concentric systems (figure 12(*a*)) claims an aperture of f/1·0 with a curved field of 35°; very similar systems have been described by McCarthy (U.S.P. 2,522,390), including

forms with aspheric field lenses adjacent to the focal plane to give correction over a small flat field. Burch (1943, 1945) and Martin (1944) have investigated the possibilities of correcting the monochromatic aberrations of a single thick lens, one or both of whose surfaces may be aspheric.

Cox has described a system, of relative aperture f/1·4 covering a curved field of 32°, consisting of two spherical surfaced cemented doublets in contact, corrected, with respect to an external stop at some distance from them, for chromatic aberrations, coma and astigmatism, the spherical aberration inherent in such a system being corrected by a figured plate at the stop (B.P. 610,269). Grey (U.S.P.

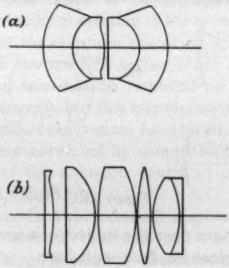

Figure 12. (The asphericities are greatly exaggerated.)

2,552,672) independently used the same principle with more complicated spherical surfaced systems, to give apertures up to f/0·65 (figure 12(*b*)). Developments of Cox's patent have been described by Warmisham (f/1·0, B.P. 619,818) and Wreathall (f/0·71, B.P. 689,110).

§ 5. Reflecting Systems

Where imaging systems of very large size are required (primarily for astronomical telescopes) mirrors are necessarily used ; glass discs of the necessary optical quality for lenses have not been produced in diameters much exceeding one metre ; and in any case lenses much larger than this would be unusable in astronomical telescopes, where the lens would have to function in varying orientations, on account of flexure effects. The freedom of reflecting surfaces from dispersion also makes them particularly suitable for large systems, where the secondary spectrum of refractors becomes serious. A second use of reflecting systems is for high aperture microscope objectives, where again the secondary spectrum associated with refracting systems assumes considerable importance, particularly for microscopes for use in the ultra-violet and infra-red ; and moreover the range of transparent refracting materials for these spectral regions is very limited.

When correction is required over at all large apertures or field angles, only systems of axial symmetry with the object and image centred on the axis need be considered, and such systems employing reflecting surfaces necessarily have physical characteristics, arising from the fact that light before and after reflection is in the same space, which limit their possible application. For a system with one mirror

(e.g. a Schmidt camera) the central part of the incident beam is obstructed by the image surface, which can therefore only have a diameter considerably less than that of the entrance pupil of the system, and is difficult of access. When two mirrors are used (e.g. Cassegrain systems) the image size is still more restricted, and unfocused light from the object reaches the image plane direct, round the edge of the secondary mirror, unless auxiliary baffles are provided. On account of these physical limitations, the use of reflecting systems has been largely confined to large telescopes for astronomy, and to high aperture microscope objectives ; a number of suggestions has been made for their use in place of wholly refracting systems as camera lenses and small telescopes, but these have not been widely adopted.

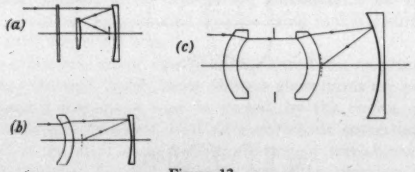

Figure 13.

Reflecting microscopes have been the subject of a recent review article by Norris (1955) ; they will not therefore be dealt with here.

Much of the recent work on reflecting systems has been devoted to overcoming various limitations of the Schmidt camera. Baker (1940) has described flat-field anastigmat systems considerably shorter than the Schmidt camera, consisting of a figured plate, a concave primary and convex secondary mirror (figure 13(*a*)) ; one or both mirrors are aspheric, the latter case giving the shortest system. Slevogt (1942), Burch (1942) and Linfoot (1944) have investigated such Schmidt–Cassegrain systems, including forms where complete correction of astigmatism and field curvature is sacrificed to allow both mirrors to be spherical. Baker (1940) suggested the use of two figured plates in contact to correct the chromatic aberration of the single figured plate, and Linfoot (1945) showed that with two separated figured plates flat field anastigmats can be designed with spherical mirrors, the axial colour being highly corrected. Wayman (1950) has investigated Schmidt–Cassegrain systems where the two mirrors are concentric, with a figured plate at the common centre ; the field is necessarily curved.

A number of systems has been described using spherical surfaced lenses in place of the aspheric plate of the Schmidt camera. Gabor (B.P. 544,694) showed that spherical aberration and coma could be corrected using a spherical mirror with a suitably placed meniscus lens, considerable chromatic aberration being introduced thereby ; and Houghton (B.P. 546,307) used two or more thin lenses in contact, forming an afocal system, in place of the figured plate at the mirror centre. The use of a meniscus lens concentric with the mirror has been suggested by a number of authors ; the first published account appears to be that of Hawkins and Linfoot (1945) ; patents have subsequently been published having earlier application dates, by Bouwers (U.S.P. 2,492,461), Dyson (B.P. 586,851), Bennett (U.S.P. 2,409,971 and 2,571,657) and Baker (U.S.P. 2,458,132).

By a suitable choice of curvatures and thickness such a meniscus can be made to give good correction of the spherical aberration of the mirror, and since the system is monocentric, the imagery at any point on the (curved) field is identical with that on the axis, all orders of oblique aberrations being absent (figure 13(*b*)). The concentric meniscus may lie on either side of the common centre of curvature. The correction of higher-order spherical aberration is improved by increasing the thickness of the meniscus corrector, but a monocentric meniscus introduces a chromatic difference of focus, which increases with meniscus thickness; for moderately low relative apertures, a meniscus thickness may be used which is small enough for the chromatic aberration to be negligible. Hawkins and Linfoot suggested correcting the chromatic aberration of the meniscus by means of a doublet afocal combination placed at the common centre of curvature, one of its surfaces being aspherized to remove the residual higher-order spherical aberration. The chromatic aberration on the axis may be removed by suitably compounding the meniscus of two glasses (Bouwers), but this introduces transverse chromatic aberration in the field. The chromatic aberration, for a given level of spherical aberration correction, is reduced but not corrected by using two menisci concentric with the mirror, one on each side of the common centre of curvature (Bennett (U.S.P. 2,571,657), Baker (U.S.P. 2,458,132)).

Another form of meniscus lens corrector for a spherical mirror which is superficially similar to the monocentric meniscus and has been frequently confused with it, but has quite different aberration characteristics, was first described in English by Maksutov in 1944. The Maksutov meniscus is achromatic for axial imagery; for a given radius of curvature for the first surface and a given thickness, the condition of axial achromatism determines the curvature of the second surface, which is such as to give a lens of slightly lower negative power than would be the case if the second surface were concentric with the first; since the lens is self-achromatic, there is no secondary spectrum, and an extremely high degree of axial achromatism is obtained. Such an achromatic meniscus can be arranged to correct the spherical aberration and coma of a spherical mirror, astigmatism and transverse colour in the field being then not fully corrected, but small when the meniscus thickness is small. As in the case of the concentric meniscus corrector, the degree of correction of higher-order spherical aberration is improved by the use of a thicker meniscus; this involves an increase in the uncorrected astigmatism and field colour. The characteristics of the two systems of spherical mirror with meniscus corrector are therefore such that the monocentric system, with its freedom from all aberrations of oblique imagery, is more suitable when relatively large field angles are to be covered, at moderately low relative apertures and small physical size so that the uncorrected chromatic difference of focus is tolerable; the Maksutov meniscus with its very high degree of correction of axial aberrations and coma is more suitable for systems of larger relative aperture and physical size (for example astronomical telescopes) over small field angles for which the residual uncorrected astigmatism and field colour are tolerable; both systems have similar field curvature.

The Maksutov achromatic meniscus also lends itself more readily to more complicated systems. Maksutov described systems where a secondary spherical mirror, of either Gregorian or Cassegrain form, is added; in the latter case field curvature and astigmatism may be corrected, but not the residual field colour. As with the

concentric meniscus system, higher order spherical aberration may be reduced by using two achromatic menisci, one on either side of and concave to the mirror centre of curvature ; in this case astigmatism and field colour can also be corrected, giving systems of large relative aperture and field (Wynne 1947 and B.P. 618,253, figure 13(*c*)).

The paraboloidal mirror of the astronomical telescope suffers from coma and astigmatism, so that the useful field size is very restricted. Ross (1935) designed doublet lenses which, located appropriately in the converging beam between mirror and focus, correct coma and astigmatism over a limited field, but which necessarily introduce spherical aberration, which for some purposes is not serious. Wynne (1949) following an unpublished suggestion by J. G. Baker, discussed systems corrected for spherical aberration, coma, astigmatism and field curvature consisting of a Ross corrector lens in the converging beam, with an aspheric plate in front of the primary parabolic mirror, and also systems with three elements in the converging beam, consisting of either a figured plate or a secondary mirror, with a doublet lens. Baker's original suggestion has been described in B.P. 696,011 (the Perkin–Elmer Corporation). Meinel (1953) has investigated the use of three aspheric elements in the converging beam.

References

Baker, J. G., 1940, *J. Amer. Phil. Soc.*, **82**, 339.

Burch, C. R., 1942, *Mon. Not. R. Astr. Soc.*, **102**, 159 ; 1943, *Proc. Phys. Soc.*, **55**, 433 ; 1945, *Ibid.*, **57**, 567.

Glancy, A. E., 1945, *J. Opt. Soc. Amer.*, **35**, 307.

Guild, J., 1951, *Proceedings of the London Conference on Optical Instruments*, 1950 (London : Chapman and Hall).

Hawkins, D. G., and Linfoot, E. H., 1945, *Mon. Not. R. Astr. Soc.*, **105**, 334.

Heavens, O. S., 1955, *Optical Properties of Thin Solid Films* (London : Butterworths Scientific Publications).

Hekker, F., 1947, *Thesis*, Delft.

Hopkins, H. H., 1950, *Wave Theory of Aberrations* (Oxford : University Press) ; 1951, *Proceedings of the London Conference on Optical Instruments*, 1950 (London : Chapman and Hall).

Lee, H. W., 1940, *Rep. Progr. Phys.*, **7**, 130 (London : Physical Society).

Linfoot, E. H., 1944, *Mon. Not. R. Astr. Soc.*, **104**, 47 ; 1945, *Proc. Phys. Soc.*, **62**, 199.

Maksutov, D. D., 1944, *J. Opt. Soc. Amer.*, **34**, 270.

Martin, L. C., 1944, *Proc. Phys. Soc.*, **56**, 104.

Meinel, A. B., 1953, *Astrophys. J.*, **118**, 335.

Norris, K. P., 1955, *Research*, **8**, 94.

Offner, A., and Decker, W. B., 1951, *J. Opt. Soc. Amer.*, **41**, 169.

Rinia, H., and van Alphen, P. M., 1947–8, *Philips Tech. Rev.*, **9**, 349.

Ross, F. E., 1935, *Astrophys. J.*, **81**, 156.

Russinov (Roossinov), M. M., and Kosyrew, A. F., 1939, *Untersuchung über Aerovermessung und Photogrammetrie, Moscow.* (Quoted in *Handbuch der Wissenschaftlichen und angewandten Photographie, Erganzungswerk*, vol. I (Wien : Springer, 1943), pp. 84, 87.)

Slevogt, H., 1942, *Z. Instrumkde.*, **62**, 312.

Slussareff, G., 1941, *J. Phys. U.S.S.R.*, **4**, 537.

Smith, T., 1945, *Proc. Phys. Soc.*, **57**, 543.

Starkie, D., 1947, *J. Televis. Soc.*, **5**, 86.

Toraldo di Francia, G., 1955, *Optica Acta*, **1**, 157.

Wayman, P. A., 1950, *Proc. Phys. Soc.* B, **63**, 553.

Wynne, C. G., 1947, *Mon. Not. R. Astr. Soc.*, **107**, 356 ; 1949, *Proc. Phys. Soc.* B, **62**, 772 ; 1951, *J. Sci. Instrum.*, **28**, 172.

PATENTS

(see footnote on p. 304)

AKLIN, G. H.			
U.S.P. 2,252,681/2	app.	17.5.40	pat. 19.8.41
2,262,985		17.5.40	18.11.41
2,336,207		8.10.41	17.12.43
2,338,614		17.6.42	4.1.44
2,343,627		8.10.41	7.3.44
2,378,170		25.6.43	12.6.45
ALTMAN, P. E.			
B.P. 563,206	app. (U.S.A.)	11.5.52	acc. 2.8.44
ANGENIEUX, P.			
B.P. 673,353	app. (France)	7.12.49	pub. 4.6.52
BACK, F. G., and LOWEN, H.			
U.S.P. 2,578,624	app.	3.5.49	pub. 11.12.51
BAKER, J. G.			
U.S.P. 2,458,132	app.	19.6.45	pat. 4.1.49
2,532,751/2		29.9.49	5.12.50
2,576,436		10.10.49	27.11.51
2,628,532		28.11.50	17.2.53
2,629,285		7.8.51	24.2.53
2,671,380		14.6.52	9.3.54
BENNETT, H. F.			
U.S.P. 2,409,971	app.	19.6.45	pat. 22.10.46
2,571,657		27.4.45	16.10.51
BEREK, M., ZIMMERMANN, O., and KLEINEBERG, G.			
U.S.P. 2,297,452	app. (Germany)	6.5.40	pat. 29.9.42
BERTELE, J. B.			
B.P. 681,456	app. (Switzerland)	11.5.49	pub. 22.10.52
696,925	„	24.6.50	9.9.53
719,162	„	12.7.51	24.11.54
BOUWERS, A.			
U.S.P. 2,492,461	app. (Netherlands)	7.7.41	pat. 27.12.49
COOK, G. H.			
B.P. 690,402–5	app.	13.2.51	pub. 22.4.53
696,159		5.6.51	26.8.53
697,336		17.8.51	23.9.53
707,943		14.5.52	28.4.54
730,411		20.11.52	25.5.55
COX, A.			
B.P. 552,024	app.	17.9.41	acc. 19.3.43
565,411		3.5.43	9.11.44
587,761		16.1.45	5.5.47
609,408		13.3.46	30.9.48
610,269		3.4.46	13.10.48
DURAND, M. A.			
U.S.P. 2,260,368	app.	21.12.40	pat. 28.10.41
2,383,115		17.4.43	21.8.45
DYSON, J.			
B.P. 586,851	app.	14.6.44	acc. 2.4.47
FREDERICK, C. W., and HERZBERGER, M. J.			
U.S.P. 2,262,998	app.	17.5.40	pat. 18.11.41
GABOR, D.			
B.P. 544,694	app.	28.1.41	acc. 23.4.42
GREY, D. S.			
U.S.P. 2,552,672	app.	18.5.46	pat. 5.5.51

HERZBERGER, M. J.			
U.S.P.	2,289,779	app. 17.5.40	pat. 14.7.42
	2,350,035	6.6.42	30.5.44
	2,466,424	18.2.46	5.4.49
HERZBERGER, M. J., and HOADLEY, H. O.			
U.S.P.	2,308,007	app. 29.10.41	pat. 12.1.43
HOUGHTON, J. L.			
B.P.	546,307	app. 7.3.41	acc. 6.3.42
KAPRELIAN, E. K.			
U.S.P.	2,424,827	app. 16.6.45	pat. 29.7.47
KINGSLAKE, R.			
B.P.	658,501	app. (U.S.A.) 17.12.48	pub. 10.10.51
KLEINEBERG, G., and ZIMMERMANN, O.			
U.S.P.	2,622,478	app. (Germany) 9.1.50	pat. 23.12.52
KODAK, LTD.			
B.P.	547,691	app. 21.5.41	acc. 7.9.42
LANGTON, B.			
B.P.	572,086	app. 9.3.44	acc. 21.9.45
LEE, H. W.			
B.P.	157,040	app. 14.8.20	acc. 20.1.21
	222,709	27.11.23	9.10.24
LEITZ, E.			
B.P.	381,135	app. (Germany) 6.6.31	acc. 29.9.32
LOTMAR, W.			
B.P.	629,167	app. (Switzerland) 30.6.45	acc. 14.9.49
MCCARTHY, E. L.			
U.S.P.	2,522,390	app. 4.7.45	pat. 12.9.50
PERKIN–ELMER CORPORATION			
B.P.	696,011	app. (U.S.A.) 15.2.51	pub. 19.8.53
RAYTON, W. B.			
U.S.P.	2,325,275	app. 12.2.42	pat. 27.7.43
RICHMOND, G. A.			
B.P.	656,011	app. 31.12.48	pub. 8.8.51
RICHTER, R.			
U.S.P.	2,247,068	app. (Germany) 18.7.38	pat. 24.6.41
ROOSSINOV (Russinov), M. M.			
B.P.	640,232	app. 24.9.46	pub. 12.7.50
SCHADE, W.			
U.S.P.	2,259,004	app. 8.6.39	pat. 14.10.41
	2,461,182	9.2.46	8.2.49
	2,541,484	17.12.48	13.2.51
	2,586,866	11.8.50	26.2.52
	2,604,013	8.8.51	22.7.52
	2,611,295	14.6.51	23.9.52
SCHADE, W., and VAN GRAAFEILAND, W. H.			
U.S.P.	2,541,485	app. 20.8.49	pat. 13.2.51
TOLLE, K.			
B.P.	671,730	app. 23.2.50	pub. 7.5.52
TRONNIER, A. W.			
B.P.	476,349	app. 31.8.36	acc. 7.12.37
U.S.P.	2,627,204/5	app. (Switzerland) 29.4.50	pat. 3.2.53
VOIGTLÄNDER, A. G.			
B.P.	677,202	app. (Switzerland) 27.1.50	pub. 13.8.52
	709,659	,, 6.12.50	2.6.54

WARMISHAM, A.

B.P. 523,061	app.	23.12.38	acc. 4.7.40
523,062		23.12.38	4.7.40
523,218		29.12.38	9.7.40
556,402		20.3.42	4.10.43
577,123		25.8.42 and 13.8.43	acc. 4.11.43
619,818		30.12.46	acc. 15.3.49
641,626		4.2.48	pub. 16.8.50

WARMISHAM, A., and WYNNE, C. G.

B.P. 547,666		app. 2.12.40	acc. 7.9.42
559,699		26.8.42	1.3.44
559,864		26.8.42	8.3.44

WILD (VERKAUFS-A.G. HEINRICH WILDS GEODATISCHE INSTRUMENTE)

B.P. 680,185	app. (Switzerland)	13.2.50	pub. 1.10.52
708,797	„	20.10.51	12.5.54

WREATHALL, W. M.

B.P. 641,069		app. 4.11.48	pub. 2.8.50
689,110		17.7.50	18.3.53

WYNNE, C. G.

B.P. 564,815	app.	29.3.43	acc. 13.10.44
575,075		25.2.44	1.2.46
575,076		25.2.44	1.2.46
577,763		8.6.44	30.5.46
604,883		7.12.45	12.7.48
618,253		1.5.46 and 1.8.46	acc. 18.2.49
689,916		15.7.50	pub. 8.4.53
696,902		15.7.50	9.9.53
697,910		15.7.50	30.9.53

ZEISS, CARL

B.P. 278,338	app. (Germany)	28.9.26	acc. 8.12.27

ZEISS–OPTON OPTISCHE WERKE, OBERKOCHEN G.M.B.H.

B.P. 723,544	app. (Germany)	25.11.50	pub. 9.2.55

THE MACROSCOPIC THEORY OF IRREVERSIBILITY

By R. O. DAVIES
Physics Department, Queen Mary College, London E.1

CONTENTS

PAGE
§ 1. Introduction 327

PART I. COMPLETE SYSTEMS UNDER NON-UNIFORM CONDITIONS: FLOW

§ 2. The theory of Onsager 329
2.1. A summary of the formal theory 329
2.2. The existence of entropy 331
2.3. Macroscopic fluctuations 332
2.4. Correlations in time 335
2.5. The reciprocity theorem 336
2.6. The Onsager fluxes and flow vectors 338
2.7. Gyroscopic forces, odd and even variables 340
§ 3. An application of Onsager's theory to discrete systems 341
3.1. The theory of plug transfer 342
3.2. The measurement of energy flow 344
3.3. Thermo-osmosis 344
3.4. The Joule–Kelvin effect 346
3.5. Multi-component systems 347
3.6. The flow of entropy 348
§ 4. An application of Onsager's theory to continuous systems 348
4.1. The theory of viscous flow in an external field 348

PART II. INCOMPLETE SYSTEMS UNDER UNIFORM CONDITIONS: RELAXATION

§ 5. The thermodynamic theory of relaxation 350
5.1. Static properties 350
5.2. Dynamic properties 354
§ 6. Some applications of relaxation theory 358
6.1. Glass formation 358
6.2. Sound absorption in fluids 360
6.3. Visco-elasticity 363
6.4. Further developments 364

PART III. BIBLIOGRAPHICAL NOTES ON SOME FURTHER TOPICS

§ 7. Other aspects of irreversibility 364
7.1. Application and development of the Onsager theory 364
7.2. The microscopic theory and fluctuations 365
References 366

Abstract. This article reviews certain aspects of irreversible thermodynamics. There are two main parts. The first part considers the Onsager theory of the approach to equilibrium of isolated systems under non-uniform conditions. The whole system is treated as being made up of macroscopic but small sub-systems, which are in ' local equilibrium ' in the sense that they can be described in terms of the same variables as are needed in equilibrium.

Applications dealt with include (*a*) the transfer of matter and energy between two phases (including the Joule–Kelvin effect); (*b*) the equations of motion of a viscous fluid in an external field. The second part considers the case of uniform systems which are not fully describable in terms of the equilibrium variables but which may still be treated phenomenologically by introducing ordering parameters. They are usually described as 'relaxing systems'. The examples discussed are (*a*) the approach to equilibrium of glass-forming liquids, (*b*) ultrasonic absorption, (*c*) visco-elasticity (which involves tensorial ordering parameters). The review concludes with bibliographical notes on those parts of irreversible thermodynamics not considered earlier.

§1. Introduction

It is generally agreed that classical thermodynamics, now a hundred years old, is one of the best established theories of nature. It contains three main strands: (*a*) it provides a macroscopic framework within which both thermal and mechanical properties of matter can be described; (*b*) it yields conditions for thermodynamic equilibrium applicable (as shown by Gibbs) even in systems of variable composition; (*c*) there are certain reciprocity rules (the Maxwell relations) connecting separately measurable thermodynamic coefficients of physical systems. It is true that there are parts of the subject (e.g. the thermodynamics of surfaces and of electrical phenomena) which do not at present fit into the classical scheme very well, but it has always been felt that it should be possible to bring these unruly elements within the law. However that may be, the classical theory deals entirely with equilibrium behaviour. The fact that in many cases the non-equilibrium behaviour of bulk matter can be simply described in thermodynamic terms suggests strongly that a generalization of the theory may be possible to deal with non-equilibrium behaviour as well.

The need for such a generalization can be seen by considering the classical theory itself. The study of statics can be founded on the principle of virtual work. Such a formulation is unsatisfactory to the physicist and he naturally prefers to regard the principle of virtual work as a consequence of Newton's second law of motion, thereby obtaining his statics as a specialization of a more general theory. In a similar way the equilibrium conditions in thermodynamics are based on the vanishing of virtual variations in the entropy of an isolated system. If, as often happens, real variations of entropy are considered then there are no dynamical laws (corresponding to Newton's law) to describe the return to equilibrium which —it is usually asserted—must take place 'sooner or later'. Recent work on the macroscopic theory of irreversibility has been concerned with establishing a suitable form for such laws. It is hoped that the results may also be applicable to steady-state, non-equilibrium phenomena and indeed the subject is sometimes called the 'thermodynamics of the steady state'.

Early writers on thermodynamics were very conscious of the necessity of generalizing the subject. Thus a number of elements of the present-day approach can be found in Bertrand (1887). His object was to trace in detail the increase in entropy (demanded by Clausius) of an isolated system. He admits that he was not able to make much headway in a subject which is 'too vague and too difficult' but cites two cases: (*a*) assuming Fourier's law of heat conduction in a solid and a suitable expression for the entropy flow, he was able to show that

entropy must be created and not destroyed in a system away from equilibrium ; (*b*) assuming the usual formulae for the thermodynamic properties of a gas he made a calculation (of a type familiar to students) of the increase in entropy associated with the adiabatic mixing of gaseous specimens at different temperatures.

Implicit in Bertrand's work is the idea of treating entropy as a ' thing '— distributed through space, flowing and being created but not destroyed. Over the next twenty years a number of continental writers (Wiedeburg, Natanson and Duhem) tried to extend Bertrand's methods as far as possible by assuming laws of viscosity, electrical conduction, etc. and attempting to find the rate of creation of entropy or the dissipation function of the system. This trend reached its culmination with the publication of Pierre Duhem's *Traité d'Énergétique* in 1911. At a more qualitative level there was a stimulating, if not always objective, book with the Victorian title : *Entropy, or Thermodynamics from an engineer's standpoint and the reversibility of thermodynamics* (1904), by an English engineer called James Swinburne.

It is clear that in the twenty years spanning 1900 there was extensive work done on irreversible thermodynamics and it is natural to ask why it is now largely forgotten and its authors' names known to only a handful of physicists. No doubt part of the reason is that concurrent discoveries in atomic physics reduced the scale, so to speak, of the physicist's main interests. Moreover Duhem at least was publicly (although not justly) associated with the ' Energetics ' school of Mach and Ostwald. More to the point, however, is the fact that one would be hard pressed to find a single new, verifiable result in all the writings indicated above. The reason for this is that the flow laws (Fourier's law, the viscosity law and so forth) are inserted into the theory *ad hoc* and used to deduce the dissipation function.

The subject was virtually refounded in 1931 when Onsager realized that by approximately reversing the older method it was possible to proceed from the entropy of an isolated system to the flow laws. By itself this would still be of limited interest but Onsager proposed further a reciprocity theorem which provides relations between flow coefficients analogous to the Maxwell relations in thermodynamics. These constitute verifiable results some of which are new, and, together with a unified way of getting at the flow equations, they give the theory its significance. The best known of the reciprocity laws is the famous Kelvin relation of thermo-electricity which relates the thermo-electric power of a pair of metals to the difference of their Thomson coefficients.

The Onsager theory and some of its applications to complete systems are considered in Part I of the present review. By the word ' complete ' it is implied that the local state of the system of interest is describable by the same number of independent thermodynamic variables as are needed to describe it in equilibrium. Indeed, it is assumed that local equilibrium subsists so that local variables are related to one another exactly as if the system were in equilibrium. Departures from equilibrium are due to non-uniformity : the temperature and/or chemical potentials are not constant throughout the system.

The opposite extreme is considered in Part II. Here it is assumed that one or more parameters (in addition to those necessary in equilibrium) are required to describe the local state of the system. Such systems may be called ' incomplete ' and we shall be mainly concerned with incomplete systems in uniform states.

In both Parts I and II some effort has been made to avoid duplicating material which is already available in reviews and monographs. As a result the present paper is not exhaustive. Since, in the opinion of the writer, a definitive form of Onsager's theory has not yet appeared this may not be altogether a bad thing. In any case an attempt has been made to offset the lack of balance by providing (in Part III) what amounts to an annotated bibliography of recent papers on selected topics not discussed earlier.

The reviews and monographs which have already appeared are by de Groot (1945), Prigogine (1947), de Groot (1951), Denbigh (1951), Haase (1952), Domenicali (1954), Montroll and Green (1954), Meixner (1954 a), Cox (1955) and Prigogine (1955). Domenicali's paper is on thermo-electric and thermo-magnetic effects; the others are more general.

It is perhaps not invidious to remark that the beginner will probably find that Denbigh's monograph and Prigogine's recent book (1955) are the most helpful.

PART I. COMPLETE SYSTEMS UNDER NON-UNIFORM CONDITIONS: FLOW

§ 2. The Theory of Onsager

2.1. *A Summary of the Formal Theory*

Recent work on macroscopic irreversibility has all been based on a formalism given by Onsager in 1931. This formalism is perfectly straightforward; the difficulties lie in making detailed applications and in justifying the work. It is therefore worth while to state Onsager's theory, explain it (at least partially) and then to consider some typical applications. The explanation will be attempted in this Section and the applications given in § 3 and § 4.

The basic assumption is that a system which is the seat of irreversibility may yet be 'sufficiently' close to equilibrium for it to be describable by thermodynamic variables. This may be achieved in two ways. Either (1) the system can be divided into sub-systems each of which can be regarded as being in local equilibrium or (2) it is possible to find one or more ordering variables which must be added to the usual independent variables of the system in order to define the instantaneous state. In Part I we shall be concerned with the first alternative.

Consider the question: how far from equilibrium is a system in a given non-equilibrium state? The only obvious answer to this question is related to the Second Law of Thermodynamics. This says that in proceeding from one equilibrium state to another, the entropy of an isolated system must increase. In this strict form the Second Law can tell us nothing about irreversible processes. If however we are prepared to consider 'freezing' the non-equilibrium state by inserting an arrangement of barriers then it may be regarded as 'represented' by an equilibrium state and the actual progress to equilibrium can be considered as the consequence of removing the barriers. The Second Law then applies and an obvious measure for the departure of the system from equilibrium is the entropy increase associated with its return to equilibrium. It might be argued that the system need not be isolated. In that case the entropy increase is partly due to the system and partly due to the surroundings although of course it may be expressed in terms of changes of the system (e.g. for a system of fixed volume which can

exchange heat with a reservoir at temperature Θ, $\Delta S_{\text{irr}} = \Delta(S - U/\Theta) \geqslant 0$ where U and S are system properties). This procedure of 'isolating' the system by adding surroundings to the original system is always used or implied when discussing irreversibility in systems which are not isolated originally.

In view of the above remarks we may conclude (with Onsager) that if the Second Law is to be used to discuss macroscopic irreversibility then we must consider an isolated system and we must use its entropy as a criterion of its departure from equilibrium.

Suppose that the instantaneous entropy S of an isolated system is fixed by n independent parameters $a_1, a_2, \ldots a_n$. Let the equilibrium values of these parameters be $a_1^0, a_2^0, \ldots a_n^0$ and the corresponding entropy be S_0. The deviations, $\alpha_i = a_i - a_i^0$, are Onsager's coordinates describing the state of the system. Since the entropy is a maximum in the equilibrium state we may assume that for states near enough to a stable equilibrium state

$$\Delta S \equiv S - S_0 = -\tfrac{1}{2} \sum_i \sum_k g_{ik} \alpha_i \alpha_k. \qquad \ldots\ldots(2.1)$$

Provided that the equilibrium state is not a thermodynamic singularity, g_{ik} is positive definite. For reasons which will be apparent presently, Onsager defines thermodynamic forces by

$$F_i = \partial \Delta S / \partial \alpha_i = -\sum_k g_{ik} \alpha_k \qquad \ldots\ldots(2.2)$$

so that, in equilibrium, both the Onsager forces and the Onsager coordinates vanish.

The next assumption is that there exists a range of states near equilibrium where the dynamic behaviour of the system is simply represented by a linear relaxation to the equilibrium state:

$$\dot{\alpha}_i = \sum_k L_{ik} F_k. \qquad \ldots\ldots(2.3)$$

The coefficients L_{ik} are called the Onsager coefficients and the final important assumption of the theory is that L_{ik} is symmetric:

$$L_{ik} = L_{ki}. \qquad \ldots\ldots(2.4)$$

This is Onsager's reciprocity theorem. The derivatives of the Onsager coordinates $\dot{\alpha}_i$ are called the Onsager fluxes or flows, often denoted by J_i.

It follows from (2.1) that the rate of irreversible production of entropy is

$$\Delta \dot{S} = \sum_i J_i F_i. \qquad \ldots\ldots(2.5)$$

This form has played an important part in applications of the theory because it is sometimes simple to calculate the rate of entropy production as the sum of products like (2.5) and then to use the form to select the Onsager fluxes and forces.

The justification for, and use of, equations (2.3), (2.4) and (2.5) make up the bulk of the literature on macroscopic irreversibility but there are two fairly important modifications which should be mentioned here:

(*a*) In the presence of an external magnetic field $\mathscr{H}$ or of uniform rotation (angular velocity ω) the reciprocity theorem must be modified to read

$$L_{ik}(\mathscr{H}, \omega) = L_{ki}(-\mathscr{H}, -\omega). \qquad \ldots\ldots(2.6)$$

Cases of this type were discussed by Meixner (1941 b) and Casimir (1945).

(*b*) The Onsager coordinates may be classified into odd or even coordinates depending on whether or not they change sign on reversal of the particle velocities. If both types are present, certain changes in the formalism are necessary (Casimir 1945, 1949, Onsager and Machlup 1953, Machlup and Onsager 1953).

For the moment we shall ignore these complications and discuss in more detail the simpler formulae given above.

2.2. *The Existence of Entropy*

We divide our isolated system into sub-systems of fixed volume and we assume that it is always possible to assign an internal energy U and a mass M to each sub-system. Because the volumes are fixed, then in equilibrium the entropy, pressure and temperature are determined by these two quantities; away from equilibrium we *define* S, p and T for each sub-system as the equilibrium values which would obtain for the given U and M of the sub-system. This is the assumption of local equilibrium. In order for the procedure to give a unique result there are three rather vague requirements which must be met: (*a*) the sub-systems must not be so small that 'surface' interactions between them swamp the volume effects; (*b*) they must be large enough to be treated as macroscopic; (*c*) they must be small enough to yield 'smooth' variations of the intensive thermodynamic properties from cell to cell—independently of the exact method of subdivision. The three requirements can be summed up by saying that the inhomogeneities which we can consider must not extend to such a small scale that they can no longer be treated macroscopically.

The assumption of local equilibrium is expressed analytically by saying that the intensive thermodynamic variables obey the Gibbs equation:

$$ds = (1/T)\,du - \sum_i (\mu_i^+/T)\,d\rho_i$$

or

$$ds^+ = (1/T)\,du^+ + (p/T)\,dv^+ - \sum_i (\mu_i^+/T)\,dm_i. \qquad \ldots\ldots(2.7)$$

(Here s, u etc. are specific quantities referred to unit volume while s^+, u^+ etc. refer to unit mass; $m_i = M_i/V$ and $m_i^+ = M_i/M$ so that only $n-1$ of the m_i^+ are independent.)

The differentials are arbitrary and may be associated with change of time, of position or both (substantive derivation).

Questions which arise immediately are: do these definitions of S, p and T have any instrumental meaning? How can they be checked? As far as pressure and temperature are concerned it is fairly clear that measured values of these properties will depend on the instrument used to carry out the measurement. This is often of little practical importance and even as a matter of principle one could imagine correction schedules to make allowance for idiosyncrasies of the instrument. Of greater importance is the fact that the pressure (as defined above) is often used to form the mechanical equations of motion of a fluid. It could be argued that a 'mechanical' pressure should be introduced (distinct from the thermodynamical pressure defined above) to deal with such cases. Prigogine has raised this question (1952) and it does not seem to be settled yet.

Whether or not an assignment of entropy is correct depends on what we mean by entropy. From a macroscopic point of view we have noted that the rigorous

version of the Second Law merely requires that the entropy of an isolated system increase in going from one equilibrium state to another. This will of course be satisfied by any definition (including ours) which reduces to the equilibrium value in equilibrium. It would be satisfied equally well if (say) grad T were added to the definition of entropy. What we hope for (and what we now assume) is that our definition of entropy must give a quantity which increases monotonically during an irreversible process in an isolated system.

The only approach to this question which can yield definite answers is to calculate theoretically the entropy (defined kinetically) during a stationary flow in gases or of electrons in a metal. Prigogine (1949) has dealt with the former case and Callen (1948) with the latter. Both workers were able to show that the local equilibrium assumption gives only a first approximation to the kinetic entropy. Since the kinetic definition of entropy away from equilibrium is also arbitrary, it is difficult to see the exact significance of such calculations. The real test would seem to be: are the consequences drawn from a definition of entropy true or not?

Finally, it should be pointed out that the existence of an entropy away from equilibrium is tacitly assumed whenever stability is discussed in classical thermodynamics. Gibbs, for example (1906, p. 56), has no hesitation in using a non-equilibrium entropy defined exactly as above.

2.3. *Macroscopic Fluctuations*

Starting from Onsager's original paper, most writers on the basis of irreversible thermodynamics have sought to connect the theory with the regression (in time) of the fluctuations about equilibrium of macroscopic variables. (Exceptional in this respect is the work of Cox (1955) and Bridgman (1932, 1950) which will not be considered here.) It is intuitively plausible that such a connection should exist. Consider the fluctuations in energy of a block of copper coated by a layer of poorly conducting material and immersed in a temperature bath. If the copper has a given non-equilibrium energy at $t = 0$, then macroscopically we know that it will relax exponentially to its equilibrium value with a time constant C/K where C is the heat capacity of the block and K the heat transfer coefficient of its coating. It seems reasonable to suggest that the *average* decay of macroscopic fluctuations in energy will also be exponential with a similar time constant. The assumption made is that the average macroscopic decay and the macroscopic decay obey *exactly* the same laws. To put the matter colloquially, it is assumed that if we were to walk into a laboratory and observe the approach to equilibrium of the copper block described above we should be unable to decide whether the initial state was produced artificially or spontaneously.

Consider first the probability distributions for macroscopic variables. According to the basic methods of statistical mechanics (see for example Schrödinger 1948) the probability that an open system in equilibrium should have an energy between E and $E+dE$ and a mass between M and $M+dM$ is

$$W(E,M)\,dE\,dM = Z^{-1}(\beta,\gamma,V)\,\Omega(E,M,V)\exp(-\beta E+\gamma M)\,dE\,dM \qquad \ldots\ldots(2.8)$$

where $\beta = 1/kT$, $\gamma = \mu^+/kT$. Z is a normalizing factor and Ω is the weight factor which gives the number of micro-states per unit range of E and M.

It follows immediately that mean values are given by

$$\langle E\rangle = -\partial \log Z/\partial\beta$$

$$\langle M\rangle = \partial \log Z/\partial\gamma$$

$$\langle \partial \log \Omega/\partial V\rangle = \partial \log Z/\partial V$$

so that $$\delta(\log Z) = -\langle E\rangle\,\delta\beta + \langle M\rangle\,\delta\gamma + \left\langle \frac{\partial \log \Omega}{\partial V}\right\rangle \delta V.$$

Comparing this with the thermodynamic formula

$$\frac{1}{k}\delta\left(S - \frac{U}{T} + \frac{\mu^+ \mathscr{M}}{T}\right) = \frac{1}{k}\delta\left(\frac{pV}{T}\right) = -U\delta\left(\frac{1}{kT}\right) + \mathscr{M}\delta\left(\frac{\mu^+}{kT}\right) + \frac{p}{kT}\delta V$$

we may identify $U = \langle E\rangle$, $\mathscr{M} = \langle M\rangle$, $p = kT\langle \partial \log \Omega/\partial V\rangle$

and $$(TS - U + \mu^+ \mathscr{M})/T = pV/T = k \log Z$$

—a Massieu function. One can go on and calculate fluctuations from equation (2.7) and this has been done by Greene and Callen (1951). However without proceeding with these details we wish to make some important observations :

(*a*) On the above scheme, the only fluctuating quantities are E, M and $\log \Omega$ (which is a function of E and M). The other properties, including T, p, μ^+ and S, are fixed once and for all. They are canonical average properties (or canonical parameters).

(*b*) It can be shown that for macroscopic systems the canonical entropy $S \equiv k \log Z + \langle E\rangle/T$ is numerically indistinguishable from $k \log \Omega(\langle E\rangle, \langle M\rangle, V)$. (See Khinchin (1949) for a lucid discussion of this point.) For this reason we are justified in calling $s \equiv k \log \Omega(E, M, V)$ the micro-canonical entropy. It is a fluctuating quantity whose *average* value is the canonical entropy. It is therefore not a maximum for $E = \langle E\rangle, M = \langle M\rangle$. The function that is maximized by this choice of E and M is $\log \Omega - E/kT + \mu^+ M/kT$ (cf. remarks made in § 2.1 concerning non-isolated systems).

(*c*) We can if we choose regard temperature, pressure and chemical potential as fluctuating variables linked to the micro-canonical entropy and hence (eventually) to the instantaneous values of E and M. Variance and covariance expressions based on this idea are given by Landau and Lifschitz (1938).

In terms of the micro-canonical entropy, the distribution function of equation (2.8) can be written as

$$W(E, M)\,dE\,dM = \exp\{(s - S)/k - \beta(E - \langle E\rangle) + \gamma(M - \langle M\rangle)\}\,dE\,dM. \qquad \ldots\ldots(2.9)$$

In future we shall contract the notation and let x stand for all additive, conserved properties of interest $(E, M, \ldots)$ and β for all intensive properties $(\beta, -\gamma, \ldots)$. For a system canonical in x we then have (2.9) in the form

$$W(x)\,dx = \exp[(s - S)/k - \beta(x - \langle x\rangle)]\,dx. \qquad \ldots\ldots(2.10)$$

Consider now a system in canonical equilibrium divided into $n+1$ sub-systems (in the manner discussed in § 2.2) whose extensive parameters are $x_1, x_2, \ldots x_{n+1}$.

Because of the macroscopic size of the sub-systems, instantaneous values of the x_i in the different sub-systems are statistically independent and the joint distribution function is

$$W(x_1, \ldots x_{n+1}) = \exp\left\{\sum_1^{n+1}(s_i - S_i)/k - \beta\sum_1^{n+1}(x_i - \langle x_i\rangle)\right\}.$$

A system like this is of course not isolated; to get the distribution function for an isolated system we have to find the marginal distribution function for n independent variables $a_1, \ldots a_n$ where we may choose $a_{n+1} = \sum_1^{n+1} x_i = \text{constant}$. Physically, this restriction can be thought of as caused by gradually 'insulating' the system from its surroundings so that fluctuations in a_{n+1} are eventually very slow and may be ignored over a long time interval. When this restriction is made, the microcanonical entropy $s = \sum_1^{n+1} s_i$ has a maximum at values of x_i equal to the full canonical means $\langle x_i\rangle$ satisfying the restriction $\sum_1^{n+1}\langle x_i\rangle = a_{n+1}$. If s_0 is the value of s in this state, $\Delta s = s - s_0$ is a negative function of $a_1, \ldots a_n$. Let the (partial) equilibrium values of a_i be a_i^0 and let the a_i be linear functions of the x_i. Then $\alpha_i = a_i - a_i^0$ $(i = 1, \ldots n)$ are Onsager's coordinates. Unlike the x_i they will not be statistically independent variables. In the neighbourhood of equilibrium Δs may be approximated by equation (2.1) and the distribution function for Onsager's variables is

$$W(\alpha_1, \ldots \alpha_n) = C\exp\left(-\frac{1}{2k}\sum_i\sum_k g_{ik}\alpha_i\alpha_k\right). \qquad \ldots\ldots(2.11)$$

Although the linear transformation from the thermodynamic variables x to Onsager's variables α is arbitrary, once it has been chosen the g_{ik} can be expressed in terms of it and of the thermodynamic coefficients. Similarly, Onsager's forces can be expressed in terms of the conjugate variables $\beta_i = \partial s_i/\partial x_i$. Also, it is clear that if the Onsager coordinates are subjected to a linear transformation $\tilde{\alpha} = T\alpha$ (say) then the forces will undergo the contragredient transformation $\tilde{F} = SF$ where $S'T = I$. This result which rests on the invariance of Δs is sometimes known as Meixner's theorem.

To show that the reduction of the thermodynamic variables just described is not trivial, consider two sub-systems 1 and 2 exchanging energy. Let their heat capacities be C_1 and C_2. Then one can easily show that in full canonical equilibrium the mean square fluctuations in energy are (apart from constants)

$$\langle\delta E_1^2\rangle = 1/C_1; \quad \langle\delta E_2^2\rangle = 1/C_2; \quad \text{also } \langle\delta E_1\,\delta E_2\rangle = 0.$$

However in the restricted equilibrium with fixed total energy, one finds

$$\langle\delta E_1^2\rangle = \langle\delta E_2^2\rangle = 1/C_1 + 1/C_2 \quad \text{and} \quad \langle\delta E_1\,\delta E_2\rangle = -(1/C_1 + 1/C_2).$$

From the distribution function of equation (2.11) it is easy to see that the second moments of the Onsager forces and coordinates are given by

$$\begin{aligned}\langle\alpha_i\alpha_j\rangle &= kg_{ij}^{-1}\\ \langle F_iF_j\rangle &= kg_{ij} \qquad \ldots\ldots(2.12)\\ \langle F_i\alpha_j\rangle &= k\delta_{ij}.\end{aligned}$$

From the first of these it follows that $\langle\Delta s^2\rangle = n.\frac{1}{2}k$, which, for macroscopic subsystems, is of course negligibly small.

2.4. *Correlations in Time*

The Onsager variables α_i fluctuate about a zero mean with an instantaneous Gaussian probability distribution in accordance with equation (2.11) above. Their complete development in time is a stationary stochastic process whose properties must now be specified. In the first place it is reasonable to assume that we have a Gaussian stochastic process. This means that for any set of variables $\alpha_i, \alpha_j, \ldots$ taken at any times $t_i, t_j, \ldots$ the joint distribution function $P(\alpha_i(t_i), \alpha_j(t_j), \ldots)$ is Gaussian. The theory and applications of Gaussian stochastic processes are well known (see Wang and Uhlenbeck 1945, Moyal 1949, Bartlett 1955 and particularly Rice 1944). The most important fact is that all probability distributions of the variables and their time derivatives can be found, once the correlation functions $\langle \alpha_i(t)\alpha_j(t+\tau)\rangle$ are known. Conversely, any information or assumption about the distribution functions restricts the possible forms for the correlation functions.

Using single variables for simplicity the macroscopic equations stated in § 2.1 are

$$F = -g\alpha$$

$$\dot{\alpha} = LF \quad \text{or} \quad F = R\dot{\alpha} \quad (R = L^{-1})$$

or

$$R\dot{\alpha} + g\alpha = 0.$$

This states that, starting from a displaced value α_0 at time 0, $\alpha(t)$ relaxes as $\alpha_0 e^{-\gamma t}$ where $\gamma = Lg$.

In virtue of the Gaussian nature of the process, from the point of view of fluctuations the joint distribution function for $\alpha(0), \alpha(t)$ is proportional to

$$\exp\left\{-\frac{1}{2}\frac{1}{V(0)^2 - V(t)^2}\left[V(0)\alpha(0)^2 - 2V(t)\alpha(0)\alpha(t) + V(0)\alpha(t)^2\right]\right\},$$

where $V(t) = \langle \alpha(0)\alpha(t)\rangle$ is the correlation function and $V(0)$ is given by equation (2.12). From this the conditional average value of $\alpha(t)$ (given $\alpha_0(0)$) is

$$\langle \alpha(t) \,|\, \alpha_0(0)\rangle = \frac{V(t)}{V(0)}\alpha_0(0).$$

If we now adopt the (very strong) assumption that the average value of the regression obeys macroscopic laws then we must have $V(t) = e^{-\gamma t}V(0)$. This immediately implies that α is a Markov process with a stochastic equation of the Langevin type :

$$\dot{\alpha} + \gamma\alpha = Z(t),$$

where $Z(t)$ is a completely random function having a white spectrum.

This frank view of the nature of the Onsager assumptions is due to Casimir (1949) and to Onsager and Machlup (1953). It should be remembered that, in a manner exactly similar to Brownian motion theory, the fluctuating variable $\dot{\alpha}$ does not really exist because of the improper nature of $Z(t)$. Its interpretation and use already implies some reasonable time averaging over a short time interval during which the system is supposed to ' forget ' its past. Casimir puts the point by saying that one must postulate the existence of a time interval (τ_1, τ_2) such that for $\tau_1 < t < \tau_2$, $\langle \alpha(t) \,|\, \alpha_0(0)\rangle - \alpha_0(0)$ is proportional to t. The constant of proportionality is what is meant by $\dot{\alpha}$.

2.5. *The Reciprocity Theorem*

The reciprocity theorem of Onsager is (in matrix notation)

$$L = L'. \qquad \ldots\ldots(2.13)$$

When the work of the previous section is written for n variables we have a matrix of correlation functions, $V(t) = \langle \alpha(0)\alpha'(t)\rangle$, and, with the same Markov assumption as before,

$$V(t) = V(0)\exp(-\gamma' t) \qquad \ldots\ldots(2.14)$$

where $\gamma = Lg$. In accordance with equation (2.12), $V(0) = kg^{-1}$. g is of course symmetric, so inserting the values of $V(0)$ and γ in (2.14) we see that the necessary and sufficient condition for L to be symmetric is that $V(t)$ should be symmetric. In other words, Onsager's theorem is equivalent to the relation

$$\langle \alpha_i(0)\alpha_j(t)\rangle = \langle \alpha_j(0)\alpha_i(t)\rangle. \qquad \ldots\ldots(2.15)$$

It has already been assumed that the fluctuations in α form a Markov process. This being so, there is a more convenient way of stating the symmetry of $V(t)$: in terms of the transition probabilities of the process. The joint distribution function for α_0 at time 0 and α_t at time $t(>0)$ can be written as

$$W(\alpha_0, 0\,;\ \alpha_t, t) = P(\alpha_0)\,T_f(\alpha_t|\alpha_0) = P(\alpha_t)\,T_b(\alpha_0|\alpha_t) \qquad \ldots\ldots(2.16)$$

where $P(\alpha)$ is the instantaneous distribution function for the α's (i.e. it is given by equation (2.11)), T_f and T_b are, respectively, the forward and backward transition probabilities, which are functions of t. (Notice that here α_0 stands for the complete set $\alpha_1(0), \alpha_2(0) \ldots \alpha_n(0)$; α_t similarly.)

In terms of these functions we may write the correlation matrix and its transpose as:

$$\langle \alpha_i(0)\alpha_j(t)\rangle = \int\ldots\int \alpha_i(0)\alpha_j(t)\,P(\alpha_0)\,T_f(\alpha_t|\alpha_0)\,d\boldsymbol{\alpha}_0\,d\boldsymbol{\alpha}_t$$

$$\langle \alpha_j(0)\alpha_i(t)\rangle = \int\ldots\int \alpha_i(t)\alpha_j(0)\,P(\alpha_0)\,T_f(\alpha_t|\alpha_0)\,d\boldsymbol{\alpha}_t\,d\boldsymbol{\alpha}_0.$$

Comparing the two integrals we see that a *sufficient* condition for them to be equal for all t is

$$P(\alpha_0)\,T_f(\alpha_t|\alpha_0) = P(\alpha_t)\,T_f(\alpha_0|\alpha_t) \qquad \ldots\ldots(2.17)$$

or

$$T_f(\alpha_t|\alpha_0) = T_b(\alpha_t|\alpha_0) \qquad \ldots\ldots(2.18)$$

or

$$W(\alpha_0, 0\,;\ \alpha_t, t) = W(\alpha_t, 0\,;\ \alpha_0, t). \qquad \ldots\ldots(2.19)$$

The relations (2.13) and (2.15) are equivalent statements of the reciprocity theorem while (2.17)–(2.19) are alternative statements of a stronger condition which implies the reciprocity theorem.

The justification for the theorem rests on the fact that in the absence of external magnetic fields or Coriolis forces the Hamiltonian of a system of particles is an even function of the momenta: $H(-p, q) = H(p, q)$. Therefore, considering Hamilton's equations ($\partial H/\partial q = -\dot{p}$, $\partial H/\partial p = \dot{q}$), we see that the transformation $p \to -p, t \to -t$ leaves them invariant. It follows that from any solution of the equations, another solution (called the *reversed* solution) is obtained from the transformation. The situation is best grasped by means of the diagram of

figure 1. This represents the path of the two solutions in phase space. The coordinates are plotted and corresponding momenta marked along the paths. Suppose now that α is an *even* function of the momenta. Then corresponding to the phase space paths of figure 1, there will be paths of the Onsager coordinates shown in figure 2. Consider now paths in Onsager space between 0 and t. A selection of possible paths and their reversals with respect to $\frac{1}{2}t$ is shown in figure 3. (In constructing this figure we have made use of the trivial possibility of time translation.) The important point is that corresponding to each path is a reversed path as shown. It is clear that, however many pairs of paths are drawn, exactly

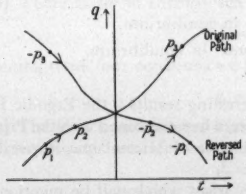

Figure 1. Two possible microscopic paths in coordinate space for a conservative non-gyroscopic system.

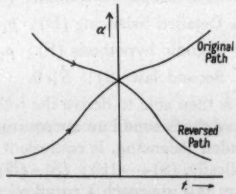

Figure 2. Two possible paths in the macroscopic space of the Onsager variables (α an even function of momenta).

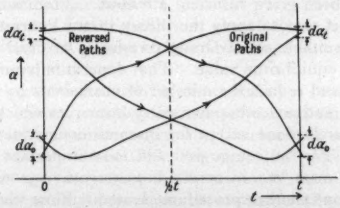

Figure 3. An illustration of possible paths in Onsager space showing how the possibility of reversal makes the reciprocity theorem plausible.

the same number of intersections will be found in $d\alpha_0$ at 0 and $d\alpha_t$ at t as are found in $d\alpha_t$ at 0 and $d\alpha_0$ at t. The probability interpretation of this is just the relation (2.19). A more rigorous discussion along these lines has been given by Wigner (1954).

It should be remarked that in this ' proof ' we have made a tacit assumption which goes beyond the phase distribution law of classical statistics. It is one thing to show the mechanical possibility of reversed paths and quite another to assert that both a given path and its reversal occur with equal probability. If this were not so we should not be entitled to draw in all the symmetric pairs of figure 3 and the whole proof would break down. (A recent, fundamental discussion has been given by Watanabe (1955).) This assumption and its consequences (equations (2.13)–(2.19)) may be called the Principle of Microscopic Reversibility or the

Principle of Detailed Balancing. From the present point of view (in which we already assume the equilibrium distribution for the instantaneous values of the macroscopic variables α) no distinction can be made between them. However from a microscopic point of view a clear distinction can be drawn. Thomsen (1953) has considered the transitions between discrete quantum levels of an isolated system. Let $p_i(t)$ be the probability of observing a state i and λ_{ij} (independent of t) be the transition probability per unit time for the transition $i \to j$. Let the entropy of the system be defined by $S = -k\Sigma p_i ln p_i$. Thomsen considers four propositions, defined as follows :

(i) Microscopic reversibility (M) : $\lambda_{ij} = \lambda_{ji}$.

(ii) Detailed balancing (D) : $p_i\lambda_{ij} = p_j\lambda_{ji}$ in equilibrium.

(iii) Ergodic hypothesis (E) : $p_i = p_j = \text{const.}$ in equilibrium.

(iv) Second law (S) : $\dot{S} \geqslant 0$.

He is then able to derive the following interesting results : the Ergodic Hypothesis and the Second Law are equivalent ; either, when combined with the Principle of Detailed Balancing, is equivalent to the Principle of Microscopic Reversibility. Symbolically, (S)$\longleftrightarrow$(E) ; (S)+(D)$\longleftrightarrow$(M).

From this approach a paradoxical situation arises which will be mentioned in § 2.7.

2.6. *The Onsager Fluxes and Flow Vectors*

We now have to consider a rather delicate problem which, in the opinion of the writer, has not been given sufficient attention. From what has been said so far, one would expect that to apply the theory in any concrete case the first task would be to find a suitable set of Onsager variables to describe the departure of the entropy from its equilibrium value. That done, it only remains to write down the linear rate laws and reduce the number of coefficients by means of Onsager's reciprocity theorem (and any other symmetry principles which may be available). In practice this is rarely done except for discontinuous systems and chemical or relaxation systems. For the commonest and most important cases involving the transport of energy, mass, etc. in continuous systems (e.g. viscous flow, thermal conductivity, diffusion) another procedure is used. Flow vectors are introduced to describe the transport of energy, mass, etc. and by means of conservation arguments an expression is found for the rate of entropy production θ_s in terms of these vectors and the space gradients of T, μ_i^+, p. The result (which is always of the form $\theta_s = \Sigma J_i F_i$) is treated as being like equation (2.5) and used to select flux and force variables to form the equations of motion. Although the variables are treated like Onsager variables, resultant equations are actually stationary state equations and not relaxation equations.

The argument can be displayed by considering the (perhaps oversimplified) case of heat conduction in solids. The conservation principles are dealt with formally by saying that, for *any* extensive property A, say, $\partial a/\partial t = -\operatorname{div} J_a + \theta_a$ where a is amount of A per unit volume, J_a is the flux of A per unit area and time and θ_a is the amount of A created per unit volume. If A is conserved, then $\theta_a = 0$.

We now have to calculate the entropy production from the formula

$$\theta_s = \operatorname{div} J_s + \partial s/\partial t. \qquad \ldots\ldots (2.20)$$

Four assumptions are made :

(i) Local equilibrium (see § 2.2) is maintained. Hence

$$\frac{\partial s}{\partial t} = \frac{1}{T}\frac{\partial e}{\partial t}. \qquad \ldots\ldots(2.21)$$

(ii) Energy is conserved ; therefore

$$\frac{\partial e}{\partial t} = -\operatorname{div} J_e. \qquad \ldots\ldots(2.22)$$

(iii) There exists an entropy flux given by

$$J_s = J_e/T. \qquad \ldots\ldots(2.23)$$

Combining these four equations we have

$$\theta_s = J_e \operatorname{grad}(1/T). \qquad \ldots\ldots(2.24)$$

(iv) The final assumption is that by the argument given above the appropriate phenomenological laws are

$$J_e = L \operatorname{grad}(1/T). \qquad \ldots\ldots(2.25)$$

Even when the details get very complicated (as they can) this basic procedure—due essentially to Prigogine (1947)—is always the same : $\partial s/\partial t$ is expressed in terms of $\partial u/\partial t, \partial \rho/\partial t, \ldots$ which in turn are calculated from conservation laws in terms of flow vectors ; an appropriate expression for the entropy flux is assumed ; whence θ_s and the macroscopic laws.

The first assumption of local equilibrium can of course be accepted since (as discussed in § 2.2) it seems at present to be a necessary assumption for any macroscopic theory of irreversibility.

The second assumption eventually involves finding a local energy balance of an arbitrary system. For a simple, one-component system the work is fairly convincing although of course it involves the (mechanical) stress tensor through the equations of motion (de Groot 1951, Prigogine 1947, 1955). For a diffusing system of more than one component the formation of the mechanical equations already involves fresh assumptions about the nature of the stress tensor. It is usually assumed to be a single tensor—isotropic at that—causing barycentric motion. Other possibilities exist however, as has been shown by Prigogine and Mazur (1951) who assume separate stress tensors for each component and apply their formulae to the thermohydromechanics of liquid helium II. Electrical systems are even more complicated and, of existing expositions, that of Mazur and Prigogine (1953) seems to the writer to be the most convincing.

The third assumption reflects the need for ' isolating ' the system of interest (see § 2.1). In the case above we must imagine a reversible heat reservoir placed at each element of the surface. The rate at which its entropy increases is J_e/T and it seems entirely reasonable to attribute this to entropy flow across the boundary. For a diffusing system on the other hand, I have been unable to find any similar justification for the assumption always made, viz.

$$J_s = \frac{1}{T}(J_e - \tfrac{1}{2}\mathbf{v}^2\mathbf{v} - h\mathbf{v}) - \mu_i^+ J_{\mathrm{M}i}/T \qquad \ldots\ldots(2.26)$$

where J_e is the total energy flow and $\mathbf{v}$ the barycentric velocity. The expression in the first bracket is sometimes defined as the ' heat flow ' but sometimes another combination is used for this quantity which, as has been shown by Tolhoek and de Groot (1952), is purely a matter of definition. These authors give the impression of having proved (2.26) but this is an illusion.

The justification for the last assumption was indicated by Casimir (1945). As the discussion of this point is particularly technical it will suffice to sketch his approach. It was shown in § 2.3 that to obtain Onsager variables from thermodynamic variables it is necessary to reduce the number of sub-system variables by one. Let $e(\mathbf{r})$ represent the energy density above the equilibrium value in a thermal conducting solid. Then a suitable choice of Onsager variables is obtained by forming the Fourier transform

$$\alpha(\mathbf{k}) = (1/V)(2\pi)^{-3/2}\iiint e(\mathbf{r}) \exp(-i\mathbf{k}.\mathbf{r})\, d\mathbf{r}$$

taken through the solid. (Actually one should consider discrete cells and a corresponding Fourier sum.) The reduction of the thermodynamic variables to the Onsager variables is then achieved by taking $\alpha(0) = 0$, which guarantees the overall conservation of energy. The thermodynamic conjugate variable is proportional to $-\theta(\mathbf{r})\, C(\mathbf{r})$ where $\theta(\mathbf{r})$ is the departure from the average temperature and $C(\mathbf{r})$ the heat capacity per unit volume. The Onsager conjugate variable (force) is

$$F(\mathbf{k}) \propto \iiint \{\theta(\mathbf{r})/C(\mathbf{r})\} \exp(i\mathbf{k}.\mathbf{r})\, d\mathbf{r}$$

and the appropriate rate equation is

$$\dot{\alpha}(\mathbf{k}) = \iiint L(\mathbf{k}, \mathbf{k}')\, F(\mathbf{k})\, d\mathbf{k}'. \qquad \ldots\ldots(2.27)$$

Inverting this formula one finds

$$\partial e/\partial t (\equiv -\operatorname{div} \mathbf{J}_e) = \iiint l(\mathbf{r}, \mathbf{r}')\, \theta(\mathbf{r}')\, C(\mathbf{r}')\, d\mathbf{r}' \qquad \ldots\ldots(2.28)$$

where l is the Fourier inverse of the Onsager coefficients. The reciprocity theorem yields $l(\mathbf{r}, \mathbf{r}') = l(\mathbf{r}', \mathbf{r})$ and certain further limiting operations lead to the thermal conductivity equation. The symmetry of l implies a restriction on the space derivatives of the thermal conductivity tensor which, as shown by Casimir, means that an antisymmetric component of this tensor can lead to no observable results. Casimir actually reverses the above argument, starting with the thermal conductivity equation and working back to the Onsager coefficients. A similar attack has been applied by de Groot and Mazur (1954) to more complex cases.

We may conclude that although certain progress has been made in linking the extensive applications of Onsager theory on the one hand and fluctuation analysis on the other, a great deal yet remains to be done.

2.7. *Gyroscopic Forces, Odd and Even Variables*

In the presence of a magnetic field $\mathscr{H}$ the Hamiltonian is an even function of the canonical momentum of each particle, viz. $\mathbf{p} - e\mathbf{A}/c$, where e is its charge

and **A** is the vector potential due to the external field. It follows that solutions of the equations of motion are invariant under $t \to -t$, $p \to -p$, $\mathscr{H} \to -\mathscr{H}$. A similar result holds for a system rotating with angular velocity ω, which requires $\omega \to -\omega$ for reversal. The original and reversed paths of figure 3 cannot then be considered as illustrating possible paths in a *single* system but rather in one system and in another one, identical except that $\mathscr{H}$ (or ω) is reversed. This circumstance clearly leads to the formula of equation (2.6). Important applications of this fact appear in the macroscopic theory of thermo-magnetic effects (Domenicali 1954, Callen 1952, Mazur and Prigogine 1951, Meixner 1941 b) and in sedimentation equilibrium (Hooyman 1955). (The last author also gives a particularly clear discussion of the transformation properties of the Onsager theory, including the effect of linear restraints on the reciprocity theorem.)

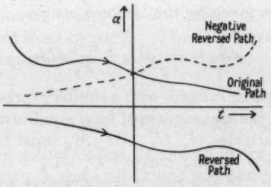

Figure 4. Two possible paths in the macroscopic space of the Onsager variables together with the negative of the reversed path (α an odd function of momenta).

The other modification of the reciprocity formulae appears when an Onsager coordinate is an odd function of the momenta. The effect is illustrated in figure 4 from which it will be clear that, if ϵ_i is defined as $+1$ for α_i even and -1 for α_i odd, then

$$L_{ik}(\mathscr{H}, \omega) = \epsilon_i \epsilon_k L_{ki}(-\mathscr{H}, -\omega). \qquad \ldots\ldots(2.29)$$

Equation (2.29) is a complete statement of the reciprocity theorem.

Finally, reference should be made to the paradox noted by Thomsen (1953). Working from microscopic transition probabilities, we recorded in § 2.5 that the reciprocity theorem was implied by $\lambda_{ij} = \lambda_{ji}$. It is a remarkable fact (see Dirac 1947, p. 174) that to the first order in time this equality holds independently of the form of the Hamiltonian. Therefore first order transition probability theory is not competent to account for the observed facts associated with gyroscopic coordinates (van Kampen 1954). Some attempts have been made to remove this difficulty by extending the time order of the transition probability calculation but the problem is not yet fully solved.

§ 3. An Application of Onsager's Theory to Discrete Systems

In this section we propose to consider an application of Onsager's theory to discrete systems—in particular to the system consisting of two uniform phases interchanging mass and energy. This problem has been widely discussed in the literature and reference may be made to the monographs of Denbigh (1951) and

de Groot (1951) and an article by Keenan (1955), where further references will be found. The obvious reason for its popularity is that it appears to provide the simplest case in which the reciprocity theorem leads to a non-trivial result. A more fundamental reason is that the theory connected with it seems to give a plausible reason for using the expression of equation (2.26) for the entropy flow in continuous systems. As we saw in § 2.6, this expression is fundamental in Prigogine's method of treating continuous systems with diffusion. For this reason the barrier transfer problem is still worth discussing.

3.1. *The Theory of Plug Transfer*

Consider two one-constituent phases, A and B, which can exchange energy and mass through a plug or membrane between them. They are to constitute the two sub-systems of an isolated system to which we apply Onsager's theory. Changes in entropy of phase A are given by the Gibbs equation

$$dS_{\mathrm{A}} = \frac{1}{T_{\mathrm{A}}}\, dU_{\mathrm{A}} - \frac{\mu^{+}_{\mathrm{A}}}{T_{\mathrm{A}}}\, dM_{\mathrm{A}} \qquad \ldots\ldots(3.1)$$

(since the volume of the phase is fixed) with a similar expression applying to phase B. These equations express the assumption of local equilibrium. In accordance with § 2.3, the two pairs of variables $U_{\mathrm{A}}, U_{\mathrm{B}}$; $M_{\mathrm{A}}, M_{\mathrm{B}}$ must be reduced in number by one each since (neglecting kinetic energy) $U_{\mathrm{A}} + U_{\mathrm{B}} = \text{const.}$, $M_{\mathrm{A}} + M_{\mathrm{B}} = \text{const.}$, by the conservation laws. In this case it is convenient to treat U_{B} and M_{B} as the a_i of § 2.3 and their departure from equilibrium as the Onsager coordinates :

$$\alpha_{\mathrm{E}} = U_{\mathrm{B}} - U_{\mathrm{B}}^{0}, \quad \alpha_{\mathrm{M}} = M_{\mathrm{B}} - M_{\mathrm{B}}^{0}. \qquad \ldots\ldots(3.2)$$

Using the Gibbs equations and the conservation laws, the departure of the entropy of the system from its equilibrium value is

$$\Delta S = \int_{U_{\mathrm{B}}^{0}}^{U_{\mathrm{B}}} \left(\frac{1}{T_{\mathrm{B}}} - \frac{1}{T_{\mathrm{A}}}\right) dU_{\mathrm{B}} - \int_{M_{\mathrm{B}}^{0}}^{M_{\mathrm{B}}} \left(\frac{\mu^{+}_{\mathrm{B}}}{T_{\mathrm{B}}} - \frac{\mu^{+}_{\mathrm{A}}}{T_{\mathrm{A}}}\right) dM_{\mathrm{B}} \qquad \ldots\ldots(3.3)$$

and this can be written to the second order in departures as the bilinear form

$$\Delta S = \frac{1}{2}\left\{\left(\frac{1}{T_{\mathrm{B}}} - \frac{1}{T_{\mathrm{A}}}\right)(U_{\mathrm{B}} - U_{\mathrm{B}}^{0}) + \left(\frac{\mu^{+}_{\mathrm{B}}}{T_{\mathrm{B}}} + \frac{\mu^{+}_{\mathrm{A}}}{T_{\mathrm{A}}}\right)(M_{\mathrm{B}} - M_{\mathrm{B}}^{0})\right\}. \qquad \ldots\ldots(3.4)$$

Comparing this with equations (2.1) and (2.2) we see that the Onsager forces conjugate to α_{E} and α_{M} are

$$F_{\mathrm{E}} = \left(\frac{1}{T_{\mathrm{B}}} - \frac{1}{T_{\mathrm{A}}}\right) \equiv \delta\left(\frac{1}{T}\right), \quad F_{\mathrm{M}} = -\frac{\mu_{\mathrm{B}}}{T_{\mathrm{B}}} + \frac{\mu_{\mathrm{A}}}{T_{\mathrm{A}}} \equiv \delta\left(-\frac{\mu^{+}}{T}\right) \qquad \ldots\ldots(3.5)$$

where the δ symbol refers to the differences in properties in proceeding from phase A to phase B.

The thermodynamic equations of motion can now be written down from equation (2.3) :

$$\begin{aligned} \frac{dU_{\mathrm{B}}}{dt} &= \dot{\alpha}_{\mathrm{E}} \equiv J_{\mathrm{E}} = L_{\mathrm{EE}}\,\delta\left(\frac{1}{T}\right) + L_{\mathrm{E1}}\,\delta\left(-\frac{\mu^{+}}{T}\right) \\ \frac{dM_{\mathrm{B}}}{dt} &= \dot{\alpha}_{\mathrm{M}} \equiv J_{\mathrm{M}} = L_{1\mathrm{E}}\,\delta\left(\frac{1}{T}\right) + E_{11}\,\delta\left(-\frac{\mu^{+}}{T}\right). \end{aligned} \qquad \ldots\ldots(3.6)$$

The Onsager reciprocity theorem (2.4) gives

$$L_{E1} = L_{1E}. \qquad \ldots\ldots(3.7)$$

This completes the formal theory, which says that the total flow of energy (A→B) and the mass flow (A→B) are linear functions of the differences in $1/T$ and $-\mu^+/T$ with a certain cross-connection between the coefficients.

Before discussing the physical significance of these results there is a characteristic complication which must be faced. The total flow of energy across a surface is only defined up to an arbitrary choice of the internal energy zero (per unit mass, say). Similarly, the chemical potential is defined up to arbitrary constants in both internal energy and entropy (per unit mass). Hence, of the forces and flows appearing in equation (3.6), J_E and $\delta(-\mu^+/T)$ are not uniquely defined. However a change in the zero of entropy does not affect $\delta(-\mu^+/T)$, so it is sufficient to consider a change in the zero of internal energy per unit mass. Let such a change increase the internal energy per unit mass by Δu^{+0}. The new flows and forces will be given by the following set of equations :

$$\begin{aligned} J_E^* &= J_E + \Delta u^{+0} J_M & F_E^* &= F_E \\ J_M^* &= J_M & F_M^* &= -\Delta u^{+0} F_E + F_M. \end{aligned} \qquad \ldots\ldots(3.8)$$

(The Onsager coordinates will of course be altered in the same way.) Inspection of the coefficients appearing in these equations and comparison with the remarks after equation (2.11) show that a change in zero of internal energy can be regarded as a linear transformation of forces and flows which leaves the entropy, the entropy production and the reciprocal theorem invariant, i.e. the matrices of (3.8) satisfy Meixner's condition. Physically this result is reasonable, because it simply means that the Onsager theory is independent of the choice of the zero of internal energy.

We now adopt a convention which is used almost universally : let the energy zero be shifted so that average enthalpy per unit mass of the two containers is zero ; the corresponding average internal energy per unit mass is then the average value of $-pv^+$. This means that in terms of the original quantities we take

$$\Delta u^{+0} = -\bar{h}^+ \equiv -\tfrac{1}{2}(h^+_A + h^+_B)$$

in equations (3.8). In accordance with the above remarks, the procedure can be interpreted as choosing a new flow $J_E^* = J_E - \bar{h}^+ J_M$ and a corresponding new force

$$F_M^* = \delta(-\mu^+/T) + \bar{h}^+ \delta(1/T) = -(\delta\mu^+)_T/\bar{T}.$$

(This point of view is emphasized particularly by de Groot.)

For our one-component system $-(\delta\mu^+)_T/T = -\bar{v}^+ \delta p/T$ so we may write the equations of motion (3.6) as

$$\begin{aligned} J_E^* &= -L_{EE}^*(\delta T/\bar{T}^2) - L_{E1}^*(\bar{v}^+ \delta p/\bar{T}) \\ J_M^* &= -L_{1E}^*(\delta T/\bar{T}^2) - L_{11}^*(\bar{v}^+ \delta p/\bar{T}), \end{aligned} \qquad \ldots\ldots(3.9)$$

with $L_{E1}^* = L_{1E}^*$.

The advantages of this new choice of zeros (or transformed Onsager coordinates) are : (*a*) All quantities appearing in the equations (including the Onsager coefficients) are uniquely defined *without* separately specifying the choice of internal energy zero.

(*b*) If a fluid in equilibrium is simply transported across a plane, the flow of energy is h^+J_M. The use of J_E^* seems to mean that we have discarded this rather uninteresting contribution to the energy flow; J_E^* represents a genuine 'conduction' of energy rather than mere convection. This notion will be made more precise presently.

3.2. *The Measurement of Energy Flow*

Although we have used the idea of energy flow quite freely we have not yet provided a definition of this concept. It is possible to do this with reasonable rigour because energy is a conserved property. Suppose that one side of a surface of interest is provided with reservoirs, pistons, etc. to receive the matter and heat transported across the surface. One then imagines that an account is made of the total energy of the reservoirs, engines, etc. before and after a unit interval of time. The difference is defined to be the flow of energy across the surface per unit time. The answer will be unique (apart from arbitrary zeros of internal energy) because of the conservation of energy. This procedure will work as long as the energy can be localized well enough to know to which side of the surface it must be assigned. This excludes long-range forces, unless they can be treated as 'internal' and associated with conservative fields. (For this reason, there are subtleties in the treatment of electrical systems by 'electrostatic' methods.)

The Onsager theory of the previous paragraphs can now be given a broader physical interpretation by allowing the energy and mass to be supplied to the barrier in any way, i.e. by destroying the isolation of the whole system. We suppose that pistons and reservoirs are attached to A and B; we call the heat flow *into* A per unit time q_A and the heat flow *out of* B, q_B. The energy flow across the barrier $(A \rightarrow B)$ can be reckoned from either side and we thus find

$$J_E - h_B{}^+ J_M = T_B M_B ds_B{}^+/dt + q_B$$
$$J_E - h_A{}^+ J_M = -T_A M_A ds_A{}^+/dt + q_A.$$

The terms involving ds^+/dt can be expressed in terms of the thermodynamic properties of the material together with the rate of change of p and T. Hence J_E (and J_E^*) can in principle be found by thermal measurements.

For a *stationary* state $ds_A{}^+/dt = ds_B{}^+/dt = 0$ and we have the specially simple relations

$$J_E^* \equiv J_E - \bar{h}^+ J_M = \tfrac{1}{2}(q_A + q_B) \qquad \ldots\ldots(3.10)$$
$$\delta h^+ J_M = q_A - q_B. \qquad \ldots\ldots(3.11)$$

The first of these equations says that *in a stationary state* J_E^* is just the average heat flow through the system. The second equation merely expresses the conservation of energy.

3.3. *Thermo-Osmosis*

Now that we have seen how J_E^* can be measured we shall return to discuss the physical meaning of the Onsager equations of motion (3.9). For this purpose it is convenient to rewrite the equations in the form

$$\left.\begin{aligned} J_E^* &= -k\,\delta T + Q^* J_M \\ J_M &= -K\,\delta p - (KQ^*/\bar{v}^+\bar{T})\,\delta T \end{aligned}\right\} \qquad \ldots\ldots(3.12)$$

where $Q^* \equiv L_{1E}^*/L_{11}^* = L_{E1}^*/L_{11}^*$, the ' heat of transport ',

$k \equiv (L_{EE}^* - L_{11}^* Q^{*2})/\overline{T}^2$, a ' thermal conductivity ',

and $K \equiv L_{11}^* \overline{v}/\overline{T}$, a ' permeability coefficient ',

are three convenient independent transport coefficients to describe the properties of the barrier. It should be noted particularly that the heat of transport is defined as the *isothermal* ratio of J_E^*/J_M ; the thermal conductivity is the heat flow per unit temperature difference at *zero mass flow* ; the permeability is the *isothermal* mass transport per unit pressure head.

The most important deduction to be made from these equations is that in a state of zero mass flow (i.e. the condition required for the measurement of thermal conductivity) there is a thermo-osmotic pressure head induced by an applied temperature difference and given by

$$\frac{\delta p}{\delta T} = -\frac{Q^*}{\overline{T}\overline{v}^+}. \qquad \ldots\ldots(3.13)$$

This is the thermo-mechanical effect, which appears in all systems having a non-vanishing heat of transfer. Equation (3.13) was discovered by Eastman (1926) who used pseudo-thermodynamic reasoning. It was derived from the Onsager theory by Meixner (1941 a).

There is a close analogy between thermo-osmosis and thermo-electricity noted by Kennard as long ago as 1932. Consider a ' circuit ' consisting of a set of membranes of type 1 connected in series with another set of type 2 and filled with fluid. Let the two chambers where the ' joins ' occur be maintained at temperatures T_0 and T and then insert an impermeable barrier into one of the chambers of the circuit. A pressure difference δp will appear between the two parts of this chamber. By integrating equation (3.13) round the circuit and then differentiating with respect to T one finds

$$\frac{d\delta p}{dT} = \frac{Q_1^* - Q_2^*}{\overline{v}^+ \overline{T}}. \qquad \ldots\ldots(3.14)$$

Also, the heat that must be supplied per unit mass flow when fluid is forced isothermally through the junction of 1 and 2 is clearly $Q_1^* - Q_2^*$. Thus Q^* is analogous to the thermo-electric power, and dQ^*/dT is analogous to the Thomson coefficient. For detailed information about the Onsager theory of thermo-electricity see the review of Domenicali (1954).

We have noted earlier that the definition of J_E^* excludes the energy of bulk transfer from the total flow of energy. We may therefore expect that with bulk transfer, Q^* will be zero. This has not been proved rigorously and the point deserves further attention. Systems known to exhibit thermo-mechanical effects include :

(*a*) Gas chambers separated by porous barriers whose passages are small in width compared with the mean free path of the gas molecules.

(*b*) Systems in which the transfer process consists of molecules dissolving in the barrier on one side (thereby disgorging heat), diffusing through it and escaping from solution on the other side (with the help of more heat).

(*c*) The transfer of liquid He II through very narrow capillaries ($\lesssim 30\mu$ in diameter).

The first case is well known and a detailed molecular theory can be given (for apertures of simple geometry) which confirms the Onsager theory. The cause of the effect is that the average energy per molecule of molecules crossing a given plane is less than the average enthalpy per molecule in the bulk gas.

An interesting study of the second case has been made by Denbigh and Raumann (1951). They measured the thermo-osmotic pressure head developed across a rubber membrane by gaseous CO_2, N_2 and H_2. In the absence of calorimetric measurements it is not possible to verify equation (3.13). However they were able to conclude that the heat of solution alone is not sufficient to account for the values of Q^* deduced from (3.13). They were led to postulate the existence of a heat of transport associated with the diffusion process inside the rubber. In order of magnitude, it is comparable with the heat of solution and it may be roughly accounted for by simple kinetic arguments of a type invented by Wirtz to deal with thermal diffusion in liquids.

In the case of liquid He II, equation (3.13) is very similar to London's formula for the fountain effect in which Q^* is replaced by $-Ts^+$. Indeed, attempts have been made to reduce (3.13) to London's formula by making special assumptions about the ' solution properties ' of the two-fluid model (de Groot, Jansen and Mazur 1950). Of greater interest is the fact that, in virtue of the calorimetric measurements of Meyer and Mellink (1947) and Kapitza (1941), the capillary flow of liquid He II is the only case for which equation (3.13) has been verified.

3.4. *The Joule–Kelvin Effect*

The Onsager theory of plug transfer has an interesting bearing on the classical theory of the Joule–Kelvin effect. Suppose that we have a stationary state of flow with particular values of δp and δT. Then reference to equations (3.10) and (3.11) shows that in such a state the heat flows into cylinder A and out of cylinder B are given by

$$q_A = J_E^* + \tfrac{1}{2}\delta h^+ J_M, \quad q_B = J_E^* - \tfrac{1}{2}\delta h^+ J_M, \qquad \ldots\ldots (3.15)$$

J_E^* and J_M being determined by the thermodynamic equations of motion. On the right-hand side of these equations the first term, J_E^*, is of the first order in $\delta p, \delta T$ and the second term (involving the Joule–Kelvin coefficient) is of the second order. The theory of the infinitesimal Joule–Kelvin effect assumes that we have (i) a stationary state and (ii) adiabatically insulated cylinders ($q_A = q_B = 0$). We then require the value of δT appropriate to a given value of δp. There are two cases to consider :

(*a*) If one at least of the parameters k, Q^* is non-vanishing, then it is clear that (ii) cannot be satisfied to the second order and so no stationary state can exist. However with sufficiently small values of δp and δT we may neglect the second order terms so that δT is determined by $J_E^* = 0$, or in analogy with equation (3.13),

$$\delta T/\delta p = -M^* v^+ T. \qquad \ldots\ldots (3.16)$$

$M^* \equiv L_{1E}^*/L_{EE}^*$ describes the transport of mass under *isobaric* conditions, when $J_M = M^* J_E^*$. It can of course be expressed in terms of k, Q^* and K. The neglected terms give rise to a secular variation in ambient conditions (Davies 1952).

(*b*) If k and Q^* both vanish, or (more realistically) we are in a region where the second term of (3.15) dominates the expression, then δT is determined by the Joule–Kelvin condition, $\delta h^+ = 0$. The first term now gives rise to a secular variation which of course will vanish in the limiting case of $k = Q^* = 0$.

To sum up: The orthodox derivation of the Joule–Kelvin formula *assumes* the existence of a stationary state with adiabatically insulated cylinders. This is possible only if the thermal conductivity and heat of transport of the barrier are rigorously zero. Failing that, there are two regions of approximately stationary states: (*a*) for sufficiently small δp, one has a mechano-thermal effect described by equation (3.16); (*b*) for sufficiently large δp, the Joule–Kelvin formula again gives the values of δT.

3.5. *Multi-component Systems*

With more than one constituent present, the work can be carried through in close analogy with the one-constituent case. Instead of equation (3.4) we have for the entropy and the entropy production in an isolated n-constituent system

$$\left.\begin{aligned} \Delta S &= \frac{1}{2}\left\{\delta\left(\frac{1}{T}\right)\Delta U_{\mathrm{B}} + \sum_{i=1}^{n}\delta(-\mu_i^+/T)\,\Delta M_{i\mathrm{B}}\right\} \\ \Delta\dot{S} &= \delta\left(\frac{1}{T}\right)J_{\mathrm{E}} + \sum_{i=1}^{n}\delta(-\mu_i^+/T)\,J_{\mathrm{M}i}. \end{aligned}\right\} \quad \ldots\ldots(3.17)$$

The removal of the arbitrary constants in the total energy flow proceeds as in § 3.1 by introducing

$$\left.\begin{aligned} J_{\mathrm{E}}^* &= J_{\mathrm{E}} - \sum_{i=1}^{n}\bar{h}_i^+ J_{\mathrm{M}i} \\ F_{\mathrm{M}i}^* &= -(\delta\mu_i^+)_T/\overline{T}, \end{aligned}\right\} \quad \ldots\ldots(3.18)$$

and the final form of the equations of motion can be written like equation (3.12):

$$\left.\begin{aligned} J_{\mathrm{E}}^* &= k\delta\left(\frac{1}{T}\right) + \sum_i Q_i^* J_i \\ J_{\mathrm{M}i} &= \sum_j L_{ij}^*\left[-\frac{(\delta\mu_j)_T}{\overline{T}} + Q_j^*\,\delta\left(\frac{1}{T}\right)\right] \end{aligned}\right\} \quad \ldots\ldots(3.19)$$

where L_{ij}^* $(= L_{ji}^*)$ are generalized coefficients of permeability,

$Q_i^* = \sum_j L_{ij}^{-1} L_{j\mathrm{E}}^*$ are '*heats of transport*',

$k = L_{\mathrm{EE}}^* - \sum_i \sum_j Q_i^* L_{ij}^* Q_j^*$ is a '*thermal conductivity*'.

We do not wish to discuss further details except to observe that a stationary state in which all the mass flows $J_{\mathrm{M}i}$ vanish requires in general the satisfaction of n equations

$$-(\delta\mu_j^+)_T/\overline{T} + Q_j^*\,\delta(1/T) = 0. \quad \ldots\ldots(3.20)$$

This is the generalization of (3.13) and means that the assignment of a non-zero value in any *one* of the increments in pressure, temperature and the $n-1$ independent concentrations also fixes the remaining n of those quantities. The formula thus

leads to relations between various thermal-mechanical-diffusion effects. Ordinary osmosis appears as a special case when sufficient of L_{ij}* vanishes to permit $\delta(1/T)$ and one or more of the $(\delta\mu_i{}^+)_T/T$ to vanish simultaneously.

3.6. *The Flow of Entropy*

The special interest to us of the previous section lies in the fact that the formula (3.17) for the rate of entropy production provides some insight into why the entropy flow in diffusing systems is assigned the value of equation (2.26). In our case, it is clear that since we have neglected kinetic energy, (2.26) must be specialized to read

$$J_s = J_E/T - \sum_i (\mu_i{}^+/T)J_{Mi}. \qquad \ldots\ldots(3.21)$$

The use of this does indeed give $\Delta\dot{S}$ the value of (3.17) above and from this point on Prigogine's method can be applied. However it still remains true that alternative choices could be made in our problem. For the one-constituent case

$$J_s' = \frac{1}{T}(J_E - h^+ J_M) - p\left(\frac{vJ_M}{T}\right) \qquad \ldots\ldots(3.22)$$

is one such choice, as can be seen from the change of variables discussed in § 3.1. The orthodox form (3.21) is certainly more elegant and once the connection $J_s = J_Q/T$ is required at a fixed boundary, the alternative form (3.22) must be discarded in the one-constituent case. In the case of a diffusing system, there seems to be no way of identifying J_E* by heat flows (cf. Tolhoek and de Groot 1952) and so the choice remains open.

Having admitted (3.21) it is still necessary to allow for the fact that kinetic energy contributes to the flow of energy but not the flow of entropy. Equation (2.26) says that it is the barycentric kinetic energy which must be thus excluded. This in turn seems to be connected with the mechanical assumption made by Prigogine (1947, p. 89) which says that it is barycentric motion which obeys the laws of mechanics.

Enough has been said to make it clear that this reviewer at least is unable to justify equation (2.26). It should however be possible—perhaps by an extension of Casimir's methods (§ 2.6)—to formulate the theory without using the entropy production in order to choose the Onsager forces and flows. This is highly desirable —especially in view of the fact that a wrong choice of force and flux (e.g. choosing J_1 as a 'force' and F_1 as a 'flux' in the formula (2.5)) gives incorrect reciprocity rules.

§ 4. An Application of Onsager's Theory to Continuous Systems

4.1. *The Theory of Viscous Flow in an External Field*

As an example of the way in which Prigogine's method is used to obtain macroscopic equations of motion in a continuous medium, we shall obtain complete formulae for the viscous laws appropriate to an isotropic fluid in a rotating system or a uniform field. Diffusion is excluded so that the difficulties mentioned in § 3.6 do not arise. This work is due to Hooyman (1955).

In accordance with the explanation given in § 2.6 we proceed to find the rate of production of entropy per unit volume θ_s in the following steps: (*a*) By the assumption of local equilibrium $\partial s/\partial t$ is expressed as

$$\frac{1}{T}\frac{\partial u}{\partial t}-\frac{g}{T}\frac{\partial \rho}{\partial t}. \qquad \ldots\ldots(4.1)$$

(*b*) $\partial u/\partial t$ is re-expressed in the form $\partial e/\partial t-\partial k/\partial t$ where e is the total energy density and k the kinetic energy density. (*c*) With the help of the mechanical equations of motion and the conservation of energy $\partial \rho/\partial t$, $\partial e/\partial t$ and $\partial k/\partial t$ are written in terms of flows. (*d*) J_s is expressed in terms of other flow vectors. The crucial steps are (*c*) and (*d*). To deal with (*c*) we start with the conservation of momentum and mass

$$\frac{\partial \rho \mathbf{v}}{\partial t}=-\frac{\partial}{\partial \mathbf{x}}.(\rho \mathbf{v}\mathbf{v})-\frac{\partial}{\partial \mathbf{x}}.\mathbf{P} \qquad \ldots\ldots(4.2)$$

$$\frac{\partial \rho}{\partial t}=-\frac{\partial}{\partial \mathbf{x}}.\rho \mathbf{v}. \qquad \ldots\ldots(4.3)$$

Combining these two equations we find

$$\frac{\partial k}{\partial t}=-\frac{\partial}{\partial \mathbf{x}}.(\mathbf{J}_k)-\mathbf{v}\frac{\partial}{\partial \mathbf{x}}:\mathbf{P} \qquad \ldots\ldots(4.4)$$

where $k=\frac{1}{2}\rho \mathbf{v}^2$ is the density of kinetic energy and $\mathbf{J}=k\mathbf{v}$ is the flow of kinetic energy. Since the total energy is conserved,

$$\frac{\partial e}{\partial t}=-\operatorname{div}\mathbf{J}_k. \qquad \ldots\ldots(4.5)$$

We *define* a heat flow J_q by the relation

$$\mathbf{J}_e=\mathbf{J}_k+\mathbf{P}.\mathbf{v}+u\mathbf{v}+\mathbf{J}_q \qquad \ldots\ldots(4.6)$$

and for (*d*) we *assume* that

$$\mathbf{J}_s=s\mathbf{v}+\mathbf{J}_q/T. \qquad \ldots\ldots(4.7)$$

Combining equations (4.1)–(4.7) we finally obtain

$$\theta_s=J_q\nabla\left(\frac{1}{T}\right)-\frac{1}{T}(\mathbf{P}-p\mathbf{I}):\frac{\partial \mathbf{v}}{\partial \mathbf{x}} \qquad \ldots\ldots(4.8)$$

where p is the thermodynamic pressure determined by u and ρ. It has no *a priori* connection with the stress-, or rather, pressure-tensor $\mathbf{P}$, which is defined by the equations of motion (4.2).

Neglecting the possibility of coupling between heat flow and velocity, we may consider the second term alone—which is associated with viscous dissipation. It is convenient to introduce the viscosity tensor $\pi=\mathbf{P}-p\mathbf{I}$ and the rate of strain tensor $\dot{e}_{ij}=\frac{1}{2}(\partial \mathbf{v}_i/\partial \mathbf{x}_j+\partial \mathbf{v}_j/\partial \mathbf{x}_i)$. In the same way as for elasticity theory we may specify these symmetric tensors by their six independent components $(\pi_1 \ldots \pi_6)$, $(\dot{e}_1 \ldots \dot{e}_6)$ where $\pi_1\equiv\pi_{11}, \pi_4\equiv\pi_{23}, \dot{e}_1\equiv\dot{e}_{11}, \dot{e}_4\equiv\dot{e}_{23}$, etc. We are then led to assume that the π_k are linear functions of the $\dot{e}_k$, the connecting coefficients being L_{kl} (say).

The whole question now is: to what extent can the number of independent components of L_{kl} be reduced by the symmetry of the problem and by Onsager's

reciprocity theorem? Let the coordinates be relabelled x, y and z (in order) and let the direction of the field or axis of rotation be along OZ. Considering first the geometrical symmetries, (i) invariance under rotation about OZ implies that L_{ik} is of the form:

	$\dot{e}_1$	$\dot{e}_2$	$\dot{e}_3$	$2\dot{e}_4$	$2\dot{e}_5$	$2\dot{e}_6$
$-\pi_1$	A	B	C	.	.	F
$-\pi_2$	B	A	C	.	.	$-F$
$-\pi_3$	D	D	E	.	.	.
$-\pi_4$	.	.	.	G	H	.
$-\pi_5$	.	.	.	$-H$	G	.
$-\pi_6$	$-F$	F	.	.	.	$\frac{1}{2}(A-B)$

(ii) for the rotating system of angular velocity ω, since L_{ik} must be invariant under $z \to -z$, $x \to -x$, $y \to y$, $\omega \to -\omega$, we have

$$\begin{aligned} &A(-\omega) = A(\omega), \quad B(-\omega) = B(\omega), \quad C(-\omega) = C(\omega), \\ &D(-\omega) = D(\omega), \quad E(-\omega) = E(\omega), \quad G(-\omega) = G(\omega), \quad \ldots\ldots (4.9) \\ &F(-\omega) = -F(\omega), \quad H(-\omega) = -H(\omega). \end{aligned}$$

The same relations hold in the magnetic and electric field cases, with $\mathscr{H}$ or E replacing ω.

(iii) Finally the reciprocity theorem must be applied. The cases of (*a*) rotation or magnetic field and (*b*) electric field must now be distinguished:

(*a*) By equation (2.6) we have $L_{ik}(\omega) = L_{ki}(-\omega)$ (and the same for $\mathscr{H}$), so that

$$\begin{aligned} &A(-\omega) = A(\omega), \quad B(-\omega) = B(\omega), \quad D(-\omega) = C(\omega), \quad E(-\omega) = E(\omega), \\ &G(-\omega) = G(\omega), \quad F(-\omega) = -F(\omega), \quad H(-\omega) = -H(\omega). \quad \ldots\ldots (4.10) \end{aligned}$$

The only fresh information not already included in equations (4.9) is that $C = D$. We are then left with seven independent coefficients, five even and two odd.

(*b*) For the case of the electric field, the Onsager relations are $L_{ik} = L_{ki}$. Hence we find $C = D$ and $F = H = 0$. There are now only five independent viscosity coefficients, all even functions of E.

It is pointed out by Hooyman that the above scheme for a magnetic field is in slight disagreement with the results of a kinetic treatment given by Chapman and Cowling (1952).

In the absence of fields or rotation one easily obtains, from geometrical symmetry only, $B = C = D$, $E = A$, $G = \frac{1}{2}(A-B)$ and $F = H = 0$. The scheme then reduces to the ordinary Stokes' formula for the viscous stress in a moving fluid. The Onsager reciprocity theorem is not required.

PART II. INCOMPLETE SYSTEMS UNDER UNIFORM CONDITIONS: RELAXATION

§5. The Thermodynamic Theory of Relaxation

5.1. *Static Properties*

In the systems considered so far the thermodynamic state even away from equilibrium has been specified by variables which are—in principle—measurable

by macroscopic methods. In contrast we now turn to the second of the two broad possibilities mentioned at the beginning of § 2.1.

In many cases transformations on a microscopic scale take place within a material which can be measured (if at all) only by x-ray or other structural investigations. In considering such systems it is convenient to think of chemically reacting systems as prototypes. Indeed such systems form a kind of half-way house between systems having external parameters only and those having internal parameters as well, for it could evidently be argued that the measurement of concentrations is a microscopic operation. Consider for simplicity the closed chemical reaction between constituents X_i and specified by

$$\nu_1 X_1 + \nu_2 X_2 - \nu_3 X_3 - \nu_4 X_4 = 0 \qquad \ldots\ldots(5.1)$$

where the ν_i are stoichiometric coefficients and the reaction proceeds from $X_3, X_4 \rightarrow X_1, X_2$. If N_i are the number of moles of X_i present in the system and μ_i the chemical potentials then a change in internal energy of the system is given by

$$dU = TdS - pdV + \sum_i \mu_i dN_i. \qquad \ldots\ldots(5.2)$$

If one is given the initial contents of the system it is clearly possible to introduce a ' degree of reaction ' z such that the change in mole numbers is $dN_i = \nu_i dz$. Then we may write

$$dU = TdS - pdV - Adz \qquad \ldots\ldots(5.3)$$

where $A = -\sum_i \mu_i \nu_i$ is the ' chemical affinity ' of the system and in chemical equilibrium, $A = 0$. This type of approach to chemical reactions is due mainly to de Donder and the Belgian school of thermodynamicists (see Prigogine and Defay (1954) for a systematic treatment). If dQ is the heat flow from the surroundings then the First Law gives $dU = dQ - pdV$. The entropy increase in the surroundings is $dS_e = -dQ/T$. Hence the rate of entropy production due to a chemical reaction is

$$\theta_s = \frac{dS}{dT} + \frac{dS_e}{dT} = \frac{A}{T}\frac{dz}{dt} \geqslant 0. \qquad \ldots\ldots(5.4)$$

As long as the system remains closed z and A can be treated as conjugate thermodynamic variables on the same footing as the other variables. This simplifies the description of the reaction. For example, $\lambda_{Hz} = (\partial H/\partial z)_{pT}$ is the heat of reaction, $\lambda_{Uz} = (\partial U/\partial z)_{VT}$ the energy of the reaction, $\lambda_{Vz} = (\partial V/\partial z)_{pT}$ the volume change of reaction, etc. (Only two of these reaction coefficients are independent and relations between them can be found by the usual methods.) In the case of the ' thermodynamic coefficients ' (such as C_p, α, κ) one must distinguish between ' frozen ' coefficients (such as $(\partial V/\partial T)_{pz}$) in which the reaction is not allowed to proceed and ' equilibrium ' coefficients (such as $(\partial V/\partial T)_{pA}$) which are evaluated at constant affinity. At or near equilibrium the latter are the coefficients which would be measured with an equilibrium system when the presence of the reaction can be ignored. Finally, we have an ' ordering coefficient ' $\beta = \partial A/\partial z$. If the chemical potentials of the constituents are known β can be written explicitly in terms of their derivatives with respect to the concentration (Prigogine and Defay 1954). For a system in stable equilibrium β is necessarily negative. This follows because the virtual infinitesimal change in an appropriate free energy in passing from the equilibrium state is given by $\delta F = -\beta \delta z^2 \geqslant 0$. A complete thermodynamic

description of the reacting system (including the reaction itself) thus requires six coefficients : three thermodynamic coefficients (frozen or equilibrium), two reaction coefficients and an ordering coefficient. If however one excludes chemical measurements on the reaction and wishes to consider physical measurements only, then a knowledge of five coefficients is enough. To see this, it is convenient to distinguish equilibrium coefficients by means of a bar and write

$$\overline{C_p} = T(\partial S/\partial T)_{p,A}, \quad C_p = T(\partial S/\partial T)_{p,z}, \text{ etc.}$$

Use p and T as independent variables and define $\Delta C_p = \overline{C_p} - C_p$, etc. Now

$$\left(\frac{\partial S}{\partial T}\right)_{pA} = \left(\frac{\partial S}{\partial T}\right)_{pz} - \left(\frac{\partial S}{\partial z}\right)_{pT}\left(\frac{\partial z}{\partial A}\right)_{pT}\left(\frac{\partial A}{\partial T}\right)_{pz}$$

$$= \left(\frac{\partial S}{\partial T}\right)_{pz} - \left(\frac{\partial S}{\partial z}\right)_{pT}\left(\frac{\partial z}{\partial A}\right)_{pT}\left(\frac{\partial S}{\partial z}\right)_{pT}$$

and so
$$\Delta C_p = -T\lambda_{Sz}\beta^{-1}\lambda_{Sz}.$$

Similarly
$$\Delta\alpha = -\frac{1}{V}\lambda_{Vz}\beta^{-1}\lambda_{Sz}$$

$$\Delta\kappa = -\frac{1}{V}\lambda_{Vz}\beta^{-1}\lambda_{Vz}. \qquad \text{.....(5.5)}$$

From these equations we may conclude :
(i) The ' incremental ' thermodynamic quantities ΔC_p, etc., are closely related to the heat and volume change of the reaction ; (ii) since β is negative, ΔC_p and $\Delta\kappa$ are necessarily positive although $\Delta\alpha$ is of indeterminate sign ; (iii) the three incremental quantities satisfy

$$\Delta\kappa\Delta C_p = TV\Delta\alpha^2. \qquad \text{.....(5.6)}$$

The last result justifies the statement made above, namely, that a thermodynamic description of the system *without* chemistry is provided by five thermodynamic coefficients such as $\alpha, \kappa, C_p, \Delta\kappa, \Delta\alpha$.

The above formalism may be extended to deal with an arbitrary finite number (n, say) of reactions described by degrees of reaction z^i and corresponding affinities A_i. The whole theory may then be considered to apply to any system with internal ordering processes—not only to systems with chemical reaction. This approach to the subject of relaxation is due to Frenkel (1946), Prigogine and Defay (1954) and Meixner (1953, 1954 c). For example, we may attempt to deal with the changes of structure occurring in liquids, with order–disorder transitions in alloys, with dielectric and paramagnetic ordering and so forth. Although it is true that some approximate theories of ordering introduce explicit parameters (the simplest example is the Bragg–Williams theory of order–disorder in alloys), we wish to take a purely phenomenological view and consider the z^i as *undefined* parameters. Let us take ν independent thermodynamic variables x^α and suppose that changes in the appropriate thermodynamic potential F are given by

$$-dF = X_\alpha dx^\alpha + A_i dz^i. \qquad \text{.....(5.7)}$$

(We shall use the summation convention for repeated suffixes unless it is suppressed by brackets.) The coefficients connected with the system are of the same three types as noted above :

(i) Frozen thermodynamic coefficients, $c_{\alpha\beta} = \partial X_\alpha/\partial x^\beta$

(ii) Reaction coefficients, $\lambda_{\alpha i} = \partial X_\alpha/\partial \dot{z}^i = \partial A_i/\partial x^\alpha$

(iii) Order coefficients, $\beta_{ij} = \partial A_i/\partial z^j$.

The Maxwell relations for the above Pfaffian imply that $c_{\alpha\beta}$ and β_{ij} are symmetric in their indices : $c_{\alpha\beta} = c_{\beta\alpha}$, etc.

It is important to notice that the choice of the z^i is not unique. (For chemical systems this means merely that the stoichiometric formulae can be combined linearly in an infinite number of ways.) We consider homogeneous linear transformations of the z^i. The A_i must transform in such a way as to leave the rate of production of entropy invariant, i.e. $\theta_s = A_i \dot{z}^i$ is invariant. Using now a matrix notation, we see that under the transformation $z \to z^+ = Tz$ we must have $A^+ = T'^{-1}A$, $\beta^+ = T'^{-1}\beta T^{-1}$, $\lambda^+ = \lambda T^{-1}$, etc. (The position of the latin indices indicates their tensorial nature.)

By an extension of the one-parameter argument it can be shown that β is a negative definite matrix. Since a transformation of z induces a congruent transformation of β, it follows that β can always be reduced to -1. Such a reduction is not unique but it is sometimes useful because it gives us a set of *independent* ordering parameters which we may call a normal set with respect to x.

By a Legendre transformation from z to A we find that the equilibrium thermodynamic coefficients $\bar{c}_{\alpha\beta} = (\partial X_\alpha/\partial x^\beta)_{zA}$ are given by

$$\bar{c} = c + \Delta c = c - \lambda\beta^{-1}\lambda'. \qquad \ldots\ldots(5.8)$$

$\Delta c_{(\alpha\alpha)}$ is positive.

If z is normal with respect to x, Δc can be written as the sum of n terms

$$\Delta^{(i)} c_{\alpha\beta} = \lambda_{\alpha(i)}\lambda_{(i)\beta} \quad (i = 1 \ldots n).$$

This matrix may be called the contribution of the nth ordering process to c. It is clearly determined by the vn reaction coefficients $\lambda_{\alpha i}$ and we have the identities

$$\Delta^{(i)} c_{(\alpha\alpha)} \Delta^{(i)} c_{(\beta\beta)} = \Delta^{(i)} c_{\alpha\beta}{}^2 \qquad \ldots\ldots(5.9)$$

so that $\Delta^{(i)} c_{(\alpha\alpha)}$ is positive.

It must be emphasized that because the choice of a normal z is not unique the splitting of Δc into n parts is also not unique, although equation (5.8) shows that Δc itself is. By applying the Schwarz inequality we find from the above relations that

$$\Delta c_{(\alpha\alpha)} \Delta c_{(\beta\beta)} \geqslant \Delta c_{\alpha\beta}{}^2 \qquad \ldots\ldots(5.10)$$

a result discovered by Meixner (1952 a).

The reason we say that a normal choice of z is ' with respect to a given x ' is that a Legendre transformation on one or more of the x^i alters the value of β and indeed of λ. For a complete change to independent variables X_α the process is exactly analogous to that described by equation (5.8). In fact the new matrix $\beta_{ij}{}^+ \equiv (\partial A_i/\partial z^j)_{sX}$ is given by

$$\beta^+ = \beta - \lambda' c^{-1} \lambda. \qquad \ldots\ldots(5.11)$$

It follows, in particular, that a set z normal with respect to x is no longer normal with X for the independent variables. β ceases to be diagonal. Of course a linear transformation of x does not affect β, although the other coefficients are altered in a way indicated tensorially by their suffixes. Such changes are not of much physical interest although they sometimes occur. An example is provided by the case when the x^α are components of geometrical tensors, such as electric and magnetic fields, stress and strain.

On account of the lack of uniqueness in the choice of ordering parameters, purely static studies of relaxing systems are of very limited value. Since we assume that direct measurements of the z^i are impossible, the best that can be hoped for is a set of measurements giving both the ' frozen ' coefficients $c_{\alpha\beta}$ and the ' equilibrium ' coefficients $\bar{c}_{\alpha\beta}$. Given such a set, it is possible to see how close to being satisfied is the equality sign of equation (5.10). A ' good ' fit implies that the system should be describable by means of a single ordering parameter. The results of such a test for a number of glass-forming systems will be given in § 6.1.

5.2. *Dynamic Properties*

We now apply the method of irreversible thermodynamics to the system with internal ordering parameters discussed in the previous paragraph. As in § 4.1 we adopt Prigogine's procedure. This consists of first using the expression for the rate of production of entropy in order to arrive at a suitable linear rate hypothesis and then applying the Onsager reciprocity theorem. By the generalization of equation (5.4), the rate of production of entropy is $\theta_s = A_i \dot{z}^i/T$ and so we assume that

$$\dot{z}^i = L^{ij} A_j \qquad \ldots\ldots(5.12)$$

where L is a linear operator—possibly depending on time—and where $L' = L$. The temperature is already included in L. To form the thermodynamic equations of motion it is convenient to introduce $\mathscr{L} = L^{-1}\, d/dt$, a positive definite symmetric operator, and write

$$\begin{aligned} \dot{X} &= c\dot{x} + \lambda\dot{z} \\ \dot{A} &= \lambda'\dot{x} + \beta\dot{z} \\ \dot{A} &= \mathscr{L}\dot{z}. \end{aligned} \qquad \ldots\ldots(5.13)$$

The first two sets of equations come from the static formula (5.7) which means physically that the thermodynamic state of the system is fixed by ν independent thermodynamic variables x^α and n ordering variables z^i. The third equation is the linear rate hypothesis.

Eliminating z and A from equations (5.13) we find that the thermodynamic variables themselves satisfy

$$\dot{X} = c^*\dot{x} \qquad \ldots\ldots(5.14)$$

where

$$c^* = c - \lambda\beta^{-1}(1 - \mathscr{L}\beta^{-1})^{-1}\lambda'.$$

$c_{\alpha\beta}{}^*$ can be regarded as a ' dynamic ' thermodynamic coefficient. It is usually specified by means of an impedance function connecting the Fourier transforms of X and x (e.g. complex elastic moduli and dielectric constants). By using the symmetry of $\mathscr{L}$ it can be shown that $c_{\alpha\beta}{}^* = c_{\beta\alpha}{}^*$.

It is convenient to define $\mathscr{T}$ and τ by means of the relations $\mathscr{T} = -\mathscr{L}\beta^{-1} = \tau d/dt$. Then with the help of equation (5.8) the dynamic coefficients can be expressed in terms of either the instantaneous or the delayed coefficients in the forms

$$c^* = c - \lambda\beta^{-1}(1+\mathscr{T})^{-1}\lambda' \equiv c + \Delta^* c \qquad \ldots\ldots(5.15)$$

or

$$c^* = \bar{c} + \lambda\beta^{-1}\frac{\mathscr{T}}{1+\mathscr{T}}\lambda' \equiv \bar{c} - \delta^* c.$$

Here $\Delta^* c$ represents the dynamic addition to the ' instantaneous ', ' frozen ' or ' infinite-frequency ' coefficients which is permitted by a relatively slow process; similarly $\delta^* c = \Delta c - \Delta^* c$ is the dynamic expression for the amount which must be taken away from the ' equilibrium ' or ' zero-frequency ' coefficient $\bar{c}$ due to the partial freezing of the material associated with a relatively fast process.

We have already seen that, by means of a linear transformation $z^+ = Tz$, β can be reduced to -1 and that this can be done in an infinite number of ways. The corresponding transformation induced in L is $L^+ = TLT'$ so that L^+ is also symmetric. It follows that after this reduction has been found, a further orthogonal transformation can be made which leaves β^+ diagonal and equal to -1 but which reduces L to diagonal form. $\mathscr{T}$ is therefore diagonal and can be written as diag $t^{(i)}$.

The $t^{(i)}$ are in fact just the eigenvalues of $\mathscr{T}$, i.e. the roots of $|\mathscr{T} - t1| = 0$. It is important to notice that, in contrast to the static diagonalization, this reduction of $\beta, L, \mathscr{T}, \tau$, etc. and the corresponding choice of z is uniquely determined by the choice of x. The z^i can be called the *proper* ordering variables with respect to x^α and the corresponding $\lambda_{\alpha i}$ the *proper* reaction coefficients. It is sometimes convenient to denote the proper parameters with respect to x by a superscript in the style ${}^{(x)}\lambda, {}^{(x)}\tau, {}^{(x)}\mathscr{T}$, etc.

It follows from these considerations that the contributions to $\Delta^* c$ from the various proper relaxation processes are uniquely determined. The dynamic coefficients can then be expressed in the forms

$$c^*{}_{\alpha\beta} = c_{\alpha\beta} + \sum_i \frac{{}^{(x)}\lambda_{\alpha(i)}\,{}^{(x)}\lambda_{(i)\beta}}{1+{}^{(x)}t^{(i)}} = c_{\alpha\beta} + \sum_i \frac{\Delta^{(i)}c_{\alpha\beta}}{1+{}^{(x)}t^{(i)}} \qquad \ldots\ldots(5.16)$$

or

$$c^*{}_{\alpha\beta} = \bar{c}_{\alpha\beta} - \sum_i \frac{{}^{(x)}\lambda_{\alpha(i)}\,{}^{(x)}\lambda_{(i)\beta}}{1+{}^{(x)}t^{(i)}} = \bar{c}_{\alpha\beta} - \sum_i \frac{\Delta^{(i)}c_{\alpha\beta}\,{}^{(x)}t^{(i)}}{1+{}^{(x)}t^{(i)}}.$$

The relations of equation (5.9) still subsist between the static contributions to the thermodynamic coefficients from the ith proper ordering variable. Therefore a complete description of the system seems to be provided by a knowledge of $\bar{c}_{\alpha\beta}$, ${}^{(x)}t^{(i)}$ and $\Delta^{(i)}c_{(\alpha\alpha)}$. There remains an ambiguity in sign since

$$\Delta^{(i)}c_{\alpha\beta} = \pm\sqrt{(\Delta^{(i)}c_{(\alpha\alpha)}\,\Delta^{(i)}c_{(\beta\beta)})}$$

and it is not clear whether this can be removed without appealing to experimental results.

In many cases an impracticably large number of ordering parameters is required in order to describe the system with reasonable accuracy. This may be because there is, in effect, a continuous distribution of ordering variables and relaxation times. This is likely to occur, for example, with structural changes in amorphous materials. To make the transition from equation (5.16) it is convenient to suppose

first that the relaxation times are numbered in increasing order of magnitude. Suppose that, of the relaxation times, a fraction $f(\tau)\,d\tau$ lie in the range $(\tau, \tau+d\tau)$. The contributions to Δc from the proper ordering processes having relaxation times in this range will be the sum of values $\Delta^{(i)}c$ taken over a certain range of i. There is, however, no necessity for these values to be identical. One could obviously go on to discuss the distribution of the $\Delta^{(i)}c$ within the range $d\tau$, but there is little point in doing so because there is no method of separating out these contributions. They all relax together. Indeed, not even $f(\tau)$ can be separated. All that can be said is that there is an average contribution from the range $(\tau, \tau+d\tau)$ of $\overline{\Delta c}(\tau)\,d\tau$ such that the impedance function representation of c is

$$c^*(\omega) = \bar{c} - \int_0^\infty \frac{\overline{\Delta c}(\tau)\, i\omega\tau\, d\tau}{1+i\omega\tau}. \qquad \ldots\ldots(5.17)$$

The problem of working back from an experimental knowledge of $c^*(\omega)$ to the value of $\overline{\Delta c}(\tau)$ has been advanced recently by (among others) Gross (1953) and Schwarzl (1951). Further information may be found in books by Alfrey (1948), Gross (1953) and Muller (Ed.) (1953). As long as this process is regarded simply as providing an alternative specification of $c^*(\omega)$ then no objection can be raised. Before any further conclusions can be drawn there are a number of difficulties to be faced:

(i) Contrary to a widespread belief, $\overline{\Delta c}(\tau)$ is not a distribution of relaxation times. As indicated above, it is the product of a certain limiting average of the $\Delta^{(i)}c$ occurring in $d\tau$ and the distribution of relaxation times $f(\tau)$. It follows that before either factor can be found an assumption must be made about the other. This fact is recognized in an instructive paper by Gevers and du Pré (1946). They actually reverse the procedure and, after making reasonable assumptions about both factors, synthesize $c^*(\omega)$. Their work is concerned with dielectric relaxation.

(ii) Because of the averaging that has been carried out over the $\Delta^{(i)}c$, the only *a priori* link between the relaxation properties of different thermodynamic coefficients is the inequality $\overline{\Delta c}_{(\alpha\alpha)}(\tau)\,\overline{\Delta c}_{(\beta\beta)}(\tau) \geqslant \overline{\Delta c}_{\alpha\beta}(\tau)^2$. The equality sign holds if all the $\Delta^{(i)}c$ in the range $(\tau, \tau+d\tau)$ are equal. In either case $\overline{\Delta c}_{(\alpha\alpha)}(\tau)$ and $\overline{\Delta c}_{(\beta\beta)}(\tau)$ are independent of one another so that a knowledge of one component of $\overline{\Delta c}(\tau)$ implies nothing about any other component.

In spite of these grave difficulties of principle the resolution into $\overline{\Delta c}(\tau)$ has been of considerable qualitative value—particularly when performed over a range of temperature. This is probably because in many cases the averaged value of $\Delta^{(i)}c$ does not vary greatly with either τ or temperature. As far as this is true $\overline{\Delta c}(\tau)$ is in fact a measure of $f(\tau)$ over a reasonable range of temperature.

We now return to the case of a finite number of ordering variables to discuss the effect of choosing different independent thermodynamic variables. The most important fact follows from equation (5.11) which gives the change in β due to a Legendre transformation from independent variables x^α to X_α; $\mathscr{L}$ is unchanged by such a transformation but, since $\mathscr{T} = -\mathscr{L}\beta^{-1}$, a $\mathscr{T}$ matrix which is diagonal for x^α is no longer diagonal for X_α—unless of course there is only a single ordering parameter involved. It is possible to find a fresh set of ordering variables which restores the diagonal properties and such a set could be called a proper set with

respect to the variables X_α. The general investigation of such changes is quite straightforward but the formulae are complicated and it seems sufficient here to note that the relaxation times of a system can be defined only with respect to a definite choice of independent thermodynamic variables. It should be added that in practice the changes involved are often small because according to equations (5.8) and (5.11) the numerical corrections are proportional to terms like $c^{-1}\Delta c$ which are often small compared with unity. When this is the case simple approximate formulae can sometimes be given. Suppose for example that we start with a proper set of ordering parameters with respect to x^α. According to equations (5.16) we then have for the dynamic coefficients

$$c^* = \bar{c} - \lambda R \lambda' \qquad \ldots\ldots(5.18)$$

where $\Delta c = \lambda\lambda'$ and R is a time-dependent relaxation operator.

With X for the thermodynamic variables, the dynamic coefficients may be found by simply inverting this expression (with a change of sign from the Legendre transform) :

$$c^{+*} = -c^{*-1} = -(1 - \bar{c}^{-1}\lambda R \lambda')^{-1}\bar{c}^{-1}. \qquad \ldots\ldots(5.19)$$

Now if the elements of Δc are all small with respect to those of $\bar{c}$, we may expand the bracket to obtain

$$c^{*-1} \simeq \bar{c}^{-1} + \bar{c}^{-1}\lambda R(\bar{c}^{-1}\lambda)'. \qquad \ldots\ldots(5.20)$$

It can be shown that the new reaction coefficients $\lambda^+_{\alpha i} \equiv (\partial(-X_\alpha)/\partial z^i)_{X_\beta}$ are given by $\lambda^+ = c^{-1}\lambda \simeq \bar{c}^{-1}\lambda$ and so the result can be stated as the following theorem : the form (5.18) for c^* is always valid with fixed R (i.e. constant relaxation times) provided that $\bar{c}$ and λ are evaluated for the variables actually being used and that Δc is small compared with c.

So far we have tacitly assumed that all the variables involved are scalars. On the other hand, we know that a thermodynamic treatment of elasticity and electricity requires tensorial thermodynamic variables and coefficients. It is natural to ask whether such systems require tensorial ordering parameters in order to describe relaxation effects. Consider an isotropic solid exhibiting delayed elasticity. Let us try to describe such a system by a single scalar ordering parameter. If the Voigt moduli of the material are s_{ij} and $s_{ij} + \Delta s_{ij}$ $(i, j = 1 \ldots 6)$ then from equation (5.9) we have $\Delta s_{(ii)}\Delta s_{(jj)} = \Delta s_{ij}{}^2$.

If the s_{ij} are replaced by expressions involving only the two independent moduli necessary for the isotropic case (e.g. Lamé's modulus and the shear modulus) then it is easy to see that the relations just given can be satisfied only if the instantaneous and delayed shear moduli are equal. Therefore a single scalar ordering coefficient is incompetent to represent a delayed shear. (Incidentally, the formula given above holds if the Δs_{ij} represent the difference between isothermal and adiabatic elastic moduli. The argument therefore verifies the known fact that the adiabatic and isothermal shear moduli are equal.) We may conclude that the representation of delayed elastic effects should be helped by the introduction of a tensorial ordering parameter. Later we shall show that the introduction of such a parameter does lead to a reasonable description of delayed elasticity in terms of well-known models.

The instantaneous rate of production of entropy in a relaxing system is $\theta_s = A'\dot{z}$. If we consider steady state sinusoidal variations in a system near equilibrium, then we may put

$$-\dot{F} = X'\dot{x} + A'\dot{z}.$$

in accordance with equation (5.7). It follows that the average rate of production of entropy is

$$\langle\theta_s\rangle = \langle A'\dot{z}\rangle = -\langle X'\dot{x}\rangle.$$

This can be neatly expressed in terms of the independent thermodynamic variables only by making use of the dynamic equation $X = c^* x$ together with the fact (proved earlier) that c is a symmetric matrix. It is then seen that

$$\langle\theta_s\rangle = -\tfrac{1}{2}\omega\bar{x}'(\mathscr{I}c^*)x$$
$$= -\tfrac{1}{2}\omega\left\{\sum_{\alpha=1}^{\nu}\mathscr{I}(c_{(\alpha\alpha)}^*)\,|x^\alpha|^2 + 2\sum_{\alpha>\beta=1}^{\nu}\mathscr{I}(c_{\alpha\beta}^*)\,|x^\alpha||x^\beta|\cos\theta_{\alpha\beta}\right\} \quad \ldots\ldots(5.21)$$

where $\mathscr{I}$ stands for 'the imaginary part of' and $\theta_{\alpha\beta}$ is the phase angle between x^α and x^β. In many cases only one of the thermodynamic variables is fluctuating because the process is practically adiabatic. Only one term of the first summation remains and the result is well known.

§ 6. Some Applications of Relaxation Theory

6.1. *Glass Formation*

The simplest system having a single ordering parameter is a system containing a single chemical reaction. We prescind from this case and consider a system which can be described only approximately by means of a single parameter: the case of glass formation. When a suitable liquid is cooled down below its melting point it may, in the absence of crystallization, become so viscous that the internal changes of structure associated with the change in temperature are unable to be completed within a reasonable time. One is then said to have formed a 'glass'. (It has been suggested that this *apparent* second-order transition should be called a 'relaxation transition'.) For a detailed account of glass formation from the present, thermodynamic point of view the reader may be referred to papers by Kauzmann (1948), Jones and Simon (1949), Davies and Jones (1953).

The basic Pfaffian for such a system comes from equation (5.7) with p and T as independent thermodynamic variables:

$$d(-G) = SdT - Vdp + Adz. \quad \ldots\ldots(6.1)$$

The matrix of instantaneous (or 'glassy') thermodynamic coefficients is

$$c = \begin{bmatrix} C_p/T & -V\alpha \\ -V\alpha & V\kappa \end{bmatrix}. \quad \ldots\ldots(6.2)$$

The first question to settle is whether or not the static identity of equation (5.6) is satisfied. The experimental data bearing on this point are scanty and in no case have all three properties ($\Delta\alpha$, $\Delta\kappa$ and ΔC_p) been measured by the same workers with the same specimen. The following figures taken from Davies and Jones (1953) must therefore be treated with reserve.

(c.g.s. units)	T(°K)	V	$10^4\Delta\alpha$	$10^{-6}\Delta C_p$	$10^{12}\Delta\kappa$	$\dfrac{\Delta\kappa\Delta C_p}{TV\Delta\alpha^2}$
Colophonium	300	0·93	~3	0·55	~10	~0·2
Selenium	300	0·24	2·5	1·9	5·8	2·4
Glucose	300	0·66	2·6	7·7	6·1	3·7
Rubber	320	1·1	3·1	6·0	37	8·3
Polystyrene	350	1·0	2·0	2·9	75	16

If equation (5.6) were true for these materials the numbers in the last column would be 1. The fact that they are not merely means that a single scalar ordering parameter does not provide an adequate description of the relaxation mechanism involved in glass formation. This is not very surprising. The qualitative explanation of glass formation is that the local structure of the material becomes frozen-in at the apparent transition temperature ; one would not expect to be able to describe the local structure in terms of a single scalar ordering parameter. Let us however ignore this for the moment and consider the isotropic behaviour of an idealized one-parameter system.

The reaction coefficients are

$$\lambda = \begin{bmatrix} (\partial S/\partial z)_{pT} \\ -(\partial V/\partial z)_{pT} \end{bmatrix} \qquad \ldots\ldots(6.3)$$

i.e. the entropy and volume changes of the ' reaction '.

The static relations between ΔC_p etc. and the reaction coefficients have already been given in equations (5.5). The thermodynamic equations of motion (with z chosen as a proper ordering parameter with respect to p, T) come from equation (5.14) :

$$\begin{aligned} \dot{S} &= \left[(\bar{C}_p/T) - \frac{\Delta C}{T} R\right] \dot{T} + [-V\bar{\alpha} + V\Delta\alpha R]\,\dot{p} \\ -\dot{V} &= [-V\bar{\alpha} + V\Delta\alpha R]\,\dot{T} + [V\bar{\kappa} - V\Delta\kappa R]\,\dot{p} \end{aligned} \qquad \ldots\ldots(6.4)$$

in which R stands for the operator $(\tau_{pT}\,d/dt)/(1+\tau_{pT}\,d/dt)$. These equations are sufficient to predict the behaviour of the system when the heat exchange with the surroundings and the impressed mechanical changes are given. Perhaps the simplest case occurs when the temperature is kept fixed. The second equation then yields (with $d \equiv \delta V/V$ for the dilatation)

$$1 + \tau_{pT}\left(\frac{d}{dt}\right) d + \left(\bar{\kappa} + \kappa\tau_{pT}\frac{d}{dt}\right) p = 0. \qquad \ldots\ldots(6.5)$$

This means for example that the isothermal application of a fixed pressure p to the system results in an instantaneous response in strain of $-\kappa p$ and a delayed response, reached by an exponential decay, of $-\bar{\kappa}p$.

Suppose now that one is interested in the adiabatic behaviour of the system ($\dot{S} = 0$). The *simplest* description is then given in terms of the proper ordering parameter with respect to (p, S) and the corresponding relaxation time. Instead of (6.5) we now find

$$\left(1 + \tau_{pS}\frac{d}{dt}\right) d + \left(\bar{\kappa}_S + \tau_{pS}\kappa_S\frac{d}{dt}\right) p = 0 \qquad \ldots\ldots(6.6)$$

where $\bar{\kappa}_S, \kappa_S$ are adiabatic compressibilities and $\tau_{pS} = C_p\tau_{pT}/\bar{C}_p$. The last statement exemplifies the remark made earlier to the effect that when (in this case) $\Delta C_p/C_p \ll 1$ the various proper relaxation times can be taken as equal.

It is sometimes useful to have the exact relations between the different relaxation times available. They are given by the following equations :

$$\tau_{pT} = \frac{\bar{\kappa}}{\kappa}\tau_{VT} = \frac{\bar{C}_p}{C_p}\tau_{pS} = \frac{\bar{\kappa}\bar{C}_V}{\kappa C_V}\tau_{VS} = \frac{\bar{\alpha}}{\alpha}\tau_{pV} = \frac{\bar{\alpha}}{\alpha}\tau_{TS} \qquad \ldots\ldots(6.7)$$

and may be found by elementary thermodynamic manipulations.

There exists a more general formula which covers changes of the thermodynamic variables other than the Legendre transformations implied by (6.7). Suppose we change the independent thermodynamic variables from x^α to $y^\alpha = f^\alpha(x^1, \ldots x^r, z)$. Then it can be shown (Davies and Lamb 1956) that

$$\tau_{y^1 \ldots y^r} = \tau_{x^1 \ldots x^r}\left[1 - \sum_{\alpha,\beta} \frac{\partial \bar{x}^\alpha}{\partial y^\beta} \Delta\left(\frac{\partial y^\beta}{\partial x^\alpha}\right)\right]. \qquad \ldots\ldots(6.8)$$

(The symbol $\partial \bar{x}^\alpha / \partial y^\beta$ means the equilibrium thermodynamic coefficient,

$$(\partial x^\alpha / \partial y^\beta)_{y^1 \ldots y^{\beta-1} y^{\beta+1} \ldots, A}.)$$

It may be verified that (6.8) reduces to (6.7) when $y^\alpha = X_\alpha$.

With the help of formulae of the type (5.5) and (5.11) it is also possible to express the λ and Δc appropriate to one set of thermodynamic variables in terms of those appropriate to another set.

The relaxation behaviour of glasses is only very approximately described by equations like (6.5). This fact (like the departures from the static formulae) is to be attributed to the multiplicity of ordering parameters which are actually present. If one is prepared to fit the data, somehow, into the 'straitjacket' of (6.5) then the relaxation time evidently gives a measure of the fractional resistance associated with volume flow. It is, of course, possible to introduce a bulk (or volume) viscosity to describe the effect but some care is necessary here because (*a*) one must distinguish between isothermal and adiabatic behaviour and (*b*) a volume viscosity is often introduced into hydrodynamics by means of a thermodynamic equation of motion equivalent to

$$\left(1 + \kappa\zeta \frac{d}{dt}\right) d + \kappa p = 0 \qquad \ldots\ldots(6.9)$$

(ζ being the bulk viscosity). Equation (6.9) can be regarded as the low frequency limit of (6.5) or (6.6) provided we identify ζ with $\tau\Delta\kappa/\kappa^2$. There is some evidence that, for structural relaxation in glasses, the bulk viscosity (defined in this way) varies with temperature in the same way as the shear viscosity.

6.2. *Sound Absorption in Fluids*

Consider now the propagation of small disturbances in a fluid medium. It can be shown by using a combination of the equations of motion, the continuity equation and the viscosity law that such disturbances can be described by an 'acoustic' linearization :

$$\rho \dot{d} = -\nabla^2 p + (\mu' + 2\mu)\nabla^2 \dot{d} \qquad \ldots\ldots(6.10)$$

where d is the dilatation, μ the coefficient of shear viscosity and μ' a second viscosity coefficient introduced into the viscosity law (Rosenhead 1954). Now by using equations similar to (6.4) the thermodynamic equation of state can be written as

$$\begin{aligned} \alpha^* \dot{T} &= \kappa^* \dot{p} + \dot{d} \\ T\alpha^* \dot{S} &= C_p^*(\kappa_S^* \dot{p} + \dot{d}). \end{aligned} \qquad \ldots\ldots(6.11)$$

Finally, the thermal conduction in the medium determines the change of entropy in accordance with

$$T\dot{S} = VK\nabla^2 T \qquad \ldots\ldots(6.12)$$

where K is the coefficient of thermal conductivity.

Combining these equations (and neglecting the difference between partial and substantive derivatives, as is tacitly done in forming (6.10)), we find

$$\rho\kappa_S^*\ddot{\psi}-(\mu'+2\mu)\kappa_S^*\nabla^2\ddot{\psi}-\nabla^2\dot{\psi}$$
$$=\frac{K}{\rho C_p^*}\{\rho\kappa^*\nabla^2\ddot{\psi}-(\mu'+2\mu)\kappa^*\nabla^4\dot{\psi}-\nabla^2\psi\} \qquad \ldots\ldots(6.13)$$

where ψ is any one of p, T, ρ, etc.

Apart from the use of operators for thermodynamic variables, this equation is identical with the propagation equation of Stokes and Kirchhoff (see Truesdell (1953) for a modern discussion).

Now let us seek solutions proportional to $\exp i(\omega t-kx)$ with ω real. The characteristic equation is

$$iH(\Gamma^{-1}+iV)X^2-(1+iV+iH)X+1=0 \qquad \ldots\ldots(6.14)$$

where
$$H=\omega K\kappa^*/C_p^*, \qquad V=\omega(\mu'+2\mu)\kappa_S^*$$
$$\Gamma=\kappa^*/\kappa_S^*, \qquad X=k^2/\rho\omega^2\kappa_S^*.$$

Under most experimental conditions $|V|\ll 1$ and $|H|\ll 1$, so we may expand the undamped (acoustic) solution to obtain

$$\frac{k^2}{\omega^2}=\rho\kappa_s^*\{1-V-H(1-\Gamma^{-1})\}+\mathrm{O}(H)+\mathrm{O}(V). \qquad \ldots\ldots(6.15)$$

The physical meaning of this equation is the following: let α be the amplitude absorption coefficient, v the phase velocity, λ the wavelength and let

$$k^2/\omega^2=|k^2/\omega^2|\exp i\theta.$$

Then
$$v=\frac{|\omega/k|}{|\cos\frac{1}{2}\theta|}; \qquad \frac{\alpha\lambda}{2\pi}=|\tan\tfrac{1}{2}\theta|. \qquad \ldots\ldots(6.15\,a)$$

The terms in V and H give rise to 'classical absorption' associated with shear viscosity and heat flow, respectively. It is clear that they are modified by the presence of relaxation effects but we do not wish to discuss this further here. There remain the terms coming from κ_S^* itself.

In the general case we have from equation (5.16)

$$\kappa_S^*(\omega)=\bar{\kappa}_S\left(1-\sum_i\frac{\Delta^{(i)}\kappa_S}{\bar{\kappa}_S}\frac{i\omega\tau_{pS}^{(i)}}{1+i\omega\tau_{pS}^{(i)}}\right) \qquad \ldots\ldots(6.16)$$

where $\tau_{pS}^{(i)}$ are the proper relaxation times with respect to p, S. Therefore experimental measurements on sound absorption over a wide range of frequencies can be expected to yield *two* parameters for each relaxation mechanism, viz. $\Delta^{(i)}\kappa_S$ and $\tau^{(i)}$. For the purpose of considering possible mechanisms for the reaction it seems best to re-write these parameters in terms of p, T variables because it might be hoped that the reaction coefficients $(\partial V/\partial z)_{pT}$ and $(\partial S/\partial z)_{pT}$ are easier to think of than the corresponding (p, S) coefficients. There are two cases:

(*a*) For a single ordering parameter it can be shown that

$$\frac{\Delta\kappa_S}{\bar{\kappa}_S}=(\bar{\gamma}-1)\frac{\bar{C}_p}{C_p}\left(\frac{\Delta\alpha}{\bar{\alpha}}-\frac{\Delta C_p}{\bar{C}_p}\right)^2\Big/\frac{\Delta C_p}{\bar{C}_p}=\frac{V\bar{C}_p}{\beta\bar{\kappa}_S C_p}\left\{\frac{1}{V}\left(\frac{\partial V}{\partial z}\right)_{pT}-\frac{\bar{\alpha}T}{\bar{C}_p}\left(\frac{\partial S}{\partial z}\right)_{pT}\right\}^2$$

and
$$\tau_{Sp}=C_p\tau_{pT}/\bar{C}_p. \qquad \ldots\ldots(6.17)$$

Two special cases are of interest: (i) for isomeric reactions in an ideal gas $(\partial V/\partial z)_{pT} = \Delta\alpha = 0$ and the formulae reduce to those of Herzfeld and Rice (1928); (ii) for water at 4°C, $\bar{\alpha} = 0$ and we have a special case considered by Hall (1948). Formulae similar to (6.17) are provided by Meixner (1952 b).

(*b*) For more than one ordering parameter it was shown in § 5 that the general conversion formulae are rather complicated. But assuming that the incremental variables are small we may expand to the first order in $\Delta\alpha/\alpha$, etc. and (as in equation (5.20)) recover

$$\kappa_S^*(\omega) = \bar{\kappa}_S\left[1 - \sum_i \frac{V}{\beta^{(i)}\bar{\kappa}_S}\left(\frac{1}{V}\left(\frac{\partial V}{\partial z^i}\right) - \frac{\bar{\alpha}T}{\bar{C}_p}\left(\frac{\partial S}{\partial z^i}\right)_{pT}\right)^2 \frac{i\omega\tau^{(i)}}{1+i\omega\tau^{(i)}}\right] \quad \ldots\ldots(6.18)$$

where now, as part of the approximation, the diagonal elements $\tau^{(i)}$ and $\beta^{(i)}$ are independent of the choice of thermodynamic variables.

Sound absorption due to relaxation effects has been found to be present in both gases and liquids. The study of gases is largely due to Kneser and he has reviewed the subject fairly recently (1949). In most cases the ' reactions ' involved are the isomeric reactions associated with the change in vibrational energy levels of the gas molecules. It is usually possible to describe the results by means of a single relaxation time and the thermodynamic part of the relaxation formulae checks well with the known statistical mechanics of molecular excitation. The relaxation time is difficult to calculate and indeed difficult to measure because it seems to be very sensitive to the presence of impurities. The theoretical problem is of course one of reaction kinetics.

The case of liquids is of more current interest. Until recently there has been a large unexplained discrepancy between the observed value of the absorption coefficient and the ' classical ' contribution due to thermal conductivity and viscosity. Typical figures for $(\alpha/\omega^2)_{\text{exp}}/(\alpha/\omega^2)_{\text{theor}}$ are: carbon disulphide 1200, toluene 26, acetic acid 5300, water 3.

In 1942 Tisza noticed that the presence of a ' second ' viscosity μ' in the viscosity law could be used to account for the discrepancy. The term has usually been ignored in hydrodynamics, either because the flow considered was incompressible or because it was assumed that $\mu' + \frac{2}{3}\mu = 0$. The latter assumption seems to be true for gases. Compressible viscous fluid flow in liquids has rarely been considered (except in sound propagation) and it is precisely for such flows that the second viscosity could be important. Support for this explanation was thought to be given by experiments of Liebermann (1949), who verified the existence of an acoustic streaming effect predicted by Eckart (1948), and linked by him with the second viscosity coefficient; the values of this coefficient as found by Liebermann were consistent with values found from the ultrasonic absorption data. However, Lamb and Pinkerton discovered in 1949 that acetic acid showed a variation of α with ω which could be explained as a relaxation effect. It was then realized that *any* absorption could give streaming effects. It will be seen from (6.15) that for $\omega\tau \ll 1$, $\alpha/\omega^2 \sim \Delta\kappa_S\tau/\kappa_S$. Hence the second viscosity would be regarded as a low frequency ' tail ' of relaxation effects centred at higher frequencies. Further work, particularly by Lamb and his collaborators, has established the relaxation in other liquids. The question as to whether the second viscosity should always be regarded as being due to relaxation effects will be considered in the next section.

The exact nature of the relaxation effects has not been established in all cases (in carbon disulphide it is due to vibrational relaxation (Lamb and Andreae 1951)) and the problem of relaxation times is virtually untouched.

6.3. *Visco-elasticity*

We have already seen that it is not possible to account for shear relaxation by means of a scalar ordering parameter. Suppose therefore that we introduce a tensorial ordering parameter z_{ij}, which we take to be a symmetric cartesian tensor of the second order. Let there be a corresponding symmetric tensorial affinity A_{ij}. β becomes a fourth order tensor $\beta_{rs,kl}$ and for an isotropic material we may take β^{-1} to be of the form

$$\beta^{-1}{}_{rs,kl} = A\delta_{rs}\delta_{kl} + B(\delta_{rk}\delta_{sl} + \delta_{rl}\delta_{sk}). \qquad \ldots\ldots(6.19)$$

By a similar argument to that given above one finds

$$c_{\alpha\beta}{}^{*} = \bar{c}_{\alpha\beta} + \lambda_{\alpha,rs}\beta^{-1}{}_{rs,kl}R_{kl,mn}\lambda_{mn,\beta} \qquad \ldots\ldots(6.20)$$

where $R_{kl,mn}$ is of similar form to β and is made up of time-dependent operators of the type $(\tau d/dt)/(1+\tau d/dt)$; $\lambda_{\alpha,rs}$ is symmetric in r and s because of the assumed symmetry of z_{ij} and by the Onsager theorem $c_{\alpha\beta}{}^{*} = c_{\beta\alpha}{}^{*}$. If the isotropic expressions for β^{-1} and R are introduced into the second term in equation (6.20) it can be thrown into the form

$$c_{\alpha\beta}{}^{*} = \bar{c}_{\alpha\beta} - \frac{\Delta_{\alpha\beta}{}^{(1)}\tau_1 d/dt}{1+\tau_1 d/dt} - \frac{\Delta_{\alpha\beta}{}^{(2)}\tau_2 d/dt}{1+\tau_2 d/dt} \qquad \ldots\ldots(6.21)$$

where

$$\Delta_{\alpha\beta}{}^{(1)} = -(3A+2B)\lambda_{\alpha,nn}\lambda_{\beta,mm}$$

$$\Delta_{\alpha\beta}{}^{(2)} = -4B\lambda_{\alpha,rs}\lambda_{\beta,rs} - 2A\lambda_{\alpha,nn}\lambda_{\beta,mm}.$$

Notice that $\Delta_{\alpha\beta}{}^{(1)}$ satisfies the static identity (5.9) but $\Delta_{\alpha\beta}{}^{(2)}$ does not. If this formula is applied to either adiabatic *or* isothermal straining we may neglect the coupling between thermal and elastic variables and the equations of elasticity become

$$\sigma_{ij} = \left(\bar{\lambda} + \frac{\Delta^{(1)}\lambda}{1+\tau_1 d/dt}\tau_1\frac{d}{dt} + \frac{\Delta^{(2)}\lambda}{1+\tau_2 d/dt}\tau_2\frac{d}{dt}\right)\delta_{ij}e_{kk} + 2\left(\bar{\mu} + \frac{\Delta^{(2)}\mu}{1+\tau_2 d/dt}\tau_2\frac{d}{dt}\right)e_{ij} \qquad \ldots\ldots(6.22)$$

where $\bar{\lambda}$ and $\bar{\mu}$ are the equilibrium Lamé and rigidity moduli, σ_{ij} is the stress tensor and e_{ij} the strain tensor.

We may draw the following conclusions:

(i) Associated with a tensorial ordering parameter there are two relaxation times and three elastic moduli.

(ii) The modulus $\Delta^{(i)}\lambda$ and the relaxation time τ_1 are present for the purely scalar processes considered in the previous section.

(iii) With $\bar{\mu} \neq 0$ the equations describe the behaviour of a relaxing solid.

(iv) With $\bar{\mu} = 0$ we have a generalized liquid: for 'slow' processes the third and fifth terms become $\Delta^{(2)}\lambda\dot{e}_{\alpha\alpha}\delta_{ij}$ and $2\Delta^{(2)}\mu\tau_2\dot{e}_{ij}$. Hence the shear viscosity coefficient is $\Delta^{(2)}\mu\tau_2$ and the second viscosity coefficient is $\Delta^{(2)}\lambda\tau_2$. This means

that the ordinary shear viscosity coefficient and the second viscosity coefficient can be regarded as low-frequency ' reflections ' of a relaxation process with a comparatively short relaxation time. This merely represents a refinement of the well known model of Maxwell. Meixner (1954 b) has reached similar conclusions to the above starting from rather different premisses.

It should be added that one can obtain systems showing both delayed elasticity and shear flow by taking two or more tensorial ordering parameters into the system. The visco-elastic behaviour of glasses is actually of this type : reference may be made to Jones (1948–49).

6.4. *Further Developments*

It is clear that for electrical systems one must introduce a vectorial ordering parameter in order to achieve a description of magnetic and electric relaxation. The end result is again a purely phenomenological description of the system in terms of time independent coefficients (Davies 1955). However, as long as the restriction to linear behaviour is borne in mind this may well be of considerable value. The method is of little help in dealing with hysteresis. Some recent attempts to cover this field by means of similar notions have been made by Everett and his collaborators (1952, 1954). It is difficult to make much progress here because the pure thermodynamic theory does not allow us to extract any information about the internal ordering variables from the experimental data unless further assumptions are made (for instance, that there is only one internal parameter). It is true that dynamic experiments (sound absorption, for example) give such information but this is only because a linear rate hypothesis has already been made. Such an hypothesis is clearly unsuitable for systems exhibiting hysteresis.

From this point of view we may conclude that a purely thermodynamic theory of internal parameters is empty unless supplemented by the linear rate hypothesis (and Onsager relations) of irreversible thermodynamics or by a kinetic identification of the ordering parameters.

PART III. BIBLIOGRAPHICAL NOTES ON SOME FURTHER TOPICS

§ 7. Other Aspects of Irreversibility

7.1. *Application and Development of the Onsager Theory*

Most of the applications of Onsager's theory are considered in the reviews and monographs listed in § 1. Electrochemistry, thermo-electric effects and thermo-magnetic effects are the commonest fields of study. Recent references which, with the help of the reviews, will give a lead to the literature include : de Groot, Mazur and Tolhoek (1953), Prigogine, Mazur and Defay (1953) on the electrochemistry of bulk processes ; Holtan, Mazur and de Groot (1953) on thermocouples and thermocells ; Mazur and Prigogine (1951) on thermo-magnetic effects. Newer applications include the work of Hooyman, Holtan, Mazur and de Groot (1953) on irreversibility in rotating systems—an application to the centrifuge ; Mazur (1952 a) on electro-kinetic effects.

Perhaps the most notable recent advance in the theory is the attempt of Kluitenberg and de Groot to throw it into a relativistically invariant form (1953 a, b,

1954, 1955 a, b). On the basis of their work they find the Abraham stress tensor to be preferable to that of Minkowski. It is however not clear just to what extent symmetry of the stress tensor has been excluded by thermodynamic assumptions introduced early in their argument.

As was recognized by Onsager himself, the linear symmetric form of the thermodynamical equations of motion admit a variational treatment. Prigogine has developed this idea very extensively. His approach is to consider the stationary state to be partially constrained and to correspond to a minimum rate of production of entropy, subject to the constraints. Recent work on this topic includes : Mazur (1952 b) on minimum principles in continuous systems, Prigogine (1954) on the stability of the stationary state, Klein and Mayer (1954), Prigogine and Mayer (1955) on fluctuations in Knudsen transfer in relation to minimum entropy production, Biot (1955) on minimum principles in visco-elastic systems.

Two authors have recently attempted to found the Onsager formalism including the reciprocity theorem on equilibrium thermodynamic theory. They are : Wundheimer (1954) and Popov (1955).

7.2. *The Microscopic Theory and Fluctuations*

A number of attempts have been made to bring Onsager's theory closer to microscopic physics. None has been wholly successful but such attempts are important because they may give a lead towards more general microscopic methods than gas-kinetic theory and its derivatives.

The most suggestive (and least microscopic) work has been concerned with making the fluctuation part of Onsager's theory into an example of Brownian movement. Onsager and Machlup (1953) found formulae which give the probability for a set of Onsager coordinates to take a prescribed path in time. Hashitzume (1952) showed that the transition probability T of § 2.4 satisfies a generalized Fokker–Planck equation. This has also been recovered from a different point of view by Yamamoto (1953). Green (1952) paid special attention to the possibility of defining the macroscopic variables as phase functions. He suggests that an acceptable macroscopic variable must be, in some sense, an approximate integral of the motion.

Callen and Welton (1951) proposed that the macroscopic variables could be represented as time-dependent perturbations of the form $V(t)\,Q(x)$ in the quantum-mechanical Hamiltonian. ($V(t)$ is to be regarded as a generalized coordinate and $Q(x)$ as a generalized force.) They proceeded to define an admittance function connecting V and Q which they found to be connected with the power spectrum of Q by means of a generalized Nyquist theorem. This type of work has been further developed by Callen, Barasch and Jackson (1952) and Takehasi (1952).

An entirely different approach to the theory (which by-passes fluctuations) is to be found in the work of Bergmann and his collaborators (Bergmann 1951, Bergmann and Thomson 1953, Bergmann and Lebowitz 1955). The object here is to construct a generalization of the canonical distribution which is appropriate when two or more reservoirs at different temperatures are in interaction. The Onsager reciprocity theorem has been recovered. The programme has some points in common with that of Cox (1955).

References

Alfrey, T., 1948, *Mechanical Properties of High Polymers* (New York : Interscience).

Bartlett, M. S., 1955, *Stochastic Processes* (Cambridge : University Press).

Bergmann, P. G., 1951, *Phys. Rev.*, **84**, 1026.

Bergmann, P. G., and Lebowitz, J. L., 1955, *Phys. Rev.*, **99**, 578.

Bergmann, P. G., and Thomson, A. C., 1953, *Phys. Rev.*, **91**, 180.

Bertrand, J. L. F., 1887, *Thermodynamique* (Paris : Gauthier-Villars).

Biot, M. A., 1955, *Phys. Rev.*, **97**, 1463.

Bridgman, P. W., 1932, *Proc. Nat. Acad. Sci., Wash.*, **18**, 242 ; 1950, *Rev. Mod. Phys.*, **22**, 56.

Callen, H. B., 1948, *Thesis*, Massachusetts Institute of Technology ; 1952, *Phys. Rev.*, **85**, 16.

Callen, H. B., Barasch, M., and Jackson, J., 1952, *Phys. Rev.*, **88**, 1382.

Callen, H. B., and Welton, T. A., 1951, *Phys. Rev.*, **83**, 34.

Casimir, H. B. G., 1945, *Rev. Mod. Phys.*, **17**, 343 ; 1949, *Nuovo Cim. Suppl. No.* 2, 227.

Chapman, S., and Cowling, T. G., 1952, *The Mathematical Theory of Non-uniform Gases*, 2nd Edn. (Cambridge : University Press).

Cox, R. T., 1955, *Statistical Mechanics of Irreversible Change* (Baltimore : Johns Hopkins Press).

Davies, R. O., 1952, *Physica*, **18**, 270 ; 1955, *Conf. de Physique des basses Temperatures, Paris* (Paris : International Union of Pure and Applied Physics), p. 489.

Davies, R. O., and Jones, G. O., 1953, *Advanc. Phys.* (*Phil. Mag.* Suppl.), **2**, 370.

Davies, R. O., and Lamb, J., 1956, *Proc. Phys. Soc.* B, **69**, 293.

Denbigh, K. G., 1951, *The Thermodynamics of the Steady State* (London : Methuen).

Denbigh, K. G., and Raumann, G., 1951, *Proc. Roy. Soc.* A, **210**, 377, 518.

Dirac, P. A. M., 1947, *Quantum Mechanics*, 3rd Edn. (Oxford : University Press).

Domenicali, C. A., 1954, *Rev. Mod. Phys.*, **26**, 167.

Duhem, P., 1911, *Traité d'énergétique* (Paris : Gauthier-Villars).

Eastman, E. D., 1926, *J. Amer. Chem. Soc.*, **48**, 1482.

Eckart, C., 1948, *Phys. Rev.*, **73**, 68.

Everett, D. H., and Smith, F. W., 1954, *Trans. Faraday Soc.*, **50**, 187.

Everett, D. H., and Whitton, W. I., 1952, *Trans. Faraday Soc.*, **48**, 749.

Frenkel, J., 1946, *Kinetic Theory of Liquids* (Oxford : University Press).

Gevers, M., and du Pré, F. K., 1946, *Trans. Faraday Soc.*, **42A**, 47.

Gibbs, J. W., 1906, *Scientific Papers of J. Willard Gibbs* (London : Longmans).

Green, M. S., 1952, *J. Chem. Phys.*, **20**, 1281.

Greene, R. F., and Callen, H. B., 1951, *Phys. Rev.*, **83**, 1231.

de Groot, S. R., 1945, *L'effet Soret* (Amsterdam : North-Holland) ; 1951, *Thermodynamics of Irreversible Processes* (Amsterdam : North-Holland).

de Groot, S. R., Jansen, L., and Mazur, P., 1950, *Physica*, **16**, 691.

de Groot, S. R., and Mazur, P., 1954, *Phys. Rev.*, **94**, 218, 224.

de Groot, S. R., Mazur, P., and Tolhoek, H. A., 1953, *Physica*, **19**, 549.

Gross, B., 1953 (*Actualités Sci. industr. No.* 1190), Mathematical Structure of the Theories of Visco-elasticity (Paris : Hermann).

Haase, R., 1952, *Ergebn. exakt. Naturw.*, **22**, 56.

Hall, L., 1948, *Phys. Rev.*, **73**, 775.

Hashitzume, N., 1952, *Progr. Theor. Phys., Univ. Kyoto*, **8**, 461.

Herzfeld, K. F., and Rice, F. O., 1928, *Phys. Rev.*, **31**, 691.

Holtan, H., Mazur, P., and de Groot, S. R., 1953, *Physica*, **19**, 1109.

Hooyman, G. J., 1955, *Thesis*, University of Leiden.

Hooyman, G. J., Holtan, H., Mazur, P., and de Groot, S. R., 1953, *Physica*, **19**, 1095.

Jones, G. O., 1948–9, *Rep. Progr. Phys.*, **12**, 133 (London : Physical Society).

Jones, G. O., and Simon, F. E., 1949, *Endeavour*, **8**, 175.

Kapitza, P. L., 1941, *Phys. Rev.*, **60**, 354.

Kauzmann, W., 1948, *Chem. Rev.*, **43**, 219.

Keenan, J. H., 1955, *Appl. Mech. Rev.*, **8**, 49.

KENNARD, E. H., 1932, *Proc. Nat. Acad. Sci., Wash.*, **18**, 237.
KHINCHIN, A. I., 1949, *Mathematical Foundations of Statistical Mechanics* (New York : Dover).
KLEIN, M. J., and MAYER, P. H. E., 1954, *Phys. Rev.*, **96**, 250.
KLUITENBERG, G. A., and DE GROOT, S. R., 1953 a, *Physica*, **19**, 689 ; 1953 b, *Ibid.*, **19**, 1079 ; 1954, *Ibid.*, **20**, 199 ; 1955 a, *Ibid.*, **21**, 148 ; 1955 b, *Ibid.*, **21**, 169.
KNESER, H. O., 1949, *Ergebn. exakt. Naturw.*, **22**, 121.
LAMB, J., and ANDREAE, J. H., 1951, *Nature, Lond.*, **167**, 898.
LAMB, J., and PINKERTON, J. M. M., 1949, *Proc. Roy. Soc.* A, **199**, 114.
LANDAU, L. D., and LIFSHITZ, E., 1938, *Statistical Physics* (Oxford : University Press).
LIEBERMANN, L. N., 1949, *Phys. Rev.*, **75**, 1415.
MACHLUP, S., and ONSAGER, L., 1953, *Phys. Rev.*, **91**, 1512.
MAZUR, P., 1952 a, *J. Chim. Phys.*, **49**, 130 ; 1952 b, *Bull. Acad. Belg. Cl. Sci.*, **38**, 182.
MAZUR, P., and PRIGOGINE, I., 1951, *J. Phys. Radium*, **12**, 616 ; 1953, *Mem. Acad. R. Belg. Cl. Sci.*, **28**, 1.
MEIXNER, J., 1941 a, *Ann. Phys., Lpz.*, **39**, 333 ; 1941 b, *Ibid.*, **40**, 165 ; 1952 a, *Changements de phases* (Paris : Société de Chimie-physique) ; 1952 b, *Acustica*, **2**, 101 ; 1953, *Kolloidzschr.*, **134**, 3 ; 1954 a, *Thermodynamik der irreversiblen Prozesse* (Aachen) (Collected reprints of published papers) ; 1954 b, *Proc. Roy. Soc.* A, **226**, 51 ; 1954 c, *Z. Naturf.*, **9a**, 654.
MEYER, L., and MELLINK, J. H., 1947, *Physica*, **13**, 197.
MONTROLL, E. W., and GREEN, M. S., 1954, *Annu. Rev. Phys. Chem.*, **5**, 449.
MOYAL, J. E., 1949, *J. R. Statist. Soc.* B, **11**, 150.
MULLER, F. H. (Ed.), 1953, *Discussion on Relaxation*, Suppl. to *Kolloidzschr.*, **134**.
ONSAGER, L., 1931 a, *Phys. Rev.*, **37**, 405 ; 1931 b, *Ibid.*, **38**, 2265.
ONSAGER, L., and MACHLUP, S., 1953, *Phys. Rev.*, **91**, 1505.
POPOV, K., 1955, *J. Exp. Theor. Phys.*, **28**, 257.
PRIGOGINE, I., 1947, *Étude thermodynamique des phénomènes irréversibles* (Liége : Desoer) ; 1949, *Physica*, **15**, 272 ; 1952, *Het Colloquium over Ultrasonore Trillingen*, p. 113 ; 1954, *Bull. Acad. Belg. Cl. Sci.*, **40**, 471 ; 1955, *Introduction to Thermodynamics of Irreversible Processes* (Oxford : Blackwell).
PRIGOGINE, I., and DEFAY, R., 1954, *Chemical Thermodynamics* (London : Longmans Green).
PRIGOGINE, I., and MAYER, G., 1955, *Bull. Acad. Belg. Cl. Sci.*, **41**, 22.
PRIGOGINE, I., and MAZUR, P., 1951, *Physica*, **17**, 661.
PRIGOGINE, I., MAZUR, P., and DEFAY, R., 1953, *J. Chim. Phys.*, **50**, 146.
RICE, S. O., 1944, *Bell Syst. Tech. J.*, **23**, 133.
ROSENHEAD, L., 1954, *Proc. Roy. Soc.* A, **226**, 1.
SCHWARZL, F., 1951, *Physica*, **17**, 832, 923.
SCHRÖDINGER, E., 1948, *Statistical Thermodynamics* (Cambridge : University Press).
SWINBURNE, J., 1904, *Entropy, or Thermodynamics from an Engineer's Standpoint and the Reversibility of Thermodynamics* (London : Constable).
TAKEHASI, H., 1952, *J. Phys. Soc. Japan*, **7**, 439.
THOMSEN, J. S., 1953, *Phys. Rev.*, **91**, 1263.
TISZA, L., 1942, *Phys. Rev.*, **61**, 531.
TOLHOEK, H. A., and DE GROOT, S. R., 1952, *Physica*, **18**, 780.
TRUESDELL, C., 1953, *J. Rat. Mech. Anal.*, **2**, 643.
VAN KAMPEN, N. G., 1954, *Physica*, **20**, 603.
WANG, MIN CHEN, and UHLENBECK, G. E., 1945, *Rev. Mod. Phys.*, **17**, 323.
WATANABE, S., 1955, *Rev. Mod. Phys.*, **27**, 26.
WIGNER, E. P., 1954, *J. Chem. Phys.*, **22**, 1912.
WUNDHEIMER, A. W., 1954, *Proc. Nat. Acad. Sci., Wash.*, **40**, 844.
YAMAMOTO, T., 1953, *Progr. Theor. Phys., Univ. Kyoto*, **10**, 11.